

DATING THE BRITISH TERTIARY IGNEOUS PROVINCE IN IRELAND

BY THE  $^{40}\text{Ar}$ - $^{39}\text{Ar}$  STEPWISE DEGASSING METHOD

Thesis submitted in accordance with the requirements of the University  
of Liverpool for the degree of Doctor in Philosophy

by  
Paul Thompson

August, 1985



## **IMAGING SERVICES NORTH**

Boston Spa, Wetherby  
West Yorkshire, LS23 7BQ  
[www.bl.uk](http://www.bl.uk)

**CONTAINS MICROFICHE**

**To be added at a later  
date**

## ABSTRACT

K-Ar dates for Irish Tertiary igneous rocks suggest that activity may have occurred between 26 and 82 Ma ago. However, studies in other parts of the British Tertiary Igneous Province (BTIP) have shown that such dates are unreliable. The preferred approach for dating rocks from the BTIP is to use a technique which allows self-consistency checks on the data to be made. The only such technique which is applicable to all the different rock types found in the BTIP is the  $^{40}\text{Ar}$ - $^{39}\text{Ar}$  stepwise degassing technique. The aim of this investigation was to assign reliable ages to Tertiary igneous rocks from Ireland by the use of the  $^{40}\text{Ar}$ - $^{39}\text{Ar}$  stepwise degassing technique. Special emphasis was placed on rocks which had given ages outside the range of reliable age estimates for the BTIP as a whole (52 - 63 Ma).

45 samples, mainly whole-rocks, were dated in this study. Although only seven of these gave well-defined absolute age estimates, the best age estimates for the samples as a whole suggest that the majority of Tertiary igneous activity in Ireland occurred in the interval 58 - 62 Ma. This includes rocks which had given ages which were clearly anomalous in the context of reliable age estimates for the BTIP. The results in this study also indicate that the Tertiary granites of Ireland, found in the Mourne Mountains, constitute a phase of igneous activity which occurred significantly later, at around 52 - 55 Ma ago. The age estimates for Tertiary igneous activity in Ireland, produced in this study, are consistent with reliable dates for other areas of the BTIP. Across the whole province, extrusive volcanism (represented by plateau basalts and the volcanic central complexes), and the intrusion of all the major dyke swarms, seems to have occurred in the earlier time interval (58 - 62 Ma). Several plutonic granite intrusions (plus some acidic volcanism) have been reliably dated in the

52 - 55 Ma interval - the Mourne, Skye Eastern Red Hills, Lundy and St. Kilda.

This investigation has again demonstrated that the  $^{40}\text{Ar}$ - $^{39}\text{Ar}$  stepwise degassing technique is superior to the conventional K-Ar method. The comparison of the  $^{40}\text{Ar}$ - $^{39}\text{Ar}$  best age estimates produced in this study with complementary K-Ar analyses clearly demonstrates this point.

The dates produced in this study are not only consistent with those reliable ones for the rest of the BTIP, but are seen to be geologically sound where stratigraphic controls exist.

In this study, the chronological interpretation of  $^{40}\text{Ar}$ - $^{39}\text{Ar}$  stepwise degassing data has been aided by extracting large numbers of steps from each sample (more than 20), complementary petrographic and scanning electron microscope observations, and careful consideration of the physical processes involved.

### ACKNOWLEDGEMENTS

I am indebted to all the members of the Department of Geophysics at Liverpool University, and all the staff at the Herald reactor, AWRE Aldermaston, for their invaluable assistance and guidance. Special thanks go to Dr. A. E. Mussett, who supervised this research project, Mr. B. Moss, who provided invaluable assistance in the laboratory, Mr. A. G. McCormack, who wrote the two Algol 68 programs and who was always available for consultation about matters relating to computers and computer programming, and my mother who showed great resilience in typing this thesis. Additional thanks go to Professor P. Mohr and Dr. J. Preston for their important contributions to the geological aspects of this study, Mr. D. C. Rex, who kindly performed the K-Ar analyses quoted in the thesis, Dr. P. Beahan, who supervised my scanning electron microscope work, my wife Lynne, who provided valuable secretarial assistance, and many others too numerous to mention.

This research was supported financially by the Natural Environmental Research Council.

TO LYNNE

## CONTENTS

	<u>Page</u>
<u>CHAPTER ONE - INTRODUCTION</u>	1
<u>CHAPTER TWO - THE <math>^{40}\text{Ar}</math>-<math>^{39}\text{Ar}</math> STEPWISE DEGASSING TECHNIQUE</u>	4
2:1 Introduction	5
2:2 The principles of $^{40}\text{Ar}$ - $^{39}\text{Ar}$ dating	5
2:2:1 Comparison of the $^{40}\text{Ar}$ - $^{39}\text{Ar}$ and K-Ar dating techniques	5
2:2:2 Producing a $^{40}\text{Ar}$ - $^{39}\text{Ar}$ age	7
2:3 The stepwise degassing technique	10
2:4 Summary	13
<u>CHAPTER THREE - PRESENTATION OF INTERPRETATION OF STEPWISE DEGASSING DATA</u>	14
3:1 Introduction	15
3:2 Age spectrum plot	15
3:3 Two-dimensional isotope correlation diagram (ICD2)	17
3:4 Three-dimensional isotope correlation diagram (ICD3)	22
3:5 The chronological interpretation of $^{40}\text{Ar}$ - $^{39}\text{Ar}$ stepwise degassing data	24
<u>CHAPTER FOUR - THE PHYSICAL INTERPRETATION OF DISTURBED <math>^{40}\text{Ar}</math>-<math>^{39}\text{Ar}</math> AGE SPECTRA</u>	27
4:1 Introduction	28
4:2 Volume diffusion	28
4:3 Effects of irradiation	37
4:3:1 Patterns of release for natural argon isotopes	38
4:3:2 Recoil of argon isotopes produced by neutron interaction	39
4:4 Atmospheric and initial argon	43
4:5 Summary	47

	<u>Page</u>
<u>CHAPTER FIVE - <math>^{40}\text{Ar}</math>-<math>^{39}\text{Ar}</math> EXPERIMENTAL TECHNIQUES</u>	49
5:1 Introduction	50
5:2 Standard	50
5:3 Samples	50
5:4 Sample and standard irradiation	52
5:4:1 Neutron flux variations	52
5:4:2 Interference reaction corrections	55
5:4:3 Loss of radiogenic argon during the irradiation	57
5:5 Gas extraction line	58
5:6 Mass spectrometer argon analysis	59
5:7 Data analysis	61
<u>CHAPTER SIX - <math>^{40}\text{Ar}</math>-<math>^{39}\text{Ar}</math> DATES FOR IRISH TERTIARY IGNEOUS ROCKS</u>	64
6:1 Introduction	65
6:1:1 Background to this study	65
6:1:2 The Tertiary igneous geology of Ireland	65
6:1:3 Presentation and interpretation of results	67
6:2 Results	68
6:2:1 The Kerry dyke system	68
6:2:2 The intrusive systems of west-central Ireland	73
6:2:3 The Droimchogaidh sill	79
6:2:4 The Lough Key dyke	91
6:2:5 Killala Bay	93
6:2:6 The Blind Rock dyke	114
6:2:7 The Antrim Lava Group	117
6:2:8 The Mourne Mountains	127
6:2:9 The Carlingford Complex	140
6:3 Conclusions	145



	<u>Page</u>
<u>CHAPTER SEVEN - DISCUSSION</u>	147
<u>APPENDIX 1 - CONSTANTS USED IN THIS <math>^{40}\text{Ar}</math>-<math>^{39}\text{Ar}</math> DATING STUDY</u>	154
<u>APPENDIX 2 - <math>^{40}\text{Ar}</math>-<math>^{39}\text{Ar}</math> STEPWISE DEGASSING ARRHENIUS DIAGRAMS</u>	156
<u>APPENDIX 3 - INTERFERENCE REACTIONS AND ARGON ISOTOPE RECOIL ENERGIES</u>	163
<u>APPENDIX 4 - THE IMPORTANCE OF THE INTERFERENCE CORRECTIONS AND THE POSSIBLE EFFECTS OF ERRORS IN, OR VARIATIONS FROM, THE ADOPTED VALUES</u>	175
<u>APPENDIX 5 - COMPUTER PROGRAM LISTINGS AND EXAMPLE OUTPUTS</u>	178
<u>APPENDIX 6 - SCANNING ELECTRON MICROSCOPY</u>	180
<u>APPENDIX 7 - PETROGRAPHIC SAMPLE DESCRIPTIONS</u>	188
<u>APPENDIX 8 - THE <math>^{40}\text{Ar}</math>-<math>^{39}\text{Ar}</math> STEPWISE DEGASSING DATA TABLES FOR THE SAMPLES ANALYSED IN THIS STUDY</u>	198
<u>REFERENCES</u>	200

CHAPTER ONE

Introduction

The Irish Tertiary igneous rocks are part of the British Tertiary Igneous Province (BTIP) - see Fig. 1:1. However, in this context they are quite distinct in terms of their association. In north-west Scotland, lavas and dyke swarms are usually found adjacent to the igneous centres, e.g. Skye and Mull. In Ireland, however, the lava pile (which is by far the largest remnant of Tertiary igneous activity in the British Isles) is not directly associated with a centre of activity and the dyke swarms, although dense in the vicinity of the centres, are widely distributed.

Of all the areas within the British Tertiary Igneous Province, Ireland has the least geochronological coverage, with the majority of dates available having been obtained by the conventional K-Ar method. Work in the BTIP as a whole has shown that such K-Ar dates are often not consistent with the known sequence of geological events and are therefore unreliable e.g. Purdy et al., (1972), Mussett et al., (1973). The preferred approach in dating the BTIP is to use a technique which offers the possibility of making internal self-consistency checks (Mussett, 1982). Two such methods only are applicable to dating the relatively young BTIP: the  $^{40}\text{Ar}-^{39}\text{Ar}$  stepwise degassing and the Rb-Sr techniques. For rocks of this age the Rb-Sr method is practical for acidic rocks only, so for a broad geochronological study of Irish Tertiary igneous rocks, which are largely basic in nature, the best method is the  $^{40}\text{Ar}-^{39}\text{Ar}$  stepwise degassing technique.

Reported K-Ar dates for Ireland suggest that Tertiary activity may have occurred during the interval 26-82 Ma (Horne & Macintyre, 1975; Macintyre et al., 1975). This apparent span of over 50 Ma contrasts markedly with accurate dates (determined by the  $^{40}\text{Ar}-^{39}\text{Ar}$  stepwise degassing and Rb-Sr techniques) for the rest of the British Tertiary Igneous Province (52-63 Ma: Mussett, 1980; Dickin & Jones, 1983; Dagley & Mussett, 1985). Clearly, a systematic  $^{40}\text{Ar}-^{39}\text{Ar}$  dating study

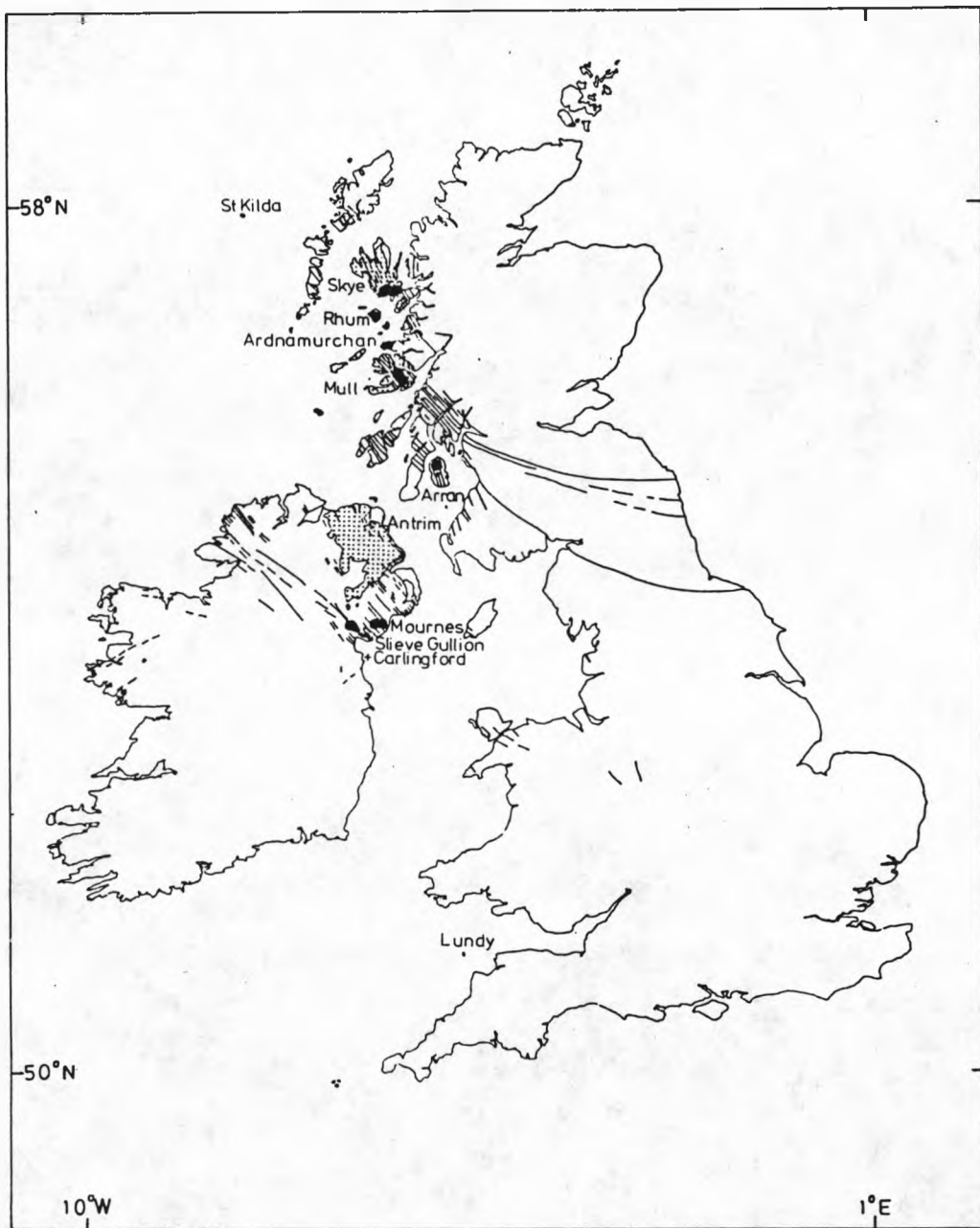


Fig. 1:1 The British Tertiary Igneous Province: stippled areas-lavas; black-centres; lines-dykes (adapted from Macintyre et al., 1975)

was required for the Irish Tertiary igneous rocks, to ascertain whether the reported age spread is real or just an artefact of non-ideal K-Ar systematics.

Because many of the Irish Tertiary igneous rocks are fine-grained, in this  $^{40}\text{Ar}-^{39}\text{Ar}$  stepwise degassing study it has been necessary to use whole-rock samples rather than mineral separates. Although the former have not been used often in terrestrial  $^{40}\text{Ar}-^{39}\text{Ar}$  dating studies because complex patterns of gas release are expected for multi-phase samples, several authors have demonstrated that whole-rock sample dates are consistent with the geological succession e.g. Mussett et al., (1980), Mussett (1985).

Chapters 2 - 5 outline the basic theoretical and experimental principles of the  $^{40}\text{Ar}-^{39}\text{Ar}$  stepwise degassing technique, with the approach to interpretation being discussed in Chapters 3 and 4. In an attempt to extract the most information from the  $^{40}\text{Ar}-^{39}\text{Ar}$  data in this study, and to make chronological interpretation more certain, several types of data presentation have been used, including one developed in this thesis (see Chapter 3). In addition, the interpretation of  $^{40}\text{Ar}-^{39}\text{Ar}$  data has been aided by supplementary sample investigations involving petrography and scanning electron microscope studies (see Appendix 6 for the latter). The results and interpretation of the  $^{40}\text{Ar}-^{39}\text{Ar}$  data for the Irish Tertiary igneous rocks are discussed area by area in Chapter 6. The discussion in Chapter 7 considers, in the light of this study, the implications for the  $^{40}\text{Ar}-^{39}\text{Ar}$  stepwise degassing technique and the regional geological interpretation of the BTIP.

The objective of this study can be summarised as follows: to date accurately Tertiary igneous activity in Ireland with special emphasis on localities that have given ages outside the range of reliable dates for the BTIP.

CHAPTER TWO

The  $^{40}\text{Ar} - ^{39}\text{Ar}$  Stepwise Degassing Technique

2:1 Introduction

This chapter is split up into two sections. The first describes the principles of  $^{40}\text{Ar}$ - $^{39}\text{Ar}$  dating and the second deals in detail with the stepwise degassing technique. A primary concern is to emphasise the advantages of the  $^{40}\text{Ar}$ - $^{39}\text{Ar}$  stepwise degassing technique when compared with the conventional K-Ar and  $^{40}\text{Ar}$ - $^{39}\text{Ar}$  fusion methods. These advantages proved to be vital for dating Irish Tertiary rocks.

2:2 The Principles of  $^{40}\text{Ar}$ - $^{39}\text{Ar}$  Dating

2:2:1 Comparison of the  $^{40}\text{Ar}$ - $^{39}\text{Ar}$  and K-Ar dating techniques

The  $^{40}\text{Ar}$ - $^{39}\text{Ar}$  dating technique is a development of the conventional potassium-argon (K-Ar) method.

The basic equation for K-Ar dating is (Dalrymple & Lanphere, 1969):

$$t = \frac{1}{\lambda_e + \lambda_\beta} \text{Log}_e \left( 1 + \frac{^{40}\text{Ar}^*}{^{40}\text{K}} \frac{\lambda_e + \lambda_\beta}{\lambda_e} \right)$$

where  $t$  = age to be calculated

$^{40}\text{Ar}^*$  = number of atoms of radiogenic  $^{40}\text{Ar}$  per gram of sample

$^{40}\text{K}$  = number of atoms of  $^{40}\text{K}$  per gram of sample

$\lambda_e$  = decay constant of  $^{40}\text{K}$  for positron emission and electron capture (the decay of  $^{40}\text{K}$  in this manner produces  $^{40}\text{Ar}^*$ )

$\lambda_\beta$  = decay constant of  $^{40}\text{K}$  for electron emission (the decay of  $^{40}\text{K}$  in this manner produces  $^{40}\text{Ca}^*$ )

For this method, measurements of both  $^{40}\text{Ar}^*$  and  $^{40}\text{K}$  are required to calculate an age and these must be made on separate aliquots. The amount of  $^{40}\text{K}$  in a sample can be measured in several ways (see Dalrymple & Lanphere, 1969) and  $^{40}\text{Ar}^*$  is measured in a mass spectrometer after sample fusion.

The  $^{40}\text{Ar}$ - $^{39}\text{Ar}$  technique which was first explicitly outlined by Merrihue (1965), differs from the K-Ar method in that the amount of  $^{40}\text{K}$  is measured indirectly. A fraction of the  $^{39}\text{K}$  present in a sample, which

is assumed to be present in a fixed ratio with  $^{40}\text{K}$ , is converted to  $^{39}\text{Ar}$  by irradiation with fast neutrons. This  $^{39}\text{Ar}$  is then measured in a mass spectrometer in the same way as the  $^{40}\text{Ar}^*$ . The fraction of  $^{39}\text{K}$  converted to  $^{39}\text{Ar}$  is determined by including samples of known K-Ar age in the same irradiation. These are called standards or monitors.

$$t_{\text{standard}} = \frac{1}{\lambda_e + \lambda_\beta} \text{Log}_e \left[ 1 + J \left( \frac{^{40}\text{Ar}^*}{^{39}\text{Ar}_K} \right)_{\text{standard}} \right]$$

where  $J$  = irradiation parameter (J-value)

$^{39}\text{Ar}_K$  = potassium-derived  $^{39}\text{Ar}$

$$\text{Therefore } J = \frac{\exp [ t_{\text{standard}} \cdot (\lambda_e + \lambda_\beta) ] - 1}{\left( \frac{^{40}\text{Ar}^*}{^{39}\text{Ar}_K} \right)_{\text{standard}}} \quad (1)$$

$$\text{and } t_{\text{sample}} = \frac{1}{\lambda_e + \lambda_\beta} \text{Log}_e \left[ 1 + J \left( \frac{^{40}\text{Ar}^*}{^{39}\text{Ar}_K} \right)_{\text{sample}} \right] \quad (2)$$

The advantage of the  $^{40}\text{Ar}$ - $^{39}\text{Ar}$  technique is that all the measurements required can be made on the gas released from a single sample in a mass spectrometer. This means that:

- i) the problems of sample inhomogeneity are circumvented
- ii) only isotopic ratios, rather than absolute quantities, need be measured
- iii) the sample can be degassed in a series of steps of increasing temperature rather than simply being fused in a single step. This is stepwise degassing. Such a procedure offers several advantages which are vital to this project and these will be explained in Section 2:3.

Several dating studies have demonstrated the equivalence of fusion  $^{40}\text{Ar}$ - $^{39}\text{Ar}$  and K-Ar ages, e.g. Mitchell (1968), Miller et al., (1970), Dalrymple & Lanphere (1971), McDougall & Roksandic (1974). However, as more recent work has shown, in certain circumstances, ages



determined by the  $^{40}\text{Ar}$ - $^{39}\text{Ar}$  technique can be significantly older than the corresponding K-Ar ages, e.g. Clague et al (1975), Dalrymple & Clague (1976), Dalrymple et al., (1977), Ozima et al., (1977), Seidemann (1978), Feraud et al., (1982). This behaviour is explained in terms of an irradiation-induced artefact which causes some of the  $^{39}\text{Ar}_K$  produced to be lost from the rock sample (see Section 4:3:2). Having lost some fraction of its  $^{39}\text{Ar}_K$ , the sample's  $^{40}\text{Ar}^*/^{39}\text{Ar}_K$  is obviously enhanced and thus the calculated age will be too high. The types of sample affected by  $^{39}\text{Ar}_K$  loss are usually those which contain fine-grained potassium-bearing phases (often found as a result of alteration). The likelihood of this problem affecting a particular sample may be ascertained by petrographic observation. Recognition of this irradiation-induced artefact, in situations where complementary K-Ar ages do not exist, is discussed in Section 4:3:2.

#### 2:2:2 Producing a $^{40}\text{Ar}$ - $^{39}\text{Ar}$ age

The introduction gives only a simplistic view of  $^{40}\text{Ar}$ - $^{39}\text{Ar}$  dating and in reality many factors have to be considered and quantified when producing a  $^{40}\text{Ar}$ - $^{39}\text{Ar}$  age.

#### The Standard

Alexander & Davis (1974) have discussed the requirements of a  $^{40}\text{Ar}$ - $^{39}\text{Ar}$  standard. The most important qualities that a standard must possess are that it has a known and repeatable  $^{40}\text{Ar}^*/^{40}\text{K}$  ratio (equivalent to the K-Ar age), and that it should be of a composition and grain size such that irradiation-induced artefacts are negligible. When choosing a standard it is important to bear in mind the ages of the samples to be dated and their potassium contents, as these place limitations on the range of useful fluxes received during neutron irradiation. Normally this involves choosing a standard with an age similar to the samples being dated. Often a standard with low calcium and chlorine contents is preferred so that interfering argon isotopes

are reduced to a minimum (see below). Ideally, large quantities of the chosen standard should be available so that it can be used for a whole dating study. The uncertainty in the age of the standard then adds only a systematic error, which, for the purposes of internal comparison, can be ignored.

#### The Irradiation

Because of the presence of fast neutron flux gradients in reactors (on the scale of centimetres), several standard samples are enclosed within a single irradiation package. In this way, the flux received in different parts of the package can be closely monitored. It is usually necessary to interpolate the J-values measured at standard locations to the sample locations.

The fast neutron flux received by a set of samples during an irradiation can be optimized in two ways (Turner, 1971a). By ensuring that:

- i) the  $^{40}\text{Ar}^*/^{39}\text{Ar}_K$  ratio is of the right order for the most accurate measurement on the mass spectrometer recording system
- ii) the interference reaction contributions to the measured argon isotopes (from neutron interactions on potassium, calcium and chlorine) are kept to a minimum.

The choice of the optimum irradiation dose obviously depends on the sample age and composition. It is thus advantageous to have all the samples in an irradiation package of similar age and composition.

#### Calculation of the $^{40}\text{Ar}^*/^{39}\text{Ar}_K$ ratio (also expressed herein as $40^*/39_K$ )

To calculate the  $40^*/39_K$  ratio for a sample or standard, the measured  $^{40}\text{Ar}$  and  $^{39}\text{Ar}$  isotopes have to be corrected for other contributions.

These are:

- i) initial argon (argon incorporated at the time of crystallisation) which, for terrestrial samples, is usually assumed to be of atmospheric composition

- ii) atmospheric argon derived from the sample and/or extraction line
- iii) argon produced by neutron interactions on potassium isotopes
- iv) argon produced by neutron interactions on calcium isotopes
- v) argon produced by neutron interactions on chlorine isotopes

} These are the  
interference  
reactions

To permit all the corrections to be made, five argon isotopes have to be measured:

$$^{40}\text{Ar} \quad 40_{\text{total}} = 40^* + 40_{\text{atm}} + 40_{\text{init}} + 40_{\text{K}} + 40_{\text{Ca}}$$

$$^{39}\text{Ar} \quad 39_{\text{total}} = 39_{\text{K}} + 39_{\text{Ca}}$$

$$^{38}\text{Ar} \quad 38_{\text{total}} = 38_{\text{atm}} + 38_{\text{init}} + 38_{\text{K}} + 38_{\text{Ca}} + 38_{\text{Cl}}$$

$$^{37}\text{Ar} \quad 37_{\text{total}} = 37_{\text{Ca}}$$

$$^{36}\text{Ar} \quad 36_{\text{total}} = 36_{\text{atm}} + 36_{\text{init}} + 36_{\text{Ca}} + 36_{\text{Cl}}$$

where atm refers to atmospheric argon ,

init refers to initial argon ,

K, Ca, Cl refer to argon produced by neutron interactions on potassium, calcium and chlorine respectively.

The conversion of argon isotopes to other isotopic species due to neutron interactions is not considered significant. This is because of the low cross sections involved (Turner, 1971a) and the very low Ar/K ratios in rocks and minerals (Brereton, 1970). Tetley et al., (1980) showed that, experimentally, the isotopic composition of atmospheric argon was unaffected by neutron irradiation. All other possible interactions are considered to be negligible due to insignificant cross sections, low interacting particle fluxes or long decay times (see Appendix 3).

The complex business of reducing the above equations to give an expression for  $40^*/39_{\text{K}}$  can be followed in the "DATING" computer program (Appendix 5); only the result is quoted here:

$$\frac{40^*}{39_K} = \frac{40_{total} - \left(\frac{40}{36}\right)_{atm} \cdot (36_{total} - 36_{Cl}) - \left[ \frac{40 - \left(\frac{40}{36}\right)_{atm} 36}{37} \right]_{Ca} \cdot 37_{total}}{39_K} - \left[ \frac{40}{39} \right]_K \quad (3)$$

where,

$$36_{Cl} = \left\{ \left(\frac{38}{36}\right)_{atm} \cdot 36_{total} - 38_{total} + \left[ \frac{38}{39} \right]_K \cdot 39_K + \left[ \frac{38 - \left(\frac{38}{36}\right)_{atm} 36}{37} \right]_{Ca} 37_{total} \right\} \\ \times \frac{\left[ \frac{36}{38} \right]_{Cl}}{\left(\frac{38}{36}\right)_{atm} \left[ \frac{36}{38} \right]_{Cl} - 1}$$

and

$$39_K = 39_{total} - \left[ \frac{39}{37} \right]_{Ca} \cdot 37_{total}$$

$\left(\frac{40}{36}\right)_{atm}$ ,  $\left(\frac{38}{36}\right)_{atm}$  are the isotope ratios for atmospheric argon. The quantities inside the square brackets refer to interference reactions and they are constants calculated from the analysis of irradiated salt samples (see Section 5:4:2). A full list of all the constants used in this  $^{40}\text{Ar}-^{39}\text{Ar}$  study is presented in Appendix 1.

In many cases, the correction for chlorine-derived interference is negligible and the above expression is reduced to:

$$\frac{40^*}{39_K} = \frac{40_{total} - \left(\frac{40}{36}\right)_{atm} \cdot 36_{total} - \left[ \frac{40 - \left(\frac{40}{36}\right)_{atm} 36}{37} \right]_{Ca} \cdot 37_{total}}{39_K} - \left[ \frac{40}{39} \right]_K \quad (4)$$

Many authors use this type of equation to calculate  $40^*/39_K$ ; however, in this work the standard age calculation procedure utilised equation (3).

Having calculated the sample's J-value and  $40^*/39_K$  ratio, its  $^{40}\text{Ar}-^{39}\text{Ar}$  age can be derived from equation (2).

### 2:3 The Stepwise Degassing Technique

The principle advantage of the  $^{40}\text{Ar}-^{39}\text{Ar}$  dating method lies in the use

of the stepwise degassing technique, an approach to  $^{40}\text{Ar}$ - $^{39}\text{Ar}$  dating first described by Merrihue & Turner (1966).

For an ideal sample, the age of each of the heating steps is expected to be identical, with this age representing the true age of the event. The ideal sample and the true age are two important concepts that must be explained. An ideal sample is one which has remained closed with respect to argon and potassium since the event to be dated. It also contains no argon at the time of closure other than that of atmospheric composition. The true age is the age representing the time of closure of the potassium-argon system.

Dalrymple & Lanphere (1974) tested the  $^{40}\text{Ar}$ - $^{39}\text{Ar}$  stepwise degassing technique on a series of presumed ideal samples with well-determined ages from 40-1700 Ma, as defined by other dating techniques. Each sample gave a near-ideal "age spectrum" with the only deviation from constant age being for the very small low temperature steps, which were explained in terms of slight argon loss and possible gas fractionation. Dalrymple & Lanphere (1974) concluded that ideal samples give a "plateau" of ages (i.e. a series of steps giving statistically the same age) that reveals the true age, with only minor discrepancies for the lowest temperature steps.

Non-ideal samples do not, in general, produce internally concordant age spectra. However, the establishment of a plateau over a significant proportion of the gas release (> 50% of the  $^{39}\text{K}$  released) is often taken as meaning that the plateau age has a real geochronological significance (see Section 3:2).

The  $^{40}\text{Ar}$ - $^{39}\text{Ar}$  stepwise degassing technique has several advantages over the total fusion method, the latter being really applicable only to ideal samples (in the same way as the K-Ar method). These advantages arise because of the separation of the various gas components con-

tained within rock/mineral samples.

i) If a sample has been subjected to an "event" of some kind (e.g. thermal, deformational or chemical), or if it has been affected by irradiation induced artefacts, then this disturbance may be limited to a particular portion of the gas release. Often, it is the low temperature steps which are predominantly affected by such disturbances (see Sections 4:2 and 4:3) and meaningful geochronological information may be obtained from the higher temperature steps. A total fusion date (or K-Ar date) would, on the other hand, just give an average age for the whole gas release which would be of no geological significance.

ii) Atmospheric argon contained within rocks and minerals is often concentrated over particular portions of the gas release. A not uncommon pattern is for there to be high atmospheric levels at low and high temperatures with reduced levels for the intermediate gas fractions. A significant reduction in the levels of atmospheric argon for a particular portion of the gas release (compared to total fusion) means that the  $^{40}\text{K}/^{39}\text{K}$  ratios for the corresponding steps can be determined to a much higher precision than the total gas  $^{40}\text{K}/^{39}\text{K}$ . Thus, ages determined from stepwise degassing data may be of a significantly higher precision than those calculated in total fusion experiments. A further discussion about atmospheric argon in rocks and minerals is presented in Section 4:4.

iii) Because, in stepwise degassing, we are producing a series of ages for the same sample (perhaps representing the gas release from different mineral phases; or at least from different physical or geometric locations within the same mineral; see Section 4:2), we are in a position to make statistical self-consistency checks on the data to assess its significance. The statistical criteria for the acceptance of a plateau age as meaningful are considered in Chapter 3. Such internal

checks on the consistency of data are not possible in either total fusion  $^{40}\text{Ar}$ - $^{39}\text{Ar}$  dating or K-Ar dating.

#### 2:4 Summary

In this dating study I have used the  $^{40}\text{Ar}$ - $^{39}\text{Ar}$  stepwise degassing technique. This approach offers several distinct advantages over both the conventional K-Ar method and the  $^{40}\text{Ar}$ - $^{39}\text{Ar}$  fusion technique. The  $^{40}\text{Ar}$ - $^{39}\text{Ar}$  technique (simple fusion or stepwise degassing) is superior to the K-Ar method as the problems of sample homogeneity are circumvented and isotopic ratios, rather than absolute quantities, only need be measured. The stepwise degassing version of the  $^{40}\text{Ar}$ - $^{39}\text{Ar}$  technique is an improvement on the simple fusion approach as, for the former, the various gas components contained within rock/mineral samples are, to some extent, separated. Calculating  $^{40}\text{Ar}$ - $^{39}\text{Ar}$  ages is complex, with many corrections to be taken account of. However, where a single standard is used, computed age uncertainties may be at a significantly lower level than those achieved in K-Ar work.

CHAPTER THREE

Presentation and Interpretation of Stepwise Degassing Data



### 3:1 Introduction

In this  $^{40}\text{Ar}$ - $^{39}\text{Ar}$  stepwise degassing dating study, I will use three types of data presentation for chronological interpretation. The first two, the age spectrum plot and the two-dimensional isotope correlation diagram (ICD2), are those commonly found in the literature. The third, the three-dimensional isotope correlation diagram (ICD3), is a mode of presentation which has not been used before for the  $^{40}\text{Ar}$ - $^{39}\text{Ar}$  dating of terrestrial samples. In terms of age calculation, these three types of data presentation make different sets of assumptions. The age spectrum plot, which is the data plot most commonly presented, makes the most assumptions of the three but is often preferred because of its visual simplicity. The ICD2 and ICD3 make one and two less assumptions respectively than the age spectrum plot and are used to test for hypothetical argon components. Because of the uncertainties involved in each plot, the approach to the interpretation of  $^{40}\text{Ar}$ - $^{39}\text{Ar}$  stepwise degassing data preferred in this study involves the use of all three types of presentation. After describing the three types of plot, I will discuss in detail the approach to chronological interpretation of  $^{40}\text{Ar}$ - $^{39}\text{Ar}$  stepwise degassing data adopted in this thesis.

### 3:2 Age Spectrum Plot (Fig. 3:1)

The apparent age of each heating step is plotted against the cumulative percentage of  $^{39}\text{K}$  released. The vertical extent of each age box indicates plus and minus one standard deviation from the calculated age (the systematic J-value error is omitted). This presentation was first used by Turner et al., (1966) and it is preferred to a simple apparent age v. step number plot e.g. Fitch et al., (1969) because the latter gives no indication of the relative size of steps. Clearly, in terms of size, we are most interested in  $^{39}\text{K}$ , which is the measure

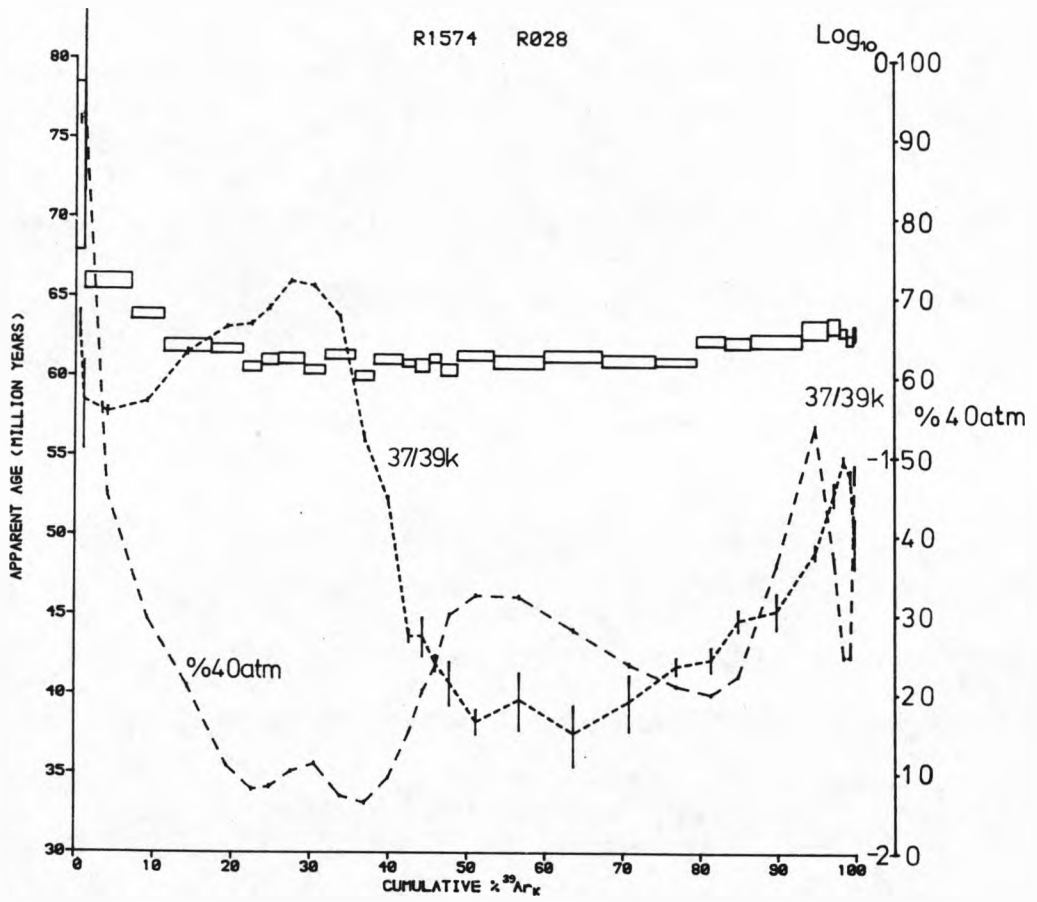


Fig. 3:1 The age spectrum plot

of effective  $^{40}\text{K}$  content and is not subject to geological processes. Included on the age spectrum plot are two other graphs. The  $\%40_{\text{atm}}$  graph shows the variation in the percentage of naturally occurring  $^{40}\text{K}$ , which is assumed to be of atmospheric origin in the age calculation (note that  $\%40_{\text{atm}} = 100 - \%40^*$ ). The  $^{37}/^{39}\text{K}$  graph gives a direct representation of the Ca/K ratio for each step; this may be useful in the identification of minerals which dominate particular phases of the gas release (see Section 4:2). The derivation of all these parameters can be followed in the "STEPAGE" computer program (Appendix 5).

In terms of geochronological interpretation, the most important age spectrum feature is the plateau. Usually, for a plateau age to be accepted as meaningful certain criteria have to be met (e.g. Fleck et al., 1977, Mussett et al., 1980). Although the precise criteria applied vary, they can be summarised as follows:

- i) The plateau must consist of several consecutive steps which constitute a significant proportion of the  $^{39}\text{K}$  released from the sample (usually taken as  $> 50\%$ ).
- ii) All plateau steps must possess statistically the same age.

Dalrymple & Lanphere (1974) proposed that steps containing less than 4 - 5% of the  $^{39}\text{K}$  released should be ignored in the analysis of age spectra because such steps were observed in some cases to give anomalous ages. They suggest that this phenomenon may be the result of experimentally introduced isotopic fractionation effects, which are presumed to be only significant where the amount of gas released from the sample is small. However, Roddick et al., (1980) suggested that the rejection of small steps was unwarranted, as they had observed that all but the very smallest of fusion steps ( $\approx 0.1\% ^{39}\text{K}$ ) gave consistent ages.

Where a plateau is accepted, the normal procedure is to calculate a mean age for the steps involved (called a plateau age). The mean can be calculated in a number of ways and in this dating study, two plateau ages are quoted:

- i) Total gas age - the argon isotopes released in each step are added together and a single age is calculated.
- ii) Weighted mean age - the expressions used in the calculation of the weighted mean age and its error (see "STEPAGE" computer program - Appendix 5) are a derivation of those presented by Topping (1972). Each step age is weighted by the reciprocal of its variance.

If at all possible, any "meaningful" plateau age (as defined above) must be assessed geologically. If the inferred age is inconsistent with the known geology, then it must be viewed with some scepticism. Examples of "false" plateaux are to be found in Pankhurst et al, (1973), Berger (1975), Hanson et al., (1975), Albarede et al, (1978), Roddick et al., (1980), Dallmeyer & Rivers (1983).

### 3:3 Two-dimensional Isotope Correlation Diagram - ICD2 (Fig. 3:2)

The precise details of the plotted ratios are given in Table 3:1, but essentially ICD2 can be thought of as a  $^{39}\text{K}/^{40}\text{v. }^{36}/^{40}$  plot in which 36 and 40 have been corrected for their respective interference reactions.

For an ideal sample, data points will lie along a straight line, with the y intercept giving the true  $^{40}\text{*}/^{39}\text{K}$  ratio and the x intercept giving  $(^{40}/^{36})_0 = (^{40}/^{36})_{\text{atmospheric}}$ .

In constructing the age spectrum plot, it was necessary to make the assumption that any initial argon present had an atmospheric composition. For ICD2, however, this is not necessary. As long as the atmospheric and initial argon form a component of constant isotopic

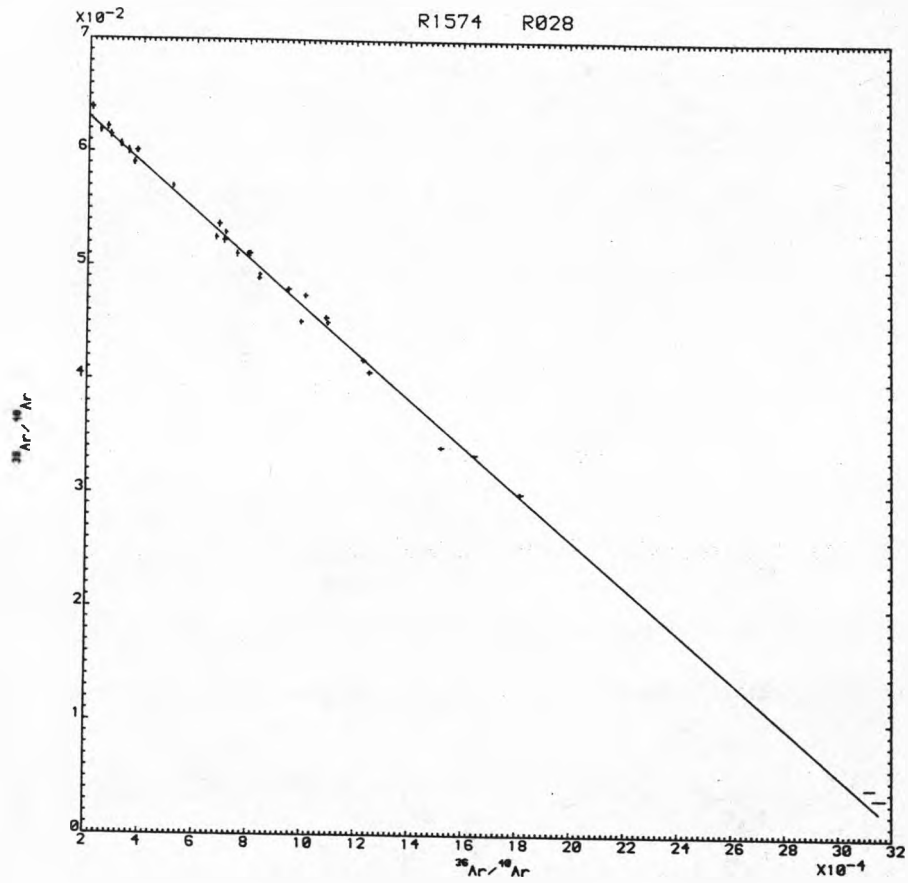
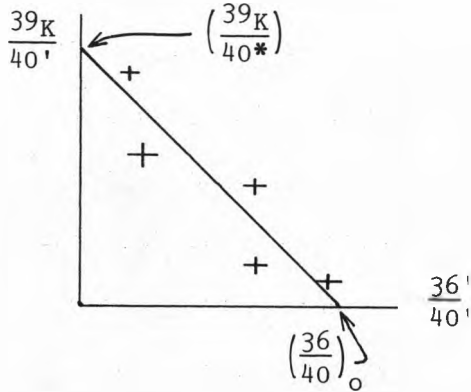


Fig. 3:2 The two-dimensional isotope correlation diagram (ICD2)

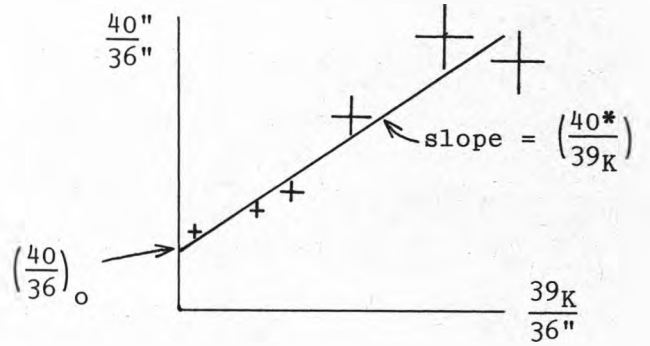
$$\left(\frac{40}{36}\right)_o \frac{36'}{40'} + \left(\frac{40^*}{39K}\right) \frac{39K}{40'} = 1$$

$$a \quad x + \quad b \quad y = 1$$



$$\left(\frac{40^*}{39K}\right) \left(\frac{36}{40}\right)_o \frac{39K}{36''} - \left(\frac{36}{40}\right)_o \frac{40''}{36''} = -1$$

$$a \quad x - \quad b \quad y = -1$$



where  $36' = 36_{total} - 36_{Cl}$

$$40' = 40_{total} - 40_K - \left[ \frac{40 - (40/36)_{atm} \cdot 36}{37} \right]_{Ca} 37_{total}$$

$$36'' = 36_{total} - \left[ \frac{36}{37} \right]_{Ca} 37_{Ca}$$

$$40'' = 40_{total} - 40_K$$

$36_{Cl}$  and  $40_{Ca}$  are assumed to be negligible

Table 3:1 Comparison of ICD2 and isochron plots

composition, ICD2 will reveal the true age and the composition of the mixed component. In some cases, especially where corrections for system atmospheric blank have been made, the atmospheric argon may be negligible, and thus ICD2 would reveal the true age and  $(40/36)_0 = (40/36)_{\text{initial}}$ . In plotting data points on an ICD2 and fitting the best straight line (see below), one is, in effect, making the assumption that natural non-radiogenic argon constitutes a hypothetical component with a fixed 40/36 ratio.

Comparing the age spectrum plot with this isotope correlation diagram, the advantage of the latter is that one less assumption is required and that two, rather than one, unknowns can be calculated. The drawback of isotope correlation diagram data analysis is that the data points say nothing about the size of the corresponding steps.

ICD2 as described here is almost identical to the isotope correlation diagram used by authors such as Davis (1977), Stettler & Bochsler (1979), Roddick et al., (1980), McDougall (1981) and Radicati di Brozolo et al., (1981). The use of 40 as the reference isotope was first proposed by Turner (1971) in a discussion of multi-dimensional isotope correlation diagrams. This approach is nowadays often preferred to the more traditional isochron plot (first described by Merrihue & Turner, 1966) in which 36 is the reference isotope (Table 3:1). The problem with using 36 as the reference isotope (described in detail by Roddick et al., 1980) is that it is usually the smallest and least accurately measured argon isotope. This results in the correlation of x and y errors due to data point positioning and error, being dominantly controlled by the 36. Where 40 is the reference isotope, correlation of errors is insignificant because 40 is usually the largest and most accurately measured argon isotope (in this case data point errors are largely a function of the 36 and  $^{39}\text{K}$  errors). Fig. 3:3, which is the isochron plot equivalent

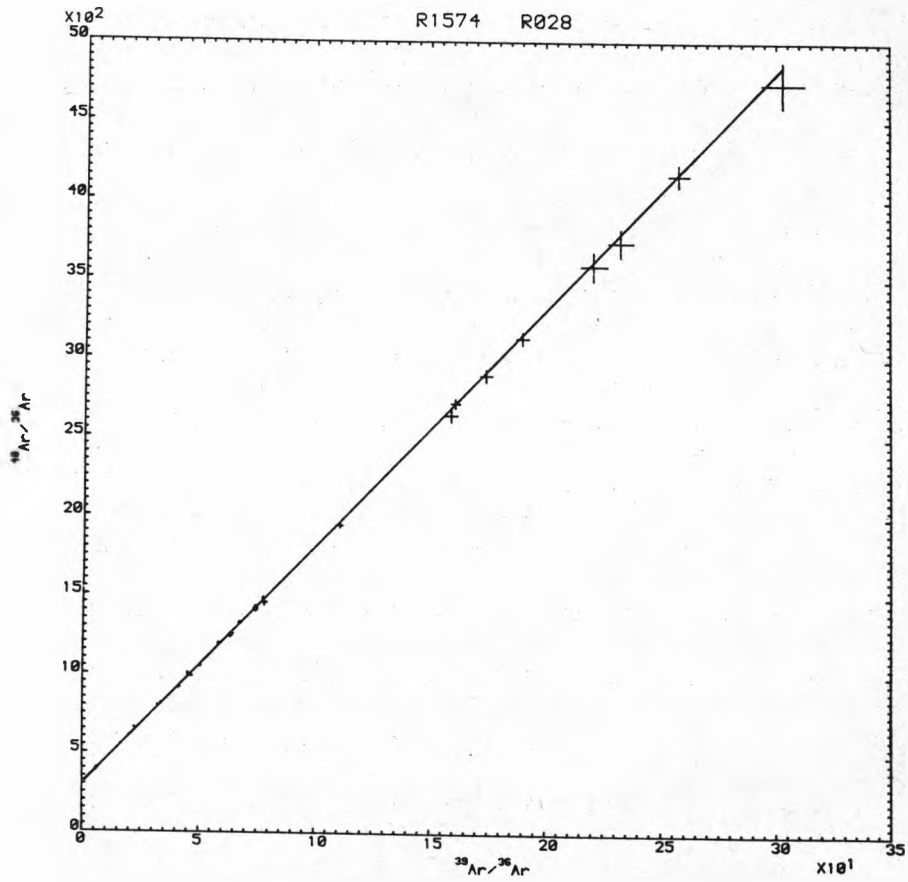


Fig. 3:3 The isochron plot



to the ICD2 of Fig. 3:2, displays clearly the symptoms of correlated errors i.e. large errors for high (x,y) values.

In order to calculate the best fitting straight line for a set of data points on ICD2 or an isochron plot, a least squares regression technique is employed (see Section 5:7). The quality of the fit is best assessed by the calculation of a parameter called the Mean Standard Weighted Deviate (MSWD) - McIntyre et al., (1966). It is possible to take account of the correlated error problem, described for the isochron plot, in the least squares routine (York, 1969) and ideally all isochron plots should utilise this approach. If, however, the latter approach is not used, deduced isochron parameters should be viewed with some scepticism as, if errors are correlated, the least squares fit is often artificially good. Table 3:2 illustrates this point by comparing the parameters calculated from ICD2 and an isochron plot of the same data (graphically displayed in Fig. 3:2 and Fig. 3:3 respectively). The MSWD values indicate that the fit for the isochron is very much better than for the ICD2 (see below).

Whether the age or  $(40/36)_o$  value calculated from an ICD2 or isochron plot are of any real significance is assessed with reference to:

- i) the MSWD value
- ii) the age spectrum plot
- iii) geological/isotopic considerations

i) The MSWD has an expectation value of  $\leq 1$  where regression is based on a large number of data points and the assigned experimental errors have been calculated from a large number of replicate analyses. MSWD = 1 is the "cut-off" level and where MSWD > 1 an invalid plot is indicated i.e. the scatter of data points is not accounted for by assigned experimental error. Brooks et al., (1972), recognising that in most cases the ideal condition of large numbers of replicates and data points is not met, suggested that a cut-off of 2.5 should be

	ICD2	Isochron
Age (Ma)	$60.9 \pm 0.6$	$61.4 \pm 0.6$
$(40/36)_o$	$306.2 \pm 4.2$	$301.7 \pm 1.7$
MSWD	9.0	1.4

Table 3:2 Comparison of least squares fits in which the correlation of errors is not taken into account

used for Rubidium-Strontium work. Saito & Ozima (1977) and Ozima et al., (1977) preferred a value of 3.5 for their  $^{40}\text{Ar}-^{39}\text{Ar}$  work because number limitations were more severe than for Brooks et al.'s (1972) Rb-Sr work. However, because of a mistake in the MSWD expression (explained by Roddick, 1978), these authors were in fact using a cut-off of  $\approx 12$ . Brooks et al.'s (1972) cut-off level is used by many authors discussing  $^{40}\text{Ar}-^{39}\text{Ar}$  data, but a higher level can be justified following the reasoning of Saito & Ozima (1977). In respect of this, the MSWD cut-off adopted in this study is 3.5.

ii) Certain disturbances are more easily recognised with reference to an age spectrum plot than they are to ICD2 or an isochron plot. For instance, the loss of radiogenic argon from a sample is often represented by a pattern of increasing ages in the age spectrum plot (Section 4:2). However, the same data on ICD2 or an isochron plot may indicate a simple single stage history (Lanphere & Dalrymple, 1978; Ozima et al., 1979).

It is recommended policy that  $^{40}\text{Ar}-^{39}\text{Ar}$  data should be assessed with reference to both age spectrum plots and ICD2/isochron plots to avoid possible ambiguities (Lanphere & Dalrymple, 1978).

iii) In the same way as with ages deduced from the age spectrum plot, isotope correlation diagram and isochron ages must be assessed geologically, if at all possible, before any real meaning can be attached to them. In some cases, apparently acceptable isochron ages have been shown to be geologically meaningless, e.g. Brereton (1972), Seidemann (1978), so geological assessment is very important.

Initial argon of non-atmospheric composition is undoubtedly a reality in some cases (see Section 4:4). However, before an ICD2/isochron which indicates  $(40/36)_O \neq (40/36)_{\text{atm}}$  can be interpreted literally, two important points have to be considered:

a) Such plots may be the result of artefacts of the stepwise degassing procedure. For example, a sample subjected to  $40^*$  loss may give a spurious ICD2 or isochron indicating  $(40/36)_o < (40/36)_{atm}$  (Lanphere & Dalrymple, 1978; Ozima et al., 1979).

b) Atmospheric argon from the sample and/or extraction line may be present in significant amounts. Its presence would undoubtedly have a corrupting influence on an ICD2 or isochron plot (Berger, 1975; Roddick, 1978). Where  $(40/36) \neq (40/36)_{atm}$  is indicated, the importance of extraction line atmospheric blanks (Section 5:5) must be assessed.

The quality of fit parameter (MSWD) may be useful in distinguishing the spurious and corrupted straight line correlation from the true ones. The former might be reasonably expected to give a greater scatter of the data points about the best fitting line (Lanphere & Dalrymple, 1978; Roddick, 1978).

Lanphere & Dalrymple (1978) proposed that a meaningful age is only obtained from an isochron (or ICD2) if the calculated  $(40/36)_o$  approximately equals the atmospheric composition. However, as Seidemann (1978) observed, in the situation where  $(40/36)_o = (40/36)_{atm}$ , the inferred age may not necessarily be meaningful.

Seidemann (1978) suggested that such an isochron (or ICD2) could be the result of 40 and 39 being released in constant proportions and variable atmospheric contamination from the extraction line.

Several authors believe that isochrons with  $(40/36)_o \neq (40/36)_{atm}$  may sometimes be interpreted literally with the calculated  $40^*/39_K$  giving the true age and  $(40/36)_o = (40/36)_{initial}$  e.g. Saito & Ozima (1977), Jessberger (1977). The latter approach is not favoured in this dating study because of the number of assumptions that need to be fulfilled (see above). I will adopt Lanphere & Dalrymple's (1978) more conservative criterion, that meaningful ages are only obtained

from an ICD2 with  $(40/36)_O \approx (40/36)_{atm}$ . To reduce to a minimum the chances of producing spurious isochrons with  $(40/36) = (40/36)_{atm}$ , blanks are maintained at the lowest possible level.

### 3:4 Three-dimensional Isotope Correlation Diagram (ICD3)

This is a logical extension of ICD2. Instead of plotting two isotopic ratios, fitting the best line and calculating two unknowns, for ICD3 we plot three isotopic ratios, fit the best plane and calculate three unknowns.

The parameters calculated are an age,  $(40/36)_O$  and a third unknown, which can be a hypothetical component of 40 in proportion to either  $^{37}Ca$  (Plot 1) or  $^{36}Cl$  (Plot 2). Alternatively, the third parameter can be used to check the value of  $\left[ \frac{40 - (40/36)_O \cdot 36}{37} \right]_{Ca}$ , which in this dating study is the most important of all the interference corrections (Appendix 4). The ratios plotted and the parameters calculated are explained in Table 3:3. ICD3 parameters are assessed in the same way as those calculated from ICD2.

A simple graphical representation of the data points and the best fitting plane is not easily achieved. However, where one parameter is very much smaller than the other two, a fairly simple graph can be constructed e.g. Fig. 3:4(a) which is normally applicable to ICD3 Plots 1 and 3. Fig. 3:4(a) displays the distribution of data points as projected perpendicularly onto the best fitting plane. The axes in this graph are the lines of intersection between the best fitting plane and the plane containing the (X1,Y) and (X2,Y) axes - Fig. 3:4(b). The construction of a series of two-dimensional graphs representing data projections onto the plane formed by X1, X2 and Y axes (Mussett & McCormack, 1978) is not favoured here in the interests of simplicity and completeness.

The details of ICD3 data analysis and presentation can be followed in

	a	+	X1	+	b	+	X2	+	c	=	Y	=	1
Plot 1	$\left(\frac{40}{36}\right)_O$	+	$\frac{36'}{40'}$	+	$\left(\frac{40_x}{37Ca}\right)$	+	$\frac{37Ca}{40'}$	+	$\left(\frac{40^*}{39K}\right)$	=	$\frac{39K}{40'}$	=	1
Plot 2	$\left(\frac{40}{36}\right)_O$	+	$\frac{36'}{40'}$	+	$\left(\frac{40_x}{36Cl}\right)$	+	$\frac{36Cl}{40'}$	+	$\left(\frac{40^*}{39K}\right)$	=	$\frac{39K}{40'}$	=	1
Plot 3	$\left(\frac{40}{36}\right)_O$	+	$\frac{36'}{40''}$	+	$\left[\frac{40 - (40/36)_O \cdot 36}{37}\right] Ca$	+	$\frac{37Ca}{40''}$	+	$\left(\frac{40^*}{39K}\right)$	=	$\frac{39K}{40''}$	=	1

where

X1, X2, Y are the plotted parameters

a, b, c are the calculated parameters

and

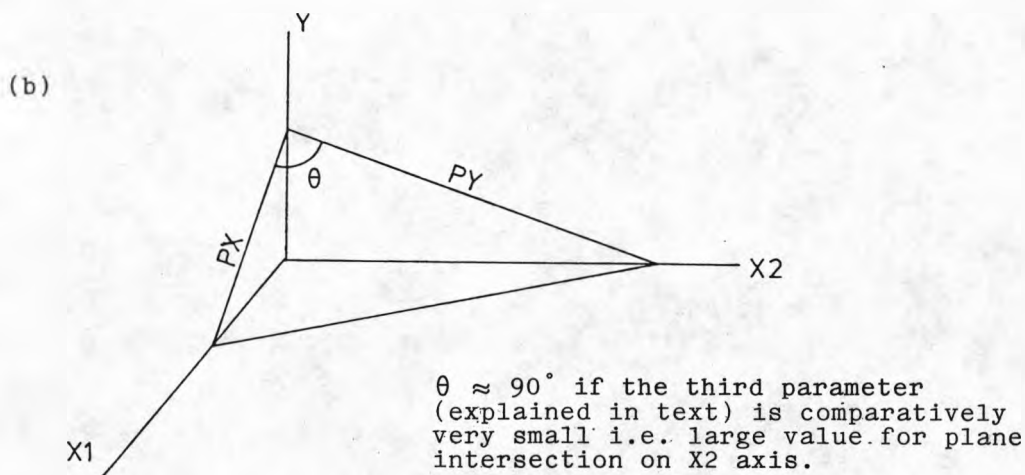
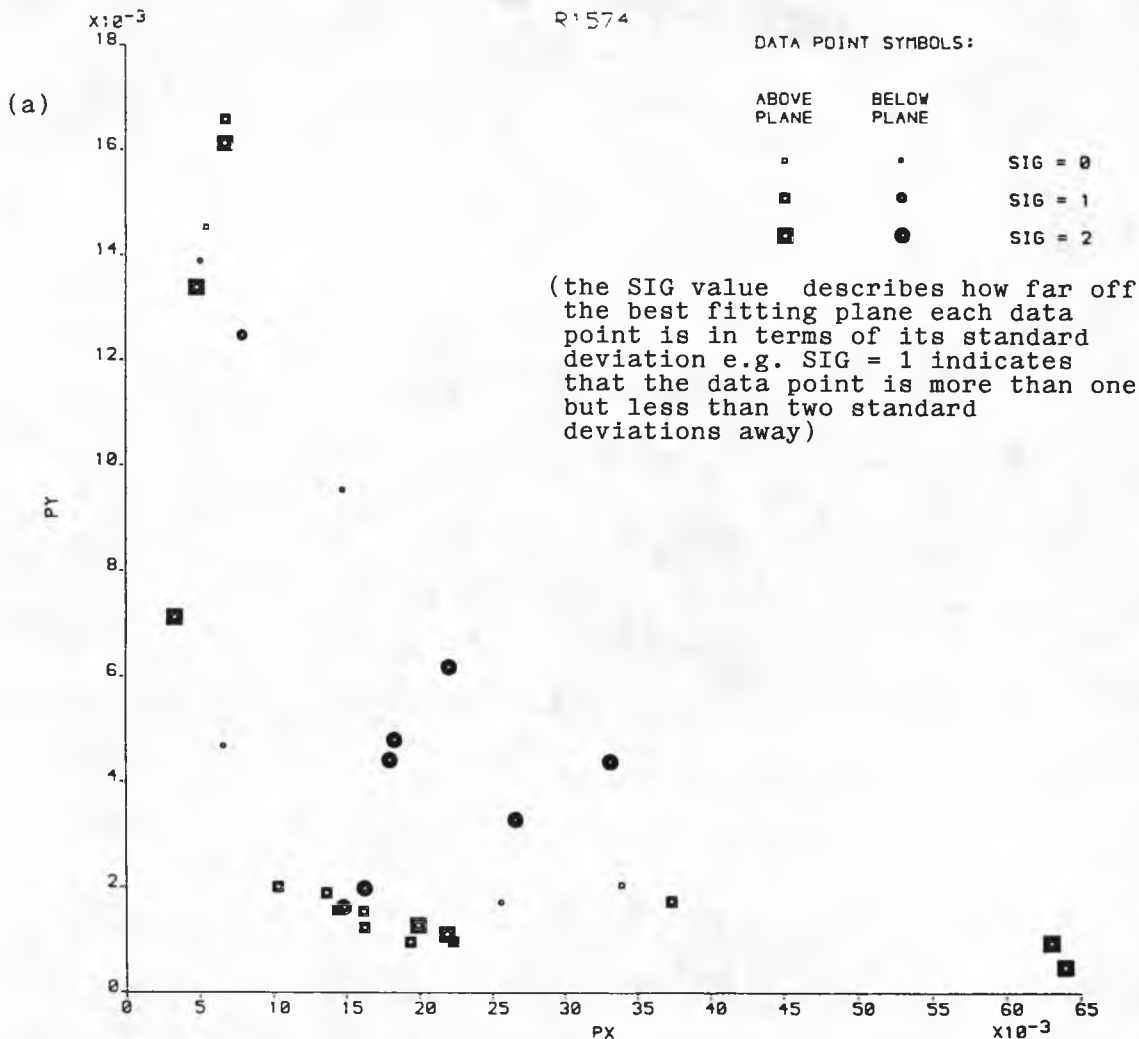
$$36' = 36_{total} - 36Cl$$

$$40' = 40_{total} - 40K - \left[ \frac{40 - (40/36)_{atm} \cdot 36}{37} \right] Ca$$

$$40'' = 40_{total} - 40K$$

40<sub>x</sub> = hypothetical component of 40

Table 3:3 Three-dimensional isotope correlation diagrams



**Fig. 3:4** Graphical representation of the 3-dimensional isotope correlation diagram (ICD3)

the "FITPLANE" computer program (Appendix 5). The value of ICD3 to the  $^{40}\text{Ar}$ - $^{39}\text{Ar}$  dating of terrestrial rocks is totally unproven. However, for each of the three plots, the choice of the third parameter can be justified.

Plot 1 - For age spectrum plots it is not uncommon for apparent age variations to be matched in some way by  $^{37}\text{Ca}/^{39}\text{K}$  variations, e.g. Bogard et al., (1976), Mussett (1985), this thesis.

Plot 2 - In terms of initial argon, it is perhaps reasonable to suggest that argon is incorporated into minerals in proportion to chlorine, as both apparently behave in a similar manner. (Work in this thesis indicates that both initial argon and chlorine are predominantly concentrated in the residual liquid phases of a crystallising melt).

Plot 3 - The age correction introduced by  $\left[ \frac{40 - (40/36)_{\text{atm}} \cdot 36}{37} \right] \text{Ca}$  is often highly significant, especially for the high temperature gas releases. Its value is subject to some uncertainty (Section 5:4:2). Ideally, this correction factor should allow for the possibility of non-atmospheric initial argon i.e.  $\left[ \frac{40 - (40/36)_{\text{o}} \cdot 36}{37} \right] \text{Ca}$ . This is the quantity that is calculated as the third parameter in ICD3 - Plot 3. Isotope correlation diagrams have been used before to calculate the values of interference correction terms (Turner, 1970 and 1971b).

The idea of multi-dimensional isotope correlation diagrams for data analysis is not new. Reynolds & Turner (1964) first introduced a multi-component isotopic analysis that has since been used routinely for the interpretation of gas release from extra-terrestrial samples. The systematics of multi-component mixing in the context of isotopic ratio correlation diagrams were described by Turner (1971b). He went on to analyse  $^{40}\text{Ar}$ - $^{39}\text{Ar}$  data from lunar samples on a three-dimensional plot, similar to the one described here. However, this is the first



time that an attempt has been made to use an ICD3 for the interpretation of terrestrial sample  $^{40}\text{Ar}-^{39}\text{Ar}$  data.

3:5 The Chronological Interpretation of  $^{40}\text{Ar}-^{39}\text{Ar}$  Stepwise Degassing Data

The statistical criteria for a meaningful age that are adopted in this thesis are as follows:

For combined age spectrum and ICD2 analysis (Lanphere & Dalrymple, 1978), the steps considered must:

- i) form an age spectrum plateau consisting of more than 3 consecutive steps
- ii) represent a significant proportion of the  $^{39}\text{K}$  released from the whole sample (ideally > 50%)
- iii) give an ICD MSWD of less than the adopted cut-off value of 3.5
- iv) give an ICD  $(40/36)_o$  not significantly different from the atmospheric  $40/36$  ratio (at the  $1\sigma$  level)
- v) give concordant plateau and ICD2 ages

For ICD3 analysis, the steps considered must fulfil criteria (ii), (iii) and (iv) above, and the third parameter must be physically

meaningful. For instance, a value of  $\left[ \frac{40 - (40/36)_o 36}{37} \right] \text{Ca}$  deduced from ICD3-Plot 3 can be checked against the values calculated

for other samples in the same irradiation batch. One would expect that samples in the same batch would be subject to almost identical interference reaction corrections (especially in the case of the calcium reactions which are activated by fast neutrons alone - see Appendix 4).

However, as I have stressed throughout the chapter, the fulfilment of these criteria does not imply that the age deduced is geologically meaningful. As noted earlier in this chapter, there are many examples of plateau/isochron ages which are totally meaningless in the context

of the known geology. Where possible, therefore, ages must be assessed geologically before any real meaning is attached to them (for instance, are the ages consistent with the basic geological contact relationships?)

For a series of steps yielding a statistically meaningful age, it is important to consider the influence of any disturbances which apparently only affect other parts of the gas release. Huneke (1976) has stressed that any disturbance will affect the whole gas release and that age spectrum segments apparently yielding statistically meaningful ages may suffer from some modification due to the disturbance(s). To assess the significance of such modifications, it is necessary to appreciate the underlying physical processes in  $^{40}\text{Ar}$ - $^{39}\text{Ar}$  stepwise degassing. These are the subject of the next chapter.

Where a sample produces no statistically meaningful age, it may still be possible to make some sort of chronological interpretation. This usually entails setting a minimum or maximum age estimate. Again, an appreciation of the physical processes involved is essential for the assessment.

It is not always possible to identify positively particular disturbances from the  $^{40}\text{Ar}$ - $^{39}\text{Ar}$  stepwise degassing data alone. To help with the identification, both petrographic and scanning electron microscope sample observations have been made in this dating study. The petrography involves identifying the various minerals present in a sample, observing their state of alteration and establishing their typical grain sizes. The scanning electron microscope work (see Appendix 6) was only conducted on selected samples and specifically investigates the location of the potassium in a sample and the sizes of the potassium-rich and potassium-poor zones.

Concluding, the approach to the interpretation of  $^{40}\text{Ar}$ - $^{39}\text{Ar}$  stepwise

degassing data adopted in this study is to pool all the available information and not to rely simply on a statistical assessment.

CHAPTER FOUR

The Physical Interpretation of Disturbed  $^{40}\text{Ar} - ^{39}\text{Ar}$  Age Spectra

#### 4:1 Introduction

Before commencing the chronological interpretation of  $^{40}\text{Ar}$ - $^{39}\text{Ar}$  stepwise degassing data it is important to be familiar with the physical mechanisms and processes involved and how they relate to age spectrum disturbances. In the interests of visual simplicity, discussions in this chapter will be focused on the age spectrum plot rather than the isotope correlation diagrams. A 'disturbed' age spectrum is generally one which does not give the same age for all the steps.

Sections 4:2 to 4:4 describe in detail the physical mechanisms and processes particularly important to a discussion of  $^{40}\text{Ar}$ - $^{39}\text{Ar}$  stepwise degassing data. Section 4:5 considers the age spectrum patterns commonly encountered in  $^{40}\text{Ar}$ - $^{39}\text{Ar}$  dating work and their physical interpretation. The implications for geochronological interpretation are also noted.

#### 4:2 Volume Diffusion

The mechanisms of argon loss from a mineral/rock during stepwise degassing or geologic reheating are not fully understood. However, in certain circumstances, argon loss can be successfully modelled by thermally activated volume diffusion. This mechanism may not quantitatively model argon loss in many cases but it does lead us towards several qualitative ideas considered to be generally valid.

The mathematical expression of volume diffusion is based on Fick's Law which states that, for an ideal gas, the rate of flow of molecules through an imaginary surface is proportional to the concentration gradient across the surface. Its one dimensional mathematical expression is (for the dimension x):

$$\frac{\delta n}{\delta t} = -D \cdot \frac{\delta c}{\delta x}$$

where  $n$  = number of molecules crossing unit area of surface

$t$  = time

$c$  = concentration measured in molecules per unit volume

$D$  = constant of proportionality - the diffusion constant

Fick's Law can be solved for various idealised geometries (assuming an isotropic and homogeneous substance) - Mussett (1969), Crank (1975).

It is usual to assume that the diffusing isotopic species has an initial uniform concentration within the grains and a zero concentration outside the grains. The latter assumption implies an infinite sink or reservoir for the diffusing isotopic species to be lost to. The general solution of Fick's Law under these conditions (Dodson, 1973) is:

$$\phi = \sum_{n=1}^{\infty} (B/\alpha_n^2) \exp(-\alpha_n^2 Dt/a^2)$$

where  $\phi$  = fraction of diffusant remaining in the system after a time  $t$

$a$  = characteristic dimension of the assumed diffusion geometry

and the constant  $B$  and the terms  $\alpha_n$  depend on the diffusion

geometry.

For geological materials, volume diffusion processes are usually taken to be thermally activated, being governed by the Arrhenius equation (Dodson, 1973):

$$D = D_0 \exp(-E/RT)$$

where  $D$  = diffusion coefficient at absolute temperature  $T$

$D_0$  =  $D$  at  $T = \infty$  (physically  $D_0$  is a constant relating to the distribution of "diffusion sites" - Mussett, 1969)

$E$  = activation energy (per mole) for the diffusion process

(physically the activation energy is the energy required to dislodge the diffusing species from a "diffusion site"

- Mussett, 1969)

$R$  = gas constant

As  $D = f(T)$  then  $\phi$ , the fraction remaining, is a function of temperature, time and the characteristic diffusion dimension  $a$ .

In a diffusion experiment, the diffusion coefficient  $D$  is calculated at a series of temperatures using the appropriate solution to Fick's Law. The various techniques used in diffusion experiments are discussed by Mussett (1969). However, a more recent development, not discussed in this review paper, is the calculation of diffusion data as a by-product of  $^{40}\text{Ar}$ - $^{39}\text{Ar}$  stepwise degassing (Turner, 1971; Turner et al., 1971b) - see Appendix 2.

Re-arranging the above equation:

$$D = \frac{-E}{R} \frac{1}{T} + D_0$$

which is of the form,

$$y = m x + c$$

Where thermally activated volume diffusion is the critical process, the plot of  $\text{Log}_e D$  v.  $1/T$  is linear. The activation energy is calculated from the slope and  $D_0$  is the y-value at  $x = 0$ . This plot is called an Arrhenius diagram and most diffusion data is graphically represented in this way.

Examples of this idealised volume diffusion behaviour for a variety of geological materials can be found in Mussett (1969), Turner et al. (1973), Foland (1974), Giletti (1974), Turner et al. (1978), Ozima & Takigami (1980), Harrison (1981), Harrison & McDougall, (1982). Some  $^{40}\text{Ar}$ - $^{39}\text{Ar}$  diffusion studies only produce a linear correlation over a limited portion of the gas release e.g. Berger & York (1981), Lopez-Martinez & York (1983). In these circumstances, simple volume diffusion is assumed to be only applicable over this part of the gas release, with other mechanisms being important over the remaining temperature intervals. For discussion of mechanisms of argon loss other than volume diffusion, see Mussett (1969) and Brereton (1972).

If a linear correlation does exist on an Arrhenius diagram, it is

possible to calculate an effective closure or blocking temperature using the computed diffusion parameters (Dodson, 1973). The term 'effective closure temperature' was defined by Dodson (1973) as "the temperature of the system at the time represented by its apparent age".

$$T_c = \frac{E}{R \cdot \text{Log}_e \left[ \frac{A R T_c^2 (D_0/a^2)}{E (\delta T/\delta t)} \right]}$$

where  $T_c$  = closure temperature

A = numerical constant depending on the diffusion geometry

$\delta T/\delta t$  = geological cooling rate

and the other symbols are as defined previously.

As  $T_c$  appears on both sides of the above expression, the calculation of closure temperature is an iterative procedure (the initial value of  $T_c$  only needs to be a rough estimate). To calculate a closure temperature, it is necessary to set values for 'a' and  $\delta T/\delta t$  in addition to the diffusion parameters E and  $D_0$ . Often the characteristic diffusion dimension 'a' will be taken as the observed grain size, where the geometry is spherical or cylindrical. However, where  $^{40}\text{Ar}-^{39}\text{Ar}$  stepwise degassing data is plotted on an Arrhenius diagram, the parameters calculated from a linear correlation are E and  $D_0/a^2$ . Thus a value of 'a' is not required. The value of  $\delta T/\delta t$  is not critical to the calculation of a closure temperature because of the large value of the logarithmic term (Dodson, 1973). Therefore, an intuitive estimate of the cooling rate is probably sufficient - the cooling rates for rocks analysed in this study are discussed in Appendix 2.

Table 4:1 lists the closure temperatures calculated for minerals commonly used in  $^{40}\text{Ar}-^{39}\text{Ar}/\text{K}-\text{Ar}$  dating. It includes estimates based on methods other than that described above:- borehole data, e.g.



Mineral	Calculated closure Temperature (°C)	References
Hornblende	400-700	Dallmeyer (1978) Berger et al., (1979) Harrison & McDougall (1980a) Berger & York (1981) Harrison (1981) Dallmeyer & Rivers (1983) Lopez-Martinez & York (1983)
Muscovite	300-400	Jager (1973) Purdy & Jager (1976) Wagner et al., (1977)
Biotite	225-400	Jager (1973) Purdy & Jager (1976) Turner & Forbes (1976) Wagner et al., (1977) Dallmeyer (1978) Harrison et al., (1979) Berger & York (1979) Harrison & McDougall (1980a) Berger & York (1981) Del Moro et al., (1982) Cliff (1985)
Plagioclase	200-260	Harrison et al., (1979) Berger & York (1981) Lopez-Martinez & York (1983)
Potassium feldspar (orthoclase, microcline)	130-230	Foland (1974) Harrison et al., (1979) Harrison & McDougall (1980a) Berger & York (1981) Harrison & McDougall (1982)

Table 4:1 Mineral closure temperatures for argon

Turner & Forbes (1976), metamorphic facies arguments, e.g. Wagner et al., (1977); cooling curve interpolation e.g. Harrison et al. (1979). This table of mineral closure temperatures is consistent with the accepted scale of mineral retentivity for thermal events (Dalrymple & Lanphere, 1969). It also conforms to the generally accepted ideas of those minerals which are most suitable for K-Ar or  $^{40}\text{Ar}-^{39}\text{Ar}$  total fusion dating and those which are not. Suitable minerals are hornblende, micas and high temperature feldspars, which have high closure temperatures. Unsuitable minerals are low temperature feldspars and glasses, which have low closure temperatures.

Reiterating the first sentence of this section - the mechanisms of argon loss from a mineral during stepwise degassing or geologic reheating are not fully understood. Thermally activated volume diffusion is only sometimes a good quantitative approximation; however, the more qualitative implications of volume diffusion are thought to be valid generally. It is possible to make several predictions of importance for the interpretation of stepwise degassing data:

1. Mineral grain outgassing in response to a thermal stimulus.

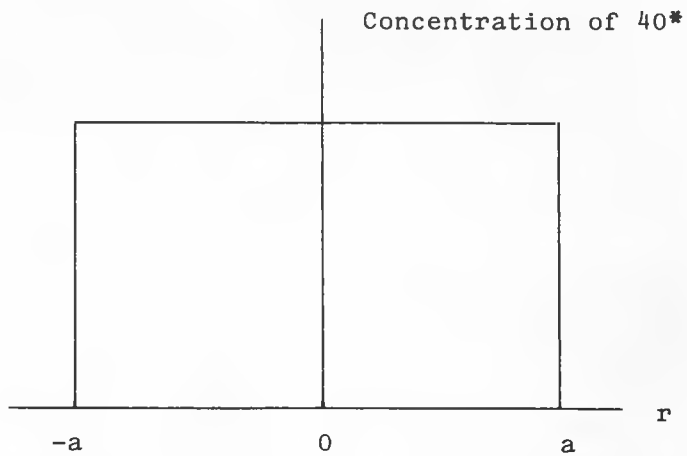
The surface regions of grains are expected to be outgassed first, with the centres of the grains outgassed last (Turner et al., 1966) - see Fig. 4:1. Albarede (1978) has described a mathematical technique which allows the spatial distribution of argon isotopes to be deciphered from  $^{40}\text{Ar}-^{39}\text{Ar}$  stepwise degassing data.

2. Grain size effect. The smaller the grain size of a given mineral,

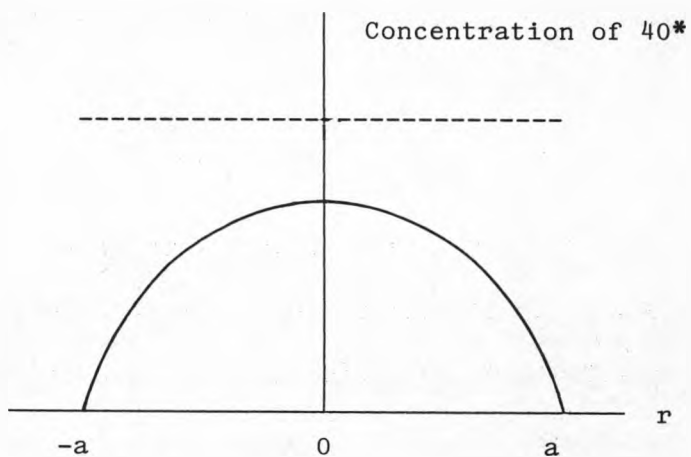
- the faster it outgasses during stepwise degassing or geologic reheating (Turner et al., 1966)

- the lower the effective retentivity/closure temperature

Pre-heating



Post-heating



where  $r$  = radial distance across grain

$a$  = grain radius

Fig. 4:1 Outgassing of an idealised spherical mineral grain in response to a thermal stimulus as predicted by volume diffusion theory

- the greater any  $^{40}\text{Ar}$  loss is during a thermal event.

These expectations are based on the assumption that the characteristic diffusion dimension is directly dependent on mineral grain size.

The predicted grain size effect has been observed by several authors e.g. Hart (1964), Foland (1974), Horn et al., (1975), Jessberger et al., (1975), Huneke & Smith (1976) and Del Moro et al., (1982).

Foland's (1974) orthoclase feldspar diffusion experiments produced similar diffusion parameters for various grain sizes. Horn et al., (1975) and Jessberger et al., (1975) found that for plagioclase separates, the  $^{40}\text{Ar}$ - $^{39}\text{Ar}$  argon isotope release curves (isotopic amounts v. temperature) were shifted towards lower temperatures for the samples of finer grain size. Hart (1964) and Del Moro et al., (1982) found that biotite separates of smaller grain size gave lower K-Ar ages. On the other hand, Purdy & Jager (1976) observed similar K-Ar ages on metamorphic biotites of widely different grain sizes.

It seems that, in this case, either the characteristic diffusion dimension is less than the smallest grain size, or volume diffusion is not the most important mechanism controlling argon retention/loss.

Several authors prefer to talk in terms of an "effective diffusion dimension" which may or may not equal the grain size, e.g. Foland (1974), Harrison & McDougall (1980b), Harrison & McDougall (1982).

In some cases an effective diffusion dimension less than the grain size may be physically meaningful. For instance, Foland (1974) suggested that for perthitic feldspars, the effective diffusion dimension may be controlled by the sizes of the perthite lamellae. Support for this comes from the work of Harrison & McDougall (1982), who performed a  $^{40}\text{Ar}$ - $^{39}\text{Ar}$  stepwise degassing diffusion experiment on a microcline feldspar. Using the inferred diffusion parameters and an expression relating to  $D_0$  to E (Hart, 1981), they were able to calculate the effective diffusion dimension. It was found to be of

the same order as the perthite lamellae widths observed in thin section. On the other hand, Harrison & McDougalls' (1980b) chosen effective diffusion dimension does not appear to have any physical meaning.

3. Partition of gas release in stepwise degassing of multi-phase samples. Particular minerals are expected to outgas over particular temperature ranges and thus portions of the stepwise gas release may be dominated by a single mineral phase. The sequence of mineral outgassing is expected to be controlled by closure temperature and grain size. The most useful parameter for identifying mineral phases of importance in particular sections of the gas release is the  $^{37}/^{39}\text{K}$  ratio (which is directly related to the Ca/K ratio). If the minerals present possess distinct Ca/K ratios, then the portions of the gas release in which they are dominant will be marked by correspondingly different  $^{37}/^{39}\text{K}$  ratios. By studying  $^{37}/^{39}\text{K}$  variations with temperature, several authors have been able to identify the minerals contributing over different sections of the gas release e.g. Bogard et al., (1976), Turner et al., (1978), Walker & McDougall (1982). However, gas release from the various phases present within whole-rock samples are likely to overlap, and this, combined with possible irradiation induced effects (see below) could make mineral identification difficult.

4. Geological argon loss in the otherwise ideal single-phase sample. Turner (1968) and Huneke (1976) have presented model  $^{40}\text{Ar}$ - $^{39}\text{Ar}$  age spectra for hypothetical mineral samples which have, during a brief event, suffered varying degrees of radiogenic argon loss. The hypothetical mineral samples considered consist of uniform spheres and, in some cases, they may be analogous to mineral separate samples. These model spectra display a pattern of increasing age over the initial portions of gas release and a segment of constant

age over at least the last 15% of  $^{39}\text{K}$  release (Huneke, 1976) - see Fig. 4:2. This plateau records an age less than the true age, the magnitude of the depression being determined by the total amount of  $^{40}\text{K}$  loss. The extrapolation of the age pattern to 0%  $^{39}\text{K}$  gives the age of the argon loss event. In ideal circumstances, therefore, where a  $^{40}\text{Ar}$ - $^{39}\text{Ar}$  age spectrum records  $^{40}\text{K}$  loss, it should be possible to deduce both the crystallisation and argon loss ages.

The application of the argon loss models to extra-terrestrial samples has apparently been quantitatively successful in many cases, e.g. Turner (1968), Turner (1969), Turner (1971b), Podosek & Huneke (1973), Jessberger et al., (1974), Huneke (1976), Wang et al., (1980). However, for terrestrial samples, success has been more limited. Lanphere & Dalrymple (1971), Berger (1975) and Hanson et al., (1975) all concluded that samples subjected to geologic reheating did not quantitatively fit Turner's (1968) model. On the other hand, Harrison & McDougall (1980b) and Harrison (1981) both produced hornblende age spectra consistent with the argon loss model in situations where the geological history was well known. Several terrestrial  $^{40}\text{Ar}$ - $^{39}\text{Ar}$  studies have produced age spectra which are qualitatively consistent with the theoretical patterns of ages (in some cases, only if the lowest temperature steps are ignored) e.g. Fitch et al., (1969), Lanphere & Dalrymple (1971), Berger (1975), Hanson et al., (1975), Albarede et al., (1978), Dallmeyer (1979), Walker & McDougall (1982), this thesis (see Section 6:2:3). Where this type of age spectrum is produced, it is possible to make two tentative conclusions (Fitch et al., 1969, Lanphere & Dalrymple, 1971, Miller & Sutter, 1982):

- i) the low temperature age minimum is a maximum estimate for the age of the geologic reheating (argon loss event)
- ii) the high temperature age plateau or age maximum is a minimum estimate for the crystallisation age (or for a sample having a

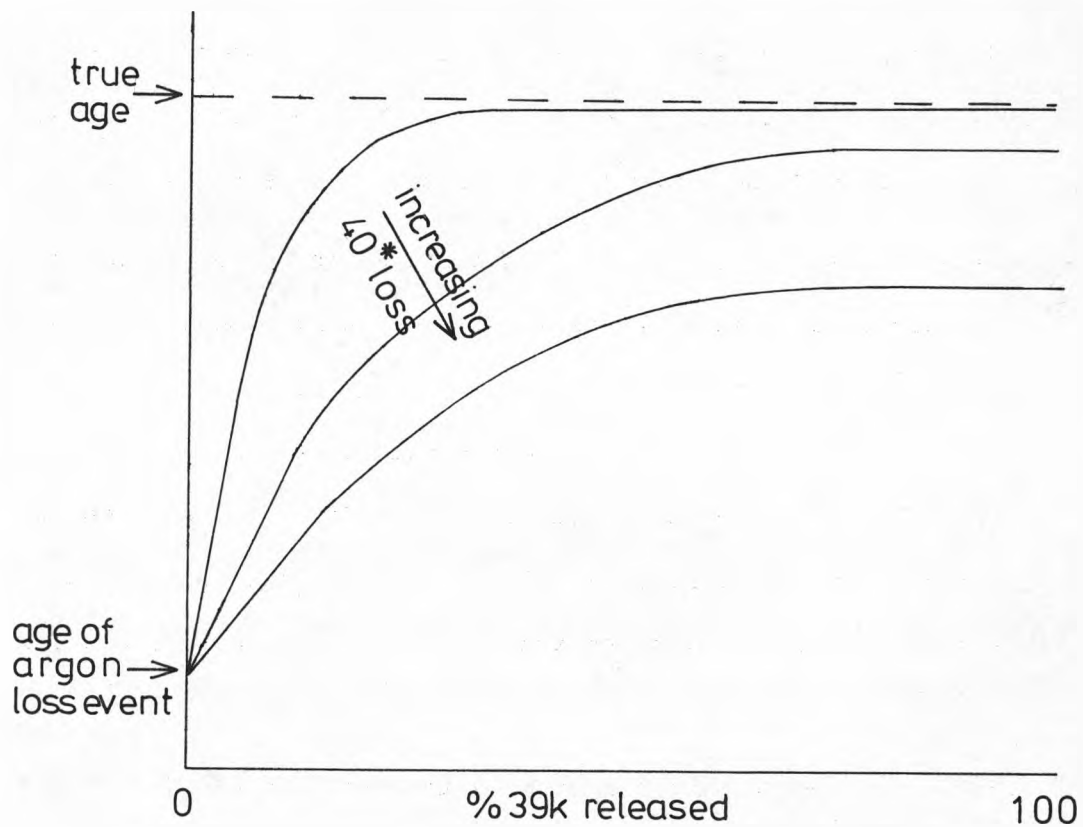


Fig. 4:2 Model argon loss age spectra

multi-stage history, the age when the K-Ar system was last totally reset).

In some cases, terrestrial samples that give an age spectrum which, for the most part, shows the pattern of increasing ages characteristic of argon loss, also display anomalously high ages for the lowest temperature steps. This can be explained in terms of a further modification to the lowest retentivity locations, e.g. "excess" argon  $^{40}$  contamination (see below, and Section 4:4),  $^{39}\text{K}$  recoil loss (see Section 4:2:2).

A tentative explanation can be given as to why extra-terrestrial samples have been more amenable to argon loss modelling. In meteoric and lunar samples, the majority of the potassium is contained within very homogeneous glass phases, which are probably the nearest thing to the idealised isotropic and homogeneous medium in volume diffusion theory (Dallmeyer, 1979). In terrestrial samples, the potassium is usually located in more complex crystal structures. Also, for extra-terrestrial samples, the assumption of an infinite sink or reservoir for loss of  $^{40}\text{Ar}$  might be more completely fulfilled. For terrestrial samples, argon is probably lost to an argon rich aqueous or gaseous phase (the concentration of  $^{40}\text{Ar}$  in this phase could well be much higher than in the minerals themselves). In this case, a significant diffusion of argon into the grains is not unreasonable. (This type of "excess" argon contamination probably explains why many terrestrial samples suffering from a geologic reheating display anomalously high ages in the low temperature steps - see above). For extra-terrestrial samples however, the medium to which  $^{40}\text{Ar}$  is lost is more like the idealised infinite sink in which the effective concentration of argon is zero. In this case, there would be no such reversed diffusion process.

Cliff (1985) has noted that metamorphism under conditions of low water



activity results in high levels of "excess" argon 40 (Foland, 1979; Harrison & McDougall, 1981) and that argon transport at grain boundaries may be dependent on water activity. Many of Harrison & McDougall's (1981)  $^{40}\text{Ar}$ - $^{39}\text{Ar}$  mineral age spectra are not even qualitatively consistent with the model argon loss spectra of Turner (1968) and Huneke (1976). This would seem to suggest that minerals metamorphosed under conditions of high water activity might be more likely to yield the idealised argon loss spectra. However, where water activity is high, mineral re-crystallisation can be expected to be important; thus all record of the rock's previous history may well be completely lost. These observations perhaps explain why terrestrial metamorphic rocks in general do not produce age spectra that quantitatively conform with Turner's (1968) and Huneke's (1976) model spectra.

#### 4:3 Effects of Irradiation

Neutron irradiation, which is essential to the  $^{40}\text{Ar}$ - $^{39}\text{Ar}$  method, may introduce a series of unwanted side-effects. Mussett (1969) discussed the effects of neutron irradiation with respect to diffusion measurements made using neutron activation. He states "Neutron activation suffers from the disadvantage that it may displace argon and lattice atoms" and goes on to say that (referencing Hart, 1960) "argon may be diffusing not only from an atypical position but in an atypical structure". Where fast neutrons are involved, the displacement of argon and lattice atoms is expected to be significant (Mussett, 1969). In  $^{40}\text{Ar}$ - $^{39}\text{Ar}$  dating, fast neutrons are essential for the  $^{39}\text{K}$  to  $^{39}\text{Ar}$  conversion; thus irradiation damage may be very important (see discussions presented in Brereton, 1972; and Horn et al., 1975).

The discussion of the effects of neutron irradiation in  $^{40}\text{Ar}$ - $^{39}\text{Ar}$  dating can be divided into two sections. The first deals with the

natural argon isotopes, the second with recoil of argon isotopes produced by neutron irradiation.

#### 4:3:1 Patterns of release for natural argon isotopes

In several  $^{40}\text{Ar}$ - $^{39}\text{Ar}$  studies, where unirradiated and irradiated samples have been compared, shifts in the argon isotope release curves (isotopic amount v. temperature) have been observed. However, no entirely consistent pattern emerges and this points towards there not being a unique irradiation effect. Davis et al., (1971) and Alexander et al., (1973) found that the temperature of maximum  $^{40}\text{Ar}$  release was significantly reduced if the whole-rock samples were irradiated. On the other hand, Turner et al., (1974), Jessberger et al., (1975) and Horn et al., (1975) found the opposite effect for mineral separate samples. However, Kaneoka (1974), Horn et al., (1975) and Roddick et al., (1980) found that the  $^{40}\text{Ar}$  release curves (also the atmospheric  $^{36}\text{Ar}$  release curves for the latter reference) were unaffected by irradiation (whole-rock and mineral separate samples). Several, rather hypothetical, mechanisms have been suggested in an attempt to explain observed shifts in the release patterns of the natural argon isotopes. Jessberger et al., (1975) postulates that increased  $^{40}\text{Ar}$  retentivity in mineral separates due to irradiation, may be the result of the argon collecting in "radiation damage traps". They also suggest that the opposite effect in whole-rock samples may be related in some way to the presence of fine-grained and/or interstitial components. Stettler & Bochsler (1979), observing the atmospheric argon  $^{36}\text{Ar}$  release pattern shifting to higher temperatures with irradiation, suggested that the argon was originally absorbed on microcracks which were annealed during step-wise degassing.

Even though the argon isotope release curves may be affected by irradiation, evidence does suggest that mineral  $^{40}\text{Ar}/^{39}\text{Ar}$  ages are not

influenced by this phenomenon (Jessberger et al., 1975; Horn et al., 1975). This is consistent with the idea that  $^{40}\text{K}$  and  $^{39}\text{K}$  occupy identical sites/locations within minerals. For whole-rock samples though, the  $^{40}\text{Ar}-^{39}\text{Ar}$  age spectrum may be irradiation dependent if the mineral phases present suffer differing shifts in their argon isotope release curves (Horn et al., 1975). Stettler & Bochsler (1979), in a study of zero age sea-floor basalt glass containing "excess" argon 40 (see Section 4:4), observed that the  $^{40}\text{Ar}-^{39}\text{Ar}$  step ages were irradiation dependent. A plausible explanation for this involves the excess argon 40 and potassium-derived 39 occupying distinct sites/locations which are affected in different ways by the irradiation.

#### 4:3:2 Recoil of argon isotopes produced by neutron interaction

Implicit to  $^{40}\text{Ar}-^{39}\text{Ar}$  dating is the assumption that corresponding  $^{40}\text{K}$  and  $^{39}\text{K}$  argon isotopes (both are produced from the potassium host) occupy similar physical locations or sites. It follows, therefore, that the  $^{40}\text{K}$  and  $^{39}\text{K}$  isotopes are expected, as a whole, to be distributed in a similar way amongst all possible locations. If this condition is not met, we cannot expect to obtain, in a simple way, any meaningful chronological information from stepwise degassing data. As noted previously, Dalrymple & Lanphere (1974) have demonstrated that ideal samples do give a concordant age spectrum which is of real chronological significance. Thus, for these samples,  $^{40}\text{K}$  and  $^{39}\text{K}$  must have been distributed amongst the various locations in a similar way and our assumption is vindicated. However, in less ideal situations this assumption may not be valid. In this context, it is necessary to consider the influence of interaction recoil in the production of  $^{40}\text{K}$  and  $^{39}\text{K}$  from potassium.

Brandt & Voronovsky (1967) calculated a recoil energy of 28 eV for  $^{40}\text{K}$  produced by the natural decay of  $^{40}\text{K}$  and they suggested that such

a recoil energy is sufficient to produce a random distribution of  $^{40}\text{Ar}^*$  in a mineral homogeneous in potassium. However, the recoil energy of  $^{39}\text{Ar}$ , which is produced during neutron irradiation via the  $^{39}\text{K}(n,p)^{39}\text{Ar}$  interaction, was calculated by Mitchell (1968) to be 300 keV. Such an energy may mean that the recoiled  $^{39}\text{K}$  travels some significant distance: Mitchell (1968) estimated that the range of  $^{39}\text{K}$  in a typical mica lattice would be as much as  $0.1\mu$ .

The difference in the recoil energies of  $^{40}\text{Ar}^*$  and  $^{39}\text{K}$  is considerable (a factor of 10,000), and this may result in the assumption of occupancy in identical locations being invalid. The recoil effect will be important where the  $^{39}\text{K}$  recoil range is significant in comparison to the sizes of the zones of uniform potassium concentration. An important point to bear in mind is that individual mineral phases may be subject to some sort of compositional variations e.g. exsolution features, mineral zoning. Where potassium is involved in such compositional variations, the dimensions of the zones of uniform potassium concentration may be much smaller than the mineral grain size.

$^{39}\text{K}$  in the marginal areas of potassic zones is most at risk to relocation. If  $^{39}\text{K}$  is lost from the host potassic zone, it can be either:

- a) lost from the entire rock sample, or
- b) implanted into the marginal zone of an adjacent mineral phase/compositional zone.

In case (a), for an otherwise ideal mineral sample, volume diffusion predicts that in a stepwise degassing experiment, the initial steps will give an anomalously high age. This is because the gas released comes from marginal locations that have lost  $^{39}\text{K}$ . Progressively higher temperature steps will produce a decreasing pattern of ages, perhaps reaching a plateau. However, as in the case of  $^{40}\text{Ar}^*$  loss, the plateau age will not equal the true age unless loss is small.

In general, where  $^{39}\text{K}$  loss is important, the plateau age will be too high and thus it will only be a maximum estimate of the true age.

Harrison & McDougall (1980b) have interpreted a hornblende separate age spectrum displaying this pattern of ages in terms of a  $^{39}\text{K}$  recoil loss effect. However, most examples of the theoretical  $^{39}\text{K}$  recoil loss age spectrum are for whole-rock samples e.g. Turner & Cadogan (1974), Ozima et al., (1977), Seidemann (1978), Feraud et al., (1982). This observation can be explained because in whole-rock samples, the small mineral grains, which are more susceptible to a  $^{39}\text{K}$  recoil loss, can usually be expected to outgas in the initial steps of an incremental heating experiment.

The  $^{39}\text{K}$  recoil loss effect may be recognised in several ways:

- i) By comparing the  $^{40}\text{Ar}-^{39}\text{Ar}$  total gas age with a complementary K-Ar age determination. If the recoil loss effect is important the  $^{40}\text{Ar}-^{39}\text{Ar}$  total gas age will be significantly greater than the K-Ar one.
- ii) By measuring  $^{39}\text{K}$  loss directly. Samples are enclosed in evacuated breakseal vials prior to irradiation e.g. Seidemann (1978).
- iii) By comparing potassium contents calculated from the amount of  $^{39}\text{K}$  released during sample fusion and from flame photometer analysis e.g. Dalrymple & Clague (1976), Ozima et al., (1977), Dalrymple et al., (1977).
- iv) By the pattern of decreasing ages produced during stepwise degassing e.g. McDougall (1981), Feraud et al., (1982).

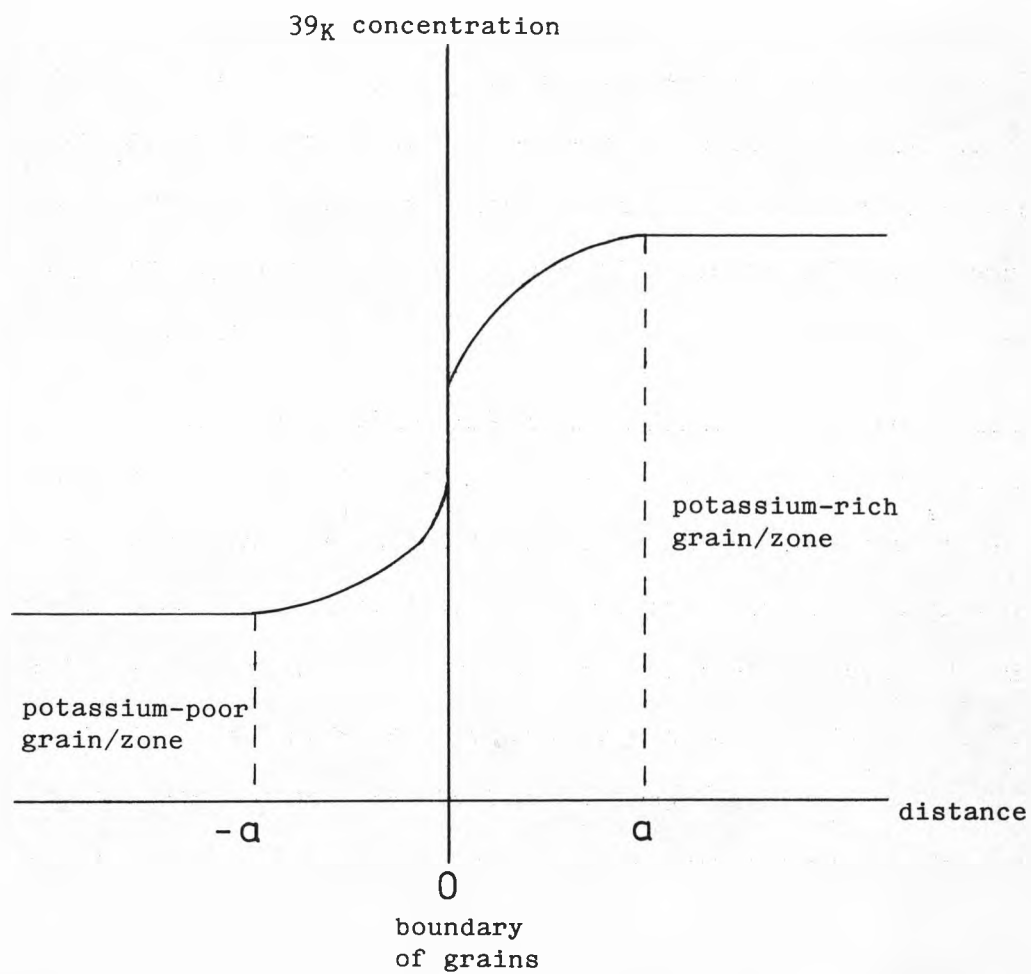
However, this type of age pattern is not without ambiguity and it must not be regarded as diagnostic of  $^{39}\text{K}$  loss (see Table 4:3).

Several authors have associated a high release of  $^{39}\text{K}$  in the low temperature steps with  $^{39}\text{K}$  recoil loss e.g. Dalrymple & Clague (1976), Seidemann (1978), Feraud et al., (1982).

Case (b), recoil re-distribution, has been considered in detail by Turner & Cadogan (1974), Huneke (1976) and Huneke & Smith (1976b). In a whole-rock (or mineral) sample consisting of discrete potassium-rich and potassium-poor grains (zones), we can envisage a  $^{39}\text{K}$  surface depletion layer in the former, and a  $^{39}\text{K}$  surface enhancement layer in the latter (see Fig. 4:3). The extent of these layers will be dependent on the recoil range. As different minerals have different activation energies for argon diffusion, it can be expected that the re-distributed  $^{39}\text{K}$  will be released at a different temperature to the corresponding  $^{40}\text{Ar}$ . For unaltered igneous rocks, the potassium-poor minerals are usually the more retentive phases, so that anomalously low ages can be expected at high temperatures and anomalously high ages at low temperatures. As with recoil loss, the development of recoil re-distribution effects will be dependent on mineral grain size (assuming the grains are of uniform potassium concentration) and they are likely to be best developed where the mineral grains are most disparate in potassium contents. For  $^{39}\text{K}$  recoil re-distribution in a sample that is otherwise ideal, the true age will equal the  $^{40}\text{Ar}$ - $^{39}\text{Ar}$  total gas age.

$^{39}\text{K}$  recoil re-distribution has been experimentally demonstrated by Huneke & Smith (1976a) and two basic types of age spectrum have been identified with this phenomenon:

1. A staircase pattern of decreasing age with temperature - e.g. Turner & Cadogan (1974), Huneke & Smith (1976b), Turner et al., (1978), Walker & McDougall (1982).
2. A high temperature decrease in age from an apparent plateau - e.g. Turner & Cadogan (1974), Huneke (1976). Several authors have associated a high temperature age decrease with the outgassing of pyroxene (a low potassium mineral), e.g. Huneke et al., (1972), Turner et al., (1972), Jessberger et al., (1974). This observation is consistent with a  $^{39}\text{K}$  recoil re-distribution phenomenon. The



where 'a' is a distance of the order of the recoil range

Fig. 4:3 Schematic representation of  $^{39}\text{K}$  recoil re-distribution

apparent plateau may be subject to some degree of age enhancement due to the  $^{39}\text{K}$  recoil re-distribution (Huneke, 1976).

This discussion of recoil effects has been limited to  $^{40}\text{K}$  and  $^{39}\text{K}$ ; however, it can be expected that all the other argon isotopes produced by neutron interaction will experience some degree of recoil. Brereton (1972) calculated the maximum recoil energy for three interference reactions and found that the energies involved were in each case greater than for the  $^{39}\text{K}(n,p)^{39}\text{Ar}$  interaction. Interference reactions sometimes result in large age corrections, and in these cases, it is necessary to consider the importance of recoil effects for the interactions involved. The age correction due to calcium interference is especially important in some dating studies; however, no recoil effect has been reported for the principal calcium-derived argon isotope ( $^{37}\text{Ar}$ ) - Turner & Cadogan (1974), Cadogan & Turner (1976). Appendix 3 details the various interference reactions, considers the maximum recoil energies involved, and discusses the possibility of recoil effects for argon isotopes other than  $^{39}\text{K}$ .

#### 4:4 Atmospheric and Initial Argon

In the past, atmospheric argon was simply regarded as a low temperature component absorbed on the surfaces of mineral grains. This contamination was thought to be due to exposure to the present day atmosphere. However, Mussett & Dalrymple (1968) showed that the atmospheric argon contained in a rock sample was not acquired in the laboratory. This work, together with that of Lanphere & Dalrymple (1971) and Kaneoka (1975) indicated that a significant proportion of atmospheric argon is apparently tightly held within mineral lattices. It is generally assumed that this high temperature argon must have been included into minerals at the time of crystallisation, i.e. it is initial argon. This assumption prompts the question - Has the



isotopic composition of the atmosphere changed in geological time? Lippolt (1970), Ozima (1973), Ozima (1975), Kaneoka (1975), Sarda et al., (1985) have discussed this question and available data suggests that the isotopic composition of the atmosphere has not changed significantly for the last 2 Ga - Hunziker (1979), Turner et al., (1983), Sarda et al., (1985). Therefore, for the Tertiary rocks dated in this thesis, any "atmospheric" initial argon can reasonably be assumed to have an isotopic composition similar to today's atmosphere (assuming no isotopic fractionation - see below).

High temperature atmospheric argon often combines with a presumed present day atmospheric contamination at low temperature to give a saddle-shaped release with reduced atmospheric levels at intermediate temperatures.

Introduction of atmospheric argon has been shown to occur during irradiation (Bernatowicz et al., 1978; Stettler & Bochsler, 1979; Walker & McDougall, 1982; Roddick, 1983) and sample crushing (Hall & York, 1978). It might be expected that this atmospheric contamination would simply affect the lowest temperature steps. However, in some cases e.g. Roddick (1983), it appears that the levels of atmospheric argon in the higher temperature steps are enhanced; thus, some of the introduced atmospheric argon may actually be tightly held. This phenomenon may be explained by the absorption of atmospheric argon into microcracks which anneal during stepwise degassing (Stettler & Bochsler, 1979).

Baksi (1974) has described an instance in which loosely held atmospheric argon affected the calculation of K-Ar ages for whole-rock basalt samples. Uncrushed whole-rock samples gave inconsistent, anomalously high ages and also high atmospheric argon levels. Crushed samples, on the other hand, produced both a consistent age that was geologically meaningful and low atmospheric argon levels.

Baksi (1974) explained the behaviour of the uncrushed samples in terms of a fractionation of loosely-held atmospheric argon which perhaps took place during the extraction line bake-out. For the crushed samples, which have a high surface area per unit mass, Baksi (1974) considered that all such loosely-held argon was removed in the bake-out. Baksi (1974) speculated that the loosely-held atmospheric argon was probably associated with fine-grained clay mineralisation.

This effect could clearly be important in  $^{40}\text{Ar}$ - $^{39}\text{Ar}$  dating. If this was the case one would expect the initial gas release in a stepwise degassing analysis to yield anomalously high ages, with only the higher temperature steps giving a meaningful age estimate. Such an age spectrum is very similar to that expected for other types of disturbances (see Table 4:3); therefore it would not be diagnostic of a fractionation of loosely-held atmospheric argon. Mussett (1985) has tentatively suggested that a basalt sample from the British Tertiary Igneous Province, which gave this type of age spectrum, may have suffered from such a fractionation effect.

The occurrences of initial argon of non-atmospheric composition can be divided into four geological environments (Table 4:2). In most cases, initial argon  $40/36$  ratios very much greater than the atmospheric value are indicated. This is consistent with the observation that magmatic argon and argon in old rocks have  $40/36$  much greater than  $(40/36)_{\text{atm}}$  (for the former, see Dymond & Hogan, 1973; Sarda et al., 1985). Initial argon with  $40/36 < (40/36)_{\text{atm}}$  has been reported for some historical subaerial volcanics - Dalrymple (1969), Krummenacher (1970), Kaneoka (1980). This phenomenon is probably explained in terms of a fractionation of atmospheric argon prior to crystallisation (Krummenacher, 1970; Kaneoka, 1980).

Where the conventional atmospheric argon correction would result in ages that are too old, the non-atmospheric initial argon is often

Geological environment	Source of non-atmospheric initial argon	References
Subaerial volcanic	Magmatic*	Dalrymple (1969) McDougall et al., (1969) Krummenacher (1970) Mellor & Mussett (1975)
	Atmospheric fractionation	Krummenacher (1970) Kaneoka (1980)
Submarine volcanic	Magmatic*	Dalrymple & Moore (1968) Dymond & Hogan (1973) Seidemann (1978) Stettler & Bochsler (1979) Sarda et al., (1985)
Intrusive igneous	Magmatic*	Damon et al., (1967) Kaneoka (1974) Lanphere & Dalrymple (1976)
	Country rock	Briden et al., (1971) Dalrymple et al., (1975)
Metamorphic	Inherited <sup>+</sup>	Dallmeyer (1975) Roddick et al., (1980) Harrison & McDougall (1981) Dallmeyer & Rivers (1983)

\* The isotopic composition of true magmatic argon may be modified by the assimilation of country rock

<sup>+</sup> This term is explained in the text.

Table 4:2 The occurrences of initial argon of non-atmospheric composition

referred to as extraneous argon (Dalrymple & Lanphere, 1969). This is subdivided into inherited argon, where the  $^{40}\text{Ar}$  enhancement is due to radiogenic argon produced in situ before the event to be dated, and excess argon, which covers all other possibilities.

There are several age spectrum patterns associated with extraneous argon (see Table 4:3):

- i) A pattern of decreasing ages at low temperature perhaps with a plateau of ages at higher temperature, e.g. Harrison & McDougall (1980b), Dallmeyer & Rivers (1983). This is analagous to the argon loss patterns discussed in Section 4:2 except that in this case  $^{40}\text{Ar}$  diffusion is into, rather than out of, the minerals. This extraneous argon contamination is clearly excess argon.
- ii) The so-called saddle-shaped age spectrum which gives lowest ages at intermediate temperatures. This is largely associated with excess argon contamination in igneous rocks (Table 4:3 No.6), e.g. Lanphere & Dalrymple (1971), Kaneoka (1974), Dalrymple et al., (1975), Lanphere & Dalrymple (1976), Feraud et al., (1982). However, it is possible for a saddle-shaped age spectrum to be produced by a sample suffering from radiogenic argon loss and an additional excess argon contamination in low temperature steps (see Table 4:3 No.5). In this case, the saddle is partly explained in terms of inherited argon. Fitch et al., (1969), suggested that a saddle-shaped age spectrum may result from a  $^{40}\text{Ar}$  re-distribution. In this case, the age spectrum pattern would be entirely explained by inherited argon. Saddle-shaped age spectra, explained partly or wholly by inherited argon, are associated with rocks that have been reheated.
- iii) A geologically meaningless plateau over a large proportion of the gas release. This pattern has been observed for

metamorphic minerals (usually biotite), e.g. Pankhurst et al., (1973), Berger (1975), Hanson et al., (1975), Albarede et al., (1978), Roddick et al., (1980), Dallmeyer & Rivers (1983).

The extraneous argon in most of these samples is clearly excess rather than inherited argon because either ages are greater than the age of the Earth or the contamination is largely a low temperature mineral effect.

In each case the effect of extraneous argon is to make ages anomalously old. Thus in general, only a maximum estimate for the timing of geological events can be made. In case (i) the high temperature plateau may be a good approximation to a meaningful age. In case (ii), for a saddle-shaped age spectrum explained at least partly in terms of inherited argon, the high temperature age maximum is probably a minimum estimate for the crystallisation age.

The presence of initial argon of a non-atmospheric but constant isotopic composition may be indicated by a step-age v.  $^{40}\text{Ar}_{\text{atm}}$  correlation in the age spectrum plot (see Section 3:2). However, available evidence suggests that, in many cases, excess argon may not maintain a constant isotopic composition in a given rock or mineral sample. For instance, the data points in isochron plots for igneous rock samples with saddle-shaped age spectra are usually very scattered.

#### 4:5 Summary

Table 4:3 displays the commonly encountered disturbed age spectra and lists the physical mechanisms (which have been discussed in the preceding sections) that researchers have invoked to explain them. The implications for geochronological interpretation are noted at the bottom of each column.

As is apparent from Table 4:3, particular age spectra may have more

Age spectrum patterns	(1)	(2)	(3)	(4)
Physical interpretation	Loss of 40* e.g. Turner (1968), Huneke (1976)	(i) 39K recoil loss e.g. Harrison & McDougall (1980b) Ozima et al. (1977), Seidemann (1978), Feraud et al., (1982) (ii) Excess 40 contamination e.g. Harrison & McDougall (1980b), Dallmeyer & Rivers (1983) (iii) Fractionation of atmospheric argon loosely held in fine-grained alteration e.g. Baksi (1974), Mussett (1985) (iv) Potassium loss - due to seawater alteration? e.g. Feraud et al., (1982)	Closed system distribution e.g. Turner & Cadogen (1974), Huneke & Smith (1976b), Turner et al., (1978), Walker & McDougall (1982) (i) 40* re-distribution e.g. Fleck et al., (1977) - due to the devitrification of glassy phases; Bottomley & York (1976)	(i) 39K recoil redistribution (plus some 40* loss?) e.g. Turner & Cadogen (1974), Huneke (1976) (ii) 40* loss plus conversion of sites from low to high argon retentivity (devitrification of glassy phases for instance) e.g. Turner (1971b), Kirsten et al., (1972)
Geochronological interpretation	(a) The maximum age is a minimum estimate of crystallisation or total resetting age + (b) The minimum age may record a maximum estimate for timing of the argon loss event.	High temperature minimum age is a maximum estimate of the crystallisation age	Total gas age $\approx$ crystallisation age	Plateau age may be a slightly enhanced value

+ K-Ar system is reset if minerals are totally outgassed of 40\*. For crystallisation age, in each case, also read total resetting age.

Table 4:3 Disturbed age spectra


Age spectrum patterns	(5)	(6)	(7)	(8)
Physical interpretation	<p>(i) 40* loss plus excess 40 contamination e.g. Albarede et al., (1973), Berger (1975), Dallmeyer (1979), Harrison &amp; McDougall (1980b), Miller &amp; Sutter (1982)</p> <p>(ii) 40* redistribution from sites of high to those of low retentivity e.g. Fitch et al., (1969), Berger (1975)</p>	<p>Excess 40 contamination e.g. Lanphere &amp; Dalrymple (1971), Kaneoka (1974), Dalrymple et al., (1975), Lanphere &amp; Dalrymple (1976), Feraud et al., (1982)</p>	<p>Metamorphic rocks - usually observed for biotite</p> <p>Excess 40 contamination e.g. Pankhurst et al., (1973), Berger (1975), Hanson et al., (1975), Albarede et al., (1978), Roddick et al., (1980), Dallmeyer &amp; Rivers (1983)</p>	<p>(i) 40* loss plus contamination of sites from low to high argon retentivity (due to irradiation) e.g. Horn et al., (1975)</p> <p>(ii) 40* loss plus 39K redistribution e.g. Hanes &amp; York (1979), Harrison &amp; McDougall (1981)</p> <p>(iii) 40* loss plus 39K recoil loss e.g. Turner &amp; Cadogan (1974)</p>
Geochronological interpretation	<p>(a) High temperature maximum age is minimum estimate of crystallisation age</p> <p>(b) The minimum age may record a maximum estimate for timing of argon loss/redistribution event</p>	<p>"Saddle" minimum gives a maximum estimate for time of crystallisation</p>	<p>None possible</p>	<p>The lowest temperature steps are likely to give a maximum estimate for timing of argon loss event</p> <p>For (i) and (ii) intermediate temperature age peak is considered to be a minimum estimate of crystallisation age. For (iii) the high temperature minimum age is a maximum age estimate.</p>
<p>These two age spectrum patterns may be confused</p>				
<p>geologically unreasonable plateau age</p>				
				

Table 4:3 continued

than one physical explanation e.g. see disturbed age spectra Nos. 8, 2 & 3, 5 & 6. This may or may not affect the geochronological interpretation.



CHAPTER FIVE

$^{40}\text{Ar} - ^{39}\text{Ar}$  Experimental Techniques

### 5:1 Introduction

This chapter outlines the experimental techniques employed in this  $^{40}\text{Ar}$ - $^{39}\text{Ar}$  dating study. The various sub-headings follow the natural progression, starting with the choice of standard and sample and finishing with the techniques of data analysis.

### 5:2 Standard

The standard used throughout this  $^{40}\text{Ar}$ - $^{39}\text{Ar}$  dating study was Bern biotite 4B. It fulfils all the requirements of an ideal  $^{40}\text{Ar}$ - $^{39}\text{Ar}$  standard (see Section 2:1:2).

The K-Ar age of Bern biotite 4B has been calculated from the data presented in Flisch (1982). Using average values for the concentrations of potassium and radiogenic argon, an age of  $17.2 \pm 0.3$  Ma was calculated. However, because of the possibility of slight variations in potassium concentration in the various aliquots analysed, a more rigorous way to calculate the age is to average the ages of the individual analyses. Such an approach yields an age of  $17.19 \pm 0.12$  Ma which is the value adopted in this study. The calculated error sets the systematic sample age error, for comparisons with other dating work, at 0.7% (this translates into an age error of  $\approx 0.4$  Ma for a typical British Tertiary igneous rock of age 60 Ma).

The standard was packed in high purity quartz vials for inclusion into the irradiation package, with the amount of material in each vial being typically about 0.04g.

### 5:3 Samples

Three types of rock sample have been used in this dating study: whole-rock, crushed whole-rock and mineral separate.

In their successful application of  $^{40}\text{Ar}$ - $^{39}\text{Ar}$  stepwise degassing to whole-rock dating, both Mussett et al., (1980) and Mussett (1985)

found that there was no correlation between the level of sample alteration and production of a statistically meaningful age plateau. Therefore, in this dating study, whole-rock samples have been simply selected on the basis of being free from weathered material and obvious fracturing.

Five doleritic/gabbroic whole-rock samples have been crushed with the 500 - 1400 $\mu$  size fraction being chosen for  $^{40}\text{Ar}$ - $^{39}\text{Ar}$  analysis. Baksi (1974) found that, for whole-rock basalt samples, loosely-held atmospheric argon, associated with fine-grained alteration, could be effectively removed by sample crushing. He found that the optimum size fraction was 10 - 30 mesh, which is virtually equivalent to 500 - 1400 $\mu$ . Where loosely-held atmospheric argon is not removed, possible isotopic fractionation problems may result (Baksi, 1974). In order to investigate the importance of loosely-held atmospheric argon in two Irish dolerites, both uncrushed and crushed samples were analysed. Because of the nature of the rock material available, three other crushed whole-rock samples were analysed.

For rock samples having a sufficiently coarse grain size, mineral separates in preference to whole-rock samples were prepared for analysis (using magnetic and hand-picking separation techniques). The maximum practical grain size was used, for each of the separates prepared, to reduce to a minimum possible  $^{39}\text{K}$  recoil loss (see Section 4:3:2).

For the measurement of argon isotopic ratios to be at the optimum precision, the argon released in a single step should fill the mass spectrometer, such that the minimum possible amplification levels can be used. With the desire to fulfil this criterion for all the samples analysed, the amount of rock/mineral needed is essentially determined by the sample potassium content and the number of steps required (the age and K/Ca ratio set the irradiation dose - see Turner, 1971a). In this dating study, sample potassium content was

found to be adequately determined from a general consideration of rock/mineral type, and each sample was required to provide at least 20 steps. Pilot samples in this thesis work were generally out-gassed in a series of up to ten steps, but, because of the complexity of the gas release patterns, no firm geochronological interpretations could be made. Thus, in an attempt to resolve the various influences affecting the gas release, I decided that samples should provide at least 20 steps.

For the more basic rocks, which constitute the majority of samples dates in this study, typically 6 - 10g of material was analysed, and for the more acidic rocks about half this amount was used. For the potassium-rich mineral separates (biotite and orthoclase feldspar) just 0.2g of sample was estimated to be adequate. However, for the potassium-poor separates (plagioclase feldspar and pyroxene) it was not possible to prepare the calculated optimum sample amounts because of a shortage of material. For these, only just over 1g of sample was analysed.

#### 5:4 Sample and Standard Irradiation

The packages containing samples and standards (placed in a 30cm long x 2cm diameter cylindrical aluminium reactor can) were irradiated at the Herald reactor AWRE Aldermaston between February, 1980 and March, 1984. The fast neutron flux received in these irradiations varied from  $1.5 - 5.5 \times 10^{17} \text{ n cm}^{-2}$ ; this range is consistent with the optimum values recommended by Turner (1971a) for rock with an age range that covers the standards and samples analysed in this study.

##### 5:4:1 Neutron Flux Variations

The fast neutron flux within a nuclear reactor is not homogeneous. Therefore, the possibility of variations in the neutron flux received by different parts of the irradiation package must be considered.

- i) Neutron flux variations along the reactor can

Several standards (usually eight) were arranged along each irradiation package because of the presence of neutron flux gradients along the reactor can. The J-values calculated for each standard sample were used to plot a J-value v. position along reactor can curve from which the sample J-values were calculated. The samples dated in this study were neutron irradiated in six individual irradiation packages. The J-value curves for five of these are presented in Figs. 5:1 to 5:5 (standard and sample data points are labelled by 'S' and 'R' numbers respectively). For the first irradiation batch (containing several pilot samples), it was not possible to plot a J-value curve because of the poor quality of the data for the standards. In this instance, sample J-values were estimated from a hand-drawn J-value curve. The standard and sample J-values for all six irradiation packages are listed in Tables 5:1 to 5:6.

The method used to fit the best J-value curve to the data of the standard samples are discussed in the data analysis section later in this chapter. The curve fitted in each case is a quadratic function. The staff at Aldermaston suggested that the fast neutron flux for the reactor positions used in this study should be symmetrical about the core centre line. They further suggested that this be approximately described by a cosine function. However, because of periodicity problems, it is difficult to fit a cosine function to a small number of data points. The easily fitted quadratic function is a very good approximation to a cosine when, as here, the lowest recorded values are no more than 15% below the peak value.

The quality of fit parameter (MSWD) for the J-value curves, listed in Tables 5:2 to 5:6, shows that, in most cases, the scatter of the data points is not wholly accounted for by the assigned experimental errors (i.e. MSWD  $\gg 1$ ). This inaccuracy is taken into account in the assigned sample J-value errors, which are directly proportional to

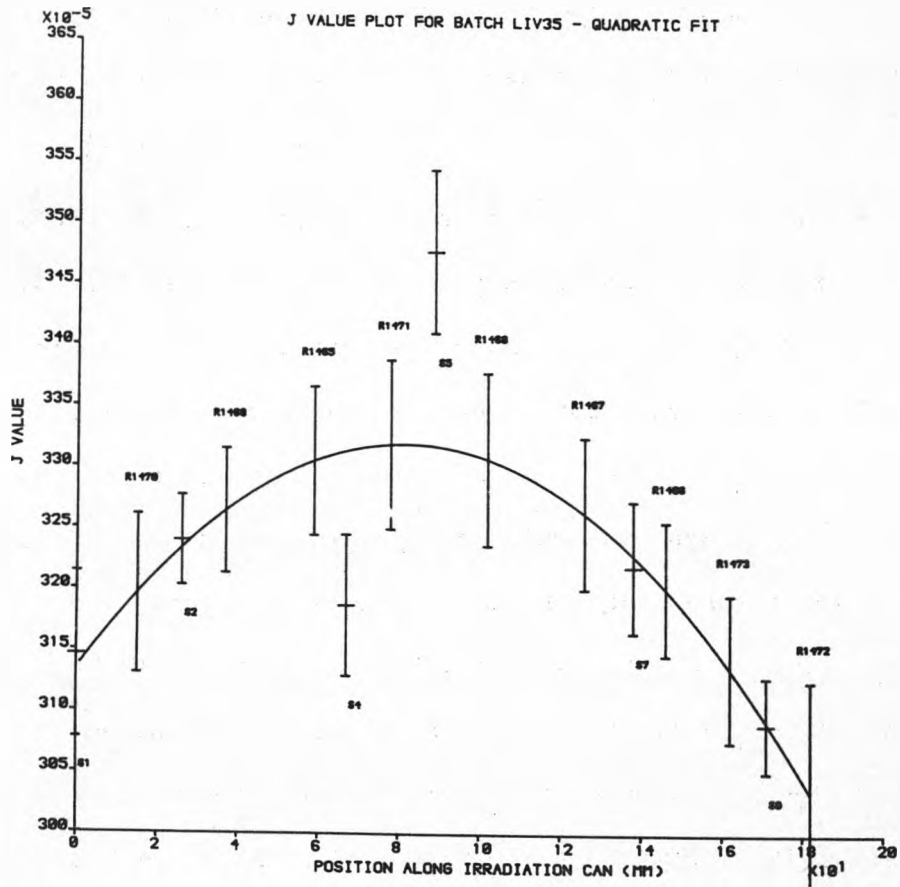


Fig. 5:1 J-value curve for irradiation batch LIV35

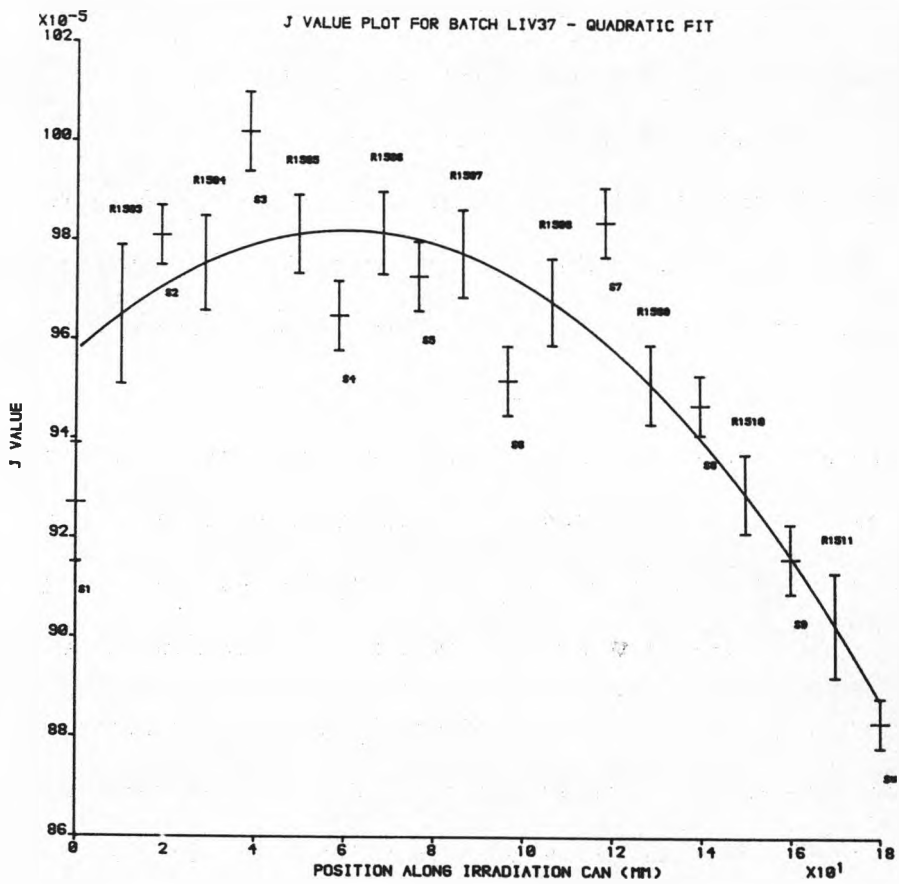


Fig. 5:2 J-value curve for irradiation batch LIV37

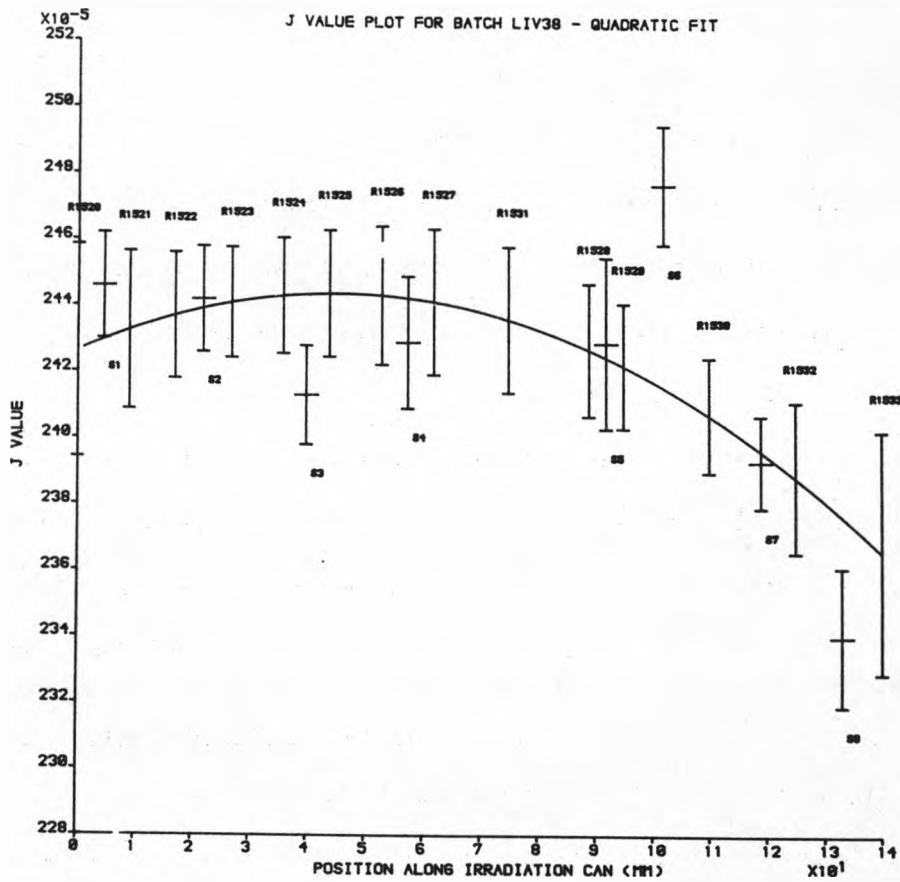


Fig. 5:3 J-value curve for irradiation batch LIV38



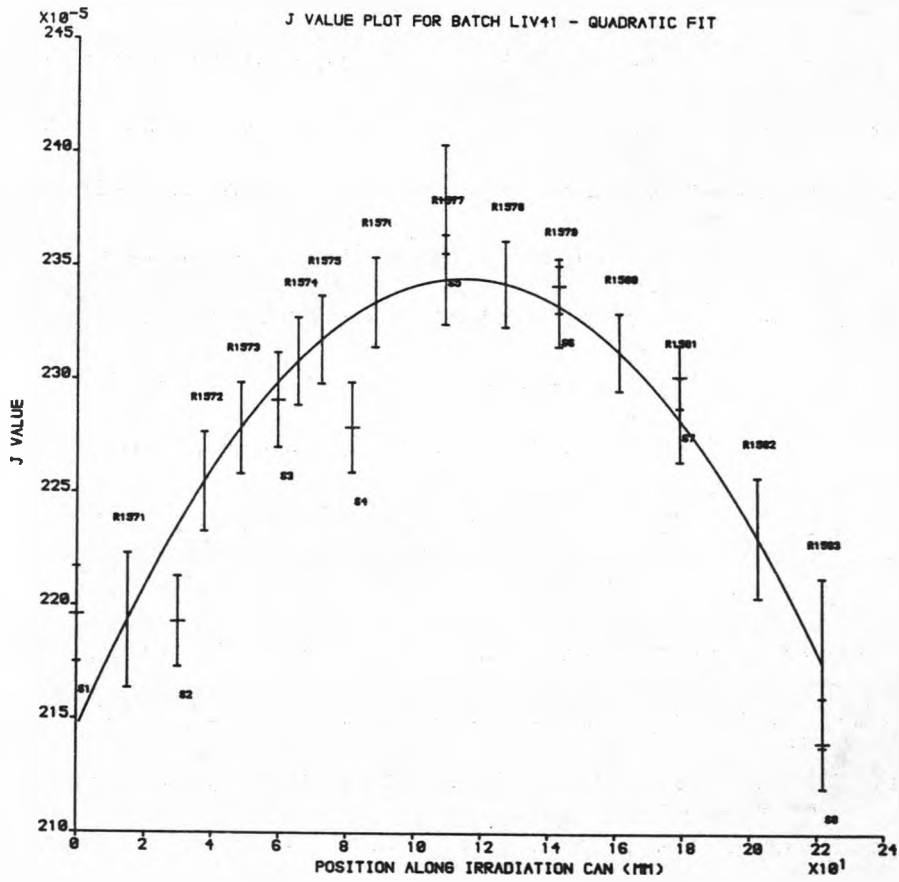


Fig. 5:4 J-value curve for irradiation batch LIV41

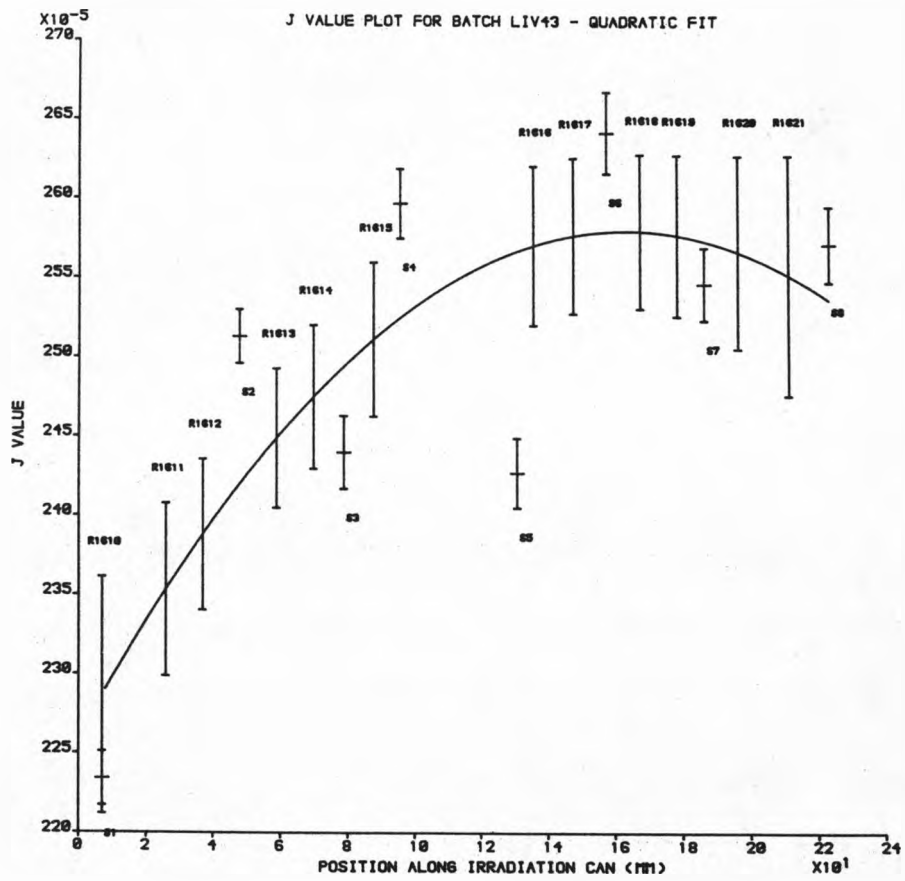


Fig. 5:5 J-value curve for irradiation batch LIV43

J VALUE CURVE FITTING AND INTERPOLATION  
\*\*\*\*\*

IRRADIATION BATCH LIV29  
\*\*\*\*\*

INPUT DATA  
\*\*\*\*\*

STANDARD AGE = 17.20 ERROR = 0.10

STANDARD NO	POSITION	ERROR	J-VALUE	ERROR
1	5.0	2.0	0.001180	0.000120
2	25.0	2.0	0.001279	0.000027
3	50.0	2.0	0.001211	0.000054
4	65.0	2.0	0.001272	0.000038
5	95.0	2.0	0.001257	0.000013
6	115.0	2.0	0.001309	0.000053
7	135.0	2.0	0.001298	0.000037
8	170.0	2.0	0.001316	0.000068

Estimated sample J-values

SAMPLE NO	POSITION	J-VALUE	ERROR
R1379	20.0	0.001270	0.000019
R1380	45.0	0.001258	0.000012
R1381	60.0	0.001255	0.000010
R1382	90.0	0.001259	0.000009
R1383	110.0	0.001269	0.000009
R1384	130.0	0.001285	0.000014
R1385	165.0	0.001326	0.000034
R1386	200.0	0.001386	0.000066

Table 5:1 J-value table for irradiation batch LIV29

J VALUE CURVE FITTING AND INTERPOLATION  
 \*\*\*\*\*

IRRADIATION BATCH LIV35  
 \*\*\*\*\*

INPUT DATA  
 \*\*\*\*\*

STANDARD AGE = 17.20 ERROR = 0.10

STANDARD NO	POSITION	ERROR	J-VALUE	ERROR
1	0.0	2.0	0.003146	0.000068
2	26.0	2.0	0.003240	0.000037
4	67.0	2.0	0.003187	0.000058
5	89.0	2.0	0.003477	0.000067
7	138.0	2.0	0.003219	0.000054
9	171.0	2.0	0.003090	0.000039

FIT TYPE : QUADRATIC  
 \*\*\*\*\*

NUMBER OF ITERATIONS = 4  
 MSWD = 3.51

J VALUE CURVE INTERPOLATION  
 \*\*\*\*\*

SAMPLE NO	POSITION	J-VALUE	ERROR
R1465	59.0	0.003305	0.000061
R1466	146.0	0.003201	0.000055
R1467	126.0	0.003263	0.000062
R1468	37.0	0.003264	0.000051
R1469	102.0	0.003307	0.000071
R1470	15.0	0.003196	0.000065
R1471	78.0	0.003319	0.000069
R1472	182.0	0.003034	0.000092
R1473	162.0	0.003136	0.000060

Table 5:2 J-value table for irradiation batch LIV35

J VALUE CURVE FITTING AND INTERPOLATION  
 \*\*\*\*\*

IRRADIATION BATCH LIV37  
 \*\*\*\*\*

INPUT DATA  
 \*\*\*\*\*

STANDARD AGE = 17.20 ERROR = 0.10

STANDARD NO	POSITION	ERROR	J-VALUE	ERROR
1	0.0	2.0	0.000927	0.000012
2	19.0	2.0	0.000981	0.000006
3	39.0	2.0	0.001002	0.000008
4	59.0	2.0	0.000965	0.000007
5	77.0	2.0	0.000973	0.000007
6	97.0	2.0	0.000952	0.000007
7	119.0	2.0	0.000984	0.000007
8	140.0	2.0	0.000947	0.000006
9	160.0	2.0	0.000916	0.000007
10	180.0	2.0	0.000883	0.000005

FIT TYPE : QUADRATIC  
 \*\*\*\*\*

NUMBER OF ITERATIONS = 5  
 MSWD = 6.73

J VALUE CURVE INTERPOLATION  
 \*\*\*\*\*

SAMPLE NO	POSITION	J-VALUE	ERROR
R1503	10.0	0.000965	0.000014
R1504	29.0	0.000975	0.000010
R1505	50.0	0.000981	0.000008
R1506	69.0	0.000982	0.000008
R1507	87.0	0.000978	0.000009
R1508	107.0	0.000968	0.000009
R1509	129.0	0.000951	0.000008
R1510	150.0	0.000929	0.000008
R1511	170.0	0.000903	0.000011

Table 5:3 J-value table for irradiation batch LIV37

J VALUE CURVE FITTING AND INTERPOLATION  
\*\*\*\*\*

IRRADIATION BATCH LIV38  
\*\*\*\*\*

INPUT DATA  
\*\*\*\*\*

STANDARD AGE = 17.20 ERROR = 0.10

STANDARD NO	POSITION	ERROR	J-VALUE	ERROR
1	4.5	2.0	0.002446	0.000016
2	22.0	2.0	0.002442	0.000016
3	40.0	2.0	0.002413	0.000015
4	57.5	2.0	0.002429	0.000020
5	92.0	2.0	0.002429	0.000026
6	102.0	2.0	0.002477	0.000018
7	119.0	2.0	0.002393	0.000014
8	133.0	2.0	0.002340	0.000021

FIT TYPE : QUADRATIC  
\*\*\*\*\*

NUMBER OF ITERATIONS = 5  
MSWD = 4.05

J VALUE CURVE INTERPOLATION  
\*\*\*\*\*

SAMPLE NO	POSITION	J-VALUE	ERROR
R1520	0.0	0.002426	0.000032
R1521	9.0	0.002433	0.000024
R1522	17.0	0.002437	0.000019
R1523	27.0	0.002441	0.000017
R1524	36.0	0.002443	0.000018
R1525	44.0	0.002444	0.000019
R1526	53.0	0.002443	0.000021
R1527	62.0	0.002441	0.000022
R1528	89.0	0.002427	0.000020
R1529	95.0	0.002422	0.000019
R1530	110.0	0.002407	0.000017
R1531	75.0	0.002436	0.000022
R1532	125.0	0.002388	0.000023
R1533	140.0	0.002366	0.000037

Table 5:4 J-value table for irradiation batch LIV38

J VALUE CURVE FITTING AND INTERPOLATION  
 \*\*\*\*\*

IRRADIATION BATCH LIV41  
 \*\*\*\*\*

INPUT DATA  
 \*\*\*\*\*

STANDARD AGE = 17.20 ERROR = 0.10

STANDARD NO	POSITION	ERROR	J-VALUE	ERROR
1	0.0	2.0	0.002196	0.000021
2	30.0	2.0	0.002193	0.000020
3	60.0	2.0	0.002291	0.000021
4	82.0	2.0	0.002279	0.000020
5	110.0	2.0	0.002380	0.000024
6	144.0	2.0	0.002342	0.000012
7	180.0	2.0	0.002302	0.000014
8	222.0	2.0	0.002140	0.000020

FIT TYPE : QUADRATIC  
 \* \*\*\*\*\*

NUMBER OF ITERATIONS = 5  
 MSWD = 4.59

J VALUE CURVE INTERPOLATION  
 \*\*\*\*\*

SAMPLE NO	POSITION	J-VALUE	ERROR
R1571	15.0	0.002193	0.000030
R1572	38.0	0.002255	0.000022
R1573	49.0	0.002279	0.000020
R1574	66.0	0.002308	0.000019
R1575	73.0	0.002318	0.000019
R1576	89.0	0.002334	0.000020
R1577	110.0	0.002345	0.000020
R1578	128.0	0.002343	0.000019
R1579	144.0	0.002333	0.000018
R1580	162.0	0.002313	0.000017
R1581	180.0	0.002283	0.000019
R1582	203.0	0.002231	0.000027
R1583	222.0	0.002176	0.000037

Table 5:5 J-value table for irradiation batch LIV41

J VALUE CURVE FITTING AND INTERPOLATION  
 \*\*\*\*\*

IRRADIATION BATCH LIV43  
 \*\*\*\*\*

INPUT DATA  
 \*\*\*\*\*

STANDARD AGE = 17.20 ERROR = 0.10

STANDARD NO	POSITION	ERROR	J-VALUE	ERROR
1	7.0	2.0	0.002234	0.000017
2	48.0	2.0	0.002513	0.000017
3	79.0	2.0	0.002440	0.000023
4	96.0	2.0	0.002597	0.000022
5	131.0	2.0	0.002427	0.000022
6	158.0	2.0	0.002642	0.000026
7	187.0	2.0	0.002546	0.000023
8	224.0	2.0	0.002571	0.000024

FIT TYPE : QUADRATIC  
 \*\*\*\*\*

NUMBER OF ITERATIONS = 6  
 MSWD = 20.10

J VALUE CURVE INTERPOLATION  
 \*\*\*\*\*

SAMPLE NO	POSITION	J-VALUE	ERROR
R1610	7.0	0.002287	0.000075
R1611	26.0	0.002353	0.000055
R1612	37.0	0.002388	0.000048
R1613	59.0	0.002449	0.000044
R1614	70.0	0.002475	0.000045
R1615	88.0	0.002511	0.000049
R1616	136.0	0.002570	0.000050
R1617	148.0	0.002577	0.000049
R1618	168.0	0.002579	0.000049
R1619	179.0	0.002577	0.000051
R1620	197.0	0.002566	0.000061
R1621	212.0	0.002552	0.000076

Table 5:6 J-value table for irradiation batch LIV43



the calculated MSWD value.

ii) Neutron flux variations across the reactor can

A neutron flux gradient across the diameter of the reactor can was also expected. It was assumed to vary linearly and to minimise its effect, each reactor can was rotated through  $180^\circ$  (about its long axis) half-way through the irradiation period.

To minimise the effect of any residual flux gradient, great care was taken to ensure that all samples and standards were positioned as close as possible to the long axis of the reactor can. This ensures that if a linear flux gradient does exist, each assigned sample J-value represents the average fast neutron flux received by that sample as a whole.

To monitor possible neutron flux gradients across the reactor can, four nickel wires were placed at  $90^\circ$  intervals around the outside of the samples/standards package approximately half-way along its length. Neutron flux measurements from these nickel wires, which were made by the staff at Aldermaston, were used to calculate a maximum fast flux variation per millimetre (assuming the variation is linear). The calculated maximum fast flux gradient for each of the irradiation packages is listed in Table 5:7. Note that these values in no way correlate with the J-value curve MSWD values. This indicates that the scatter of data points in the J-value plots (see MSWD values) cannot be reasonably explained in terms of misalignment of standard samples off the reactor can axis.

iii) Self-shielding

Neutron flux variation due to sample shielding has been discussed by Mitchell (1968). He found that there was no difference in the neutron flux received by the inner and outer portions of a sphere of muscovite mica 10 mm in diameter. Samples in this study were of a similar dimension and generally of a less hydrated nature than muscovite

Irradiation batch	Maximum fast neutron flux gradient across the reactor can ( $\%mm^{-1}$ )
LIV29	0.08
LIV35	0.31
LIV37	0.68
LIV38	1.01
LIV41	0.44
LIV43	0.36

Table 5:7 Calculated maximum fast neutron flux gradients

(i.e. reduced flux moderation). Thus "self-shielding" is assumed to be unimportant.

#### 5:4:2 Interference Reaction Corrections

Available data (see for example, Roddick, 1983) suggests that all the interference reaction correction terms (see Section 2:2:2) except  $[40/39]_K$  are reasonably constant. This is true for repeated measurements in the same reactor and also, to a lesser extent, for analyses from reactor to reactor. This constancy is explained by the activation of the reactions involved being mainly due to fast neutrons (see Appendix 3). We know that the thermal to fast neutron flux ratio is variable within a single reactor core position and significantly more so from reactor to reactor. Variation in the measured value of  $[40/39]_K$  is thus not surprising as the reactions responsible for the production of  $^{40}K$  and  $^{39}K$  are activated largely by thermal and fast neutrons respectively (see Tetley et al., 1980).

In an attempt to measure the interference reaction correction constants appropriate to the sample/standard irradiations performed in this study, a package containing high purity potassium and calcium salts was also irradiated.

Each of the four salt samples irradiated ( $K_2SO_4$ ,  $K_2CO_3$ ,  $CaF_2$ ,  $CaCO_3$ ) were packed in evacuated break-seal vials. This was done in an attempt to allow any isotopic recoil loss effects to be monitored by the measurement of the argon in the evacuated space of the vial. However, two of the break-seal tips were smashed in transit and, for another salt, the argon in the evacuated space was, to some extent, lost due to a technical problem.

The values of the interference reaction correction terms calculated from the analyses of the irradiated salt samples are presented in Table 5:8. The values of the interference reaction corrections

	R1559 (K <sub>2</sub> SO <sub>4</sub> )	R1560 (CaF <sub>2</sub> )	R1561 (K <sub>2</sub> CO <sub>3</sub> )	R1562 (CaCO <sub>3</sub> )	Turner et al. (1978)	Roddick (1983)	Values adopted in this study
$\left[ \begin{smallmatrix} 40 \\ 39 \end{smallmatrix} \right] \text{K}$	0.0267 +0.0020		-0.016 +0.058		0.012	0.016	0.015
$\left[ \begin{smallmatrix} 38 \\ 39 \end{smallmatrix} \right] \text{K}$	0.010951 +0.000032		0.0010815 +0.0000081		0.011 +0.001	0.0107	0.011
$\left[ \frac{40-(40/36)\text{atm.36}}{37} \right] \text{Ca}$		-0.113 ± 0.022		-0.069 ± 0.013	-0.074 ± 0.015 <sup>+</sup>	-0.0742 ± 0.0006 <sup>+</sup>	-0.074
$\left[ \begin{smallmatrix} 39 \\ 37 \end{smallmatrix} \right] \text{Ca}$ (× 10 <sup>-4</sup> )		7.12 ± 0.15		6.32 ± 0.12	6.7 ± 0.3	6.44 ± 0.04	6.65
$\left[ \frac{38-(38/36)\text{atm.36}}{37} \right] \text{Ca}$ (× 10 <sup>-5</sup> )		75.4 ± 5.5		-1.2 ± 1.1	5.3 ± 5.1 <sup>+</sup>	-0.88 ± 0.21 <sup>+</sup>	-1.0

\* Calculated from the data presented in the publication

Table 5:8 Values for the interference reaction correction terms

adopted in this dating study are actually a compromise between these and others reported by Turner et al., (1978) and Roddick (1983) for similar core positions in the same reactor (see Table 5:8). This is because the values measured here were subject to inconsistency (possibly due to mass spectrometer backgrounds in the critical m/e range) and, in some cases, rather large errors. Thus, they alone were not considered reliable enough to set the correction terms for the whole dating study. Although I have mentioned that the value of  $[40/39]_K$  can be variable within even a single reactor core position, the value adopted is not critical (see Appendix 4). The importance of each of the interference corrections and the possible effects of errors in (or real variations from) the adopted values are considered, in the context of this dating study, in Appendix 4.

In the analysis of the  $K_2SO_4$  sample, it was possible to estimate a value for the previously ignored interference reaction correction term  $[37/39]_K$  (for the  $K_2CO_3$  sample, the  $^{37}Ar$  background due to the previously run  $CaF_2$  was unacceptably high). Having shown that any  $^{37}Ar$  due to calcium impurity in the  $K_2SO_4$  salt (quoted at 2ppm) was negligible ( $< 5\%$ ), a value of  $(3.5 \pm 0.2) \times 10^{-5}$  was calculated. This confirms the assumption that potassium-derived  $^{37}Ar$  is of no great significance for most samples (Section 2:2:2). Where  $^{37}K$  is not negligible, the correction due to the supposed calcium interferences will be minimal and thus its presence will not be important.

The vials that remained unbroken prior to loading in the gas extraction line yielded some interesting results. The gas released by smashing the break-seal tip of R1559 ( $K_2SO_4$ ) contained  $\approx 0.3\%$  of the  $^{39}K$  released in salt fusion. Whilst the amounts of argon released were insufficient to significantly affect the calculated correction terms, they do indicate an apparent "fractionation" effect between potassium-derived 38 and 39. A  $[38/39]_K$  ratio of  $0.04225 \pm 0.00063$  indicates a

$^{38}\text{K}$  enhancement relative to  $^{39}\text{K}$  for the argon in the evacuated space of the vial. This argon can either be due to outgassing of the salt sample as a result of heating during the irradiation and/or pre-fusion extraction line bakeout or recoil loss. Outgassing is unlikely to produce an isotopic fractionation, so recoil loss is favoured as being the dominant contributor. This apparent "fractionation" is consistent with the maximum recoil energy for the interaction producing  $^{38}\text{K}$  being greater than that for the interaction responsible for  $^{39}\text{K}$  (see Appendix 3). The fine-grained nature of the  $\text{K}_2\text{SO}_4$  salt sample might have led one to predict such a recoil loss effect.

The gas released by the smashing of the break-seal tip of R1560 ( $\text{CaF}_2$ ) was, to some extent, lost due to a technical problem. However,  $^{37}\text{Ar}$  amounting to at least 1% of that released during sample fusion was contained in the evacuated space of the vial containing this  $\text{CaF}_2$  salt sample. The hypothesised recoil loss effect appears to be more significant here than for the  $\text{K}_2\text{SO}_4$  salt. This is consistent with the very high maximum recoil energy for the calcium interaction producing  $^{37}\text{Ar}$  (Appendix 3) and the more fine-grained nature of the  $\text{CaF}_2$  salt sample (the manufacturers quoted a "mean volume diameter" of  $2\mu$  for the  $\text{CaF}_2$  salt and  $30\mu$  for the  $\text{K}_2\text{CO}_3$  salt, and the  $\text{K}_2\text{SO}_4$  salt was visibly coarser than the  $\text{K}_2\text{CO}_3$ ). The calculations of maximum recoil energies presented in Appendix 3 suggest that a significant "fractionation" effect between calcium-derived  $^{36}\text{Ar}$  and  $^{37}\text{Ar}$  can be expected. However, no such effect is likely between calcium-derived  $^{39}\text{Ar}$  or  $^{40}\text{Ar}$  and  $^{37}\text{Ar}$  because the calculated maximum recoil energies are very similar.

#### 5:4:3 Loss of Radiogenic Argon During the Irradiation

Experiments carried out by Mitchell (1968) and Ross (1976) suggested that samples etc. may be heated, during irradiation in the Herald reactor, to temperatures not in excess of  $200^\circ\text{C}$ . They both concluded

that this was insufficient to cause any significant loss of  $^{40}\text{K}$  from samples or standards (the temperatures experienced during irradiation are probably, in most cases, no greater than those experienced during extraction line bake-outs).

#### 5:5 Gas Extraction Line

The gas extraction line used in this study was similar to the one described by Ross (1976). Each sample was placed in a molybdenum crucible, which was heated by radio-frequency (r.f.) induction. The sample temperature was monitored by either a thermocouple, an optical pyrometer, or an infra-red detector. The heating schedule used for each sample was based upon the desire to keep individual steps at about the same size (in term of  $^{39}\text{K}$  release) and was largely a matter of experience. For each heating step, the extraction line and crucible can be expected to add a component of argon presumed to be of atmospheric composition. This is the so-called blank and it was minimised in two ways:

- i) Each crucible was outgassed at the highest possible r.f. setting for approximately 15 minutes prior to sample loading (the latter involves breaking the furnace vacuum). Baksi (1973) has discussed various crucible preparation techniques and he concluded that such a procedure was probably the optimum. It would probably be possible to reduce crucible blank levels even more if the sample was loaded directly into the crucible without breaking the furnace vacuum. However, this was not practical for the large (up to 10g) samples commonly used in this dating study.
- ii) In addition to the extraction line bake-out following sample loading, a similar bake-out was performed after each day's step-heating runs. The temperature of these bake-outs was typically  $\approx 150^\circ\text{C}$ .

To test the assumption that the blank component is of an atmospheric composition, and also to ascertain what levels of blank contribution

can be expected, crucibles have been stepwise degassed. Fig. 5:6 displays the results of one of these blank runs. It is apparent that the calculated step  $40/36$  ratios are approximately equal to the measured  $40/36$  ratios for air, so vindicating our assumption. Step  $40/36$  ratios were, in fact, observed to be systematically slightly below  $(40/36)_{\text{air}}$ ; this can probably be explained in terms of a small mass spectrometer background at  $m/e = 36$ , which is only significant where the amounts of gas are low. The pattern of  $^{40}\text{Ar}$  release displays low and high temperature peaks. The former probably represents atmospheric argon absorbed onto the crucible after degassing whilst the latter may indicate that all the tightly held atmospheric argon was not removed by the outgassing procedure.

The total amount of  $^{40}\text{Ar}$  released during stepwise and single step degassing of a crucible was variable. 500 - 1000 units seemed to be typical (25,000 units is a mass spectrometer's full), but where the crucible was initially poorly outgassed, amounts as high as 2,500 have been recorded. The level of  $^{36}\text{Ar}$  in a sample due to blank contributions (up to  $2500/(40/36)_{\text{atm}} \approx 10$  units) was generally very small compared with the total amount of natural  $^{36}\text{Ar}$  (typically 1000 units). Thus, the majority of the measured natural  $^{36}\text{Ar}$  was sample derived.

If the blank contribution is significant, then only where a sample's initial argon has a non-atmospheric composition will it be important in terms of age calculation (see Section 3:3). Where a sample's initial argon has an atmospheric composition, then obviously the presence of a blank contribution is purely academic (except that it has the effect of increasing the error in the calculated age).

#### 5:6 Mass Spectrometer Argon Analysis

Before starting the  $^{40}\text{Ar}$ - $^{39}\text{Ar}$  stepwise degassing analyses in this study, checks were made to ensure that the chart recorder and mass spectrometer amplifier were operating in a linear fashion. These checks were



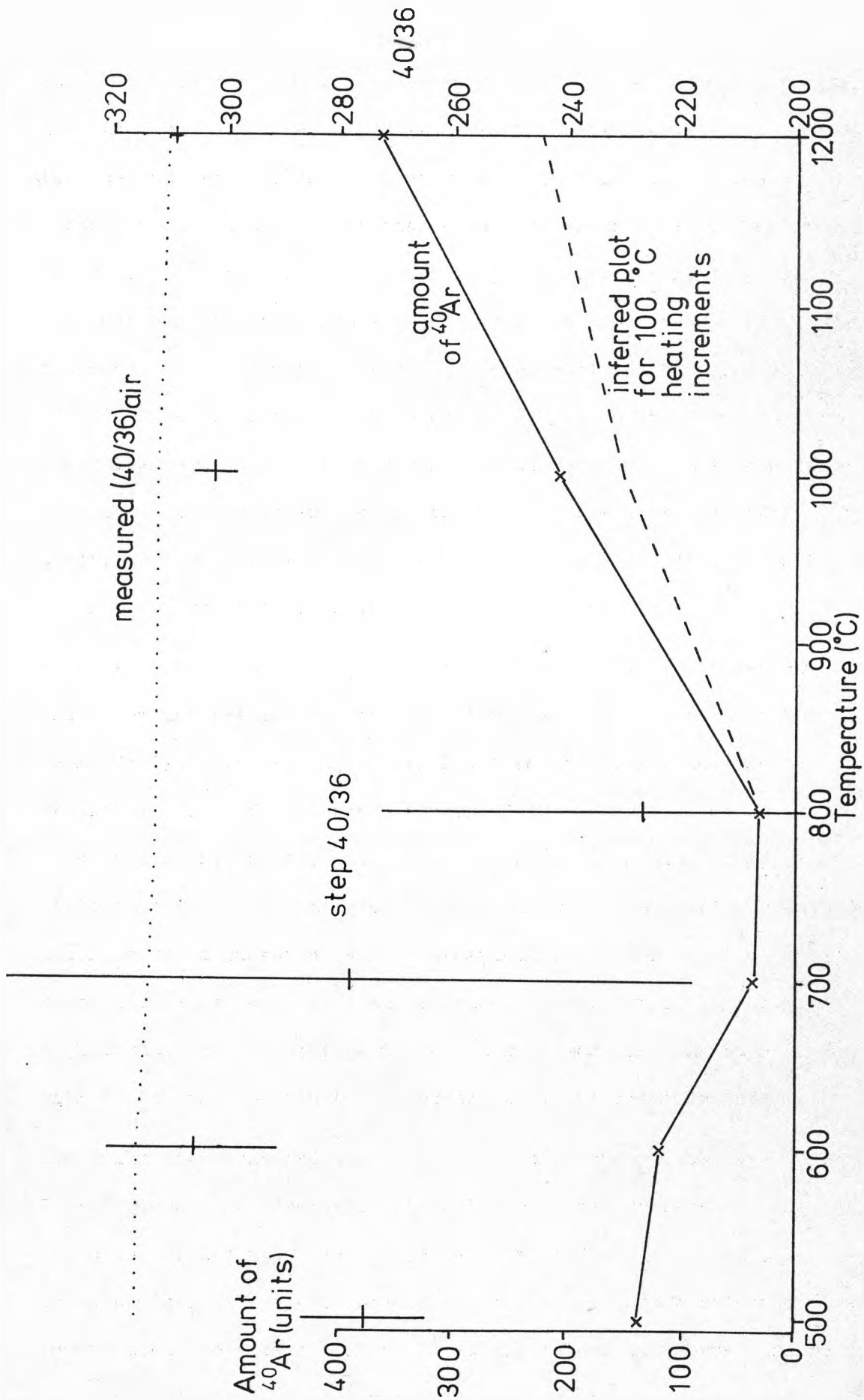


Fig. 5:6 Example of a blank run

repeated about half-way through the period in which experimental measurements were made.

After gas equilibration in the mass spectrometer, sample or standard gas analysis commenced. The five argon isotopes were measured sequentially, starting with that of lowest mass. This procedure was repeated three times. For each isotope peak, the maximum possible amplifier gain was used to maximise peak measuring precision. Every other day, aliquots of atmospheric argon from a large reservoir were analysed to ascertain quantitatively the mass discrimination effect of the mass spectrometer. Acting as an argon spike, the analyses of these aliquots also gave information about changes in the mass spectrometer sensitivity. Over most of the life of the filament mass spectrometer sensitivity was constant to within 10%. However, towards the end of its life, sensitivity changed markedly, but as the mass discrimination was also then subject to significant day-to-day variations, all analyses were ceased. Argon analysis recommenced only when a new filament had been fitted.

A recurring problem with new filaments was the presence of small mass spectrometer backgrounds at  $m/e = 36$  and  $38$ . The relative isotopic proportions suggested that this background was caused by a HCl contamination. However, within a week or so of having fitted the new filament, this background would entirely disappear and analyses were re-commenced. An occasional problem encountered in mass spectrometer argon analysis was a "hydrocarbon" contamination. This was recognised by the presence of mass spectrometer peaks which decay rapidly in a static system and probably results from a poor gas clean-up. The peak decay was interpreted as a cracking process instigated by the hot filament. Where such a contamination was present, gas analysis was commenced only when the "hydrocarbons", at  $m/e$  values corresponding to the argon isotopes, had been entirely broken down.

Argon isotopes analysed in a static mass spectrometer are subject to

a "memory" effect which entails the isotopic peak height gradually changing with time. The magnitude and sense of the effect is dependent on the argon isotopes present in the mass spectrometer volume prior to a given analysis. With low argon levels in the pumped mass spectrometer volume and at least half an hour's interval between separate gas analyses, the memory effect was usually negative and small (i.e. peak height gradually decreased with time).

#### 5:7 Data Analysis

Fig. 5:7 presents a simplified flow diagram of the stages in the calculation of a  $^{40}\text{Ar}$ - $^{39}\text{Ar}$  step age. The mathematics involved can be followed in the appropriate computer program listings (see below).

All quoted errors are standard deviation estimates, i.e.  $1\sigma$  level.

The isotopic ratio errors are based on the replication errors of the three scans (having taken account of any memory effect) but also include a minimum error based on the examination of many scans.

Total gas calculation (i.e. where the basic data for a number of individual steps are summed) assume constant sensitivity of the mass spectrometer. As noted above, the mass spectrometer sensitivity is probably constant to within 10%, however, it is not thought that such a variation in sensitivity will significantly affect the total gas calculations.

Eight computer programs for data analysis have been written as part of this thesis and five of them utilise a generalised least squares regression routine ("WOLBRG"), outlined by Wolberg (1967). All are written in Fortran 77 except two, "DATING" and "JVALUE", which are written in Algol 68. Brief descriptions of each of the computer programs are given below with listings and example outputs being presented in Appendix 5.

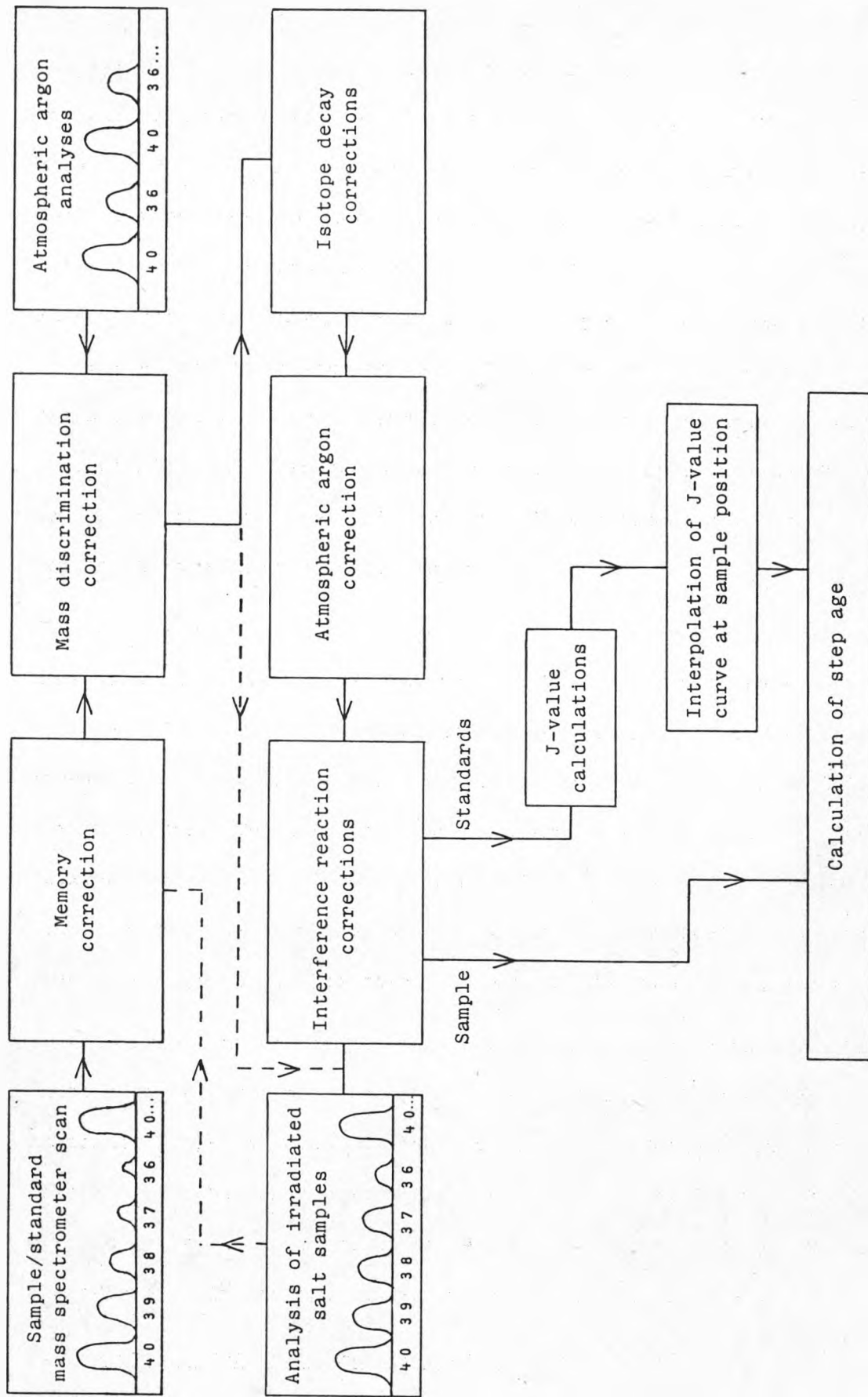


Fig 5:7 Flow diagram for the calculation of a  $^{40}\text{Ar}$ - $^{39}\text{Ar}$  step age

## Computer Programs for the Basic Data Analysis

### For Data Produced by Samples

"DATING": This program is for the input of sample data. It performs the basic age calculation for individual steps and creates the data file for the main program ("STEPAGE").

"STEPAGE": This is the main program for the analysis of  $^{40}\text{Ar}$ - $^{39}\text{Ar}$  step-wise degassing data. It consists of 14 modules and uses the basic data file produced by "DATING". "STEPAGE" calculates plateau ages and ICD2/ isochron parameters (for the latter, the generalised least squares regression routine "WOLBRG" is used) and also plots the age spectrum, ICD2 and the isochron diagrams either on the computer terminal or a graph plotter, e.g. Figs. 3:1 to 3:3. The basic data files for the Arrhenius diagram program ("ARRHENUS") and ICD3 data analysis ("FITPLANE") are created in "STEPAGE".

### For Data Produced by Standards

"JVALUE": This is very similar to "DATING" in structure. "JVALUE" calculates the standard J-values and creates the data files for the curve fitting and interpolation program "JCURVE".

"JCURVE": Using the data files produced by "JVALUE", this program calculates the best fitting cosine, quadratic or cubic curve to the standard J-value data. The best curve is found by using the "WOLBRG" routine and J-value interpolation at sample positions follows the procedure described by Wolberg (1967). "JCURVE" produces a graphical plot of the standard J-values, the best fitting curve and the interpolated sample J-values (e.g. Fig. 5:1).

### For Data Produced by Salts

"SALTS": The basic data file for this program is produced by "DATING". "SALTS" calculates the interference reaction correction terms for irradiated potassium or calcium salts.

Additional Programs

"FITPLANE": This program calculates the best fitting plane for the ICD3 (using "WOLBRG") and thus an age, a  $(40/36)_0$  and one other parameter (see Section 3:4). "FITPLANE" also produces the graphical representation of the best fitting plane and data points described in Section 3:4 (see Fig. 3:4). The data necessary for the running of this program is produced in "STEPAGE".

"ARRHENUS": Using the data file produced by "STEPAGE", this program draws an Arrhenius diagram assuming either a spherical or planar symmetry (see Appendix 2). "WOLBRG" is called to calculate the best fitting straight line to a chosen series of data points; from this, an activation energy and a  $D_0/a^2$  value can be computed. The diffusion parameters and an assumed cooling rate lead to the calculation of a closure temperature.

"NIFIT": This program calculates a maximum fast neutron flux gradient across a reactor can from the nickel wire flux measurements. A standard geometrical arrangement of the nickel wires is assumed and the calculation utilises "WOLBRG" to fit a plane to the data.

CHAPTER SIX

$^{40}\text{Ar}$ - $^{39}\text{Ar}$  Dates for Irish Tertiary Igneous Rocks

## 6:1 Introduction

### 6:1:1 Background to this study

As pointed out in Chapter 1, the available dates for Tertiary activity in Ireland were determined largely by the conventional potassium-argon method. Experience in the rest of the BTIP suggests that such dates are unreliable (Mussett, 1982). Several of the Irish K-Ar ages are much younger or older than reliable dates reported for other areas of the BTIP. A primary aim of this project was to check the validity of these results. The  $^{40}\text{Ar}$ - $^{39}\text{Ar}$  stepwise degassing technique is the only dating method that is versatile enough to apply to all the rock types found in the BTIP and which also circumvents the limitations of the conventional K-Ar approach (see Chapter 1). This method was therefore essential for the accurate dating of Tertiary igneous rocks from Ireland.

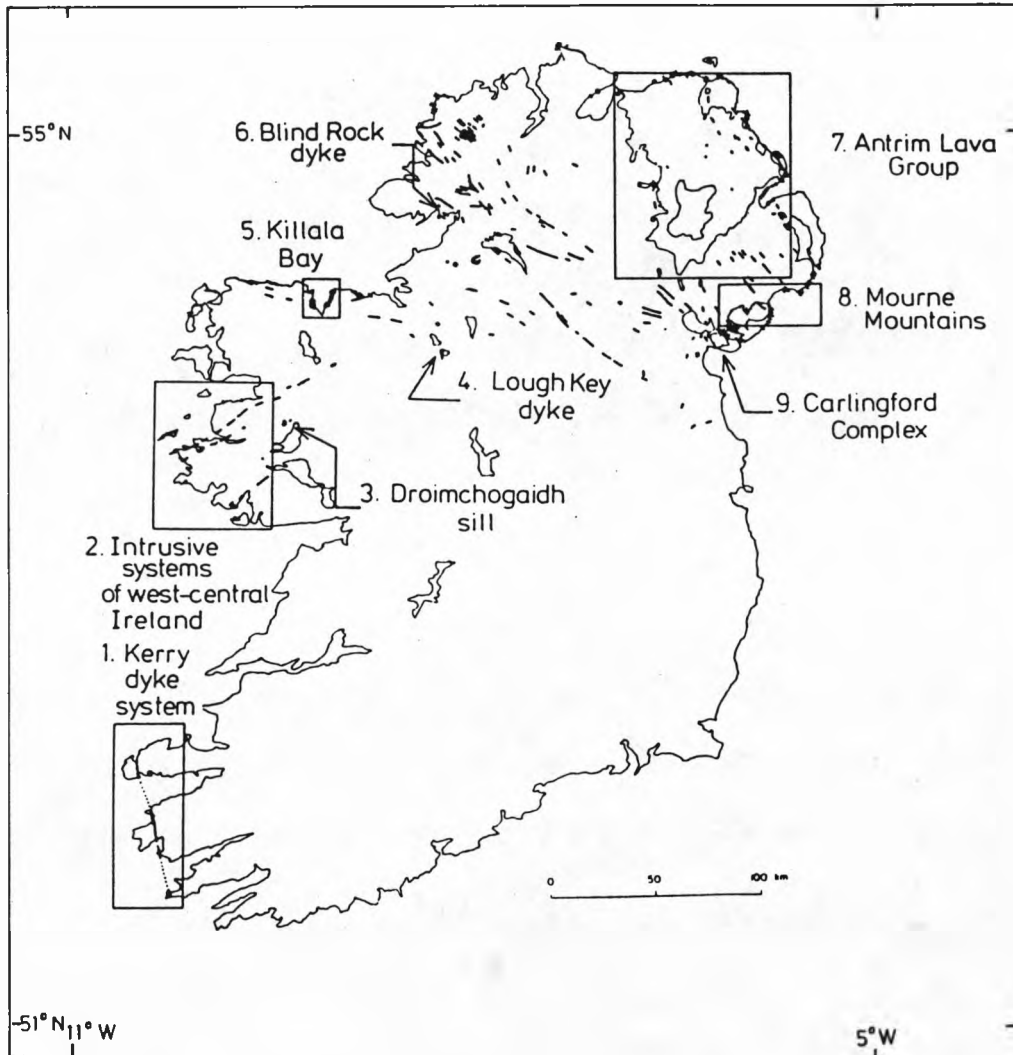
### 6:1:2 The Tertiary Igneous Geology of Ireland

Fig. 6:1 shows the distribution of Tertiary igneous rocks in Ireland (the numbered areas were investigated in this study). A discussion of the geology can be divided conveniently into three sections - the Antrim plateau basalts, the central complexes (the Mourne mountains, Carlingford and Slieve Gullion), and the minor intrusives which are widely distributed (see Fig. 6:1). Brief details only are presented here and for a deeper insight into the igneous geology of Tertiary Ireland, the reader should refer to Preston (1981).

#### The Antrim Plateau Basalts

Covering 4000 km<sup>2</sup>, the Antrim lavas are the largest remnant of Tertiary igneous activity in the British Isles. The maximum exposed thickness of lavas is 300 m (Walker, 1959) and the Langford Lodge borehole passed through over 750 m of basalts (Fowler, 1957). It is thought, however, that the original pile thickness may have been considerably greater (Walker, 1960). Individual lava flows average just under 7 m in





**Fig. 6:1** The Tertiary igneous geology of Ireland (the numbered locations were investigated in this study) - adapted from Mohr (1982)

thickness and in some cases they can be traced as far as 10 km (Walker, 1959). The lava pile, which consists mainly of olivine basalt, is essentially divided into two by the Interbasaltic Formation, representing a period of relative volcanic quiescence. This formation is marked by the weathered remnants of earlier basalt flows, tholeiitic lavas (including the Giant's Causeway), and acidic volcanic rocks (mainly at Tardree - see Fig. 6:42). It is thought that the Antrim lavas were extruded subaerially in fissure-type eruptions and there are at least two examples showing dykes directly feeding lava flows (Walker, 1959; Preston, 1981). The 30 or so doleritic plugs that cut the Antrim lavas may represent feeders to lava flows long since removed by erosion (Walker, 1959). Many basalts of the Antrim Lava Group are strongly altered, displaying vesicles in-filled with zeolites and other amygdale minerals. This is thought to indicate a regional hydrothermal metasomatism which commenced after a rapid accumulation of a great thickness of lavas (Walker, 1960).

#### The Central Complexes

The Carlingford and Slieve Gullion Complexes are thought to represent the remnants of a single volcanic centre which migrated in a southeasterly direction (see Fig. 6:1). They consist of both acidic and basic intrusive bodies, as well as small patches of basaltic lavas. The Carlingford and Slieve Gullion volcanoes are not considered responsible for the plateau lavas in Antrim. This is because lavas in Antrim do not thicken to the south and individual flows of the Antrim pile do not extend far (Walker, 1959).

The Mourne Complex is distinct from Carlingford and Slieve Gullion in that it is entirely intrusive in nature and largely consists of granitic rocks. The Mourne Granites consist of five separate bodies (Richey, 1928; Emeleus, 1955) which are thought to have been emplaced successively by a process of ring dyke formation and cauldron

subsidence (Macintyre, 1973). Gravity anomalies suggest that the granites are underlain by a large mass of basic rocks (Preston, 1981).

### The Minor Intrusives

Many of the Tertiary dyke swarm/systems in Ireland are not associated with central complexes and do not show any marked focus of concentration. This is in strong contrast to the Hebridean dyke swarms such as those in Skye and Mull. Not all the dyke swarms/systems display the typical British NW-SE trend e.g. Killala Bay E-W; west-central Ireland NE-SW (see Fig. 6:1). These notable exceptions, which are found on the west coast of Ireland, may be related to a hypothesised offshore Tertiary centre (Mohr, 1982). Several feeder dykes and plugs have been recognised on the west coast of Ireland (Preston, 1965; Macintyre, 1973). These probably represent the remnants of extrusive activity in the west of Ireland (Preston, 1965, 1981).

### 6:1:3 Presentation and Interpretation of Results

The results of this dating study are discussed area by area in Section 6:2. The basic raw data for the 45 samples analysed can be found in Appendix 8 and only plateau and ICD (isotope correlation diagram) ages are listed in the main text. As ICD3 data analysis was not very helpful in this investigation, interpretation is based largely on the age spectrum and ICD2 plots. For each of the samples, the results of age spectrum and ICD2 data analysis for all the extracted steps are given. Usually, the parameters calculated for one or two selected segments of the gas release are also given. The criteria for a statistically meaningful age, based on combined age spectrum and ICD2 data analysis, have been discussed in Section 3:5. All the ages quoted in this work have been calculated or re-calculated using the decay constants etc. recommended by the International Union of Geological Sciences - Subcommittee on Geochronology (Steiger & Jäger, 1977). All errors quoted for results in this study are at the 1 $\sigma$

level of confidence. Those for published dates are either at the 1 $\sigma$  level, or assumed to be at this level, if not stated by the original authors.

Analyses R1381 (238P), R1382 (124NA), R1383 (105A), R1384 (253) and R1473 (238P) were the pilot samples for this dating study. As these analyses consist of only small numbers of steps and have not been corrected for chlorine interferences (see Section 2:1:2) or the memory effect (see Section 5:6), they are considered as giving rough age estimates only.

It has been possible to plot Arrhenius diagrams only where step temperature information is available. As stated in Appendix 2, only the cases where the Arrhenius diagrams yield apparently meaningful results are they discussed in detail in the text. All the Arrhenius diagrams presented in this thesis assume a spherical diffusion geometry unless otherwise stated. The assignment of geological cooling rates for closure temperature calculations undertaken in this work are discussed in Appendix 2. Appendix 7 gives brief petrographic sample descriptions, together with the grid references of sampling locations.

## 6:2 Results

### 6:2:1 The Kerry Dyke System

The NNW trending Kerry dyke system represents the most southerly expression of Tertiary igneous activity in Ireland and in the context of the whole British Isles, only Lundy is further south.

The line of the dyke system (see Fig. 6:2) was mapped by ground magnetic surveying (Morris, 1974) and it is at least 70 km in length, with possible extensions offshore. There are, in fact, only four known exposures of the Kerry dyke system - these are indicated by arrows in Fig. 6:2. Samples from all these localities are lithologically similar (doleritic), with a consistent palaeomagnetic direction (Morris, 1974). Mohr (1982) has related the Kerry dyke system and other dolerite

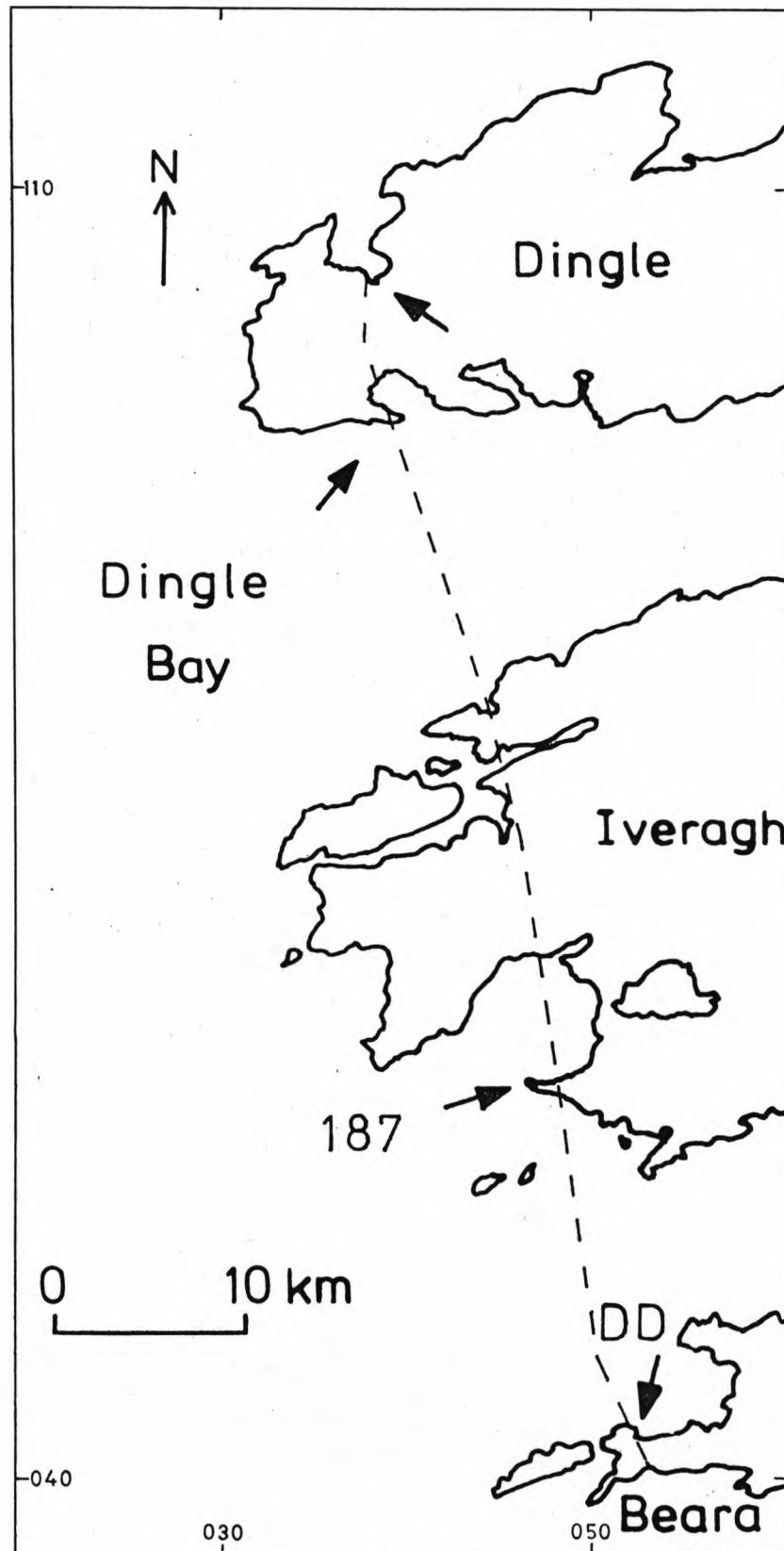


Fig. 6:2 The Kerry dyke system - known exposures, inferred line and sampling locations (adapted from Morris, 1974)

intrusions in Galway (see Section 6:2:2) to the geophysically identified Brendan igneous centre (Riddihough & Max, 1976). This hypothesised offshore Tertiary centre lies 100 km north-west of the most northerly outcrop of the Kerry dyke system.

The Tertiary age of this dyke system is apparent from the lithology, freshness and undeformed nature of its exposures, and from its palaeomagnetic characteristics: strong intensity/steep inclination/reversed direction (Morris, 1974; Horne & Macintyre, 1975). Four whole-rock K-Ar dates have been reported for the Kerry dyke system (Horne & Macintyre, 1975; Mitchell & Mohr, 1985). Horne & Macintyre (1975) produced ages of 26, 43 and 44 Ma for samples from the Dingle peninsula (see Fig. 6:2). They interpreted these ages as meaningful because of the apparent freshness of samples, and concluded that the 26 and 43 Ma ages may be related to changes in the pattern of sea-floor spreading in the NE Atlantic. Mitchell & Mohr (1985), report an age of  $39.0 \pm 1.0$  Ma for the dolerite exposed at Hog's Head on the Iveragh peninsula (Fig. 6:2). As a whole, their K-Ar study of Tertiary dykes in the west of Ireland gave ages between 63-27 Ma. Mitchell & Mohr (1985) on geological grounds, did not favour the idea that these ages represent an extended duration of magmatism. They preferred the hypothesis of a single brief episode of intrusion (55-59 Ma) with the K-Ar ages being explained by a failure of the potassium-argon system to remain closed. Mitchell (1980) briefly refers to a 17 Ma age for a dyke system in SW Ireland but quotes no reference.

In this  $^{40}\text{Ar}$ - $^{39}\text{Ar}$  stepwise degassing study of dolerites from the Kerry dyke system, three whole-rock samples have been dated. Two are from the dyke exposed on the Beara peninsula (labelled DD) and the other is from the dyke at Hog's Head on Iveragh (187) - see Fig. 6:2. The Beara dyke DD has been sampled at its fine-grained margin (DDF) and in the coarse-grained interior (DDC). All three  $^{40}\text{Ar}$ - $^{39}\text{Ar}$  analyses give age spectra that are similar in general form to spectrum No.8 of

Table 4:3. Dyke rock samples R1614, R1615 and R1620 from the Mourne granite's metamorphic aureole also produce age spectra of this shape.

The age of the dyke intrusion inferred from these  $^{40}\text{Ar}$ - $^{39}\text{Ar}$  analyses is very much greater than Horne & Macintyre (1975) suggested from their K-Ar data. The best age estimate of  $59 \pm 1$  Ma is consistent with Mitchell & Mohr's (1985) contention that dyke intrusions in the west of Ireland represent a single brief igneous episode between 55 and 59 Ma.

#### R1470 (DDF)

The age spectrum for R1470 is shown in Fig. 6:3. The age correction due to calcium interferences varies from 2 to 5 Ma over the first 85% of  $^{39}\text{K}$  release but over the remaining three steps it increases markedly. The calcium age correction for the last step is 14 Ma. Only the very lowest temperature steps, that give anomalously low ages, have a chlorine interference age correction greater than 0.05 Ma.

ICD2 data analysed did not provide any meaningful ages where a reasonable number of steps were selected e.g. see Table 6:1 for the ICD2 parameters of steps 9-14 (in this case the  $(^{40}/^{36})_0$  is significantly less than 295.5). The use of the three-dimensional isotope correlation diagrams was not helpful for data analysis. Bearing in mind the possible interpretations for this type of age spectrum (see Table 4:3 No.8), it is best to note both the intermediate temperature maximum age of 62.8 Ma and the high temperature minimum age of 58.6 Ma. The question of chronological interpretation will be returned to in the conclusions section for the Kerry dyke system.

#### R1575 (DDC)

Fig. 6:4 displays the age spectrum for R1575. The difference in age between the intermediate temperature age maximum and high temperature age minimum is more pronounced for R1575 than it was for R1470. The former has a value of  $\approx 64$  Ma and the latter a value of  $\approx 59$  Ma. The

Irradiation no. (Locality no.)	Steps	% <sup>39</sup> K	Total gas age (Ma)	Mean age (Ma) (step ages weighted by 1/variance)	Age (Ma)	ICD2 parameters (40/36) <sub>O</sub>	MSMD
R1470(DDF)	A11(1-15)	100	54.2 ± 1.3	60.7 ± 2.7	62.6 ± 1.4	285.6 ± 4.9	6.4
	9-14	35	60.3 ± 1.2	60.3 ± 1.5	62.8 ± 1.6	281.2 ± 11.4	2.7
R1575(DDC)	A11(1-29)	100	59.2 ± 0.5	61.0 ± 4.6	66.4 ± 1.5	275.5 ± 11.4	27.6
	ex 3,13						
	9-21 23-29	40 47	63.6 ± 0.6 59.6 ± 0.5	63.7 ± 1.1 59.8 ± 0.9	65.7 ± 1.2 59.5 ± 0.9	288.0 ± 10.1 296.6 ± 8.5	2.0 3.0
R1579(187 <sup>+</sup> )	A11(1-22)	100	58.7 ± 0.6	60.8 ± 2.3	62.5 ± 1.0	287.1 ± 9.2	16.7
	7-16	58	62.1 ± 0.5	62.0 ± 1.1	58.3 ± 0.9	318.0 ± 9.6	1.3
	17-22	24	57.9 ± 0.5	58.3 ± 0.8	58.8 ± 0.8	292.3 ± 7.5	1.7

+ denotes crushed sample

Table 6:1 Parameters calculated for the Kerry dyke system samples



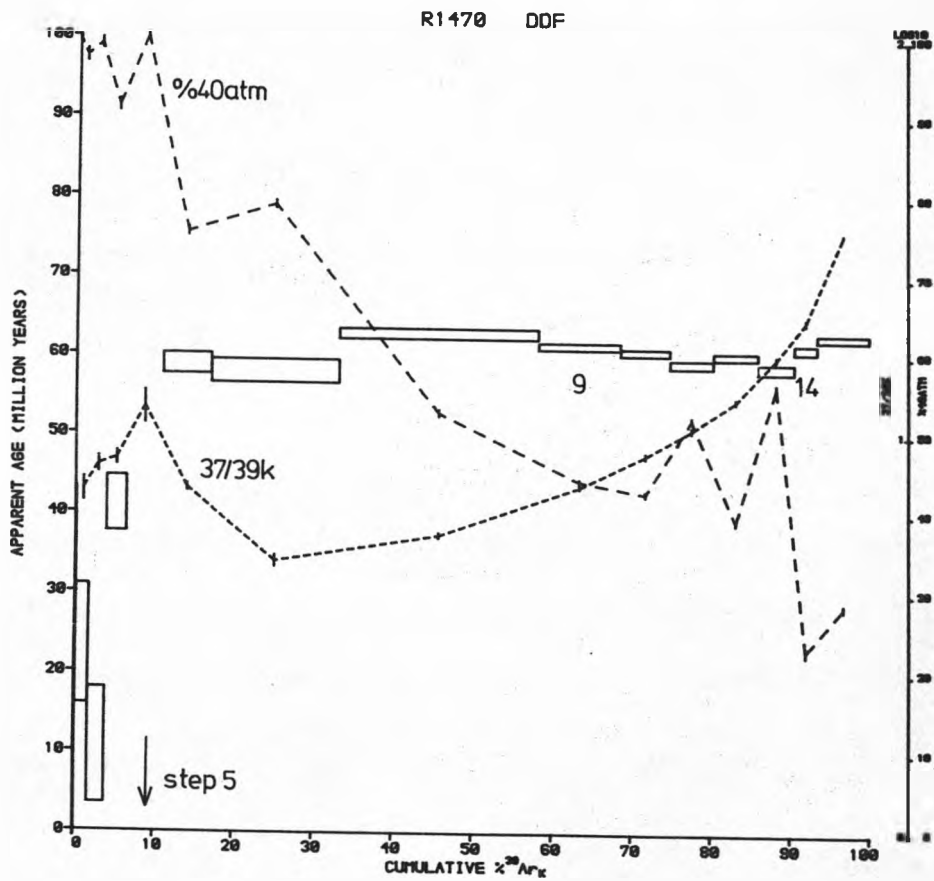


Fig. 6:3 Age spectrum for the Kerry dyke sample R1470 (DDF)

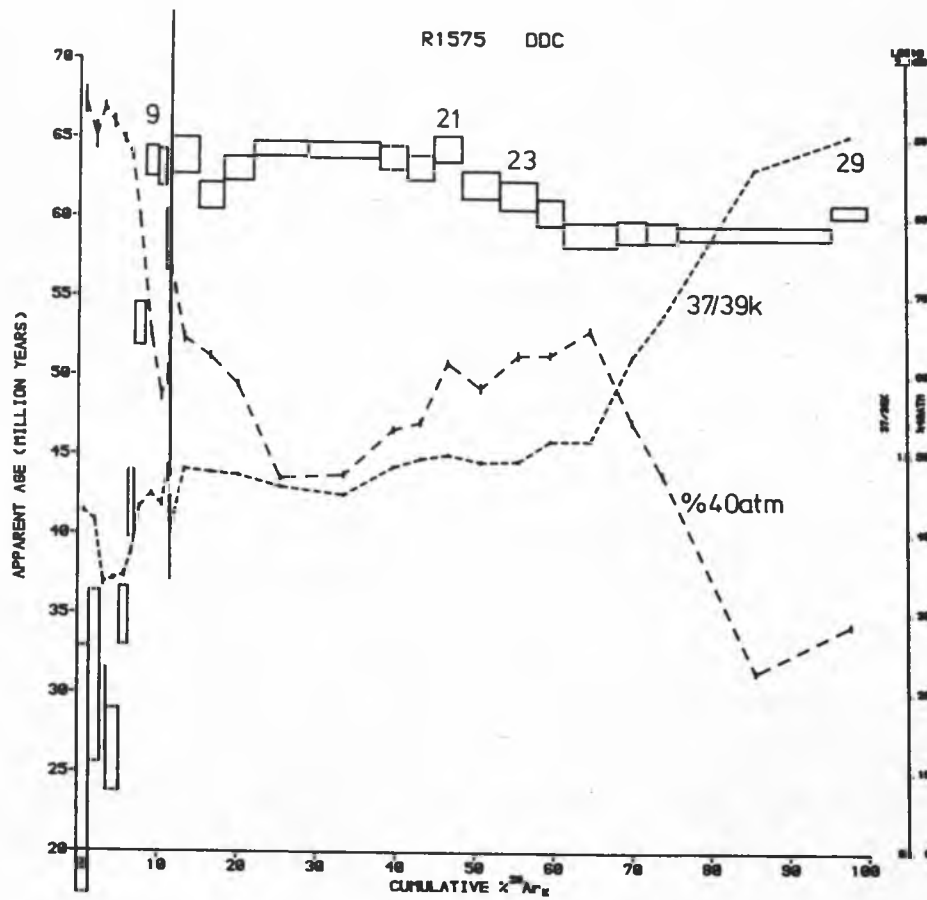


Fig. 6:4 Age spectrum for the Kerry dyke sample R1575 (DDC)

calculated calcium age corrections for R1575 show a similar pattern to those for R1470, with a marked increase only over the last four steps (the last step records the highest value of 21 Ma). The chlorine interference age correction is negligible for all steps.

Steps 9-21 and 23-29 both give apparently meaningful ICD2s (see Table 6:1), indicating ages of  $65.7 \pm 1.2$  and  $59.5 \pm 0.9$  Ma respectively. It is unlikely both ages could have real geological meaning as the highest age is given by the lowest temperature plateau. Chronological interpretation of the Kerry dyke samples as a whole will be discussed at the end of this section. It is interesting to note that when steps 23-29 are plotted on ICD3 - Plot 3 they give a better MSWD than in the corresponding ICD2. For the ICD3 an age of  $56.2 \pm 2.2$  Ma and a

$\left[ \frac{40-(40/36)_0 \cdot 36}{37} \right]_{Ca}$  value of  $-0.06383 \pm 0.00474$  are calculated with  $(40/36) \approx 295.5$ . This age is significantly less than the ICD2 age for the same steps, however it is not considered meaningful because other samples in the same batch as R1575 do not support the inferred

$\left[ \frac{40-(40/36)_0 \cdot 36}{37} \right]_{Ca}$  value.

The Arrhenius plots for R1575 do not yield any geologically meaningful information. Those for  $40^*$  and  $39_K$  release are very similar (see Fig. 6:5); thus it is not possible to make any inferences from them about possible disturbances affecting sample R1575.

#### R1579 (187)

For R1579 the intermediate temperature age maximum is  $\approx 63$  Ma and the high temperature age minimum is 57 Ma (see Fig. 6:6). The calcium and chlorine interference age corrections follow a pattern very similar to those for R1470 and R1575.

Steps 7-16 yield an ICD2 with an age similar to the high temperature age minimum and  $(40/36)_0 = 318 \pm 10$  (Table 6:1). However, this ICD2 is not considered meaningful because of the implied presence of

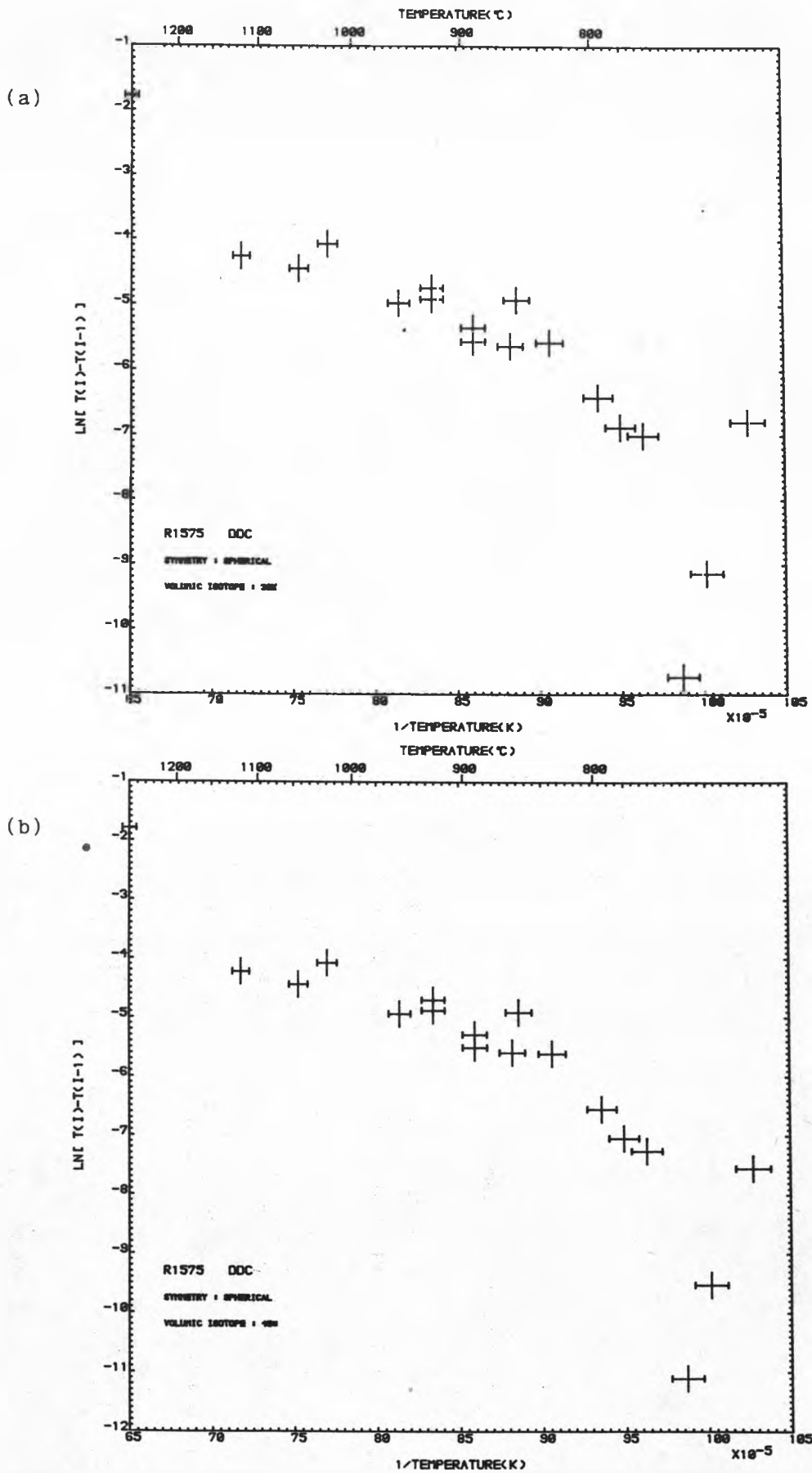


Fig. 6:5 Arrhenius diagrams for the Kerry dyke sample R1575 (DDC)  
 (a) 39K (b) 40\*

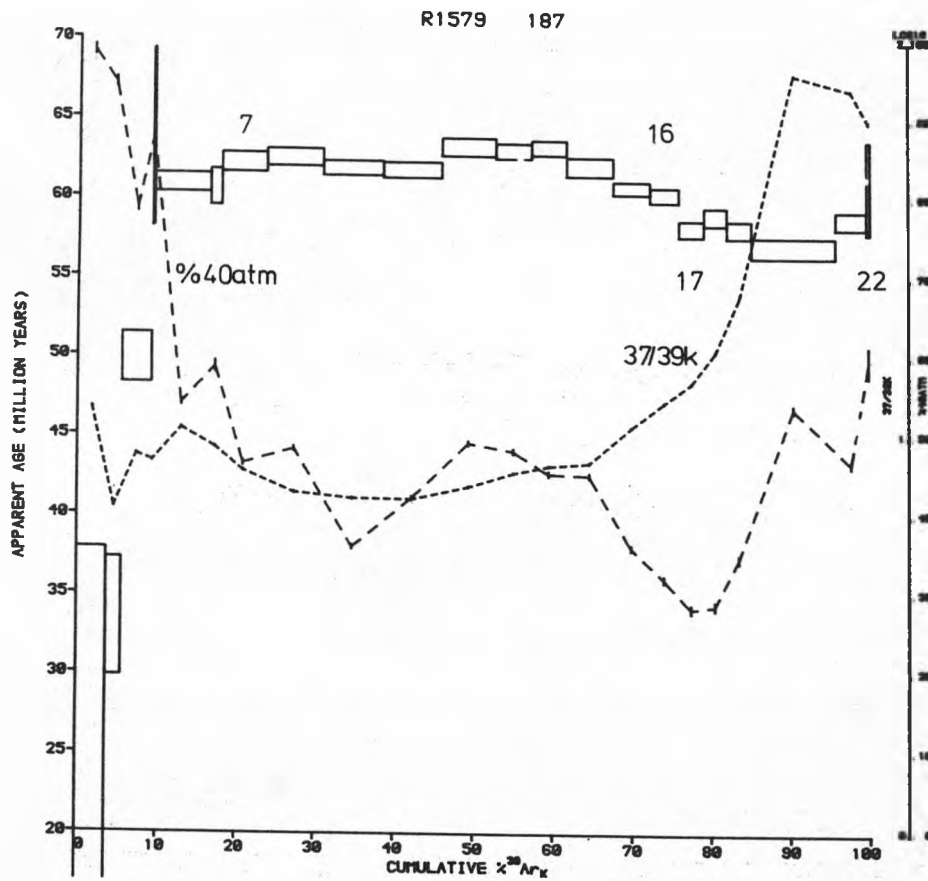


Fig. 6:6 Age spectrum for the Kerry dyke sample R1579 (187)

Sample	Intermediate temperature age maximum (Ma)	High temperature age minimum (Ma)
R1470(DDF)	62.8	58.6
R1575(DDC)	~64 Plateau ICD2: 65.7 ± 1.2	~59 Plateau ICD2: 59.5 ± 0.9
R1579(187)	~63 Plateau ICD3: 58.3 ± 0.9	57.0 Plateau ICD2: 58.8 ± 0.8

Table 6:2 Comparison of ages calculated for Kerry dyke system samples

excess argon. Mitchell & Mohr's (1985) K-Ar analysis of dyke 187, which gave an age of 39 Ma, suggested that argon loss, rather than excess, would be a problem. The correspondence between the ICD2 age and the high temperature age minimum must therefore be fortuitous.

Steps 17-22 give an apparently meaningful ICD2 (Table 6:1) indicating an age of  $58.8 \pm 0.8$  Ma. ICD3 analyses of steps 7-22 all give MSWDs less than the cut-off of 3.5 (the corresponding ICD2 gave MSWD = 16.8). However, in each case,  $(40/36)_0$  is significantly greater than the 40/36 ratio for atmospheric argon and the third ICD3 parameter is not physically acceptable. Therefore, the calculated ages are not regarded as meaningful.

#### Conclusions for the Kerry Dyke System

Table 6:2 lists the calculated age maxima and minima for Kerry dyke samples R1470, R1575, R1579. The latter are considered to give meaningful estimates for the timing of emplacement as they show very little scatter and are consistent with age estimates for other Tertiary igneous activity in the west of Ireland presented in this thesis e.g. Droimchogaidh sill (Section 6:2:3), Killala Bay (Section 6:2:5). The age of emplacement of the Kerry dyke system is taken to be  $59 \pm 1$  Ma. An age of 59 Ma is considerably greater than the K-Ar dates reported by Horne & Macintyre (1975) and Mitchell & Mohr (1985). However, it is in agreement with the hypothesis preferred by Mitchell & Mohr (1985) that Tertiary igneous activity in the west of Ireland occurred during a single brief episode between 55 and 59 Ma. In the Kerry dyke rocks, the potassium-argon system is subject to a high degree of radiogenic argon loss as witnessed by the K-Ar dates. This radiogenic argon loss is probably due to leakage from poorly retentive products of a deuteric alteration (there is no geological evidence for an argon loss event as such). An important point to note is that the  $^{40}\text{Ar}-^{39}\text{Ar}$  total gas ages of R1470, R1575 and R1579 ( $54.2 \pm 1.3$ ,  $59.2 \pm 0.5$  and  $58.7 \pm 0.6$  Ma

respectively) are very much greater than the reported K-Ar dates. In fact, in two cases, they approximately equal the accepted age of emplacement and thus are not apparently subject to radiogenic argon loss. It is thought that this correspondence in age is fortuitous due to the combined effects of radiogenic argon loss and  $^{39}\text{K}$  recoil loss. Such an interpretation is consistent with the age spectrum shape (see Table 4:3) and with the preponderance of fine-grained alteration in the Kerry dyke system samples (see thin section descriptions in Appendix 7). The slight increase in age observed at very high temperatures for the Kerry dyke samples probably reflects a conversion of sites from low to high retentivity induced by the irradiation (see also the conclusions for the Mourne Swarm dykes - Section 6:2:8). However, it is perhaps feasible that this increase in age may be due to the  $^{36}\text{Ca}$  recoil effect hypothesised in Appendix 3.

#### 6:2:2 The Intrusive Systems of West-Central Ireland

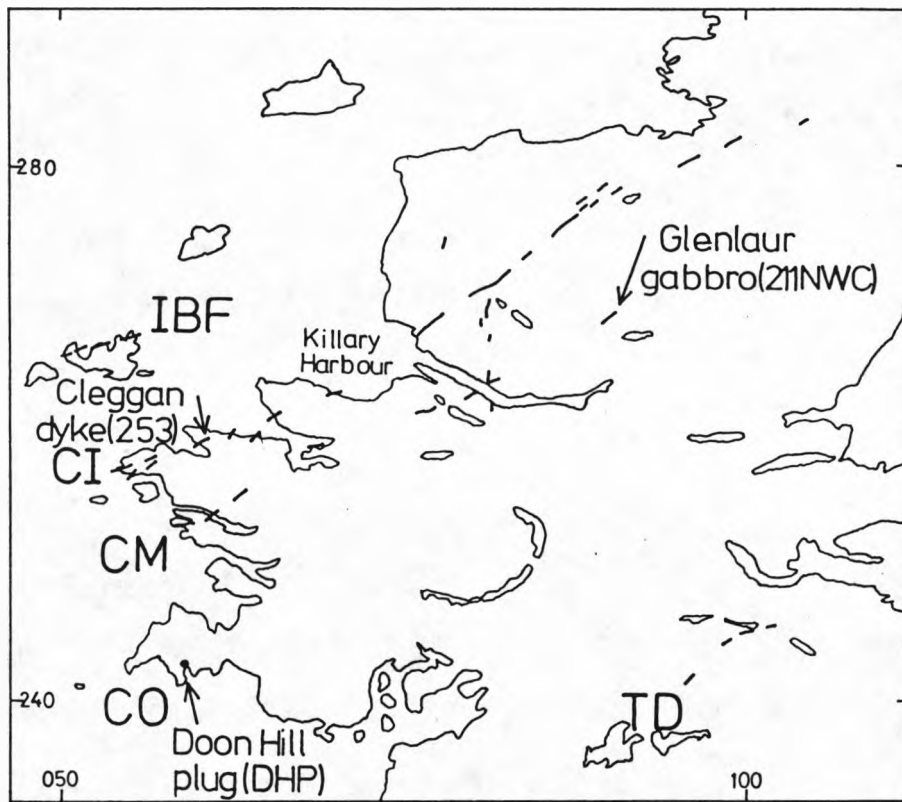
Three bodies from Mohr's (1982) series of linear intrusive systems in west-central Ireland have been dated in this study (see Fig. 6:7 for locations). These systems trend in a NE-SW direction which is perpendicular to the direction commonly associated with Tertiary dyke swarms in the British Isles.

##### a) The Doon Hill Plug

Intruding Dalradian migmatites, this gabbroic plug lies along the line of Mohr's (1982) CO dyke system. The 60 m high Doon Hill is found 15 km south-west of Clifden on the County Galway coast (see Fig. 6:7).

Two K-Ar whole-rock analyses have been reported for the Doon Hill plug. Macintyre et al., (1975) calculated an age of 61.5 Ma and they considered that this was a reliable estimate for the timing of emplacement because of the freshness of their rock sample. Mitchell & Mohr (1985) report an age of  $68.5 \pm 0.7$  Ma and they suggest that this reflects an excess argon contamination probably derived from the plug's





**Fig. 6:7** The intrusive systems of west-central Ireland: sampling locations (adapted from Mohr, 1982)

metamorphic aureole.

In this study a whole-rock sample collected from the southern margin of the plug has been dated. The best age estimate for this sample is consistent with Macintyre et al.'s (1975) contention that the Doon Hill plug was intruded  $\approx$  61.5 Ma ago.

#### R1576 (DHP)

The age spectrum of R1576 (Fig. 6:8) shows a very pronounced pattern of decreasing age. The first step gives an age of 368 Ma, whilst the last gives 59 Ma. Regardless of the physical interpretation of this age pattern, the high temperature ages will probably give a maximum estimate for the age of emplacement (see below). The calcium interference age correction is less than 3 Ma for all but the last three steps. For these, the age corrections are 6, 24 and 25 Ma respectively. The chlorine age correction reaches 0.3 Ma over the early part of the gas release but on the whole it is insignificant.

ICD2 analysis of steps 23-28, which form a high temperature plateau, does not give a meaningful age because the  $(40/36)_o$  value is significantly less than 295.5. (Table 6:3). Nevertheless, the best estimate of the timing of plug intrusion is probably given by the mean total gas age for these steps. Because of the shape of the age spectrum this age of  $62.3 \pm 0.7$  Ma is regarded as a maximum estimate. None of ICD3 data analysis techniques were found to be helpful.

The total gas age of  $94.9 \pm 0.8$  Ma is much greater than the K-Ar dates reported by Macintyre et al., (1975) and Mitchell & Mohr (1985). This suggests that  $^{39}K$  recoil loss is important for R1576 and the latter conjecture is consistent with the observed age spectrum shape and the occurrence of significant amounts of fine-grained alteration in the geological thin-section (see Appendix 7). The possibility of excess argon discussed by Mitchell & Mohr (1985) could have a similar effect

Irradiation no. (Locality no.)	Steps	% <sup>39</sup> K	Total gas age (Ma)	Mean age (Ma) (step ages weighted by 1/variance)	Age (Ma)	ICD2 parameters (40/36) <sub>0</sub>	MSWD
R1576(DHP)	All(1-28) 23-28	100	94.9 ± 0.8	70.5 ± 16.7	67.0 ± 3.9	383.4 ± 49.3	972.3
		15	62.2 ± 0.6	62.4 ± 0.7	63.0 ± 0.6	285.9 ± 2.5	0.4
R1384(253)	All(1-10, ex 8,9) 6,7,10	100	50.1 ± 4.1	60.4 ± 22.8	81.7 ± 11.9	269.0 ± 64.0	15.9
		69	60.5 ± 2.9	60.3 ± 1.4	59.9 ± 2.4	296.6 ± 19.1	0.2
R1504(253)	All(1-34) 20-27	100	47.4 ± 1.1	58.0 ± 3.1	59.8 ± 0.9	285.0 ± 7.4	14.6
		18	57.9 ± 0.6	57.8 ± 0.9	57.3 ± 0.8	298.1 ± 5.6	0.9
R1610(211MNC <sup>+</sup> )	All(1-21) 9-17 6-10	100	66.1 ± 2.1	64.0 ± 4.0	61.3 ± 2.0	326.6 ± 6.6	9.7
		63	62.9 ± 2.0	62.9 ± 2.2	63.5 ± 2.6	285.4 ± 34.0	8.4
		30	64.1 ± 2.1	64.3 ± 2.5	59.4 ± 2.2	339.3 ± 16.7	1.6

+ denotes crushed sample

Table 6:3 Parameters calculated for samples from the intrusive systems of west-central Ireland

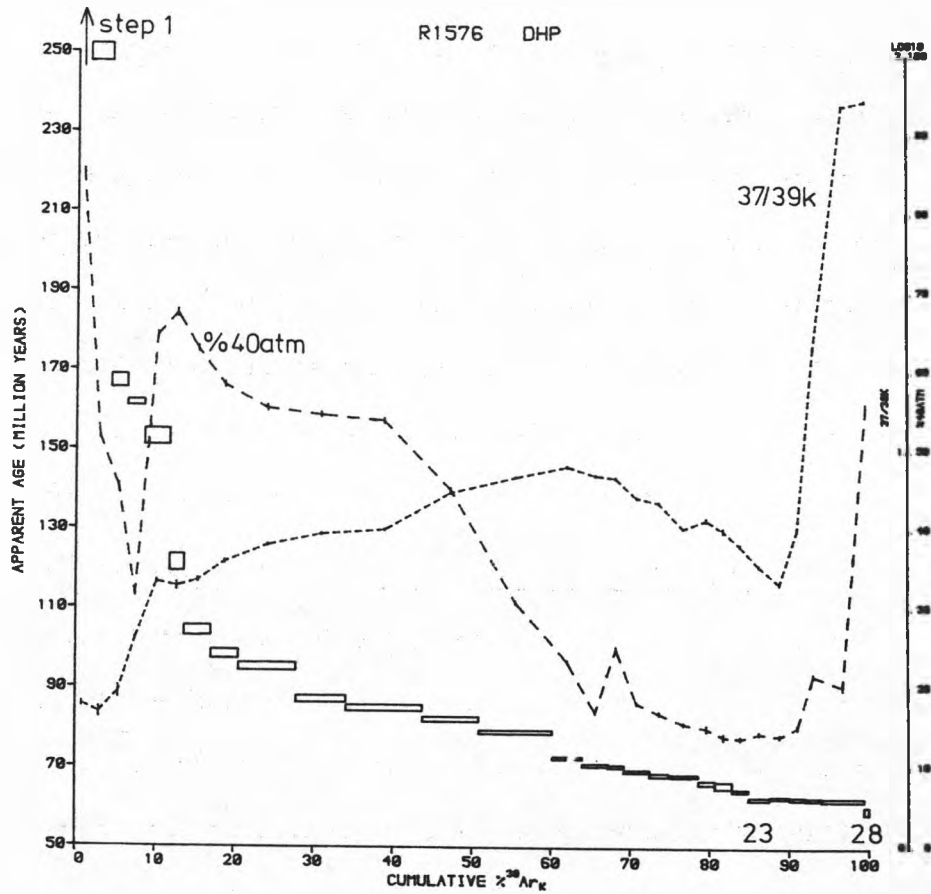


Fig. 6:8 Age spectrum for the Doon Hill plug sample R1576 (DHP)

to  $^{39}\text{K}$  recoil loss on the age spectrum shape (see Table 4:3).

No geologically meaningful linear correlations are observed in the Arrhenius diagrams for R1576. The  $^{40}\text{Ar}$  and  $^{39}\text{K}$  diagrams are very similar, even though the age spectrum is greatly disturbed (presumed to be largely the result of  $^{39}\text{K}$  recoil loss).

#### Conclusions for the Doon Hill Plug

The best estimate for the timing of plug intrusion from the data of sample R1576 is  $62.3 \pm 0.7$  Ma. Because of the shape of the age spectrum, this age is regarded as a maximum estimate. This interpretation is consistent with Macintyre et al.'s (1975) conclusion that the Doon Hill plug was intruded approximately 61.5 Ma ago.

#### b) The Cleggan Dyke

Part of Mohr's (1982) NE trending CI system, the Cleggan dyke is found on the Connemara coast, near Cleggan, (Fig.6:7). It has a dolerite composition and intrudes Dalradian quartzites. The Cleggan dyke is 8 m in width.

Mitchell & Mohr (1985) report a whole-rock potassium-argon date for the Cleggan dyke of  $42.0 \pm 0.6$  Ma. They suggest that their western Connacht samples, as a whole, are subject to varying degrees of argon loss, and that the age of emplacement probably lies between 55 and 59 Ma.

Two samples of the dyke-rock have been dated in this study.

#### R1384 (253)

This is a pilot sample from which only eight steps were recovered. Three of the steps give negative ages and the last three steps (6,7, 10) form a plateau which constitutes  $\approx 70\%$  of the  $^{39}\text{K}$  release (see Fig. 6:9). The age correction due to calcium interferences is  $\approx 1$  Ma, except in the case of the last step for which it is 8 Ma.

ICD2 analysis of steps 6,7 and 10 yields an apparently meaningful age

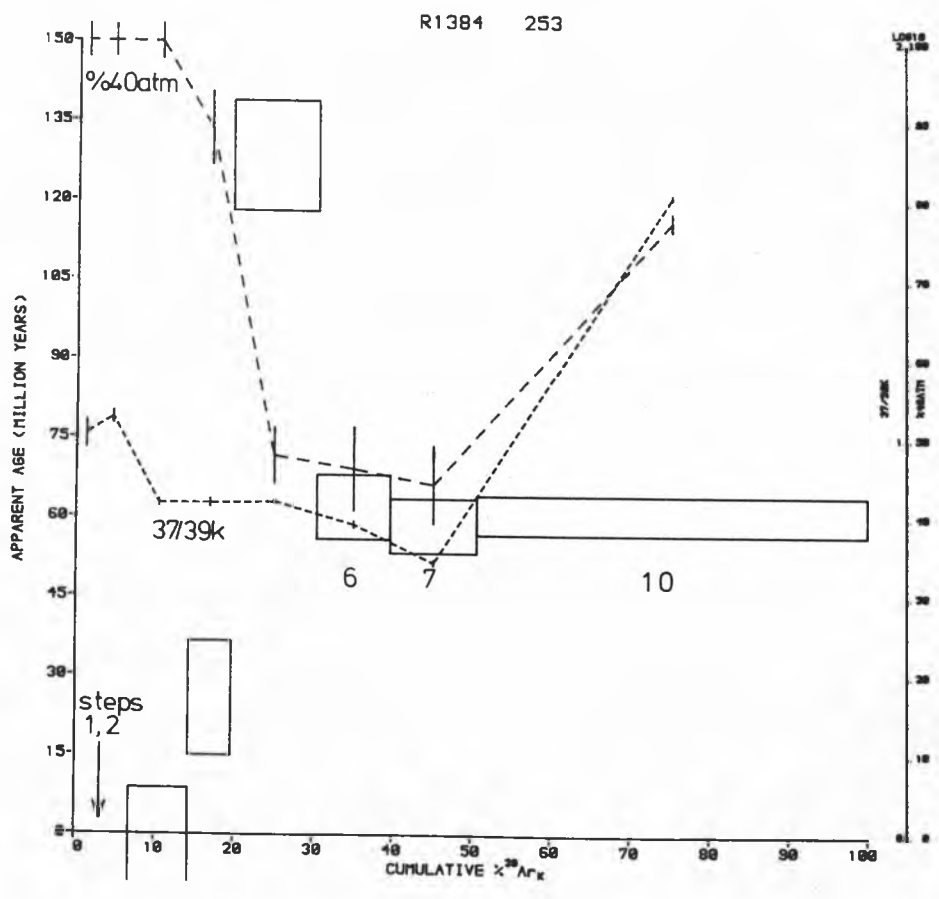


Fig. 6:9 Age spectrum for the Cleggan dyke sample R1384 (253)

of  $59.9 \pm 2.4$  Ma (Table 6:3). However, because of the small number of steps involved and as step 10 constitutes  $\approx 50\%$  of the gas release, the assigned age must be viewed cautiously.

The negative ages calculated for the first three steps apparently reflect some sort of fractionation effect or the presence of a mass spectrometer background at  $m/e = 36$ .

#### R1504 (253)

Fig. 6:10 shows that the age spectrum of sample R1504 is complicated, with very high levels of  $^{39}\text{K}$  release for the first three steps. The total gas age of  $47.4 \pm 1.1$  Ma is similar to Mitchell & Mohr's (1985) K-Ar date. The calcium interference age correction is between 1 and 3 Ma for steps 1-22, but is typically  $\approx 10$  Ma for the remaining 12 steps. The chlorine age correction is negligible for all steps.

ICD2 analysis of the last seven steps to contain significant amounts of the total  $^{39}\text{K}$  release (20-27) gives a MSWD less than the cut-off,  $(40/36)_o \approx (40/36)_{\text{atmospheric}}$ , and an age of  $57.3 \pm 0.8$  Ma (see Table 6:3). However, this age must only be considered as a tentative estimate for the timing of intrusion because steps 20-27 contain only 18% of the total  $^{39}\text{K}$  release.

The discordancy of the age spectrum is probably the result of the combined effects of radiogenic argon loss (low total gas age),  $^{39}\text{K}$  recoil loss (high levels of  $^{39}\text{K}$  release at low temperatures) and  $^{39}\text{K}$  recoil re-distribution (anomalously low ages for steps 15-17).

#### Conclusions for the Cleggan Dyke

R1384 and R1504 both give rather tentative estimates of the emplacement age for the dyke at Cleggan. It was probably intruded about between 57 and 60 Ma ago.

#### c) The Glenlaur Gabbro

This 100m wide body is part of Mohr's (1983) NE trending CM Tertiary

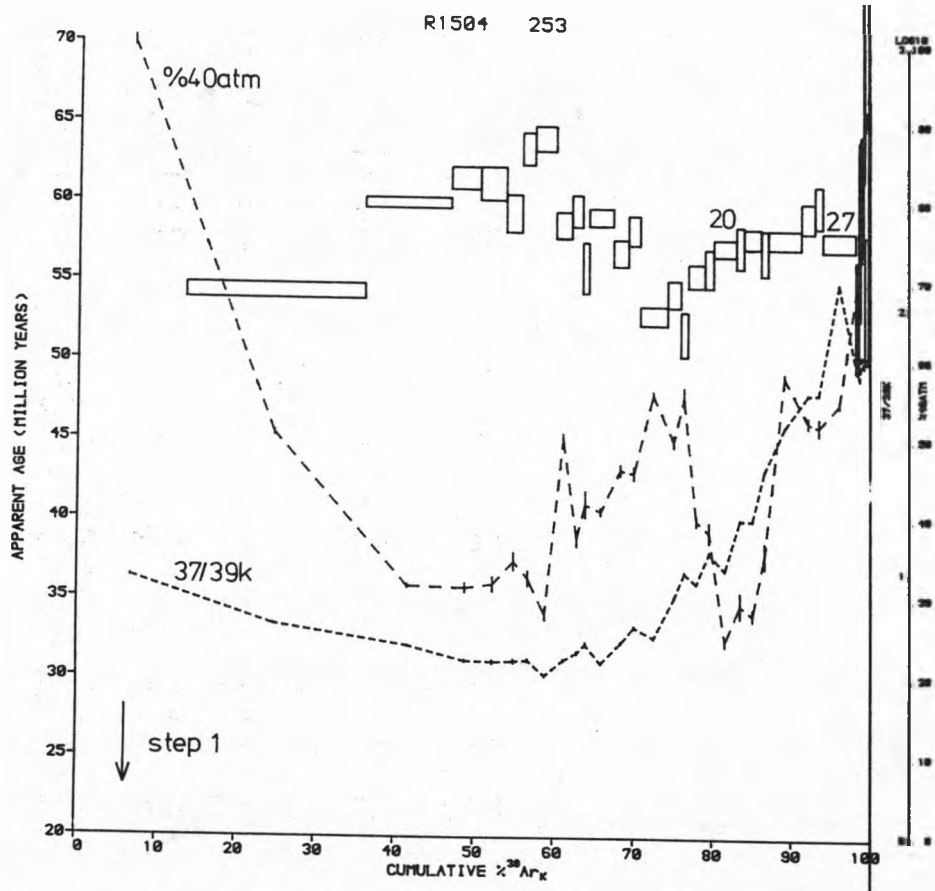


Fig. 6:10 Age spectrum for the Cleggan dyke sample R1504 (253)



intrusive system. The Glenlaur gabbro lies slightly to the north-west of Lough Tawnyard in Connacht and about 20 km from Ireland's west coast (see Fig. 6:7). A single crushed whole-rock sample has been analysed in this dating study.

#### R1610 (211NWC)

The age spectrum of R1610 (Fig. 6:11) displays the saddle-shaped form, which is thought to be diagnostic of excess argon (see Table 4:3). The saddle minimum, which constitutes more than 50% of the  $^{39}\text{K}$  release, has an age of approximately 63 Ma. The %  $^{40}\text{Ar}_{\text{atmospheric}}$  curve also defines a saddle shape and the  $^{37}/^{39}\text{K}$  curve possesses two peaks, probably corresponding to plagioclase feldspar and pyroxene outgassing (see Killala Gabbro mineral separate samples R1571 and R1621). The age correction due to calcium interference is less than 5 Ma for all but the last four steps. These steps constitute the high age part of the high temperature release and their associated calcium age correction is as high as 30 Ma. The age correction due to chlorine interference is insignificant.

ICD2 analysis of the steps forming the saddle minimum (9-17) does not give an MSWD below the 3.5 cut-off (see Table 6:3). Only where small numbers of steps are selected is the MSWD calculated to be below the required level e.g. steps 6-10 - see Table 6:3. However, for these ICD2s the  $(^{40}/^{36})_0$  values are significantly greater than the atmospheric ratio. Thus, the calculated ages (which lie between 58 - 59 Ma) are not considered meaningful. Although ICD2 data analysis does not produce a conclusive age, it does indicate that excess argon is probably important over the whole gas release. Thus, the saddle minimum age of  $62.9 \pm 2.1$  Ma (steps 9-17 total gas/mean age - see Table 6:3) must be interpreted simply as a maximum estimate for the timing of the intrusion. The physical interpretation of saddle-shaped age spectra is discussed in the Killala Bay section (6:2:5). ICD3 data

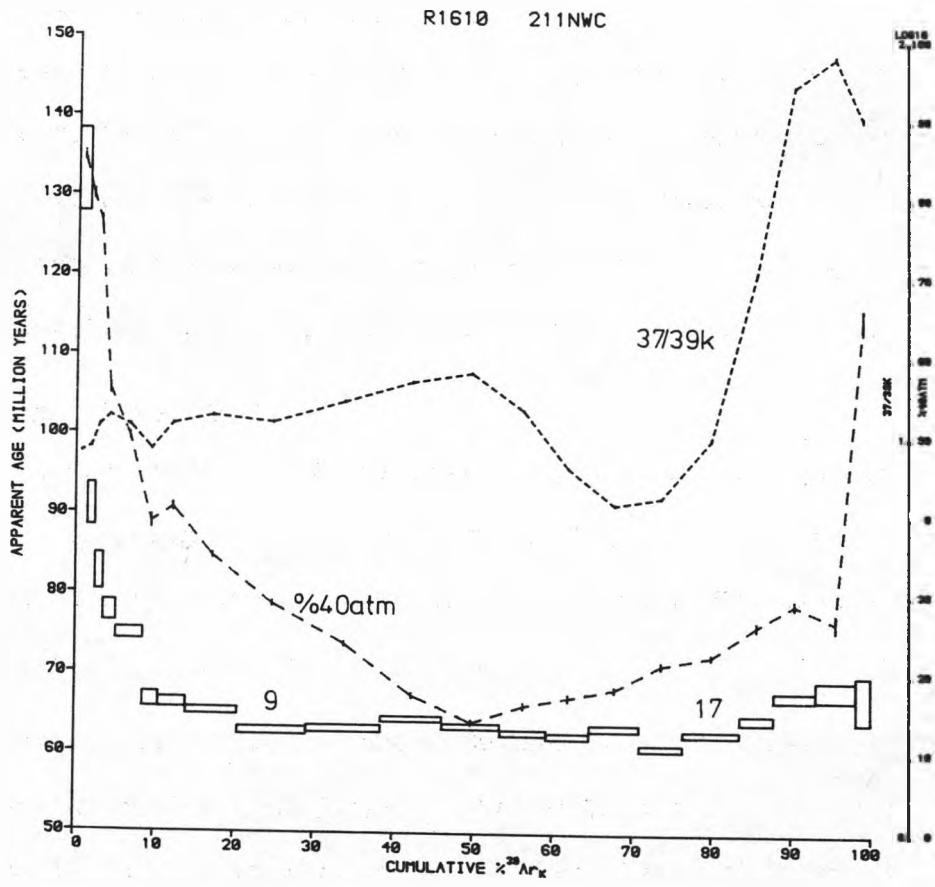


Fig. 6:11 Age spectrum for the Glenlaur gabbro sample R1610 (211NWC)

analysis was not helpful for the chronological interpretation, even though there was some evidence for an apparent age -  $37/39_K$  correlation.

Of the Arrhenius's diagrams, only the one for 37 release gives linear correlations which may have some physical meaning (see Fig. 6:16). For steps 9-12  $E = 26 \text{ kcal mol}^{-1}$ ,  $D_0/a^2 = 0.11 \text{ s}^{-1}$ ,  $\text{MSWD} = 0.1$  and  $T_c = 220^\circ\text{C}$  (assumed cooling rate of  $10^4 \text{ }^\circ\text{C Ma}^{-1}$ ). These steps correspond to the rising edge of the intermediate temperature  $37/39_K$  peak, which is thought to be associated with plagioclase outgassing. The inferred closure temperature is compatible with published values for plagioclase (see Table 4:1). For steps 17-20, the calculated parameters are  $E = 108 \text{ kcal mol}^{-1}$ ,  $D_0/a^2 = 1.1 \times 10^{11} \text{ s}^{-1}$ ,  $\text{MSWD} = 1.3$  and  $T_c = 730^\circ\text{C}$ . Steps 17-20, which are marked by the high temperature increase in  $37/39_K$ , are thought to represent pyroxene outgassing.

#### Conclusions for the Glenlaur Gabbro

The best estimate for the timing of gabbro intrusion is  $62.9 \pm 2.1 \text{ Ma}$ . This must be treated as a maximum age estimate, as the age spectrum shape of R1610 implies the presence of excess argon.

#### Conclusions for the Intrusive Systems of West-Central Ireland

A summary of the best age estimates for the Doon Hill, Cleggan and Glenlaur samples is presented in Table 6:4. Unfortunately, all the samples yielded severely disturbed age spectra, thus it was only possible to make rather tentative age estimates. These ages range from 57- 63 Ma. Mohr (1982) suggested that the intrusive systems of west-central Ireland, together with the Kerry dyke system, may be related to the offshore Brendan centre (Riddihough & Max, 1976). The best age estimate of  $59 \pm 1 \text{ Ma}$  for the Kerry dyke system (see Section 6:2:1) lies within the range of age estimates for the samples dated in this section. A 59.Ma date of intrusion is probably applicable also to the intrusive

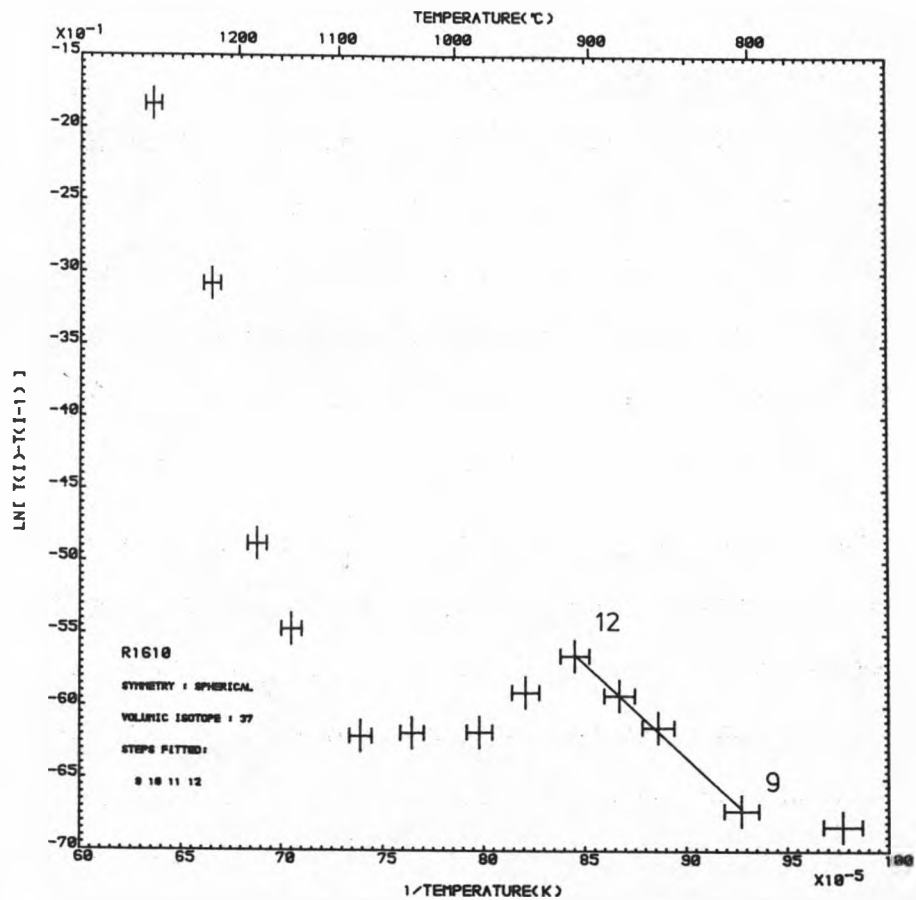


Fig. 6:12 Arrhenius diagram for the 37 release of Glenlair gabbro sample R1610 (211NWC)

Intrusive body	Sample	System (Mohr, 1982)	Best age estimate (Ma)
Doon Hill plug	R1576(DHP)	CO	< 62.3 ± 0.7
Cleggan dyke	R1384(253) R1504(253)	CI	between 57 and 60 ?
Glenlaur gabbro	R1610(211NWC)	CM	< 62.9 ± 2.1

Table 6:4 Summary of best age estimates for the samples from the west-central Ireland intrusive systems

systems of west-central Ireland.

### 6:2:3 The Droimchogaidh Sill

The Droimchogaidh sill, which lies to the north-west of Lough Mask (see Fig. 6:1) has been studied in detail by Mohr et al., (1984).

This sill has a maximum thickness of about 100 m and its arcuate outcrop is over 4 km long. The predominant rock type is an olivine gabbro; however, there are also syenitic differentiates and a basal picritic cumulate. A presumed satellite sill, found slightly to the north of the main sill, consists of olivine dolerite and is 3-4m thick. This has been named by Mohr et al., (1984) the Bohaun-Srah sill.

Mohr et al., (1984) presented two  $^{40}\text{Ar}$ - $^{39}\text{Ar}$  stepwise degassing analyses of a potassic syenite. They concluded that the sill was intruded  $55 \pm 1$  Ma ago. I have re-assessed the  $^{40}\text{Ar}$ - $^{39}\text{Ar}$  data which was produced by the Liverpool laboratory, using improved data analysis techniques and a revised value for the standard age. In addition to the re-worked data, new  $^{40}\text{Ar}$ - $^{39}\text{Ar}$  analyses for the syenite, olivine gabbro, picrite and for the satellite sill dolerite are also presented in this thesis. This work shows that Mohr et al.'s (1984) 55 Ma date is too young and that the age of Droimchogaidh sill is constrained to lie between 58 and 61 Ma.

#### a) The Potassic Syenite (238P)

Samples R1381 and R1473 are those presented by Mohr et al., (1984).

R1612 is a new  $^{40}\text{Ar}$ - $^{39}\text{Ar}$  analysis.

#### R1381

The age spectrum for this sample (Fig. 6:13a) shows that for the majority of the steps, the level of radiogenic  $^{40}\text{Ar}$  is greater than 90% ( $\%^{40}\text{Ar}^* = 100 - \%^{40}\text{Ar}_{\text{atm}}$ ). Lower values corresponding to the low age intermediate temperature steps are explained by the exposure of the sample and crucible to the atmosphere. This dip in the age pattern is

related to a breakdown of the mass spectrometer system. Calcium-derived argon was only recorded for a single step. However, the age correction that this induced was only 0.02 Ma so calcium-derived argon is effectively insignificant.

The shape of the age spectrum for R1381 suggests that this sample has suffered  $^{40}\text{Ar}$  loss (see Section 4:5). The pattern of ages is, in fact, very similar to the volume diffusion model for identical spheres assuming a total  $^{40}\text{Ar}$  loss of  $\approx 5\%$  (Turner, 1968; Huneke, 1976). This model predicts that the high temperature plateau age should approximately equal the emplacement age because argon loss is only slight.

The mean, total gas and ICD2 ages for the plateau steps are consistent (Table 6:5) indicating an age of  $55.3 \pm 0.5$  Ma. As the plateau steps represent  $> 50\%$  of the  $^{39}\text{K}$  released, the ICD2  $(^{40}/^{36})_0 \approx (^{40}/^{36})_{\text{atm}}$  and the ICD2 MSWD is significantly less than the adopted cut-off of 3.5, then all the criteria for a statistically meaningful age are fulfilled. From the ICD2 analysis of data points, two points are worthy of note:

- i) In the ICD2 for the plateau steps (Fig. 6:13b), step 20 exerts a strong influence over the data point linear correlation because of its relatively high level of atmospheric  $^{40}\text{Ar}$ . However, as the omission of step 20 from the ICD2 analysis does not significantly alter the calculated parameters, this effect is not important.
- ii) The ICD2 for all the steps gives an age approximately equal to the plateau age, a  $(^{40}/^{36})_0$  slightly less than the atmospheric  $^{40}/^{36}$  ratio, and a poor MSWD. This is consistent with the observations made by Lanphere & Dalrymple (1978) and Ozima et al., (1979) for samples suffering from  $^{40}\text{Ar}$  loss.

Continuing with the simple volume diffusion interpretation, one would expect the initial steps to date the timing of the argon loss event - 45 Ma (step 1 is ignored because of its large associated error).

Irradiation no. (Locality no.)	Steps	% <sup>39</sup> K	Total gas age (Ma)	Mean age (Ma) (step ages weighted by 1/variance)	Age (Ma)	ICD2 parameters (40/36) <sub>0</sub>	MSWD
R1381(238P)	A11(1-23, ex <sub>4</sub> ) 15-23	100	53.9 ± 0.5	54.8 ± 1.5	55.2 ± 0.6	271.6 ± 16.4	15.7
		56	55.2 ± 0.4	55.2 ± 0.5	55.3 ± 0.5	288.9 ± 7.1	1.1
R1473(238P)	A11(1-15) 3-15	100	55.9 ± 1.1	55.4 ± 2.2	57.3 ± 1.1	212.7 ± 11.4	4.2
		95	56.3 ± 1.1	55.5 ± 1.9	58.0 ± 1.2	184.0 ± 15.7	3.1
R1612(238P)	A11(1-27) 21-27	100	55.3 ± 1.1	54.5 ± 2.6	55.5 ± 1.2	256.2 ± 11.7	67.3
		48	57.3 ± 1.1	57.1 ± 1.2	57.9 ± 1.2	233.8 ± 32.8	3.4

Table 6:5 Parameters calculated for the Droimchogaidh sill potassic syenite sample 238P



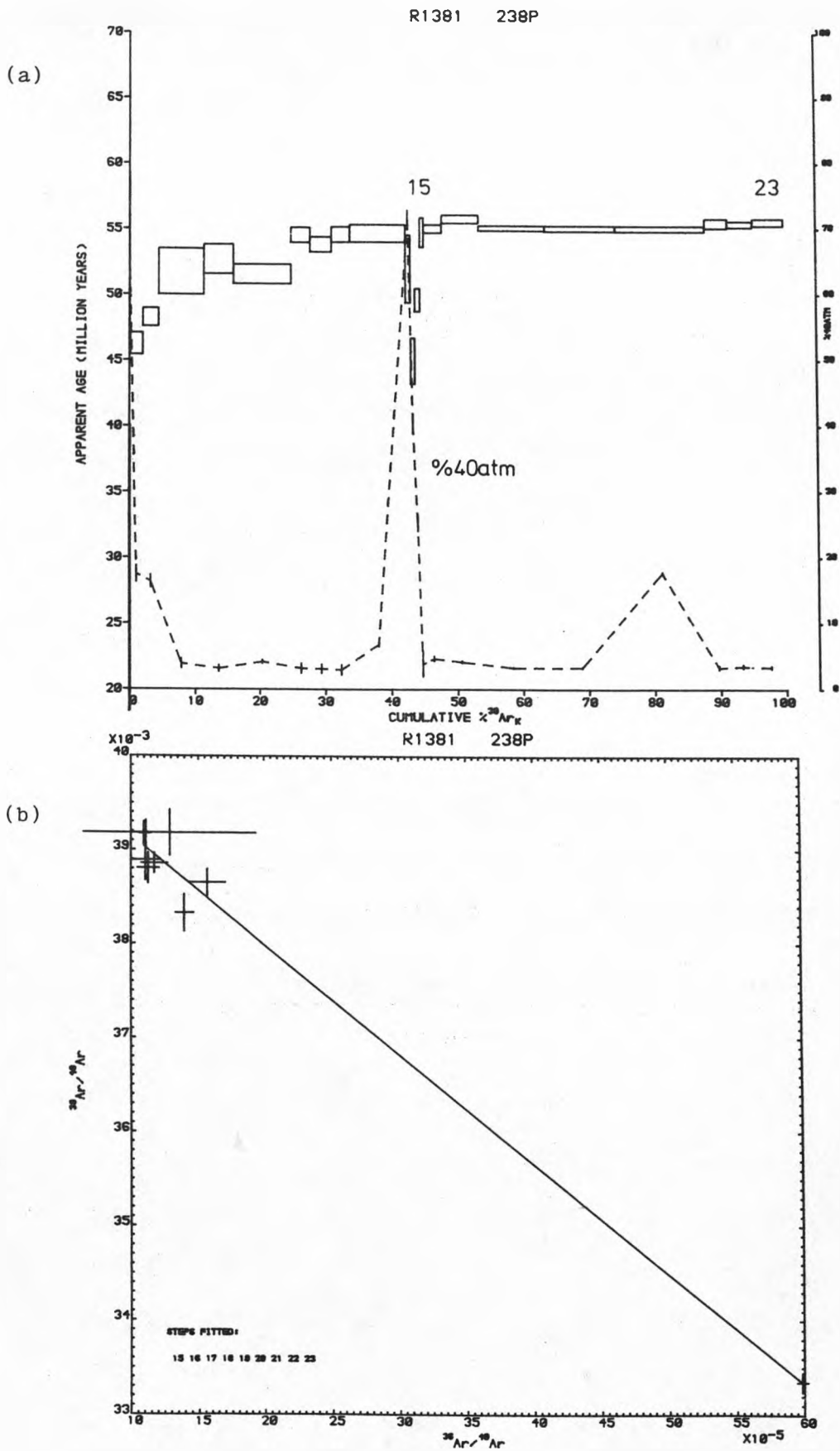


Fig. 6:13 Age spectrum (a) and ICD2 steps 15-23 (b) for the Droimchogaidh sill sample R1381 (238P)

R1473

The age spectrum plot of this sample (Fig. 6:14) differs from that of R1381 in two ways. Firstly there is no well-developed high temperature plateau. Instead the steps gradually increase in age over most of the gas release, and the last step is marked by an age decrease. Secondly,  $^{37}\text{Ar}$  is recorded for the majority of the steps. Even so, the age correction due to calcium-derived isotopes in all cases is  $< 0.1$  Ma and thus insignificant.

Steps 3-15 give an ICD2 with an MSWD of 3.1 but a  $(40/36)_0$  very much less than the atmospheric  $40/36$  ratio, thus, in keeping with the criteria outlined in Section 3:5, the ICD2 age is not accepted as meaningful. The low value of  $(40/36)_0$  probably indicates that argon loss is an important feature of steps 3-15. ICD2 analysis of steps 10-15 gives similar results (see Table 6:5).

The trend for steps 1-14 is of increasing age. However, step 15 (the last step) is marked by an age decrease and this corresponds to a notable increase in  $^{37}/^{39}\text{K}$  (see Fig. 6:14). Possible explanations for a high temperature age decrease are outlined in Table 4:3 and the most reasonable alternative in this case is a  $^{39}\text{K}$  recoil re-distribution. This interpretation is justified by the coincidence of the age decrease with an increase in  $^{37}/^{39}\text{K}$ . The latter undoubtedly indicates that the calcium-rich pyroxene within the sample is outgassing (see Appendix 7 for this section description). The scanning electron microscope work (Appendix 6) clearly shows that pyroxene grains are surrounded by potassium-rich feldspar, thus a significant re-location of feldspar-derived  $^{39}\text{K}$  into the rims of the pyroxene is not unreasonable.

Regardless of the physical interpretation of this high-temperature age decrease, the implication for geochronological interpretation is still

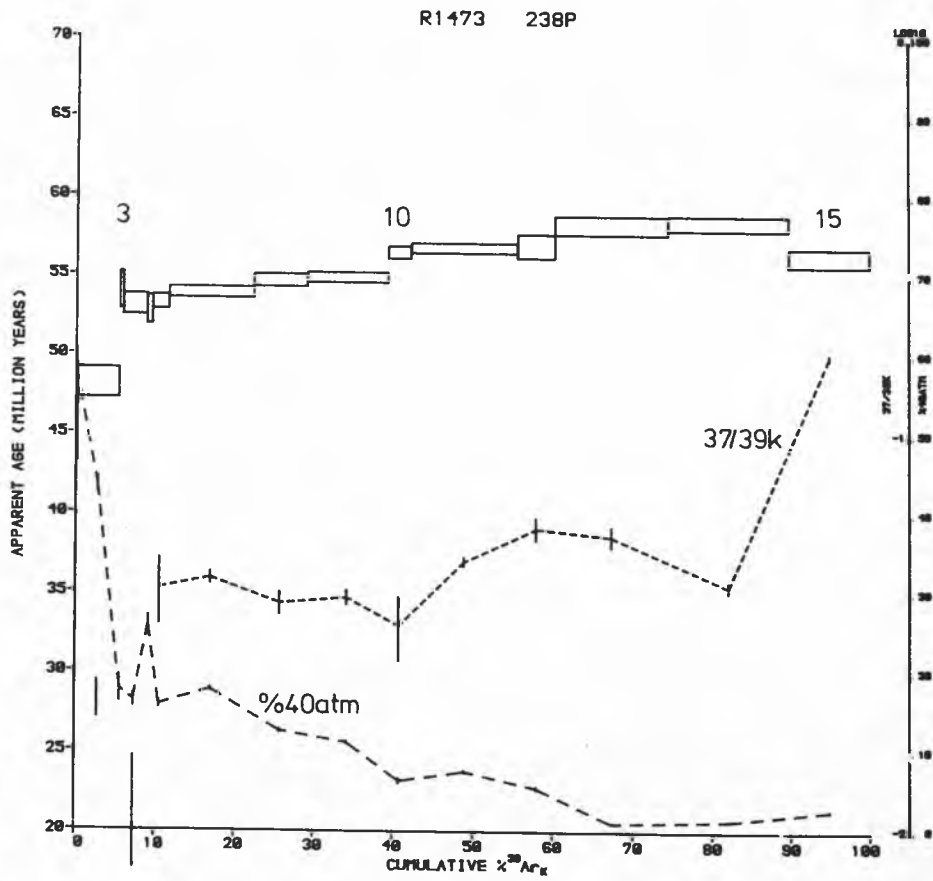


Fig. 6:14 Age spectrum for the Droimchogaidh sill sample R1473 (238P)

the same i.e. the "plateau" age may be a slightly enhanced value. However, for this sample there is no well-formed plateau, presumably because of a high level of  $^{40}\text{Ar}$  loss. The effect of argon loss is to make all ages too young and this is thought to be the more dominant influence on the plateau as the decrease in age for the last step is small. Therefore, the step giving the highest age of  $58.5 \pm 0.5$  Ma is considered to give a minimum estimate of the emplacement age.

The pattern of ages produced by R1473 suggests that argon loss is more important here than for R1381. However, this is not supported by a comparison of the respective best estimates for the emplacement age (58.5 and 55.3 Ma respectively). The lowest temperature step for R1473 gives an age of 46 Ma, which is similar to that observed for R1381.

#### R1612

In an attempt to resolve the discrepancies between analyses R1381 and R1473, a third analysis of sample 238P was undertaken as part of this work. To obtain a greater definition of the age trends, R1612 was out-gassed over a particularly large number of steps in comparison to R1381 and R1473.

The age spectrum for R1612 (Fig. 6:15) is similar in shape to that produced by R1473. The high temperature age decrease is observed for the last three steps and, again, this feature corresponds to high  $^{37}/^{39}\text{K}$  levels. R1612 gives the highest recorded  $^{37}/^{39}\text{K}$  values of all the 238P samples and the age correction due to calcium interferences is as high as 0.2 Ma. The lowest temperature step for R1612 gives an age of 39 Ma.

The last seven steps give an ICD2 with an acceptable MSWD value but a  $(^{40}/^{36})_0$  value less than  $(^{40}/^{36})_{\text{atm}}$  at the  $1\sigma$  level of confidence (Table 6:5). This indicates that argon loss is probably important

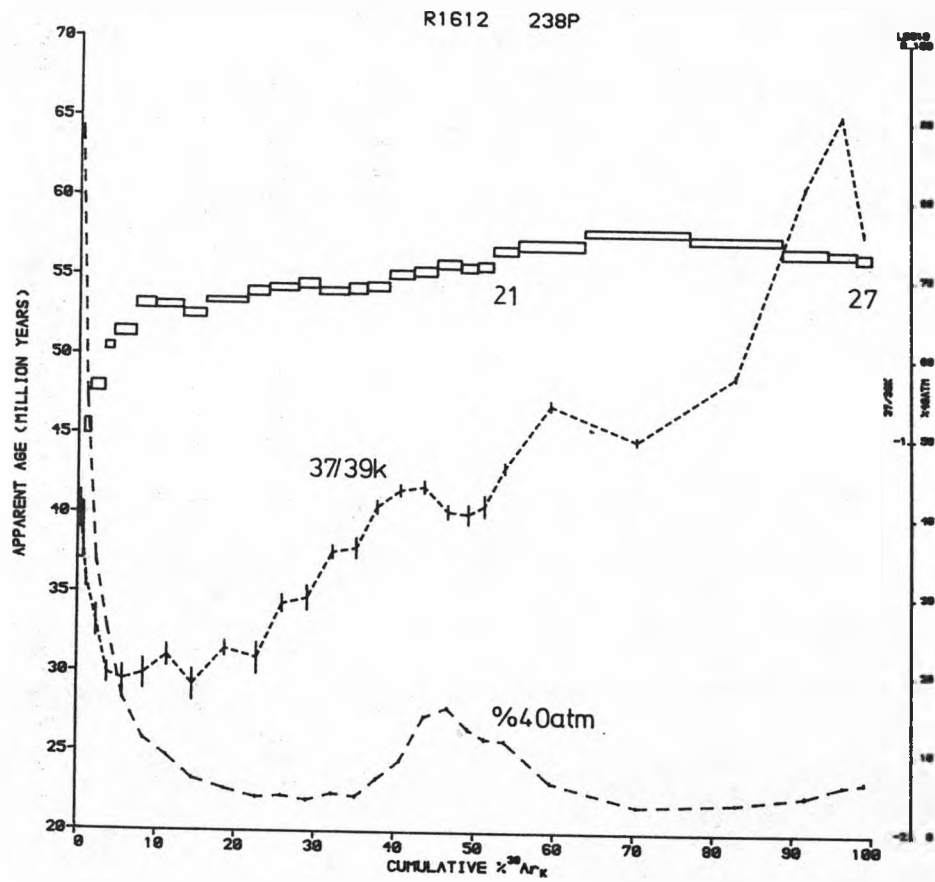


Fig. 6:15 Age spectrum for the Droimchogaidhsill sample R1612 (238P)

for these high temperature steps which could also be disturbed by the  $^{39}\text{K}$  recoil re-distribution phenomenon outlined for R1473. The step giving the highest age (No.23) is taken as setting a minimum estimate for the true age -  $57.9 \pm 0.2$  Ma. This is similar to that deduced for R1473.

The ICD3s were not useful for the interpretation of the  $^{40}\text{Ar}-^{39}\text{Ar}$  stepwise degassing data for R1612. The Arrhenius diagrams for the release of argon isotopes  $^{39}\text{K}$ ,  $^{40}\text{*}$  and 37 are presented in Fig. 6:16 all show two regimes of gas release. The low temperature linear correlation for 37 probably represents plagioclase outgassing, whereas the high temperature one undoubtedly relates to pyroxene outgassing. The former interpretation is supported by the closure temperature estimate for steps 3-12 presented in Table 6:6 (see Table 4:1 for published values of plagioclase closure temperatures). The  $^{39}\text{K}$  and  $^{40}\text{*}$  plots (which are virtually identical) should be simply related to the outgassing of the potassium feldspar, which constitutes the majority of sample 238P. The low and high temperature linear correlations may thus be related to the outgassing of the interstitial potassium feldspar and of the large zoned feldspar crystals respectively (see Appendix 7). However, the calculated closure temperatures for both low and high temperature linear correlations (see Table 6:6 for  $^{39}\text{K}$  values) do appear to be rather high for potassium feldspar (see Table 4:1). This may be explained by the relatively rapid assumed cooling rate. The similarity between  $^{39}\text{K}$  and  $^{40}\text{*}$  Arrhenius diagrams is not fully understood, bearing in mind that 238P is believed to be suffering from  $^{40}\text{*}$  loss. The similarity of  $^{40}\text{*}$  and  $^{39}\text{K}$  Arrhenius diagrams is, in fact, a common feature of samples with disturbed age spectra.

#### Conclusions for the Potassic Syenite

The three  $^{40}\text{Ar}-^{39}\text{Ar}$  analyses for sample 238P are not wholly consistent

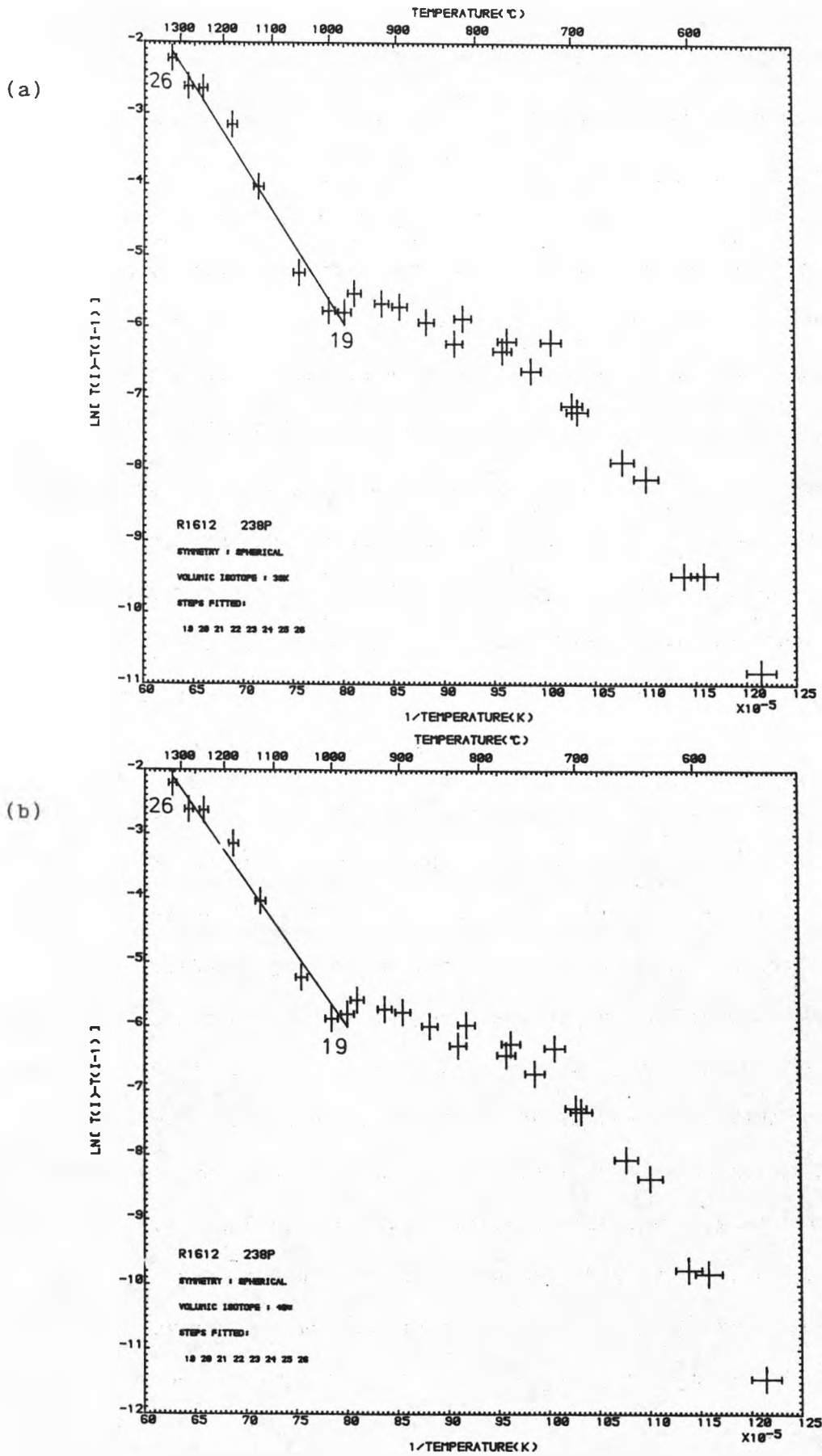


Fig. 6:16 Arrhenius diagrams for the Droimchogaidh sill sample R1612 (238P) (a) 39K (b) 40\* (c) 37

(c)

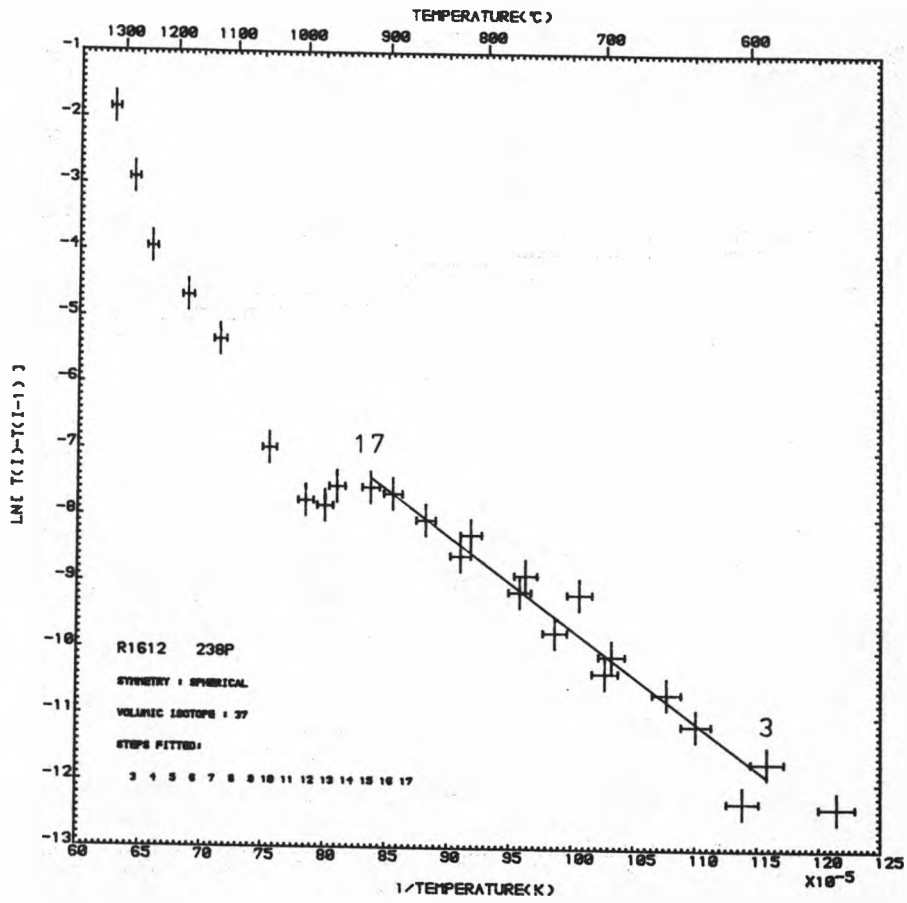


Fig. 6:16 continued



Isotope release	Steps	E (kcal mol <sup>-1</sup> )	Do/a <sup>2</sup> (s <sup>-1</sup> )	MSWD	Closure temperature (°C) - cooling rate assumed to be 10 <sup>4</sup> °C Ma <sup>-1</sup>
39K	3-12	33	1.1 * 10 <sup>1</sup>	3.3	260
	19-26	44	6.9 * 10 <sup>1</sup>	3.8	395
37	3-17	28	4.2 * 10 <sup>-2</sup>	4.3	270
	19-26	69	1.4 * 10 <sup>5</sup>	5.7	575

Table 6:6 Diffusion parameters and closure temperatures calculated for Droimchogaidh sample R1612 (238P)

although they are all interpreted as suffering from argon loss. The data for R1612 is considered the most reliable because no experimental problems were encountered during the stepwise degassing procedure and also because of the large number of steps extracted from that sample. My interpretation of the data for R1612 suggests a minimum estimate of the emplacement age for the Droimchogaidh sill of  $57.9 \pm 0.2$  Ma. This is significantly higher than Mohr et al.'s (1984) age of  $55 \pm 1$  Ma, but is similar to the majority of dates reported in this thesis for Tertiary igneous activity in Ireland.

The initial steps for the  $^{238}\text{P}$  samples range from 39 - 46 Ma and assuming argon took place during a discrete event this gives a maximum estimate for the timing of the argon loss event. There is, in fact, no geological evidence for any sort of thermal event in the west of Ireland in mid-Tertiary time (Mitchell & Mohr, 1985). Rather than envisaging a discrete argon loss event, it is perhaps more reasonable to consider a continuous  $^{40}\text{Ar}$  loss process. The syenite, as observed in this section (Appendix 7), consists of  $\approx 80\%$  feldspar which often has a very mottled appearance. This feldspar has thus probably been subjected to a secondary (probably deuteric) alteration process in which fine-grained sericite is one of the products. Such fine-grained alteration can be expected to be "leaky" with respect to radiogenic  $^{40}\text{Ar}$  (see Section 4:2). This second alternative is certainly plausible as Mohr et al., (1984) consider that the formation of the syenitic rocks was in fact aided by late-stage hydrothermal metasomatism.

b) The Olivine Gabbro - R1530 (238)

This sample, poorer in potassium than the syenite, gives percentage radiogenic  $^{40}\text{Ar}$  levels typically between 50 - 70%. Over much of the gas release, the calcium interference age correction is 2 - 4 Ma; however, for the last two steps the corrections are 24 and 31 Ma respectively. The chlorine interference age correction at its greatest

only reaches 0.1 Ma. In the initial steps of the gas release, the apparent age decreases rapidly and step ages are roughly constant (or slightly decreasing) over the last 80% of  $^{39}\text{K}$  release (see Fig. 6:17a). Steps 14-26, which constitute the last 80% of  $^{39}\text{K}$  release, give an ICD2 with a large MSWD value of 9.2. However, analysis of steps 14-22 gives a meaningful ICD2 (Fig. 6:17b) indicating an age of  $61.1 \pm 0.7$  Ma (see Table 6:7), a value consistent with the total gas and mean ages for these steps. Steps 23-26 give an age slightly below the plateau value and this may be explained by a  $^{39}\text{K}$  recoil re-distribution, in the same way as the high temperature age decrease observed for  $^{238}\text{P}$ . These low age steps are again seen to correspond with high  $^{37}/^{39}\text{K}$  levels. This might mean that the plateau age is, in fact, a slightly enhanced value. The pattern of ages for the initial steps, regardless of their physical interpretation, also indicates that any inferred age should be treated as a maximum estimate for the crystallisation age (see Section 4:5). A likely explanation for the low temperature steps, bearing in mind the proposed interpretation of the highest temperature steps, is a  $^{39}\text{K}$  recoil loss effect.

A second plausible chronological interpretation involves treating the plateau as part of a gradually decreasing pattern of ages. In this case the highest temperature steps would give a maximum age estimate -  $59.4 \pm 0.3$  Ma. The first interpretation is, in fact, preferred as a statistically meaningful age was produced and because it is a more conservative explanation. Thus, the maximum estimate for the emplacement age of the Droimchogaidh sill from sample R1530 is  $61.1 \pm 0.7$  Ma. Data analysis using ICD3 did not, in most cases, produce significantly different results to the ICD2 approach. ICD3 - Plot 2 (hypothetical component of  $^{40}\text{Ar}$  in proportion to  $^{36}\text{Cl}$ ) for steps 14-26 did give an MSWD below the cut-off. However, the deduced  $^{40}\text{Ar}/^{36}\text{Cl}$  ratio was negative and this is not physically acceptable.

Irradiation no. (Locality no.)	Steps	%39K	Total gas age (Ma)	Mean age (Ma) (step ages weighted by 1/variance)	Age (Ma)	ICD2 parameters (40/36) <sub>0</sub>	MSWD
R1530(238)	A11(1-26)	100	64.7 ± 0.5	62.3 ± 4.0	59.3 ± 0.8	315.8 ± 7.0	20.4
	14-26	80	61.3 ± 0.4	61.3 ± 1.1	61.2 ± 0.8	296.8 ± 8.1	9.2
	14-22	53	62.1 ± 0.5	61.8 ± 0.8	61.1 ± 0.7	301.6 ± 8.0	3.2
R1583(243)	A11(1-28)	100	66.4 ± 1.4	66.1 ± 4.0	66.8 ± 1.5	293.7 ± 8.4	27.5
	11-23	85	67.0 ± 1.2	66.2 ± 3.5	67.2 ± 2.6	290.8 ± 23.7	49.1
R1506(234)	A11(1-40)	100	65.0 ± 0.6	63.2 ± 4.3	62.5 ± 1.0	306.0 ± 10.1	45.5
	14-37	66	61.7 ± 0.5	61.8 ± 1.2	62.2 ± 0.6	290.9 ± 4.6	4.5
	14-26	41	61.8 ± 0.5	62.0 ± 0.9	62.2 ± 0.6	293.6 ± 4.0	2.4
R1581(234 <sup>+</sup> )	A11(1-22)	100	68.1 ± 0.6	63.8 ± 4.0	62.3 ± 1.8	313.5 ± 23.2	108.8
	9-18	42	62.3 ± 0.5	62.4 ± 0.7	63.1 ± 0.6	287.3 ± 6.3	2.1

+ denotes crushed sample

Table 6:7 Parameters calculated for Droimchogaidh sill samples 238, 243 and 234

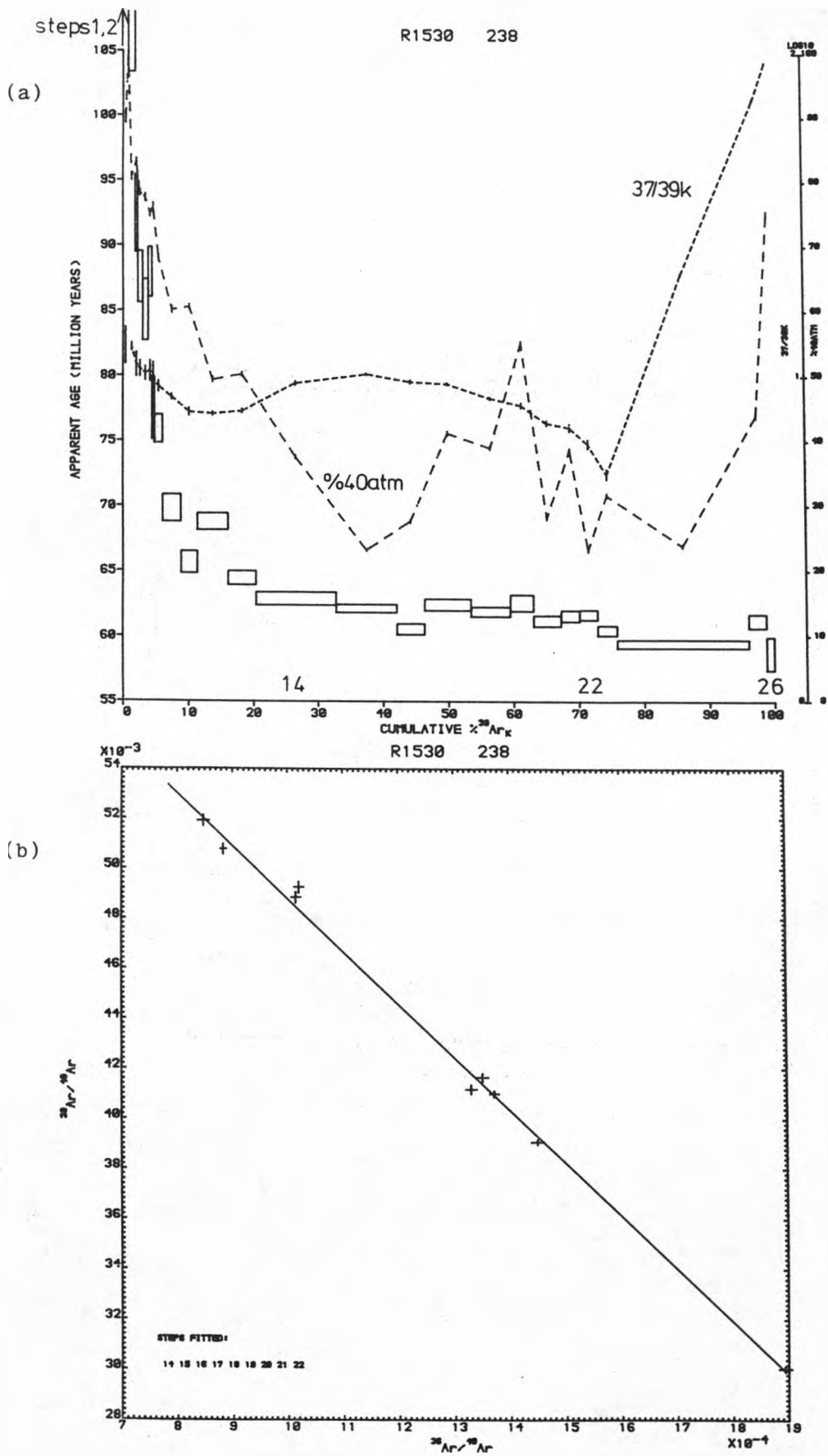


Fig. 6:17 Age spectrum (a) and ICD2 steps 14-22 (b) for the Droimchogaidh sill sample R1530 (238)

c) The Picrite - R1583 (243)

Although the radiogenic  $^{40}\text{Ar}$  level for the combined steps is only 19%, intermediate temperature steps attain values of 50 - 60%. This clearly demonstrates one of the advantages of the  $^{40}\text{Ar}$ - $^{39}\text{Ar}$  step heating method compared to the total fusion version (see Section 2:3). The majority of the atmospheric argon is contained within the disturbed low temperature steps. The age correction due to calcium interferences is typically 2 - 4 Ma. However, for the last two significant steps (in terms of  $^{39}\text{K}$  release) the correction is 11 and 53 Ma respectively. This undoubtedly represents pyroxene outgassing. The chlorine interference age correction is less than 0.1 Ma for all steps that contribute more than 0.1% of the  $^{39}\text{K}$  released.

Ignoring the first 20% of gas released, the steps display a pattern of decreasing age (see Fig. 6:18). This pattern could be interpreted as being the result of either of two quite different types of disturbance - Table 4:3 Nos. 2 and 3. In the former case ( $^{39}\text{K}$  recoil loss, excess  $^{40}\text{Ar}$  contamination ) the high temperature steps would be taken as giving a maximum age estimate -  $60.6 \pm 0.6$  Ma. In the latter case (closed system re-distribution) the total gas age would be the best estimate of the crystallisation age -  $\approx 67$  Ma (see Table 6:7 for analysis of steps 11-23). The former interpretation is preferred because it is consistent with the results for R1530 (238). Isotope correlation diagram data analysis was not found to be useful.

A point to note is that the total gas age (all steps) for R1583 (243) is greater than that for R1530 (238). This suggests that  $^{39}\text{K}$  recoil loss (the most likely explanation of the age patterns) or excess contamination etc. is greatest for the former. We would therefore expect that the maximum age estimate R1583 (243) produced to be greater than that for R1530 (238). The reverse is observed and this may be taken as evidence supporting the choice of the highest temperature

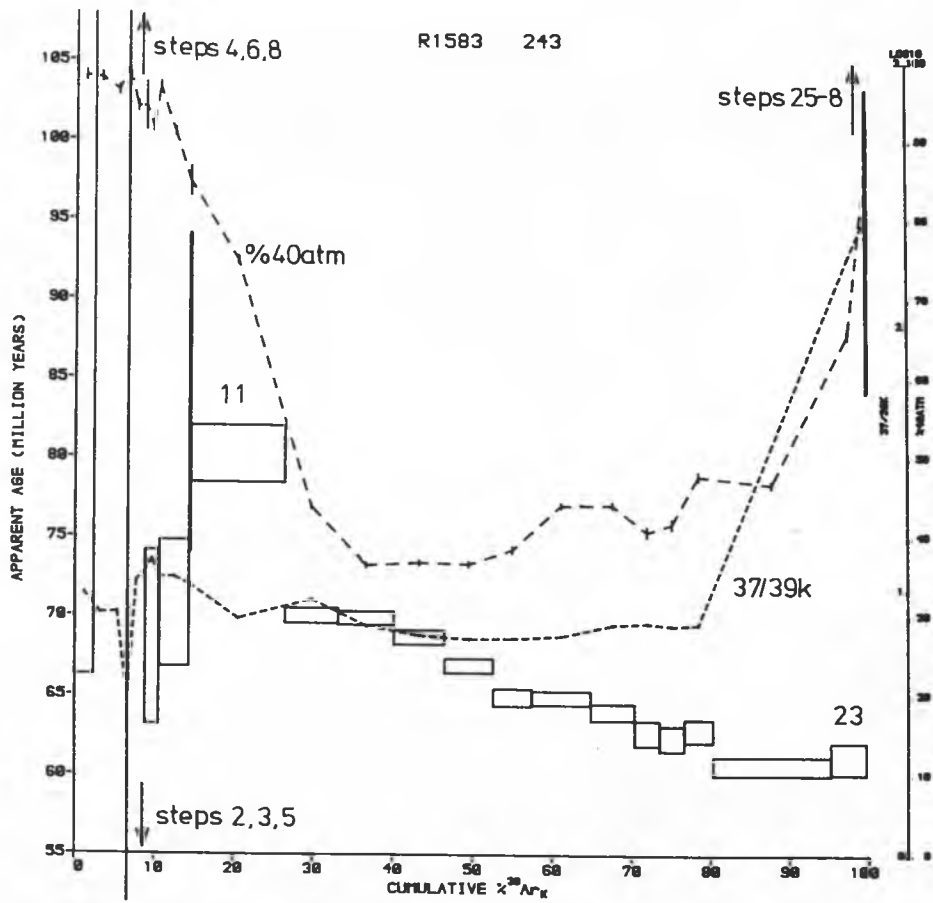


Fig. 6:18 Age spectrum for the Droimchogaidh sill sample R1583 (243)

steps, rather than the intermediate temperature plateau, as giving the best maximum age estimate for R1530 (238). However, alternatively this observation may be explained in terms of differences in the two samples e.g. grain sizes. Therefore the original interpretation of R1530's age spectrum is still preferred.

d) The Satellite Sill Dolerite

Two whole-rock samples of this dolerite have been analysed. The second of these, numbered R1581, was crushed prior to irradiation.

R1506 (234)

This sample gives an age spectrum (Fig. 6:19a) similar in general form to the one produced by R1530 (238) except that, in this case, the intermediate temperature plateau spans 60% of the  $^{39}\text{K}$  release. The peaks in the %  $^{40}\text{Ar}_{\text{atmospheric}}$  curve in the earlier parts of the gas release correspond to exposures of the sample and crucible to the atmosphere (the result of technical problems). The age correction due to calcium-derived argon isotopes is  $\approx 1$  Ma over most of the age spectrum; however, for the last five steps it is from 15 - 30 Ma. Three of these steps contribute  $< 0.2\%$   $^{39}\text{K}$  and thus are not regarded as significant.

ICD2 analysis of all the steps beyond the marked low temperature age decline (14-37) gives an MSWD greater than the adopted cut-off of 3.5 (see Table 6:7). However, by restricting the steps considered to 14-26 a statistically meaningful age is produced -  $62.2 \pm 0.6$  Ma (the isotope correlation diagram is presented to Fig. 6:19b). The strong influence exerted by step 16 on the ICD2 linear correlation (due to its high level of atmospheric  $^{40}\text{Ar}$ ) does not greatly affect the calculated parameters. ICD2 analysis of steps 17-26 gives almost identical results to that for 14-26. An interesting point to note is that many of the steps that constitute the plateau contain less than



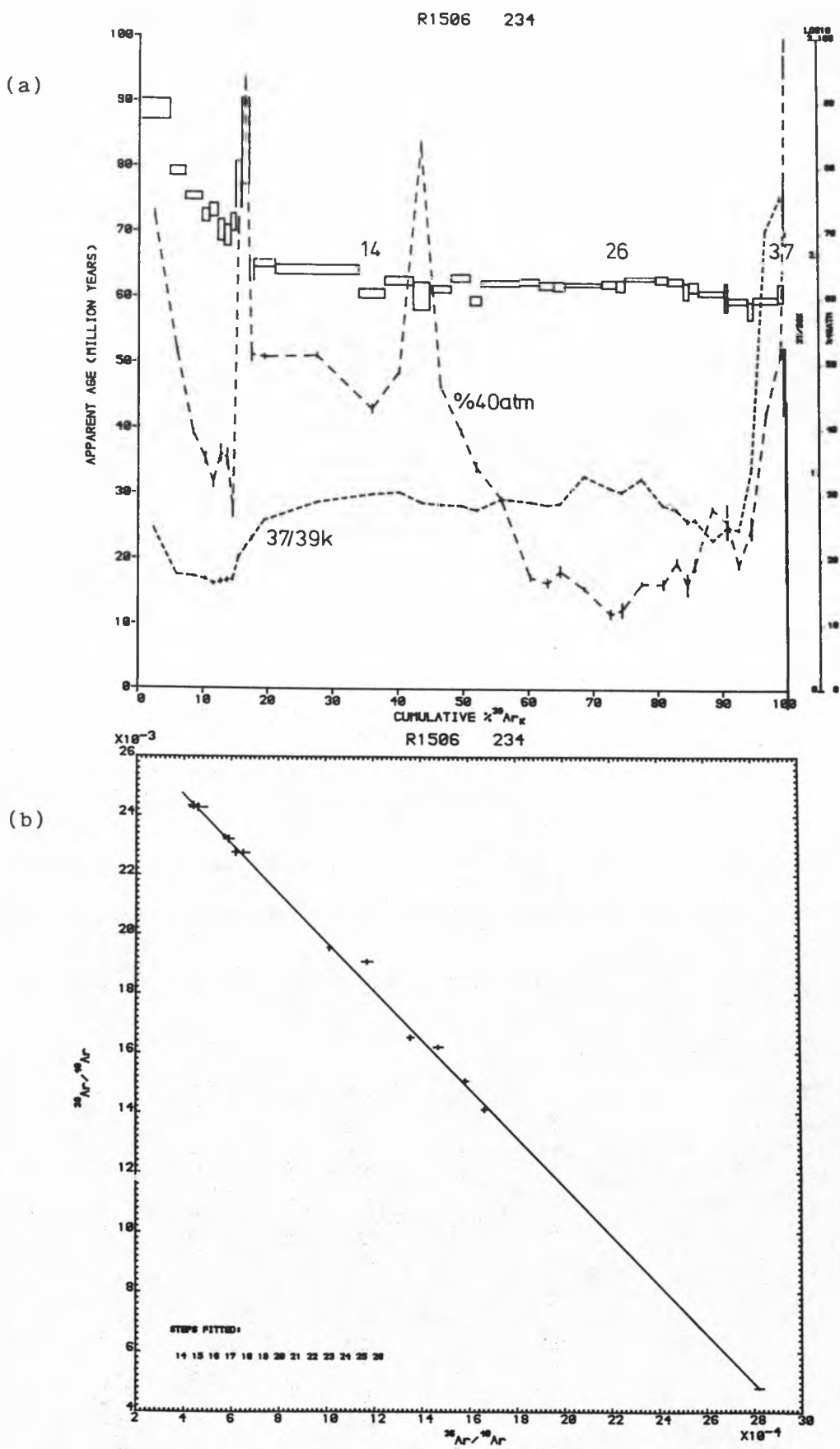


Fig. 6:19 Age spectrum (a) and ICD2 steps 14-26 (b) for the Droimchogaidh satellite sill sample R1506 (234)

5% of the total  $^{39}\text{K}$  released (a feature that is common to many of the samples analysed in this work). This is firm evidence supporting Roddick et al.'s (1980) contention that Dalrymple & Lanphere's (1974) rejection of small steps is unwarranted.

Beyond this plateau, the higher temperature steps increase slightly in age and then decrease to a level below the plateau (steps 27-37).

This feature could be explained in terms of a  $^{39}\text{K}$  recoil re-distribution from potassium-rich phases to potassium-poor minerals. Such an interpretation is justified by the equivalence of the total gas ages for steps 14-26 (the plateau) and 27-37. The  $^{37}/^{39}\text{K}$  peak (pyroxene outgassing) does not, in fact, wholly coincide with the high temperature age decrease. This could be because of  $^{39}\text{K}$  recoil into the rims of olivine grains, which do not contain appreciable potassium or calcium, as well as into pyroxene.

As stated in the introduction to this chapter, ICD3 data analysis does not, in general, result in significant improvement in MSWD levels.

However, for steps 14-37, plot 3 did give an MSWD less than the cut-off. As in the case of R1530 (238) though, the calculated  $^{40}\text{Ar}/^{36}\text{Cl}$  ratio was negative and physically unacceptable.

As the low temperature disturbance (again probably due to a  $^{39}\text{K}$  loss) is restricted to the first 15% of  $^{39}\text{K}$  release, the plateau age of  $62.2 \pm 0.6$  Ma is thought to be a good approximation to the emplacement age.

#### R1581 (234)

The age spectrum for the crushed 234 sample R1581 (Fig. 6:20a) is similar in general form to that produced by R1506. However, the low temperature disturbance is more pronounced and it extends over 50% of the gas release. Also, the highest temperature steps record a simple age decline rather than an increase from the plateau, followed by a

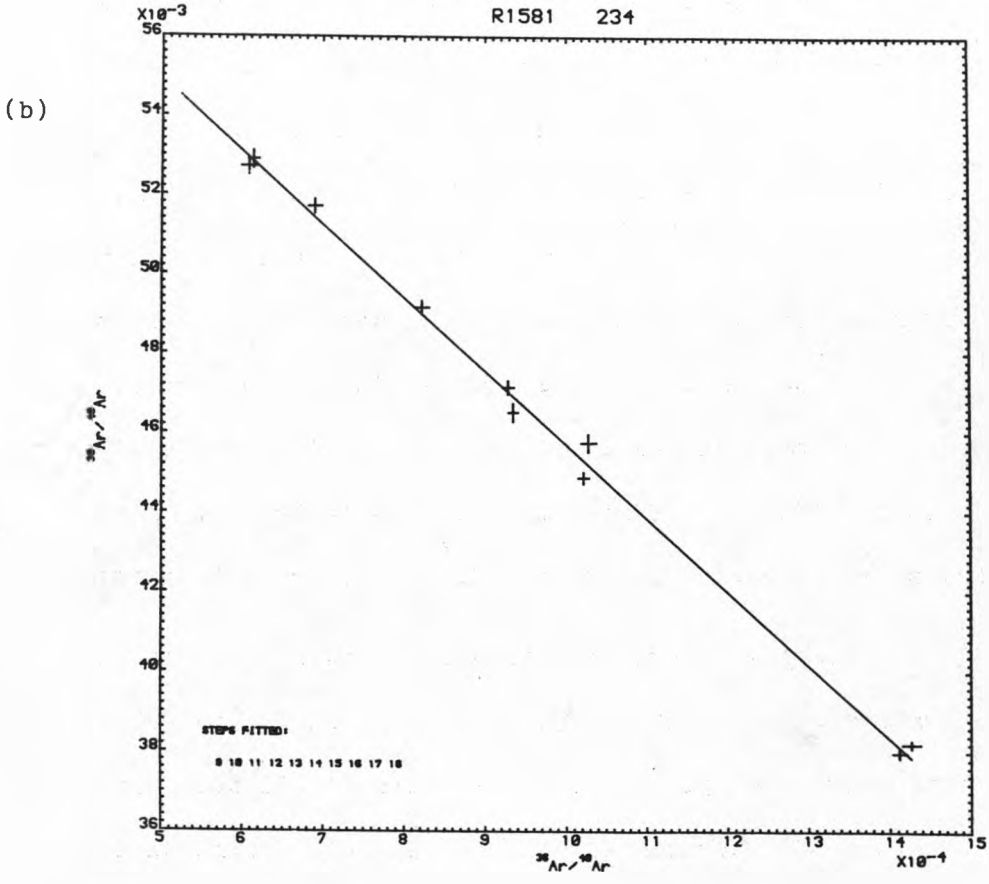
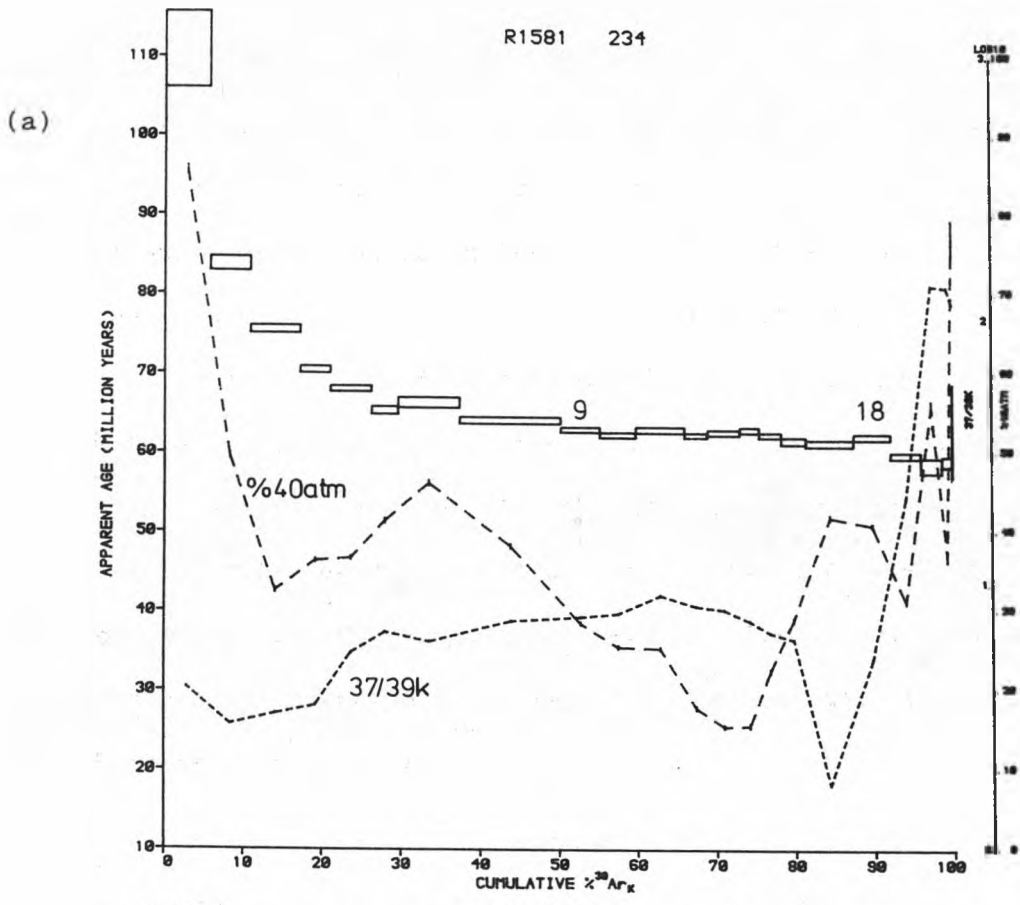


Fig. 6:20 Age spectrum (a) and ICD2 steps 9-18 (b) for the Droimchogaidh satellite sill sample R1581 (234)

decline. The latter difference may be explained by the outgassing procedure adopted for R1581 - this sample was outgassed in a series of 22 steps whereas R1506 produced 40. A  $^{39}\text{K}$  recoil re-distribution is however still thought to explain the anomalous pattern of ages at the high temperatures. The age correction related to calcium interference reactions is 1 - 3 Ma over most of the steps; however for the last three it reaches 40 Ma. This is similar to the pattern observed for the uncrushed sample R1506.

Steps 9-18 give a statistically meaningful plateau age of  $63.1 \pm 0.6$  Ma (Table 6:7) but they only constitute 42% of the  $^{39}\text{K}$  released.

Bearing in mind the extent of the low temperature disturbance, this age is treated as a maximum estimate of the emplacement age. The latter interpretation is consistent with that for R1506.

The greater extent of the low temperature disturbance for R1581 compared to R1506 is probably explained by an increased  $^{39}\text{K}$  recoil loss effect. Such a phenomenon certainly seems plausible, bearing in mind that R1581 is a crushed whole-rock sample. This contention is supported by a comparison of total gas ages (all steps) for the two samples: R1581 gives the greater age. Levels of radiogenic  $^{40}\text{Ar}$  for the total gas release of both samples are similar. However, R1581 was not subject to atmospheric exposures and thus, sample crushing has apparently led to an increase in atmospheric argon contamination. This is in contrast to expected results if the fractionation of loosely-held atmospheric argon (during extraction line bake-out etc.) were important in the uncrushed sample (Baksi, 1974). It is possible that atmospheric argon added by crushing may suffer from a fractionation. This effect may contribute to the explanation of the anomalously high ages at low temperatures.

The  $^{37}/^{39}\text{K}$  patterns for R1506 and R1581 are very similar, although the total gas levels differ significantly. This difference could conceivably be explained by recoil loss effects but the most likely

reason for it involves slight compositional variations between the two samples.

ICD3 data analysis was also carried out for R1581. Although this did not help in the interpretation of this sample's  $^{40}\text{Ar}$ - $^{39}\text{Ar}$  stepwise degassing data, it does illustrate the sort of results this analysis typically produces. ICD3-Plot 3 was used to check whether the high temperature age decrease (which corresponds to rising  $37/39\text{K}$  values) can be explained by the adoption of an inaccurate  $\left[ \frac{40-(40/36)_{\text{atm}}^{36}}{37} \right]_{\text{Ca}}$  value. Choosing steps 9-22 for analysis, an MSWD value of 5.0 is calculated which is unacceptably high (see Table 6:8). Thus the high temperature decrease cannot realistically be attributed to this cause. Whereas the ICD3-Plot 3 for steps 9-22 does not produce an MSWD value significantly less than that for the corresponding ICD2, ICD3-Plot 2 does (Table 6:8). The MSWD in this case is calculated to be 3.5, which is equal to the adopted cut-off level. However, the ICD3-Plot 2 is not physically meaningful because the calculated  $^{40}\text{Ar}/^{36}\text{Cl}$  ratio is negative. For this sample, as with many others, ICD3 data analysis is not helpful for the interpretation of  $^{40}\text{Ar}$ - $^{39}\text{Ar}$  stepwise degassing data.

Fig. 6:21a shows the Arrhenius diagram plotted for the  $39\text{K}$  release of sample R1581. The linear correlation of steps 12-21 indicates an activation energy of  $31 \text{ kcal mol}^{-1}$  and a  $D_0/a^2$  of  $8.4 \text{ s}^{-1}$  (MSWD = 4.8). Using a cooling rate of  $10^6 \text{ }^\circ\text{C Ma}^{-1}$ , a closure temperature of  $315^\circ\text{C}$  is calculated. This figure is considerably larger than others reported for alkali feldspar (see Table 4:1), which is probably the dominant source of  $39\text{K}$  (and  $40^*$  - see below) in this sample, however this may be explained by the relatively rapid assumed cooling rate. The  $40^*$  Arrhenius diagram is almost identical to the one for  $39\text{K}$ , however the diagram for  $^{37}\text{Ar}$  release is distinctly different (Fig. 6:21b). The

	Age (Ma)	(40/36) <sub>o</sub>	MSWD
ICD2	63.4 ± 0.7	281.7 ± 6.3	5.6
ICD3-Plot 3	63.1 ± 0.7	286.8 ± 8.2	5.0
		$\left[ \frac{40}{37} - \frac{(40/36)_o \cdot 36}{37} \right] \text{Ca}$	
		-0.0779 ± 0.0037	
		$\frac{40x}{36c1}$	
ICD3-Plot 2	63.4 ± 0.6	286.8 ± 5.4	3.5
		(-8.9 ± 3.3) * 10 <sup>3</sup>	

Table 6:8 Comparison of ICD parameters calculated for Droimchogaidh satellite sill sample R1581 (234) steps 9-22

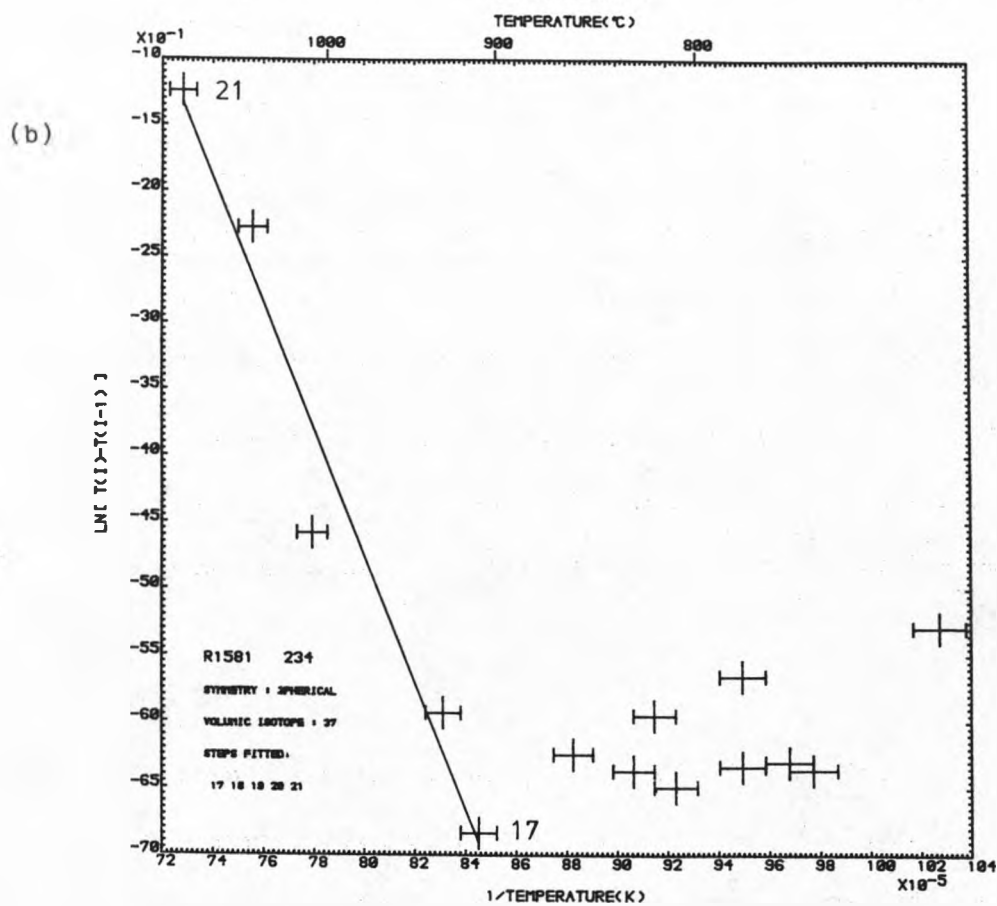
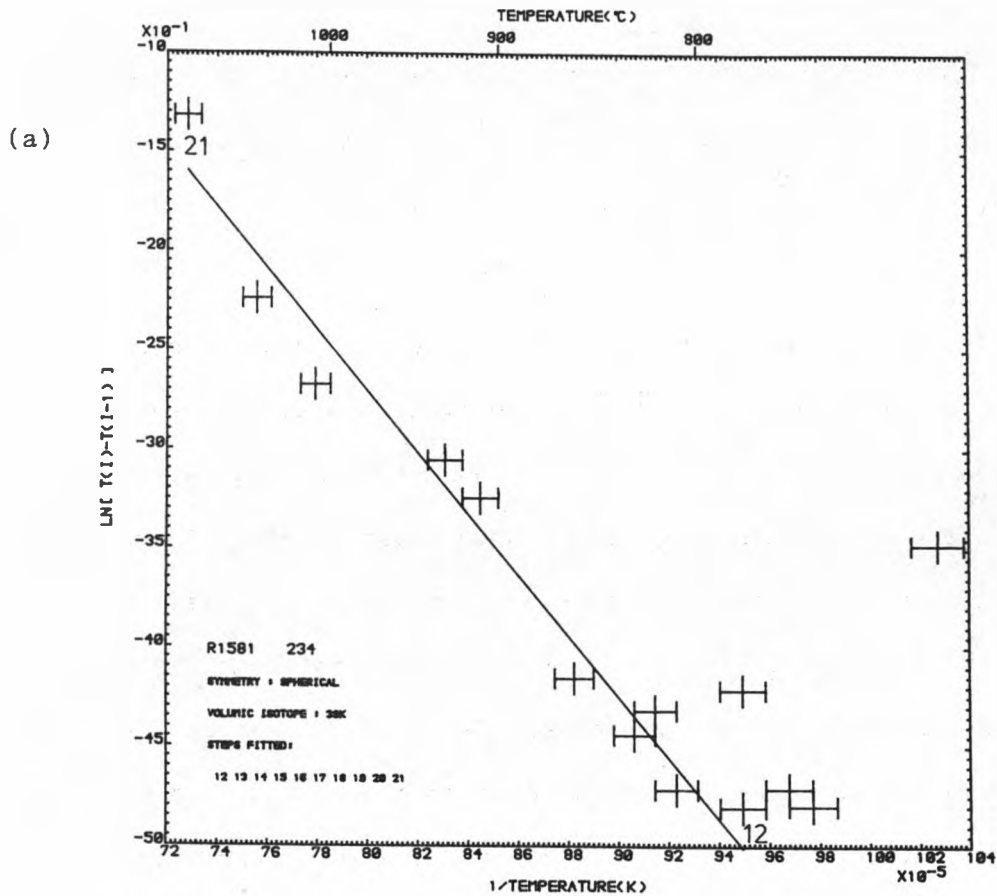


Fig. 6:21 Arrhenius diagrams for the Droimchogaidh satellite sill sample R1581 (234) (a) 39K (b) 37

only linear correlation for the 37 release is for steps 17-21 and the activation energy is calculated to be  $95 \text{ kcal mol}^{-1}$  with a  $D_0/a^2$  of  $1.8 \times 10^{+11} \text{ s}^{-1}$  (MSWD = 3.6). This segment undoubtedly corresponds to pyroxene outgassing and a closure temperature of nearly  $680^\circ\text{C}$  is indicated. Because no temperature information is available for the first eight steps of R1581, the possible effects of the proposed  $39\text{K}$  loss on the Arrhenius diagram could not be observed.

#### Conclusions for the Satellite Sill Dolerite

The best estimate of the emplacement age of the satellite sill is  $62.2. \pm 0.6 \text{ Ma}$ .

#### Conclusions for the Droimchogaidh Sill

Table 6:9 gives a summary of chronological interpretation for the Droimchogaidh samples. As discussed previously R1612 is considered to be the most reliable of the 238P analyses, thus the age of the Droimchogaidh sill is constrained to lie between 58 and 61 Ma. The results in Table 6:9 suggest that the Droimchogaidh satellite sill, at 62 Ma, may be a little older than the main body. However, if the Droimchogaidh sill itself is most accurately dated by the more basic rocks (R1530 and R1583 give ages of 61 Ma) then there is no significant age difference between this and the satellite sill.

#### 6:2:4 The Lough Key Dyke

This rather isolated dyke outcrop is found on the west side of Lough Key in County Roscommon (see Fig. 6:1). Because of its apparent freshness this dolerite dyke was assumed to be of Tertiary age. Samples of this dyke rock were collected as part of an Irish Tertiary palaeomagnetic investigation. When analysed at the Liverpool laboratory they were found to possess a normal magnetisation as opposed to the reversed direction found for all the other Irish Tertiary samples. As a consequence of this anomalous observation a whole-rock sample of the Lough Key dyke has been dated as part of this study.



Sample	Rock type	Best age estimate (Ma)
R1381(238P)	Potassic syenite	55.3 ± 0.5
R1473(238P)	Potassic syenite	> 58.5 ± 0.5
R1612(238P)	Potassic syenite	> 57.9 ± 0.2
R1530(238)	Olivine gabbro	< 61.1 ± 0.7
R1583(243)	Picrite	< 60.6 ± 0.6
R1506(234)	Satellite sill dolerite	62.2 ± 0.6
R1581(234)	Satellite sill dolerite	< 63.1 ± 0.6

Table 6:9 Summary of best age estimates for the Droimchogaidh sill samples

Irradiation no. (Locality no.)	Steps	%39k	Total gas age (Ma)	Mean age (Ma) (step ages weighted by 1/variance)	Age (Ma)	ICD2 parameters (40/36) <sub>0</sub>	MSWD
R1611(G048)	All(1-32)	100	310.8 ± 6.7	313.3 ± 11.6	317.4 ± 7.0	260.3 ± 10.2	47.9
	10-23	41	313.8 ± 6.7	314.2 ± 6.9	315.3 ± 6.9	282.2 ± 14.1	2.2
	24-32	54	313.4 ± 6.7	316.6 ± 9.8	318.9 ± 10.0	257.1 ± 144.7	45.5

Table 6:10 Parameters calculated for the Lough Key dyke sample

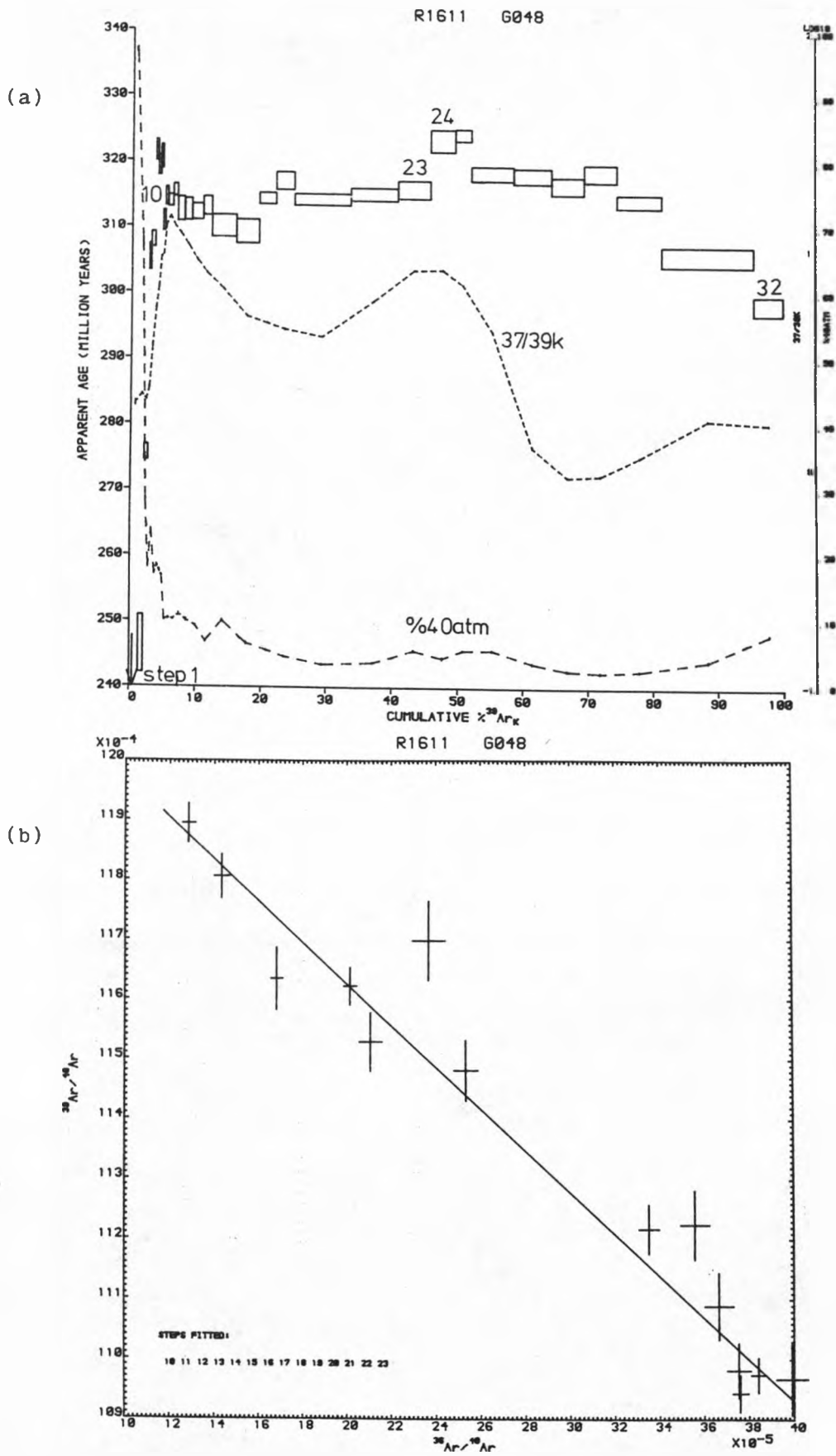


Fig. 6:22 Age spectrum (a) and ICD2 steps 10-23 for the Lough Key dyke sample R1611 (G048)

R1611 (G048)

The age spectrum for sample R1611 is given in Fig. 6:22a. One immediately sees that the majority of ages lie between 300 and 320 Ma; therefore dyke G048 is apparently of a Carboniferous age rather than Tertiary.

The total gas %  $^{40}\text{Ar}^*$  is 81% and for the majority of the steps the level is greater than 90%. The  $^{37}/^{39}\text{K}$  curve displays a peak at  $\approx 50\%$  release which probably corresponds to plagioclase outgassing. The lack of a distinct  $^{37}/^{39}\text{K}$  peak at high temperatures indicates that pyroxene is probably not a major constituent of this dyke rock. Such a conjecture is supported by petrographic observations (Appendix 7). The age correction due to calcium interference reactions is  $\leq 6$  Ma for all steps, whereas that for chlorine interferences is  $\leq 0.03$  Ma for all steps.

The results of several ICD2 analyses are presented in Table 6:10. Steps 10-23 give an apparently meaningful age of  $315 \pm 7$  Ma (Fig. 6:22b). Steps 24-32, which show a pattern of decreasing age in the age spectrum plot (Fig. 6:22a), do not give a meaningful ICD2 age as the MSWD value is very high. However, it is interesting to note that the calculated total gas age for steps 10-23 and 24-32 are almost identical. This is strong evidence to support the hypothesis that the decreasing pattern of ages over steps 24-32 is due to a  $^{39}\text{K}$  recoil re-distribution. This hypothesis certainly seems plausible because of the highly altered condition of the dyke rock (as observed in thin section - see Appendix 7). Alteration often leads to the formation of fine-grained secondary minerals which may be susceptible to recoil effects.

The ICD3 plots and the Arrhenius diagrams for R1611 do not appear to give meaningful results.

Conclusions for the Lough Key Dyke

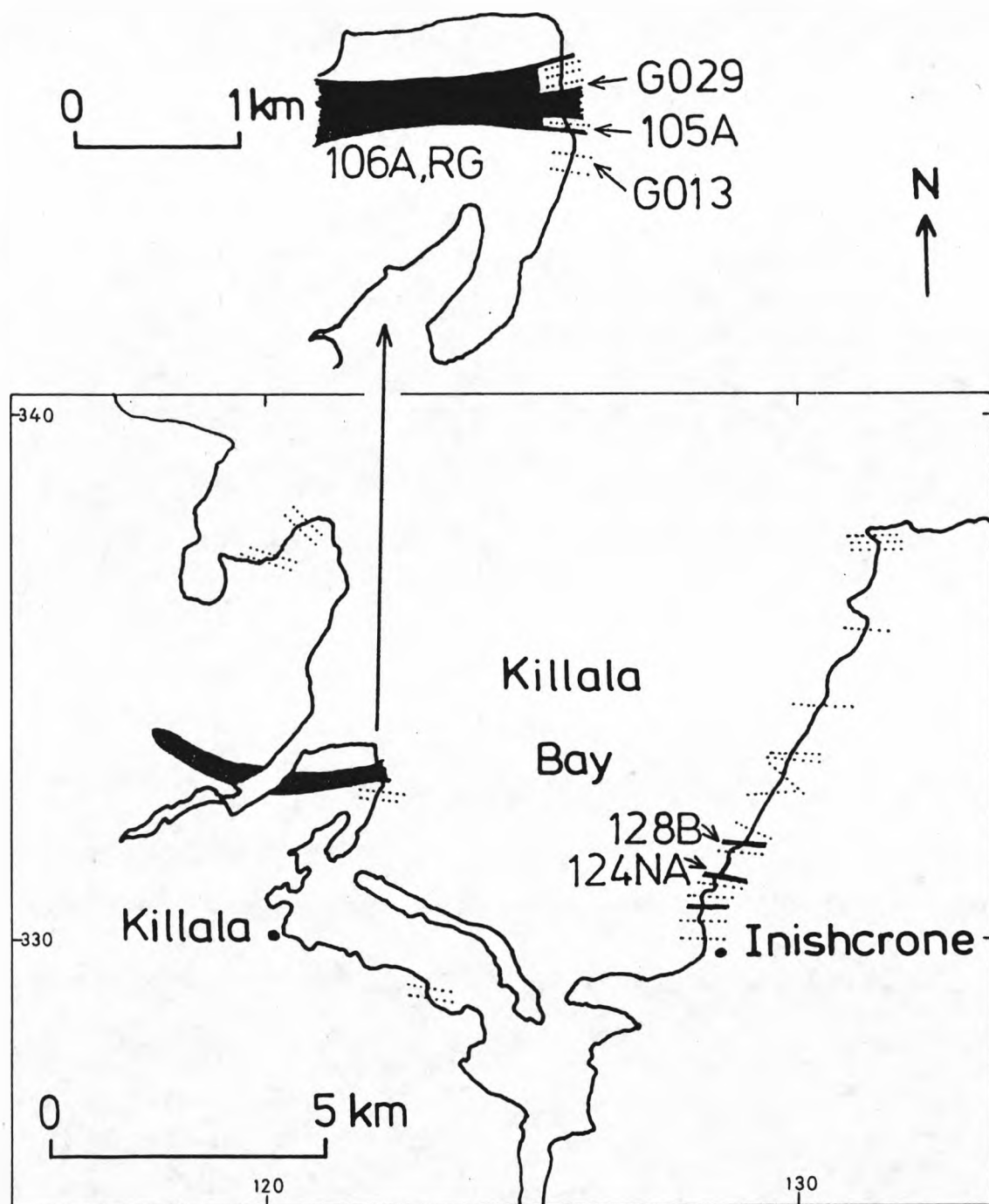
In the absence of any geological controls,  $315 \pm 7$  Ma is taken as the

the best estimate for the age of emplacement of the Lough Key Dyke. It is clear that the Lough Key Dyke is of an Upper Carboniferous age rather than Tertiary and thus the anomalous "Tertiary" palaeomagnetic result for this intrusion is explained.

#### 6:2:5 Killala Bay

Killala Bay is found on the north coast of Counties Mayo and Sligo. Here, Tertiary intrusives follow an east-west trend which is distinct from the north-westerly direction followed by most of the Tertiary dyke swarms in Ireland (and indeed the rest of the British Tertiary Igneous Province). The largest intrusion is the Killala Gabbro which is found on the west side of the bay. More than 400 m wide, it has doleritic chilled margins and a core of laminated gabbros and anorthosites (Preston, 1981). On the east side of Killala Bay, the gabbro is represented by a series of feeder dykes (5-20m thick) which have pyroxenite margins against the country rock limestone (Preston, 1965). A swarm of doleritic flash injections intruded after the gabbro are represented on both east and west sides of the bay (some of them are observed to cross-cut the earlier gabbro). These bodies are typically 1m thick. Fig. 6:23 shows the location of the main gabbro body, feeder dykes, and flash injections in the Killala Bay area. The latter are numerous and are thus only displayed diagrammatically.

Macintyre et al., (1975) presented several potassium-argon analyses of Killala Bay Tertiary igneous rocks. Pyroxene separated from the pyroxenite margin of one of the feeder dykes on the east side of the bay gave ages of about 52 Ma. Whole-rock analyses of a fresh dolerite cutting the Killala Gabbro gave consistent ages of  $\approx 59.5$  Ma. The latter dates were taken as establishing the true age of the flash injections and a minimum age for the Killala Gabbro. Macintyre et al.'s (1975) K-Ar results for the gabbro itself (whole-rock and mineral separate) were thought to reflect the presence of excess  $^{40}\text{Ar}$ .



**Fig. 6:23** Tertiary igneous intrusions around Killala Bay: sampling locations (solid shading - gabbro; dotted lines - doleritic flash intrusions) - adapted from a personal communication (P. Mohr)

However, they did suggest that the gabbro was probably emplaced  $\approx 82$  Ma ago.

On the basis of geological field evidence alone, it is possible to show that the doleritic flash injections and the Killala Gabbro must be of essentially the same age (P. Mohr pers. comm.). Dykes intruding the core of the gabbro have flow banded, non-chilled margins and a non-linear strike. Therefore, when the flash injection took place the gabbro must still have been hot. Only the dykes intruded into the edge of the Killala Gabbro are fine-grained, indicating that at the time of intrusion the gabbro was cold at its margins. Thus, Macintyre et al.'s (1975) age estimates are not consistent with the known geology.

In this  $^{40}\text{Ar}$ - $^{39}\text{Ar}$  dating study, 12 samples from the Killala Bay area have been analysed. They fall into several categories (numbers of samples given in brackets)

- Whole-rock samples of the later doleritic dykes (3)
- Whole-rock sample of a small felsic dykelet which cross-cuts the Killala Gabbro but is cross-cut itself by one of the doleritic dykes (1)
- Whole-rock samples of the Killala Gabbro (2)
- Mineral separate samples extracted from the Killala Gabbro (2)
- Whole-rock samples of the gabbroic feeder dykes (4)

As the gabbroic feeder dykes are thought to be the frayed edges of the Killala Gabbro and many of the age spectra have a similar form, the last three sample categories are considered together. The dates presented here resolve the anomaly apparent in Macintyre et al.'s (1975) K-Ar study and suggest that activity in the whole Killala Bay area took place around 58 Ma ago.

a) The Doleritic Dykes

Two whole-rock samples of the dyke 105A, which cuts the Killala Gabbro, and one of G013, which does not, have been analysed (see Fig. 6:23).

R1383 (105A)

This is one of the pilot samples which was prepared as part of the preliminary  $^{40}\text{Ar}$ - $^{39}\text{Ar}$  investigation of Irish Tertiary rocks. It was outgassed in only nine steps and shows a generally decreasing pattern of ages (Fig. 6:24). Stepwise degassing of R1383 was carried out about 500 days after irradiation; in consequence the majority of the calcium-derived  $^{37}\text{Ar}$  had decayed away before sample analysis ( $^{37}\text{Ar}$  has a half life of only 35 days). Thus, it was not possible to make an accurate correction for the calcium interference reactions.  $^{37}\text{Ar}$  was, in fact, only recorded for two steps and in each case at the minimum possible level. The age correction due to calcium interference was, in these two cases, calculated to be 20 and 40 Ma. R1383 can therefore be expected to give only a rough guide to the age of sample 105A. Steps 8 and 9, which constitute more than 60% of the  $^{39}\text{K}$  release, give ages of 62 and 58 Ma respectively. Taking a simple average, sample 105A is probably, therefore, about 60 Ma old.

R1503 (105A)

The  $^{40}\text{Ar}$ - $^{39}\text{Ar}$  total gas age for R1503 ( $61.5 \pm 0.9$  Ma) is consistent with the K-Ar dates reported by Macintyre et al., (1975) for the doleritic dykes. However its age spectrum is rather complicated (Fig.6.25), with only small sections of the gas release displaying constant age. The  $^{37}/^{39}\text{K}$  curve shows the increasing importance of the calcium-interference age correction with temperature which is 1 - 2 Ma for steps 1-9 and up to 5 Ma for the remaining steps.

ICD2 analyses of steps forming the two four-step "plateau segments" (see Fig. 6:25) both give MSWDs below the cut-off value but different ages, and  $(^{40}/^{36})_{\text{O}}$  ratios greater than  $(^{40}/^{36})_{\text{atm}}$  (see Table 6:11). Steps 6-16, which consist of the last 60% of  $^{39}\text{K}$  release, give an ICD2 with  $(^{40}/^{36})_{\text{O}} \approx 295.5$  but an MSWD of 4.7, which is unacceptably high. However, ICD3-Plot 3 analysis of the same steps gives an MSWD



Irradiation no. (Locality no.)	Steps	% <sup>39</sup> K	Total gas age (Ma)	Mean age (Ma) (step ages weighted by 1/variance)	Age (Ma)	ICD2 parameters (40/36) <sub>O</sub>	MSWD
R1383(105A)	All(2-10)	100	64.9 ± 1.0	59.7 ± 5.1	58.1 ± 3.1	315.3 ± 36.6	15.3
R1503(105A)	All(1-16)	100	61.5 ± 0.9	62.6 ± 1.8	62.9 ± 1.1	293.1 ± 7.9	16.1
	2-5	30	64.6 ± 0.9	64.3 ± 1.0	63.8 ± 1.0	301.0 ± 4.2	1.0
	6-9	30	61.6 ± 0.9	61.6 ± 0.9	60.9 ± 0.9	307.1 ± 5.9	0.2
R1526(G013)	All(1-30)	100	70.2 ± 0.6	62.9 ± 18.4	81.7 ± 5.7	217.1 ± 62.4	3056.6
R1613(G029)	All(1-30)	100	60.1 ± 1.1	61.3 ± 1.6	62.0 ± 1.1	289.7 ± 2.8	4.5
	21-30	70	59.8 ± 1.1	60.2 ± 1.3	57.8 ± 1.6	306.4 ± 13.2	1.8

Table 6:11 Parameters calculated for the Killalala Bay doleritic dykes and the Killalala Gabbro felsic dykelet

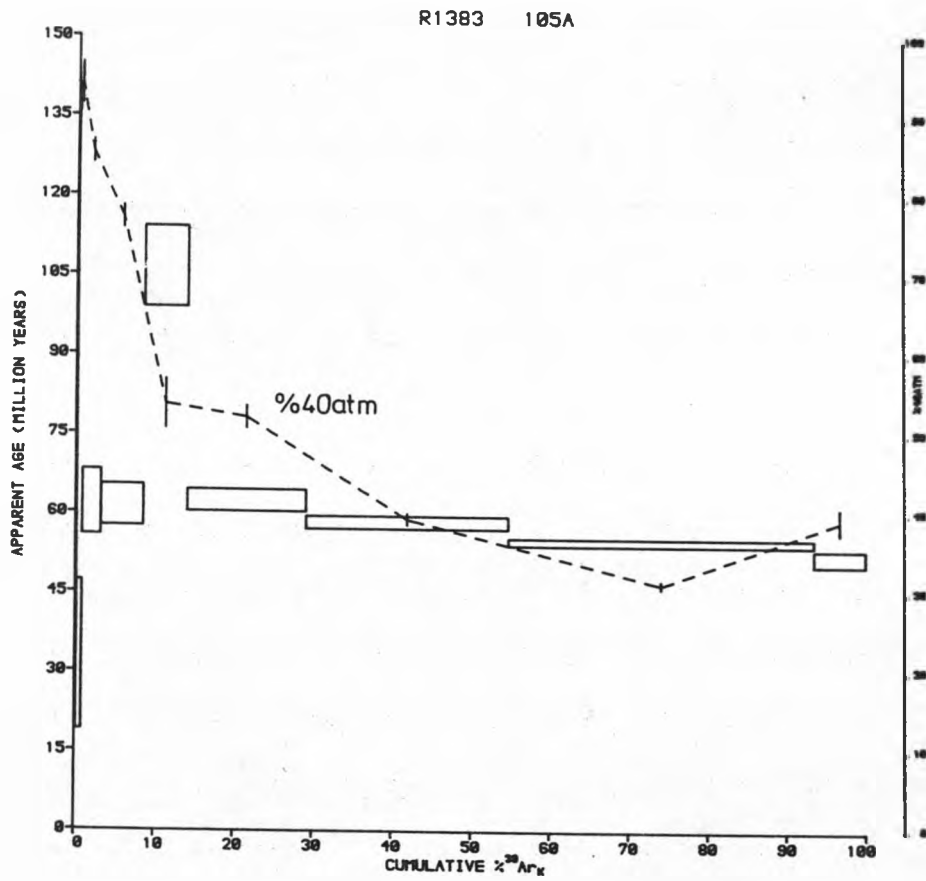


Fig. 6:24 Age spectrum for the Killala Bay doleritic dyke sample R1383 (105A)

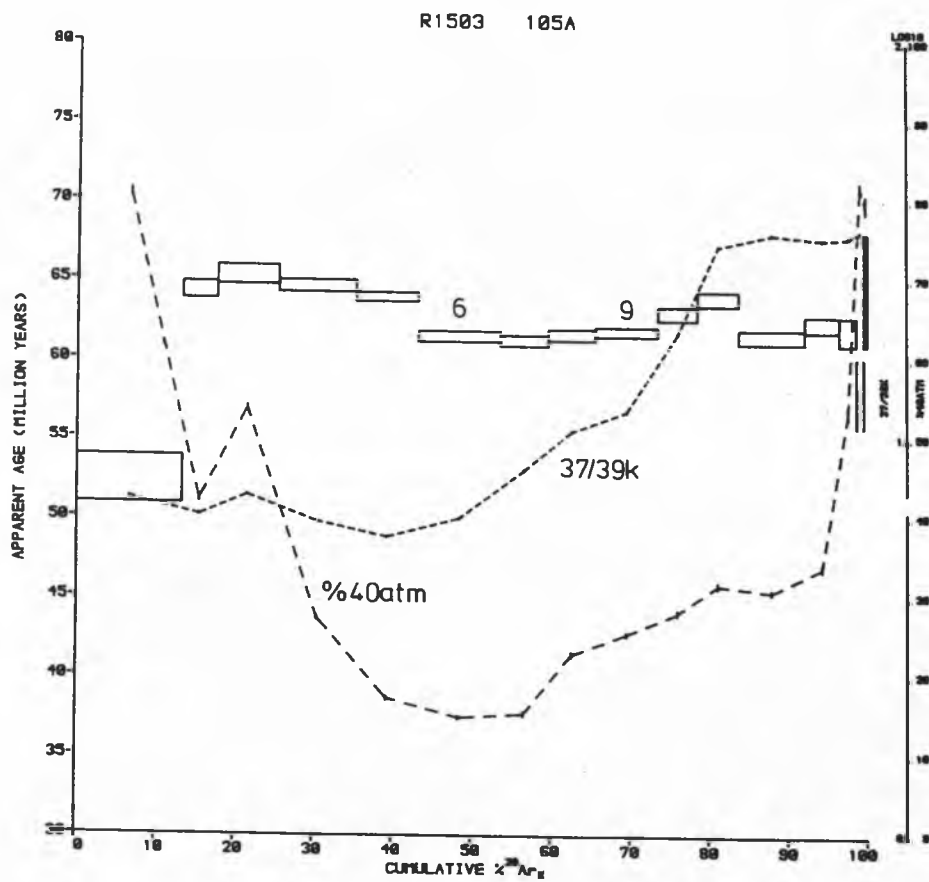


Fig. 6:25 Age spectrum for the Killala Bay doleritic dyke sample R1503 (105A)

below the cut-off level, a  $(40/36)_O \approx 295.5$ ,  $^{40}\text{Ar}/^{36}\text{Cl} = (2.3 \pm 1.0) \times 10^5$  and an age of  $59.3 \pm 1.4$  Ma. In the absence of evidence from other samples for  $^{40}\text{Ar}$  being incorporated into rocks in proportion to  $^{36}\text{Cl}$ , this result must be viewed with scepticism. Thus, it appears that no conclusive age interpretation can be reached for R1503. Before attempting a more qualitative interpretation, it is necessary to discuss the possible physical mechanisms that makes this sample's age spectrum so complicated.

The anomalous low age recorded for step 1 probably records a minor loss of radiogenic  $^{40}\text{Ar}$ . The remaining steps form a pattern which is fairly similar to others produced in this Killala Bay work (see whole-rock analyses of gabbroic feeder dyke 124NA for instance). In these cases, samples are thought to be subject to excess  $^{40}\text{Ar}$  contamination because of the saddle-shaped pattern of ages they produce (see Table 4:3). Excess argon in the doleritic dyke 105A is certainly plausible because the gabbro into which it is intruded undoubtedly contains excess argon (Macintyre et al., 1975 and this work). Excess argon could be released from the gabbro due to heating by the intruding dyke and it is possible that this argon would find its way into the crystallising dyke rock. An example of excess argon being incorporated into dykes, due to country-rock outgassing, has been presented by Dalrymple et al., (1975). If excess argon is the explanation for the age pattern produced by R1503, then the intermediate temperature age minimum (steps 6-9) gives a maximum estimate for the intrusion age (Table 4:3). Steps 6-9 give mean and total gas ages of  $61.6 \pm 0.9$  Ma (Table 6:11). As discussed above, ICD2 analysis of steps 6-9 gives a  $(40/36)_O > 295.5$ . and this may be considered as supporting evidence for the incorporation of excess argon in sample R1503. The calculated ICD2 age is  $60.9 \pm 0.9$ . However, as one of the criteria for a statistically meaningful age is that  $(40/36)_O$  should equal  $(40/36)_{\text{atm}}$ , the mean/total

gas age for these steps of  $61.6 \pm 0.9$  Ma is the preferred best (maximum) age estimate.

The possibility of R1503's age spectrum reflecting  $^{39}\text{K}$  recoil effects cannot be discounted because of the very fine-grained nature of this sample (see thin section description in Appendix 7). However, the age patterns do not conform to those usually reported for such effects.

Arrhenius diagrams have been plotted for sample R1503, however, they are all rather complicated with no well-defined linear correlations.

#### R1526 (G013)

The age spectrum for this sample is very intricate (Fig. 6:26). Thin-section examination shows that R1526 is subject to a high degree of alteration (see Appendix 7) and the high levels of chlorine-derived argon (the step chlorine age correction is up to 1.2 Ma) suggest a sea-water alteration. The age correction due to calcium interferences is 1 - 2 Ma for steps 1-25 but rises to 15 Ma for the last five steps. Bearing in mind the state of alteration of this sample, it is surprising that radiogenic  $^{40}\text{Ar}$  levels are over 80% for most of the gas release (total gas level equals 76%). As the alteration has not apparently added atmospheric argon, one might be tempted to suggest that radiogenic  $^{40}\text{Ar}$  has not been disturbed to any great extent.

The expected 60 Ma age of emplacement (typical age for Tertiary rocks in Britain) is apparently preserved at two points in the gas release - steps 18-20 and 29-30. The remaining steps give ages above and below this level - the highest and lowest recorded ages are 101 and 28 Ma respectively. All ICD2s plotted give MSWDs very much greater than the cut-off level (see Table 6:11 for the data analysis of all the steps). ICD3 was not useful for the interpretation of the data.

The observed pattern of ages may be explained in several ways. For ages less than 60 Ma:

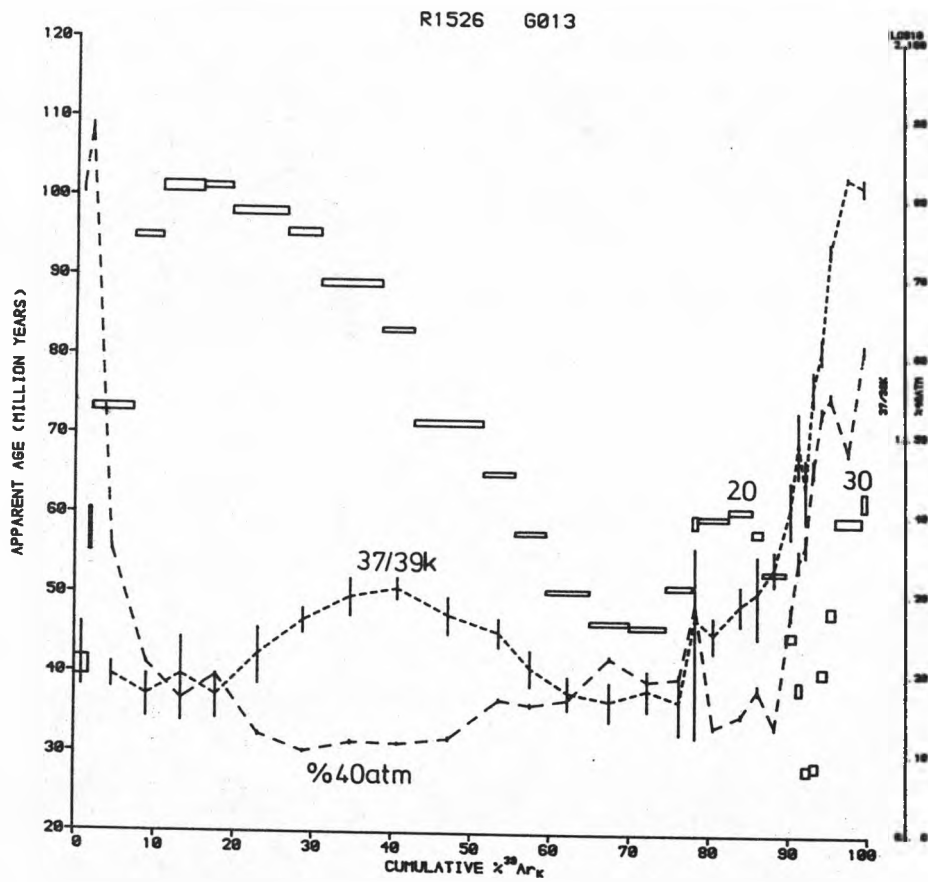


Fig. 6:26 Age spectrum for the Killala Bay doleritic dyke sample R1526 (G013)

- i)  $^{39}\text{K}$  recoil re-distribution
- ii)  $^{40}\text{Ar}$  loss, plus conversion of sites from low to high argon retentivity (perhaps due to alteration or irradiation effects)
- iii) Potassium addition due to sea water alteration. The total gas  $^{37}/^{39}\text{K}$  for R1526 ( $5.38 \pm 0.09$ ) is very much lower than that for the comparable dyke rock sample R1503 ( $13.45 \pm 0.02$ ); however this may simply represent compositional differences. One might expect that, if this were important, large amounts of atmospheric argon would also be added. Such atmospheric argon contamination is not observed.

For ages greater than 60 Ma:

- i)  $^{39}\text{K}$  recoil re-distribution/loss
- ii) Excess  $^{40}\text{Ar}$  contamination. Such excess would have to be magma-dissolved because dyke G013 intrudes argon-poor sedimentary strata rather than the excess-rich Killala Gabbro.

The favoured explanation for the pattern of ages is of the recoil re-distribution/loss of  $^{39}\text{K}$  with minor loss of  $^{40}\text{Ar}$  at low temperatures. The most prominent drop in age below 60 Ma coincides with an increase in the  $^{37}/^{39}\text{K}$  level which is thought to be related to pyroxene out-gassing (see Fig. 6:26). This observation supports the  $^{39}\text{K}$  recoil hypothesis because  $^{39}\text{K}$  captured in the marginal locations of pyroxene grains may well be reflected by an age decline. It is thought that the total gas age (all steps) of  $70.2 \pm 0.6$  Ma indicates that there is a net loss of  $^{39}\text{K}$ .

#### Conclusions for the Doleritic Dykes

None of the three samples gives a conclusive chronological interpretation. The best age estimate comes from R1503, which gives  $61.6 \pm 0.9$  Ma as a maximum value. This is consistent with the K-Ar whole-rock analyses presented by Macintyre et al., (1975) for similar rock samples.

b) The Killala Gabbro Felsic Dykelet

The dykelet rock, which consists of more than 80% untwinned feldspar, cross-cuts the Killala Gabbro and is itself cross-cut by one of the doleritic flash intrusions (see Fig. 6:23 for location). It is of the order of 10cm thick.

R1613 (G029)

The age spectrum of this potassium-rich sample is presented in Fig. 6:27a and it displays a pattern of gradually decreasing age over the majority of the gas release. The  $37/39_K$  peak at relatively low temperatures indicates the probable outgassing of minor plagioclase feldspar (see Killala Gabbro mineral separate sample R1621). It is interesting to note that the percentage radiogenic  $^{40}Ar$  reaches its highest levels in the segment of gas release corresponding to the  $37/39_K$  peak. Over the last 70% of  $^{39}Ar_K$  release, the age corrections due to calcium interferences are less than 0.1 Ma. However, where the  $37/39_K$  curve peaks, this correction reaches 0.6 Ma. The chlorine interference age correction is effectively zero for all steps.

The last ten steps give an apparently meaningful ICD2, indicating an age of  $57.8 \pm 1.6$  Ma (see Fig. 6:27b and Table 6:11). Although the  $(40/36)_O$  is not significantly greater than 295.5, it does have the effect of making the ICD2 age lie below each of the apparent step ages. This is due to the low radiogenic argon levels of the last ten steps (45 - 50%). Because of this and also the observation that step age is, in fact, noticeably declining over steps 21-30, the age of the large penultimate step is preferred as the best estimate for the emplacement age -  $58.7 \pm 1.1$  Ma. This must be regarded as a maximum estimate because of the generally declining pattern of ages. ICD3 data analysis was not found to be helpful.

As dykelet G029 is intruded into the Killala Gabbro (which is known to contain excess argon) and because it was probably derived from the same



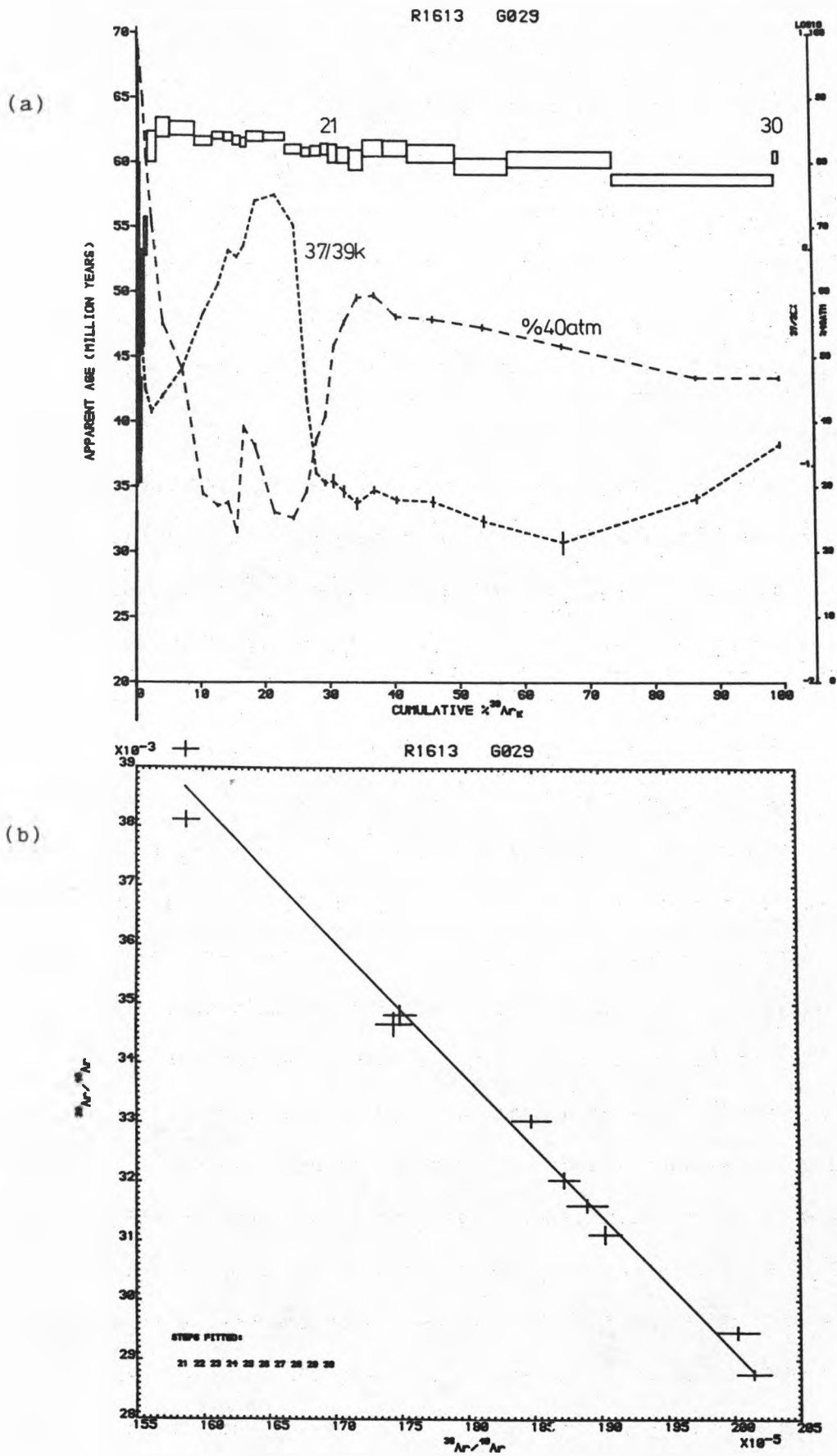


Fig. 6:27 Age spectrum (a) and ICD2 steps 21-30 (b) for the Killala Gabbro felsic dykelet sample R1613 (G029)

magma source as the Gabbro, the most likely explanation for R1613's age pattern is excess argon contamination. Recoil effects are unlikely to be important for a sample consisting largely of a single mineral with a typical grain size of 0.5 mm (see Appendix 7). The anomalously low ages recorded for the first 15% of  $^{39}\text{K}$  release probably indicate slight loss of radiogenic  $^{40}\text{Ar}$ . If this sample does indeed contain excess argon, why does it not produce a saddle-shaped age spectrum like many of the gabbro samples? (see below). The answer to this may lie in the pattern of  $^{39}\text{K}$  release which peaks markedly in the last few steps (thus any high temperature excess argon may be swamped by true radiogenic argon) or in the absence of mineral exsolution features (see description of Killala Gabbro plagioclase feldspar separate sample R1621). The recorded pattern of ages for R1613 largely conforms to that expected for simple excess argon contamination at grain margins e.g. Harrison & McDougall (1980b), Dallmeyer & Rivers (1983). Such an interpretation is supported by the observation that the highest ages are recorded as the  $^{37}/^{39}\text{K}$  level steeply rises. The latter marks the onset of plagioclase outgassing and this mineral is thought to constitute the rims of the zoned feldspar observed in thin-section (see Appendix 7). A similar zoning to this was observed for Droimchogaidh sample 238P, in which the feldspar grain rims were positively identified as plagioclase feldspar.

The  $^{39}\text{K}$  and  $^{40}\text{K}$  Arrhenius diagrams for R1613 were very similar, giving linear correlations consisting of a few steps only. Parameters deduced from these Arrhenius diagrams are not apparently meaningful. However, the  $^{37}\text{K}$  Arrhenius diagram (see Fig. 6:28) gives a strong linear correlation for steps 5-16, which constitute the rising edge of the  $^{37}/^{39}\text{K}$  peak. The calculated activation energy of  $62 \text{ kcal mol}^{-1}$  and  $D_0/a^2$  of  $2.5 \times 10^7 \text{ s}^{-1}$  (MSWD = 1.0) are used to calculate a closure temperature of  $410^\circ\text{C}$  (assuming a cooling rate of  $10^4^\circ\text{C Ma}^{-1}$ ). This value is very

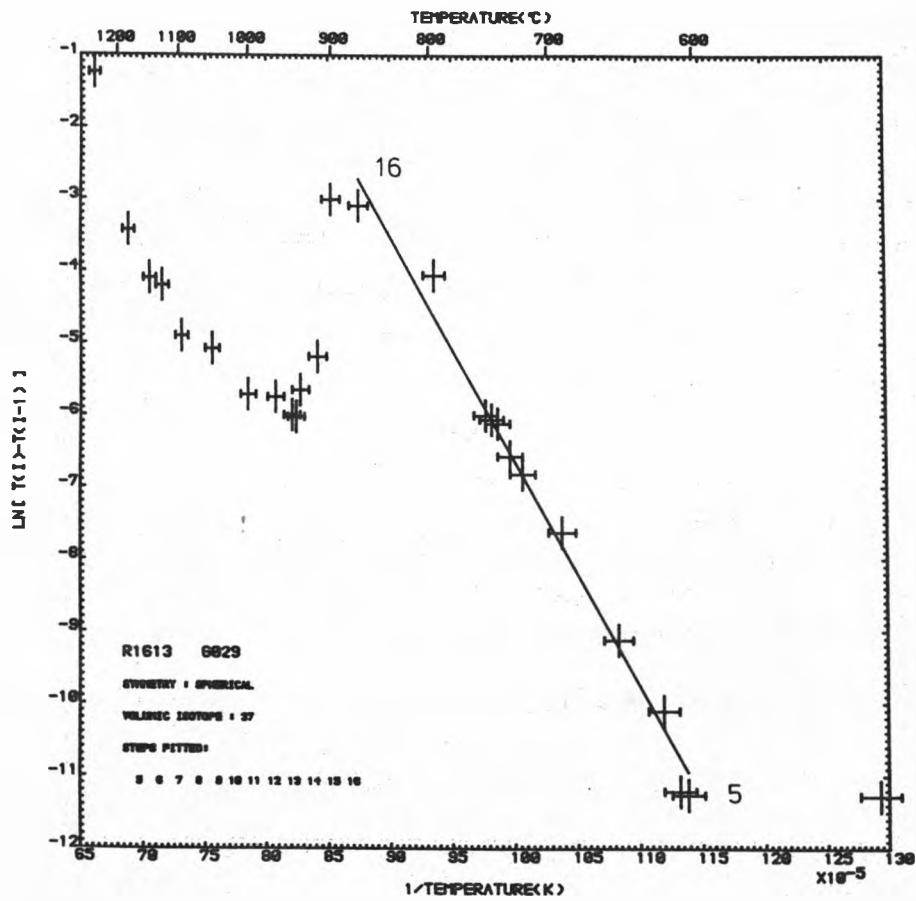


Fig. 6:28 Arrhenius diagram for the 37 release of the Killala Gabbro felsic dykelet sample R1613 (G029)

high compared to expected values for the plagioclase feldspar with which the  $37/39\text{K}$  peak is identified (see Table 4:1). The high calculated closure temperature is probably explained by the rapid cooling rate which is assumed for the dykelet.

#### Conclusions for the Killala Gabbro Felsic Dykelet

The best age estimate for sample R1613 is  $58.7 \pm 1.1$  Ma. Because of the shape of the age spectrum and the likely presence of excess argon, this age is treated as a maximum estimate for the age of intrusion. This interpretation is consistent with that for the younger doleritic dykes for which the best maximum age estimate was  $61.6 \pm 0.9$  Ma.

#### c) The Gabbro Analyses

R1466 (106A), R1520 (RG), R1571 (RG-pyroxene) and R1621 (RG-plagioclase feldspar) are samples from the Killala Gabbro itself, whereas R1382 (124NA), R1505 (124NA), R1577 (124NA) and R1467 (128B) are samples from the feeder dykes on the east side of Killala Bay. Sampling locations are displayed in Fig. 6:23.

Six of the above samples give a saddle-shaped age spectrum which is thought to be diagnostic of excess argon (Table 4:3). Anomalously high ages at high temperatures are not thought to indicate a multi-stage history because there is no geological evidence for a metamorphism of the gabbro and country rock (P. Mohr, pers. comm.). Where a sample gives a saddle-shaped age spectrum, the intermediate temperature age minimum is expected to give a maximum estimate for the time of crystallisation (Lanphere & Dalrymple, 1976). The chronological interpretation of the  $^{40}\text{Ar}-^{39}\text{Ar}$  data from the gabbro analyses is discussed at the end of this section.

#### Killala Gabbro Whole-Rock Samples

##### R1466 (106A)

This sample gives a saddle-shaped age spectrum (see Fig. 6:29a) with

Irradiation no. (Locality no.)	Steps	% <sup>39</sup> K	Total gas age (Ma)	Mean age (Ma) (step ages weighted by 1/variance)	Age (Ma)	ICD2 parameters (40/36) <sub>0</sub>	MSWD
R1466(106A)	Al(1-19) 4-11	100	87.0 ± 1.5	73.5 ± 13.0	63.9 ± 3.3	329.0 ± 27.9	65.8
		60	69.9 ± 1.3	68.6 ± 2.7	64.8 ± 1.6	310.2 ± 10.7	3.3
R1520(RG)	Al(1-31) 15-27	100	70.7 ± 0.9	66.4 ± 4.0	63.0 ± 1.2	326.2 ± 11.2	43.3
		54	64.7 ± 0.9	63.7 ± 1.2	62.8 ± 0.9	305.7 ± 5.7	3.4
R1571(RG- pyroxene)	Al(1-18) 13-18	100	129.6 ± 5.7	84.5 ± 47.5	57.0 ± 8.3	310.6 ± 66.1	2.0
		48	137.0 ± 7.4	81.1 ± 48.4	42.4 ± 5.1	318.5 ± 55.6	0.7
R1621(RG- plagioclase feldspar)	Al(1-20) 10-16	100	78.3 ± 2.5	62.1 ± 8.1	57.4 ± 2.8	308.6 ± 20.0	20.0
		39	57.6 ± 1.7	57.5 ± 1.8	58.0 ± 2.2	294.3 ± 13.4	0.5
R1382(124NA)	Al(1-9) 3-9 5-9	100	65.8 ± 0.6	63.3 ± 5.3	60.8 ± 1.0	318.9 ± 9.3	5.1
		99	65.1 ± 0.6	63.3 ± 4.9	60.0 ± 0.7	326.9 ± 6.7	1.7
		87	62.3 ± 0.6	62.2 ± 1.2	60.4 ± 1.6	320.1 ± 28.5	1.6
R1505(124NA)	Al(1-18) 2-10	100	66.8 ± 0.9	65.8 ± 3.6	63.4 ± 1.2	306.2 ± 10.7	14.8
		70	63.9 ± 0.7	63.8 ± 1.0	64.2 ± 0.8	293.2 ± 6.6	2.2
R1577(124NA <sup>+</sup> )	Al(1-21, ex 17) 3-6	100	78.2 ± 1.9	66.5 ± 2.4	65.2 ± 0.7	302.0 ± 3.1	3.1
		31	66.2 ± 0.6	66.1 ± 0.6	65.5 ± 0.6	300.3 ± 3.7	0.1
R1467(128B)	Al(1-13) 2-5 6-10	100	62.6 ± 1.3	61.8 ± 2.2	62.3 ± 1.4	292.2 ± 8.3	14.1
		30	59.7 ± 1.2	59.6 ± 1.4	59.6 ± 1.4	295.5 ± 8.8	3.1
		44	63.6 ± 1.2	63.3 ± 1.4	61.3 ± 1.2	320.4 ± 5.4	0.2

+ denotes crushed sample

Table 6:12 Parameters calculated for gabbroic samples from Killala Bay

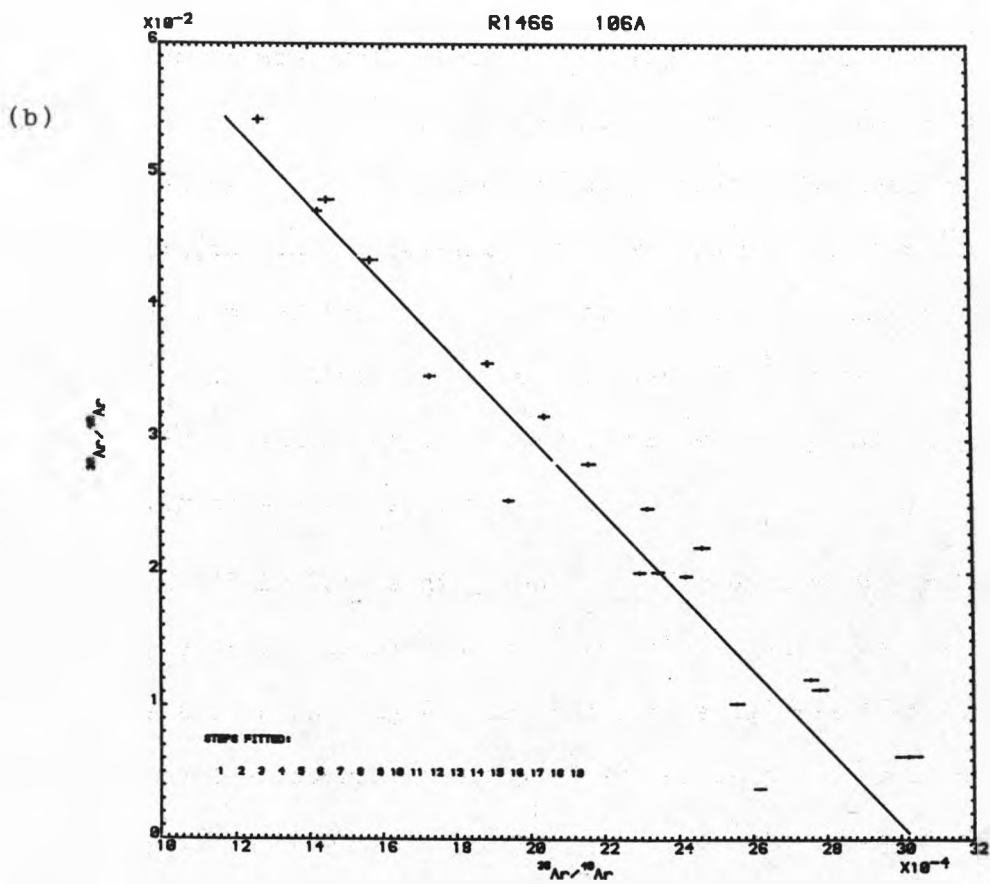
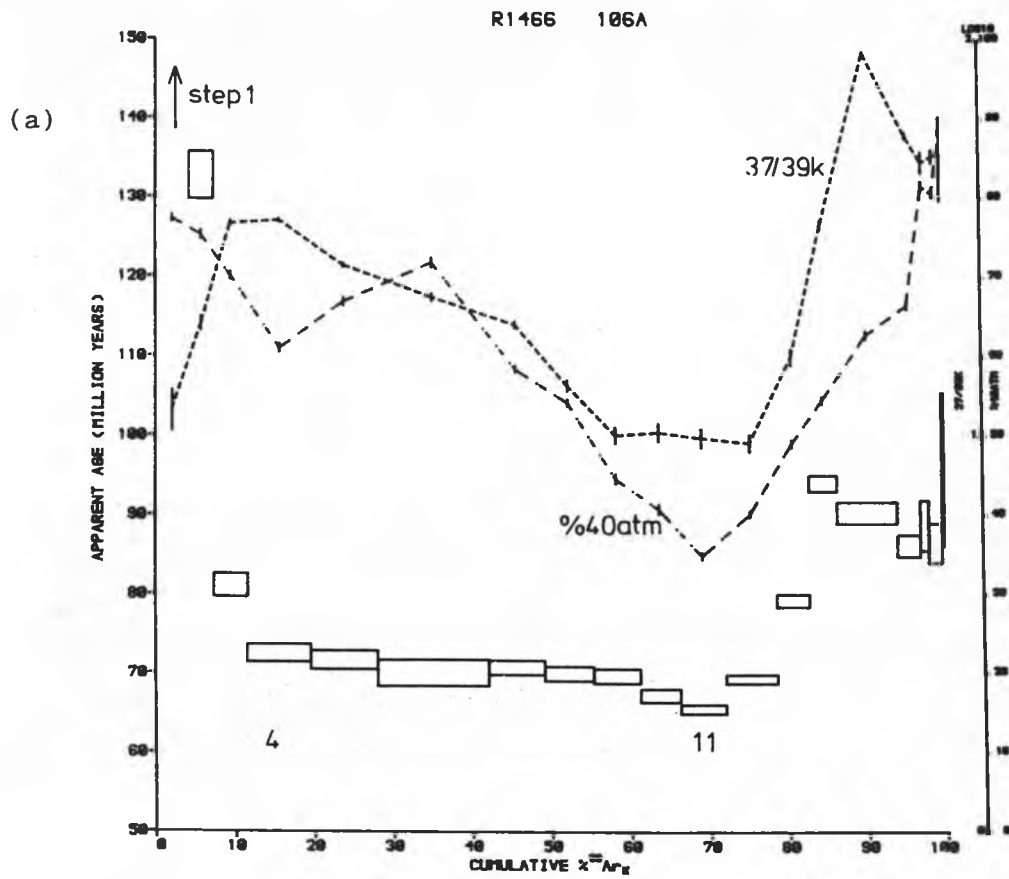


Fig. 6:29 Age spectrum (a) and ICD2 steps 1-19 (b) for the Killala Gabbro whole-rock sample R1466 (106A)

a saddle minimum of  $65.5 \pm 1.2$  Ma. The total gas age (all steps) is  $87.0 \pm 1.5$  Ma. The age correction due to calcium interferences is as high as 15 Ma for the initial steps,  $\approx 5$  Ma for the intermediate temperature steps and up to 40 Ma for the last six steps. The chlorine age correction is as high as 0.5 Ma in some cases but is generally negligible. The  $^{37}/^{39}\text{K}$  pattern (Fig. 6:29a) with peaks at low and high temperatures indicates that the whole-rock sample is dominated by plagioclase and pyroxene (see section on Killala Gabbro mineral separates below). Over much of the gas release the  $^{37}/^{39}\text{K}$  and  $\%^{40}\text{Ar}_{\text{atmospheric}}$  curves follow the age variation. The latter correlation is often indicative of initial argon on a non-atmospheric composition.

The two-dimensional isotope correlation diagram for all the steps is very scattered (see Fig. 6:29b and Table 6:12). This is a common feature of these gabbro analyses and is expected where a sample contains excess argon. ICD2 analysis of steps 4-11 gives an MSWD  $< 3.5$  but a  $(^{40}/^{36})_0$  greater than the atmospheric ratio (Table 6:12) which makes the calculated age unacceptable. Other step selections with an MSWD below the cut-off are unacceptable due to this and/or the small percentage of  $^{39}\text{K}$  involved. ICD3-Plot 2 shows significantly reduced MSWD values compared with ICD2 and the other three-dimensional isotope correlation diagrams. However, where MSWD  $< 3.5$  either  $^{40}\text{Ar}/^{36}\text{Cl}$  is negative or the calculated age is geologically meaningless. Thus ICD3 analysis adds nothing to the interpretation of R1466's data.

The Arrhenius diagrams for R1466 are very complex and many of the data point linear correlations give geologically unacceptable closure temperatures (in some cases the calculated closure temperature is negative). The  $^{40}\text{Ar}$  and  $^{39}\text{K}$  Arrhenius diagrams are very similar and thus of no use in deciding which of the isotopes is disturbed (see Appendix 2).

R1520 (RG)

This sample has the highest potassium content and lowest total gas  $37/39\text{K}$  of all the gabbroic samples giving saddle-shaped spectra (the former was deduced from the comparison of total gas  $39\text{K}$  levels). R1520 has a total gas age of  $70.7 \pm 0.9$  Ma and a saddle-minimum age of  $63 \pm 1$  Ma. Age variation is largely followed by the %  $^{40}\text{Ar}$  atmospheric curve (Fig. 6:30). The age correction due to calcium interferences is less than 2 Ma for all steps, whereas that for chlorine interferences is less than 0.1 Ma for the majority of steps (the highest recorded value is 0.27 Ma).

The ICD2 for all steps is again scattered but analysis of steps 15-27 gives an MSWD < 3.5 (Table 6:12). However,  $(40/36)_o = 305.7 \pm 5.7$  is significantly greater than 295.5 ( $1\sigma$  level) and thus the age of  $62.8 \pm 0.8$  Ma is not considered meaningful. It is possible to pick out several linear correlations on an ICD2 plot of all steps. However, they only consist of a small number of steps, constituting a small percentage of the total  $39\text{K}$  release, and often give unacceptable ICD2 ages and/or  $(40/36)_o$  values. Such linear correlations are therefore not considered to be geologically meaningful. ICD3 analysis of sample data was not found to be useful.

Killala Gabbro Mineral Separate SamplesR1571 (RG-pyroxene)

This potassium-poor mineral separate gives the highest total gas age of all the gabbro samples -  $129.6 \pm 5.7$  Ma. However, it also gives the lowest recorded saddle minimum age of  $50 \pm 15$  Ma (see Fig. 6:31). The calcium interference age correction is  $\approx 1$  Ma ( $37/39\text{K} < 10$ ) over the first 14 steps but dramatically increases over the remaining four steps to reach 640 Ma ( $37/39\text{K}$  over 4000). The marked upturn in the  $37/39\text{K}$  curve undoubtedly represents the onset of argon release from the true pyroxene, which was identified as augite. The majority of the  $39\text{K}$  release probably corresponds to argon released from the often



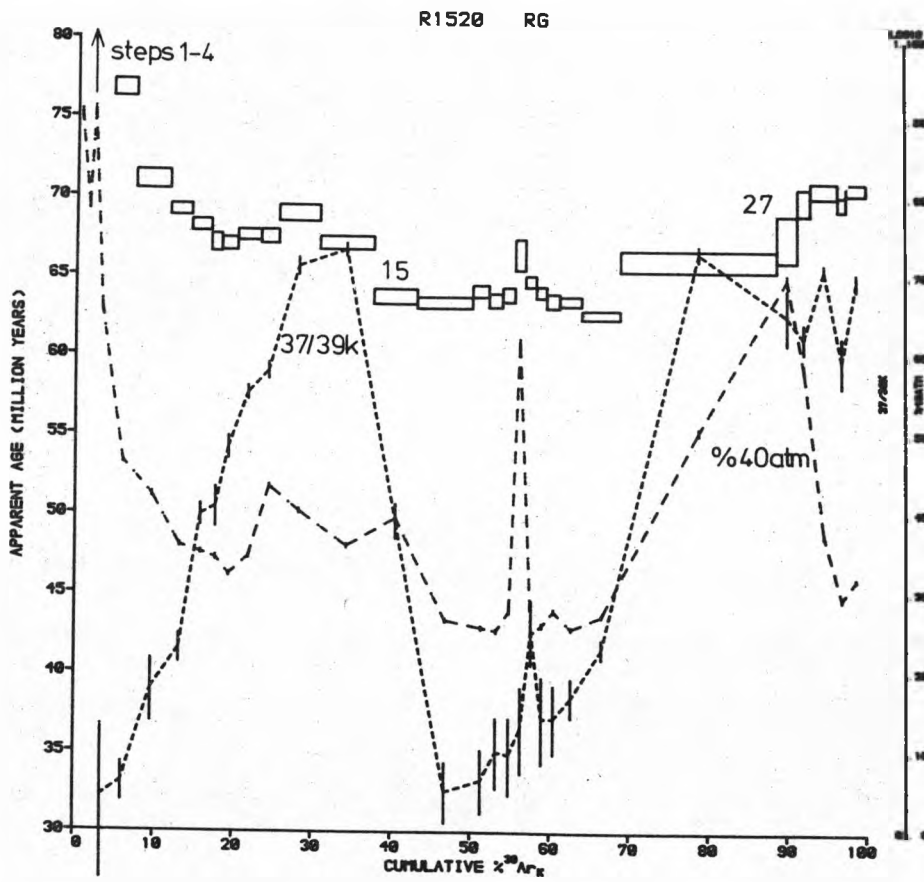


Fig. 6:30 Age spectrum for the Killala Gabbro whole-rock sample R1520 (RG)

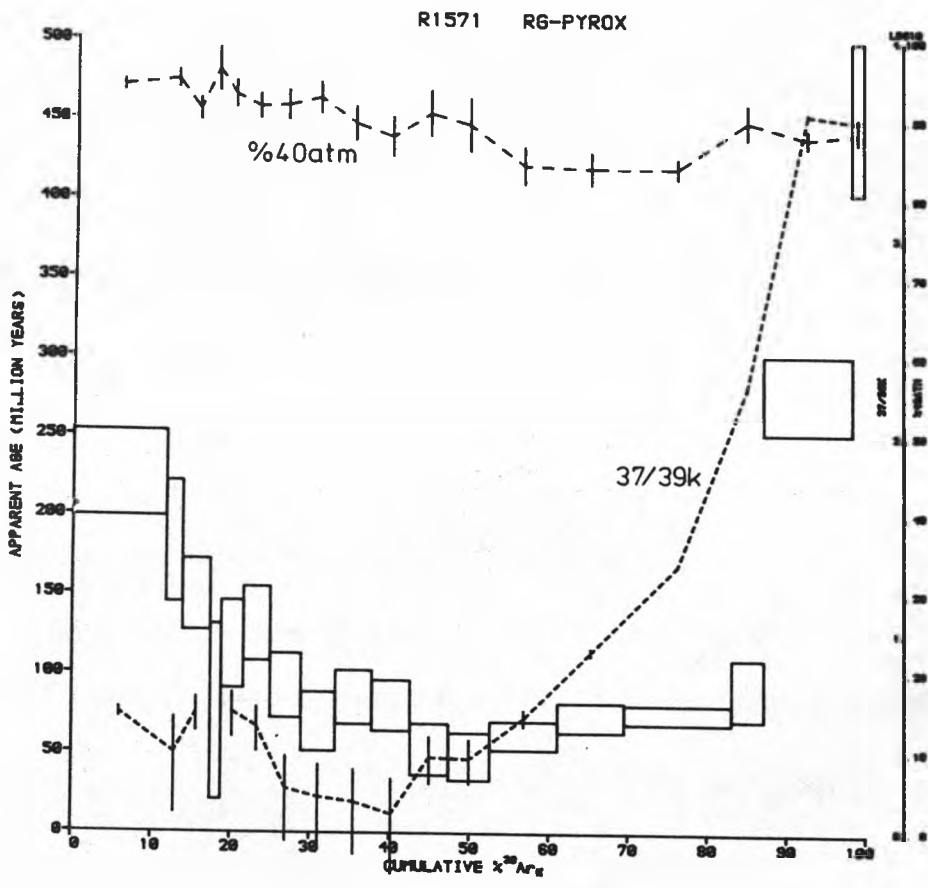


Fig. 6:31 Age spectrum for the Killala Gabbro mineral separate sample R1571 (RG-pyroxene)

potassium-rich alteration which is found in the cracks of the pyroxene grains - see scanning electron microscope work for sample 124NA in Appendix 6. This material corresponds in its elemental contents to biotite, which was positively identified in Killala Gabbro thin sections. The level of radiogenic  $^{40}\text{Ar}$  is no greater than 15% for any of the steps and this results in large errors in individual step ages (typically 20 Ma).

ICD2 analysis of all the steps gives an MSWD  $< 3.5$ ,  $(40/36)_0 \approx 295.5$  and an age of  $57.0 \pm 8.3$  Ma. This age is significantly different from the calculated total gas age which reflects the very low levels of radiogenic argon. Selecting steps giving more well-defined linear correlations, one finds that calculated ages are geologically unreasonable (see example in Table 6:12). Corresponding ICD3 analyses often give lower MSWDs, but the calculated ages are meaningless (in one case a negative age was computed). Isotope correlation diagram analysis as a whole, therefore, is not helpful for the chronological interpretation of sample R1571's  $^{40}\text{Ar}$ - $^{39}\text{Ar}$  stepwise degassing data.

The  $^{39}\text{K}$  Arrhenius diagram for R1571 displays a well-defined linear correlation over steps 4-14 (Fig. 6:32a). With an activation energy  $E = 25 \text{ kcal mol}^{-1}$  and  $D_0/a^2 = 8.4 \times 10^{-2} \text{ s}^{-1}$  (MSWD = 3.1), a closure temperature of  $205^\circ\text{C}$  is calculated for a cooling rate of  $10^4^\circ\text{C Ma}^{-1}$ .

This figure is rather low for biotite; however, this may be explained by the very small grain size of the material in the pyroxene cracks - the cracks themselves are typically only  $20\mu$  across. The observation of a relatively simple pattern of data points on the  $^{39}\text{K}$  Arrhenius diagram does suggest that this isotope is relatively undisturbed. The Arrhenius diagram for  $^{40}\text{Ar}$  release, on the other hand, produces no sizeable linear segments (Fig. 6:32b) and this is thought to be consistent with the presence of excess argon in this sample. It is only possible to plot  $^{37}\text{Ar}$  Arrhenius diagram data points for steps 15-17

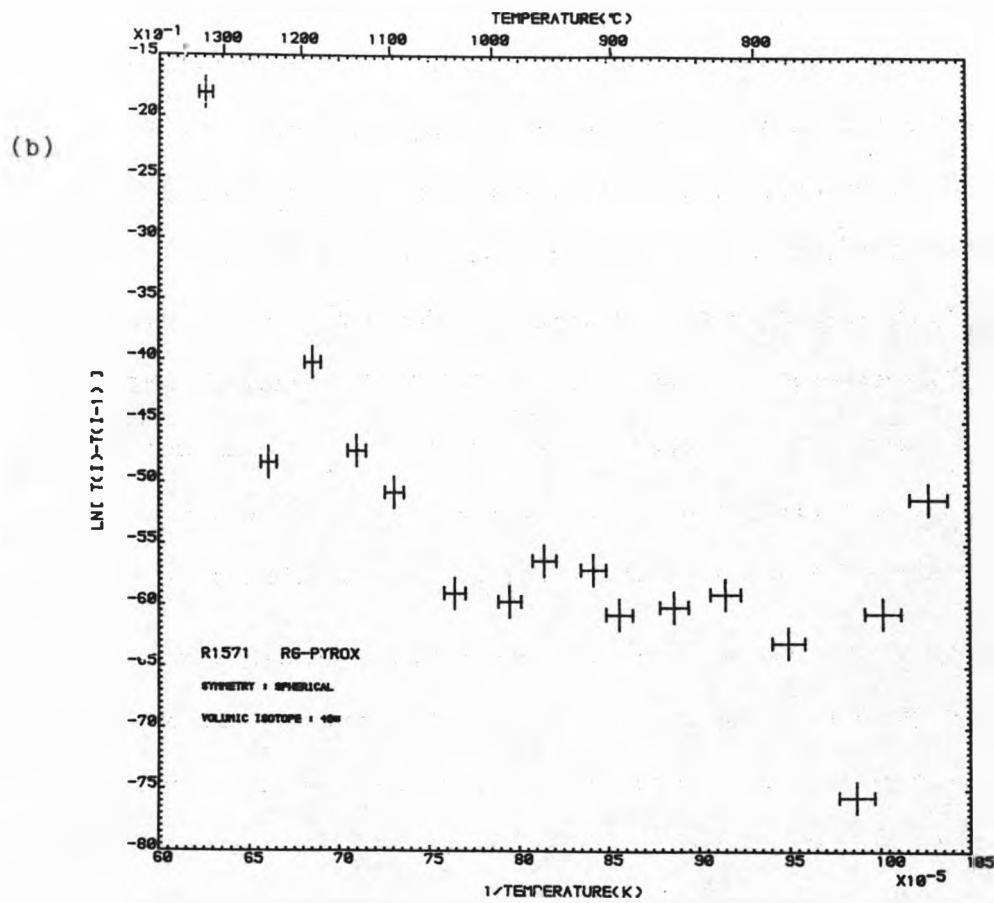
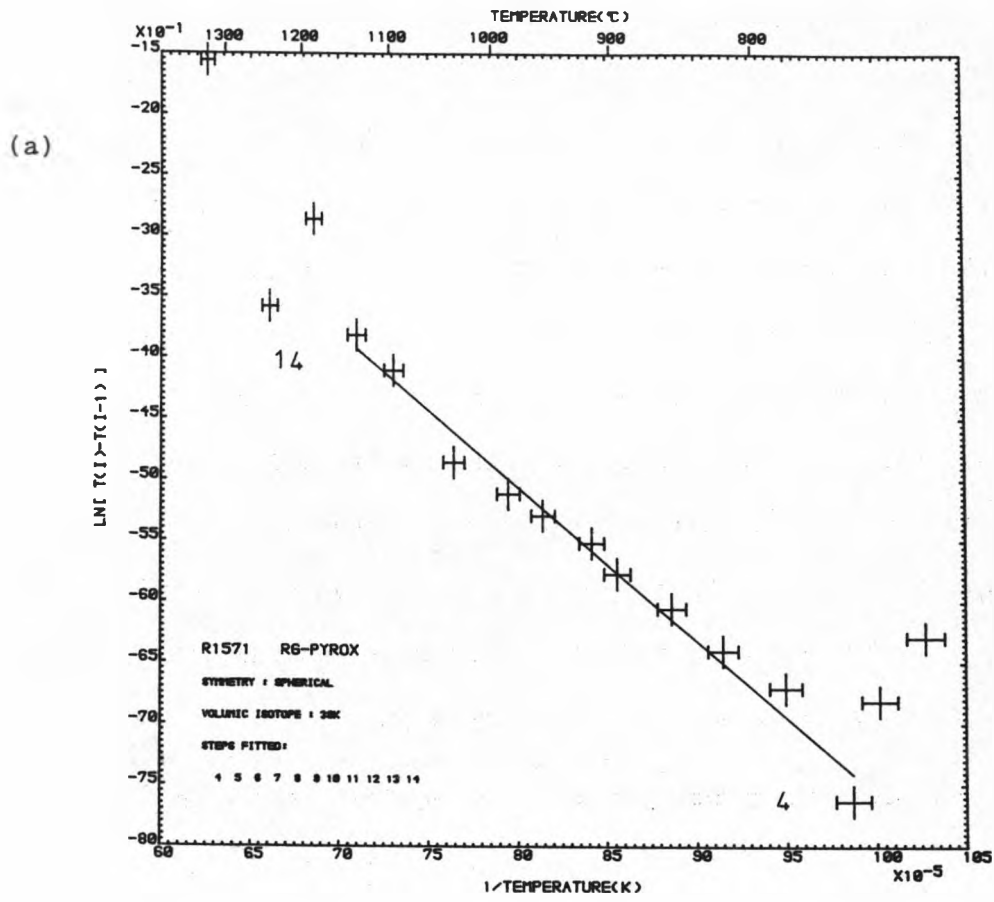


Fig. 6:32 Arrhenius diagrams for the Killala Gabbro mineral separate sample R1571 (R6-pyroxene) (a) 39K (b) 40\*

because steps 1-14 account for less than 0.5% of the total 37 release. These define an activation energy  $E = 348 \text{ kcal mol}^{-1}$ ,  $D_0/a^2 = 1.7 \times 10^{43} \text{ s}^{-1}$  and an MSWD = 8.4. For a cooling rate of  $10^4 \text{ }^\circ\text{C a}$  closure temperature of  $1055 \text{ }^\circ\text{C}$  is calculated. This very high value is consistent with the observation that pyroxene is one of the first minerals to crystallise in a basic melt.

#### R1621 (RG-plagioclase feldspar)

R1621 gives a saddle-shaped age spectrum with a saddle minimum of 56-59

Ma which accounts for nearly 40% of the  $^{39}\text{K}$  release (see Fig. 6:33a). However, the total gas age is still high at  $78.3 \pm 2.4 \text{ Ma}$ . The  $^{37}/^{39}\text{K}$  pattern is very distinct with the majority of 37 release taking place at low temperatures ( $<755 \text{ }^\circ\text{C}$ ). Similar plagioclase  $^{37}/^{39}\text{K}$  patterns have also been reported by Dalrymple & Lanphere (1974), Dalrymple et al., (1975), Harrison & McDougall (1981), Berger & York (1981) and Feraud et al., (1982). The age correction due to calcium interferences varies between 2 - 12 Ma, and that due to chlorine is typically less than 0.1 Ma and thus negligible.

The ICD2 analyses of all the steps extracted and those that constitute the saddle minimum (steps 10-16) are presented in Table 6:12. For the latter, the MSWD is less than 3.5 and the  $(^{40}/^{36})_0 \approx 295.5$ ; therefore the calculated age of  $58.0 \pm 2.2 \text{ Ma}$  is considered to be meaningful (see Fig. 6:33b for ICD2 plot). The MSWDs for ICD3-Plots 1 and 3 are generally higher than for the corresponding ICD2. On the other hand, for ICD3-Plot 2, values are found to be consistently lower. However, ages calculated from ICD3-Plot 2 are very low (down to 43 Ma) and they are not geologically meaningful.

The three Arrhenius diagrams for R1621 are presented in Fig. 6:34 and the calculated diffusion parameters and closure temperatures are listed in Table 6:13. Although the Arrhenius diagram for  $^{40}\text{*}$  release does not

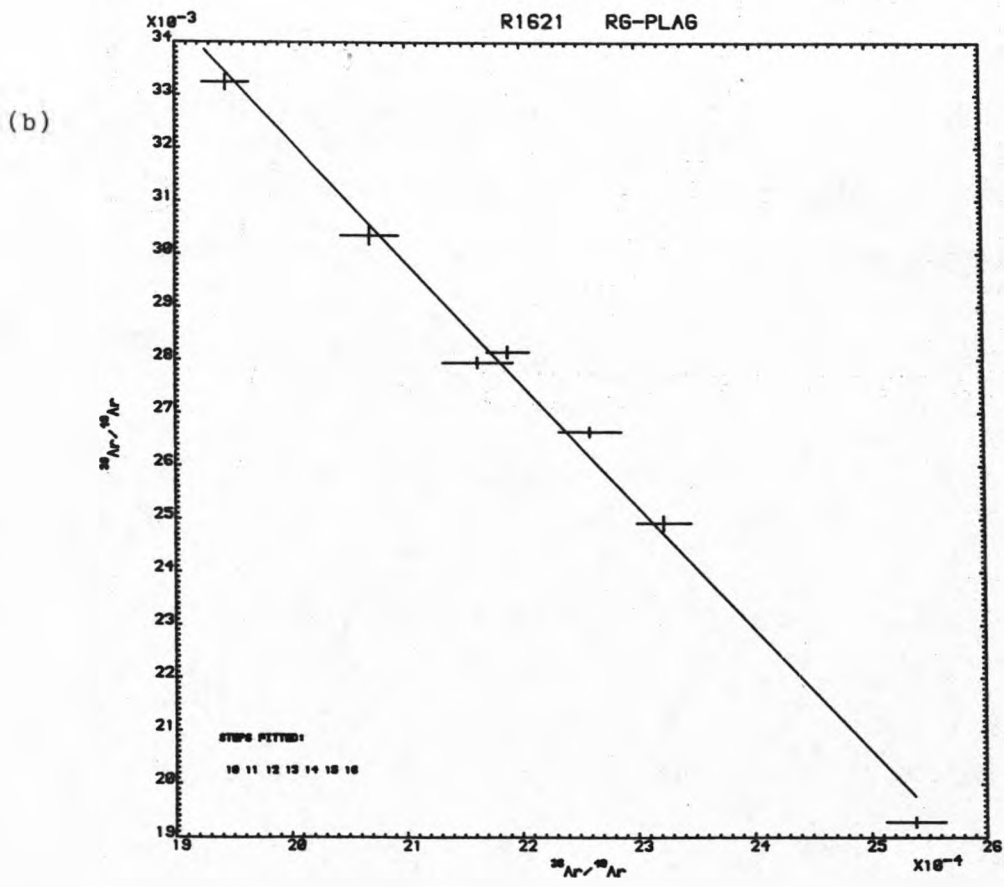
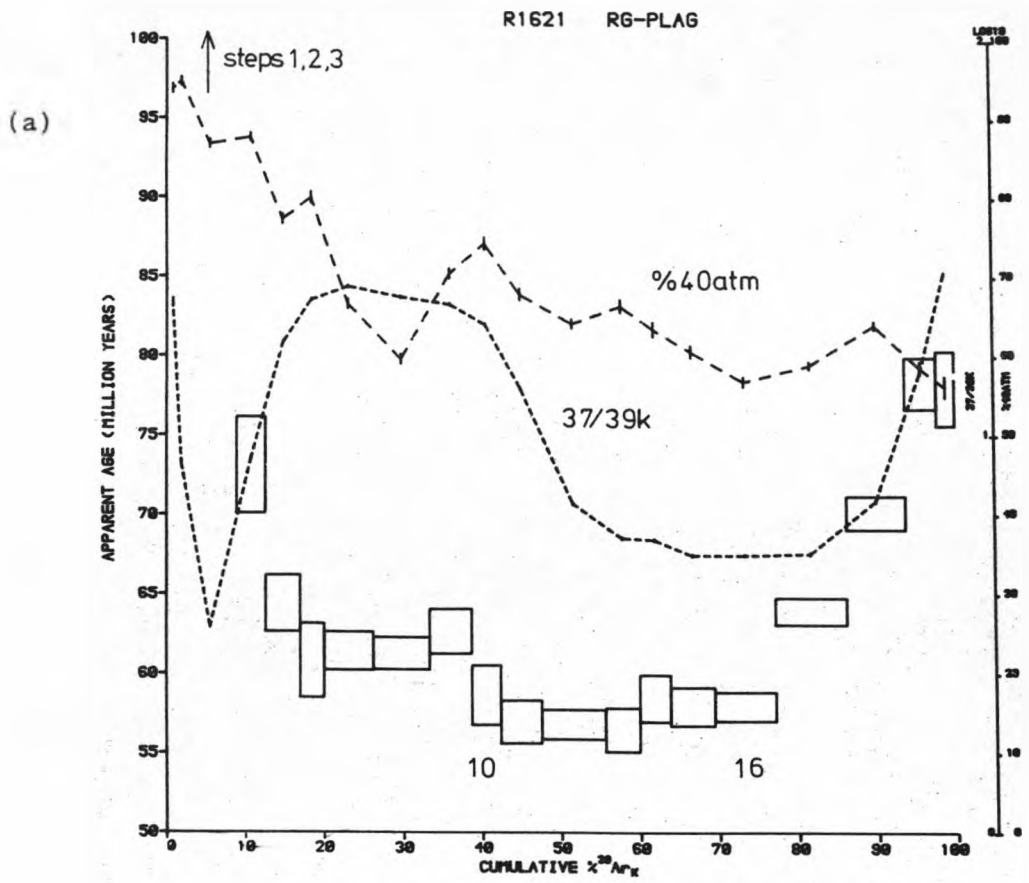


Fig. 6:33 Age spectrum (a) and ICD2 steps 10-16 (b) for the Killala Gabbro mineral separate sample R1621 (RG-plagioclase feldspar)

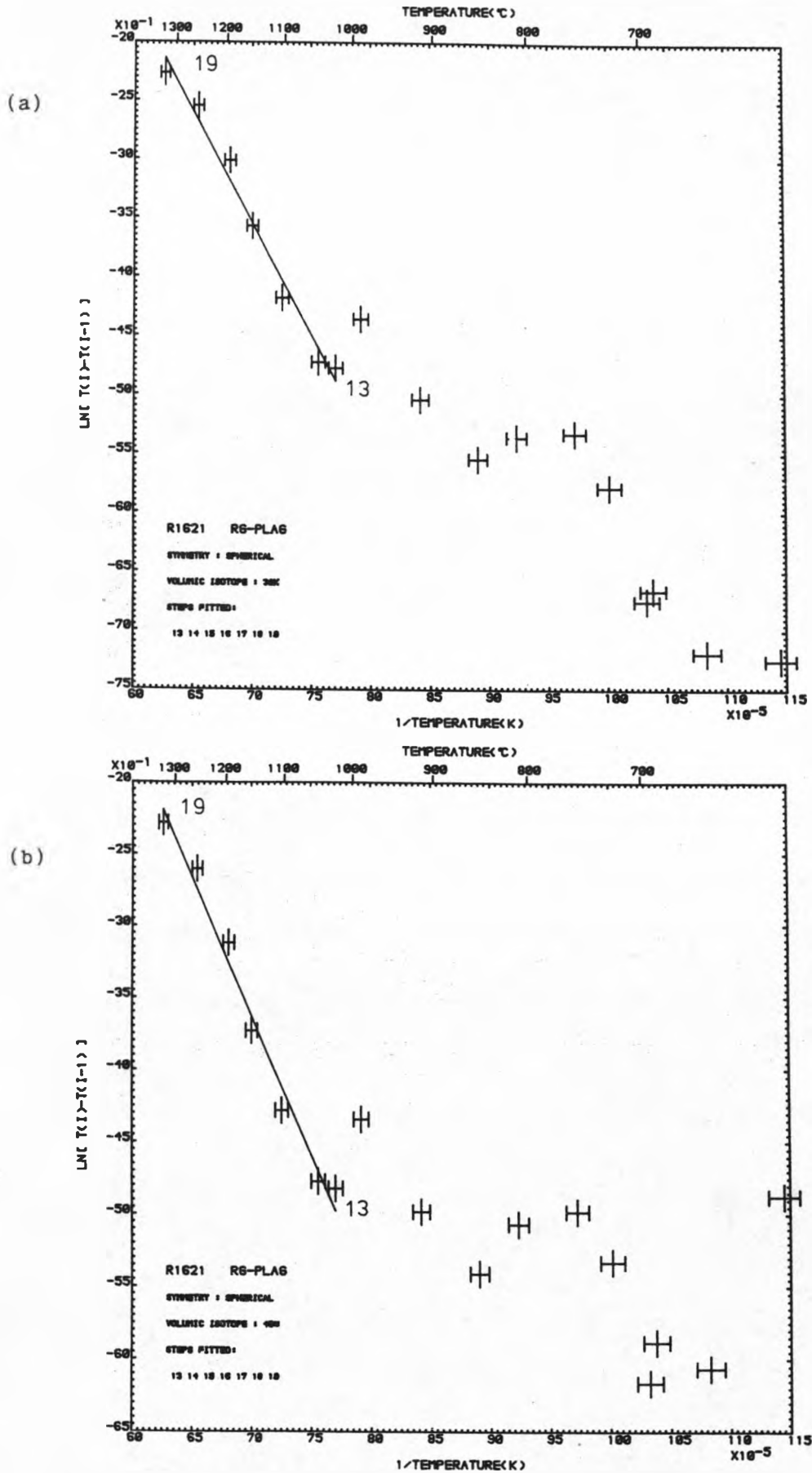


Fig. 6:34 Arrhenius diagrams for the Killala Gabbro mineral separate sample R1621 (RG-plagioclase feldspar) (a) 39K (b) 40\* (c) 37

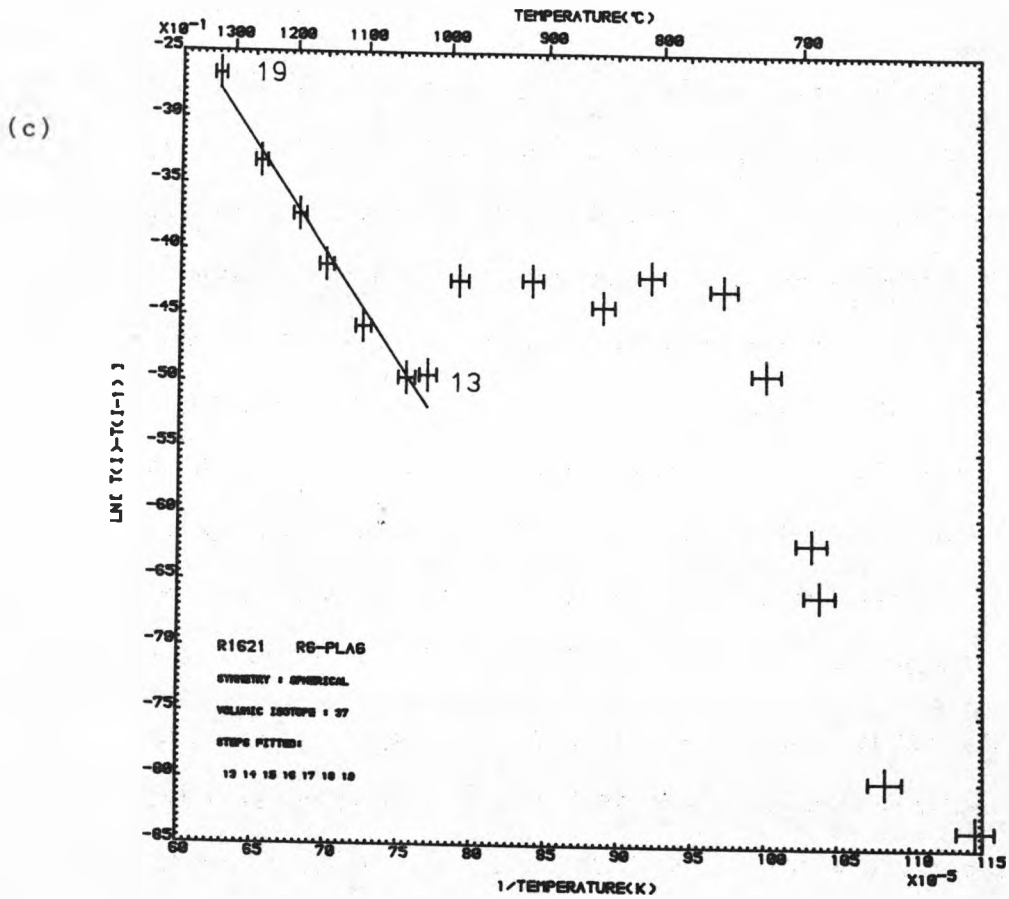


Fig. 6:34 continued



Isotope release	Steps	E (kcal mol <sup>-1</sup> )	D <sub>0</sub> /a <sup>2</sup> (s <sup>-1</sup> )	MSWD	Closure temperature (°C) - cooling rate assumed to be 10 <sup>-4</sup> °C Ma <sup>-1</sup>
39k	4-8	36	1.3 * 10 <sup>2</sup>	1.2	265
	13-19	38	9.1	2.8	340
40*	13-19	38	1.1 * 10 <sup>1</sup>	2.6	340
37	4-8	69	3.8 * 10 <sup>9</sup>	0.3	415
	13-19	33	1.1	2.8	300

Table 6:13 Diffusion parameters and closure temperatures calculated for Killala Gabbro mineral separate sample R1621 (RG-plagioclase feldspar)

give a low temperature correlation in the same way as  $^{39}\text{K}$ , it does produce a well-defined high temperature linear correlation. The calculated diffusion parameters are very similar to those computed for the  $^{39}\text{K}$  high temperature linear correlation. The inferred closure temperature may be geologically meaningful but the reason why the  $^{39}\text{K}$  and  $^{40}\text{K}$  plots are so similar, over a portion of gas release marked by an increasing pattern of ages, is not fully understood. The Arrhenius diagram for  $^{37}\text{Ar}$  release is distinctly different to the other two. Steps 4-8 define a linear correlation giving a very high activation energy and closure temperature (Table 6:13). The calculated closure temperature of  $415^\circ\text{C}$  is not compatible with published estimates for plagioclase feldspar which range between  $200 - 260^\circ\text{C}$  (see Table 4:1). However, it is comparable with the closure temperature calculated from the 37 release of sample R1613, which was also thought to be associated with plagioclase outgassing. The high temperature linear correlation for the 37 release gives a lower activation energy and closure temperature. The latter results are similar to those calculated for the corresponding  $^{39}\text{K}$  and  $^{40}\text{K}$  Arrhenius diagram high temperature linear correlations. Because of this similarity, all three argon isotopes are probably derived from the same source over the high temperature gas release.

The Arrhenius diagrams for the Killala Gabbro plagioclase are similar to those reported by Harrison & McDougall (1981) for metamorphic plagioclases in which saddle-shaped age spectra were also observed. In each case, for both the  $^{39}\text{K}$  and 37 Arrhenius diagrams, the high temperature linear correlation yields an activation energy of approximately  $35 \text{ kcal mol}^{-1}$ . Also, the ratio of low temperature activation energies for  $^{39}\text{K}$  and 37 release is, in each case, approximately 0.5. The only difference between the two sets of plagioclase Arrhenius diagrams is that for Harrison & McDougall's (1981) work the high temperature linear

correlations have an activation energy similar to the low temperature 37 release. For the Killala Gabbro plagioclase, the high temperature activation energies correspond to the low temperature 39K activation energy.

Harrison & McDougall (1981) suggested that their Arrhenius diagrams indicate the presence of more than one phase in the plagioclase feldspar. As the Killala Gabbro plagioclase Arrhenius diagrams are very similar to Harrison & McDougall's (1981), such an inference is also made in this study. Harrison & McDougall (1981) were, in fact, able to observe compositional exsolution lamellae in one of their plagioclase samples using a transmission electron microscope. The lamellae dimensions were found to be of the order of 10's nanometres. They went on to suggest that excess argon contained in lamellae peripheries may explain, not only the low temperature excess argon in a sample displaying a saddle-shaped age spectrum, but also the high temperature excess. A special type of location for diffusive excess contamination was postulated (anion vacancies) which displays rapid low temperature diffusion. However, because of the diffusion-temperature dependence, a relatively high retentivity at the temperatures used in stepwise degassing experiments was hypothesised. In this way, low temperature diffusive excess argon contamination would not be released in a stepwise degassing experiment until the high temperature steps were extracted.

This explanation of saddle-shaped age spectra may also be valid for the igneous Killala Gabbro plagioclase. That is, if the excess contamination can be considered as a diffusive process from the residual liquid phase of the crystallising melt.

It was not possible in the scanning electron microscope work of this study to directly observe exsolution features in the Killala Gabbro plagioclase. This was because the primary electron beam width used

was between 100 - 200 nm. This is very much greater than the lamellae dimensions which could be predicted from Harrison & McDougall's (1981) work. As Harrison & McDougall (1981) pointed out, pyroxenes are well known to exsolve in both igneous and metamorphic environments. Thus, the saddle-shaped age spectrum of the Killala Gabbro pyroxene separate (and all the whole-rock samples) may be explained in terms of a diffusive excess contamination at the margins of exsolution lamellae.

#### Feeder-dyke Gabbro Whole-rock Samples

Three of the four samples in this category were taken from the largest of the feeder dykes on the east side of Killala Bay. This dyke varies in width from 5 to 10 metres and is numbered 124NA. The fourth sample analysed was collected from the dyke 128B. The locations of these two dykes are marked on Fig. 6:23.

#### R1382 (124NA)

R1382 was one of the pilot samples and it was outgassed in just nine steps, 60% of the  $^{39}\text{K}$  released being contained in steps 7 and 8.

$^{37}\text{Ar}$  was recorded only for the last three steps for which the calcium-interference age correction is no more than 1.5 Ma. Even though the total gas age is quite high, at  $65.8 \pm 0.6$  Ma, this sample's age spectrum does not display a saddle-shaped form (see Fig. 6:35a). The observed pattern of declining age essentially follows the %  $^{40}\text{atmos-}$ pheric curve, which suggests the presence of initial argon with a non-atmospheric composition (see Section 4:4).

ICD2 analysis of steps 3-9 and 5-9 are presented in Table 6:12. The former constitutes  $\approx 99\%$  of the  $^{39}\text{K}$  release and gives an MSWD of 1.7. However, the  $(^{40}/^{36})_0$  is significantly greater than the atmosphere  $^{40}/^{36}$  ratio and thus the calculated age is not accepted as meaningful. The latter step selection gives a  $(^{40}/^{36})_0$  statistically indistinguishable from  $(^{40}/^{36})_{\text{atmospheric}}$  and an MSWD of 1.6 (the ICD2 is displayed

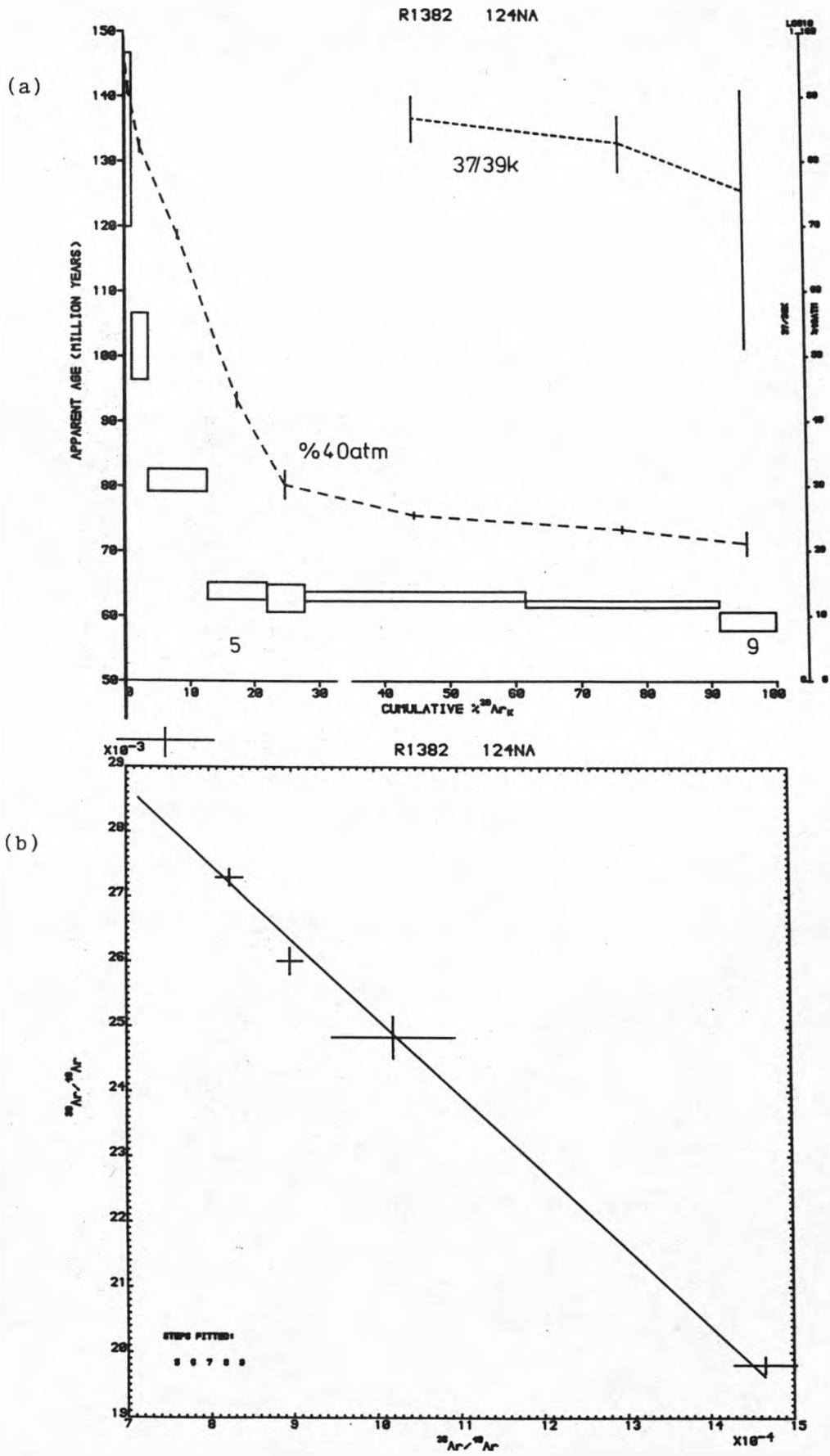


Fig. 6:35 Age spectrum (a) and ICD2 steps 5-9 (b) for the Killala Gabbro feeder dyke sample R1382 (124NA)

in Fig. 6:35b). The calculated age of  $60.4 \pm 1.6$  Ma should be treated as a maximum age estimate because of the likely importance of excess argon.

R1505 (124NA)

This sample has a total gas age of  $66.8 \pm 0.9$  Ma and it displays a saddle-shaped age spectrum (see Fig. 6:36a). The saddle minimum lies between 62 - 64 Ma. Over the first 80% of the  $^{39}\text{K}$  release, the age correction due to calcium interferences is typically 1 - 2 Ma. However, over the last 20% of  $^{39}\text{K}$  release the  $^{37}/^{39}\text{K}$  curve rises steeply (probably indicating the onset of pyroxene outgassing) and the calcium correction becomes as high as 46 Ma. The chlorine age correction is less than 0.1 Ma for all steps which is not important.

Several step selections give ICD2s with an MSWD less than the 3.5 cut-off. However, especially where the high temperature data points are involved, geologically meaningless ages are produced. The only series of steps likely to give a meaningful ICD2 are the plateau steps 2-10 (see Fig. 6:36b and Table 6:12). Here, the calculated parameters are apparently meaningful but in the presence of excess argon the age of  $64.2 \pm 0.8$  Ma must be treated as a maximum estimate for the timing of emplacement. ICD3 analysis of steps 2-10 gives slightly better MSWD values but ages are higher and the third parameter e.g.  $^{40}\text{Ar}/^{36}\text{Cl}$  is in each case physically unacceptable.

Arrhenius diagrams for R1505 do not display a simple data point distribution. The only linear correlations produce geologically unacceptable closure temperatures.

R1577 (124NA)

This crushed sample gives the highest total gas age ( $78.2 \pm 1.9$  Ma) and the lowest total gas level of radiogenic  $^{40}\text{Ar}$  (14%) of all the 124NA analyses. R1577 displays a saddle-shaped age spectrum (see

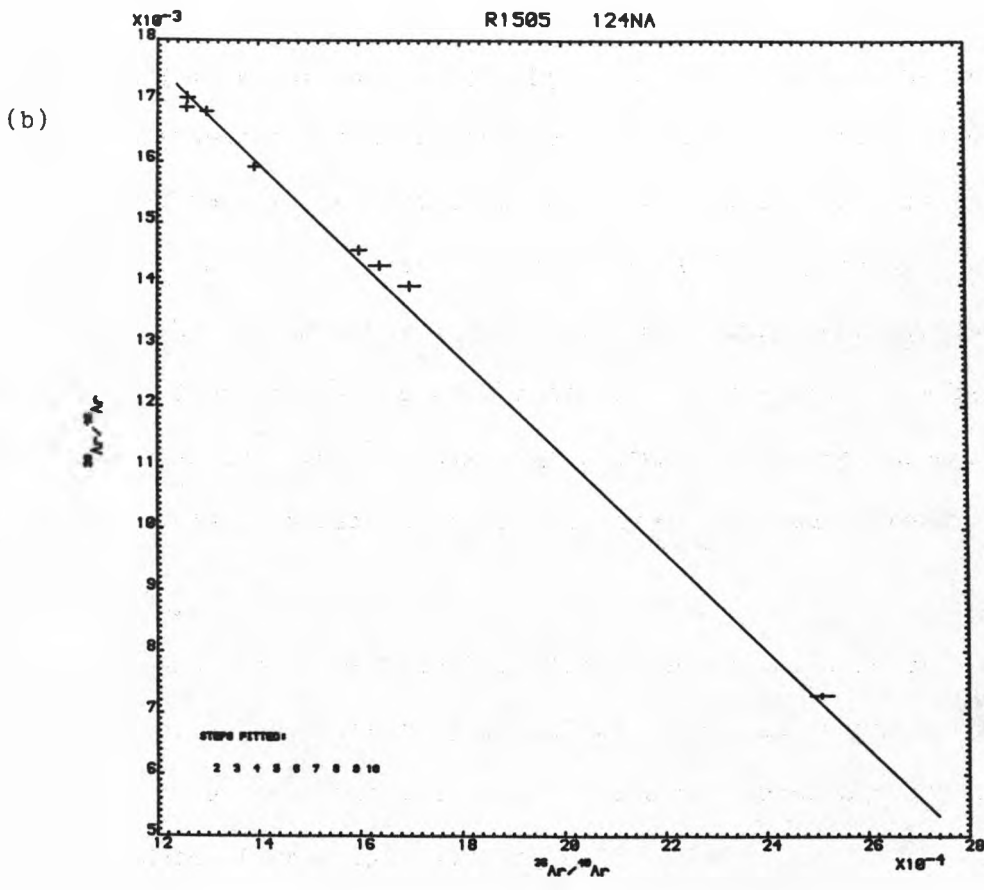
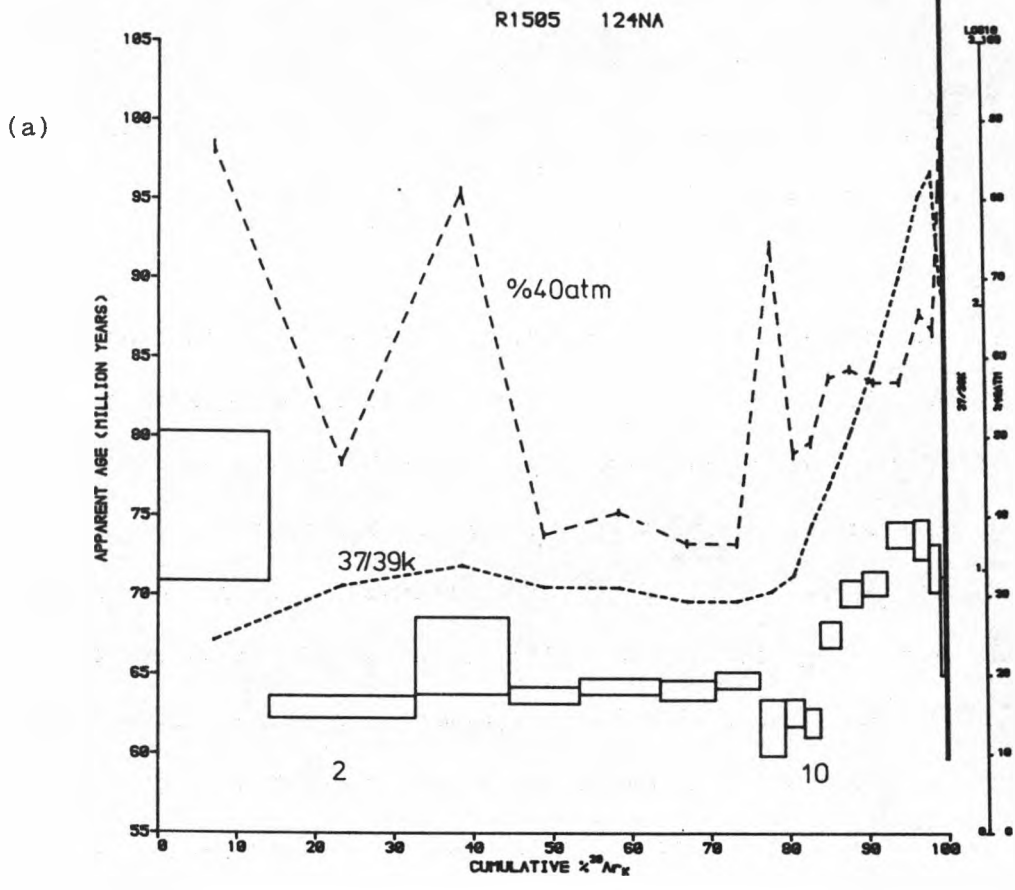


Fig. 6:36 Age spectrum (a) and ICD2 steps 2-10 (b) for the Killala Gabbro feeder dyke sample R1505 (124NA)

Fig. 6:37). As in the case of Droimchogaidh sill sample R1581 (234), crushing of the rock sample prior to irradiation leads to increased atmospheric argon levels. This atmospheric argon introduced by crushing apparently affects the majority of the gas release rather than simply the low temperature segment, as might be expected. Comparing the age spectra for R1505 (Fig. 6:36a) and R1577 (Fig. 6:37) it would seem that most of the absorbed atmospheric argon in R1577 is, in fact, released at the higher temperatures. This sort of behaviour has been noted before, as discussed in section 4:4, and may be explained by the absorption of atmospheric argon onto microcracks which anneal during stepwise degassing (Stettler & Bochsler, 1979). Such a process would potentially be more serious for crushed samples because of their large surface area for absorption.

The  $^{37}/^{39}\text{K}$  curve displays clearly the double-peaked pattern that marks samples consisting predominantly of plagioclase feldspar and pyroxene. The age correction due to calcium interferences is  $\approx 1$  Ma for the lowest temperature steps and  $\approx 4$  Ma and 1 Ma where  $^{37}/^{39}\text{K}$  peaks and troughs respectively at intermediate temperatures, and up to 38 Ma for the highest temperature steps. The chlorine interference age correction is typically  $< 0.1$  Ma.

Step age variation, which describes a saddle-shaped pattern, displays an intermediate temperature minimum of  $66 \pm 1$  Ma. The close correlation between step age and the  $\% \text{ } ^{40}\text{Ar}_{\text{atmospheric}}$  curve may help us understand why this  $^{124}\text{NA}$  sample should give the oldest total gas age. Step 7, which follows the exposure of the sample and crucible to the atmosphere, gives a very much greater age than steps 6 or 8 (which record very similar ages), and a very high  $\% \text{ } ^{40}\text{Ar}_{\text{atmospheric}}$  level. The simplest explanation of these observations involves atmospheric argon absorption by the sample and a fractionation of this loosely-held argon during the bake-out procedure (Baksi, 1974).



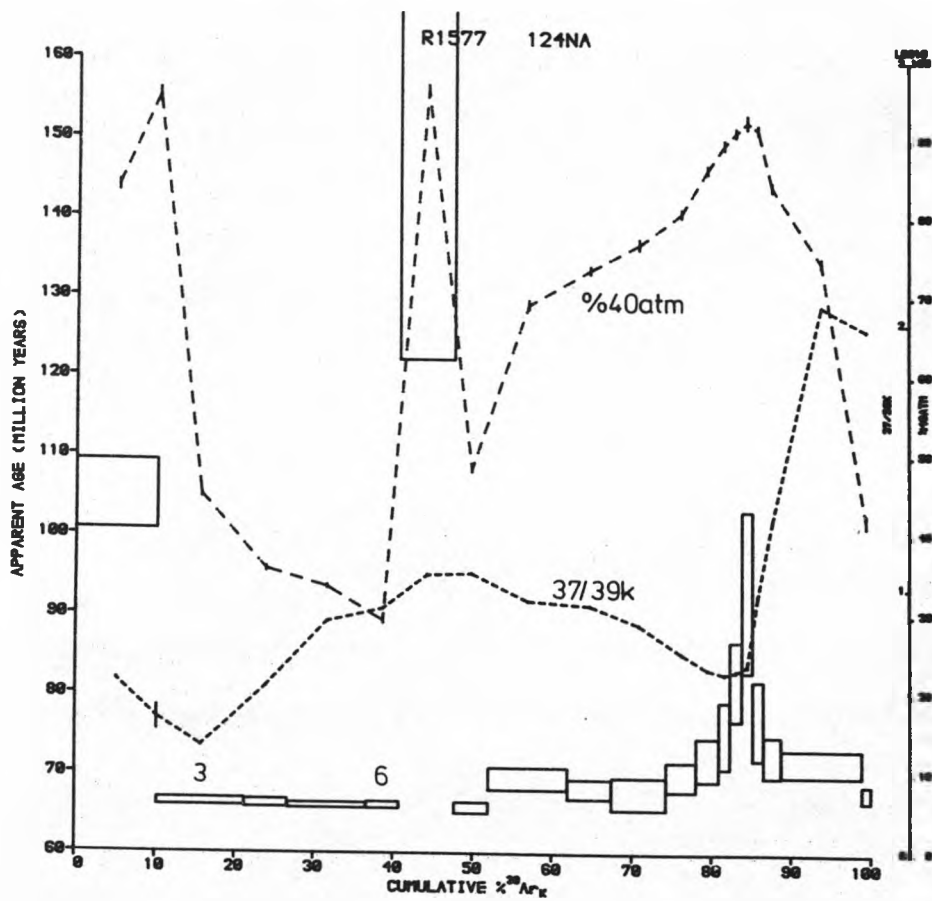


Fig. 6:37 Age spectrum for the Killala Gabbro feeder dyke sample R1577 (124NA)

$^{36}\text{Ar}$ , being lighter than  $^{40}\text{Ar}$ , would be preferentially lost from the sample during such a process; thus the remaining absorbed argon would have a 40/36 ratio greater than the atmospheric value. When released, this argon would appear as an excess argon component and the conventionally calculated step age would be anomalously old. This proposed fractionation effect may partially explain the high ages at the lowest temperatures. However, it is not thought that the observed pattern of anomalous ages at high temperatures could be explained by fractionation of atmospheric argon. The combined contributions of true excess argon and atmospheric fractionation effects probably explains why R1577 gives the oldest age of all the  $^{124}\text{NA}$  samples.

ICD2 analysis of all the steps recovered from R1577 produces an MSWD of 3.1. However, the calculated  $(40/36)_0$  value is significantly greater than the atmospheric ratio (Table 6:12); thus the computed age cannot be accepted as meaningful. Analysis of steps 3-6 which constitute the saddle minimum reveals similar results (see Table 6:12). The low MSWD values for all step selections probably reflects the high levels of atmospheric argon contamination. ICD3 data analysis was not found to be useful for the interpretation of R1577's stepwise degassing data.

#### R1467 (128B)

R1467 gives a very complex pattern of ages (see Fig. 6:38) for which there is no simple explanation. The double-peaked  $^{37}/^{39}\text{K}$  pattern is again evident. The calcium interference age correction is typically 3 - 4 Ma, but reaches 37 Ma for the last step. The chlorine age correction is  $\approx 0.8$  Ma for step 1 but decreases with temperature and is only  $\approx 0.1$  Ma for the latter steps.

Steps 2-5 (30%  $^{39}\text{Ar}_\text{K}$  release) and 6-10 (41%  $^{39}\text{Ar}_\text{K}$  release) both give an ICD2 with an MSWD < 3.5 and an age of about 60 Ma (Table 6:12).

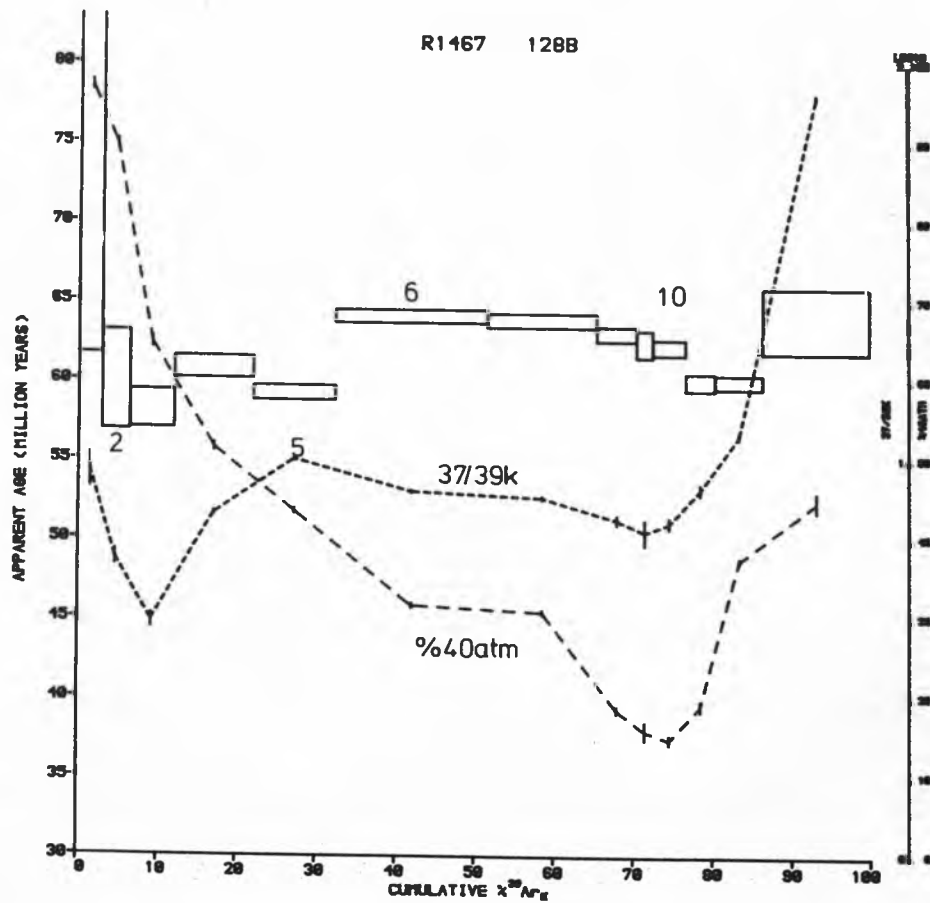


Fig. 6:38 Age spectrum for the Killala Gabbro feeder dyke sample R1467 (128B)

The  $(40/36)_0$  values are  $295.5 \pm 8.8$  and  $320.4 \pm 5.4$  respectively.

These results suggest an emplacement age of  $\approx 60$  Ma and that " excess argon (of a constant argon isotopic composition) is present in the latter series of steps. However, because of the small numbers of steps analysed, this interpretation must only be very tentative.

ICD3 data analysis was not helpful.

#### Conclusions for the Gabbro Analyses

Six out of the eight samples analysed gave the saddle-shaped age spectrum which is apparently diagnostic of excess argon. A summary of ages calculated for these is presented in Table 6:14. The J-values are also listed to show that there is no obvious correlation between flux received and calculated ages (Stettler & Bochsler, 1979 found that, for a sea-floor basalt glass containing excess argon, the saddle ages were irradiation dependant). The saddle minimum ages, which are treated as maximum age estimates, lie between 58 and 66 Ma (the 50 Ma for R1571 is ignored because of its large associated error). The  $58 \pm 2$  Ma age from R1621 is considered to be the best estimate of the emplacement age as it is the lowest saddle minimum age and because, for R1621, the saddle minimum is defined by a series of steps which give a meaningful ICD2 age. The best ages derived from the two samples not giving saddle-shaped age spectra (R1382 and R1467) are consistent with this interpretation.

Fig. 6:39 is a plot of inferred total excess argon concentration (assuming a true age of 58 Ma) versus total  $^{39}\text{Ar}_K$  concentration (normalised to  $J = 0.0025$ ) for the samples producing saddle-shaped age spectra. It is similar to Kaneoka's (1974) equivalent plot for ultramafic rocks containing excess argon and clearly shows that excess argon is concentrated in the potassium-rich mineral phases and rock samples. This is consistent with the expectation that both potassium, and any gases dissolved in the magma, will be concentrated in the

Sample	Total gas age (Ma)	Saddle minimum age (Ma)	J-Value
R1466(106A)	87.0 ± 1.5	65.5 ± 1.2	0.003201
R1520(RG)	70.7 ± 1.9	63 ± 1	0.002426
R1571(RG- pyroxene)	129.6 ± 5.7	50 ± 15	0.002193
R1621(RG- plagioclase feldspar)	78.3 ± 2.5	58 ± 2 *	0.002552
R1505(124NA)	66.8 ± 0.9	64.2 ± 0.8 *	0.000081
R1577(124NA)	78.2 ± 1.9	66 ± 1	0.002345

\* denotes 'meaningful' ICD2 age estimate

Table 6:14 Summary of results for Killala Bay gabbro samples giving saddle-shaped age spectra

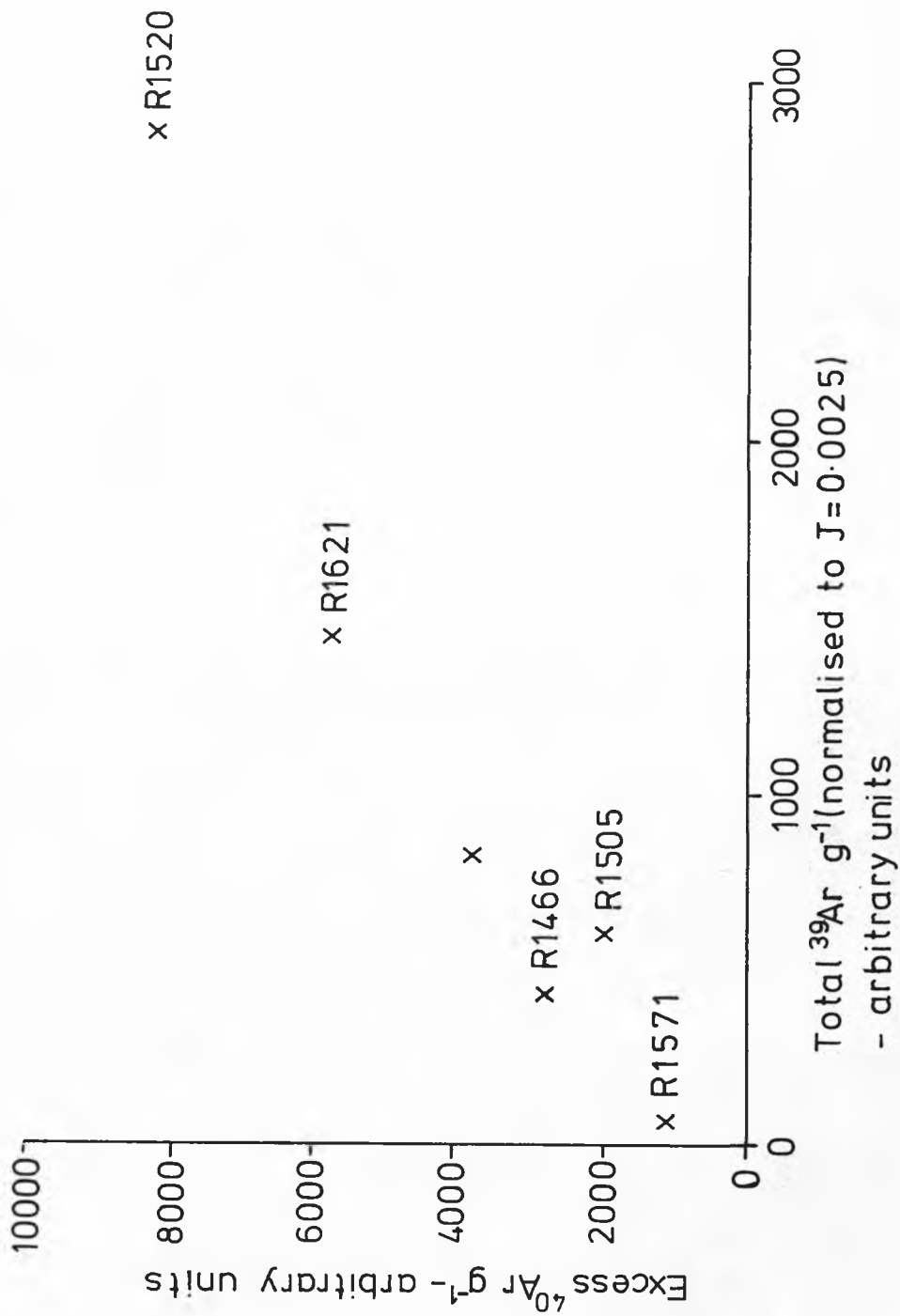


Fig. 6:39 Total excess argon concentration (assumed true age of 58 Ma) v. total  $^{39}\text{Ar}$  concentration for Killala Bay gabbro samples giving saddle-shaped age spectra

residual liquid phase of a melt as it crystallises and thus in the low temperature minerals. A similar correlation is found to exist between the concentration of total excess argon and total chlorine-derived  $^{38}\text{Ar}$ . This prompted the development of an ICD3 in which a component of  $^{40}\text{Ar}$  in proportion to  $^{36}\text{Cl}$  is hypothesised (see Section 3:4).

It is clear from the ICD2 data analyses that the excess  $^{40}\text{Ar}$  in these samples is not correlated with the  $^{36}\text{Ar}$  release. If it were, we would expect ICD2 linear correlations to give the true age and the 40/36 ratio of the excess argon. Although atmospheric blank corrections have not been made routinely for any of the stepwise degassing experiments in this study, it has been shown for the Killala Bay gabbros that they do not significantly affect the ICD2 data point distributions.

The only plausible explanation for saddle-shaped age spectra has been presented by Harrison & McDougall (1981). It is outlined in the discussion of sample R1621. The work of Dalrymple et al., (1975) has clearly shown that saddle-shaped age spectra may be entirely the result of excess argon contamination. It is thought that this is largely the case for the Killala Bay gabbro samples even though in one, R1577, the fractionation of loosely-held atmospheric argon was thought to contribute to anomalous high ages of low temperature. Recoil effects are not expected to be important for the Killala Bay gabbro samples because on both petrographic and SEM scales individual grain size is large (see Appendix 7 and 6 respectively).

#### Conclusions for Killala Bay

Cross-cutting relations establish the sequence of intrusion in the Killala Bay area. The Killala Gabbro and its associated feeder dykes were the first bodies to be intruded, closely followed by the Killala Gabbro dykelet and finally by the doleritic flash intrusions. The best

age estimates for the three events from this dating study are  $58 \pm 2$  Ma,  $58.7 \pm 1.1$  Ma(maximum) and  $61.6 \pm 0.9$  Ma(maximum) respectively. All these results are consistent with the view that igneous activity in the Killala Bay area took place around 58 Ma ago. Excess argon was positively identified in many of the Killala Bay samples and this explains Macintyre et al.'s (1975) suggested date of 82 Ma for the Killala Gabbro.

#### 6:2:6 The Blind Rock Dyke

The Blind Rock dyke is the largest of the swarm of Tertiary doleritic intrusions which are exposed on the northern shore of Donegal Bay (see Fig. 6:1). Trending NW-SE (typical direction for Tertiary dyke swarms in the British Isles) and being over 30 m wide, it possesses many features characteristic of a feeder intrusion (Preston, 1967). The petrology of the Blind Rock dyke has been described by Preston (1967) and in this  $^{40}\text{Ar}$ - $^{39}\text{Ar}$  dating study, samples of the centrally located tholeiitic dolerite (G049C) and the more marginal "normal dolerite" (G049M) have been analysed.

The Doonan Rocks intrusion, found about 10 km ENE of the Blind Rock dyke and probably part of the same dyke swarm, has been dated, using the K-Ar technique, by Macintyre et al., (1975). They report an age of  $\approx 62.5$  Ma for powdered whole-rock samples and  $\approx 73$  Ma for chipped whole-rock samples. The former is thought to give the time of emplacement whilst the latter may be subject to excess argon contamination.

#### R1524 (G049M)

This fine-grained sample produced a plateau of ages over more than 90% of the  $39\text{K}$  release with the only deviations being at the very lowest and highest temperatures (Fig. 6:40a). Percentage radiogenic  $^{40}\text{Ar}$  levels are 90%+ over the majority of the gas release. The calcium interference age correction is typically 1 - 2 Ma, but with markedly



Irradiation no. (Locality no.)	Steps	% <sup>39</sup> K	Total gas age (Ma)	Mean age (Ma) (step ages weighted by 1/variance)	Age (Ma)	ICD2 parameters ( <sup>40</sup> / <sub>36</sub> ) <sub>o</sub>	MSWD
R1524(G049M)	All(1-32) 4-29	100	61.6 ± 0.5	61.7 ± 0.7	61.8 ± 0.5	294.5 ± 2.6	4.2
		92	61.7 ± 0.5	61.7 ± 0.7	61.7 ± 0.5	295.5 ± 3.9	3.4
R1521(G049C)	All(1-31, ex 24) 3-13 14-31	100	63.7 ± 0.6	63.5 ± 1.3	63.1 ± 0.7	302.0 ± 4.3	10.6
		28	64.9 ± 0.6	64.8 ± 1.2	63.2 ± 0.8	313.4 ± 6.9	3.4
		70	62.7 ± 0.6	62.8 ± 0.8	63.0 ± 0.6	293.5 ± 2.8	2.9

Table 6:15 Parameters calculated for the Blind Rock dyke samples

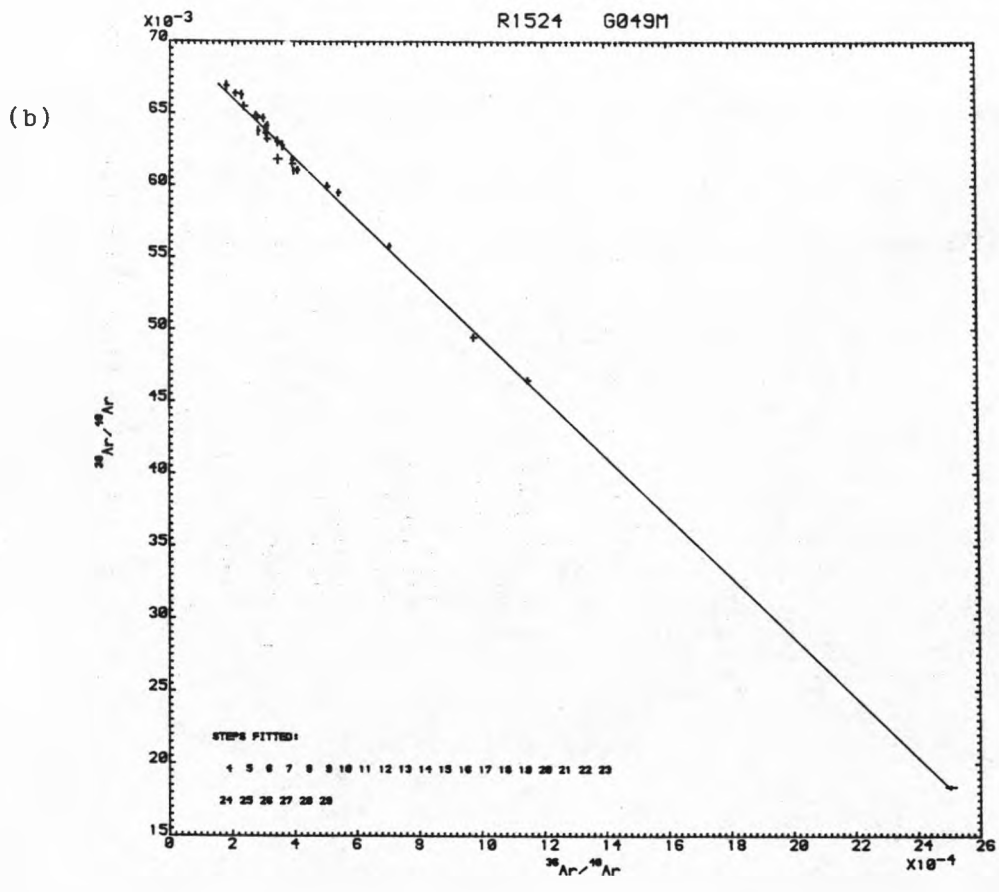
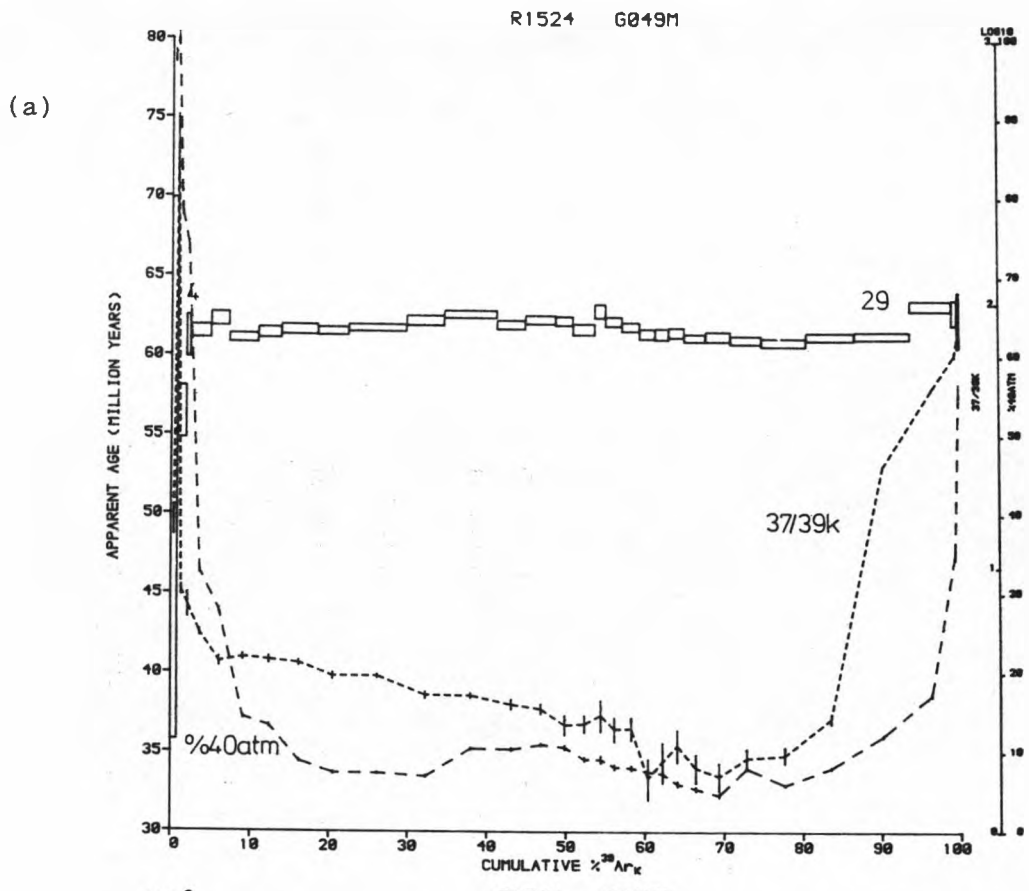


Fig. 6:40 Age spectrum (a) and ICD2 steps 4-29 (b) for the Blind Rock dyke sample R1524 (G049M)

higher values for the last four steps (up to 27 Ma). The latter feature undoubtedly indicates the importance of argon release from the mineral pyroxene (see  $^{37}/^{39}\text{K}$  curve in Fig. 6:40a). The chlorine age correction is less than 0.1 Ma for all but the last two steps.

The plateau steps (4-29) give a meaningful ICD2 (Fig. 6:40b, Table 6:15); thus the ICD2 age of  $61.7 \pm 0.5$  Ma is taken to be a reliable estimate for the timing of dyke emplacement. Low ages for the first three steps can be explained by minor radiogenic argon loss. A possible explanation for the anomalously high ages recorded by steps 30-32 is provided by ICD3-Plot 3 data analysis. Table 6:16 compares parameters calculated for steps 4-32 using ICD2 and ICD3-Plot 3. Only for the latter is the MSWD low enough to indicate a meaningful plot. ICD3-Plot 3 gives a  $\left[ \frac{^{40}-(^{40}/^{36})_{\text{O}} \cdot 36}{37} \right]_{\text{Ca}}$  value of  $-0.069 \pm 0.003$ , which is slightly below the adopted value. Thus, the anomalously high apparent ages of steps 30-32 are probably the result of using a

$\left[ \frac{^{40}-(^{40}/^{36})_{\text{O}} \cdot 36}{37} \right]_{\text{Ca}}$  value which is slightly too small. It is not possible to confirm the inferred value of  $\left[ \frac{^{40}-(^{40}/^{36})_{\text{O}} \cdot 36}{37} \right]_{\text{Ca}}$  by looking at other samples from the same irradiation batch as the difference between this value and the adopted value is only slight. Only here, where the sample is apparently almost "ideal", is such a discrepancy noticeable.

#### R1521 (G049C)

The coarser grained tholeiitic dolerite represents the last magmatic injection of the Blind Rock multiple dyke. Its coarse texture suggests intrusion whilst the marginal "normal dolerite" was still hot. The tholeiitic dolerite intrusion will therefore be slightly younger than the "normal dolerite", however, in geological terms this difference will not be significant.

Over the majority of the gas release, R1521 displays a pattern of

	Age (Ma)	$(40/36)_O$	$\left[ \frac{40 - (40/36)_O \cdot 36}{37} \right]_{Ca}$	MSWD
ICD2	$61.6 \pm 0.5$	$299.1 \pm 3.6$	_____	3.9
ICD3-Plot 3	$61.6 \pm 0.5$	$295.7 \pm 4.0$	$-0.069 \pm 0.003$	3.4

Table 6:16 Comparison of ICD parameters calculated for steps 4-32 of Blind Rock dyke sample R1524 (G049M)

gradually decreasing age (Fig. 6:41). The high temperature steps record an age of  $\approx 62$  Ma, which is approximately equal to the best age estimate for R1524. Percentage radiogenic  $^{40}\text{Ar}$  levels are lower for R1521 than for R1524 and their  $^{37}/^{39}\text{K}$  curves are distinctly different. For R1521, the  $^{37}/^{39}\text{K}$  curve displays two peaks which probably represent plagioclase and pyroxene outgassing (the intermediate and high temperature peaks respectively). For the majority of steps the calcium age correction is less than 2 Ma; however for the last four it is  $\approx 15$  Ma. The chlorine age correction is less than 0.1 Ma for all steps.

Both steps 3-13 and 14-31 give two-dimensional isotope correlation diagrams with an MSWD less than 3.5 and an age of  $\approx 63$  Ma (see Table 6:15). However, in the former case  $(^{40}/^{36})_0 = 313 \pm 7$  and in the latter  $(^{40}/^{36})_0 = 294 \pm 3$ . This suggests that the true age of emplacement is 63 Ma and that excess argon of a constant isotopic composition is important for steps 3-13. An interpretation involving excess argon is consistent with the observed age spectrum shape. Excess argon contamination is not, in fact, the preferred interpretation of the age data for sample R1521 as the calculated ICD2 ages of 63 Ma are significantly greater than the 61.7 Ma best age estimate for the older "normal dolerite". The age pattern of R1521 is believed to reflect a  $^{39}\text{K}$  recoil loss and this interpretation is supported by the scanning electron microscope work presented in Appendix 6. This work shows that the bulk of the potassium in the coarse-grained tholeiitic dolerite (R1521) is found in feldspathic zones less than  $10\mu$  across, whereas that in the fine-grained "normal dolerite" (R1524) is contained in feldspathic zones typically of the order of  $50\mu$ . These observations suggest that recoil effects will be important for the former sample because the expected order of magnitude for the  $^{39}\text{K}$  recoil range (Mitchell, 1968 estimated a  $0.1\mu$  maximum range for a

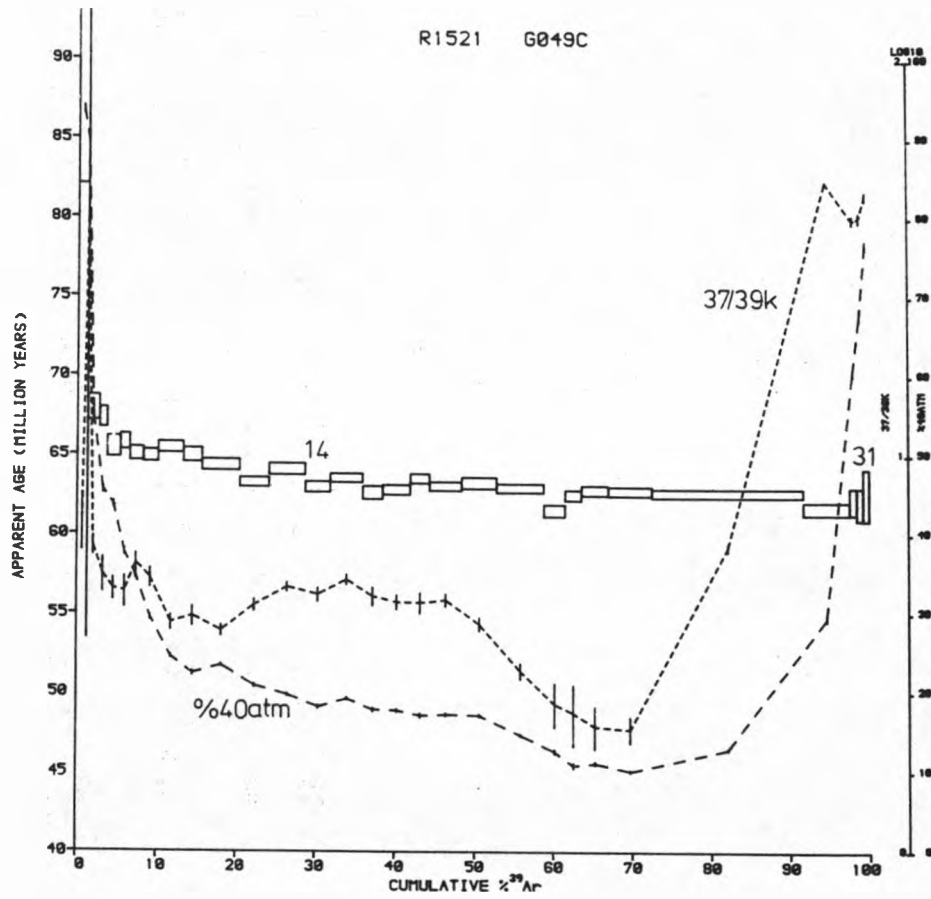


Fig. 6:41 Age spectrum for the Blind Rock dyke sample R1521 (G049C)

mica) is significant compared to the observed potassium zone size. It is not expected that recoil effects would be important for R1524 because the potassium zone size is so much greater than the expected  $^{39}\text{K}$  recoil range.

Where  $^{39}\text{K}$  recoil loss is believed to be important, the high temperature ages must only be considered as giving a maximum age estimate. This is especially the case where there is a marked pattern of decreasing age over the majority of the gas release (see Table 4:3). For R1521, the high temperature age minimum of  $62 \pm 1$  Ma is therefore treated as a maximum age estimate. This interpretation is consistent with the  $61.7 \pm 0.5$  Ma best age estimate for the older "normal dolerite" sample.

#### Conclusions for the Blind Rock Dyke

The  $^{40}\text{Ar}$ - $^{39}\text{Ar}$  data presented in this study suggests that the Blind Rock dyke, and the dyke swarm exposed on the northern shore of Donegal Bay, were intruded  $61.7 \pm 0.5$  Ma ago. This date is similar to Macintyre et al.'s (1975) estimate for the timing of emplacement of the Doonan Rocks intrusion, which is found only 10 km from the Blind Rock dyke.

#### 6:2:7 The Antrim Lava Group

The Antrim Lava Group is the largest remnant of Tertiary igneous activity in Britain. On the basis of field evidence, Old (1975) proposed splitting the Antrim Lava Group into three lithostratigraphical units (Fig. 6:42): the Lower Basalt Formation (LBF), the Interbasaltic Formation (IBF) and the Upper Basalt Formation (UBF). The IBF, which includes the Causeway Tholeiite Member (formerly termed Middle Basalts) and the Tardree Rhyolite Complex, represents a period of relative volcanic quiescence between extrusion of the younger UBF and older LBF.

Radiometric dating has provided us with quantitative estimates for the

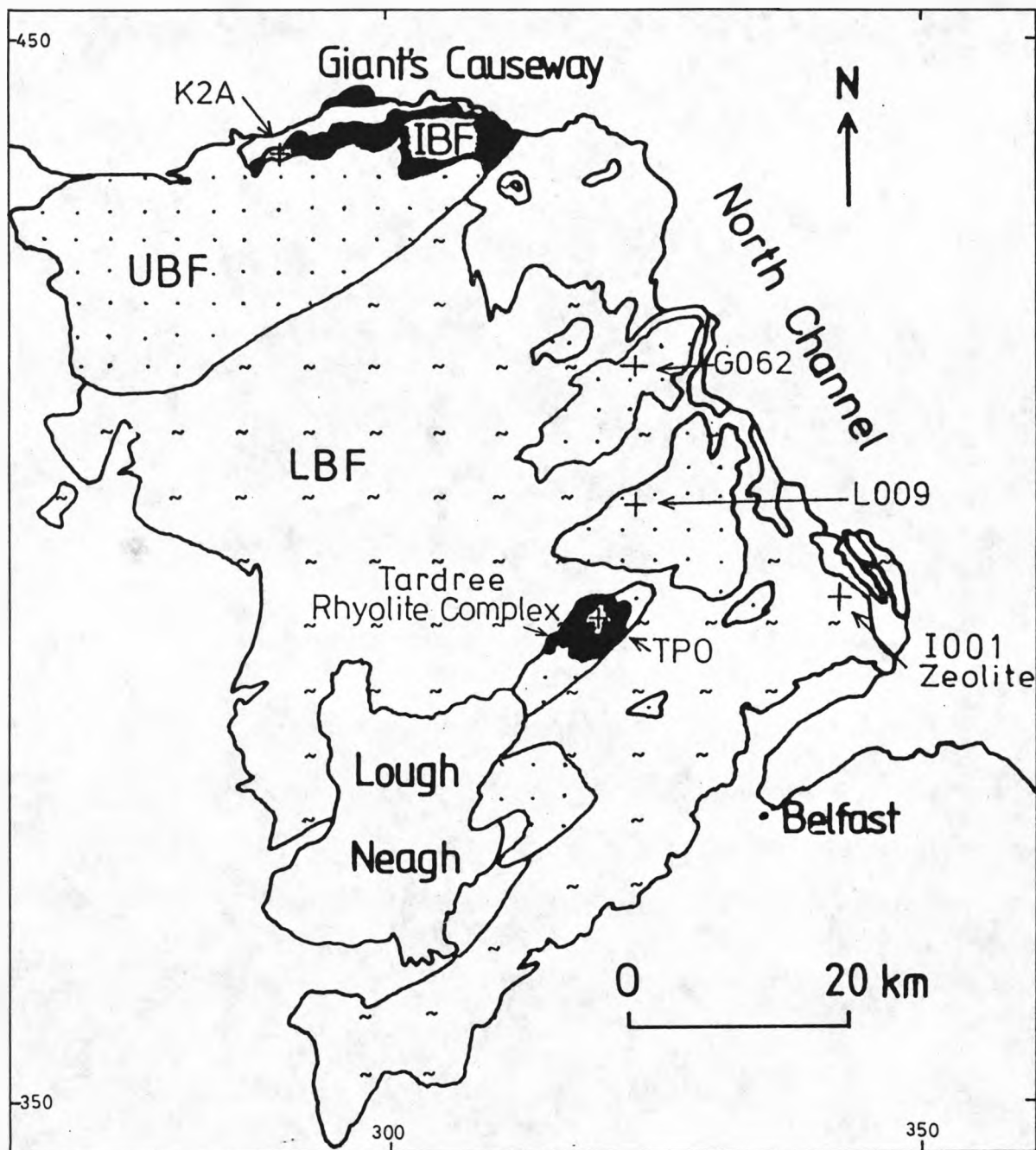


Fig. 6:42 The Antrim Lava Group (adapted from Old, 1975) -  
 LBF = Lower Basalt Formation, IBF = Interbasaltic  
 Formation, UBF = Upper Basalt Formation. Sampling  
 locations are marked by crosses.



ages of formations within the Antrim Lava Group (K-Ar dates: Purdy et al., 1972; Evans et al., 1973; Reffay et al., 1974; Mellor & Mussett, 1975; Fitch et al., 1976. Fission track date: Fitch & Hurford, 1977). However, two partially conflicting scenarios for the time and duration of activity have been proposed.

Scenario (1): Volcanic activity from 68 to 61 Ma

The conventional K-Ar results of Evans et al., (1973) are difficult to interpret (see histogram of ages presented in Fig. 6:43). They considered argon loss to be important, and thus their estimates for commencement of volcanism (67 Ma) and cessation of activity (61 Ma) are minima. However, it appears that the samples giving the estimate of the age of commencement of volcanism are in fact from the UBF. A clustering of ages around 60.5 Ma (see Fig. 6:43) was interpreted in terms of a complete overprinting metasomatic event, perhaps related to Slieve Gullion-Carlingford ring complex activity (Macintyre, 1973 suggested that this clustering age might represent the age of extrusion). Samples dated from the IBF (Causeway Tholeiite Member) yielded ages of  $\approx 52$  and 59 Ma. Such apparent ages were interpreted by Evans et al., (1973) as evidence for overprinting events. The only published age data for the Tardree Rhyolite Complex is that of Fitch & Hurford (1977). They determined a mean zircon fission track apparent age for the Tardree Rhyolite of  $65.2 \pm 0.4$  Ma, stating that this result supports the conclusion of Evans et al., (1973) that the stratigraphically older LBF activity commenced  $> 67$  Ma ago.

Scenario (2): Extrusion of the whole Antrim Lava Group within a relatively short time interval at about 60.5 Ma.

The conclusion of Macintyre et al., (1975) that the Antrim lavas are  $\approx 59.5$  Ma old was based on two pieces of evidence:

- i) The Mourne Granites and the Interbasaltic Formation rhyolites are geochemically similar (Meighan & Gamble, 1972) and are thus

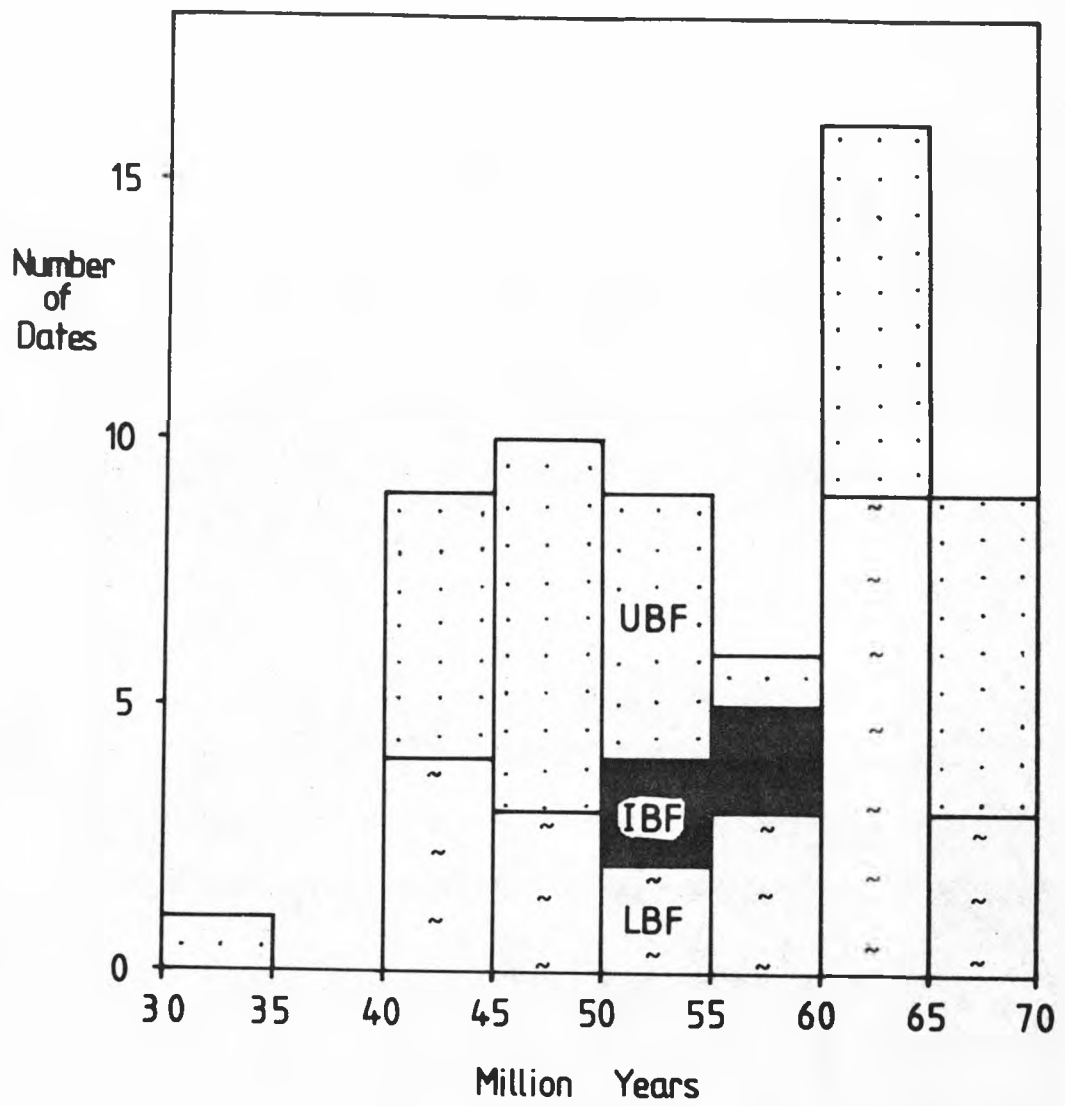


Fig. 6:43 Histogram of the K-Ar dates reported by Evans et. al., (1973) for the Antrim Lava Group

deduced to be contemporaneous. The age of the Mourne Granites was thought to be well established at about 59.5 Ma by two  $^{40}\text{Ar}-^{39}\text{Ar}$  age spectrum analyses (Evans et al., 1973)

- ii) All the Antrim lavas have a reversed direction of magnetisation (Wilson, 1970). On the polarity timescale (Fig. 6:44) an age of 59.5 Ma is consistent with a reversed direction of magnetisation. If it is assumed that the whole Antrim Lava Group was extruded in a single reversed polarity epoch, as suggested by Wilson (1970), then the time span of activity must have been  $< 2.5$  Ma and therefore considerably less than the span suggested in Scenario (1).

Independently, Mellor & Mussett (1975) and Fitch et al., (1976) re-evaluated some of the earlier K-Ar data by using a whole-rock K-Ar isochron technique. Mellor & Mussett (1975) used LBF and UBF results from Evans et al., (1973) and Purdy et al., (1972) and concluded from their six single whole-rock isochrons (data from several analyses of a single sample) that the whole Antrim Lava Group is  $\approx 61.5$  Ma old. However, Fitch et al., (1976) using only the results of Evans et al., (1973) produced similar numerical results, but interpreted their multiple whole-rock isochron (data from several samples), which gave an age of  $60.6 \pm 0.3$  Ma, in terms of a total overprinting event. This isochron plot included six LBF and one UBF sample. Most of the K-Ar isochrons of Mellor & Mussett (1975) and Fitch et al., (1976) imply the presence of initial argon with a non-atmospheric composition.

None of the arguments presented above can be considered conclusive for the following reasons:

- i) The inferred contemporaneity of the Mourne Granites and IBF rhyolites (Macintyre et al., 1975) is not fully justified.
- ii) Work presented in this thesis shows that the Mourne Granites are

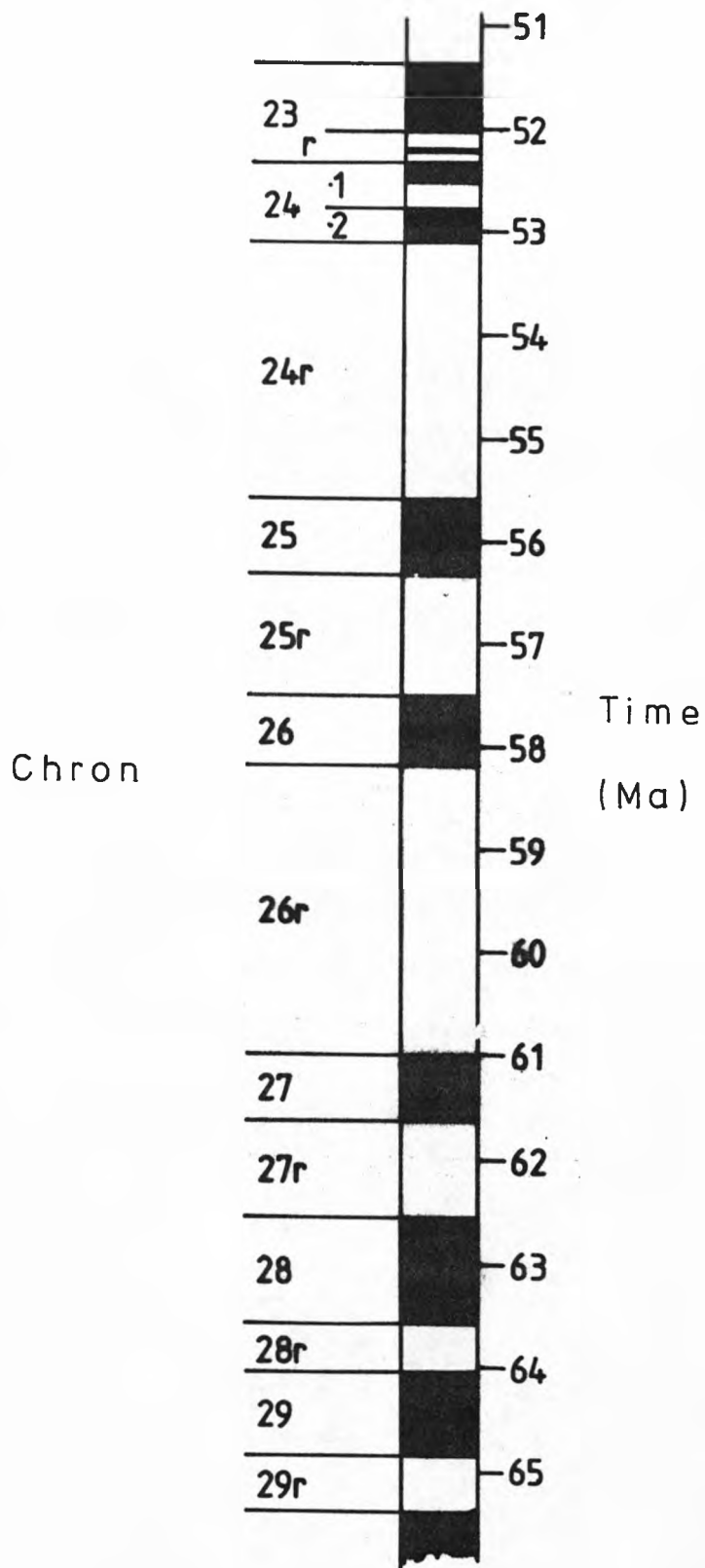


Fig. 6:44 The polarity timescale (adapted from Harland et al., 1982)

in fact no more than 55 Ma old rather than 59.5 Ma as Evans et al.'s (1973) work had suggested.

- iii) The case for extended activity in Antrim (Scenario (1)) relies partially on the inconsistent K-Ar data of Evans et al., (1973), which can be interpreted in at least two ways.
- iv) The reliability of the age determined by Fitch & Hurford (1977), by the then relatively new fission track technique, is uncertain.
- v) The meaning of K-Ar isochrons (or  $^{40}\text{Ar}$ - $^{39}\text{Ar}$  isochrons/ICDs) with non-atmospheric  $(40/36)_0$  ratios is not clear (see Section 3:3).

In this study, six samples from the Antrim Lava Group have been dated (two from each of the three formations - sampling locations are given in Fig. 6:42). The results presented here strongly support Scenario (2).

a) The Lower Basalt Formation

The two samples dated were both collected from the Magheramorne Quarry, near Larne (see Fig. 6:42). The first, an olivine basalt whole-rock sample, was from the flow lying directly on the Cretaceous Limestone and thus represents one of the oldest Tertiary lavas in N. Ireland. This basal lava flow is 19m thick. The second was a chunk of amygdaloidal zeolite extracted from one of the overlying flows.

R1527 (I001)

The age spectrum for this whole-rock basalt sample is presented in Fig. 6:45. The low temperature steps give scattered ages but from step 10 onwards there is a generally decreasing pattern of ages from 64 to 58 Ma. Although the total gas level of radiogenic argon is only 47%, intermediate to high temperature steps display levels of > 80%. This again demonstrates one of the major advantages of the  $^{40}\text{Ar}$ - $^{39}\text{Ar}$  stepwise degassing technique. The calcium interference age correction is typically less than 5 Ma for steps 1-20; however, over the last six steps the  $37/39_K$  curve rises and the correction increases in

Irradiation no. (Locality no.)	Steps	% <sup>39</sup> K	Total gas age (Ma)	Mean age (Ma) (step ages weighted by 1/variance)	Age (Ma)	ICD2 parameters (40/36) <sub>0</sub>	MSWD
R1527(1001)	A11(1-26) 12-17 20-24	100 52 24	60.8 ± 0.6 60.7 ± 0.6 58.6 ± 0.6	59.7 ± 1.7	59.5 ± 0.6	297.6 ± 3.6	9.1
				60.6 ± 0.6	60.7 ± 0.6	294.8 ± 2.3	1.0
				58.5 ± 0.7	58.4 ± 0.7	296.9 ± 6.7	2.0
R1522(K2A)	A11(1-30, ex 2) 6-24	100 63	67.3 ± 1.1 62.0 ± 0.6	60.8 ± 3.0	56.1 ± 0.9	305.4 ± 6.8	2.3
				61.8 ± 1.7	59.0 ± 1.5	300.9 ± 12.2	1.6
R1532(TP0)	A11(1-21) 2-13	100 72	60.4 ± 0.6 60.9 ± 0.6	58.7 ± 5.2	59.5 ± 1.4	307.9 ± 84.6	429.2
				61.1 ± 0.7	61.0 ± 0.6	377.9 ± 203.3	2.8
R1523(G062)	A11(1-19) 14-19	100 23	59.0 ± 0.4 58.0 ± 0.5	59.7 ± 2.1	60.5 ± 0.7	287.3 ± 6.8	26.5
				58.0 ± 0.5	58.0 ± 0.4	295.3 ± 2.2	0.6
R1617(L009)	A11(1-24) 9-23	100 77	56.7 ± 1.1 58.6 ± 1.1	58.6 ± 1.8	59.3 ± 1.2	287.5 ± 4.0	9.1
				58.6 ± 1.1	58.3 ± 1.1	300.6 ± 6.9	2.7

Table 6:17 Parameters calculated for the Antrim Lava Group samples

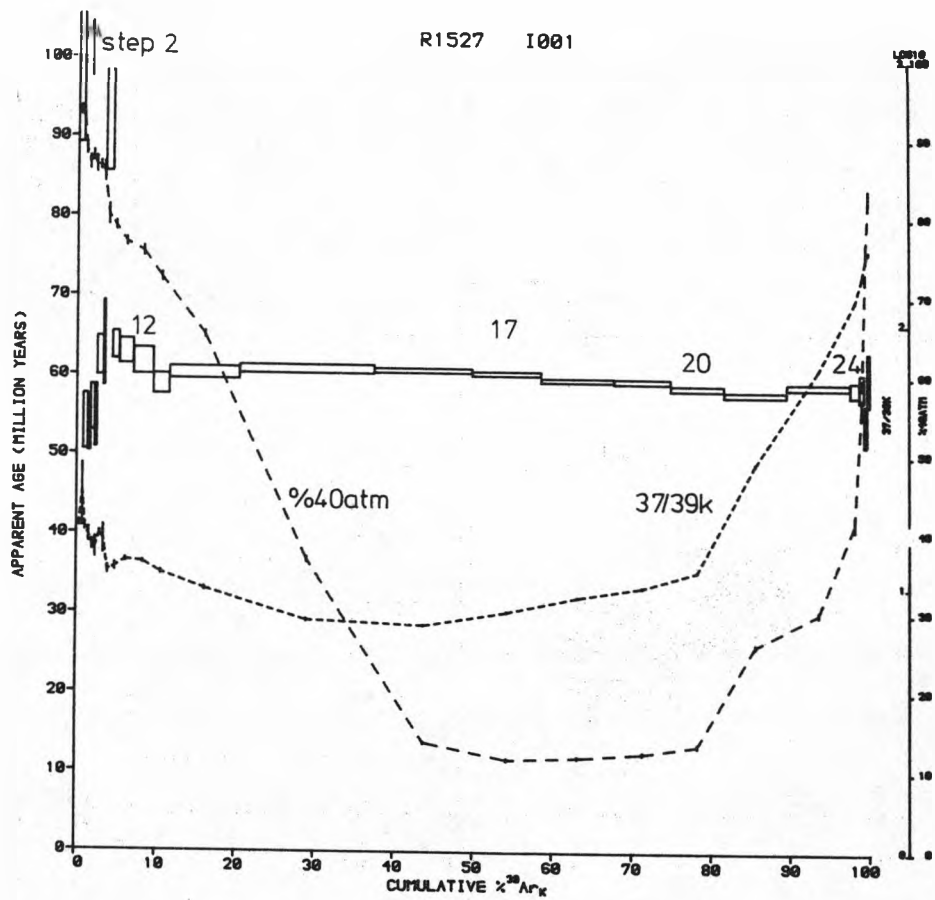


Fig. 6:45 Age spectrum for the Lower Basalt Formation sample R1527 (I001)

importance (60 Ma age correction for the last step). The age correction due to chlorine interferences is less than 0.2 Ma for all steps and is thus insignificant.

Only where small numbers of consecutive steps are selected does ICD2 analysis give meaningful ages (see Table 6:17). Although steps 12-17 constitute over 50% of  $^{39}\text{K}$  release, it is not possible to accept the  $60.7 \pm 0.6$  Ma age without reservations. Firstly, steps 20-24 also give a meaningful ICD2 but with a significantly lower age of  $58.4 \pm 0.7$  Ma. I can think of no reasonable explanation for this drop in age over the last 40% of  $^{39}\text{K}$  release unless we are witnessing a large scale  $^{39}\text{K}$  re-distribution effect (the  $^{37}/^{39}\text{K}$  level is increasing over these steps indicating that pyroxene, a possible site for  $^{39}\text{K}$  re-location, is outgassing). Secondly, the plateau formed by steps 12-17 is part of a trend of decreasing age with temperature. The preferred chronological interpretation involves taking the high temperature age minimum ( $58.4 \pm 0.7$  Ma) as a maximum age estimate. Although the statistical evidence is not clear-cut, it is apparently possible to conclude that the basal basalt of the Antrim Lava Group was extruded around 60 Ma ago and not at  $> 67$  Ma ago as Evans et al., (1973) and Fitch & Hurford (1977) suggested. However, the scanning electron microscope work for basalt I001 (see Appendix 6) shows that the majority of the potassium was contained in zeolite amygdales. Thus, the analysis of R1527 is, in fact, dating the timing of zeolitisation which may have occurred significantly later than the original extrusion. The age data for R1527 does not therefore assist in the task of dating the LBF volcanic activity.  $58.4 \pm 0.7$  Ma is taken as a maximum estimate for the timing of zeolitisation.

The zeolitisation of the Antrim basalts is a regional hydrothermal alteration thought to have taken place after the lava pile attained a critical thickness (Walker, 1960). Generally, the zeolite zones



(higher temperature species are found at greater depths) are parallel to the original top of the lava pile (Walker, 1960). However, for some of the Upper Basalts, the zones are discordant with the lava stratigraphy (Walker, 1951). Walker (1960) states that this, combined with all other geological evidence, supports the theory that zeolitisation postdates the eruption of the lavas by a substantial margin.

In an attempt to date the timing of zeolitisation precisely, a large piece of zeolite, from one of the Magheramorne Quarry lava flows, was analysed by the  $^{40}\text{Ar}$ - $^{39}\text{Ar}$  technique.

#### R1533 (Zeolite)

Unfortunately, the zeolite selected for analysis had a very low potassium content; thus none of the ten steps extracted gave a meaningful age. The ratio of naturally-occurring  $^{40}\text{Ar}/^{36}\text{Ar}$  was, in fact, approximately equal to  $(^{40}\text{Ar}/^{36}\text{Ar})_{\text{atm}}$  for all the steps. Thus, from the analysis of R1533, it was not possible to date the timing of zeolitisation.

#### b) The Interbasaltic Formation

Of the two samples dated, the first, R1522 (K2A), was a basalt from the Causeway Tholeiite Member (8m thick flow), and the second, R1532 (TPO), was a porphyritic obsidian from the Tardree Rhyolite Complex (see Fig. 6:42 for sampling locations).

#### R1522 (K2A)

Individual step ages for R1522 possess rather large errors due to the low levels of radiogenic  $^{40}\text{Ar}$  (see Fig. 6:46a). The total gas level of  $^{40}\text{Ar}^*$  is only 16% and the maximum level achieved by an individual step is 47%. The age spectrum displays a decreasing pattern of ages over the first 20% of  $^{39}\text{K}$  release, with a rough plateau over the next 60%, and ages lower than the plateau over the last 20%. This latter

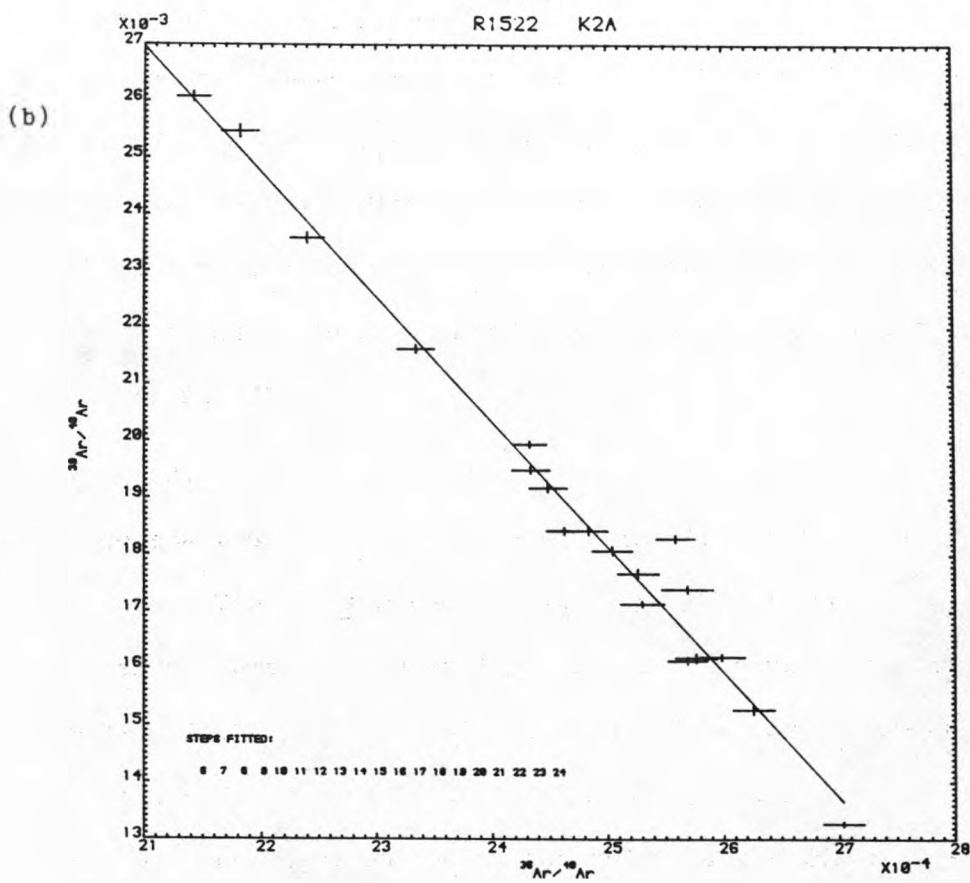
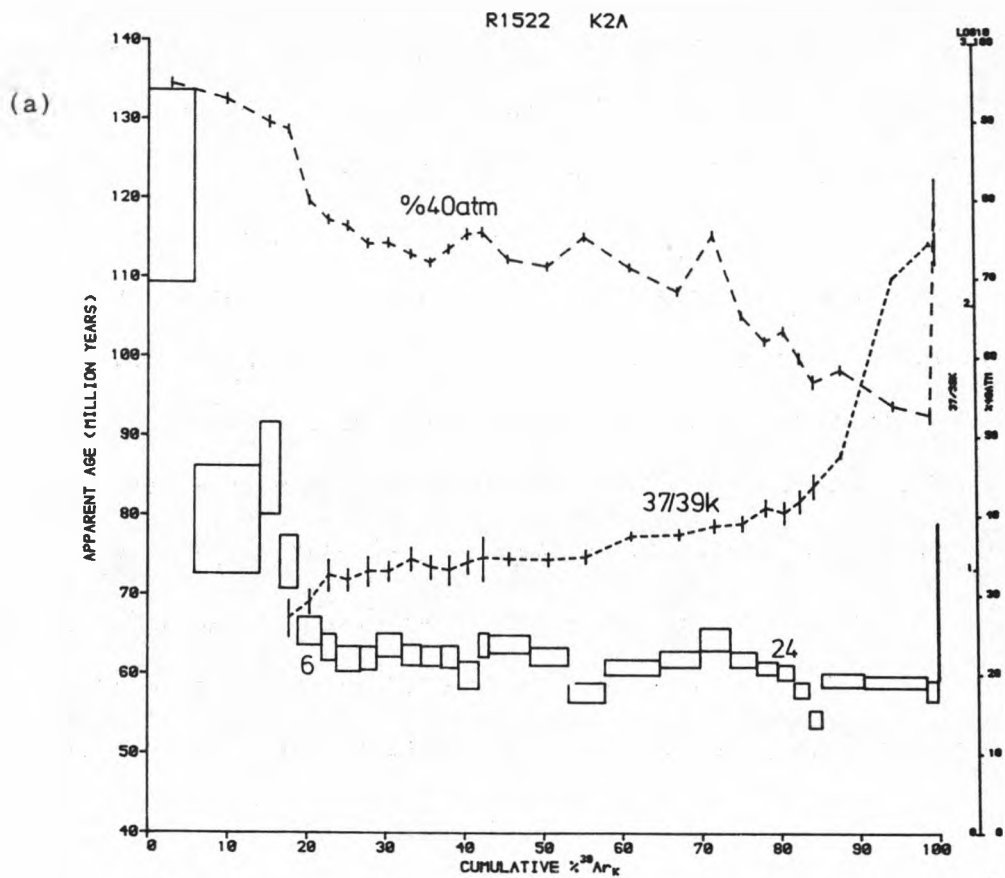


Fig. 6:46 Age spectrum (a) and ICD2 steps 6-24 (b) for the Inter-basaltic Formation sample R1522 (K2A)

feature corresponds with the peaking of the  $^{37}/^{39}\text{K}$  curve (which marks pyroxene outgassing) and the increasing importance of the calcium interference age correction. For earlier steps, the age correction is less than 6 Ma but for the last six steps it rises to 55 Ma. The chlorine interference age correction is less than 0.2 Ma for all steps and is therefore insignificant.

ICD2 analysis of all the steps extracted from R1522 yields an MSWD < 3.5 (see Table 6:17). However, the calculated age is not accepted as meaningful because the  $(^{40}/^{36})_{\text{O}}$  is greater than 295.5. Analysis of steps 6-24, which constitute the plateau observed in the age spectrum, does give a meaningful age of  $59.0 \pm 1.5$  Ma (see Table 6:17, Fig. 6:46b). Petrographic examination of a thin section, taken from the same chunk of rock as the dating sample, reveals that zeolitisation is not important in this basalt. Therefore, the 59 Ma age is taken as an estimate of the timing of lava extrusion. The very fine-grained nature of K2A suggests that the anomalous low and high temperature segments of the gas release may be explained by  $^{39}\text{K}$  recoil effects. Interpreting the high temperature age decline in terms of a  $^{39}\text{K}$  recoil re-distribution effect certainly seems plausible, as the age drop is marked by the onset of pyroxene outgassing. Because of the likelihood of such  $^{39}\text{K}$  recoil effects, the plateau age of  $59.0 \pm 1.5$  Ma must be regarded as a maximum age estimate. An age of around 59 Ma for the IBF is consistent with Scenario (2) rather than with Scenario (1).

The interpretation of the data for R1522 was not aided by ICD3 data analysis.

#### R1532 (TPO)

This porphyritic obsidian sample was collected from the Sandy Braes vent of the Tardree Rhyolite Complex (see Fig. 6:42). The geology of Sandy Braes and the Tardree Rhyolite Complex is described by Cameron &

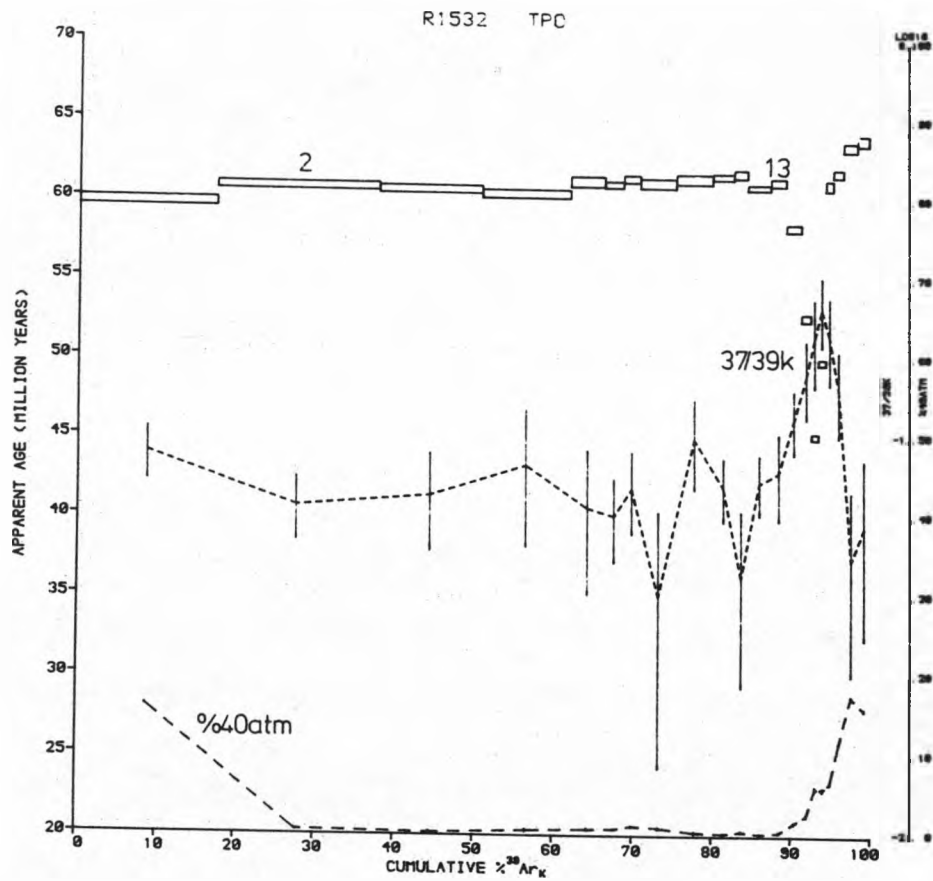


Fig. 6:47 Age spectrum for the Interbasaltic Formation sample R1532 (TPO)

Sabine (1969) and Old (1975). Although the porphyritic obsidian sample consists of about 70% glass, (which is often considered unreliable for K-Ar dating; Dalrymple & Lanphere, 1969), severe radiogenic argon loss problems were not anticipated because of the freshness of the glass. This assumption is verified by the age spectrum of R1532 (Fig. 6:47) which displays a plateau of ages constituting about 70% of the  $^{39}\text{K}$  release. Radiogenic argon loss is only apparent for step 1, which gives an age slightly below the plateau, and for steps 14-17. The dip in ages recorded by these latter steps is thought to represent the outgassing of partially sericitised feldspar phenocrysts (a feature observed in thin section - see Appendix 7). This explanation is supported by the observation that the age dip corresponds to a peak in the  $^{37}/^{39}\text{K}$  curve, and thus to the outgassing of a relatively calcium-rich phase.

Both the calcium and chlorine interference age corrections are less than 0.1 Ma for all steps and thus insignificantly small. As Fig. 6:47 shows, for the majority of the steps the level of radiogenic  $^{40}\text{Ar}$  is greater than 95%.

The ICD2 analysis of the plateau steps 2-13 yields a meaningful age of  $61.0 \pm 0.6$  Ma (see Table 6:17). This is considered to be a reliable estimate of the timing of Interbasaltic Formation volcanic activity and is consistent with the age deduced for R1522 (K2A). These ages are over 4 Ma lower than Fitch & Hurford's (1977) date of  $65.2 \pm 0.4$  Ma for the Tardree rhyolite (which was the only strong evidence for Scenario (1)). On the other hand, they are both consistent with the timing of volcanic activity as proposed by Scenario (2).

#### c) The Upper Basalt Formation

R1523 (G062) is an analysis of an olivine basalt sample collected from the fourth flow (10m thick) above the Interbasaltic Formation on the Inver River section of the Garron Plateau. R1617 (L009) is an analysis of an

olivine dolerite sample from the volcanic plug cutting the UBF on Slemish Mountain. Sampling locations are indicated on Fig. 6:42.

R1523 (G062)

Beyond the first 10% of  $^{39}\text{K}$  release, steps display a pattern of decreasing age (see Fig. 6:48). For steps 1-15, the calcium age correction is less than 5 Ma. However, for the last four steps (16-19) it reaches a level or more than 50 Ma. The chlorine age correction is negligible for all steps.

The only ICD2 yielding on  $\text{MSWD} < 3.5$  is that for steps 14-19, which constitute a high temperature plateau (see Table 6:17). However, the calculated age of  $58.0 \pm 0.4$  Ma cannot be considered as more than a maximum age estimate. This is due to preceding steps giving higher ages (probably due to  $^{39}\text{K}$  recoil loss) and steps 14-19 constituting only 23% of the  $^{39}\text{K}$  release. The calculated age probably refers to the timing of zeolitisation, rather than basalt extrusion, because amygdales containing zeolite were observed in the thin section of G062 (see Appendix 7). 58 Ma is comparable with the high temperature plateau calculated for R1527 (I001). This latter best age estimate is also thought to reflect the timing of zeolitisation rather than lava extrusion.

ICD3 data analysis was not found to be helpful for the chronological interpretation of R1523's  $^{40}\text{Ar}-^{39}\text{Ar}$  data. However, it is gratifying to notice that the ICD3-Plot 3 analysis of steps 14-19, which have calcium age corrections ranging from 2 to 57 Ma, gives very similar results to the corresponding ICD2 analysis. The inferred

$\left[ \frac{40-(40/36)_{0.36}}{37} \right]_{\text{Ca}}$  value of  $-0.074 \pm 0.003$  is identical to the adopted value.

R1617 (L009)

This sample was selected for analysis because it represents probably

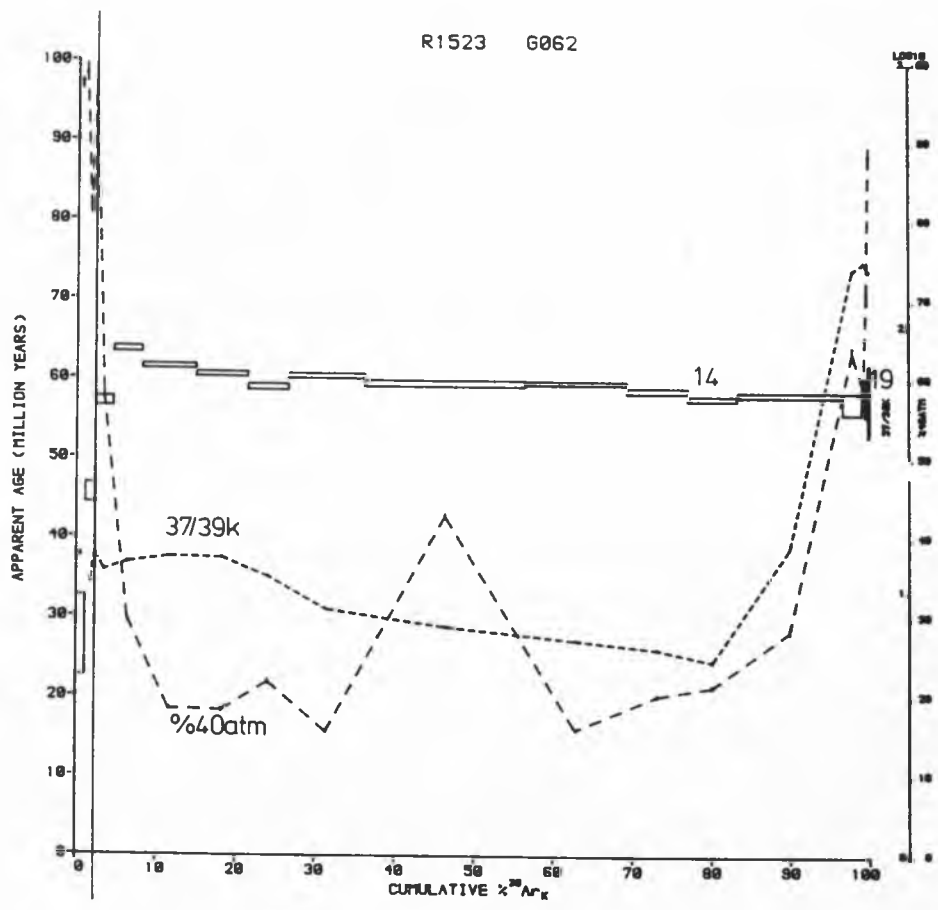


Fig. 6:48 Age spectrum for the Upper Basalt Formation sample R1523 (G062)

one of the youngest bodies of the Antrim Lava Group. The Slemish plug is thought to have been a feeder for lavas now removed by erosion.

The age spectrum for R1617 displays a well-developed plateau over the majority of the gas release (Fig. 6:49a). The low ages recorded in the first 10% of  $^{39}\text{K}$  release probably represent a minor loss of radiogenic argon from grain peripheries. The calcium interference age correction varies between 3 and 11 Ma for all but the last two steps. For these, the correction is 31 and 101 Ma respectively. The age correction due to chlorine interferences is negligible for all steps.

Steps 9-23 define a statistically meaningful ICD2 with an age of  $58.3 \pm 1.1$  Ma (see Table 6:17, Fig. 6:49b). This age is consistent with the ages of zeolitisation deduced from samples R1527 and R1523. However, the age for R1617 (L009) does not date the zeolitisation because rock sample L009 was very fresh with no signs of alteration or zeolitisation (see Appendix 7).  $58.3 \pm 1.1$  Ma is therefore taken as the emplacement age of the Slemish plug and it probably dates the youngest volcanic activity in Ireland. The coincidence of the age of the Slemish plug with the age of zeolitisation suggests that only after the cessation of volcanic activity did the lava pile cool sufficiently to stop the zeolitising hydrothermal activity.

ICD3 data analyses and the Arrhenius diagrams did not yield meaningful results.

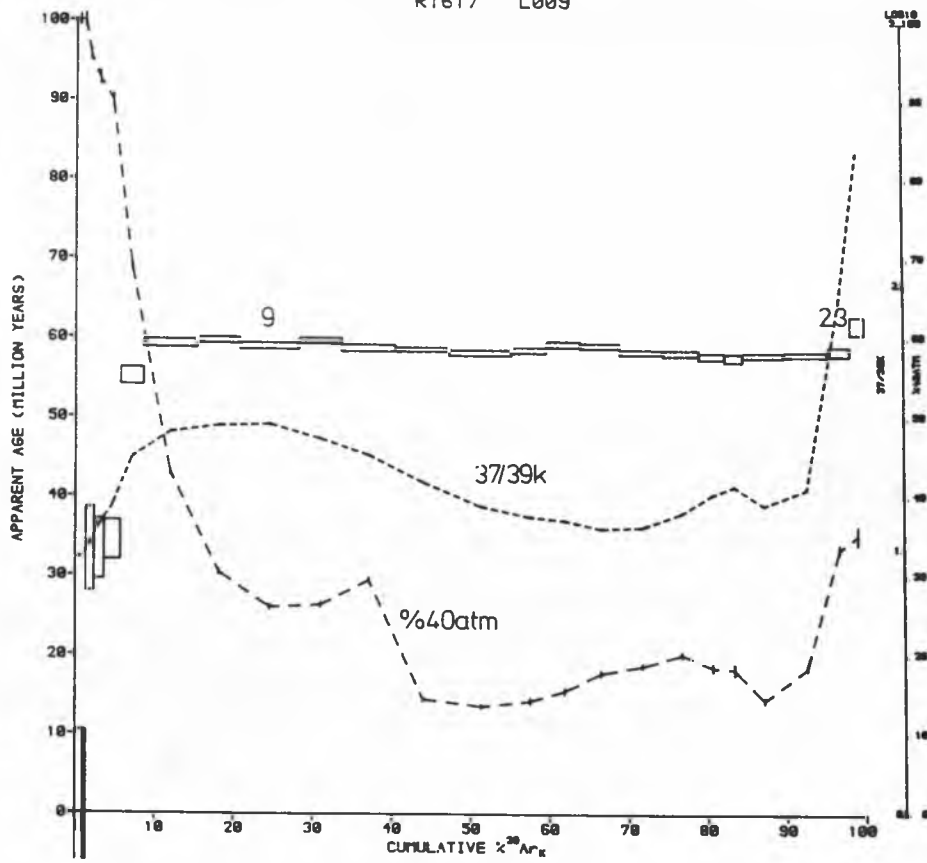
#### Conclusions for the Antrim Lava Group

Table 6:18 summarises the chronological interpretation of the Antrim Lava Group samples. The results presented here suggest that the volcanic activity in Antrim lasted from 61 to 58 Ma, which is consistent with Scenario (2). However, it has not been possible to



R1617 L009

(a)



(b)

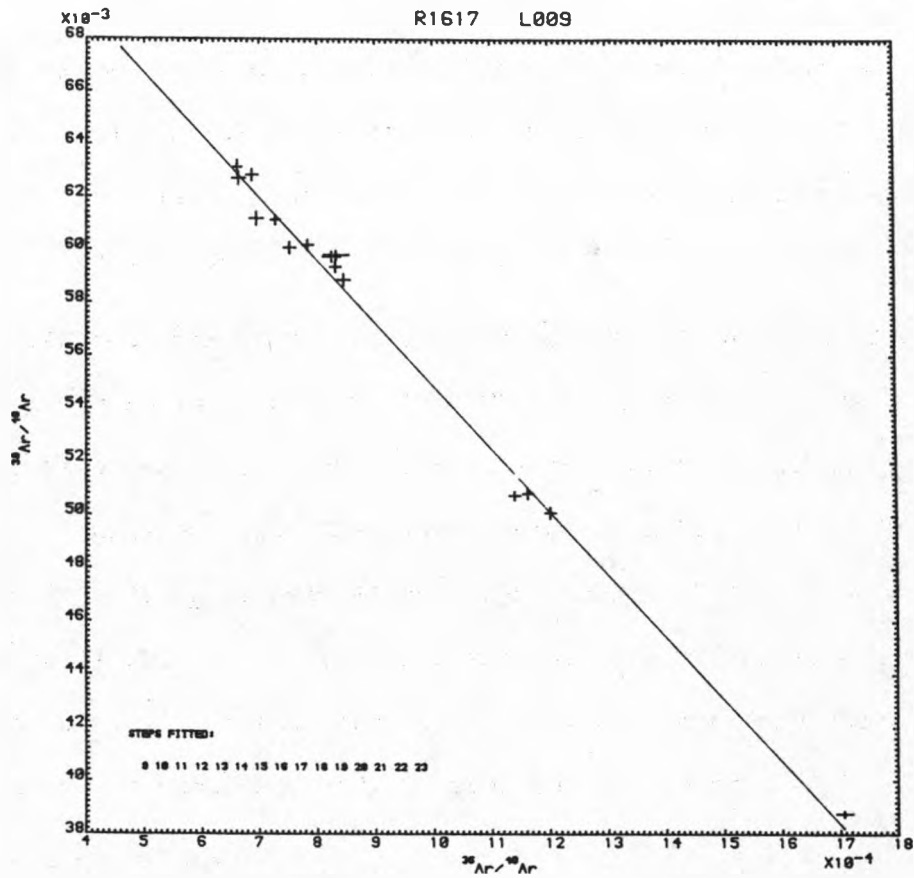


Fig. 6:49 Age spectrum (a) and ICD2 steps 9-23 (b) for the Upper Basalt Formation sample R1617 (L009)

Sample	Formation	Best age estimate (Ma)	
R1527(1001)	LBF	< 58.4 ± 0.7	probably dates zeolitization
R1533(Zeolite)	LBF	_____	
R1522(K2A)	IBF	< 59.0 ± 1.5	
R1532(TP0)	IBF	61.0 ± 0.6	
R1523(G062)	UBF	< 58.0 ± 0.4	probably dates zeolitization
R1617(L009)	UBF	58.3 ± 1.1	

Table 6:18 Summary of best age estimates for the Antrim Lava Group samples

conclusively date the Lower Basalt Formation because of the effects of zeolitisation. It is thought that the LBF is probably not much older than 61 Ma because all of the Antrim lavas possess a reversed direction of magnetisation (Wilson, 1970, and unpublished work from the Liverpool laboratory). Extrusion of the whole reversely magnetised Antrim Lava Group in the period of 58 - 61 Ma is consistent with Harland et al.'s (1982) geomagnetic polarity time scale (Fig. 6:44).

Mussett (1984), (1985) has reported  $^{40}\text{Ar}$ - $^{39}\text{Ar}$  best age estimates of 60 Ma for BTIP lavas found in Rhum and Mull respectively. It is concluded in this study that basalt extrusion in Antrim probably occurred at the same time as that in the rest of the BTIP.

The maximum age estimates for zeolitisation (R1527 and R1523 - see Table 6:18) are thought to be consistent with the cessation of volcanic activity at around 58 Ma.

#### 6:2:8 The Mourne Mountains

The Mourne Mountains of County Down are formed by five granite bodies emplaced into the Palaeozoic sedimentary country-rock by a process of ring dyke formation and cauldron subsidence (Miller & Brown, 1963). The centre of intrusion migrated with time in a westerly direction: the granite labelled G1 is the oldest and G5 the youngest (see Fig. 6:50).

The dense swarm of north-west trending dolerite dykes in the vicinity of the Mourne Mountains is largely truncated by the granite intrusions. Therefore they are, on the whole, older than the granites (although there are some dyke intrusions within the Mourne Granites which are clearly younger).

A summary of existing age data for the Mourne Mountains is presented in Table 6:19. The age of the Mourne Granites was thought to be well established by Evans et al.'s (1973) two  $^{40}\text{Ar}$ - $^{39}\text{Ar}$  step heating

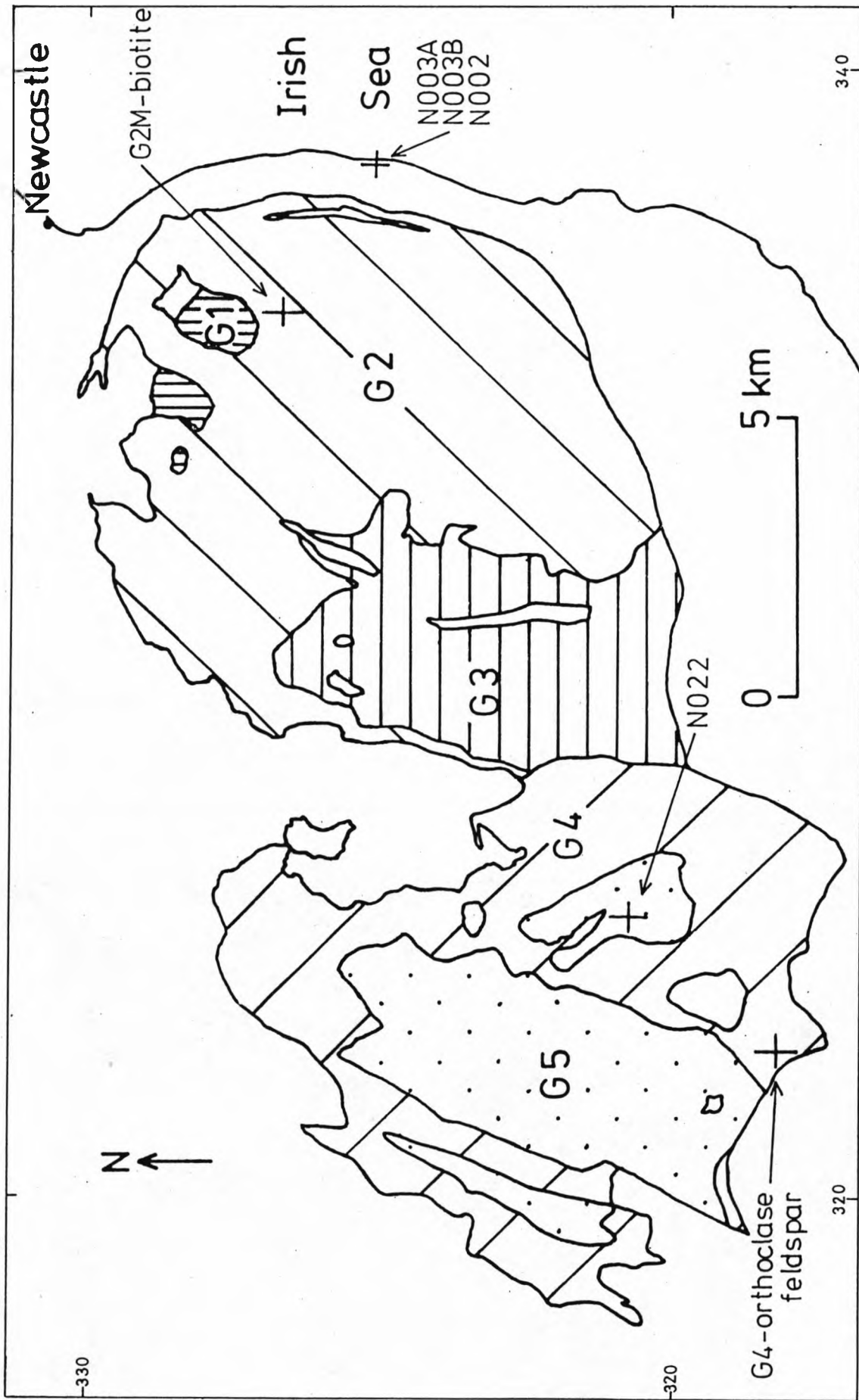


Fig. 6:50 The Mourne Granites: sampling locations

Granite	Mineral	Technique	Age (Ma)	Reference
G1	Biotite	K-Ar	77 ± 7	Miller & Brown (1963)
	K feldspar	K-Ar	57.1 ± 2.2	Beckinsale (unpublished-quoted in MacIntyre, 1973)
	Biotite	K-Ar	57.1 ± 1.9	Beckinsale (unpublished-quoted in MacIntyre, 1973)
	Biotite	K-Ar	57.6 ± 2.0	Beckinsale (unpublished-quoted in MacIntyre, 1973)
	Biotite	K-Ar	56.3	Evans et al. (1973)
G2	Biotite	K-Ar	57.5	Evans et al. (1973)
	Biotite	<sup>40</sup> Ar- <sup>39</sup> Ar step heating	59.6 ± 1.6	Evans et al. (1973)
G4	K feldspar	K-Ar	55.3 ± 2.1	Beckinsale (unpublished-quoted in MacIntyre, 1973)
	Biotite	K-Ar	60.7 ± 2.6	Beckinsale (unpublished-quoted in MacIntyre, 1973)
G5	Biotite	<sup>40</sup> Ar- <sup>39</sup> Ar step heating	59.5 ± 1.6	Evans et al. (1973)
<hr/>				
Hornfels contact of G4		K-Ar	55.7	Evans et al. (1973)
Basic dyke cutting G4		K-Ar	52.5	Evans et al. (1973)

Table 6:19 Existing age data for the Mourne Mountains

plateaux which gave concordant ages of  $59.5 \pm 1.5$  Ma (Evans et al., 1973; Macintyre, 1973; Macintyre et al., 1975). The conventional K-Ar dates would then be explained in terms of varying degrees of radiogenic argon loss (Miller & Brown's 1963 date is clearly erroneous). However, work presented in this thesis and Gibson's unpublished Rb-Sr analyses strongly suggest that the granites were emplaced significantly later than 59.5 Ma, at around 55 Ma. In this study, two granite mineral separate samples have been analysed by the  $^{40}\text{Ar}$ - $^{39}\text{Ar}$  stepwise degassing technique, together with five whole-rock samples from dykes in the vicinity of the Mourne Mountains.

a) The Granite Mineral Separates

R1572 (G2M-biotite)

This biotite separate (300 - 500 $\mu$ ) was extracted from a sample of granite G2 collected at the mafic-rich locality marked on Fig. 6:50.

R1572 displays very little age variation across the majority of the gas release (Fig. 6:51), the only discordancies being for the first two steps and for a series of three steps (13-15) at intermediate temperatures. For the majority of steps, the level of radiogenic  $^{40}\text{Ar}$  is about 90% and for those steps where  $^{37}\text{Ar}$  is recorded, the calcium interference age correction is less than 0.1 Ma and thus negligible. The chlorine age correction is typically 0.15 Ma, and therefore also insignificant.

ICD2 analysis of all steps but the first two (anomalous ages) and last two (negligible  $^{39}\text{K}$  release) only just fails to give a meaningful age, when applying the acceptance criteria outlined in Chapter 3 (see Table 6:20). However, steps 5-12 and 16-20 do give apparently meaningful ages of  $54.9 \pm 0.6$  Ma (see Fig. 6:52 for the two ICD2 plots). This age is taken as the best estimate for the time of emplacement of granite G2. It is thought that the slightly anomalous ages of steps 13-15 may be related to the dehydration processes which

Irradiation no. (Locality no.)	Steps	% <sup>39</sup> K	Total gas age (Ma)	Mean age (Ma) (step ages weighted by 1/variance)	Age (Ma)	ICD2 parameters (40/36) <sub>O</sub>	MSWD
R1572(G2M- biotite)	All(1-22)	100	55.0 ± 0.5	55.2 ± 1.3	55.2 ± 0.6	295.9 ± 5.8	11.0
	3-20	96	55.1 ± 0.5	55.2 ± 0.9	54.8 ± 0.6	313.4 ± 15.0	3.6
	5-12	38	54.9 ± 0.5	54.9 ± 0.5	54.9 ± 0.6	297.9 ± 16.9	1.4
	16-20	36	54.7 ± 0.5	54.8 ± 0.6	54.9 ± 0.7	289.8 ± 24.8	2.1
R1573(G4- orthoclase feldspar)	All(1-27)	100	54.3 ± 0.6	55.6 ± 2.7	56.6 ± 1.3	293.0 ± 10.9	6.9
	15-21	63	53.3 ± 0.7	53.3 ± 0.6	54.5 ± 0.8	293.1 ± 6.4	0.1

Table 6:20 Parameters calculated for the Mourne Granite mineral separates

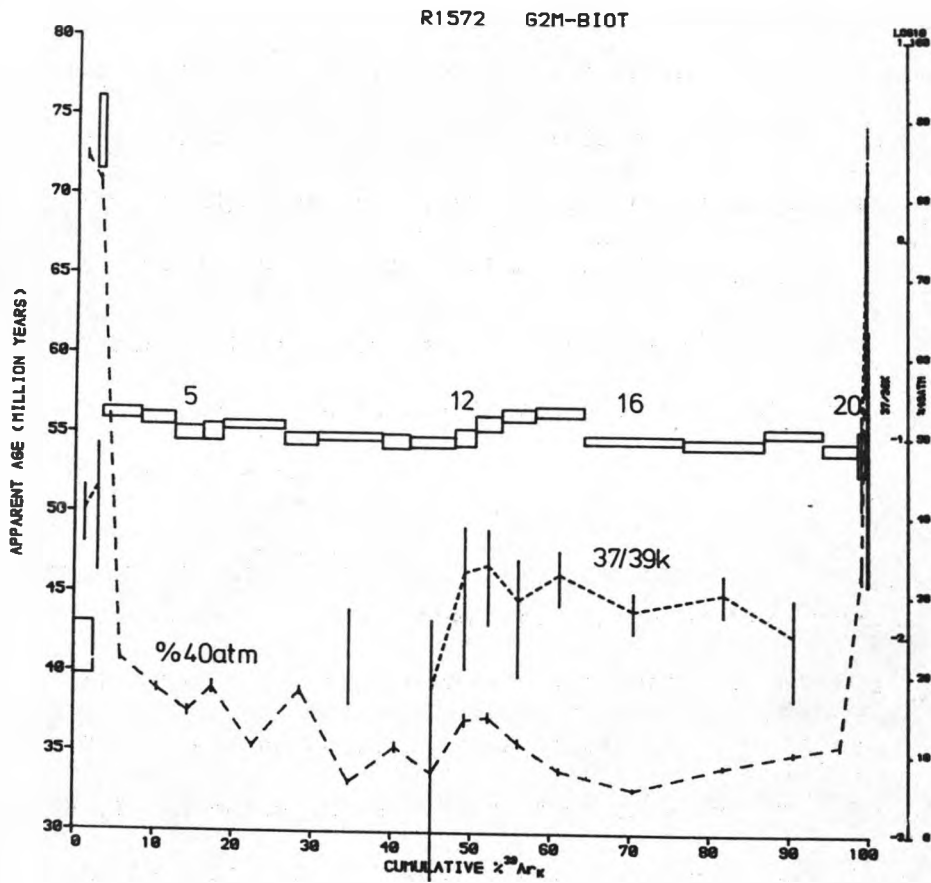


Fig. 6:51 Age spectrum for the Mourne Granite mineral separate sample R1572 (G2M-biotite)



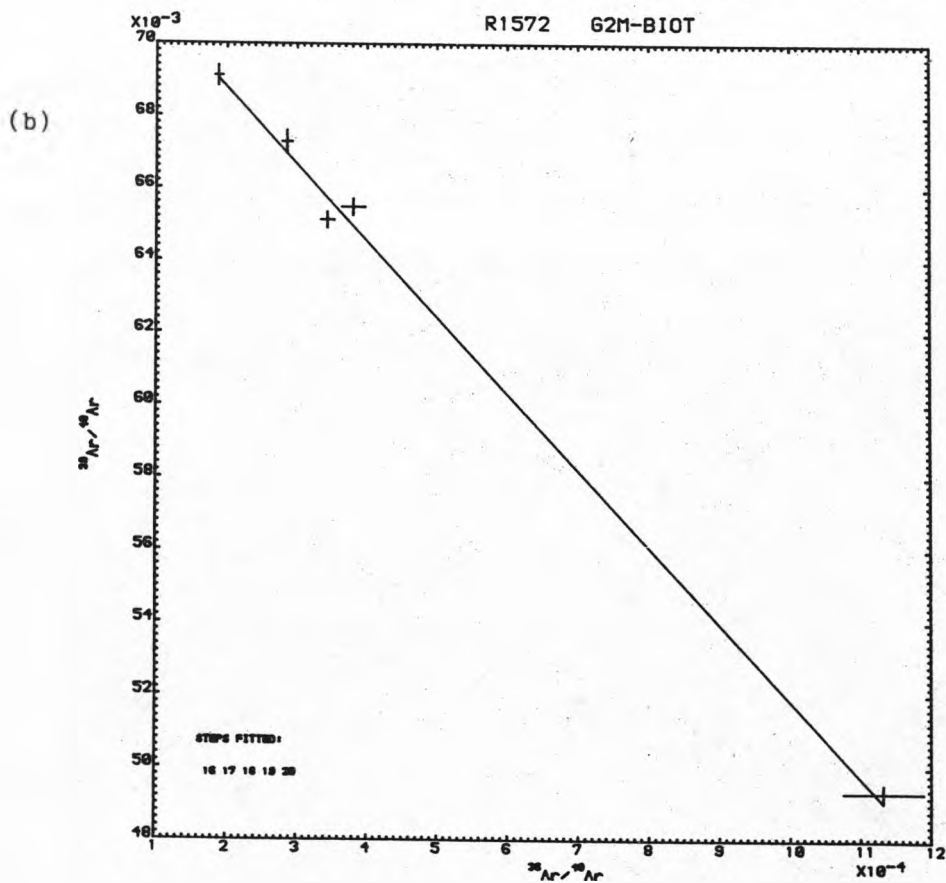
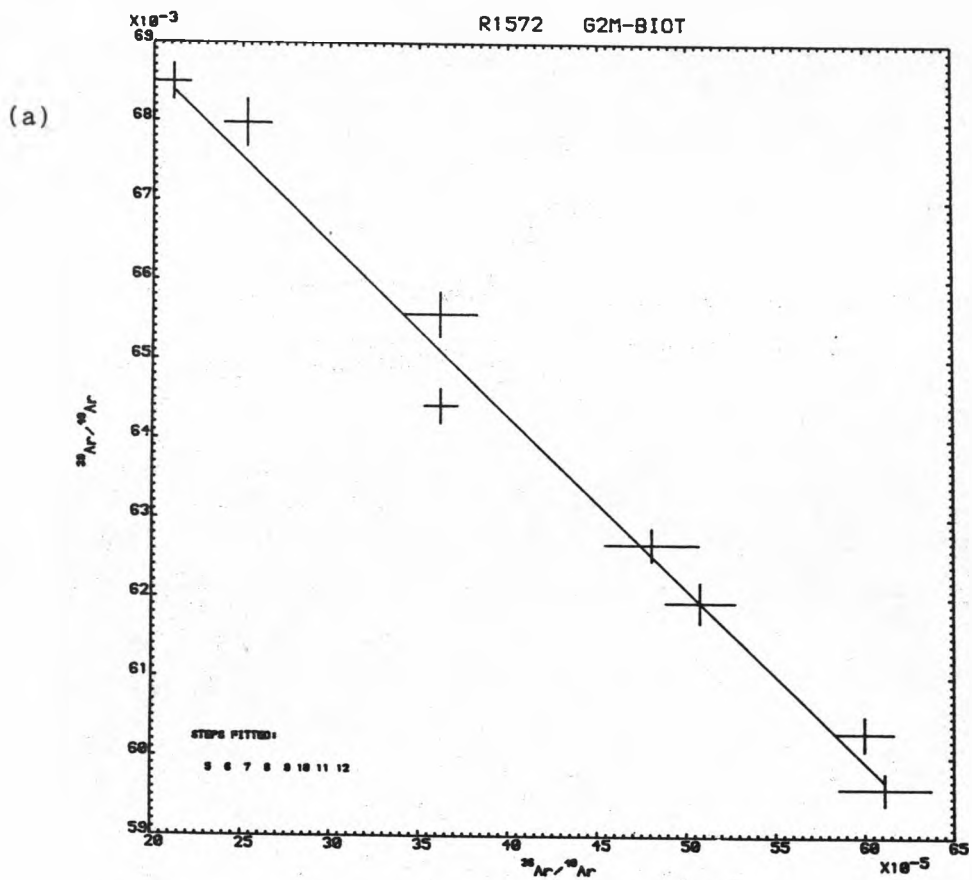


Fig. 6:52 ICD2s (a) steps 5-12 (b) steps 16-20 for the Mourne Granite mineral separate sample R1572 (G2M-biotite)

inevitably occur when a hydrated mineral is outgassed in a vacuum. Similar anomalous age segments in biotites at intermediate temperatures have also been reported by Tetley & McDougall (1978) and Berger & York (1981). Both Tetley and McDougall's (1978) and the Mourne Granite biotite are not thought to have experienced any major disturbance since crystallisation, so the observed effect appears to be a property of the mineral itself.

Unlike the corresponding ICD2, ICD3-Plot 2 analysis of steps 3-20 gave an MSWD less than 3.5. However, the calculated age of  $47.6 \pm 3.2$  Ma is not geologically acceptable in the context of the other results presented in this study. Geologically meaningless ages and good MSWDs are a common feature of ICD3-Plot 2 data analyses in this Irish Tertiary work.

The Arrhenius diagrams for  $39\text{K}$  and  $40^*$  are almost identical and the results for the former only are quoted here (the  $37$  release Arrhenius diagram was not plotted because  $^{37}\text{Ar}$  was recorded for only about half the total steps). Table 6:21 compares the diffusion parameters and closure temperatures calculated from the  $39\text{K}$  release for spherical and planar diffusion geometry (the two Arrhenius diagrams are presented in Fig. 6:53). Those computed for the planar symmetry are lower than the spherical geometry ones and the former are preferred on the grounds of mineral structure (micas are sheet silicates). The Arrhenius diagrams display two approximately parallel but offset linear segments. Such a biotite Arrhenius diagram pattern has also been observed by Berger & York (1981) who suggested that it may reflect mineral breakdown during vacuum outgassing. For the Mourne's biotite sample, the step separating the two linear segments is number 11, which just precedes the intermediate temperature age bump (steps 13-15). Thus, both effects may be intimately related, with the common denominator being mineral dehydration. The biotite Arrhenius

Diffusion geometry	Steps	E (kcal mol <sup>-1</sup> )	Do/a (s <sup>-1</sup> )	MSWD	Closure temperature (°C) - cooling rate assumed to be 1000°C Ma <sup>-1</sup>
Spherical	3-10	41	3.6 * 10 <sup>4</sup>	2.9	225
	12-19	40	5.6 * 10 <sup>4</sup>	1.1	245
Planar	3-10	35	9.3 * 10 <sup>3</sup>	4.5	190
	12-19	37	5.4 * 10 <sup>3</sup>	1.3	225

Table 6:21 Comparison of diffusion parameters and closure temperatures calculated from the 39K release Arrhenius diagrams of Mourne Granite mineral separate sample R1572 (G2M-biotite)

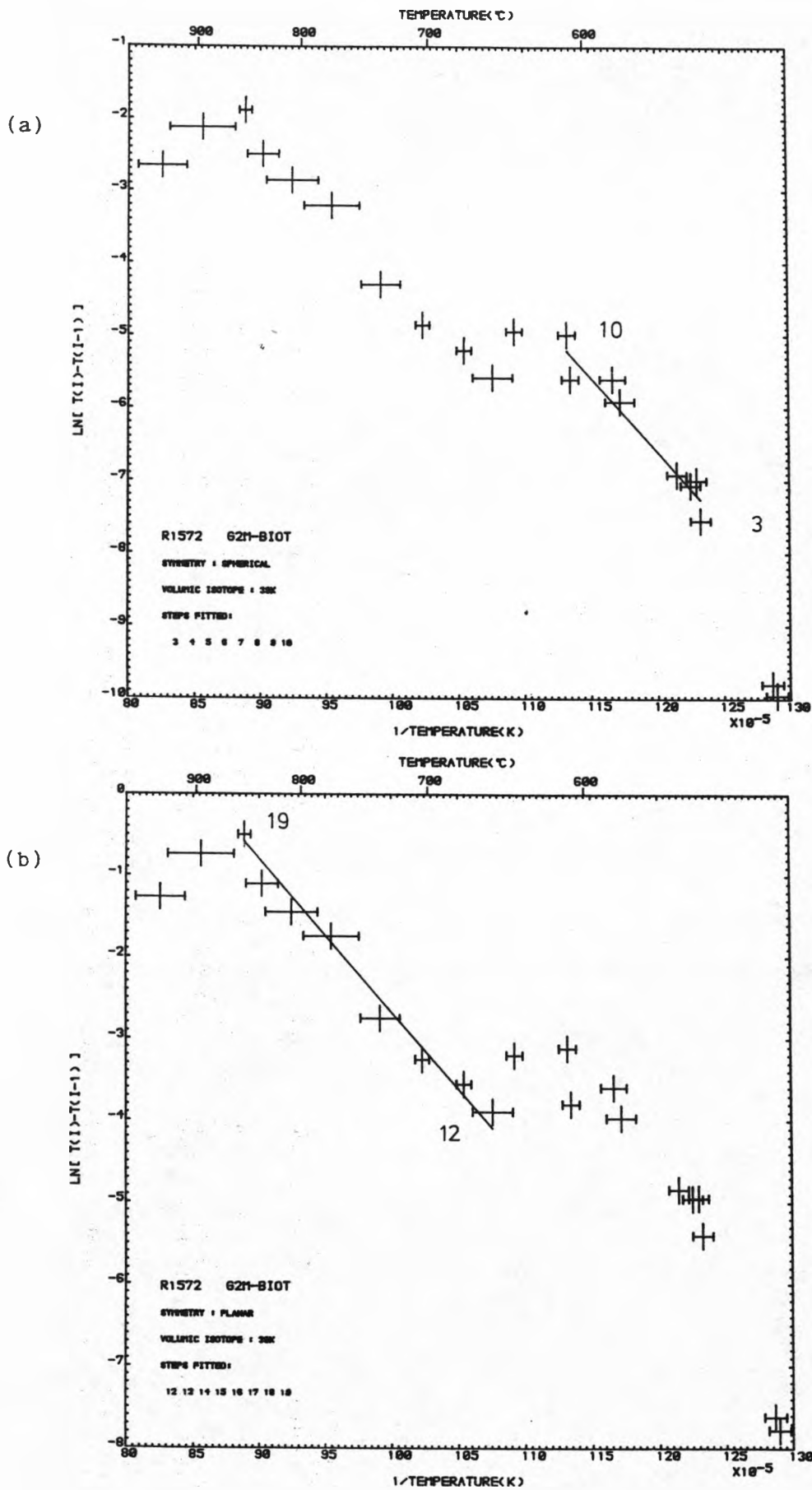


Fig. 6:53 Arrhenius diagrams for the  $^{39}\text{K}$  release of the Mourne Granite mineral separate sample R1572 (G2M-biotite) (a) spherical symmetry (b) planar symmetry

diagrams give two closure temperature estimates; one from the low and one from the high temperature linear correlations. The preferred planar symmetry Arrhenius diagram gives closure temperatures of 190 and 225°C respectively (see Table 6:21). Without presuming which of these is the most reliable, the mean is taken as the best estimate of biotite closure temperature in Mourne granite G2 (this follows the example of Berger & York, 1981). This value of 210°C lies slightly below the range of biotite closure temperatures quoted in Table 4:1.

R1573 (G4-orthoclase feldspar)

This orthoclase feldspar separate (300 - 500 $\mu$ ) was extracted from a sample of granite G4 collected at the locality marked on Fig. 6:50. The age spectrum for R1573 (Fig. 6:54a) displays a saddle shape (usually diagnostic of excess argon) with a very broad age minimum at about 53 Ma. The %  $^{40}\text{Ar}_{\text{atmospheric}}$  curve shows a very strange variation, with very low levels only at low temperatures. This may reflect a type of compositional zoning within the potassium feldspar (or perhaps a mineral separate contamination). No  $^{37}\text{Ar}$  was recorded for any of the steps of R1573; thus there is no correction for calcium-derived interferences. The chlorine age correction is less than 0.05 Ma for all steps and thus negligible.

Steps 15-21, which constitute the saddle minimum, yield a meaningful ICD2, indicating an age of  $54.5 \pm 0.8$  Ma (see Table 6:20, Fig. 6:54b). This age is essentially identical to the best age estimate for the biotite separated from G2. However, it must be realised that the ICD2 age is very sensitive to the deduced  $(40/36)_0$  because of the high %  $^{40}\text{Ar}_{\text{atmospheric}}$  levels. Although the  $(40/36)_0$  for steps 15-21 is not significantly less than 295.5., it does have the effect of making the calculated ICD2 age greater than all the individual step ages. Because of this, and the saddle shape of the age spectrum (which indicates the presence of excess argon), the age of  $54.5 \pm 0.8$  Ma

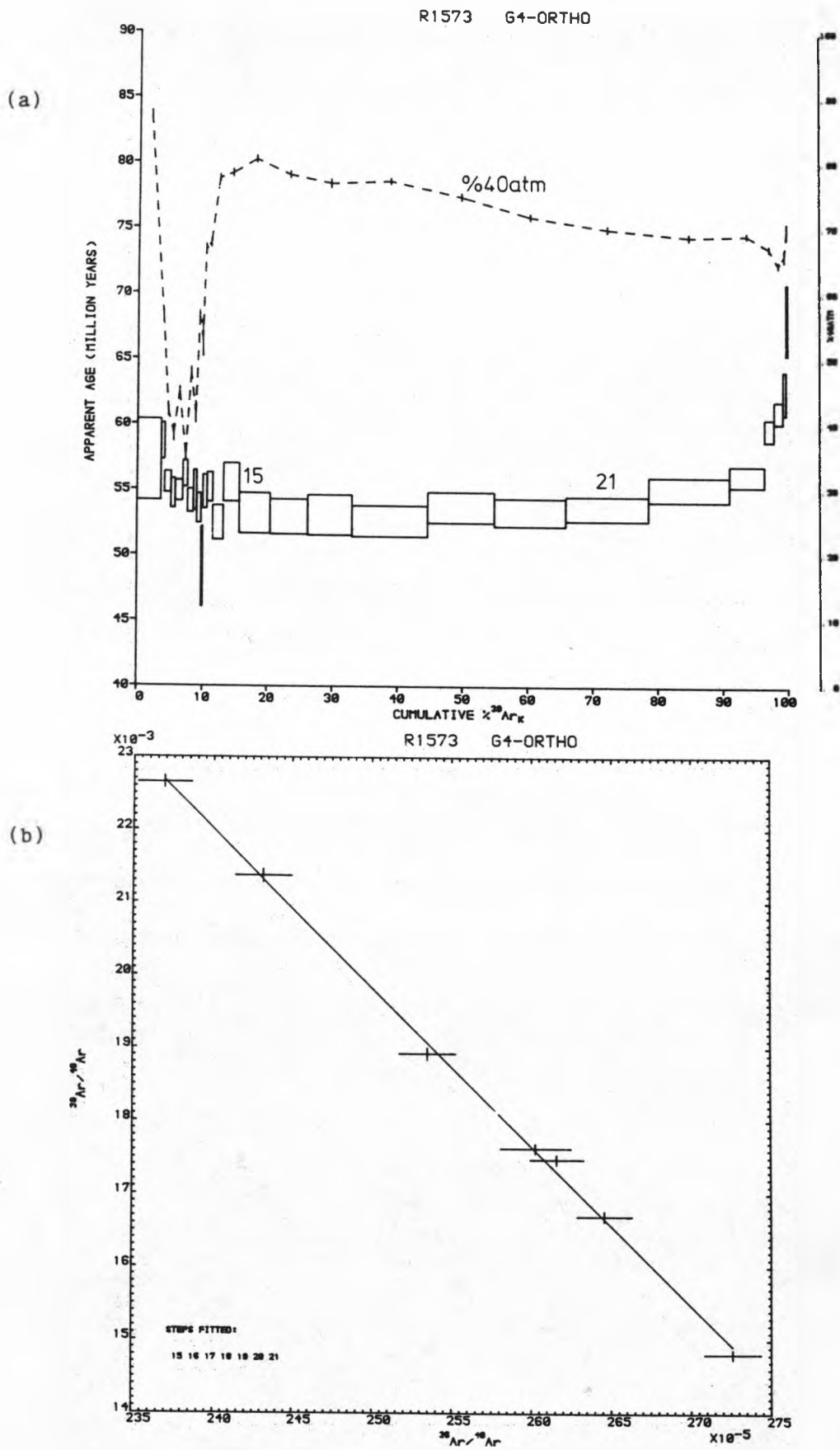


Fig. 6:54 Age spectrum (a) and ICD2 steps 15-21 (b) for the Mourne Granite mineral separate sample R1573 (G4-orthoclase feldspar)

is regarded as a maximum age estimate.

Steps 11-23 give a well-defined linear correlation on  $^{39}\text{K}$  and  $^{40}\text{K}$  Arrhenius diagrams (MSWD = 2.4). However, with  $E \approx 70 \text{ kcal mol}^{-1}$  and  $D_0/a^2 \approx 10^6 \text{ s}^{-1}$ , the implied closure temperature is calculated to be over  $500^\circ\text{C}$  (cooling rate assumed to be  $1000^\circ\text{C Ma}^{-1}$ ) which is very much greater than published closure temperature estimates for potassium feldspar ( $130 - 230^\circ\text{C}$ ). The  $^{39}\text{K}$  Arrhenius plot for R1573 is presented in Fig. 6:55.

#### Conclusions from the Mourne Granite Mineral Separate Analyses

R1572 (G2M-biotite) and R1573 (G4-Orthoclase feldspar) give ages of  $54.9 \pm 0.6 \text{ Ma}$  and  $54.5 \pm 0.8 \text{ Ma}$  (a maximum estimate) respectively, which are significantly younger than the  $^{40}\text{Ar}-^{39}\text{Ar}$  plateau ages reported by Evans et al., (1973) for Mourne Granite mineral separates. The younger granite sample, R1573, gives a slightly younger age than R1572. However, this difference is not significant due to the assigned age errors. From the analyses of these two mineral separates, it is not possible to establish the duration of granite emplacement in the Mourne Mountains because the younger sample gives only a maximum age estimate. In an attempt to place a lower age limit on granite emplacement, a dyke cutting granite G5 has been analysed.

#### b) Dyke Cutting G5

A whole-rock sample of a 0.5m thick fine-grained basaltic dyke cutting G5 has been analysed as part of the Mourne Mountain investigation (the dyke locality is marked on Fig. 6:50 as N022). The fine-grained texture of the dyke rock suggests it was intruded when granite G5 was cool.

#### R1578 (N022)

R1578 has a total gas age of  $55.7 \pm 0.5 \text{ Ma}$  and shows a decreasing pattern of ages in the age spectrum plot (Fig. 6:56). The  $^{37}/^{39}\text{K}$  curve displays a marked peak at intermediate temperatures where the

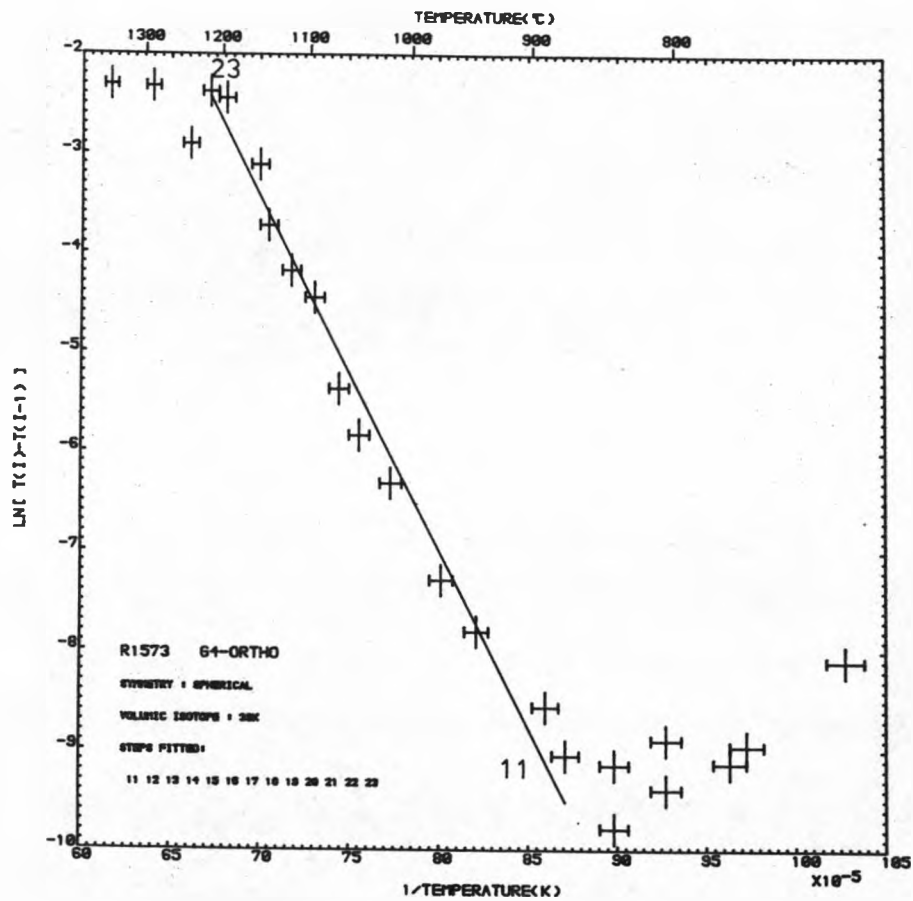


Fig. 6:55 Arrhenius diagram for the <sup>39</sup>K release of the Mourne Granite mineral separate sample R1573 (G4-orthoclase)



Irradiation no. (Locality no.)	Steps	% <sup>39</sup> k	Total gas age (Ma)	Mean age (Ma) (step ages weighted by 1/variance)	Age (Ma)	ICD2 parameters (40/36) <sub>o</sub>	MSWD
R1578(N022)	A11(2-37)	100	55.7 ± 0.5	56.1 ± 1.3	55.4 ± 0.6	300.5 ± 6.3	10.0
	9-16	8	57.2 ± 0.5	57.2 ± 0.6	53.1 ± 1.1	330.4 ± 16.4	0.3
	17-35	85	55.3 ± 0.5	55.4 ± 1.0	52.2 ± 1.0	320.8 ± 13.3	3.4
R1614(N003A)	A11(1-27)	100	57.6 ± 1.0	55.8 ± 6.1	58.8 ± 1.7	232.7 ± 31.2	532.7
R1615(N003B)	A11(1-27)	100	56.6 ± 1.1	53.7 ± 8.0	58.9 ± 1.8	52.4 ± 56.9	726.2
R1620(N002)	A11(1-26)	100	56.3 ± 1.3	54.3 ± 6.3	56.7 ± 1.9	224.2 ± 32.2	650.1
R1616(P001)	A11(1-26)	100	103.9 ± 2.0	80.9 ± 32.8	65.7 ± 8.1	348.2 ± 69.8	216.6

Table 6:22 Parameters calculated for dyke rock samples collected in the vicinity of the Mourne Mountains

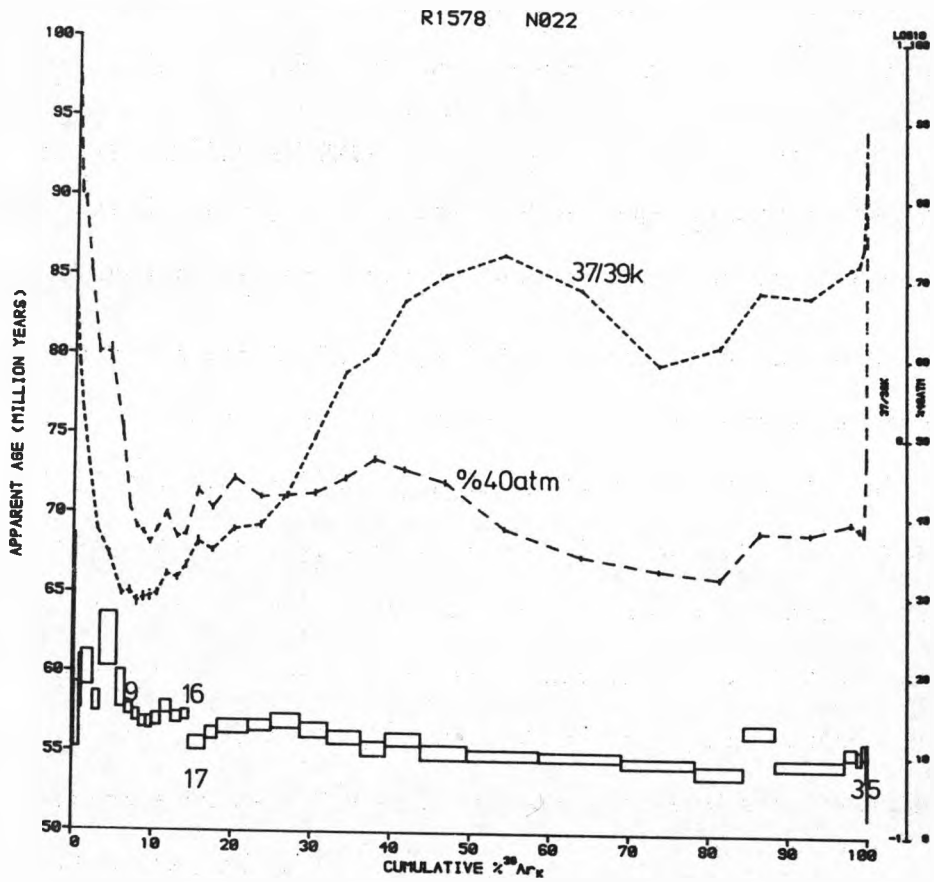


Fig. 6:56 Age spectrum for the dyke (cutting the Mourne Granite G5) sample R1578 (N022)

calcium interference age correction is as high as 1 Ma. Peaking in the same portion of the gas release is the chlorine age correction, which reaches a highest value of 1.4 Ma.

The ICD2 analyses of steps 9-16 and 17-35 are listed in Table 6:22. Both give an age of about 52 - 53 Ma with  $(40/36)_O$  greater than 295.5, and an MSWD below the cut-off of 3.5 (analysis of the combined steps 9-35 gives an unacceptable MSWD). The  $(40/36)_O$  values indicate the presence of excess argon and such an interpretation is consistent with the age spectrum shape (see Table 4:3). However, the generally adopted policy is not to accept ages as meaningful where the  $(40/36)_O$  is significantly different from the atmospheric 40/36 ratio (see Section 3:5). The high temperature ages of  $\approx 54.5$  Ma are therefore regarded as giving the best age estimate. Bearing in mind the shape of the age spectrum, the 54.5 Ma date must be regarded as a maximum age estimate. This interpretation is valid regardless of the physical explanation for the anomalously high age low temperature steps (see Table 4:3). The best age estimate for R1578 is indistinguishable from the ages determined for the Mourne Granite mineral separates. ICD3 data analysis was not found to be helpful and the Arrhenius diagrams for R1578 gave linear correlations that were defined only by a small number of steps. The deduced closure temperatures are not thought to be meaningful in the context of published estimates of mineral closure temperatures (see Table 4:1).

c) Dykes of the Mourne Swarm

All the dykes on the shore east of the Mourne Mountains are thought to be cut off by the granites and thus older than them (Tomkeieff & Marshall, 1933). In this study, I have dated three samples from Tomkeieff & Marshall's (1933) dyke number 61 which consists of a 10 m wide composite dyke and a cross-cutting hypersthene-basalt dyke (4m thick). R1614 (N003A) and R1615 (N003B) were from the composite's feldspar-

porphyry inner and hypersthene-basalt outer respectively and R1620 (N002) was from the cross-cutting dyke (all samples were whole-rocks). The sampling location is marked on Fig. 6:50. The petrology of dyke 61 is described in Tomkeieff & Marshall (1933) and a brief description of sections of the dated rocks is presented in Appendix 7. All the dykes of the Mourne Swarm are heavily altered and this may be due to the effect of the later granite intrusions (Tomkeieff & Marshall, 1933).

The three samples dated all give an age spectrum similar to one recorded for the Kerry dyke system samples and to disturbed spectrum No. 8 of Table 4:3. Bearing in mind the possible interpretations of such an age spectrum shape, both the low temperature age maximum and the high temperature age minimum are recorded for each sample. The geochronological interpretation of the  $^{40}\text{Ar}$ - $^{39}\text{Ar}$  data for the Mourne Swarm samples is discussed at the end of this section.

#### R1614 (N003A)

The age spectrum of R1614 is presented in Fig. 6:57. The low temperature age maximum and high temperature age minimum are  $61.3 \pm 1.1$  and  $54.3 \pm 1.0$  Ma respectively. The increase in age at very high temperatures corresponds to increasing  $^{37}/^{39}\text{K}$  levels. The calcium interference age correction is less than 0.4 Ma for all but the last three steps and is therefore generally insignificant. For the last three steps, this correction reaches a maximum value of 3.3 Ma. The chlorine age correction is negligible for all steps. Over the majority of the gas release, the level of radiogenic  $^{40}\text{Ar}$  is greater than 90%.

Both ICD2 and ICD3 data analyses did not produce meaningful results. The Arrhenius diagrams for R1614 are complex, with linear correlations being limited to small numbers of steps; they are therefore not presented here.

#### R1615 (N003B)

The age spectrum for R1615 (Fig. 6:58) displays a low temperature age

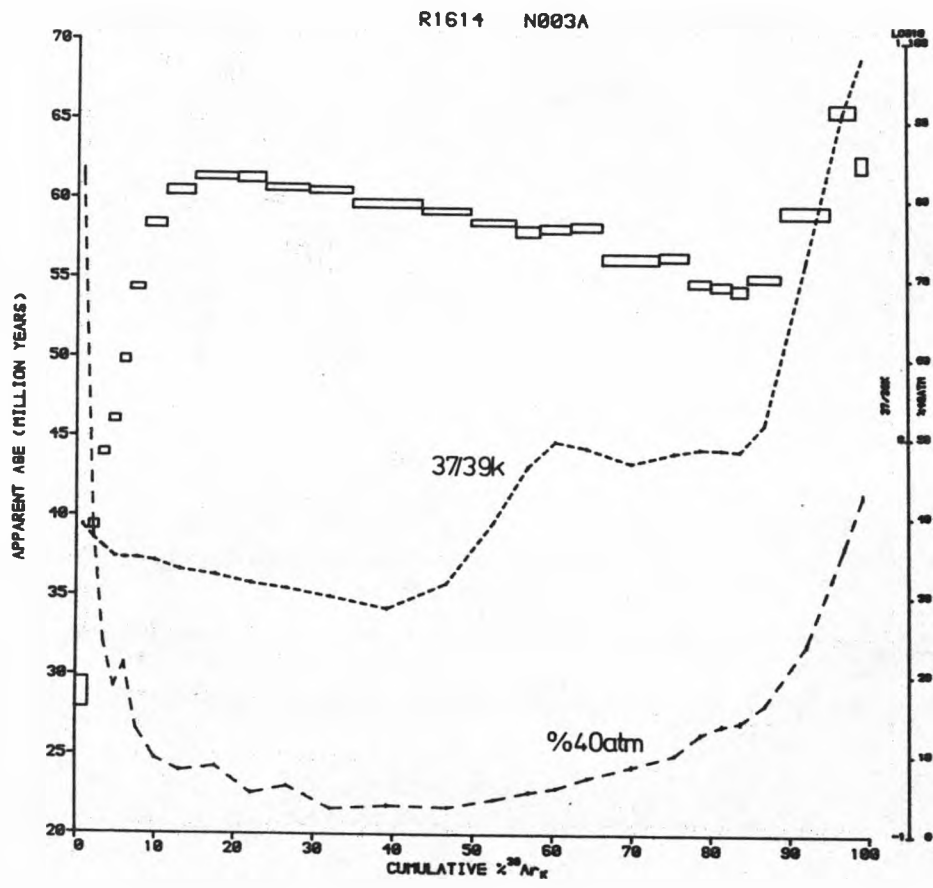


Fig. 6:57 Age spectrum for the Mourne Swarm sample R1614 (N003A)

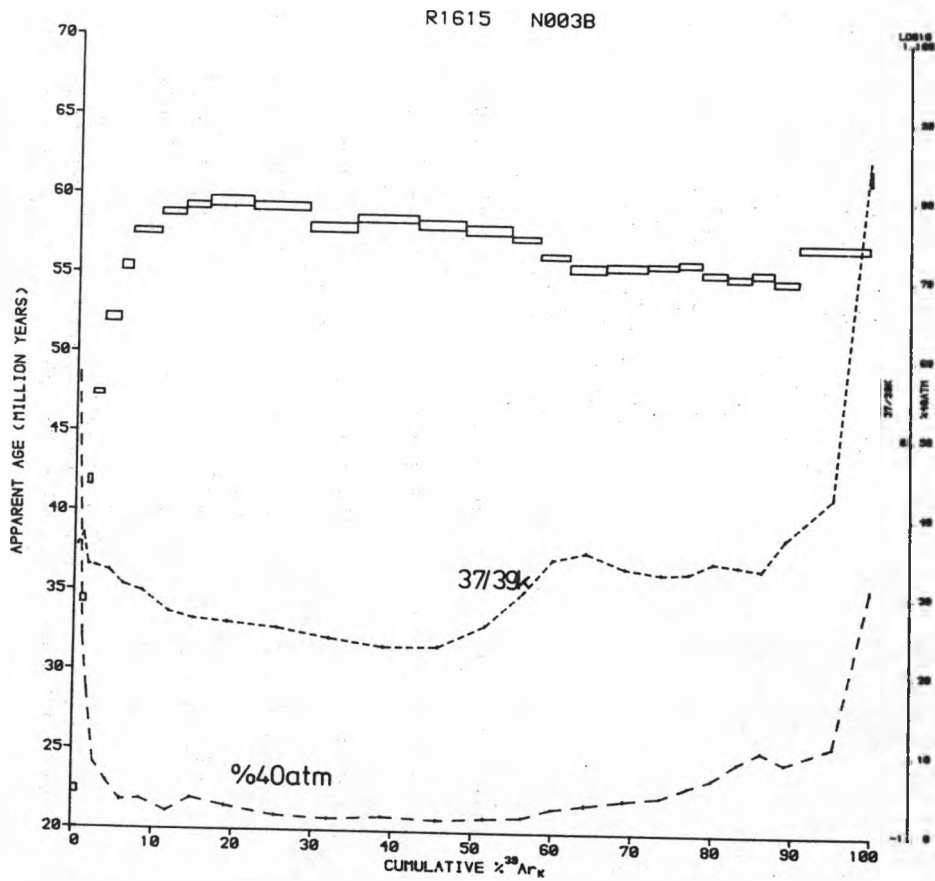


Fig. 6:58 Age spectrum for the Mourne Swarm sample R1615 (N003B)

peak of  $59.6 \pm 1.2$  Ma and a high temperature age trough of  $54.9 \pm 1.1$  Ma. Again, the increase in age at very high temperatures corresponds to rising  $37/39\text{K}$  levels. The  $37/39\text{K}$  and %  $^{40}\text{Ar}_{\text{atmospheric}}$  curves and the levels of the calcium/chlorine age corrections are very similar to those reported for R1614.

Again ICD2 and ICD3 data analysis and the Arrhenius diagrams did not produce meaningful results.

#### R1620 (N002)

The features of the age spectrum of R1620 (Fig. 6:59) are similar to those reported for R1614 and R1615. The low temperature age maximum is  $59.5 \pm 1.4$  Ma and the high temperature age minimum is  $52.9 \pm 1.3$  Ma.

ICD2 and ICD3 data analyses were not found to be helpful. The Arrhenius diagrams for  $39\text{K}$ ,  $40^*$  and 37 release are all very similar (see Fig. 6:60 for a comparison of the  $39\text{K}$  and 37 plots) with a possibly meaningful linear correlation spanning steps 4-11 in each case. The parameters calculated for these steps are listed in Table 6:23. The concordance of the closure temperature estimates suggests that all three isotopes were derived from the same mineral over steps 4-11. This mineral is tentatively identified as hornblende because in sample N003A, which is altered in the same way as N002, this was the major potassium-bearing mineral (see Appendix 6). The closure temperature estimates (Table 6:23) are rather low for hornblende, however, this could be explained by a very small effective grain size (for N003A the scanning electron microscope work showed that potassium-rich zones were typically of the order of  $25\mu$  and less). It must be noted that steps 4-11 correspond only roughly to a plateau of ages.

#### Conclusions for the Mourne Swarm Dykes

Table 6:24 compares the low temperature age maxima and high temperature age minima for samples R1614, R1615 and R1620.

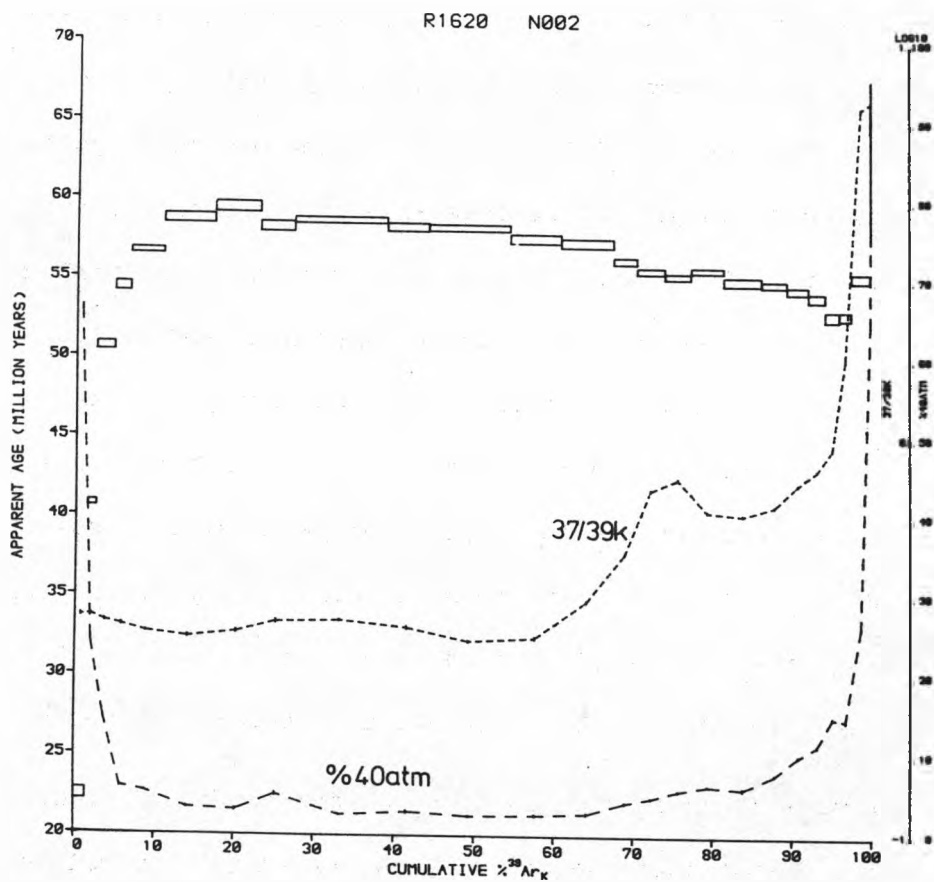
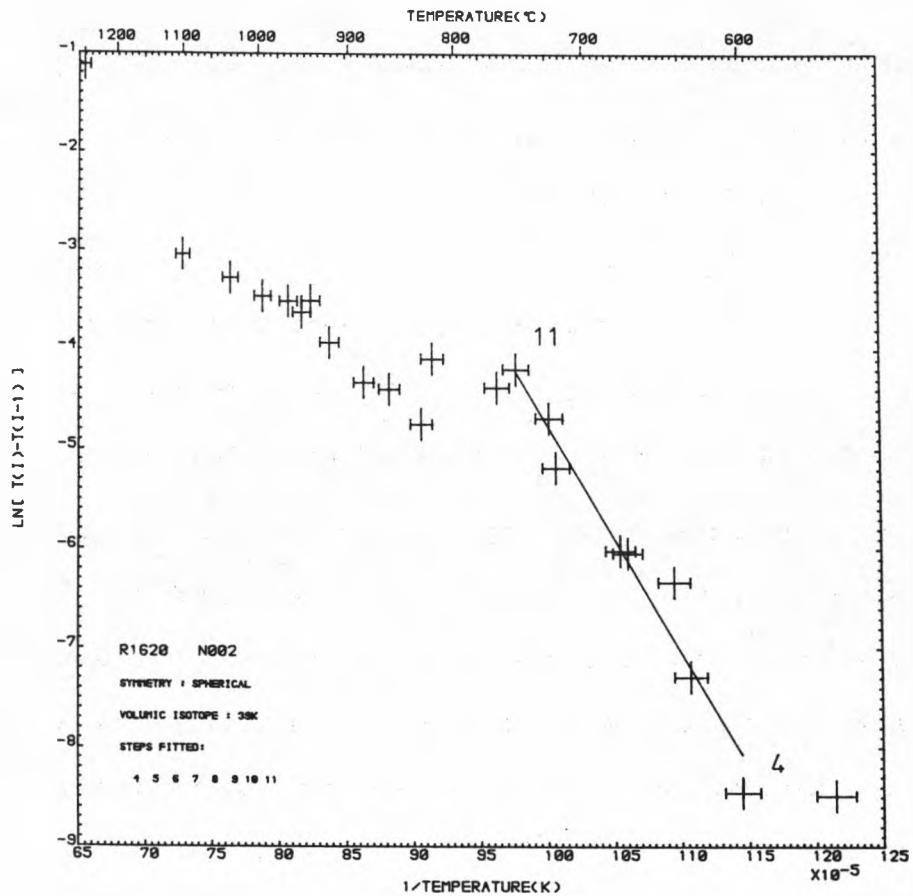


Fig. 6:59 Age spectrum for the Mourne Swarm sample R1620 (N002)



(a)



(b)

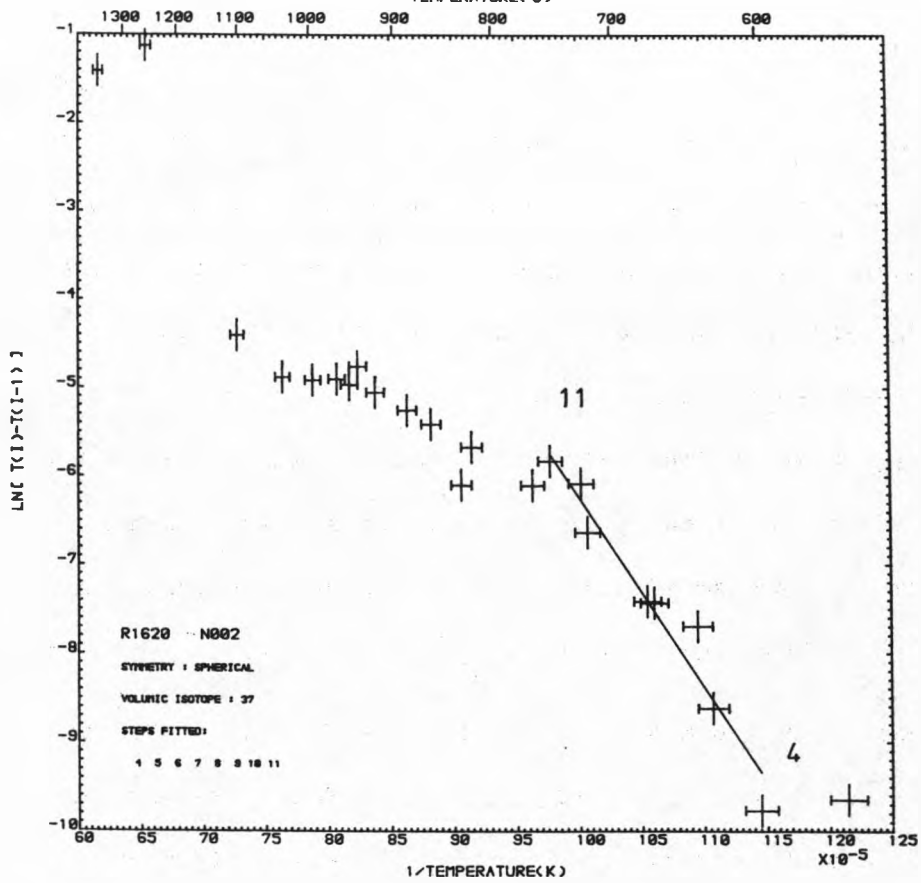


Fig. 6:60 Arrhenius diagrams for the Mourne Swarm sample R1620 (N002)  
(a) 39K (b) 37

Isotope release	E (kcal mol <sup>-1</sup> )	Do/a (s <sup>-1</sup> )	MSWD	Closure temperature (°C) - cooling rate assumed to be 10 <sup>4</sup> °C Ma <sup>-1</sup> †
39K	46	4.6 * 10 <sup>4</sup>	1.3	310
40*	50	3.5 * 10 <sup>5</sup>	1.5	330
37	43	2.2 * 10 <sup>3</sup>	1.6	315

† This is a relatively slow cooling rate for a dyke intrusion. However it is used because the major potassium (and calcium) bearing phase is a secondary mineral thought to have formed due to the heating effect caused by granite intrusion (see text). It is thought that cooling in the metamorphic aureole surrounding the Mourne Granites would be relatively slow.

Table 6:23 Comparison of diffusion parameters and closure temperatures calculated for 39K, 40\* and 37 release for steps 4-11 of Mourne Swarm sample R1620 (N002)

Sample	Low temperature age maximum (Ma)	High temperature age minimum (Ma)
R1614(N003A)	61.3 ± 1.1	54.3 ± 1.0
R1615(N003B)	59.6 ± 1.2	54.9 ± 1.1
R1620(N002)	59.5 ± 1.4	52.9 ± 1.3

Table 6:24 Comparison of the low/high temperature age maxima/minima recorded by the Mourne Swarm samples

It is tempting to conclude that these samples are subject to radiogenic argon loss (induced by the heat generated from the intruding Mourne Granites) and a conversion of sites from low to high retentivity due to irradiation e.g. Horn et al., (1975). In this case, the low temperature age maximum of  $\approx 60$  Ma would record a minimum estimate for the age of dyke emplacement. This inferred age is geologically reasonable. The anomalously low ages of the first four steps, which are not geologically meaningful, would then be explained in terms of continuous argon loss from weakly retentive alteration. The correspondence between the high temperature age minima and the age of the Mourne Granites (as inferred in this thesis) would then probably be a fortuitous feature. It is conceivable that the conversion of sites from low to high retentivity may involve a phase recording the timing of the argon loss event. However, such an interpretation is not favoured here because of the anomalously low ages given by the initial steps.

The favoured explanation for the patterns of ages recorded by R1614, R1615 and R1620 involves a total resetting of the K-Ar system, due to alteration induced by the intrusion of the granites, and a  $^{39}\text{K}$  recoil loss effect. This contention is supported by several observations:

- i) The age spectra for R1614, R1615 and R1620 very closely resemble Turner & Cadogan's (1974) for a crushed lunar basalt. Their original uncrushed sample displayed a pattern of ages symptomatic of simple radiogenic argon loss.
- ii) The scanning electron microscope work for N003A reveals that the majority of the potassium is contained in hornblende (see Appendix 6). This mineral is the product of augite alteration (Tomkeieff & Marshall, 1933).
- iii) The scanning electron microscope work also shows that the dimensions of the potassium-rich zones are typically of the

order of  $25\mu$  and less. It is thought that  $^{39}\text{K}$  recoil effects are likely to be important where the potassic phases are of this size (see Appendix 6).

Assuming this is the correct explanation of the age spectra, then the high temperature age minima give maximum estimates for the timing of the total resetting event (see Table 4:3). The 54 Ma average is consistent with the dates reported for the Mourne Granite separates (see above). The pattern of anomalously low ages for the initial steps is explained by continuous argon loss from weakly retentive mineral alteration. High ages at very high temperatures (also observed by Turner & Cadogan, 1974) may reflect the conversion of low retentivity sites suffering from  $^{39}\text{K}$  recoil loss to high-retentivity sites. It is not possible for this age increase to be explained by the  $^{36}\text{Ca}$  recoil effect hypothesised in Appendix 3, because the levels of calcium-derived isotopes are far too low. It appears, therefore, that the correspondence between increasing age and  $^{37}/^{39}\text{K}$  levels at very high temperature is not meaningful. The original emplacement age of the dykes is not clear from the analyses R1614, R1615 and R1620. In an attempt to ascertain this, a dyke from the Killough-Ardglass swarm was dated. Dykes from this swarm, lying 30 km ENE of the Mourne Granites, will probably not be subject to effects related to granite intrusion.

d) Dyke from the Killough-Ardglass Swarm

The NW trending Mourne and Killough-Ardglass dyke swarms are separated on the north coast of Dundrum Bay by sand dunes. Although mineralogically distinct, the Mourne and Killough-Ardglass dykes may be of roughly the same age, perhaps with both sets of fissures acting as feeders for lavas now removed by erosion.

There is some evidence for the age of the Killough-Ardglass dyke swarm. The swarm is marked by a strong magnetic anomaly which can be

followed in a NW direction, and near Lisburn, the dykes are seen to cut the Lower Basalt Formation of the Antrim Lava Group (Preston, 1965). The Antrim Lava Group is dated in this study at 58 - 61 Ma and the Killough-Ardglass dyke swarm is probably about the same age.

The whole-rock sample dated in this work was taken from Tomkeieff & Marshall's (1940) basalt dyke number 52 (1.5m thick), which is found close to St. John's point. Dyke 52 is described petrographically in Tomkeieff & Marshall (1940) and a brief description of the thin section taken from the dating block is given in Appendix 7.

#### R1616 (P001)

The age spectrum for R1616 (Fig. 6:61) displays a pattern of decreasing age with temperature starting at 300 Ma and finishing at 65 Ma. The penultimate step displays a slight increase in age compared to previous steps, and this corresponds to the highest  $^{37}/^{39}\text{K}$  ratios recorded. The calcium interference age correction varies between 5 and 15 Ma for steps 1-24, however for the last two steps it is 102 and 85 Ma respectively. The age correction for chlorine interferences is less than 0.05 Ma for all steps and thus insignificant.

ICD data analysis does not yield meaningful results and the only chronological interpretation possible is that the high temperature minimum age of  $65.1 \pm 1.5$  Ma gives a maximum estimate for age of emplacement (see Table 4:3).

It is thought that the pattern of ages given by R1616 probably reflects the combined effects of  $^{39}\text{K}$  recoil loss and an excess  $^{40}\text{Ar}$  contamination. This hypothesis is supported by comparing the total gas age for R1616 of  $103.9 \pm 2.0$  Ma with a complementary K-Ar analysis carried out at the Leeds laboratory which gave an age of 84 Ma (D. Rex pers. comm.). An excess  $^{40}\text{Ar}$  contamination seems plausible because the magma which gave rise to the Killough-Ardglass dykes is thought to have been rich in volatiles (Tomkeieff & Marshall, 1940).

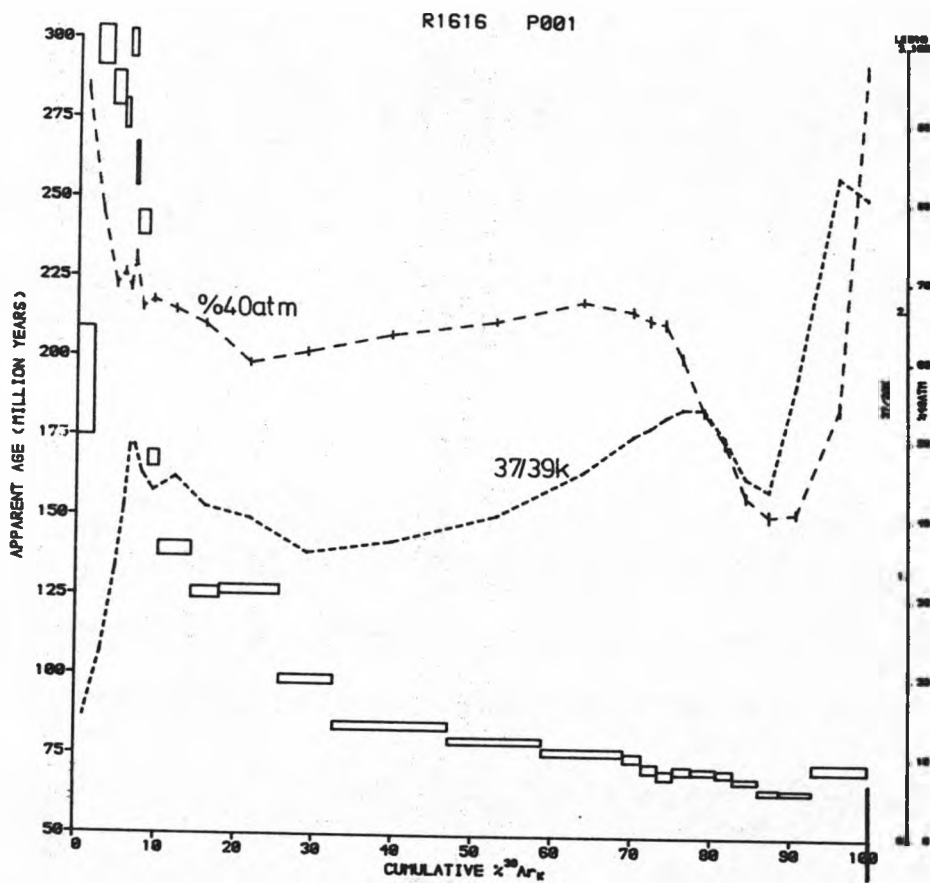


Fig. 6:61 Age spectrum for the Killough-Ardglass sample R1616 (P001)

Although the Arrhenius diagrams for R1616 yield some data point linear correlations, the calculated closure temperatures do not appear to be meaningful in the context of published estimates of mineral closure temperatures (see Table 4:1).

#### Conclusions for the Dyke from the Killough-Ardglass Swarm

The maximum age estimate of  $65 \pm 1.5$  Ma is consistent with the observed geological field relationships. It is thought that the dykes of the Killough-Ardglass swarm are probably less than 61 Ma because they are observed to cut lavas of the Lower Basalt Formation (see Section 6:2:7).

#### Conclusions for the Mourne Mountains

The best estimates for the timing of intrusion of the Mourne Granites come from the mineral separate samples R1572 (G2-biotite) and R1573 (G4-orthoclase) and the analysis of the dyke cutting granite G5 (ages of  $54.9 \pm 0.6$ ,  $< 54.5 \pm 0.8$ , and  $< 54.5 \pm 0.6$  Ma respectively). These results suggest granite intrusion commenced 55 Ma ago which is a significantly lower age than Evans et al's (1973)  $^{40}\text{Ar}$ - $^{39}\text{Ar}$  plateau ages and many of the conventional K-Ar dates for Mourne Granite mineral separates (see Table 6:19). However, for two main reasons, I feel there is a strong case for the validity of the results presented here. Firstly, because three samples are shown to give well-defined and consistent age estimates and three more (the dykes of the Mourne Swarm) present tentative support for the same age. Secondly, as recent Rubidium-Strontium results are largely in agreement with my own work (D. Gibson - unpublished work).

Unfortunately, it is not possible, from the dates presented here, to firmly establish the duration of granite emplacement as the ages for younger samples are maximum estimates only. If the ICD2 analyses of R1578, which give  $(40/36)_O > 295.5$ , are meaningful then the duration of activity is constrained to lie between 52 and 55 Ma. This is con-



sistent with Gibson's estimate for the duration of granite emplacement. Unpublished work from the Liverpool laboratory has demonstrated that granites G2 - G5, and dykes being truncated by, or intruded into, the granites are reversely magnetised. A 55 Ma age is consistent with this observation (see Fig. 6:44), however, Harland et al.'s (1982) polarity time scale suggests that a rock cooling in the interval 52 - 53.5 Ma would be more likely to possess a normal magnetisation. Combining the dates in this study with the palaeomagnetic evidence it is tempting to conclude that the Mourne Granites were intruded in the interval 53.5 - 55 Ma. However, it is recognised that the polarity time scale is not absolutely accurate chronologically, thus it may still be possible to justify activity in the Mourne Mountains until as late as 52 Ma (see Section 6:3 for a more detailed discussion of the palaeomagnetism). These results suggest that granite emplacement (52? - 55 Ma) took place significantly later than the extrusion of lavas in Antrim (58 - 61 Ma - see Section 6:2:7). This age difference is not thought to represent a protracted cooling of the granite intrusions. This is because simple heat loss models suggest that bodies such as the Mourne Granites will cool to temperatures at which the K-Ar system is effectively closed in less than 1 Ma (A.E. Mussett pers. comm.). There are in fact several acidic (mainly granitic) bodies within the British Tertiary Igneous Province (BTIP) that are dated in the range of 52 to 55 Ma - Skye Eastern Red Hills (Long, 1964; Moorbath & Bell, 1965; Kelly, 1973; Beckinsale et al., 1974; Dickin, 1981), Lundy (Miller & Fitch, 1962; Dodson & Long, 1962; Mitchell, 1968; Fitch et al., 1969), Rockall (Miller, 1965; Miller & Mohr, 1965; Jones et al., 1972, Hawkes et al., 1975), Sgurr of Eigg (Dickin & Jones, 1983) and St. Kilda (Brook, 1984). Thus the intrusion of acidic bodies in the period 52 - 55Ma appears to be a common feature of the BTIP.

The timing of emplacement of the Mourne and Killough-Ardglass dyke

swarms is constrained to lie between 55 and 61 Ma i.e. younger than the oldest of the Antrim basalts (see Section 6:2:7) but older than the Mourne Granites.

#### 6:2:9 The Carlingford Complex

The Slieve Gullion and Carlingford Complexes (see Fig. 6:1) are contiguous and may represent the remnants of a single volcanic centre in which activity migrated south-easterly (Preston, 1981).

The Carlingford Complex consists of at least two generations of gabbroic and doleritic intrusions, a central intrusion of granophyre and granite and small patches of plateau lavas which could be vestiges of the Antrim Lava Group. A system of basic cone-sheets encircles the complex and it is cut by a great number of north-westerly trending dykes. Evans et al., (1973) suggested that, as the Mourne Complex is cut by relatively few dykes, then igneous activity at Carlingford (and Slieve Gullion) occurred prior to the emplacement of the Mourne Granites.

The only radiometric date for the Carlingford Complex (there are none for Slieve Gullion) was reported by Evans et al., (1973). They dated a late basaltic sheet by the conventional K-Ar method and the calculated age of 60 Ma was thought to give a minimum estimate for the timing of activity in the Carlingford Complex.

In this study I have dated three whole-rock samples: a gabbro and a granophyre from the northern margin of the complex at Windy Gap and an early gabbro (Halsall, 1974) from the west side of the complex at Trumpet Hill. The results presented here confirm Evans et al.'s (1973) estimate for the age of the Carlingford Complex.

#### R1574 (R028)

The age spectrum of the granophyre sample R1574 (Fig. 6:62a) displays a saddle shape which appears to be diagnostic of excess argon (see Table 4:3). However, the saddle minimum is very broad, covering

Irradiation no. (Locality no.)	Steps	% <sup>39</sup> K	Total gas age (Ma)	Mean age (Ma) (step ages weighted by 1/variance)	Age (Ma)	ICD2 parameters (40/36) <sub>0</sub>	MSWD
R1574(R028)	All(1-30) 5-22	100	62.0 ± 0.5	61.5 ± 1.2	60.9 ± 0.6	306.2 ± 4.2	9.0
		68	61.1 ± 0.5	61.0 ± 0.7	60.9 ± 0.5	298.5 ± 4.9	2.4
R1618(R031)	All(1-28) 10-28	100	69.8 ± 1.7	66.3 ± 4.3	65.2 ± 1.6	299.7 ± 8.6	14.8
		93	70.2 ± 1.5	66.3 ± 4.0	63.3 ± 1.6	306.3 ± 10.1	11.6
R1619(R048)	All(1-29) 18-22 10-15	100	58.0 ± 1.2	60.1 ± 2.5	60.5 ± 1.3	293.1 ± 7.2	31.1
		20	58.6 ± 1.2	58.6 ± 1.1	58.7 ± 1.2	295.2 ± 2.7	0.2
		27	59.9 ± 1.2	60.0 ± 1.2	62.1 ± 2.2	282.9 ± 20.9	0.8

Table 6:25 Parameters calculated for the Carlingford Complex samples

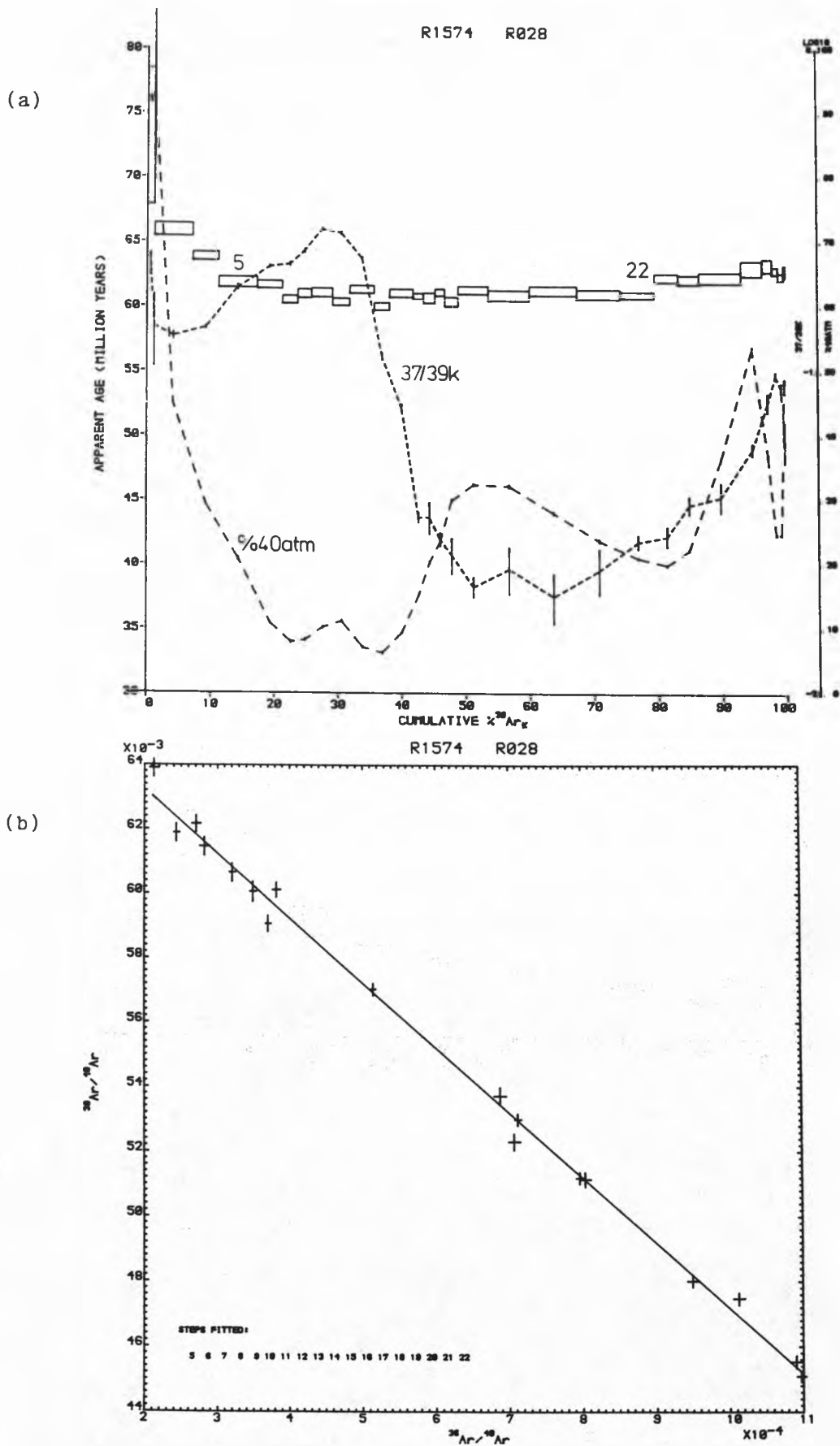


Fig. 6:62 Age spectrum (a) and ICD2 steps 5-22 (b) for the Carlingford Complex sample R1574 (R028)

about 70% of the  $^{39}\text{K}$  release, so the excess argon is probably only a minor contaminant. The peak in the  $^{37}/^{39}\text{K}$  curve at low-intermediate temperatures is thought to represent plagioclase outgassing (see Killala Bay sample R1621). In common with Killala Bay sample R1613, the  $^{37}/^{39}\text{K}$  peak corresponds with the highest recorded levels of radiogenic argon. Both the calcium and chlorine interference age corrections are less than 0.1 Ma for all steps and thus are negligible.

ICD2 analysis of the saddle minimum steps (5-22) yields a meaningful age of  $60.9 \pm 0.5$  Ma (see Table 6:25). It is suggested that this age should be regarded as a true estimate for the timing of granophyre emplacement because the anomalous segments of the gas release constitute only  $\approx 30\%$  of the total  $^{39}\text{K}$ .

ICD3 data analyses and the Arrhenius diagrams did not produce meaningful results.

#### R1618 (R031)

The age spectrum of this gabbro sample from Windy Gap is very disturbed (see Fig. 6:63). The strong correlation between step age and the level of atmospheric  $^{40}\text{Ar}$  over the majority of the gas release indicates that initial argon of a non-atmospheric composition may be important. The  $^{37}/^{39}\text{K}$  curve is saddle-shaped and the calcium age correction is around 15 Ma for the low temperature steps,  $\approx 4$  Ma at intermediate temperatures, and about 25 Ma for the last two steps. The chlorine interference age correction is not very important, with a maximum value of 0.2 Ma for the penultimate step.

ICD2 analyses do not yield meaningful results. By way of example, the results for steps 10-28, which display the strong correlation between step age and the level of atmospheric  $^{40}\text{Ar}$  noted above, are presented in Table 6:25. Because of the pattern of ages produced

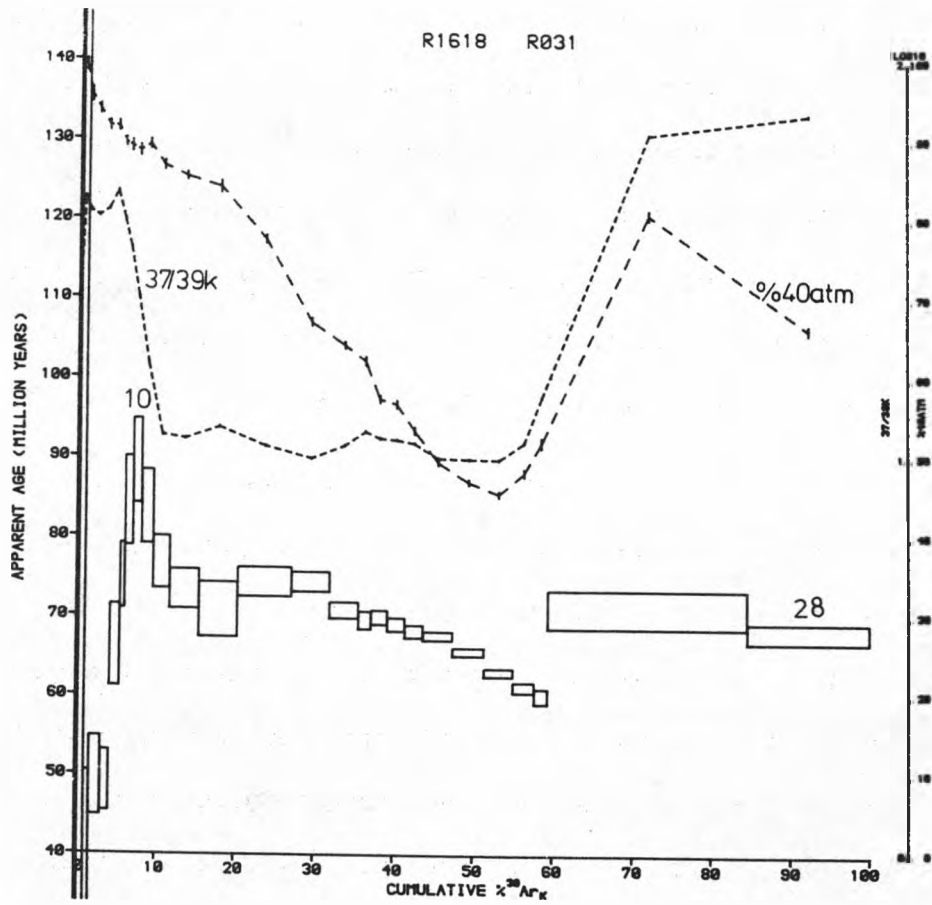


Fig. 6:63 Age spectrum for the Carlingford Complex sample R1618 (R031)

by R1618 (roughly saddle-shaped), and as R1574 was subject to an excess argon contamination, the lowest intermediate temperature step age of  $60.0 \pm 1.5$  Ma is taken as a maximum age estimate. This interpretation is consistent with the best age estimate of sample R1574.

As for R1574, ICD3 data analyses and the Arrhenius diagrams did not produce meaningful results.

#### R1619 (R048)

The age spectrum for this early gabbro sample is presented in Fig. 6:64. The marked increase in age at high temperatures corresponds to a peak in the  $37/39\text{K}$  curve, which is probably associated with pyroxene outgassing. For these high temperature steps, the calcium interference age correction reaches a maximum value of 50 Ma (step 27). Over the majority of the gas release, however, this correction is only 1 - 4 Ma. The chlorine age correction is as high as 0.4 Ma but is generally insignificant.

As the age spectrum of R1619 is saddle-shaped (ignoring the first 10% of  $39\text{K}$  release), and because excess argon has been identified in the other Carlingford samples, it might be thought that excess argon would be important for sample R1619. The low ages recorded by the first nine steps probably reflect slight radiogenic argon loss and this may explain why the low temperature side of the saddle is not marked by such high ages as the high temperature side. The excess argon interpretation implies that the intermediate temperature age minimum, defined by the ICD2 analysis of steps 18-22 (see Table 6:25), should be treated as a maximum age estimate. This age of  $58.7 \pm 1.2$  Ma is significantly lower than the age reported for the younger granophyre ( $60.9 \pm 0.5$  Ma). The latter is regarded as the best age estimate for the Carlingford Complex because the steps from which the age was calculated constitute a very large proportion of

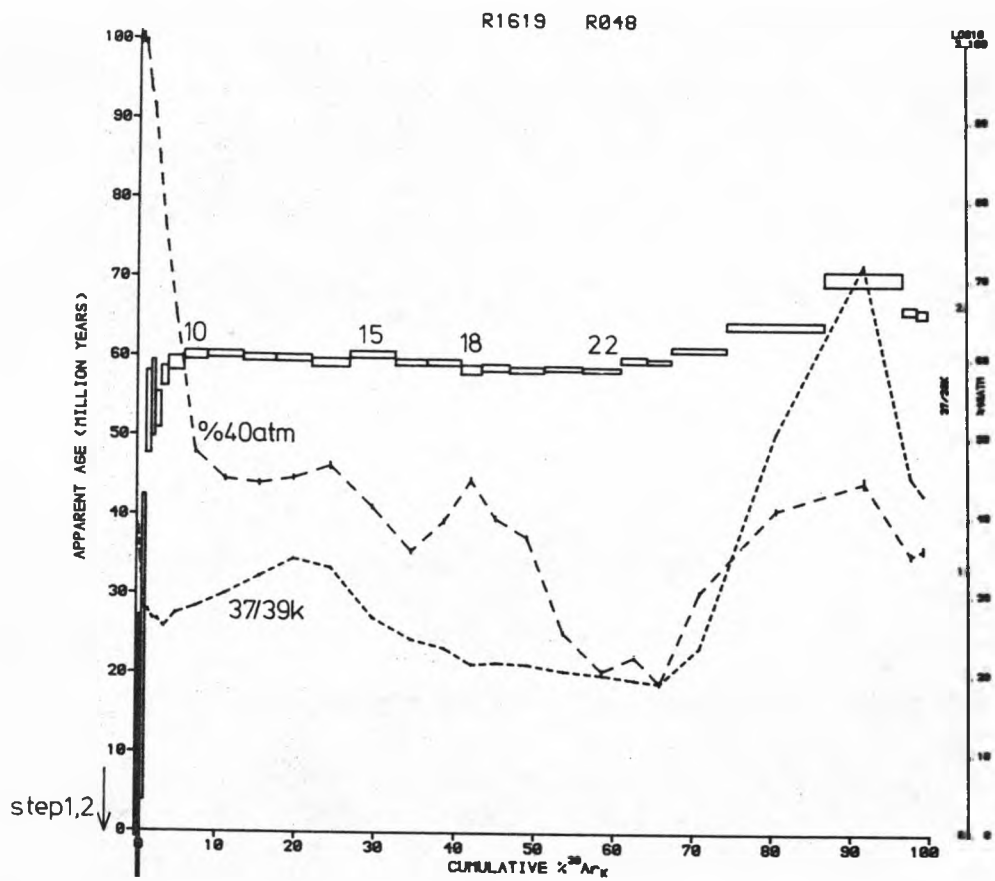


Fig. 6:64 Age spectrum for the Carlingford Complex sample R1619 (R048)



the total  $^{39}\text{K}$  release. The excess argon interpretation apparently yields an age estimate which is not geologically meaningful and therefore this explanation of R1619's age spectrum pattern is not considered valid.

An alternative explanation that does yield a geologically acceptable age estimate, invokes the  $^{36}\text{Ca}$  recoil effect hypothesised in Appendix 3. High ages at high temperatures would then be interpreted as indicating  $^{36}\text{Ca}$  loss, whilst the low ages at intermediate and low temperatures could well reflect  $^{36}\text{Ca}$  gain. This interpretation suggests that the low temperature age maximum, defined by steps 10-15 (see Table 6:25) should be regarded as a minimum estimate for the age of crystallisation (only a minimum estimate because of the possibility of  $^{36}\text{Ca}$  gain in all the low and intermediate temperature gas fractions). ICD2 analysis of steps 10-15 gives a statistically meaningful age of  $62.1 \pm 2.2$  Ma which is consistent with the well-defined age of  $60.9 \pm 0.5$  Ma calculated for the later granophyre intrusion.

A  $^{36}\text{Ca}$  recoil effect appears to be a reasonable explanation of the age pattern of R1619 because:

- i) only a small proportion of  $^{36}\text{Ca}$  would have to be re-distributed to explain the anomalously high ages for the high temperature steps. In the conventional step age calculation for these steps, the  $^{36}\text{Ca}$  accounts for a large proportion of the total amount of  $^{36}\text{Ar}$ .
- ii) although the pyroxene, with which the  $^{37}/^{39}\text{K}$  and age increase at high temperature are thought to be associated, is observed in thin section to have dimensions typically over 1 mm, it is also seen to be severely altered (see Appendix 7). This may have the effect of reducing the size of areas of uniform composition to such an extent that  $^{36}\text{Ca}$  recoil effects become

important between the different phases contained within the primary pyroxene

iii) it provides an explanation for the negative ages recorded for the first three steps. If the  $^{36}\text{Ca}$  lost from high temperature locations is partially gained by sites that out-gas in the lowest temperature steps, then the amount of atmospheric  $^{40}\text{Ar}$  for these steps, inferred from the supposed level of  $^{36}\text{Ar}_{\text{atm}}$ , may be apparently greater than the total measured amount of  $^{40}\text{Ar}$ . In this way low temperature steps could yield negative ages.

As the total gas age (all steps) of  $58.0 \pm 1.2$  Ma is less than the inferred minimum age estimate, a slight loss of radiogenic  $^{40}\text{Ar}$  must also be postulated. This does not seem unreasonable, bearing in mind the state of alteration of the thin section (see Appendix 7).

For R1619 the three-dimensional isotope correlation diagrams and the Arrhenius diagrams did not give meaningful results.

#### Conclusions for the Carlingford Complex

R1574 was the only one of the three Carlingford samples to give what is regarded as a reliable age estimate for the timing of igneous activity. Interpretation of the other two samples is rather tentative because of the complexity of the age spectrum patterns. For R1619, it was based on the assumption that the true age of igneous activity was recorded by R1574. The best age estimate of  $60.9 \pm 0.5$  Ma from the granophyre sample R1574 is consistent with Evans et al.'s (1973) proposal that the age of the Carlingford Complex was 60.5 Ma. The Carlingford Complex is thought to be of roughly the same age as the older Antrim lavas (see Section 6:2:7) but significantly older than the Mourne Granites, which are found about 15 km to the north-east of Carlingford (see Section 6:28).

### 6:3 Conclusions

Table 6:26 summarises the best age estimates for the rocks dated in this study. These are also shown on Fig. 6:65 which in addition displays the previous age estimates in brackets.

This work indicates strongly that the majority of Tertiary igneous activity in Ireland occurred between 58 and 62 Ma. All the rocks which had given anomalous old or young K-Ar ages (in the context of reliable dates for the rest of the BTIP), e.g. Kerry dyke system (Horne & Macintyre, 1975), Killala Bay (Macintyre et al., 1975), Antrim Lava Group (Evans et al., 1973; Fitch & Hurford, 1977), have been dated in the 58 - 62 Ma bracket. This work has also shown that the Mourne Granites (and their cross-cutting intrusions) are significantly younger than 58 - 62 Ma, with activity there probably occurring between 52 and 55 Ma. The Lough Key dyke which was assumed to be of a Tertiary age on geological grounds has been shown to be of Carboniferous age and therefore it is not part of the British Tertiary Igneous Province.

Work conducted at the Liverpool laboratory has shown that all the Tertiary igneous rocks dated in this study, together with all (but two) of those analysed palaeomagnetically alone, possess a reversed direction of magnetisation. This observation and the ages for Tertiary activity given above appear to be consistent with Harland et al.'s (1982) geomagnetic polarity time scale (Fig. 6:44) with the earlier activity taking place during chron 26r and the later activity occurring in chron 24r. One might have expected that if some of the Mourne Mountain intrusives were as young as 52 Ma they would show a normal magnetisation (see Fig. 6:44). The two samples giving a normal magnetisation are, in fact, from the Mourne Mountains (a felsic vein in granite G5 and a dyke), however, the granites themselves all give a reversed magnetisation (the oldest granite was not sampled). As pointed out in Section 6:2:8, the polarity timescale does not give an absolute

Area	Best age estimate (Ma)
1. Kerry dyke system	59 ± 1
2. Intrusive systems of west-central Ireland	Doon Hill Plug: < 62.3 ± 0.7 Cleggan dyke: between 57 and 60? Glenlaur gabbro: < 62.9 ± 2.1
3. Droimchogaidh sill	Main sill: between 58 and 61 Satellite sill: 62.2 ± 0.6
4. Lough Key dyke	315 ± 7
5. Killala Bay	Gabbro emplacement: 58 ± 2 Gabbro dykelet: < 58.7 ± 1.1 Doleritic flash intrusions: < 61.6 ± 0.9
6. Blind Rock dyke	61.7 ± 0.5
7. Antrim Lava Group	Interbasaltic Formation: 61.0 ± 0.6 Upper Basalt Formation: 58.3 ± 1.1 (Zeolitisation: 58?)
8. Mourne Mountains	Granite G2: 54.9 ± 0.6 Granite G4: < 54.5 ± 0.8 Dyke cutting G5: < 54.5 ± 0.6 Metamorphism of dykes of the Mourne Swarm: 54? Killough-Ardglass dyke: < 65 ± 1.5 (inferred to be less than 61 Ma old because dykes of the same swarm cut the Lower Basalt Formation)
9. Carlingford Complex	Granophyre 60.9 ± 0.5

Table 6:26 Summary of best age estimates

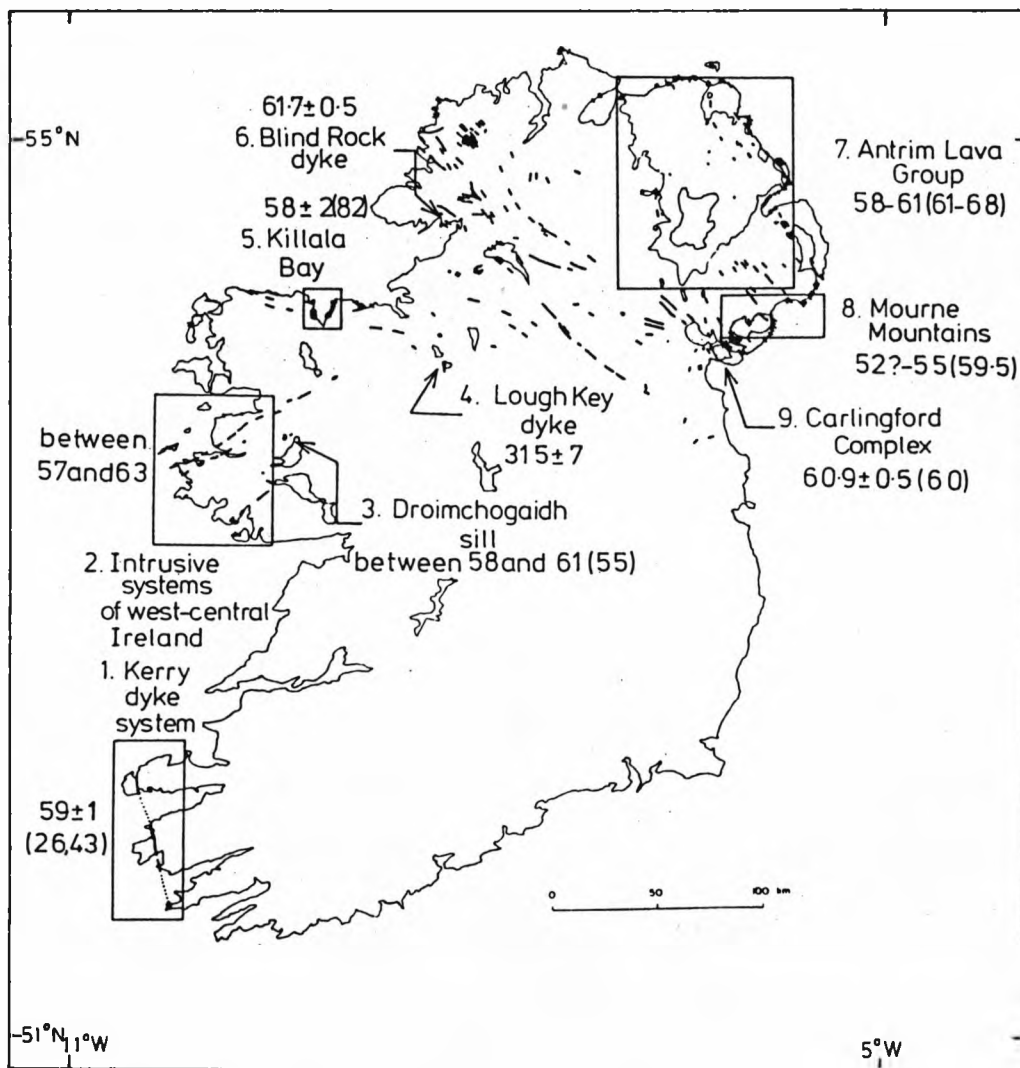


Fig. 6:65 Best age estimates for the Irish Tertiary igneous rocks dated in this study (previous age estimates given in brackets)

chronology; the age error is thought to be as much as 1 Ma. Thus, a 52 - 55 Ma age for the Mourne Granites may not be inconsistent with their observed reversed magnetisation.

The timing of Tertiary igneous activity, as defined above, is comparable with reliable estimates for the rest of the British Tertiary Igneous Province (see Fig. 6:66). This study has conclusively shown that previously reported K-Ar dates (see above), which seemed to suggest that Tertiary activity in Ireland was more prolonged than elsewhere, have no chronological significance.

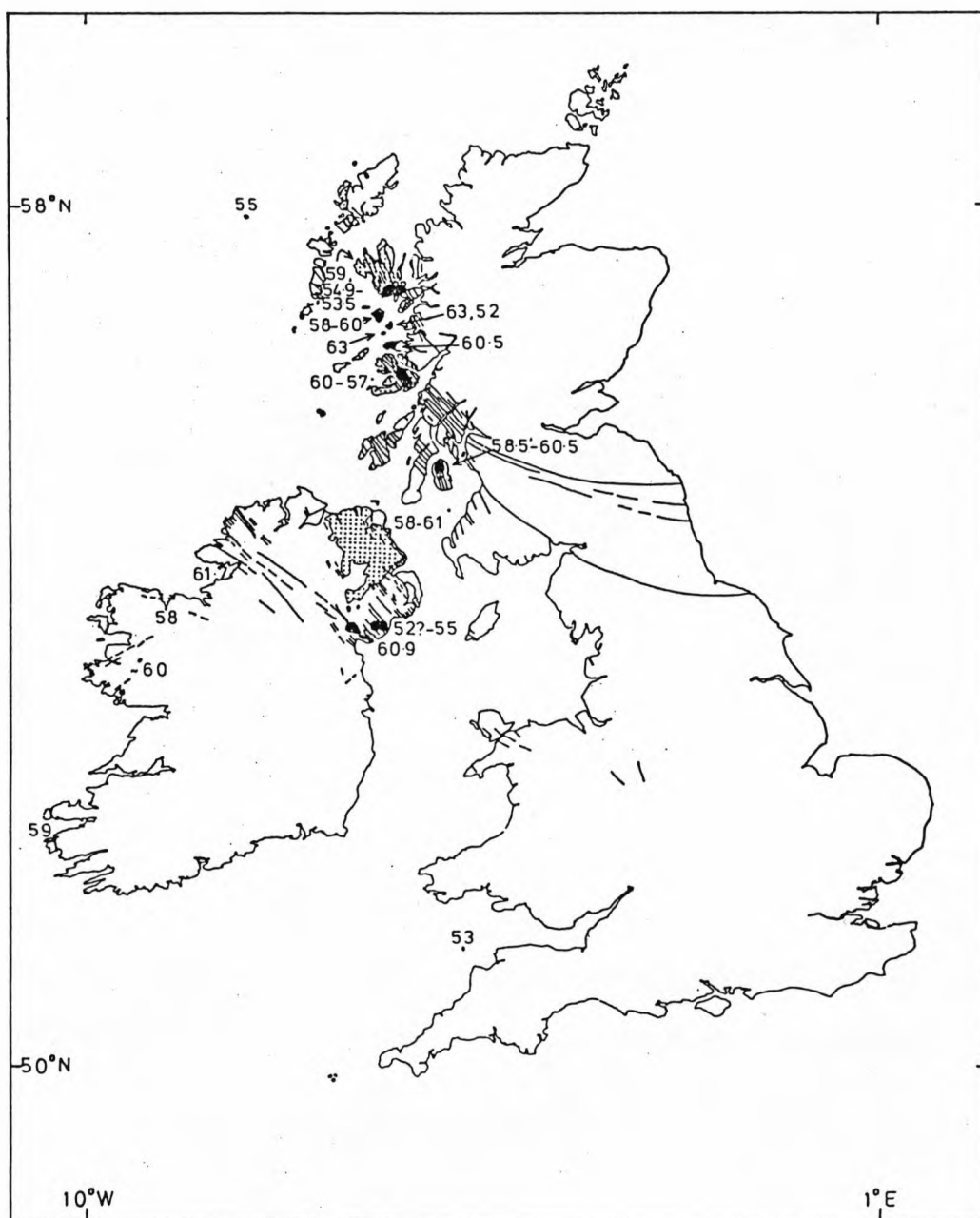


Fig. 6:66 Reliable age estimates for the British Tertiary Igneous Province (Ireland - this thesis. Mull - Walsh et al., 1979, Mussett, 1985. Ardnamurchan - Beckinsale, unpublished. Arran - Evans et al., 1973, Mussett, unpublished. Lundy - Dodson & Long, 1962, Mitchell, 1968. St. Kilda - Brook, 1984. Muck - Dagley & Mussett, 1985. Eigg - Dickin & Jones, 1983, Dagley & Mussett, 1985. Rhum - Mussett, 1984. Skye - Dickin, 1981, Mussett, unpublished)

CHAPTER SEVEN

Discussion



## Introduction

The objective of this investigation was to date accurately Tertiary igneous activity in Ireland with special emphasis on localities that have given K-Ar ages outside the usual range of reliable dates for the British Tertiary Igneous Province (BTIP).

The  $^{40}\text{Ar}$ - $^{39}\text{Ar}$  stepwise degassing technique was used in this study for two reasons. Firstly, because it is applicable to all the types of Tertiary igneous rock found in Ireland, and secondly, because, unlike the conventional K-Ar method, it is possible to make internal self-consistency checks on the data. The latter was most important as many of the K-Ar dates for the BTIP as a whole are not consistent with the known sequence of geological events.

The results of this  $^{40}\text{Ar}$ - $^{39}\text{Ar}$  stepwise degassing investigation of Irish Tertiary igneous rocks are discussed in Section 6:2 and summarised in Section 6:3. The best age estimates are stratigraphically consistent where such controls exist and they are comparable with reliable dates for the rest of the BTIP.

Discussion in the light of this investigation is split into two sections. The first deals with the  $^{40}\text{Ar}$ - $^{39}\text{Ar}$  stepwise degassing technique and the second discusses the regional geological implications for the BTIP.

### The $^{40}\text{Ar}$ - $^{39}\text{Ar}$ Stepwise Degassing Technique

The majority of samples dated in this study have been whole-rocks. It is recognised that such multi-phase samples are likely to give a complex gas release which might make interpretation difficult. However, several studies have demonstrated that the  $^{40}\text{Ar}$ - $^{39}\text{Ar}$  step heating approach can yield geologically meaningful dates for these types of terrestrial samples, e.g. Mussett et al., (1980), Walker & McDougall (1982), Mussett (1985). The results of this study also demonstrate that geologically acceptable dates can be produced by dating whole-rock

samples by the  $^{40}\text{Ar}$ - $^{39}\text{Ar}$  stepwise degassing technique even when age spectrum patterns are complicated. Out of the total of 41 whole-rock samples analysed in this study, only 6 gave well-defined and meaningful absolute age estimates. However, a further 11 gave well-defined ages which, because of age spectrum complexities, are regarded as slightly high or low age estimates. For the remaining samples, it is apparent that best age estimates are a distinct improvement over the probable conventional K-Ar method sample ages (comparing the best age estimates with the  $^{40}\text{Ar}$ - $^{39}\text{Ar}$  total gas age for all steps, and assuming all Tertiary igneous activity in Ireland occurred within the range of reliable dates for the BTIP i.e. 52 - 63 Ma - see next section). This point is positively demonstrated for samples for which complementary K-Ar age data exists (see Table 7:1).

For the samples dated in this study there was no strong correlation between petrographic freshness and the production of a well-defined age estimate. For instance, the Lough Key dyke sample produced a well-defined and stratigraphically acceptable age (J.D.A. Piper pers. comm.) but was severely altered (see Section 6:2:4). On the other hand, most of the largely fresh Killala Bay gabbro samples gave no well-defined age estimates (see Section 6:2:5). It appears therefore, that there are no firm rules for  $^{40}\text{Ar}$ - $^{39}\text{Ar}$  (or K-Ar) sample selection where Irish Tertiary igneous rocks are dated. Mussett et al., (1973) and Mussett (1985) have also found for BTIP rocks (from Mull - conventional K-Ar and  $^{40}\text{Ar}$ - $^{39}\text{Ar}$  stepwise degassing techniques respectively) that sample freshness is no guide to whether a particular sample will produce a reliable potassium-argon age.

In this study, the chronological interpretation of complex  $^{40}\text{Ar}$ - $^{39}\text{Ar}$  age spectra has been seen to be aided by the extraction of large numbers of steps (more than 20). This is because any age trend is more well-developed in terms of the number of steps that define it. Only by

Sample	$^{40}\text{Ar}-^{39}\text{Ar}$ best age estimate (Ma)	Conventional K-Ar age (Ma)
Kerry dyke system dolerite DDC	59 ± 1	46 (D. Rex pers. comm.)
Kerry dyke system dolerite 187	59 ± 1	39 ± 1 (Mitchell & Mohr, 1985)
Cleggan dyke dolerite 253	57.3 ± 0.8	42.0 ± 0.6 (Mitchell & Mohr, 1985)
Droimchogaidh sill olivine gabbro 238	< 61.1 ± 0.7	50 ± 2 (D. Rex pers. comm.)
Antrim Lava Group olivine basalt K2A	59.0 ± 1.5	41 (D. Rex pers. comm.)
Mourne Mountain dyke feldspar porphyry N003A	≈54	54 (D. Rex pers. comm.)
Mourne Mountain dyke dolerite P001	< 65 ± 1.5	84 ± 10 (D. Rex pers. comm.)

Table 7:1 Comparison of  $^{40}\text{Ar}-^{39}\text{Ar}$  best age estimates and conventional K-Ar ages

extracting large numbers of steps has it been possible, in the instances where plateau segments extend over a limited portion of the gas release, to use a significant number of steps in the data analysis. I recommend that, where pilot dating studies produce complicated age spectra (as in this investigation), further samples should be outgassed in 20 or more steps. In this way any chronological interpretation of the age spectra will be more reliable.

The interpretation of whole-rock  $^{40}\text{Ar}$ - $^{39}\text{Ar}$  stepwise degassing data has, in this study, also benefitted from Scanning Electron Microscope (SEM) work on dated samples. From these investigations it has been possible to identify the mineral phases contributing to the release of radiogenic  $^{40}\text{Ar}$  and potassium-derived  $^{39}\text{Ar}$ . In addition, by studying mineral grain sizes, it has been possible to ascertain the likely importance of  $^{39}\text{Ar}_K$  recoil effects. This study clearly demonstrates the usefulness of SEM investigations and I believe that SEM sample examinations would be beneficial for any whole-rock  $^{40}\text{Ar}$ - $^{39}\text{Ar}$  dating project (particularly where age spectrum patterns are complicated).

The chronological interpretation of  $^{40}\text{Ar}$ - $^{39}\text{Ar}$  stepwise degassing data in this study was largely based on both the age spectrum and the 2-dimensional isotope correlation diagram (ICD2). Interpretation was not aided by the use of the 3-dimensional isotope correlation diagram (ICD3) developed in this thesis; thus:

- i) the hypothesised excess argon components (Plots 1 and 2) do not appear to have any physical meaning. Age variations corresponding to  $37/39K$  changes, for instance, have then to be explained in terms of some other mechanism e.g. recoil - see Droimchogaidh sill sample R1581 (234).
- ii) the adopted value of  $\left[ \frac{40-(40/36)atm^{36}}{37} \right]_{Ca}$  appears to be applicable to all the samples dated in this study.

It remains to be seen whether the ICD3 will be useful at all.

Arrhenius diagrams were not found, in general, to be useful for the interpretation of disturbed age spectra. Linear correlations did not correspond in any consistent fashion with age spectrum features and only in some cases did the calculated diffusion parameters and closure temperatures seem to have any geological meaning. Several alternative explanations for these observations can be given:

- i) volume diffusion may not be the major argon transport process (see Mussett, 1969 and Brereton, 1972 for discussion of mechanisms other than volume diffusion)
- ii) the argon isotopes released from the mainly multi-phase samples may be derived in significant proportions from more than one mineral (or the same mineral with variations in grain size)
- iii) neutron irradiation may have modified the argon isotope release patterns (see Section 4:3).

All three of these points may be important in reality.

In view of this inconsistency, Arrhenius diagrams, for whole-rock samples at least, cannot be regarded as reliable for closure temperature calculations or as indicators of argon isotope disturbances.

Work in this study suggests crushed whole-rock samples should be avoided unless there is very strong evidence for a loosely-held atmospheric argon component. This is because, where both uncrushed and crushed samples of the same rock were analysed, crushing led to increased atmospheric argon contamination with, in some cases, possible fractionation effects - see Killala Bay sample R1577 (124NA).

It is generally assumed that the only important argon isotopic recoil effect involves  $^{39}\text{Ar}_K$ . However, in this study, I have shown that a  $^{36}\text{Ar}_{Ca}$  recoil effect might be expected on theoretical grounds (see Appendix 3). I have suggested instances in which such an effect may explain observed age spectrum disturbances (see Section 6:2:1 and 6:2:9).

### Regional Geological Implications

Reliable age estimates ( $^{40}\text{Ar}$ - $^{39}\text{Ar}$  step heating and Rb-Sr isochron ages) suggest that the majority of activity within the BTIP took place in the interval 58 - 61 Ma (basalts, volcanic centres and the major dyke swarms - Evans et al., 1973; Walsh et al., 1979; Dickin, 1981; Mussett, 1984; Mussett, 1985 and this thesis). There is also strong evidence for a minority occurring between 52 and 55 Ma (granitic plutons, acidic volcanism and some basic dykes - Dodson & Long, 1962; Mitchell, 1968; Dickin, 1981; Dickin & Jones, 1983; Brook, 1984 and this thesis), and perhaps around 63 Ma (basalts of Eigg and Muck - Dagley & Mussett, 1985).

These reliable age estimates suggest a pulsing of Tertiary magnetic activity in the British Isles. This supports Fitch et al.'s (1978) contention that Tertiary igneous activity in the whole N.E. Atlantic province (British Isles, E. Greenland and the Faeroe Islands) was confined to a number of discrete episodes. The youngest igneous activity in the BTIP (52 - 55 Ma) apparently occurred at the same time as the basaltic outpourings in E. Greenland and the Faeroe Islands (the most reliable dates for these are presented in Fitch et al., 1978). The E. Greenland and Faeroe Islands basalts are thought to be directly associated with the initiation of rifting and the onset of spreading in the N.E. Atlantic - Brook (1973); Faller (1975); Soper et al., (1976). Fig. 7:1 shows that these eruptive rocks lie adjacent to the oldest known magnetic sea-floor anomaly which marks the earliest basalts to be extruded at the Mid-Atlantic Ridge. If the igneous activity around 52 - 55 Ma in Greenland and the Faeroe Islands and also in the BTIP is related, (responses to the same tectonic stimulus perhaps); it seems reasonable to suggest that the earlier BTIP activity is somehow related to the opening of the N.E. Atlantic. Such an idea is not new. Several authors have directly related Tertiary activity in the British Isles and also in E. Greenland and the Faeroe Islands

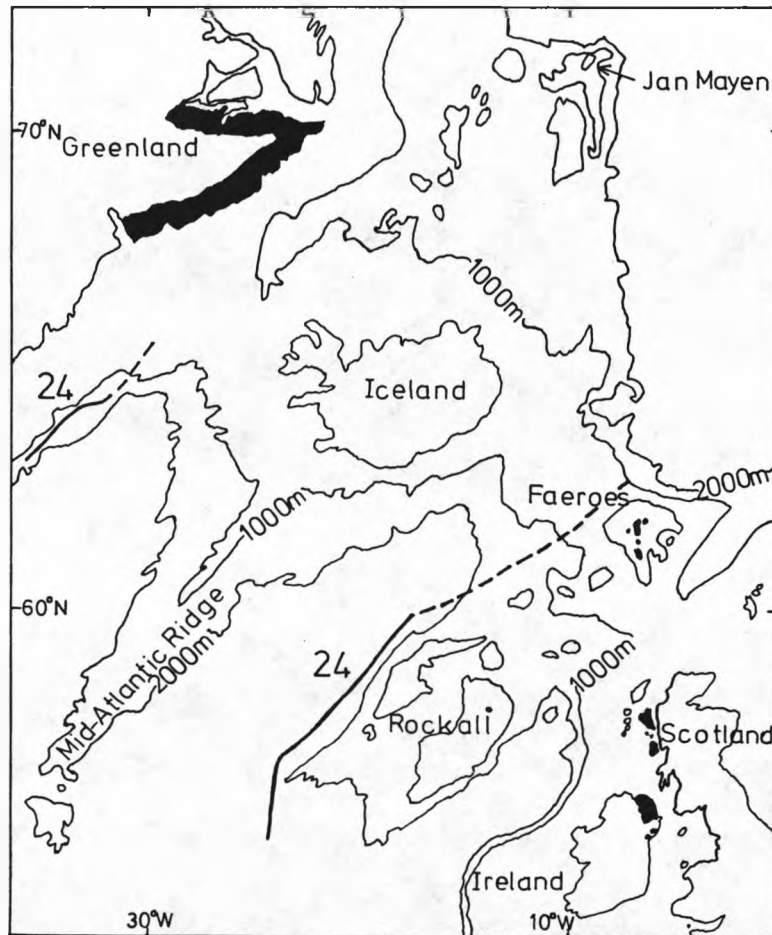


Fig. 7:1 Tertiary igneous rocks at the margins of the N.E. Atlantic (shaded areas) and sea-floor magnetic anomaly 24 (adapted from Schilling & Noe-Nygaard, 1974 and Vogt & Avery, 1974)

with the opening of the N.E. Atlantic e.g. Scrutton (1973); Macintyre (1973); Soper et al., (1976); Fitch et al., (1978); Carter et al., (1979). However, at the present time it is not possible to relate directly the Tertiary igneous activity of the British Isles with that found in E. Greenland and the Faeroe Islands because of several major geological differences between the two provinces (Mussett et al., 1980).



APPENDIX 1

Constants Used in this  $^{40}\text{Ar}$ - $^{39}\text{Ar}$  Dating Study

$\lambda_e$	=	$0.581 \times 10^{-10} \text{ a}^{-1}$	} Values recommended by the International Union of Geological Sciences - Subcommittee on Geochronology (Steiger & Jäger, 1977)
$\lambda_\beta$	=	$4.962 \times 10^{-10} \text{ a}^{-1}$	
${}^4\text{0K/K}$	=	$1.167 \times 10^{-4} \text{ atom/atom}$	
$\left(\frac{40}{36}\right)_{\text{atm}}$	=	295.5	
$\left(\frac{38}{36}\right)_{\text{atm}}$	=	0.187	

} Nier (1950)

The constancy of  ${}^4\text{0K}$  decay constants has been discussed by Gale (1982); the possibility of  ${}^4\text{0K/K}$  variations was briefly covered by Turner (1971b). They both concluded that possible variations are, in general, too small to produce significant discrepancies in calculated ages.

Three important isotopes produced during neutron irradiation are radioactive, so it is necessary to make corrections for decay. The half lives are as follows:

${}^{39}\text{Ar}$	$T_{1/2}$	=	269 years	} Weast (1983)
${}^{37}\text{Ar}$	$T_{1/2}$	=	35 days	
${}^{36}\text{Cl}$	$T_{1/2}$	=	$3 \times 10^5$ years	

Corrections for interference reactions:

$\left[\frac{36}{38}\right]_{\text{Cl}}$	=	315.8	Roddick (1983)	} Values quoted are a compromise between those measured in this study and those reported by Turner et al., (1978) and Roddick (1983) for the same reactor facility. (See Section 5:4:2).
$\left[\frac{40}{39}\right]_{\text{K}}$	=	0.015		
$\left[\frac{38}{39}\right]_{\text{K}}$	=	0.011		
$\left[\frac{40 - \left(\frac{40}{36}\right)_{\text{atm}} 36}{37}\right]_{\text{Ca}}$	=	-0.074		
$\left[\frac{39}{37}\right]_{\text{Ca}}$	=	$6.65 \times 10^{-4}$		
$\left[\frac{38 - \left(\frac{38}{36}\right)_{\text{atm}} 36}{37}\right]_{\text{Ca}}$	=	$-1.0 \times 10^{-5}$		

APPENDIX 2

$^{40}\text{Ar}$ - $^{39}\text{Ar}$  Stepwise Degassing Arrhenius Diagrams

## Introduction

Arrhenius diagrams can be plotted using  $^{40}\text{Ar}$ - $^{39}\text{Ar}$  stepwise degassing data following the example of Turner (1971b), Turner et al., (1973), Albarede (1978) etc.

This appendix is divided into three sections. The first discusses Arrhenius diagrams in published work and the second deals in detail with their use in this thesis. The third considers the assignment of cooling rates for the closure temperature calculations made in this study.

### Arrhenius diagrams in published $^{40}\text{Ar}$ - $^{39}\text{Ar}$ dating studies

Arrhenius diagrams have been plotted for the  $^{40}\text{Ar}$ ,  $^{39}\text{K}$  or  $^{37}\text{Ar}$  isotopic gas release. Turner (1971b), Turner et al., (1973), Turner et al., (1978), Turner (1979) and Ozima & Takigami (1980) preferred to use  $^{39}\text{K}$  rather than  $^{40}\text{Ar}$  because, in a particular mineral, the former can be expected to have the idealised uniform distribution prior to degassing (providing recoil effects are not important). On the other hand, the  $^{40}\text{Ar}$  in a rock or mineral is subject to geological processes and thus may not be distributed homogeneously. Berger & York (1981) and Lopez-Martinez & York (1983) plotted both the  $^{39}\text{K}$  and the  $^{40}\text{Ar}$  Arrhenius diagrams for their mineral samples. They found little difference between corresponding plots and calculated closure temperatures. This behaviour could well have been expected as many samples gave age plateau over the majority of the gas release. Berger & York (1981) suggest that  $^{40}\text{Ar}$  should be preferred for plutonic feldspars because of the probability of  $^{39}\text{K}$  recoil effects within micron-sized exsolution features. Albarede (1978), however, chose  $^{37}\text{Ar}$  for a plagioclase Arrhenius diagram on the basis that it is likely to be more homogeneously distributed than  $^{39}\text{K}$ .

The selection of the diffusion symmetry assumed in the solution of Fick's law is often based on basic mineral structure arguments (Berger & York, 1981). For example, where a mica sample is involved (these

minerals have a sheet silicate structure), a planar symmetry is generally selected. The diffusion symmetry is usually either spherical, cylindrical or planar.

There are several examples of  $^{40}\text{Ar}$ - $^{39}\text{Ar}$  Arrhenius diagrams that give a linear correlation of data points over the whole gas release e.g. Ozima & Takigami (1980), Harrison & McDougall (1982). However, such linear correlations normally only extend over a portion of the gas release e.g. Berger & York (1981), Harrison & McDougall (1981), Lopez-Martinez & York (1983). Very often it is the lowest and/or highest temperature data points in the Arrhenius diagram that are rather scattered. In these cases idealised volume diffusion is considered to be only applicable over the temperature range covered by the Arrhenius diagram linear correlation.

The majority of  $^{40}\text{Ar}$ - $^{39}\text{Ar}$  Arrhenius diagrams are for mineral samples. However, both Turner et al., (1978) and Ozima & Takigami (1980) have presented Arrhenius diagrams for whole-rock samples. These were found to give linear correlations over part or over the whole gas release. This behaviour was thought to indicate that the potassium contained within these whole-rock samples was located in a single mineral phase.

$^{40}\text{Ar}$ - $^{39}\text{Ar}$  Arrhenius diagrams have been put to several uses:

- i) Calculating mineral closure temperatures. Where a linear correlation of data points exists, it is possible to calculate a closure temperature using the computed diffusion parameters and Dodson's (1973) formula - Buchan et al., (1977), Turner et al., (1978).
- ii) Commenting on argon isotopic disturbances. By comparing their  $^{39}\text{K}$  and  $^{40}\text{K}$  Arrhenius diagrams, Ozima & Takigami (1980) were able to make two observations. Firstly, as the  $^{39}\text{K}$  plots were linear over the whole gas release they suggested that  $^{39}\text{K}$  recoil effects

were not important. Secondly, the failure of the  $^{40}\text{Ar}$  plots to give linear correlations was explained in terms of a non-uniform initial distribution of radiogenic  $^{40}\text{Ar}$ . Turner et al., (1978) suggested that where  $^{39}\text{K}$  Arrhenius diagrams give a significantly lower activation energy than the corresponding  $^{40}\text{Ar}$  ones (from linear correlations of data points), then the  $^{39}\text{K}$  may be subject to a recoil re-distribution effect.

- iii) As an aid to the identification of mineral phases, Harrison & McDougall (1981) plotted  $^{37}\text{K}$  and  $^{39}\text{K}$  Arrhenius diagrams for a plagioclase feldspar. They found that the low temperature linear correlations gave very different activation energies and that there was a distinctly different higher temperature correlation common to both isotopes. Harrison & McDougall (1981) concluded that the plagioclase must, in fact, contain more than one compositional phase.

Both Harrison & McDougall (1980b) and Cliff (1985) warn against using  $^{40}\text{Ar}$ - $^{39}\text{Ar}$  Arrhenius plots to make conclusions about argon diffusion in nature. There are three important points to consider:

- i) If  $^{39}\text{K}$  is used in plotting the Arrhenius diagram, then this reactor-produced isotope may misrepresent the transport of the natural radiogenic isotope. The pattern of  $^{39}\text{K}$  loss from a mineral during stepwise degassing may reflect recoil and lattice damage effects.
- ii) Mineral phases may be unstable during vacuum heating. One of the criteria for a successful diffusion experiment is that the mineral must remain stable (Giletti, 1974). Hydrous minerals such as biotite and hornblende are unlikely to remain stable during a  $^{40}\text{Ar}$ - $^{39}\text{Ar}$  stepwise degassing experiment. Feldspars, on the other hand, will probably not be subject to any such stability problems.

iii) In making geological interpretations, the laboratory diffusion results have to be extrapolated over many orders of magnitude.

Arrhenius diagrams in this thesis

Three types of Arrhenius diagram data file can be produced in the "STEPAGE" computer program (see Section 5:7). These are for the release of  $^{40}\text{K}$ ,  $^{39}\text{K}$  and  $^{37}\text{K}$ . There are two choices of diffusion symmetry in the "ARRHENUS" program - spherical and planar. The corresponding solutions to Fick's law are taken from Crank (1975);

$$\text{Spherical} \quad f = \frac{6}{\pi^2} \sum_{k=1}^{\infty} \frac{\exp(-k^2\pi^2\tau)}{k^2}$$

$$\text{Planar} \quad f = \frac{8}{\pi^2} \sum_{n=0}^{\infty} \frac{\exp[-(2n+1)^2\pi^2\tau/4]}{(2n+1)^2}$$

where  $f$  = fraction of isotope remaining (calculated for each step)

$$\tau = Dt/a^2$$

and  $D$  = diffusion coefficient

$t$  = duration of heating step (30 minutes)

$a$  = characteristic diffusion dimension

By separating the first term from the summation an expression for  $\tau$  is apparent;

$$\text{Spherical} \quad \tau = \frac{-1}{\pi^2} \text{Log}_e \left[ \frac{\pi^2 f}{6} - \sum_{k=2}^{\infty} \frac{\exp(-k^2\pi^2\tau)}{k^2} \right]$$

$$\text{Planar} \quad \tau = \frac{-4}{\pi^2} \text{Log}_e \left[ \frac{\pi^2 f}{8} - \sum_{n=1}^{\infty} \frac{\exp[-(2n+1)^2\pi^2\tau/4]}{(2n+1)^2} \right]$$

As  $\tau$  appears on both sides of these expressions, its calculation is an iterative operation. In the spherical case, a series of four initial guesses were determined empirically (covering the range of  $f$  values from 0 to 0.995). Expressions given in Harrison & McDougall (1981) were used as initial guesses in the planar case. In this way  $\tau$  values are calculated for each step.

The traditional Arrhenius diagram is a plot of  $\text{Log}_{10} D$  v.  $1/T$ . However, following the example of Albarede (1978), the  $^{40}\text{Ar}$ - $^{39}\text{Ar}$  Arrhenius diagram

in this study is plotted as  $\text{Log}_e[\tau_i - \tau_{i-1}]$  v.  $1/T_i$  ('i' refers to step number). An example of one of these Arrhenius diagrams is presented in Fig. A2:1. Where the data points on an Arrhenius diagram form a linear correlation, values for E (the activation energy) and  $D_0t/a^2$  are calculated from a least squares regression (Fig. A2:1 shows the best fitting straight line to a series of data points). From these, a closure temperature can be estimated if a value for the geological cooling rate is set. Errors in the calculated parameters are not quoted in this study because of the difficulty in setting realistic errors for f and T (see below). Thus, any quoted numerical quantities e.g. activation energy, closure temperature, should only be considered as estimates.

There are two reasons why it was not possible to set realistic errors for f and T in this study. Firstly, the step temperatures quoted are those as measured on the outside wall of the sample crucible. They were often only average figures because of temperature variations on the crucible wall. There is some doubt as to whether the quoted step temperatures will accurately reflect the temperature of the sample itself. Often where step temperature was monitored by more than one device, the measurements were not wholly consistent. Secondly, calculation of 'f' values assume that the mass spectrometer sensitivity was constant. Variations of up to 10% are likely, but in any given case the variation cannot be easily quantified. As there is no method of estimating meaningful errors in quoted f values, I have chosen to set no error at all, rather than using a blanket error. An error is only set for the temperature measurements (usually  $\pm 10^\circ\text{C}$ ) to facilitate the least squares regression.

Where temperature information was available for samples, all three isotopic Arrhenius diagrams were plotted. Usually, a spherical diffusion symmetry was assumed, but in some cases the planar symmetry



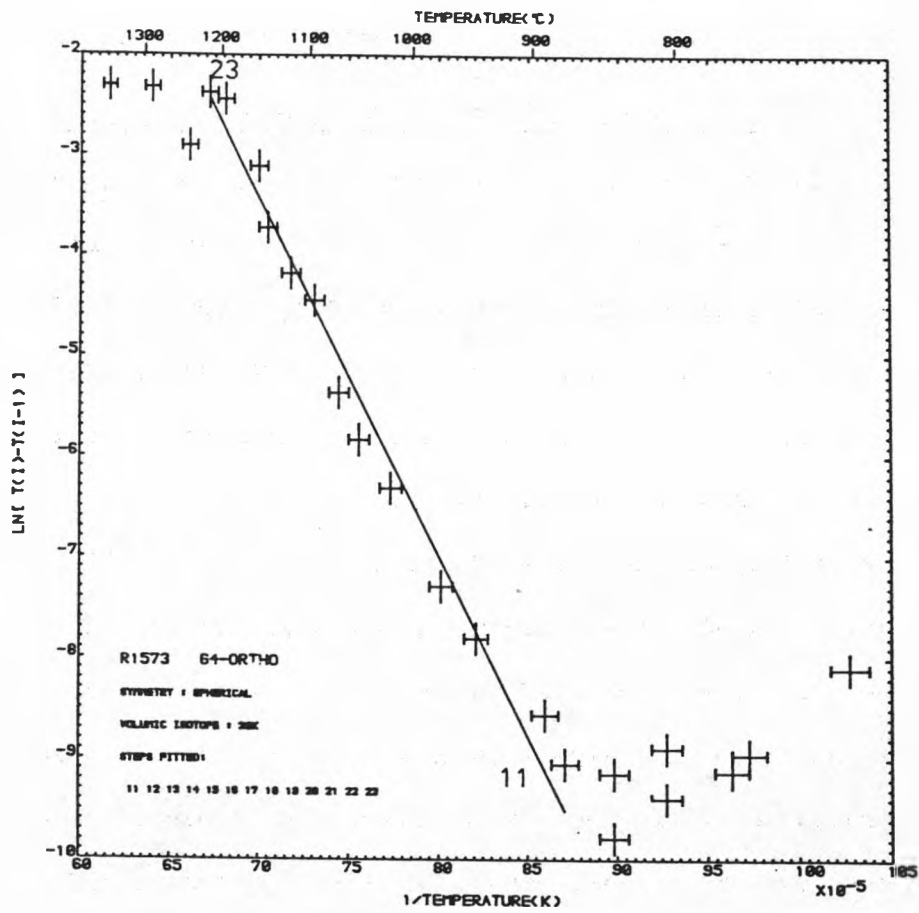


Fig. A2:1 An Arrhenius plot

was preferred after considering mineral structure. In fact, for a given sample there is little difference between diffusion parameters and closure temperatures calculated with spherical and planar symmetries (e.g. see Table 6:21 for a comparison of values calculated using the two diffusion symmetries).

The majority of samples dated in this thesis are whole-rocks and often the Arrhenius diagrams they produce are very complicated. Usually, whether age spectra are disturbed or not, the  $^{39}\text{K}$  and  $^{40}\text{*}$  plots are similar. Where linear correlations exist in the two plots they invariably give almost identical diffusion parameters. This behaviour is not entirely understood. In this study it does not appear that Arrhenius diagrams can be used reliably to differentiate  $^{39}\text{K}$  disturbances (e.g. recoil loss/re-distribution) from those of  $^{40}\text{*}$  (e.g. excess argon) as was implied by Turner et al., (1978) and Ozima & Takigami (1980). The  $^{37}\text{Ar}$  Arrhenius diagrams are usually quite different to the ones for  $^{39}\text{K}$  and  $^{40}\text{*}$ . This can probably be explained by the calcium-derived  $^{37}\text{Ar}$  originating from sources which are distinct from those producing  $^{39}\text{K}$  and  $^{40}\text{*}$ . Sometimes, calculated closure temperatures appear to be geologically meaningful but in other cases they do not.

In the absence of any consistent pattern in the results, it is difficult to make firm conclusions or observations helpful in interpreting  $^{40}\text{Ar}-^{39}\text{Ar}$  age data. Only in instances where the Arrhenius diagram information is particularly compelling and apparently meaningful will the results be discussed in the results section. A detailed interpretation of all the Arrhenius diagrams may be possible with a greater understanding of argon release from multi-phase samples and of the effects of irradiation.

Calculating closure temperatures from Arrhenius diagram parameters  
- assignment of cooling rates

The calculation of an effective closure temperature from the Arrhenius diagram parameters  $E$  and  $D_0/a^2$ , and also of a geological cooling rate, has been outlined in Section 4:2. As noted by Dodson (1973), the value of the cooling rate is not critical to the calculation of a closure temperature. The relative insensitivity of the closure temperature calculation to the value of the cooling rate is most effectively demonstrated using an example. Taking  $E = 35 \text{ kcal mol}^{-1}$  and  $D_0/a^2 = 9.3 \times 10^3 \text{ s}^{-1}$  (values calculated from the Arrhenius diagram of R1572 (G2M-biotite) - see Table 6:21) and cooling rates of (i)  $10^3$  and (ii)  $10^4 \text{ }^\circ\text{C Ma}^{-1}$ , closure temperatures of (i)  $190^\circ\text{C}$  and (ii)  $220^\circ\text{C}$  are calculated respectively. For an order of magnitude increase in cooling rate, the calculated closure temperature increases by  $30^\circ\text{C}$  only. For the estimation of a closure temperature, therefore, an intuitive estimate of the cooling rate is probably sufficient.

Simple theoretical calculations show that granite plutons such as the Mourne Mountains (10-15km across) probably cooled in less than 1 Ma (A. E. Mussett pers. comm.). Therefore a cooling rate of  $1000^\circ\text{C Ma}^{-1}$  appears to be appropriate for the Mourne Granite mineral separates dated in this thesis. The smaller, but still coarse-grained, bodies of the Glenlaur gabbro (100m wide), the Droimchogaidh sill (100m thick) and the Killala Gabbro (400m wide) are assigned tentative cooling rates of  $10^4 \text{ }^\circ\text{C Ma}^{-1}$ . The Killala Gabbro felsic dykelet is also assigned a cooling rate of  $10^4 \text{ }^\circ\text{C Ma}^{-1}$ , (which is the same as for the host body), although the intrusion concerned is of the order of only 10cm across. This choice is justified by the similar grain sizes of the dykelet and the host gabbro. These observations suggest that the felsic dykelet was intruded into the gabbro whilst it was still very hot and that the two bodies cooled at a very similar rate. A  $10^4 \text{ }^\circ\text{C Ma}^{-1}$

cooling rate has further been assigned to the dykes of the Mourne Swarm. This may seem rather slow for dykes of the order of 5m wide. However, it is thought that the major potassium-bearing phase in these rocks is a secondary mineral formed by the heating effect of the intruding Mourne Granites. A  $10^4$  °C Ma<sup>-1</sup> cooling rate in the metamorphic aureole surrounding the Mourne Granites seems reasonable considering the  $10^3$  °C Ma<sup>-1</sup> rate assumed for the granites themselves. In respect of its small size (3-4m wide), the Droimchogaidh satellite sill has been tentatively assigned a very fast cooling rate of  $10^6$  °C Ma<sup>-1</sup>.

Table A2:1 summarises the cooling rates assumed for rocks in this study for which closure temperature estimates are made.

Rock body	Samples for which closure temperature estimates are made	Size of body	Assigned cooling rate ( $^{\circ}\text{C Ma}^{-1}$ )
Glenlaur gabbro	R1610(211NWC)	100m	$10^4$
Droimchogaidh sill	R1612(238P)	100m	$10^4$
Droimchogaidh satellite sill	R1581(234)	3-4m	$10^6$
Killala Gabbro felsic dykelet	R1613(G029)	of the order of 10cm	$10^4$
Killala Gabbro	R1571(RG-pyroxene) R1621(RG-plagioclase feldspar)	400m	$10^4$
Mourne Granites	R1572(G2M-biotite) R1573(G4-orthoclase feldspar)	10-15km	$10^3$
Mourne Swarm dyke	R1620(N002)	5m	$10^4$

Table A2:1 Summary of cooling rates assumed for rocks in this study

APPENDIX 3

Interference Reactions and Argon Isotope Recoil Energies

## Introduction

The interference reactions are neutron interactions on chlorine, potassium or calcium which result in the formation of argon isotopes in the atomic mass range 36 - 40. Neutron interactions likely to be involved are listed in Table A3:1. To determine which ones are the most important, it is necessary to consider two factors:

- i) the reactor neutron energy spectrum
- ii) interaction cross-section variation with energy

i) The precise form of the neutron energy spectrum experienced by  $^{40}\text{Ar}$ - $^{39}\text{Ar}$  samples in the Herald reactor is not known. However, the fast neutron spectrum may be adequately described by the fission neutron energy spectrum. This is a reasonable assumption because the samples are positioned very close to the reactor fuel elements (the nearest fuel element being  $\approx 5\text{cm}$  away). The generally accepted mathematical expression of the fission neutron energy spectrum is (Bennett, 1972):

$$S(E) = 0.770 E^{\frac{1}{2}} e^{-0.776E} \quad (E \text{ measured in MeV})$$

For the Herald reactor core positions used in this dating study, about three times as many thermal neutrons ( $E < 0.1 \text{ MeV}$ ) than fast neutrons ( $E > 0.1 \text{ MeV}$ ) can be expected.

ii) Information about interaction cross-sections has been gathered from a number of sources (the major ones were Brookhaven National Laboratory BNL325 - 3rd edition, 1976, and the ENDF/B-IV, JENDL-2 nuclear data files).

Knowledge of factors (i) and (ii) also allows the calculation of maximum recoil energies for the argon isotopes produced by neutron interaction. The maximum recoil energy is attained if the recoiling argon isotope moves in the same direction as the incident neutron. In addition, other particle(s) produced as a result of the interaction must travel in the opposite direction. Where one other particle is produced, conservation of momentum requires that it should

Target element	$^{36}\text{Ar}$	$^{37}\text{Ar}$	$^{38}\text{Ar}$	$^{39}\text{Ar}$	$^{40}\text{Ar}$
Chlorine	$^{35}\text{Cl}(n,\gamma)^{36}\text{Cl}(\beta^-)$		$^{37}\text{Cl}(n,\gamma)^{38}\text{Cl}(\beta^-)$		
Potassium	$^{39}\text{K}(n,\alpha)^{36}\text{Cl}(\beta^-)$ $^{40}\text{K}(n,n\alpha)^{36}\text{Cl}(\beta^-)$	$[^{39}\text{K}(n,t)]$	$^{39}\text{K}(n,d)$ $^{39}\text{K}(n,np)$ $^{41}\text{K}(n,\alpha)^{38}\text{Cl}(\beta^-)$	$^{39}\text{K}(n,p)$ $^{40}\text{K}(n,d)$ $^{40}\text{K}(n,np)$	$^{40}\text{K}(n,p)$ $^{41}\text{K}(n,d)$ $^{41}\text{K}(n,np)$
Calcium	$^{40}\text{Ca}(n,n\alpha)$	$^{40}\text{Ca}(n,\alpha)$	$^{42}\text{Ca}(n,n\alpha)$	$^{42}\text{Ca}(n,\alpha)$ $^{43}\text{Ca}(n,n\alpha)$	$^{43}\text{Ca}(n,\alpha)$ $^{44}\text{Ca}(n,n\alpha)$

Table A3:1 Argon isotopes produced by neutron interactions on chlorine, potassium and calcium



travel in the opposite direction to the neutron and argon isotopes.

Because of the particle energies involved, the mathematics for the calculation of recoil energies are relativistic (expressions used are taken from French, 1968).

To simplify the mathematics, a transformation into the centre of mass reference frame is required:



Laboratory reference frame

Centre of mass reference frame

(velocity V)

$$V = \frac{p_n C^2}{E_n + E_T} = \frac{(E_n^2 - E_{n_0}^2)^{\frac{1}{2}}}{E_n + E_{T_0}} = \frac{(M_n^2 - M_{n_0}^2)^{\frac{1}{2}}}{M_n + M_{T_0}} C$$

where  $p_n$  = the momentum of the incident neutron

$E_n, E_T$  = the total energy of the neutron and target (chlorine, potassium or calcium atom)

$E_{n_0}, E_{T_0}$  = rest mass energies

$M_{n_0}, M_{T_0}$  = rest masses

$$M_n = \text{neutron mass} = M_{n_0} + \frac{K_n (\text{MeV})}{931.48}$$

$K_n$  = neutron kinetic energy

Total energy available in centre of mass for physical processes:

$$E' = (M_{n_0}^2 + M_{T_0}^2 + 2\gamma M_{n_0} M_{T_0})^{\frac{1}{2}} C^2 \quad \text{where } \gamma = E_n/E_{n_0}$$

Converting this expression into an equivalent mass we have:

$$M' = (M_{n_0}^2 + M_{T_0}^2 + 2M_n M_{T_0})^{\frac{1}{2}}$$

Considering the two outgoing particles:

Ar = argon isotope

$\Delta$  = additional particle(s) produced by neutron interaction (if there is more than one, then, as they are all travelling in the same direction, they can be thought of as a single particle).

Conservation of momentum:

$$\begin{aligned}
 p_{Ar}' &= p_{\Delta}' \\
 \frac{(E_{Ar}'^2 - E_{Ar_0}^2)^{\frac{1}{2}}}{c} &= \frac{(E_{\Delta}'^2 - E_{\Delta_0}^2)^{\frac{1}{2}}}{c} \\
 E_{Ar}'^2 - E_{Ar_0}^2 &= E_{\Delta}'^2 - E_{\Delta_0}^2
 \end{aligned}$$

Conservation of energy:

$$E' = E_{Ar}' + E_{\Delta}'$$

eliminating  $E_{\Delta}'$ :

$$E_{Ar}' = \frac{E_{Ar_0}^2 - E_{\Delta_0}^2 + E'^2}{2E'}$$

and in terms of masses:

$$M_{Ar}' = \frac{M_{Ar_0}^2 - M_{\Delta_0}^2 + M'^2}{2M'}$$

Using the energy transformation equation:

$$\begin{aligned}
 E_{Ar} &= \gamma (E_{Ar}' + v p_{Ar}') \\
 &= \frac{E_{Ar}' + \frac{v}{c} (E_{Ar}'^2 - E_{Ar_0}^2)^{\frac{1}{2}}}{\left(1 - \frac{v^2}{c^2}\right)^{\frac{1}{2}}}
 \end{aligned}$$

and the maximum argon isotope recoil energy  $K_{Ar} = E_{Ar} - E_{Ar_0}$

In terms of masses:

$$K_{Ar} = \left\{ \frac{\left[ M_{Ar}' + \frac{v}{c} (M_{Ar}'^2 - M_{Ar_0}^2)^{\frac{1}{2}} \right]}{\left(1 - \frac{v^2}{c^2}\right)^{\frac{1}{2}}} - M_{Ar_0} \right\} \times 931.48 \text{ MeV}$$

To conduct a recoil energy calculation, it is necessary to know the particle rest masses and to set an energy for the incident neutron. Particle rest masses can be calculated with reference to Wapstra & Bos (1976). The neutron energy used in these recoil calculations is a mean one. Where the interaction considered is activated mainly by fast neutrons, the mean energy can be estimated from a graph showing the  $S(E) \times$  interaction cross-section ( $\sigma$ ) variation with energy. To simplify matters, I shall take the energy at which  $\sigma S(E)$  peaks. Where thermal neutrons are thought to activate a particular inter-

action, I shall use an incident neutron energy of 0.025 eV.

Before considering the interference reactions, it is worth reassessing the recoil energies involved in the production of  $^{39}\text{K}$  and  $^{40}\text{K}$ . The plot of  $\sigma S(E)$  v.  $E$  for the  $\text{K}(n,p)$  interaction is displayed in Fig. A3:1 (all the available  $^{39}\text{K}(n,p)$  cross-sectional data for fast neutrons is quantitatively consistent with that for the natural element interaction). Choosing the energy of which the  $\sigma S(E)$  curve peaks as the mean neutron energy (3.4 MeV), a recoil energy of 371 keV is calculated, which is similar to the value computed by Mitchell (1968). Although two other interactions may produce  $^{39}\text{Ar}$  from neutron interactions on potassium, they are not considered important due to the low abundance of  $^{40}\text{K}$  (see Table A3:1).

If the incident neutron is ignored, the recoil energy of  $^{40}\text{K}$ , produced by the decay of  $^{40}\text{K}$ , can be calculated using the above equations, i.e.

$$M' = M_{\text{T}_O} = M_{^{40}\text{K}}$$

$$M_{\text{Ar}'} = \frac{M_{\text{Ar}_O}^2 - M_{\Delta_O}^2 + M_{\text{T}_O}^2}{2 M_{\text{T}_O}}$$

and

$$K_{\text{Ar}} = (M_{\text{Ar}'} - M_{\text{Ar}_O}) \times 931.48 \text{ MeV}$$

The computed value of 27 eV is in agreement with Brandt & Voronovsky's (1967) estimate of 28 eV.

Where cross-sectional information is available for the possible interference reactions, maximum recoil energies have been calculated. These are presented in Table A3:2.  $\sigma S(E)$  v.  $E$  curves for the reactions activated by fast neutrons are presented in Figs. A3:2 and A3:7.

The various interference reactions are discussed target element by target element, and argon isotope by argon isotope.

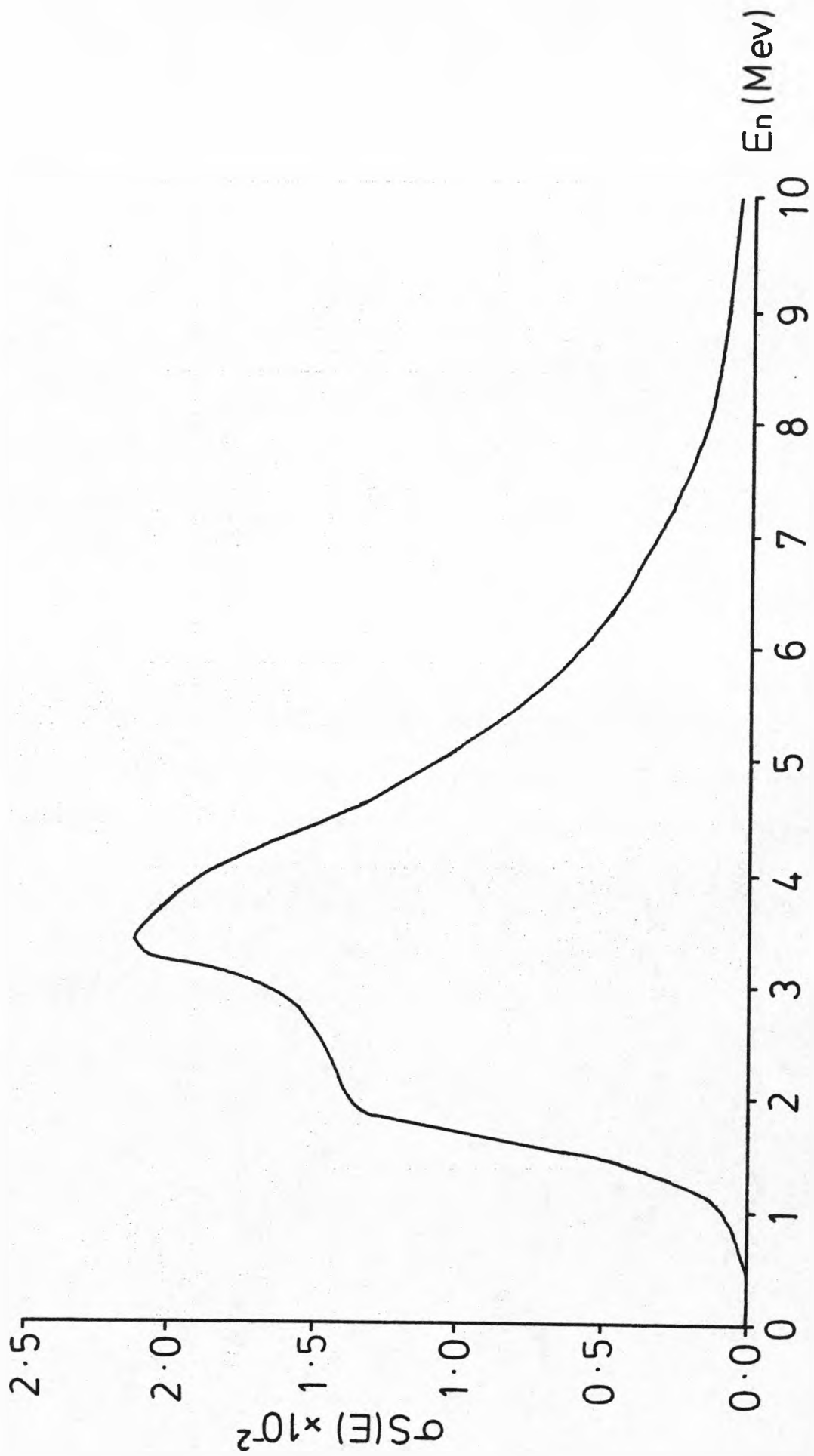


Fig. A3:1  $\sigma_S(E)$  v.  $E_n$  curve for the K(n,p) interaction

Chlorine interactions	Potassium interactions	Calcium interactions
* $^{35}\text{Cl}(n, \gamma)^{36}\text{Cl}(\beta^-)^{36}\text{Ar}$ 1096 eV 3 eV	$^{39}\text{K}(n, np)^{38}\text{Ar}$ 673 keV * $^{40}\text{K}(n, p)^{40}\text{Ar}$ 69 keV	$^{40}\text{Ca}(n, n\alpha)^{36}\text{Ar}$ 2304 keV $^{40}\text{Ca}(n, \alpha)^{37}\text{Ar}$ 1179 keV(2)
* $^{37}\text{Cl}(n, \gamma)^{38}\text{Cl}(\beta^-)^{38}\text{Ar}$ 527 eV 338 eV (1)		$^{42}\text{Ca}(n, \alpha)^{39}\text{Ar}$ 925 keV $^{43}\text{Ca}(n, \alpha)^{40}\text{Ar}$ 1148 keV

\* Interactions activated by thermal neutrons

(1) Stettler & Bochsler (1979) report 60 eV for the whole interaction

(2) Brereton (1972) reports 360 keV

Table A3:2 Calculated maximum recoil energies

Chlorine

<sup>36</sup>Ar: The ENDF/B-IV and BNL325 cross-section v. energy curves for Cl(n,γ) show that this interaction is largely activated by thermal neutrons. As the BNL325 <sup>37</sup>Cl(n,γ) curve records very much lower cross-sections, the curve for the natural element is thought to be a reasonable approximation to <sup>35</sup>Cl(n,γ).

<sup>38</sup>Ar: The BNL325 <sup>37</sup>Cl(n,γ) reaction cross-section v. energy curve follows a similar pattern to the Cl(n,γ) curve. Therefore, the <sup>37</sup>Cl(n,γ) interaction is assumed to be largely activated by thermal neutrons.

Potassium

<sup>36</sup>Ar: Of the two possible interactions listed in Table A3:1, cross-sectional information is available only for <sup>39</sup>K(n,α) - ENDF/B-IV K(n,α) evaluation (all cross-sectional data for <sup>39</sup>K(n,α) is quantitatively consistent with that for the natural element interaction). However, as the inferred [36/39]<sub>K</sub> can be shown to be negligible (see below), a recoil calculation has not been undertaken. The (n,nα) interaction will probably be less important than the (n,α) interaction because of the low natural abundance of <sup>40</sup>K.

By comparing the areas under the σS(E) v. E curves for K(n,α), and K(n,p) it is possible to calculate a theoretical [36/39]<sub>K</sub> value:

$$\left[ \frac{36}{39} \right]_K = \frac{A_\alpha}{A_p} (1 - e^{-\lambda t})$$

where  $A_\alpha$  = area under σS(E) v. E curve for K(n,α) - see Fig. A3:2  
 $A_p$  = area under σS(E) v. E curve for K(n,p) - see Fig. A3:1  
 $(1 - e^{-\lambda t})$  = term taking account of <sup>36</sup>Cl(β<sup>-</sup>)<sup>36</sup>Ar  
 $t$  = time since irradiation.

For a typical maximum value of  $t = 1$  year:

$$[36/39]_K = 6.7 \times 10^{-7}$$

Where levels of <sup>39</sup>K and <sup>36</sup>total are normal, the level of <sup>36</sup>K will be insignificant.

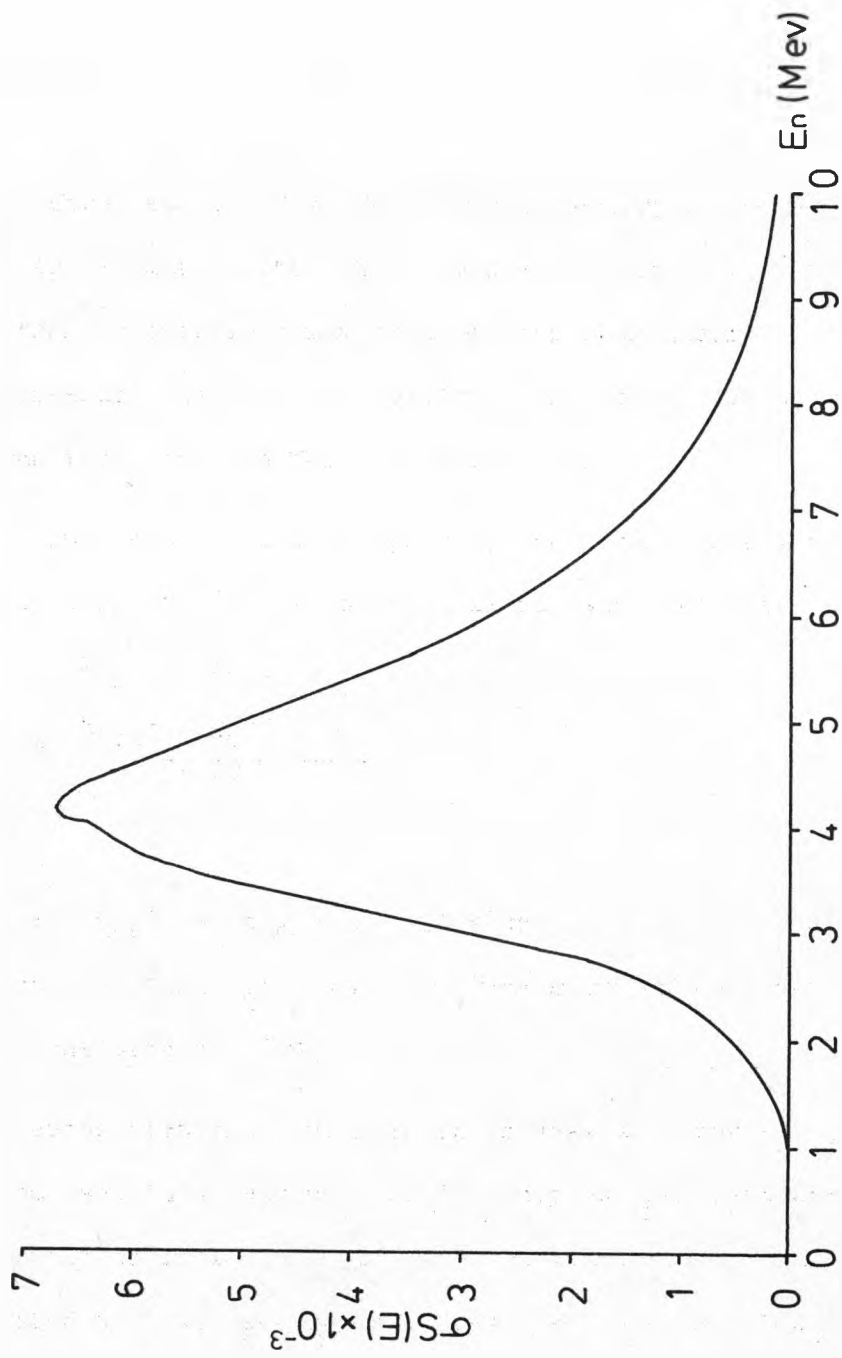


Fig. A3:2  $\sigma_S(E)$  v.  $E_n$  curve for the  $K(n,\alpha)$  interaction

Note: 
$$\frac{^{36}\text{K}}{^{36}\text{Ca}} = \left( \frac{^{39}\text{K}}{^{40}\text{Ca}} \right)_{\text{natural abundance}} \frac{A_{^{36}\text{K}}}{A_{^{36}\text{Ca}}} (1 - e^{-\lambda t})$$

where  $A_{^{36}\text{K}}$  = area under  $\sigma S(E)$  v.  $E$  curve for  $\text{K}(n,\alpha)$  - see Fig. A3:2

$A_{^{36}\text{Ca}}$  = area under  $\sigma S(E)$  v.  $E$  curve for  $^{40}\text{Ca}(n,n\alpha)$  - see Fig. A3:4

for  $t = 1$  year,  $^{36}\text{K}/^{36}\text{Ca} \approx 0.1\text{K}/\text{Ca}$

$^{37}\text{Ar}$ : Potassium-derived  $^{37}\text{Ar}$  has been measured for a  $\text{K}_2\text{SO}_4$  salt sample (Section 5:4:2). However, none of the simple neutron interactions considered would result in the production of  $^{37}\text{Ar}$  from potassium. The reaction responsible may be  $^{39}\text{K}(n,t)^{37}\text{Ar}$ , for which one cross-section datum is given in BNL325 (0.184 mb at 14.7 MeV). As discussed in Chapter 5, any potassium-derived  $^{37}\text{Ar}$  will not be important in terms of  $^{40}\text{Ar}$ - $^{39}\text{Ar}$  dating.

$^{38}\text{Ar}$ : Cross-sectional information is available for  $\text{K}(n,np)$  - ENDF/B-IV, and  $^{41}\text{K}(n,\alpha)$  - BNL325 (the former is probably dominated by  $^{39}\text{K}(n,np)$  because of the high natural abundance of  $^{39}\text{K}$ ). As reported [38/39]<sub>K</sub> values show very little scatter (see Roddick, 1983), we can infer that the majority of  $^{38}\text{K}$  must be produced by fast neutron interactions. The fast neutron cross-sections for the above interactions are of the same order. It is therefore reasonable to conclude that the  $^{39}\text{K}(n,np)$  reaction will be far more important than the  $^{41}\text{K}(n,\alpha)$ , on the basis of the relative natural abundances of the potassium isotopes.

The maximum recoil energy for  $^{39}\text{K}(n,np)^{38}\text{Ar}$  is calculated to be 673 keV. This value is similar to the maximum recoil energy of 750 keV calculated by Brereton (1972) for the  $^{39}\text{K}(n,d)^{38}\text{Ar}$  interaction. However, the possibility of a significant contribution from this source cannot be evaluated without cross-sectional information.

Comparing the areas under the  $\sigma S(E)$  v.  $E$  curves for  $\text{K}(n,np)$  and  $\text{K}(n,p)$  (see Figs. A3:3 and A3:1) a theoretical [38/39]<sub>K</sub> value of 0.0078 is calculated. This is not much smaller than the measured ratio of



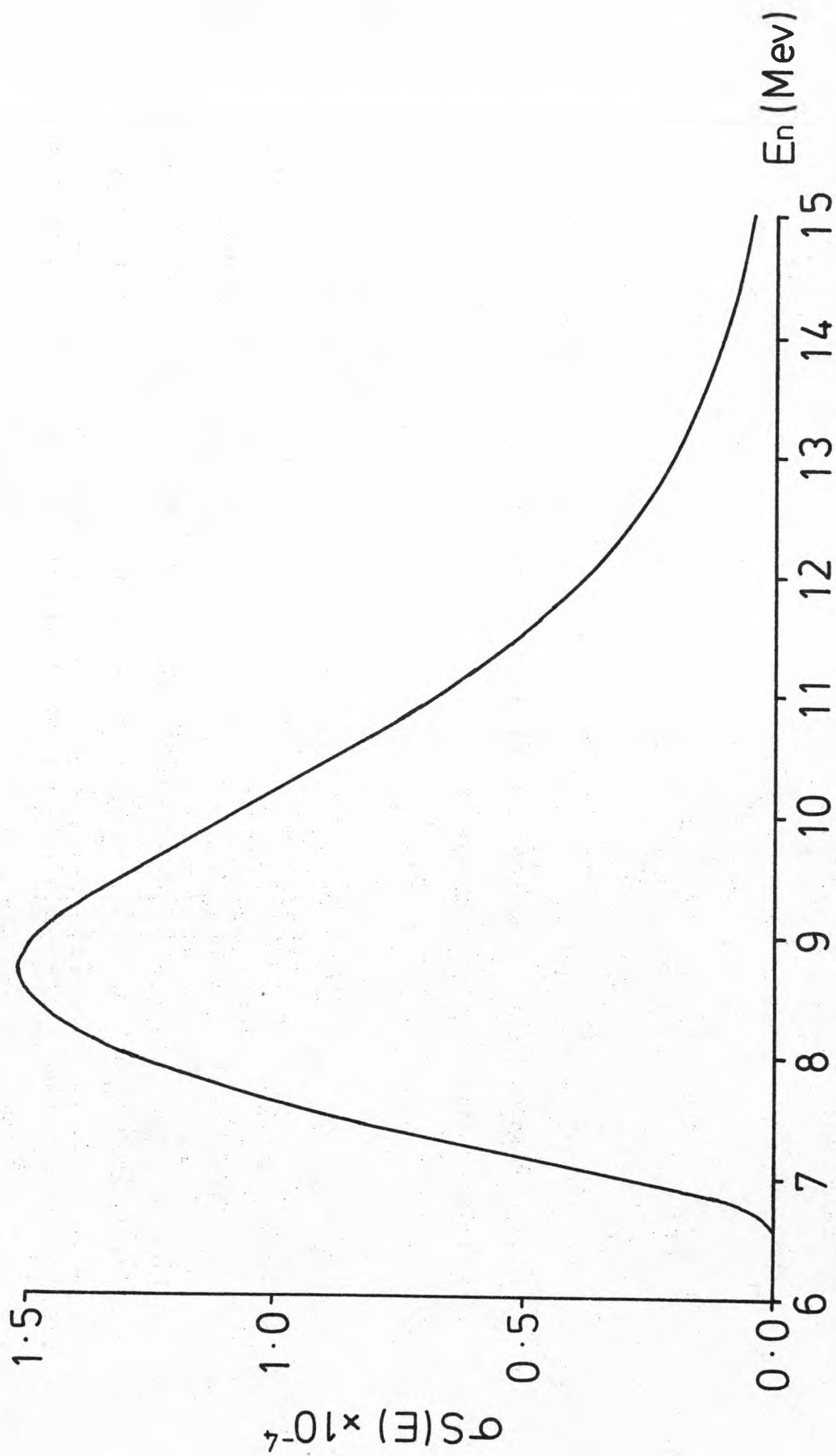


Fig. A3:3  $\sigma_S(E)$  v.  $E_n$  curve for the  $K(n,np)$  interaction

0.011 (see Section 5:4:2).

<sup>40</sup>Ar: No detailed cross-sectional information is available for the interactions listed in Table A3:1. Several studies have shown that the <sup>40</sup>K(n,p) interaction is largely thermally activated (e.g. Tetley et al., 1980); therefore an incident neutron energy of 0.025 eV was used in the calculation for maximum recoil energy.

Assuming that the <sup>40</sup>K(n,p) interaction is solely responsible for potassium-derived <sup>40</sup>Ar, it is possible to make a rough estimate of the [40/39]<sub>K</sub> value from theoretical considerations:

$$\left[ \frac{40}{39} \right]_K \approx \frac{\sigma(\text{}^{40}\text{K})}{f\sigma(\text{}^{39}\text{K})} \left( \frac{\text{thermal}}{\text{fast}} \right)_{\text{Herald}} \left( \frac{\text{}^{40}\text{K}}{\text{}^{39}\text{K}} \right)_{\text{natural abundance}}$$

where  $\sigma(\text{}^{40}\text{K})$  = thermal neutron cross-section for <sup>40</sup>K(n,p) = 4.4 b  
(BNL325)

$f\sigma(\text{}^{39}\text{K})$  = fast neutron cross-section for <sup>39</sup>K(n,p) at the energy corresponding to the peak in the  $\sigma S(E)$  curve  
= 0.208 b

$(\text{thermal/fast})_{\text{Herald}}$  = ratio of the numbers of thermal to fast neutrons in the Herald reactor  $\approx 3$

$$\left( \frac{\text{}^{40}\text{K}}{\text{}^{39}\text{K}} \right)_{\text{natural abundance}} = 1.251 \times 10^{-4} \text{ (Steiger \& J\ddot{a}ger, 1977)}$$

$$\therefore \left[ \frac{40}{39} \right]_K \approx 0.008$$

which is of the same order as the adopted value of 0.015. This suggests that, of the three possible interactions listed in Table A3:1, the <sup>40</sup>K(n,p) is probably the most important.

### Calcium

All the cross-sectional information for the calcium interactions is derived from the JENDL-2 nuclear data files.

$^{36}\text{Ar}$ : It is possible to estimate a theoretical  $[36/37]_{\text{Ca}}$  value:

$$\left[ \frac{36}{37} \right]_{\text{Ca}} = \frac{A_{n\alpha}}{A_{\alpha}}$$

where  $A_{n\alpha}$  = area under  $\sigma S(E)$  v.  $E$  curve for  $^{40}\text{Ca}(n,n\alpha)$  - see Fig. A3:4

$A_{\alpha}$  = area under  $\sigma S(E)$  v.  $E$  curve for  $^{40}\text{Ca}(n,\alpha)$  - see Fig. A3:5

Substituting the appropriate values,

$$[36/37]_{\text{Ca}} = 5.1 \times 10^{-4}$$

This value is about twice as large as the experimentally derived one that is typically quoted -  $2.5 \times 10^{-4}$  (Roddick, 1983).

$^{38}\text{Ar}$ : There is no available cross-sectional data for the  $^{42}\text{Ca}(n,n\alpha)$  interaction.

$^{39}\text{Ar}$ : No cross-sectional data is available for  $^{43}\text{Ca}(n,n\alpha)$ . However, because of the significantly lower natural abundance of  $^{43}\text{Ca}$  relative to  $^{42}\text{Ca}$ , this interaction is likely to be unimportant. Taking the  $^{42}\text{Ca}(n,\alpha)$  interaction as the sole contributor to calcium-derived  $^{39}\text{Ar}$ , we can estimate a  $[39/37]_{\text{Ca}}$  value:

$$\left[ \frac{39}{37} \right]_{\text{Ca}} = \frac{A_{\alpha 1}}{A_{\alpha 2}} \left( \frac{^{42}\text{Ca}}{^{40}\text{Ca}} \right)_{\text{natural abundance}}$$

where  $A_{\alpha 1}$  = area under  $\sigma S(E)$  v.  $E$  curve for  $^{42}\text{Ca}(n,\alpha)$  - see Fig. A3:6

$A_{\alpha 2}$  = area under  $\sigma S(E)$  v.  $E$  curve for  $^{40}\text{Ca}(n,\alpha)$  - see Fig. A3:5

$$\left( \frac{^{42}\text{Ca}}{^{40}\text{Ca}} \right)_{\text{natural abundance}} = 6.67 \times 10^{-3} \quad \text{Weast (1983)}$$

therefore  $[39/37]_{\text{Ca}} = 8.8 \times 10^{-3}$

This value is considerably greater than the adopted value of  $6.65 \times 10^{-4}$ . An  $^{39}\text{Ar}$  contribution from  $^{43}\text{Ca}(n,n\alpha)$  would only make this discrepancy greater.

$^{40}\text{Ar}$ : Of the possible interactions listed in Table A3:1 cross-sectional data is available only for  $^{43}\text{Ca}(n,\alpha)$ . The  $^{44}\text{Ca}(n,n\alpha)$  reaction may be important ( $^{44}\text{Ca}$  is the second most common calcium isotope behind  $^{40}\text{Ca}$ ) but for the purpose of this discussion it will be

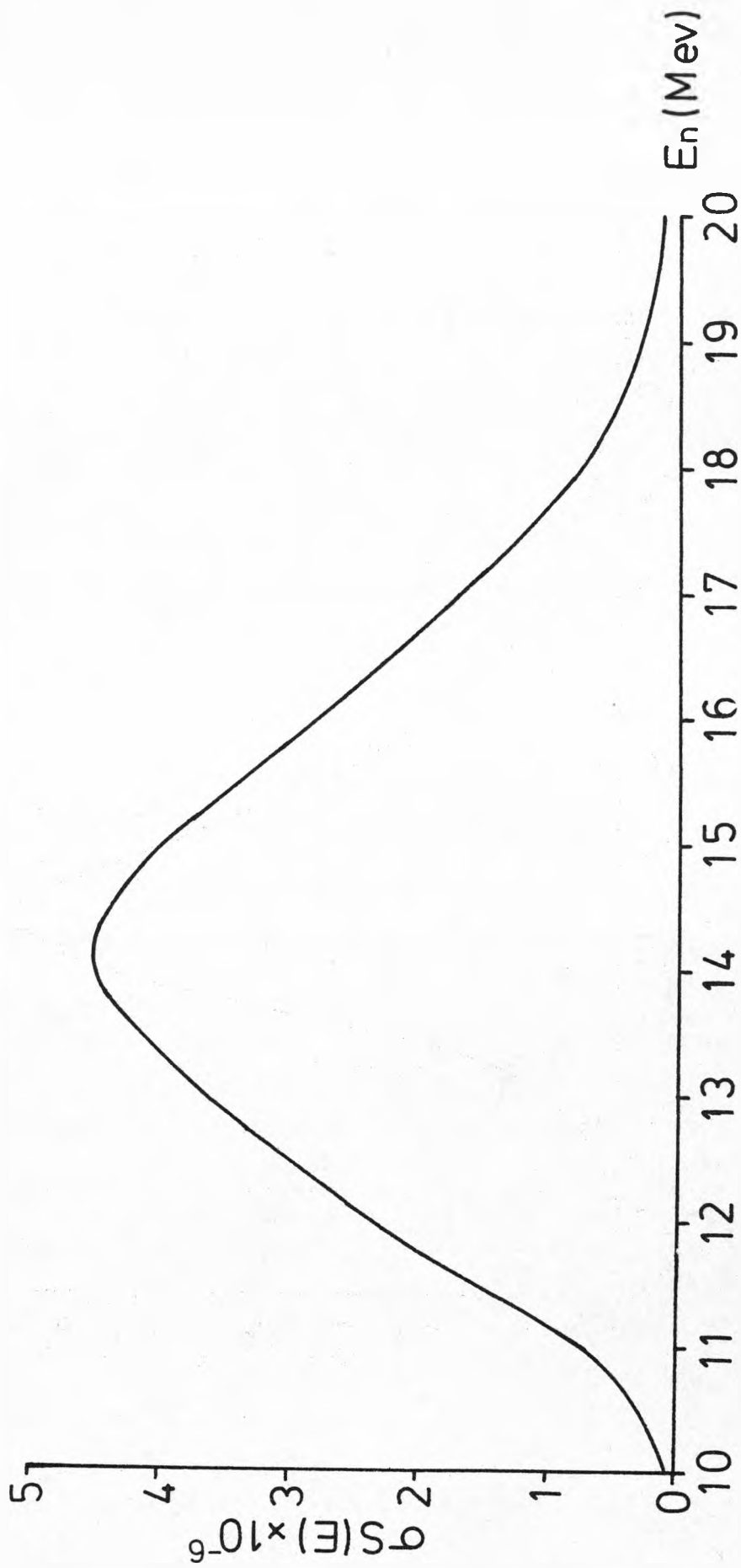


Fig. A3:4  $\sigma_S(E)$  v.  $E_n$  curve for the  $^{40}\text{Ca}(n,nd)^{36}\text{Ar}$  interaction

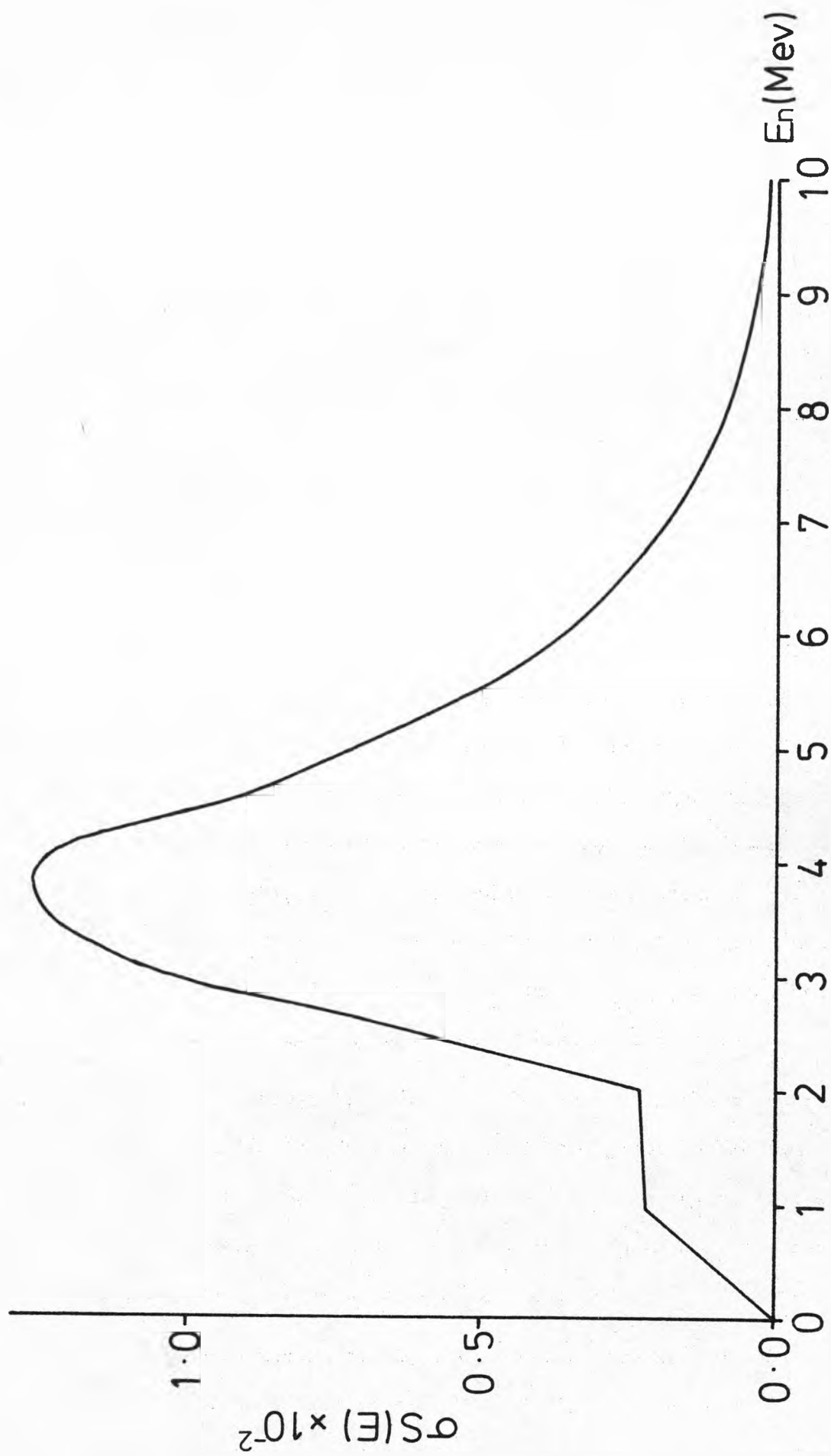


Fig. A3:5  $\sigma_S(E)$  v.  $E_n$  curve for the  ${}^4_0\text{Ca}(n,\alpha)^3_7\text{Ar}$  interaction

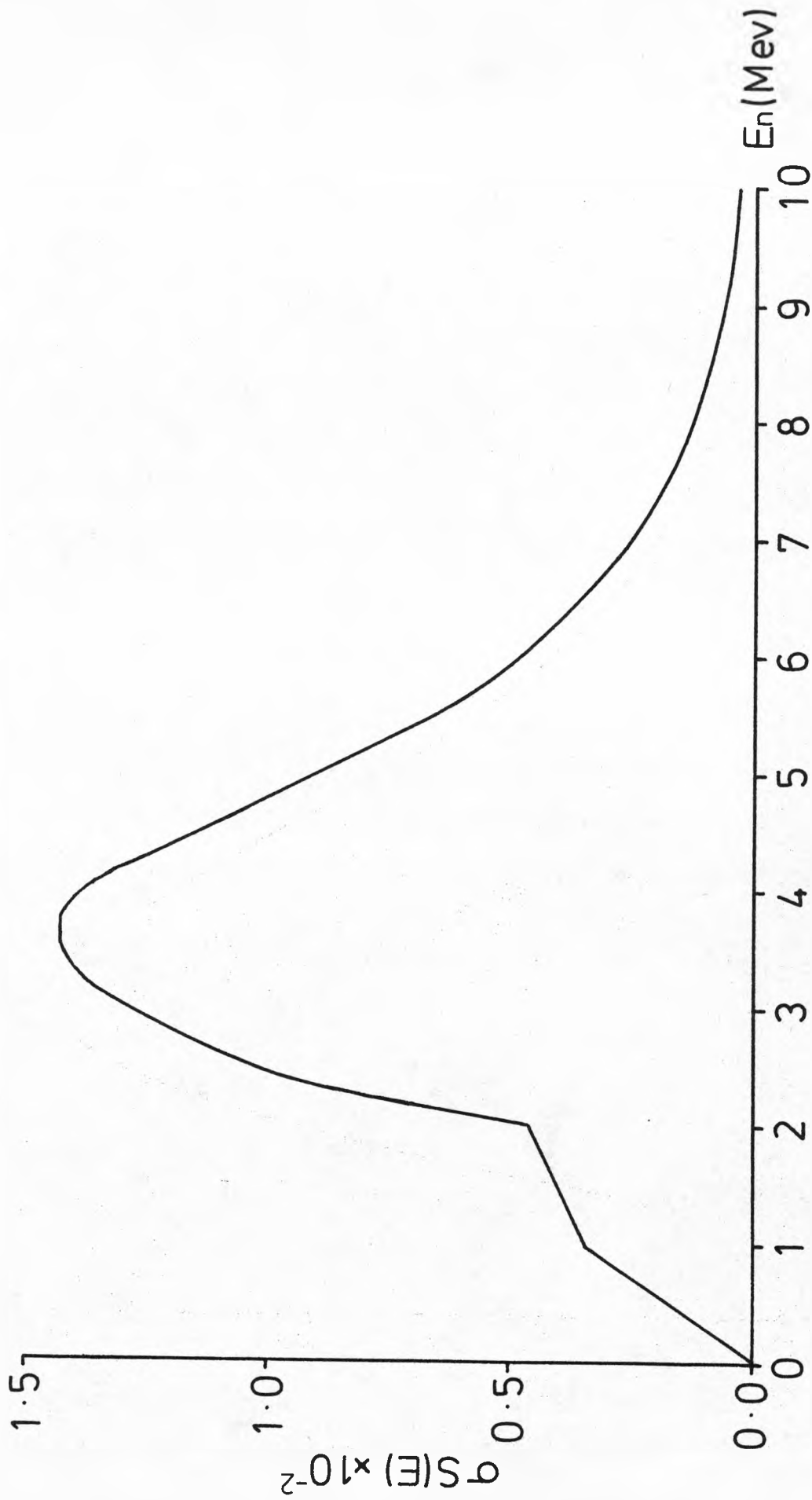


FIG. A3:6  $\sigma_S(E)$  v.  $E_n$  curve for the  $^{42}\text{Ca}(n,d)^{39}\text{Ar}$  interaction.

ignored.

Estimates of  $[40/37]_{Ca}$  and  $[40/36]_{Ca}$  can be made in the same way as described above (see Fig. A3:7 for  $\sigma S(E)$  v.  $E$  curve for the  ${}^43Ca(n,\alpha){}^40Ar$  interaction):

$$[40/37]_{Ca} = 1.1 \times 10^{-3}$$

$$[40/36]_{Ca} = 2.1$$

The inferred  $\left[ \frac{40 - (40/36)_{atm} 36}{37} \right]_{Ca}$  of -0.15 is about twice as large as the adopted value of -0.074. This essentially seems to reflect the difference between theoretical and measured values of  $[36/37]_{Ca}$ , as in the context of the  $\left[ \frac{40 - (40/36)_{atm} 36}{37} \right]_{Ca}$  term calcium-derived  ${}^40Ar$  appears to be insignificant. However, an unaccounted for contribution of  ${}^40Ar$  from the  ${}^44Ca(n,n\alpha)$  interaction could also offer an explanation for this discrepancy. It is important to bear in mind that experimentally-derived values of  $[36/37]_{Ca}$  implicitly assume that  ${}^40Ca$  is insignificant.

## Discussion

### Maximum recoil energies

The maximum recoil energies calculated for neutron interactions on a chlorine target and the recoil energies for the  $\beta^-$  decay of the chlorine isotopes to argon isotopes are insignificant compared with that computed for  ${}^{39}K$ . Recoil effects are thus not expected to be important for chlorine-derived argon isotopes.

For  ${}^{39}K(n,np){}^{38}Ar$  the calculated maximum recoil energy of 673 keV is significantly larger than 370 keV computed for  ${}^{39}K(n,p){}^{39}Ar$ .

Recoil of  ${}^{38}K$  has, in fact, been observed to be more important than for  ${}^{39}K$  in an irradiated  $K_2SO_4$  salt sample (see Section 5:4:2). Nevertheless, recoil of  ${}^{38}K$  is not expected to be important in terms of this  ${}^40Ar$ - ${}^{39}Ar$  dating study because of the small age correction that it entails. The recoil energy calculated for  ${}^40K(n,p){}^40Ar$  is approximately one fifth of that for  ${}^{39}K$ . Recoil of  ${}^{40}K$  is, therefore,

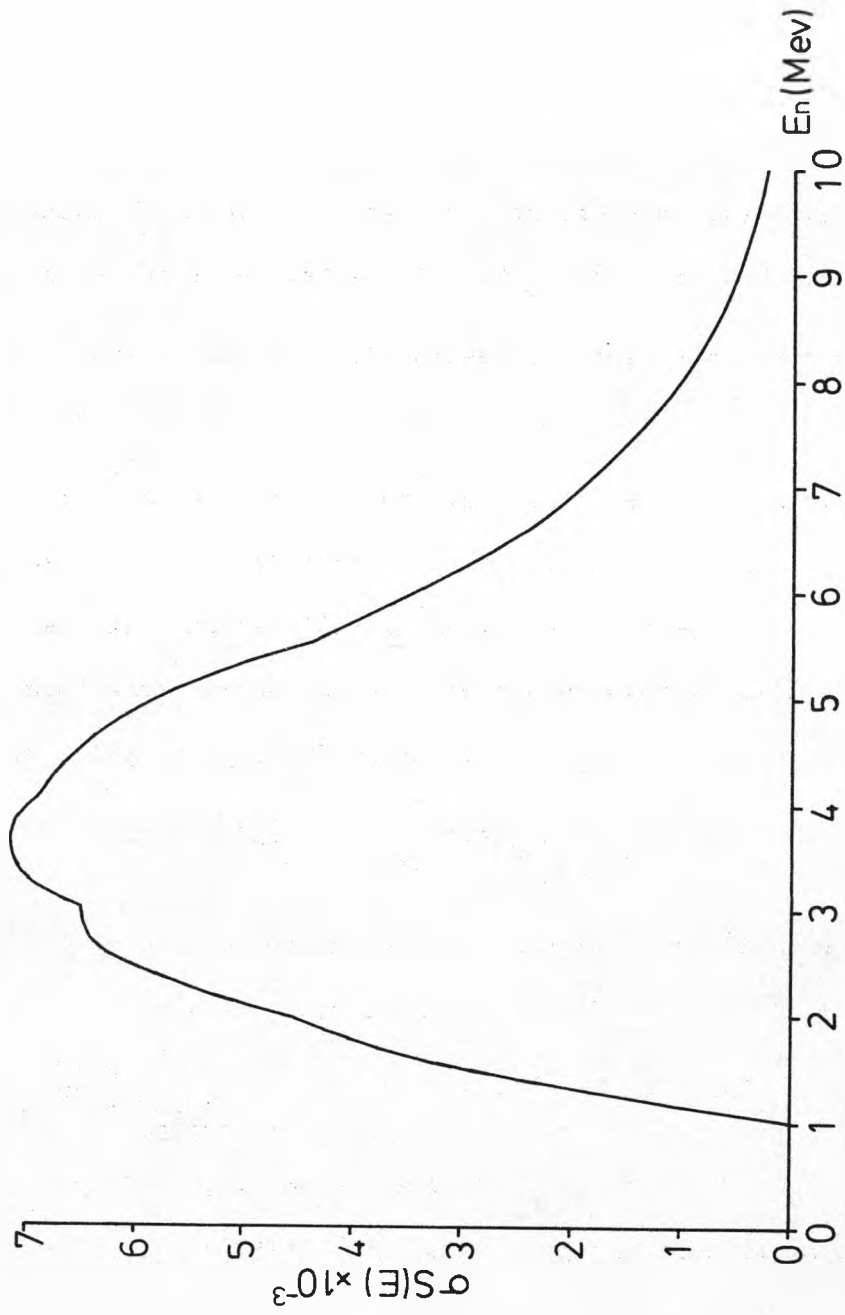


Fig. A3:7  $\sigma_S(E)$  v.  $E_n$  curve for the  $^{43}\text{Ca}(n,\alpha)^{40}\text{Ar}$  interaction.



not expected to be important.

The calculated maximum recoil energies for the calcium interactions are very much greater than the one reported for  $^{39}\text{K}(n,p)^{39}\text{Ar}$ . This would suggest that recoil loss/re-distribution effects are potentially more important for calcium-derived argon isotopes than they are for  $^{39}\text{K}$ . However, the generally accepted view is that in  $^{40}\text{Ar}$ - $^{39}\text{Ar}$  dating, recoil effects are only important for  $^{39}\text{K}$  (see Section 4:3:2). This can, perhaps, be explained by the observation that calcium phases in basic rocks (for which the majority of recoil effects have been reported) tend to be of a much greater size than the potassium phases. Thus, even though the calcium-derived argon isotopes may recoil with greater energies than  $^{39}\text{K}$ , proportionately fewer might be expected to be subject to a relocation. In addition, it is important to remember that this calcium-derived argon only results in an age correction which is often quite small. Thus, in many cases, recoil relocation of these isotopes could only result in relatively small disturbances in sample age patterns.

#### Theoretical values for interference reaction correction terms

This section is concerned with the discrepancies between theoretical and measured interference reaction correction terms (for the latter, see Section 5:4:2). Ignoring  $^{40/39}\text{K}$ , for which the theoretical value was only approximately calculated, there are several possible causes of the discrepancies.

For the theoretical values:

- i) All the calculations assume that only fast neutrons are responsible for interaction activation. There may be a significant contribution from thermal neutron interactions in some cases.
- ii) The neutron energy spectrum experienced by samples in a reactor may not be adequately modelled by the fission neutron energy spectrum.

iii) There may be argon isotopic contributions from other interactions not considered here.

For the measured values:

iv) Argon isotope recoil loss effects may be important.

It is not possible to evaluate points (ii) and (iii) with the information available.

The possibility of interaction activation by thermal neutrons may go some way towards explaining the discrepancies in the calcium terms. However, for  $[38/39]_K$ , a contribution from thermal neutrons would only make the observed discrepancy greater as such interactions are only feasible for  $^{39}K(n,p)^{39}Ar$  ( $^{39}K(n,np)^{38}Ar$  has an interaction threshold energy of 6.6 MeV).

Recoil loss effects for a potassium salt irradiated in this study are observed to be insignificant (see Section 5:4:2). However, they may be important for calcium-derived argon, specifically in terms of  $[36/37]_{Ca}$ . The calculated maximum recoil energy for  $^{36}Ca$  is twice that for  $^{37}Ca$ . Thus, it might be reasonable to expect that measured values of  $[36/37]_{Ca}$  will be too low where any recoil loss is not compensated for. This is consistent with the comparison of theoretical and measured values of  $[36/37]_{Ca}$ . Although recoil loss of  $^{37}Ca$ ,  $^{39}Ca$  and  $^{40}Ca$  is likely to be important, it is not thought that this would affect measured values of the interference reaction correction terms because similar maximum recoil energies are involved in each interaction.

It is possible that a  $^{36}Ca$  recoil loss effect (see above) might offer an explanation for age spectra which display a high temperature age increase corresponding to rising  $37/39_K$  levels e.g. Jessberger et al., (1975). No reasonable explanation for this type of age pattern has been offered.

APPENDIX 4

The importance of the interference corrections and the possible effects  
of errors in, or variations from, the adopted values

As stated in Section 2:2:2, in most cases the correction for chlorine-derived interference is negligible. Therefore, I will consider only the simplified age expression (see Section 2:2):

$$t = 1804.1 \times \text{Log}_e \left( 1 + J \cdot \frac{40^*}{39_K} \right)$$

$$\text{where } \frac{40^*}{39_K} = \frac{40_{\text{total}} - \left( \frac{40}{36} \right)_{\text{atm}} \cdot 36_{\text{total}} - \left[ \frac{40 - (40/36)_{\text{atm}} 36}{37} \right]_{\text{Ca}} \cdot 37_{\text{total}}}{39_{\text{total}} - \left[ \frac{39}{37} \right]_{\text{Ca}} \cdot 37_{\text{total}}} - \left[ \frac{40}{39} \right]_K$$

The interference reaction correction terms to be studied are:

$$\left[ \frac{40}{39} \right]_K, \left[ \frac{40 - (40/36)_{\text{atm}} 36}{37} \right]_{\text{Ca}} \text{ and } \left[ \frac{39}{37} \right]_{\text{Ca}}$$

$$\text{The first term: } \left[ \frac{40}{39} \right]_K = 0.015$$

Assuming a practical J-value, this correction term is going to be important only for very young samples. The age correction due to this term will then be:

$$\begin{aligned} \delta t &\approx 1804.1 J \left[ \frac{40}{39} \right]_K \text{ Ma} \\ &= 0.05 \text{ Ma for } J = 0.002 \end{aligned}$$

In this  $^{40}\text{Ar}$ - $^{39}\text{Ar}$  dating study (ages  $\approx 60$  Ma) the  $\left[ \frac{40}{39} \right]_K$  correction term, plus any error in its adopted value, will be insignificant.

For the rest of the discussion, the  $\left[ \frac{40}{39} \right]_K$  will be ignored.

$$\text{The second term: } \left[ \frac{40 - (40/36)_{\text{atm}} 36}{37} \right]_{\text{Ca}} = -0.074$$

Fig. A4:1 displays the importance of this correction term for a 60 Ma old rock with a range of typical J-values and  $37/39_K$  values.

For an uncertainty of  $\delta \left( \left[ \frac{40 - (40/36)_{\text{atm}} 36}{37} \right]_{\text{Ca}} \right)$ :

$$\delta t = 1804.1 \frac{J}{e^{t/1804.1}} \cdot \frac{37}{39_K} \cdot \delta \left( \left[ \frac{40 - (40/36)_{\text{atm}} 36}{37} \right]_{\text{Ca}} \right)$$

Taking typical parameters for this study:

$$t = 60 \text{ Ma}, J = 0.002, 37/39_K = 200 \text{ (maximum value)}$$

then for  $\delta t < 0.5$  Ma (i.e. for an age discrepancy of  $< 1\%$ )

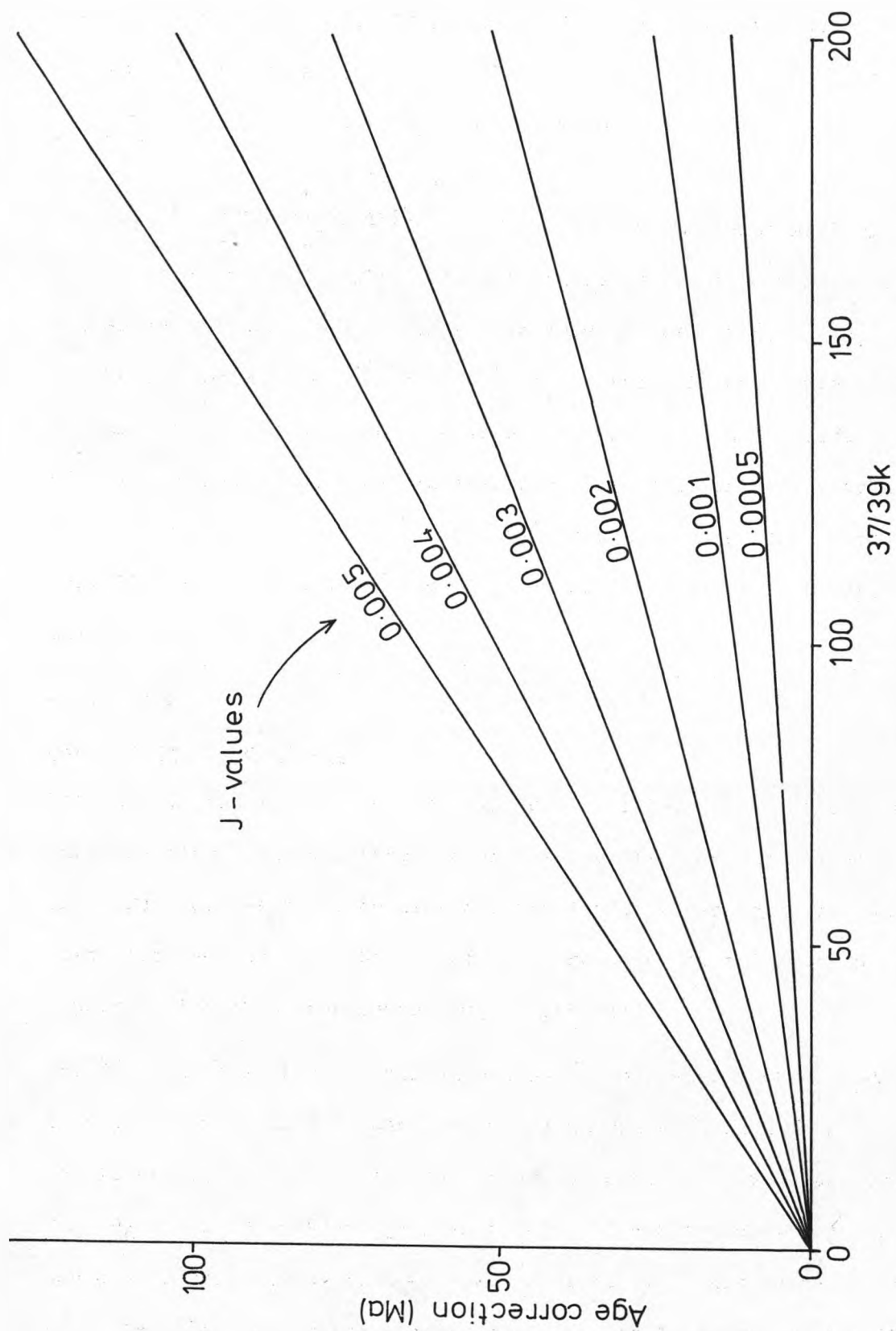


Fig. A4:1 The importance of the interference reaction correction term  $\left[ \frac{40-(40/36)atm36}{37} \right] Ca$

$$\delta\left(\left[\frac{40-(40/36)\text{atm}36}{37}\right]_{\text{Ca}}\right) < 7.2 \times 10^{-4} \approx 1\%$$

The values presented in Table 5:8 indicate that the error (or real variation) in  $\left[\frac{40-(40/36)\text{atm}36}{37}\right]_{\text{Ca}}$  may be very much greater than 1%. Thus, age discrepancies could well be important for steps with high  $37/39_{\text{K}}$  values. Age variations due to the adoption of an inaccurate  $\left[\frac{40-(40/36)\text{atm}36}{37}\right]_{\text{Ca}}$  value can be checked using ICD3-Plot 3 (see Section 3:4).

The third term:  $\left[\frac{39}{37}\right]_{\text{Ca}} = 6.65 \times 10^{-4}$

Dividing each term in the expression for  $40^*/39_{\text{K}}$  by  $39_{\text{total}}$  and rearranging:

$$\frac{40^*}{39_{\text{K}}} = \left\{ 1 + \underbrace{\left[\frac{39}{37}\right]_{\text{Ca}} \frac{37}{39_{\text{K}}}}_{\text{fractional increase in } \frac{40^*}{39_{\text{K}}} \text{ due to } \left[\frac{39}{37}\right]_{\text{Ca}} \text{ correction}} \left\{ \left(\frac{40}{39}\right)_{\text{total}} - \left(\frac{40}{36}\right)_{\text{atm}} \left(\frac{36}{39}\right)_{\text{total}} - \left[\frac{40-(\frac{40}{36})\text{atm}36}{37}\right]_{\text{Ca}} \left(\frac{37}{39}\right)_{\text{total}} \right\} \right\}$$

For  $37/39_{\text{K}} = 200$ , the increase in  $40^*/39_{\text{K}}$  due to the correction for calcium-derived 39 equals 13.3%. This implies an age correction of + 6.9 Ma for a 60 Ma old sample (regardless of J-value) which is in the same sense as the age correction involved by the second term.

For uncertainty in  $\left[\frac{39}{37}\right]_{\text{Ca}}$  :

$$\delta t = 1804.1 \frac{e^{t/1804.1} - 1}{e^{t/1804.1}} \frac{37}{39_{\text{K}}} \delta\left(\left[\frac{39}{37}\right]_{\text{Ca}}\right)$$

setting  $t = 60 \text{ Ma}$ ,  $37/39_{\text{K}} = 200$ , for  $\delta t < 0.5 \text{ Ma}$ ,

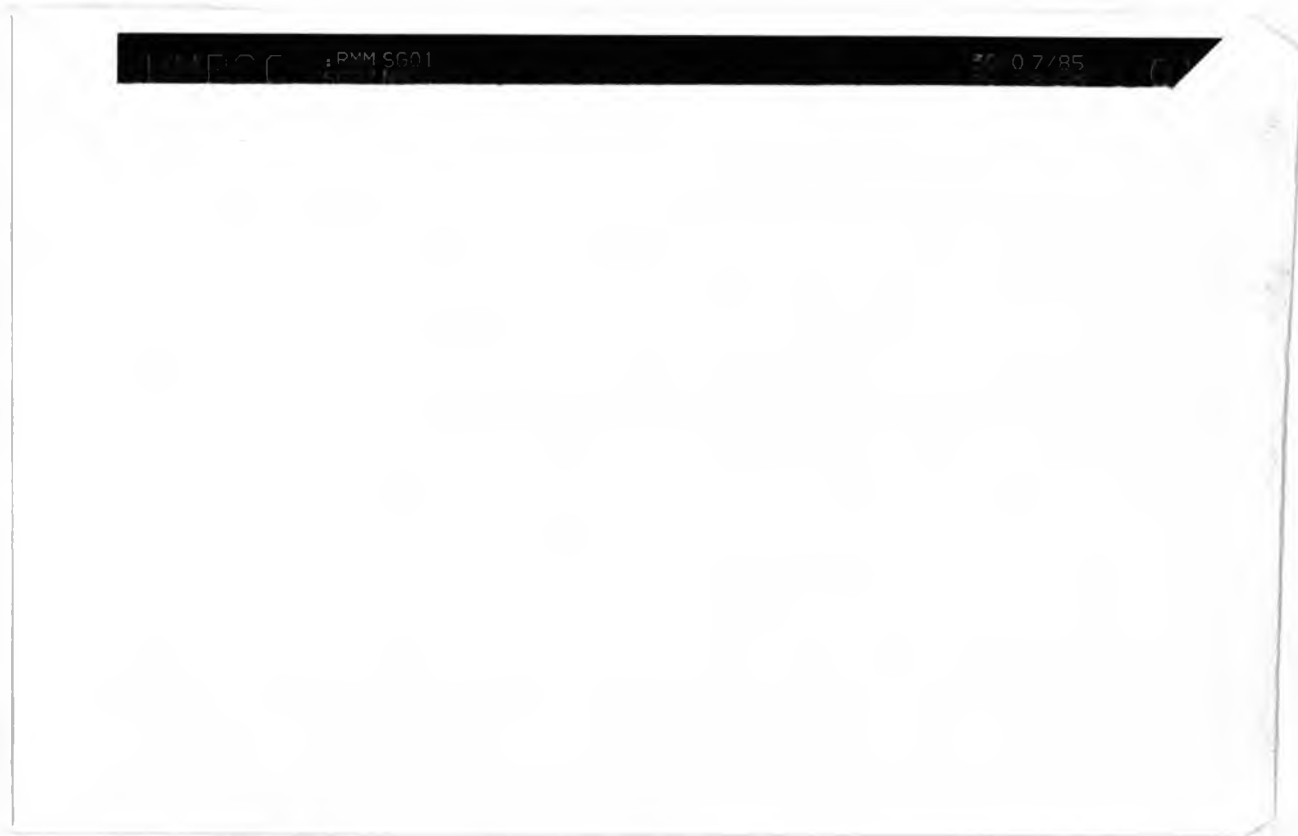
then  $\delta\left(\left[\frac{39}{37}\right]_{\text{Ca}}\right) < 0.4 \times 10^{-4} \approx 6.4\%$ .

The  $\left[\frac{39}{37}\right]_{\text{Ca}}$  values presented in Table 5:8 show a variation of about this order. Error (or variation) in the adopted value of  $\left[\frac{39}{37}\right]_{\text{Ca}}$  is not therefore expected to cause significant age discrepancies.

APPENDIX 5

Computer Program Listings and Example Outputs

Listings of the programs described in Section 5:7 are on the microfiche card contained in this pocket:



Examples of these program's data table outputs (where applicable)

are given in the following tables:

Table A5:1 "STEPAGE" data table output

Table A5:2 "JCURVE" data table output

Table A5:3 "FITPLANE" data table output

Table A5:4 "ARRENHUS" data table output



ARGON DATING PROGRAM

SAMPLE R1574 R028

DATE 30/ 7/1985

INPUT DATA  
\*\*\*\*\*

J = 0.002308 ERROR 0.000019

STEP	DATE	TEMP	T	D	ED	SCANS	DIV	ARGON 40	ARGON 39	ARGON 38	ARGON 37	ARGON 36
1	13/2/84	5.5	162.0	302.0	2.0	3	11.18	16447.33	71.97	12.23	0.62	50.16
2	13/2/84	5.5	162.0	302.0	2.0	3	1.00	10425.00	36.29	6.76	0.20	32.15
3	14/2/84	6.0	163.0	302.0	2.0	3	11.25	11358.33	384.88	8.10	1.94	16.92
4	14/2/84	6.0	163.0	302.0	2.0	3	3.40	19685.00	883.20	14.20	4.73	19.20
5	15/2/84	6.0	164.0	302.0	2.0	3	11.22	7510.33	390.28	5.49	2.73	5.20
6	15/2/84	6.0	164.0	302.0	2.0	3	3.37	14859.33	872.03	10.92	7.07	5.39
7	16/2/84	6.0	165.0	302.0	2.0	3	3.33	8517.33	526.14	6.40	4.27	2.26
8	16/2/84	6.0	165.0	302.0	2.0	3	3.36	7547.33	461.00	5.51	4.10	2.08
9	17/2/84	6.5	166.0	302.0	2.0	3	3.35	11968.33	714.47	9.06	4.10	4.09
10	17/2/84	6.5	166.0	302.0	2.0	3	3.39	9613.33	574.36	7.30	5.69	3.59
11	21/2/84	7.0	170.0	304.0	2.0	3	3.34	13501.00	828.90	10.30	6.32	3.20
12	21/2/84	7.0	170.0	304.0	2.0	3	3.37	8206.66	519.89	6.39	1.97	1.70
13	22/2/84	7.5	171.0	304.0	2.0	3	3.35	13255.33	796.97	10.37	2.05	4.13
14	22/2/84	7.5	171.0	304.0	2.0	3	1.00	20682.33	1168.93	16.18	1.37	10.35
15	23/2/84	8.0	172.0	304.0	2.0	3	3.38	7181.00	382.31	5.60	0.44	4.80
16	23/2/84	8.0	172.0	304.0	2.0	3	1.00	21254.66	1078.17	16.42	1.06	16.44
17	24/2/84	8.5	173.0	305.0	2.0	3	3.36	9688.00	455.42	7.39	0.39	9.50
18	24/2/84	9.0	173.0	305.0	2.0	3	3.37	22542.00	1006.50	17.29	0.69	23.96
19	27/2/84	9.5	176.0	306.0	2.0	3	11.48	9044.66	407.46	6.97	0.30	9.52
20	27/2/84	10.0	176.0	306.0	2.0	3	11.53	9856.00	468.24	7.61	0.28	9.03
21	28/2/84	10.5	177.0	306.0	2.0	3	11.43	8511.66	430.67	6.87	0.31	6.60
22	28/2/84	11.0	177.0	306.0	2.0	3	3.39	21616.00	1133.37	17.98	0.99	14.86
23	29/2/84	11.5	178.0	307.0	2.0	3	3.40	15101.00	784.43	12.71	0.70	9.82
24	29/2/84	12.0	178.0	307.0	2.0	3	3.38	13909.00	702.80	11.99	0.79	10.12
25	1/3/84	13.0	179.0	308.0	2.0	3	11.61	10011.00	413.30	8.37	0.48	11.82
26	1/3/84	14.0	179.0	308.0	2.0	3	3.44	23478.64	697.27	19.00	1.14	40.92
27	2/3/84	15.0	180.0	308.0	2.0	3	3.37	8270.33	332.73	8.52	0.74	9.94
28	2/3/84	16.0	180.0	308.0	2.0	3	1.00	13559.33	656.05	22.74	1.78	10.90
29	5/3/84	18.0	183.0	309.0	2.0	3	1.00	12239.00	595.72	29.36	1.39	9.84
30	5/3/84	22.0	183.0	309.0	2.0	1	1.00	6657.00	219.90	16.70	0.35	10.48

Table A5:1

"STEPAGE" data table output (TEMP - measurement of RF current used in step heating, T = number of days since irradiation, D = measured or interpolated (40/36)atmospheric, ED = error in D, DIV = gas sample division factor for total gas calculations. Errors for the argon isotope measurements are of the order of 0.5% for values >100 and 1% for values <100)

ARGON ISOTOPE RATIOS (CORRECTED FOR DISCRIMINATION AND DECAY)  
 \*\*\*\*\*

STEP	40/39	ERROR	38/39	ERROR	37/39	ERROR	36/39	ERROR
1	0.2270E+03	0.110E+01	0.1707E+00	0.104E-02	0.2136E+00	0.174E-01	0.7077E+00	0.501E-02
2	0.2854E+03	0.151E+01	0.1871E+00	0.161E-02	0.1374E+00	0.344E-01	0.8995E+00	0.712E-02
3	0.2932E+02	0.114E+00	0.2114E-01	0.144E-03	0.1283E+00	0.335E-02	0.4463E-01	0.275E-03
4	0.2214E+02	0.903E-01	0.1614E-01	0.833E-04	0.1366E+00	0.158E-02	0.2207E-01	0.143E-03
5	0.1912E+02	0.937E-01	0.1413E-01	0.135E-03	0.1620E+00	0.341E-02	0.1352E-01	0.149E-03
6	0.1693E+02	0.732E-01	0.1258E-01	0.750E-04	0.2108E+00	0.180E-02	0.6272E-02	0.692E-04
7	0.1608E+02	0.684E-01	0.1221E-01	0.997E-04	0.2149E+00	0.264E-02	0.4353E-02	0.991E-04
8	0.1626E+02	0.769E-01	0.1201E-01	0.113E-03	0.2359E+00	0.301E-02	0.4587E-02	0.113E-03
9	0.1664E+02	0.860E-01	0.1273E-01	0.908E-04	0.2756E+00	0.239E-02	0.5812E-02	0.803E-04
10	0.1663E+02	0.643E-01	0.1276E-01	0.921E-04	0.2678E+00	0.255E-02	0.6353E-02	0.942E-04
11	0.1615E+02	0.736E-01	0.1250E-01	0.784E-04	0.2240E+00	0.208E-02	0.3935E-02	0.660E-04
12	0.1566E+02	0.684E-01	0.1236E-01	0.101E-03	0.1113E+00	0.285E-02	0.3329E-02	0.996E-04
13	0.1649E+02	0.774E-01	0.1309E-01	0.829E-04	0.771E-01	0.192E-02	0.5285E-02	0.717E-04
14	0.1755E+02	0.593E-01	0.1393E-01	0.604E-04	0.3517E-01	0.129E-02	0.9031E-02	0.659E-04
15	0.1863E+02	0.945E-01	0.1474E-01	0.138E-03	0.3516E-01	0.400E-02	0.1281E-01	0.150E-03
16	0.1955E+02	0.691E-01	0.1532E-01	0.680E-04	0.3004E-01	0.142E-02	0.1556E-01	0.988E-04
17	0.2108E+02	0.849E-01	0.1634E-01	0.118E-03	0.2686E-01	0.343E-02	0.2134E-01	0.158E-03
18	0.2219E+02	0.812E-01	0.1729E-01	0.771E-04	0.2139E-01	0.155E-02	0.2434E-01	0.147E-03
19	0.2198E+02	0.948E-01	0.1723E-01	0.132E-03	0.2434E-01	0.407E-02	0.2396E-01	0.178E-03
20	0.2084E+02	0.825E-01	0.1637E-01	0.115E-03	0.1998E-01	0.354E-02	0.1978E-01	0.150E-03
21	0.1957E+02	0.864E-01	0.1607E-01	0.124E-03	0.2412E-01	0.393E-02	0.1572E-01	0.145E-03
22	0.1888E+02	0.644E-01	0.1599E-01	0.666E-04	0.2960E-01	0.150E-02	0.1344E-01	0.862E-04
23	0.1904E+02	0.878E-01	0.1634E-01	0.934E-04	0.3078E-01	0.221E-02	0.1279E-01	0.102E-03
24	0.1958E+02	0.990E-01	0.1721E-01	0.106E-03	0.3863E-01	0.247E-02	0.1479E-01	0.119E-03
25	0.2394E+02	0.970E-01	0.2044E-01	0.134E-03	0.4090E-01	0.428E-02	0.2945E-01	0.198E-03
26	0.3328E+02	0.159E+00	0.2750E-01	0.146E-03	0.5758E-01	0.255E-02	0.6046E-01	0.445E-03
27	0.2457E+02	0.118E+00	0.2583E-01	0.172E-03	0.8052E-01	0.542E-02	0.3078E-01	0.228E-03
28	0.2043E+02	0.629E-01	0.3499E-01	0.107E-03	0.9776E-01	0.277E-02	0.1712E-01	0.115E-03
29	0.2029E+02	0.672E-01	0.4977E-01	0.277E-03	0.8932E-01	0.323E-02	0.1706E-01	0.121E-03
30	0.2990E+02	0.754E-01	0.7670E-01	0.281E-03	0.6095E-01	0.871E-02	0.4922E-01	0.336E-03

ARGON DATING PROGRAM

SAMPLE R1574 R028

DATE 30/ 7/1985

STEP AGE TABLE  
\*\*\*\*\*

STEP	AGE	ERR	RERR	%40RAD	%39K	CACOR	KCOR	CLCOR	37/39K	ERROR
1	73.17	5.33	5.30	7.9	1.1	0.11	0.00	0.05	0.214E+00	0.17E-01
2	79.64	8.13	8.10	6.9	0.1	0.01	0.00	-0.03	0.137E+00	0.34E-01
3	65.92	0.73	0.50	55.0	6.0	0.04	0.00	0.00	0.128E+00	0.34E-02
4	63.87	0.61	0.33	70.5	4.1	0.04	0.00	0.00	0.137E+00	0.16E-02
5	61.90	0.64	0.40	79.1	6.0	0.06	0.00	0.00	0.182E+00	0.34E-02
6	61.71	0.57	0.28	89.1	4.1	0.07	0.00	0.00	0.211E+00	0.18E-02
7	60.59	0.57	0.30	92.0	2.4	0.07	0.00	0.00	0.215E+00	0.26E-02
8	61.05	0.60	0.33	91.7	2.1	0.08	0.00	0.00	0.236E+00	0.30E-02
9	61.13	0.60	0.34	89.7	3.3	0.10	0.00	0.00	0.276E+00	0.24E-02
10	60.42	0.56	0.28	88.7	2.7	0.09	0.00	0.00	0.268E+00	0.25E-02
11	61.38	0.58	0.29	92.8	3.8	0.08	0.00	0.01	0.224E+00	0.21E-02
12	60.05	0.57	0.30	93.7	2.4	0.04	0.00	0.00	0.111E+00	0.29E-02
13	61.10	0.58	0.30	90.5	3.7	0.03	0.00	0.00	0.771E-01	0.19E-02
14	60.86	0.54	0.23	84.7	1.6	0.01	0.00	0.00	0.352E-01	0.13E-02
15	60.72	0.64	0.41	79.6	1.8	0.01	0.00	0.00	0.352E-01	0.40E-02
16	61.16	0.56	0.26	76.4	1.5	0.01	0.00	0.00	0.300E-01	0.14E-02
17	60.44	0.61	0.37	70.0	2.1	0.01	0.00	0.00	0.269E-01	0.34E-02
18	61.35	0.58	0.30	67.5	4.7	0.01	0.00	0.00	0.214E-01	0.16E-02
19	60.94	0.64	0.41	67.7	6.5	0.01	0.00	0.00	0.243E-01	0.41E-02
20	61.33	0.61	0.36	71.9	7.4	0.01	0.00	0.00	0.200E-01	0.35E-02
21	61.04	0.62	0.37	76.2	6.8	0.01	0.00	0.00	0.241E-01	0.39E-02
22	60.99	0.55	0.25	78.9	5.3	0.01	0.00	0.00	0.296E-01	0.15E-02
23	62.32	0.60	0.33	80.0	3.7	0.01	0.00	0.00	0.308E-01	0.22E-02
24	62.18	0.62	0.36	77.6	3.3	0.01	0.00	0.00	0.386E-01	0.25E-02
25	62.32	0.66	0.42	63.6	6.6	0.02	0.00	0.00	0.409E-01	0.43E-02
26	63.04	0.77	0.58	46.3	3.3	0.02	0.00	0.00	0.576E-01	0.26E-02
27	63.27	0.71	0.50	62.9	1.5	0.03	0.00	0.00	0.805E-01	0.54E-02
28	62.87	0.58	0.28	75.2	0.9	0.04	0.00	0.01	0.978E-01	0.28E-02
29	62.39	0.58	0.29	75.1	0.8	0.03	0.00	0.02	0.893E-01	0.32E-02
30	62.81	0.70	0.48	51.3	0.3	0.02	0.00	0.03	0.609E-01	0.87E-02

TOTAL GAS CALCULATIONS  
\*\*\*\*\*

AGE = 62.0 ERROR 0.5  
%40 RADIOGENIC = 65.7  
37/39K = 0.955031E-01 ERROR 0.710614E-03

Table A5:1 continued (RERR = step age error ignoring systematic J-value error, %40RAD = %<sup>40</sup>Ar\*. CACOR, KCOR and CLCOR are the interference reaction age corrections associated with calcium, potassium and chorine respectively).

ARGON DATING PROGRAM

SAMPLE R1574 R028

DATE 30/ 7/1985

STEPS SELECTED FOR FURTHER ANALYSIS  
 \*\*\*\*\*

1	2	3	4	5	6	7	8	9	10	11	12	13	14	15	16	17	18	19	20
21	22	23	24	25	26	27	28	29	30										

PERCENTAGE OF AR39K = 100.0

WEIGHTED MEAN AGES  
 \*\*\*\*\*

STEP AGES WEIGHTED BY 1/VARIANCE 61.5 ERROR 1.2  
 STEP AGES WEIGHTED BY %39K 61.9 ERROR 1.9  
 TOTAL GAS 62.0 ERROR 0.5

ISOCHRON PLOT: 39/36 VS 40/36  
 \*\*\*\*\*  
 WOLBERG

AGE = 61.4 ERROR 0.6  
 (40/36) INIT = 301.7 ERROR 1.7  
 CORRELATION = 1.00  
 MSWD = 1.44

ISOCHRON PLOT: 36/40 VS 39/40  
 \*\*\*\*\*  
 WOLBERG

AGE = 60.9 ERROR 0.6  
 (40/36) INIT = 306.2 ERROR 4.2  
 CORRELATION = -1.00  
 MSWD = 9.04

ARGON DATING PROGRAM

SAMPLE R1574 R028

DATE 30/ 7/1985

ISOCHRON PLOT: 36/40 VS 39/40  
 \*\*\*\*\*

3D DERIVED  
 WOLBERG

AGE = 60.9 ERROR 0.6  
 (40/36)INIT = 306.2 ERROR 4.2  
 CORRELATION = -1.00  
 MSWD = 9.04

TABLE OF RESIDUALS  
 \*\*\*\*\*

STEP	39/40	ERR	RES	SIG	36/40	ERR	RES	SIG	TOTAL RES	ERR(DTR)	SIG
1	0.44038E-02	0.213E-04	0.381E-05	0	0.31170E-02	0.194E-04	0.652E-04	2	0.653E-04	0.195E-04	2
2	0.35047E-02	0.186E-04	0.169E-05	0	0.31521E-02	0.237E-04	0.567E-04	2	0.57E-04	0.237E-04	2
3	0.34113E-01	0.133E-03	-0.522E-03	2	0.15226E-02	0.991E-05	-0.595E-04	2	0.525E-04	0.732E-04	2
4	0.45169E-01	0.184E-03	-0.104E-02	2	0.99718E-03	0.596E-05	-0.224E-04	2	0.104E-02	0.153E-03	2
5	0.52307E-01	0.257E-03	-0.227E-03	0	0.70720E-03	0.822E-05	-0.480E-05	0	0.227E-03	0.214E-03	1
6	0.59064E-01	0.255E-03	-0.449E-03	1	0.37049E-03	0.401E-05	-0.227E-05	0	0.449E-03	0.243E-03	1
7	0.62170E-01	0.265E-03	0.450E-03	1	0.27067E-03	0.623E-05	0.514E-05	0	0.450E-03	0.238E-03	1
8	0.61467E-01	0.291E-03	0.697E-04	0	0.28202E-03	0.701E-05	0.834E-06	0	0.697E-04	0.261E-03	0
9	0.60062E-01	0.310E-03	0.568E-04	0	0.34913E-03	0.472E-05	0.270E-06	0	0.568E-04	0.296E-03	0
10	0.60114E-01	0.233E-03	0.626E-03	2	0.38196E-03	0.579E-05	0.799E-05	1	0.626E-03	0.207E-03	2
11	0.61891E-01	0.282E-03	-0.258E-03	0	0.24354E-03	0.404E-05	-0.109E-05	0	0.258E-03	0.271E-03	0
12	0.63900E-01	0.279E-03	0.895E-03	2	0.21272E-03	0.641E-05	0.969E-05	1	0.895E-03	0.252E-03	2
13	0.60656E-01	0.285E-03	0.626E-04	0	0.32054E-03	0.428E-05	0.290E-06	0	0.626E-04	0.272E-03	0
14	0.57028E-01	0.193E-03	0.382E-03	1	0.51503E-03	0.370E-05	0.289E-05	0	0.382E-03	0.180E-03	2
15	0.53718E-01	0.273E-03	0.490E-03	1	0.68804E-03	0.849E-05	0.975E-05	1	0.490E-03	0.230E-03	2
16	0.51181E-01	0.181E-03	0.294E-03	1	0.79645E-03	0.487E-05	0.438E-05	0	0.294E-03	0.158E-03	2
17	0.47468E-01	0.191E-03	0.642E-03	2	0.10128E-02	0.805E-05	0.233E-04	2	0.642E-03	0.145E-03	2
18	0.45086E-01	0.165E-03	0.302E-03	1	0.10975E-02	0.620E-05	0.878E-05	1	0.302E-03	0.131E-03	2
19	0.45528E-01	0.196E-03	0.218E-03	1	0.10907E-02	0.874E-05	0.174E-04	1	0.428E-03	0.145E-03	2
20	0.48015E-01	0.190E-03	0.427E-03	2	0.94958E-03	0.768E-05	0.730E-05	0	0.218E-03	0.146E-03	1
21	0.51139E-01	0.226E-03	0.327E-03	1	0.80387E-03	0.785E-05	0.812E-05	1	0.327E-03	0.184E-03	1
22	0.52993E-01	0.181E-03	0.369E-03	2	0.71222E-03	0.444E-05	0.456E-05	1	0.369E-03	0.162E-03	2
23	0.52544E-01	0.243E-03	-0.616E-03	2	0.67618E-03	0.502E-05	-0.543E-05	0	0.616E-03	0.223E-03	2
24	0.51108E-01	0.259E-03	-0.434E-03	1	0.75608E-03	0.558E-05	-0.415E-05	0	0.434E-03	0.236E-03	1
25	0.41787E-01	0.169E-03	-0.353E-04	0	0.12307E-02	0.887E-05	-0.199E-05	0	0.354E-04	0.115E-03	0
26	0.30054E-01	0.144E-03	0.678E-04	0	0.18170E-02	0.115E-04	0.895E-05	0	0.684E-04	0.752E-04	0
27	0.40715E-01	0.196E-03	-0.327E-03	1	0.12531E-02	0.999E-05	-0.175E-04	1	0.328E-03	0.136E-03	2
28	0.48955E-01	0.151E-03	-0.585E-03	2	0.83812E-03	0.598E-05	-0.190E-04	2	0.585E-03	0.117E-03	2
29	0.49302E-01	0.163E-03	-0.362E-03	2	0.84038E-03	0.633E-05	-0.112E-04	1	0.362E-03	0.128E-03	2
30	0.33457E-01	0.845E-04	0.156E-04	0	0.16461E-02	0.116E-04	0.603E-05	0	0.168E-04	0.303E-04	0

Table A5:1 continued (SIG values have been explained in Fig. 3:4, ERR(DTR) = error in the direction of the total residual)

J VALUE CURVE FITTING AND INTERPOLATION  
 \*\*\*\*\*

IRRADIATION BATCH LIV41  
 \*\*\*\*\*

INPUT DATA  
 \*\*\*\*\*

STANDARD AGE = 17.20 ERROR = 0.10

STANDARD NO	POSITION	ERROR	J-VALUE	ERROR
1	0.0	2.0	0.002196	0.000021
2	30.0	2.0	0.002193	0.000021
3	60.0	2.0	0.002291	0.000021
4	82.0	2.0	0.002279	0.000020
5	110.0	2.0	0.002380	0.000024
6	144.0	2.0	0.002342	0.000012
7	180.0	2.0	0.002302	0.000014
8	222.0	2.0	0.002140	0.000020

FIT TYPE : QUADRATIC  
 \*\*\*\*\*

NUMBER OF ITERATIONS = 5  
 MSWD = 4.59

J VALUE CURVE INTERPOLATION  
 \*\*\*\*\*

SAMPLE NO	POSITION	J-VALUE	ERROR
R1571	15.0	0.002193	0.000030
R1572	38.0	0.002255	0.000022
R1573	49.0	0.002279	0.000020
R1574	66.0	0.002308	0.000019
R1575	73.0	0.002318	0.000019
R1576	89.0	0.002334	0.000020
R1577	110.0	0.002345	0.000020
R1578	128.0	0.002343	0.000019
R1579	144.0	0.002333	0.000018
R1580	162.0	0.002313	0.000017
R1581	180.0	0.002283	0.000019
R1582	203.0	0.002231	0.000027
R1583	222.0	0.002176	0.000037

Table A5:2 "JCURVE" data table output

PLANE FITTING PROGRAM

SAMPLE R1574

DATE 30/ 7/1985

3D FIT : CHECK [(40-136)/37]CA VALUE  
 \*\*\*\*\*

INPUT DATA  
 \*\*\*\*\*

J-VALUE = 0.002308 ERROR = 0.000019

STEP	39K/40(Y)	VAR	36/40(X1)	VAR	37CA/40(X2)	VAR
1	0.440415E-02	0.455491E-09	0.311717E-02	0.378307E-09	0.940738E-03	0.585817E-08
2	0.350420E-02	0.345548E-09	0.315222E-02	0.563496E-09	0.481590E-03	0.145490E-07
3	0.341238E-01	0.177361E-07	0.152309E-02	0.983219E-10	0.437812E-02	0.131514E-07
4	0.451898E-01	0.340133E-07	0.997634E-03	0.356040E-10	0.617182E-02	0.485231E-08
5	0.523444E-01	0.659877E-07	0.707701E-03	0.677269E-10	0.953031E-02	0.330562E-07
6	0.591184E-01	0.654213E-07	0.370828E-03	0.160759E-10	0.124663E-01	0.104957E-07
7	0.622313E-01	0.702423E-07	0.270942E-03	0.389316E-10	0.133736E-01	0.292201E-07
8	0.615329E-01	0.849067E-07	0.282319E-03	0.493127E-10	0.145202E-01	0.374902E-07
9	0.601356E-01	0.966981E-07	0.349554E-03	0.222902E-10	0.165767E-01	0.183927E-07
10	0.601860E-01	0.543089E-07	0.382413E-03	0.336327E-10	0.161197E-01	0.261191E-07
11	0.619548E-01	0.799248E-07	0.243794E-03	0.163885E-10	0.138778E-01	0.155532E-07
12	0.639335E-01	0.782363E-07	0.212835E-03	0.411507E-10	0.711494E-02	0.339486E-07
13	0.606772E-01	0.812811E-07	0.320649E-03	0.182982E-10	0.467912E-02	0.134021E-07
14	0.570367E-01	0.372616E-07	0.515105E-03	0.136822E-10	0.200595E-02	0.540075E-08
15	0.537250E-01	0.744110E-07	0.688140E-03	0.720330E-10	0.188887E-02	0.461818E-07
16	0.511873E-01	0.327449E-07	0.796538E-03	0.236950E-10	0.153782E-02	0.529464E-08
17	0.474728E-01	0.366163E-07	0.101289E-02	0.647688E-10	0.127531E-02	0.264975E-07
18	0.450894E-01	0.272499E-07	0.109759E-02	0.385026E-10	0.964260E-03	0.490096E-08
19	0.455315E-01	0.386064E-07	0.109082E-02	0.763374E-10	0.110841E-02	0.343849E-07
20	0.480181E-01	0.361963E-07	0.949648E-03	0.590554E-10	0.959366E-03	0.289547E-07
21	0.511433E-01	0.511099E-07	0.803942E-03	0.616221E-10	0.123362E-02	0.404056E-07
22	0.529987E-01	0.327732E-07	0.712304E-03	0.196951E-10	0.156860E-02	0.629615E-08
23	0.525502E-01	0.588478E-07	0.676256E-03	0.252281E-10	0.161728E-02	0.134529E-07
24	0.511150E-01	0.669293E-07	0.756194E-03	0.310991E-10	0.197460E-02	0.158734E-07
25	0.417922E-01	0.287010E-07	0.123087E-02	0.786825E-10	0.170953E-02	0.319515E-07
26	0.300574E-01	0.206491E-07	0.181726E-02	0.132443E-09	0.173063E-02	0.583864E-08
27	0.407249E-01	0.384667E-07	0.125344E-02	0.597887E-10	0.327921E-02	0.488890E-07
28	0.489823E-01	0.227472E-07	0.838412E-03	0.358849E-10	0.478884E-02	0.184947E-07
29	0.493177E-01	0.267149E-07	0.840655E-03	0.400591E-10	0.440547E-02	0.254884E-07
30	0.334625E-01	0.713501E-08	0.164636E-02	0.133901E-09	0.203946E-02	0.849459E-07

Table A5.3 "FITPLANE" data table output

PLANE FITTING PROGRAM

SAMPLE R1574

DATE 30/ 7/1985

STEPS FITTED  
\*\*\*\*\*

1 2 3 4 5 6 7 8 9 10 11 12 13 14 15 16 17 18 19 20 21 22 23 24 25 26 27 28 29 30

CALCULATED PARAMETERS  
\*\*\*\*\*

AGE = 60.7 ERROR = 0.6

INITIAL RATIO = 307.1 ERROR = 5.1

$[(40-136)/37]CA = 0.34527$  ERROR = 0.53148

MSWD = 9.11



PLANE FITTING PROGRAM

SAMPLE R1574

DATE 30/ 7/1985

TABLE OF RESIDUALS  
\*\*\*\*\*

STEP	39K/40(Y)	ERR	RES	SIG	36/40(X1)	ERR	RES	SIG	37CA/40(X2)	ERR	RES	SIG
1	0.44041E-02	0.213E-04	0.430E-05	0	0.31172E-02	0.195E-04	0.740E-04	2	0.94074E-03	0.765E-04	0.129E-05	0
2	0.35042E-02	0.186E-04	0.193E-05	0	0.31522E-02	0.237E-04	0.652E-04	2	0.48159E-03	0.121E-03	0.189E-05	0
3	0.34124E-01	0.133E-03	-0.495E-03	2	0.15231E-02	0.992E-05	-0.568E-04	2	0.43781E-02	0.115E-03	-0.854E-05	0
4	0.45190E-01	0.184E-03	-0.995E-03	2	0.99763E-03	0.597E-05	-0.216E-04	2	0.61718E-02	0.697E-04	-0.331E-05	0
5	0.52344E-01	0.257E-03	-0.147E-03	0	0.70770E-03	0.823E-05	-0.313E-05	0	0.95303E-02	0.182E-03	-0.172E-05	0
6	0.59118E-01	0.256E-03	-0.312E-03	1	0.37083E-03	0.401E-05	-0.159E-05	0	0.12466E-01	0.102E-03	-0.117E-05	0
7	0.62231E-01	0.265E-03	0.582E-03	2	0.27094E-03	0.624E-05	0.668E-05	1	0.13374E-01	0.171E-03	0.564E-05	0
8	0.61533E-01	0.291E-03	0.228E-03	0	0.28232E-03	0.702E-05	0.274E-05	0	0.14520E-01	0.194E-03	0.234E-05	0
9	0.60136E-01	0.311E-03	0.298E-03	0	0.34959E-03	0.472E-05	0.142E-05	0	0.16577E-01	0.136E-03	0.132E-05	0
10	0.60186E-01	0.233E-03	0.828E-03	2	0.38241E-03	0.580E-05	0.106E-04	1	0.16120E-01	0.162E-03	0.927E-05	0
11	0.61955E-01	0.283E-03	-0.975E-04	0	0.24379E-03	0.405E-05	-0.414E-06	0	0.13878E-01	0.125E-03	-0.442E-06	0
12	0.63933E-01	0.280E-03	0.876E-03	2	0.21284E-03	0.641E-05	0.954E-05	1	0.71149E-02	0.184E-03	0.885E-05	0
13	0.60677E-01	0.285E-03	-0.596E-05	0	0.32065E-03	0.428E-05	-0.278E-07	0	0.46791E-02	0.116E-03	-0.229E-07	0
14	0.57037E-01	0.193E-03	0.274E-03	1	0.51510E-03	0.370E-05	0.208E-05	0	0.20060E-02	0.735E-04	0.924E-06	0
15	0.53725E-01	0.273E-03	0.414E-03	1	0.68814E-03	0.849E-05	0.829E-05	0	0.18889E-02	0.215E-03	0.598E-05	0
16	0.51187E-01	0.181E-03	0.217E-03	1	0.79554E-03	0.487E-05	0.325E-05	0	0.15378E-02	0.728E-04	0.816E-06	0
17	0.47473E-01	0.191E-03	0.593E-03	2	0.1C 29E-02	0.805E-05	0.217E-04	2	0.12753E-02	0.163E-03	0.999E-05	0
18	0.45089E-01	0.165E-03	0.253E-03	1	0.10976E-02	0.621E-05	0.740E-05	1	0.96426E-03	0.700E-04	0.106E-05	0
19	0.45532E-01	0.196E-03	0.385E-03	1	0.10908E-02	0.874E-05	0.158E-04	1	0.11084E-02	0.185E-03	0.798E-05	0
20	0.48018E-01	0.190E-03	0.160E-03	0	0.94965E-03	0.768E-05	0.539E-05	0	0.95937E-03	0.170E-03	0.297E-05	0
21	0.51143E-01	0.226E-03	0.254E-03	1	0.80394E-03	0.785E-05	0.635E-05	0	0.12336E-02	0.201E-03	0.468E-05	0
22	0.52999E-01	0.181E-03	0.280E-03	1	0.71230E-03	0.444E-05	0.348E-05	0	0.15686E-02	0.793E-04	0.125E-05	0
23	0.52550E-01	0.243E-03	-0.711E-03	2	0.67626E-03	0.502E-05	-0.631E-05	1	0.16173E-02	0.116E-03	-0.378E-05	0
24	0.51115E-01	0.259E-03	0.512E-03	1	0.75619E-03	0.558E-05	-0.492E-05	0	0.19746E-02	0.126E-03	-0.282E-05	0
25	0.41792E-01	0.169E-03	-0.525E-04	0	0.12309E-02	0.887E-05	-0.298E-05	0	0.17095E-02	0.179E-03	-0.136E-05	0
26	0.30057E-01	0.144E-03	0.781E-04	0	0.18173E-02	0.115E-04	0.104E-04	0	0.17306E-02	0.764E-04	0.514E-06	0
27	0.40725E-01	0.196E-03	-0.321E-03	1	0.12534E-02	0.999E-05	-0.172E-04	1	0.32792E-02	0.221E-03	-0.949E-05	0
28	0.48982E-01	0.151E-03	-0.584E-03	2	0.83841E-03	0.599E-05	-0.190E-04	2	0.47888E-02	0.136E-03	-0.111E-04	0
29	0.49318E-01	0.163E-03	-0.368E-03	2	0.84066E-03	0.633E-05	-0.114E-04	1	0.44055E-02	0.160E-03	-0.818E-05	0
30	0.33462E-01	0.845E-04	0.184E-04	0	0.16464E-02	0.116E-04	0.715E-05	0	0.20395E-02	0.291E-03	0.510E-05	0

Table A5:3 continued (SIG values have been explained in Fig. 3:4)

PLANE FITTING PROGRAM

SAMPLE R1574

DATE 30/ 7/1985

DATA TABLE FOR GRAPHICAL PROJECTION  
\*\*\*\*\*

STEP	TOTAL RESIDUAL	ERROR IN DIRECTION OF TOTAL RESIDUAL	SIG	COORDINATES FOR GRAPHICAL PROJECTION PX	COORDINATES FOR GRAPHICAL PROJECTION PY
1	0.74130E-04	0.19458E-04	2	0.63083E-01	0.94091E-03
2	0.65235E-04	0.23741E-04	2	0.63994E-01	0.48165E-03
3	0.49782E-03	0.72958E-04	2	0.33241E-01	0.43794E-02
4	0.99548E-03	0.15326E-03	2	0.22121E-01	0.61736E-02
5	0.14746E-03	0.21411E-03	0	0.14882E-01	0.95329E-02
6	0.31215E-03	0.24328E-03	1	0.80316E-02	0.12470E-01
7	0.58237E-03	0.23824E-03	2	0.48964E-02	0.13377E-01
8	0.22790E-03	0.26074E-03	0	0.55679E-02	0.14524E-01
9	0.29790E-03	0.29664E-03	1	0.69190E-02	0.16581E-01
10	0.82768E-03	0.20717E-03	2	0.68808E-02	0.16124E-01
11	0.97498E-04	0.27104E-03	0	0.51595E-02	0.13882E-01
12	0.87643E-03	0.25267E-03	2	0.33389E-02	0.71168E-02
13	0.59628E-05	0.27226E-03	0	0.66533E-02	0.46804E-02
14	0.27388E-03	0.17943E-03	1	0.10361E-01	0.20065E-02
15	0.41369E-03	0.22936E-03	1	0.13680E-01	0.18893E-02
16	0.21669E-03	0.15810E-03	1	0.16228E-01	0.15382E-02
17	0.59349E-03	0.14441E-03	2	0.19955E-01	0.12756E-02
18	0.25296E-03	0.13032E-03	1	0.22347E-01	0.96450E-03
19	0.38528E-03	0.14468E-03	2	0.21902E-01	0.11087E-02
20	0.15979E-03	0.14603E-03	1	0.19415E-01	0.95961E-03
21	0.25458E-03	0.18360E-03	1	0.16280E-01	0.12339E-02
22	0.27982E-03	0.16144E-03	1	0.14414E-01	0.15690E-02
23	0.71111E-03	0.22296E-03	2	0.14859E-01	0.16178E-02
24	0.51163E-03	0.23625E-03	2	0.16288E-01	0.19752E-02
25	0.52583E-04	0.11507E-03	0	0.25629E-01	0.17100E-02
26	0.78807E-04	0.74860E-04	1	0.37378E-01	0.17311E-02
27	0.32132E-03	0.13518E-03	2	0.26660E-01	0.32801E-02
28	0.58416E-03	0.11658E-03	2	0.18357E-01	0.47902E-02
29	0.36871E-03	0.12759E-03	2	0.18031E-01	0.44067E-02
30	0.20403E-04	0.31110E-04	0	0.33962E-01	0.20400E-02

ANGLE BETWEEN PX AND PY AXES = 91.33

Table A5:3 continued

ARRHENIUS PLOT PROGRAM

INPUT DATA  
\*\*\*\*\*

VOLUMIC ISOTOPE = 39K

SAMPLE R1574

DATE 30/ 7/1985

STEP	TEMPERATURE(C)	ERROR	FRACTION OF ISOTOPE REMAINING
10	650.0	10.0	0.681
11	700.0	10.0	0.643
12	700.0	10.0	0.618
13	750.0	10.0	0.582
14	760.0	10.0	0.565
15	810.0	10.0	0.548
16	810.0	10.0	0.533
17	830.0	10.0	0.512
18	850.0	10.0	0.465
19	880.0	10.0	0.400
20	910.0	10.0	0.326
21	940.0	10.0	0.258
22	960.0	10.0	0.205
23	980.0	10.0	0.168
24	1000.0	10.0	0.135
25	1040.0	10.0	0.069
26	1070.0	10.0	0.036
27	1100.0	10.0	0.020
28	1130.0	10.0	0.011
29	1140.0	10.0	0.003

Table A5:4 "ARRHENIUS" data table output

ARRHENIUS PLOT PROGRAM

SAMPLE R1574

DATE 30/ 7/1985

ARRHENIUS PLOT DATA TABLE  
 \*\*\*\*\*

SYMMETRY IS SPHERICAL

STEP	TOR(I)	LN[TOR(I)-TOR(I-1)]	1/TEMPERATURE(K)	ERROR
10	0.107642E-01	-4.53153	0.108319E-02	0.117330E-04
11	0.138597E-01	-5.77779	0.102754E-02	0.105583E-04
12	0.161697E-01	-6.07051	0.102754E-02	0.105583E-04
13	0.199115E-01	-5.8820	0.977326E-03	0.955166E-05
14	0.218641E-01	-6.23859	0.967867E-03	0.936766E-05
15	0.239385E-01	-6.17806	0.923190E-03	0.852281E-05
16	0.258823E-01	-6.24314	0.923190E-03	0.852281E-05
17	0.287802E-01	-5.84375	0.906454E-03	0.821659E-05
18	0.361113E-01	-4.91564	0.890313E-03	0.792658E-05
19	0.484932E-01	-4.39151	0.867152E-03	0.751953E-05
20	0.666478E-01	-4.00883	0.845165E-03	0.714305E-05
21	0.886639E-01	-3.81598	0.824266E-03	0.679415E-05
22	0.111079E+00	-3.79801	0.810898E-03	0.657556E-05
23	0.130832E+00	-3.92447	0.797957E-03	0.636736E-05
24	0.152740E+00	-3.82090	0.785423E-03	0.616888E-05
25	0.220506E+00	-2.69168	0.761498E-03	0.579880E-05
26	0.286393E+00	-2.71982	0.744491E-03	0.554266E-05
27	0.345944E+00	-2.82092	0.728226E-03	0.530313E-05
28	0.406517E+00	-2.80391	0.712657E-03	0.507879E-05
29	0.538162E+00	-2.02765	0.707614E-03	0.500717E-05

Table A5:4 continued (only the first three figures for TOR(I) and LN[TOR(I)- TOR(I-1)] values are significant)

ARRHENIUS PLOT PROGRAM

SAMPLE R1574

DATE 30/ 7/1985

STEPS FITTED  
\*\*\*\*\*

10 11 12 13 14 15 16 17 18 19 20 21 22 23 24 25 26 27 28 29

CALCULATED PARAMETERS  
\*\*\*\*\*

ACTIVATION ENERGY (KCAL/MOL) = 24.3

FREQUENCY FACTOR/(EFFECTIVE DIFFUSION RADIUS)\*\*2 = 0.2532E+00

MSWD = 47.5

INFERRED CLOSURE TEMPERATURE  
\*\*\*\*\*

FOR A COOLING RATE OF 1000 DEGREES C/MA  
THE CLOSURE TEMPERATURE IS CALCULATED TO BE 141.3 DEGREES C

Table A5:4 continued

APPENDIX 6

Scanning Electron Microscopy

## Introduction

The primary aim of this ancillary investigation is to observe the distribution of potassium (and, to some extent, calcium) in polished thin sections of dated samples. Several authors interested in such complementary studies for K-Ar or  $^{40}\text{Ar}$ - $^{39}\text{Ar}$  dating work have used a microprobe device, e.g. Dalrymple & Lanphere (1969), Mankinen & Dalrymple (1972), Stukas & Reynolds (1974), Dalrymple & Clague (1976), Hanes & York (1979), rather than a scanning electron microscope, which is the machine used in this study.

An SEM (Scanning Electron Microscope) alone is not capable of examining elemental distributions as it is essentially just an electron imaging device. The various types of electrons produced by the interaction of the scanning primary electron beam with the sample can be used to build up images of that sample. Such images may give only a rough guide to atomic number distribution. To observe elemental distributions on an SEM, it should ideally be fitted with an X-ray detection system.

In addition to electrons, X-rays are also produced by the interaction of the primary beam with the sample. The X-rays produced by a particular element are characteristic of that element in terms of their energies. Thus, where an X-ray detection system is included in an SEM, elemental distributions can be monitored. In this way the SEM becomes comparable to the conventional microprobe. The SEM used in this investigation was fitted with EDAX which stands for Energy Dispersive Analysis of X-rays.

## Basic Principles of SEM-EDAX Analysis

Only the rudimentary principles of SEM-EDAX analysis are covered here; for further details the reader should refer to Chandler (1977) or Goldstein et al., (1981).

A schematic diagram of an SEM with EDAX attachment is given in

Fig. A6:1. Electron beam-sample interactions important to the SEM apparatus used in this work are considered in Fig. A6:2.

The spatial resolution of secondary electron images is essentially determined simply by the size of the incident electron beam (0.1 - 0.2 $\mu$ ). However, as can be seen from Fig. A6:2, the X-rays emanate from a pear-shaped volume in the sample. Thus, the resolution of an X-ray image will be significantly less than in the case of the electron image. The maximum workable SEM magnification that can be used in a particular study is ultimately determined by image resolution and thus, the size of the incident electron beam. Sample composition and the accelerating voltage also have an effect because the electron range (which is a measure of how far the pear-shaped volume penetrates into the sample), is a function of both.

There are several types of X-ray detector. The SEM used in this investigation was fitted with an energy dispersive solid state detector (SSD). This consists of a silicon radiation detector between two electrodes, across which a bias voltage is applied. X-rays entering the detector create electron-hole pairs, the number of which is proportional to the X-ray energy. The charge produced by a single X-ray photon is collected at the electrodes and the output voltage is then amplified and passed to a multi-channel analyser. Here, the voltage pulses are separated in terms of their amplitude (proportional to X-ray energy) and counted. In this way, an energy spectrum can be constructed and this is displayed on a CRO or chart recorder (see Fig. A6:3). The energy spectrum represents the gross elemental composition of the area scanned by the primary electron beam. Peak identification is accomplished by comparing the observed X-ray energies with known elemental energies and peak intensities.

The X-ray detection system used in this investigation measures energies up to 20 keV. This is sufficient to cover all typical K $\alpha$  X-ray lines



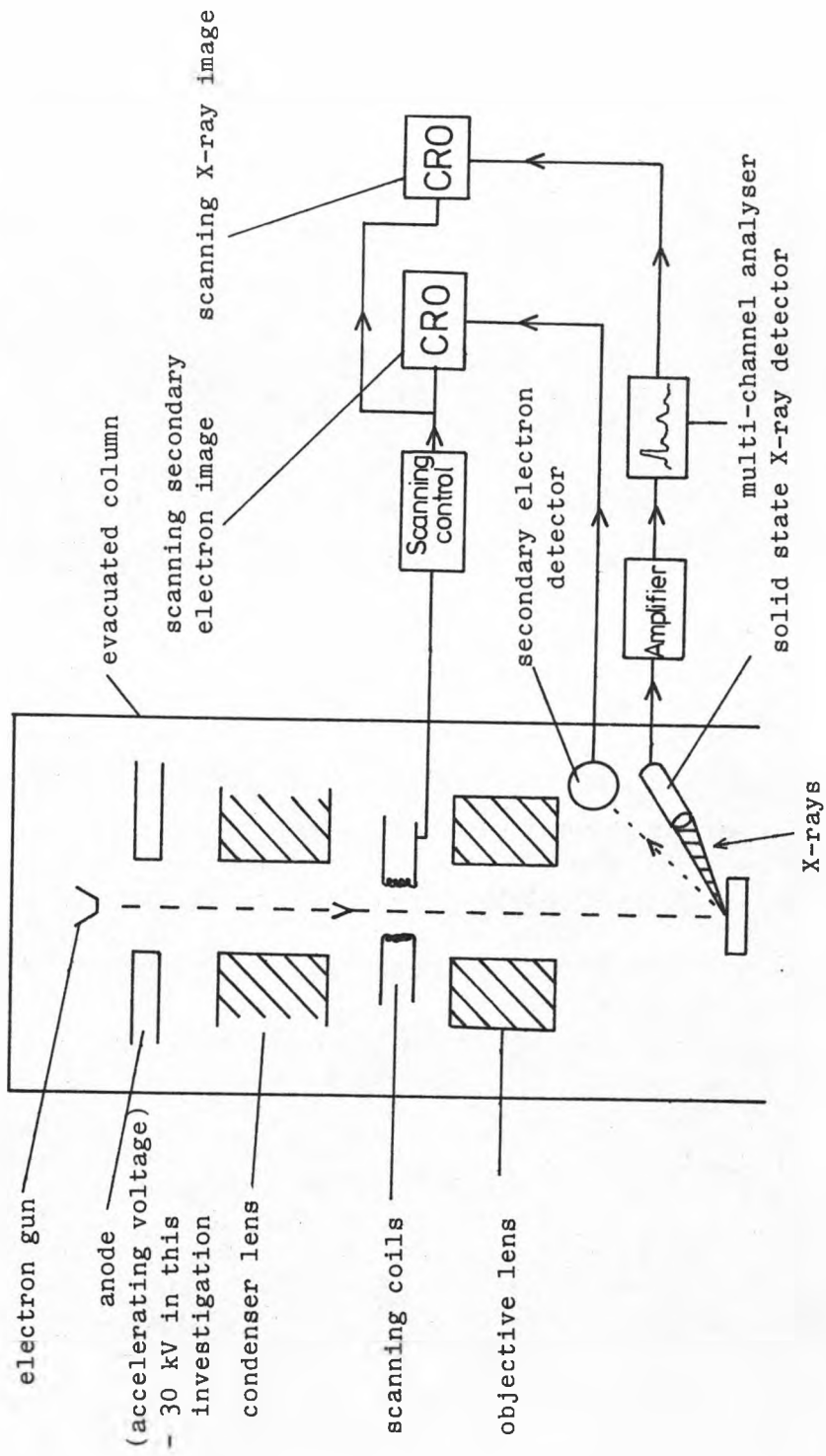


Fig. A6:1 Schematic diagram of SEM with EDAX attachment (adapted from Chandler, 1977)

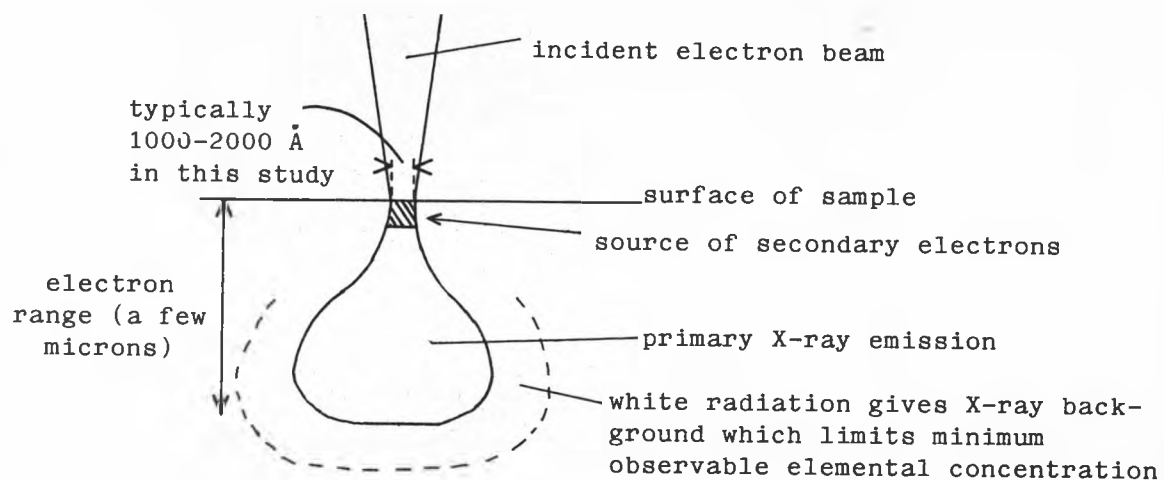


Fig. A6:2 Electron beam-sample interactions.

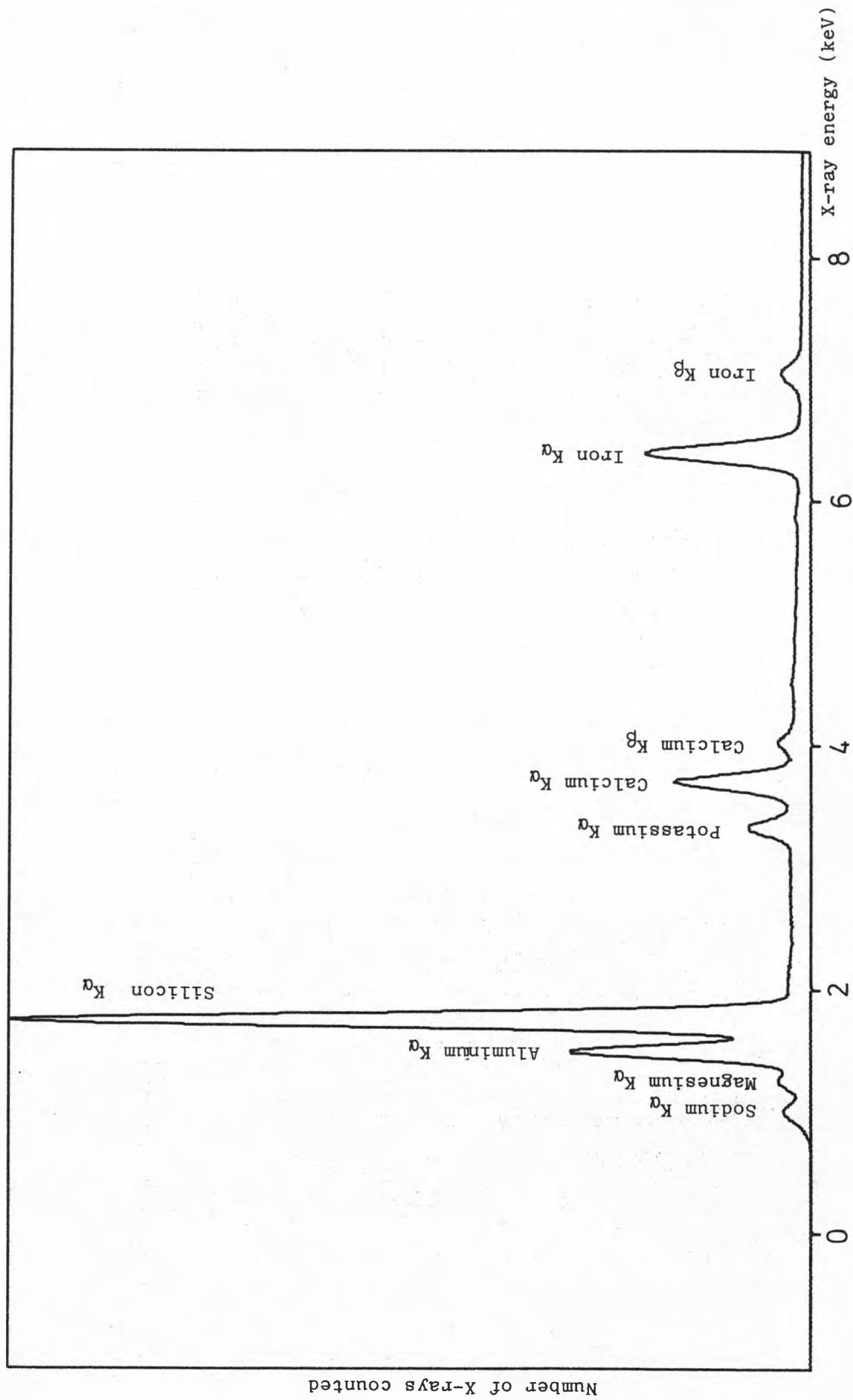


Fig. A6:3 An X-ray energy spectrum for a geological specimen

for geological materials. However, the SSD does not detect all X-ray energies with equal efficiency (see Fig. A6:4); in fact the  $K\alpha$  X-rays of elements of an atomic number less than sodium are not detected at all. The low energy limitation of the SSD is due to X-ray absorption in the detector "window" (the low efficiency at very high energies, unimportant to this investigation, is due to the X-rays passing through the detector without interaction).

Included in the EDAX package are computer programs which can convert the SSD output into numerical figures, e.g. elemental weight percentages, by making all the appropriate allowances. However, a fully quantitative analysis requires the use of standard samples of known composition. The preparation and use of such standards is very time consuming so in this study a more qualitative approach was adopted.

#### Presentation of X-ray Analyses

The most useful form of presentation for this study was the X-ray map which, in spatial terms, is a direct equivalent to the secondary electron image. The construction of an X-ray map involves setting the SSD to a single elemental  $K\alpha$  X-ray peak (Fig. A6:5) and linking the output to a CRO. Where an X-ray of the correct energy is detected at a given point in the area scan, a bright dot momentarily appears at the corresponding point on the CRO screen. The CRO screen is photographed over the duration of the scanning time and an X-ray dot map is thus built up, representing the distribution of the chosen element. The scanning time is usually linked to a preset number of X-ray counts (typically 100,000).

For a given area of interest, four X-ray maps were usually constructed - one each for potassium, calcium, aluminium and iron (see Fig. A6:6) The distributions of K and Ca are of direct interest in terms of the sizes of the areas in which they are concentrated and those in which they are not. The Fe and Al maps are of use in the

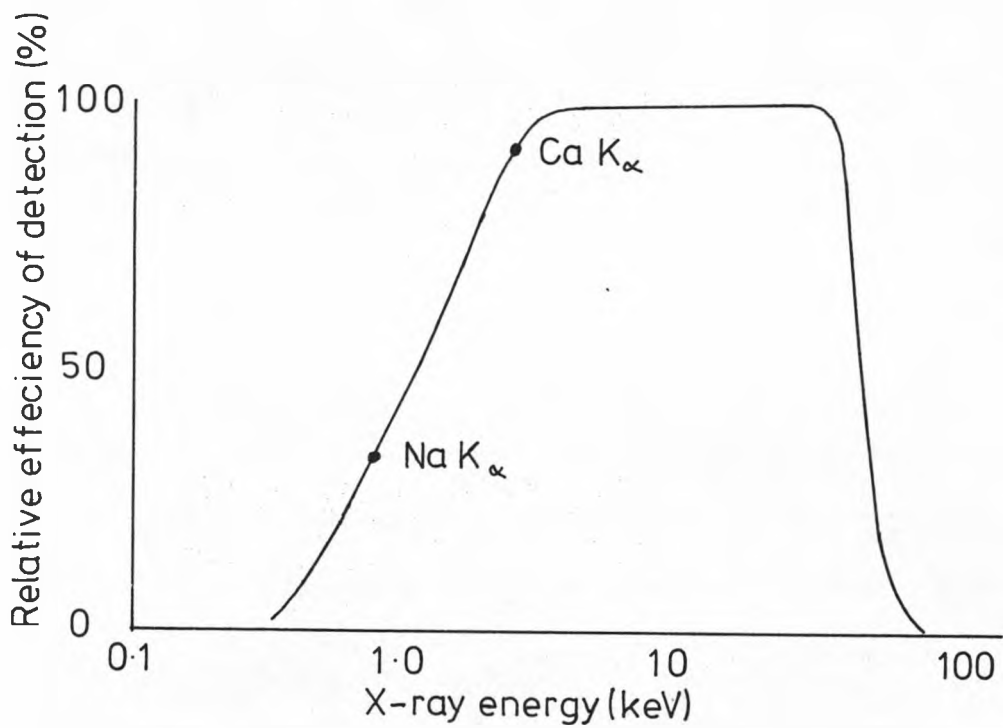


Fig. A6:4 Relative efficiency of detection for a typical SSD

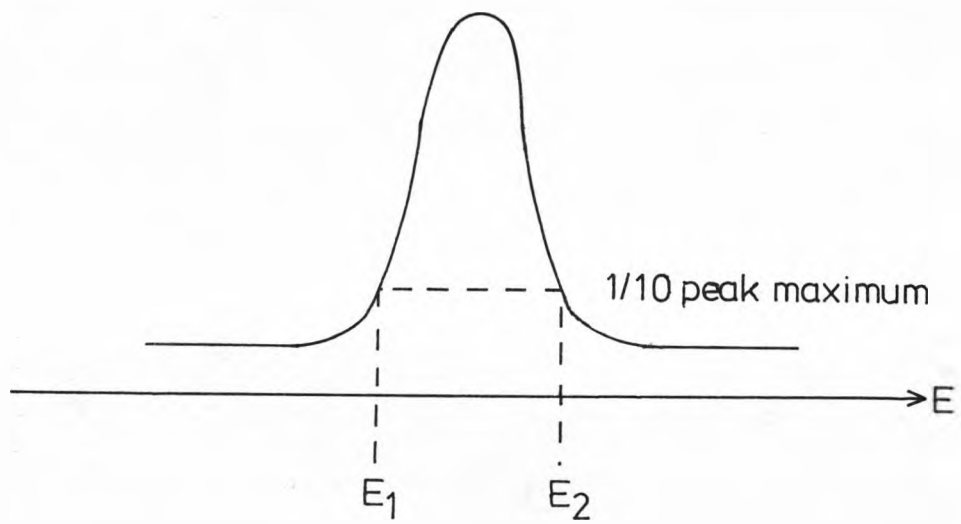
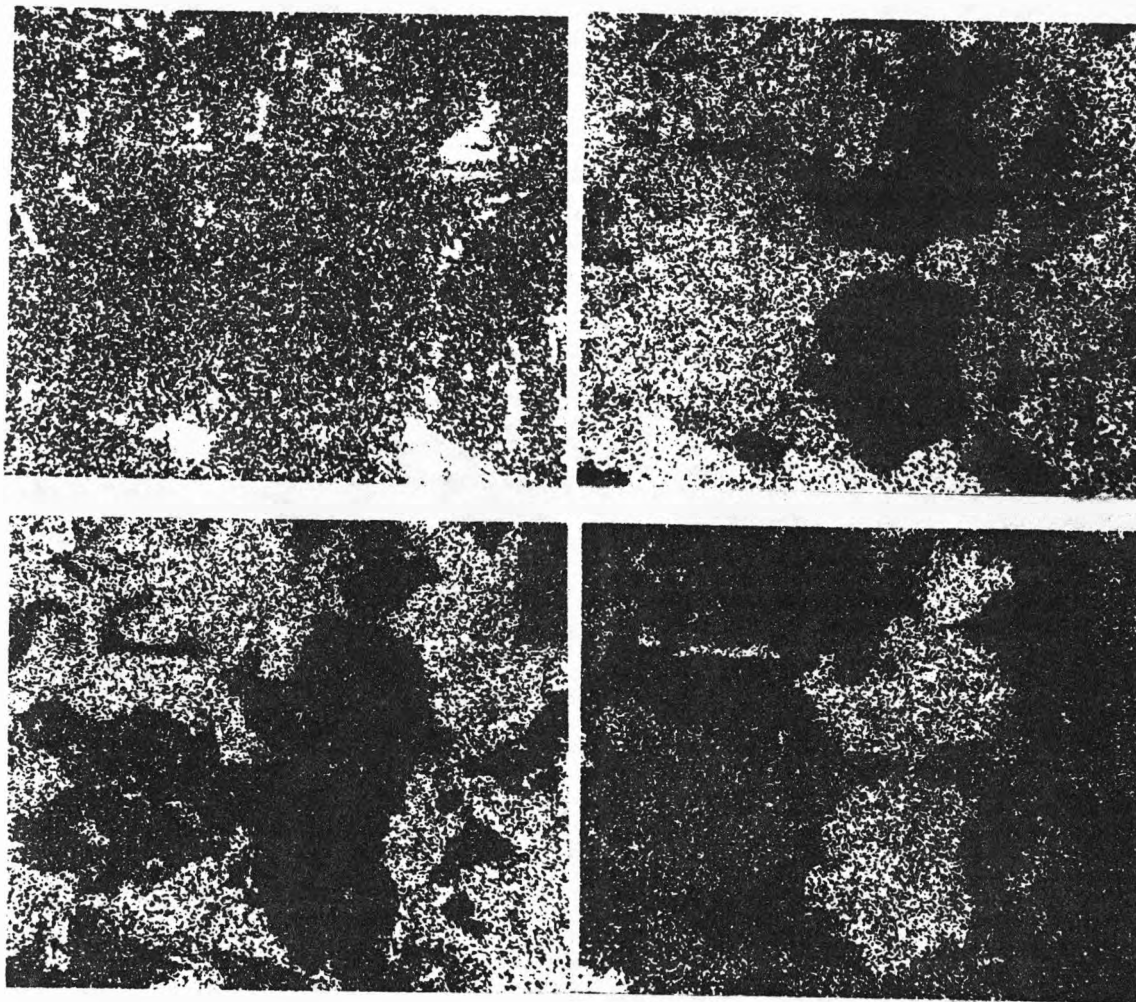


Fig. A6:5 Setting the SSD to a single elemental X-ray peak - only X-rays in the energy range  $E_1$  to  $E_2$  are monitored



Potassium	Calcium
Aluminium	Iron

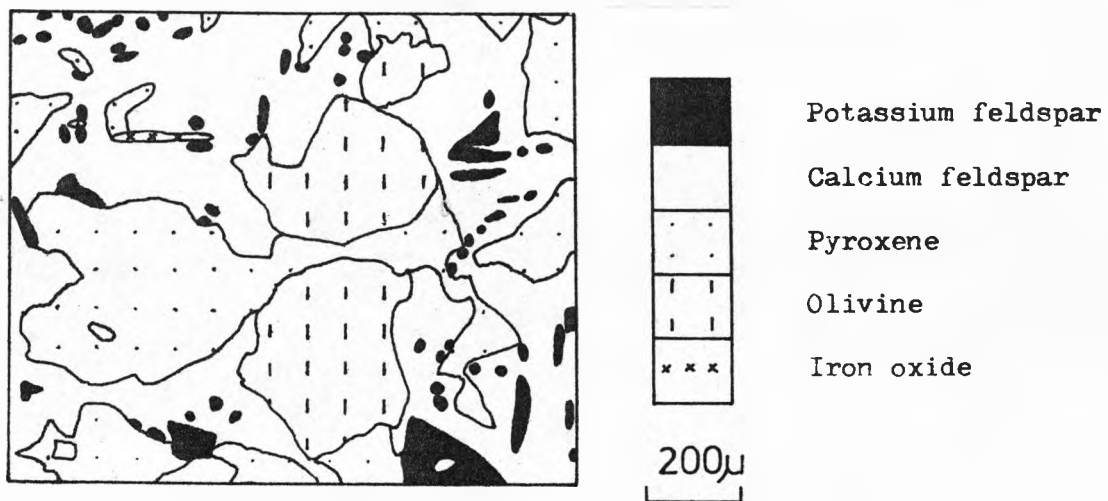


Fig. A6:6 X-ray maps showing the distribution of potassium, calcium, aluminium and iron for an area of a geological thin section

identification of the potassium and calcium bearing minerals. Initial investigations would start at low magnification (e.g. x40) to obtain an overall view of the sample and also to select areas of interest for more detailed work. Successive analyses would then be conducted at higher magnifications (up to x640).

Several authors interested in potassium distributions for K-Ar or  $^{40}\text{Ar}$ - $^{39}\text{Ar}$  dating studies have utilised the X-ray map technique before e.g. Dalrymple & Lanphere (1969), Mankinen & Dalrymple (1972), Stukas & Reynolds (1974).

An additional form of presentation occasionally employed in this study was the line-scan. Here, the electron beam is made to scan along a line on the specimen surface rather than across an area. In this way, a picture of elemental concentration variations along a linear traverse can be built up. The data file containing the number of X-ray counts at each of the discrete points along the traverse was fed into a simple computer program which produced the graphical output (for example, see Fig. A6:7)

### Results

A summary of the findings of the SEM investigations for the eight selected samples is presented below. The implications for the interpretation of the corresponding  $^{40}\text{Ar}$ - $^{39}\text{Ar}$  stepwise degassing analyses are discussed in Chapter 6.

#### Droimchogaidh sill potassic syenite sample 238P

Fig. A6:8 shows that the majority of the sample consists of a potassium-rich feldspar. The variations in potassium concentration are due either to the presence of mafic minerals, e.g. pyroxene, opaque, or feldspar zoning. The latter usually takes a rectangular form with a potassium-rich core and a potassium-poor calcium-rich rim, (the interstitial feldspar is potassium-rich but less so than the cores



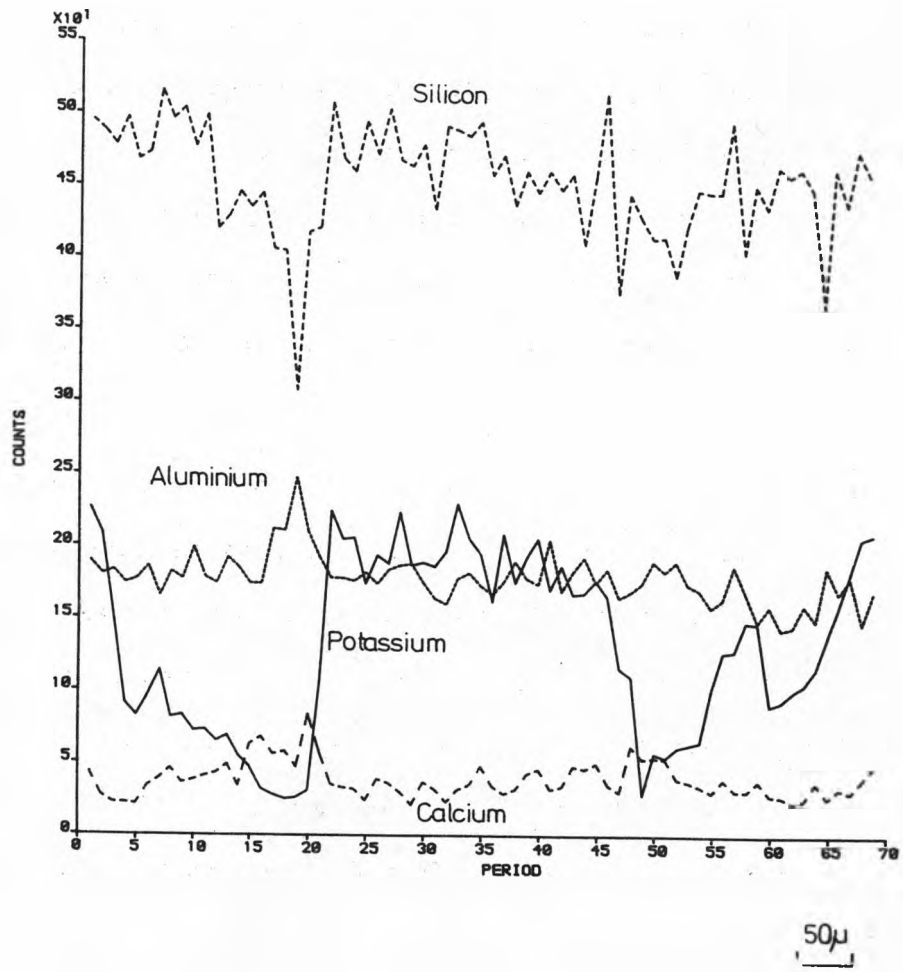
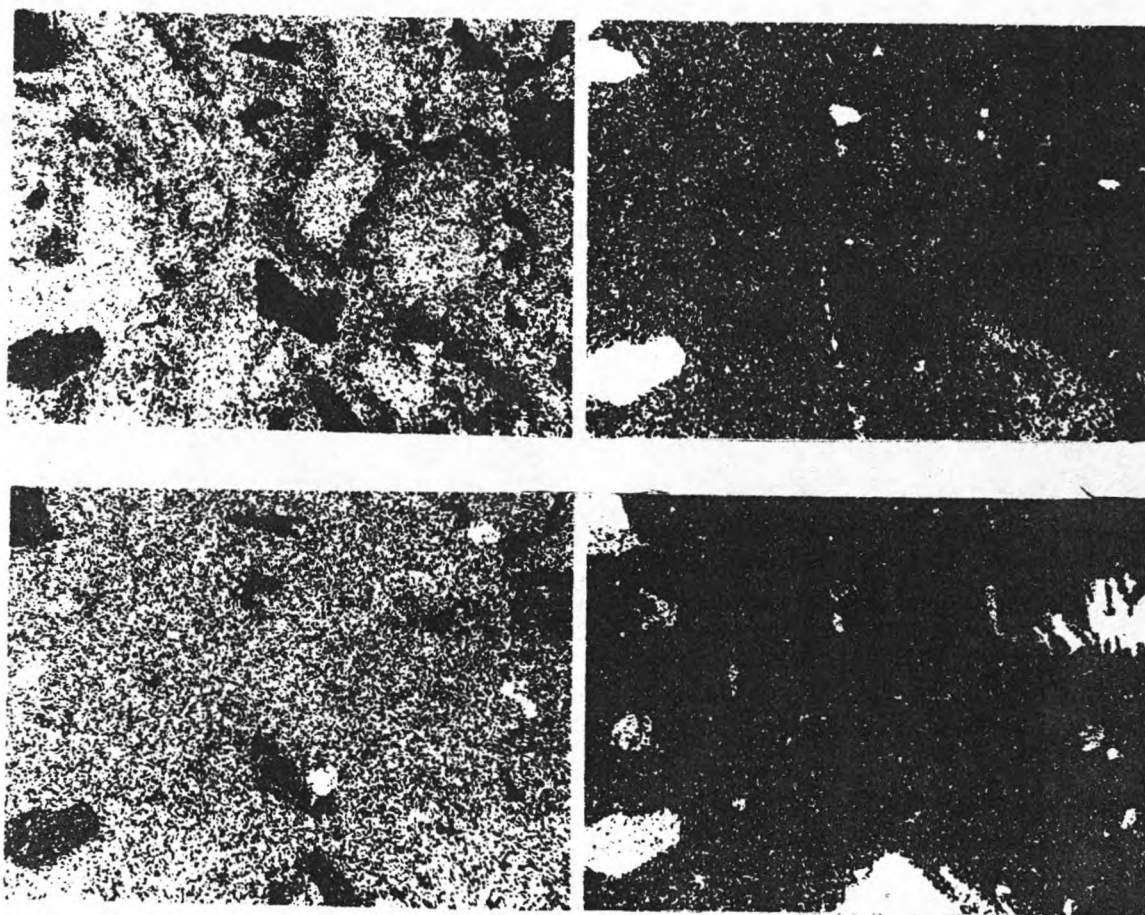
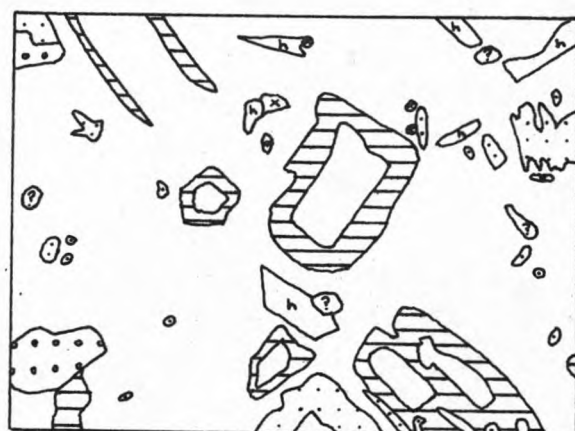


Fig. A6:7 X-ray analysis along a line-scan



K	Ca
Al	Fe



- Potassium feldspar
- Calcium feldspar
- Pyroxene
- Iron oxide
- Apatite
- Unidentified mineral
- Hole in slide

400μ

Fig. A6:8 Example X-ray maps for Droimchogaidh sill potassic syenite sample 238P

of the zoned feldspars). An example of this can be seen at the centre of the potassium X-ray map in Fig. A6:8. Fig. A6:7 displays the line-scan over this zoned feldspar.

The areas of uniform high potassium content are typically  $> 200\mu$  in dimension and the potassium-poor feldspar rims range in width from 50 -  $100\mu$ . The larger mafic crystals are  $> 200\mu$  across; however, there are some smaller ones  $< 50\mu$  in dimension.

Droimchogaidh sill olivine gabbro sample 238

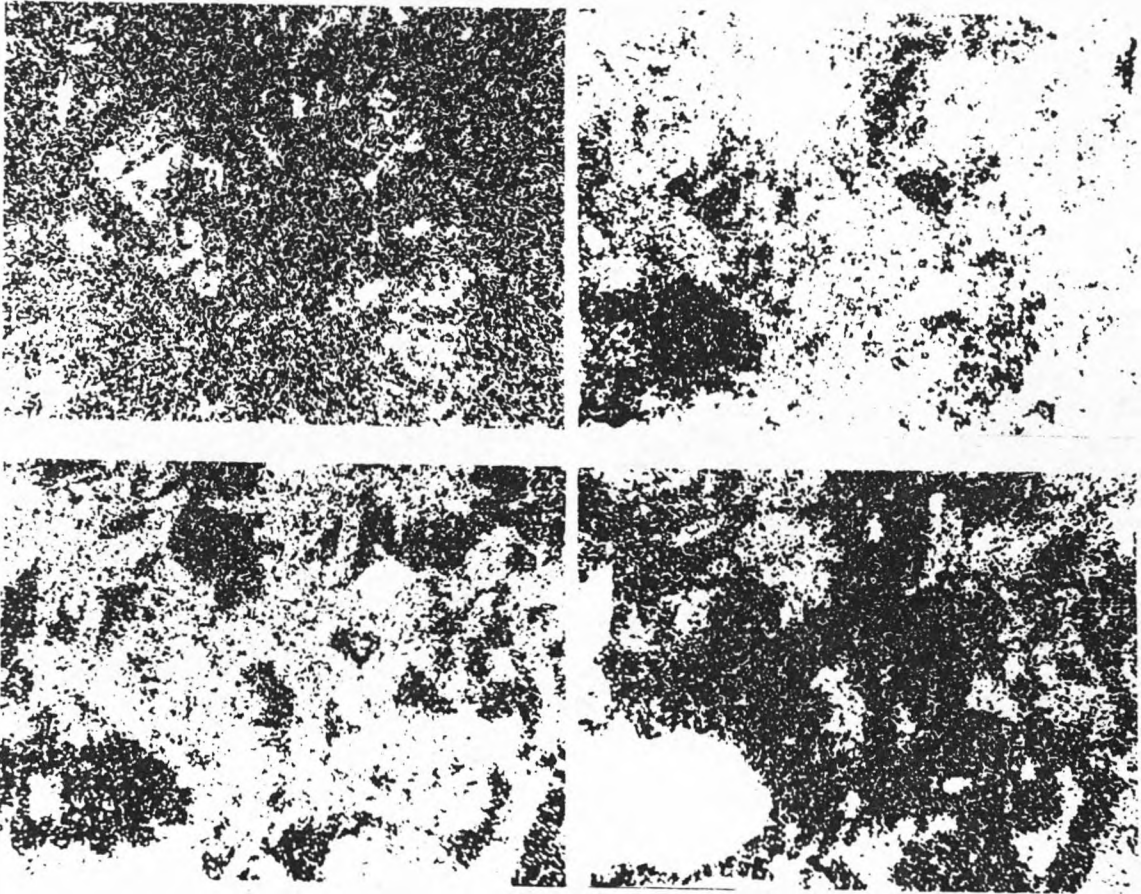
The majority of the potassium in this sample appears to reside in feldspathic area typically  $50\mu$  across, but in some cases  $100\mu$  (see Fig. A6:9). The speckly nature of most of the potassium maps produced for this sample suggests that a significant proportion of potassium may be found in very small grains ( $\ll 50\mu$ ).

Killala Bay gabbro sample 124NA

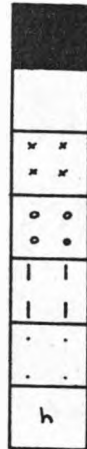
The majority of the potassium is found in the interstitial feldspar, which can be anything from 50 - several  $100\mu$  across (see Fig. A6:10 and A6:11). As Fig. A6:11 clearly shows, potassium is also found in high-potassium "spots" in the range 10 -  $25\mu$ , mafic grains ( $\approx 50\mu$ ), and the cracks of the large pyroxene grains which are less than  $10\mu$  across. The mafic potassium-bearing mineral is probably biotite, which was recognised in some of the Killala Bay gabbro petrographic thin sections.

Killala Bay gabbro sample 128B

From the X-ray maps of this sample, it is clear that there are two important types of potassium locations - mafic and feldspathic (see Figs. A6:12 and A6:13). The mafic potassium-rich areas are found on the rims of olivine grains and may represent a deuteric alteration; it is thought that the mineral concerned is biotite (see description of sample 124NA). These mafic areas are typically 5 -  $25\mu$  across. The potassium-bearing feldspar is found in areas as large as  $250\mu$ ;



K	Ca
Al	Fe



Potassium feldspar

Calcium feldspar

Sodium feldspar

Pyroxene

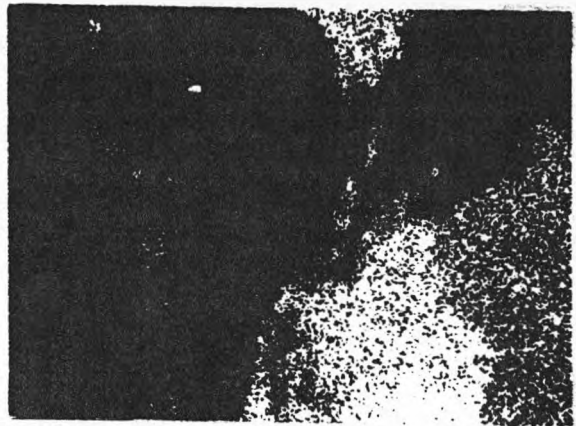
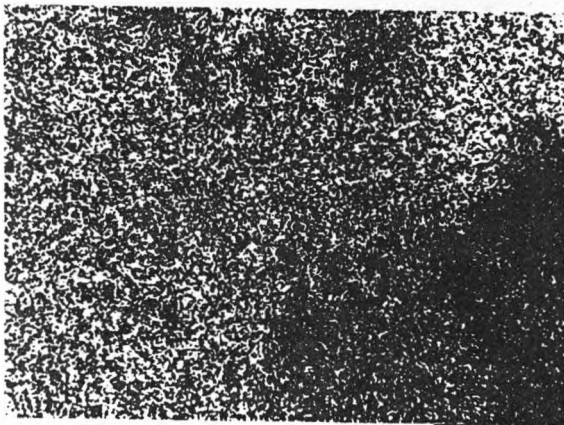
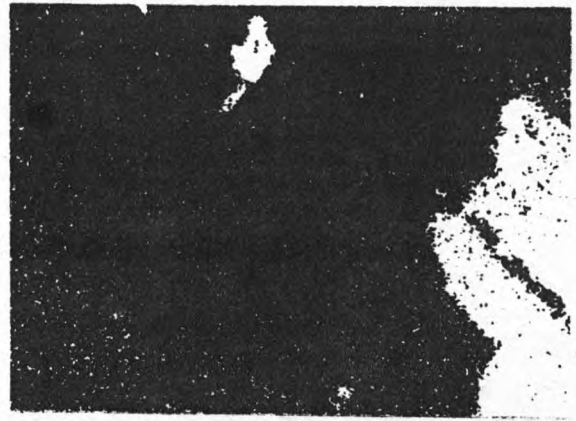
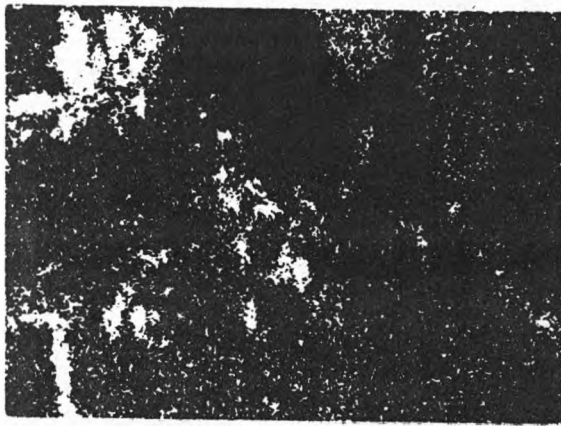
Olivine

Iron oxide

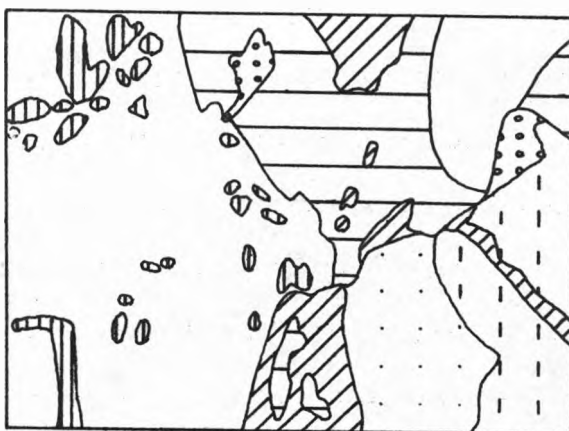
Hole in slide

400μ

Fig. A6:9 Example X-ray maps for Droimchogaidh sill olivine gabbro sample 238



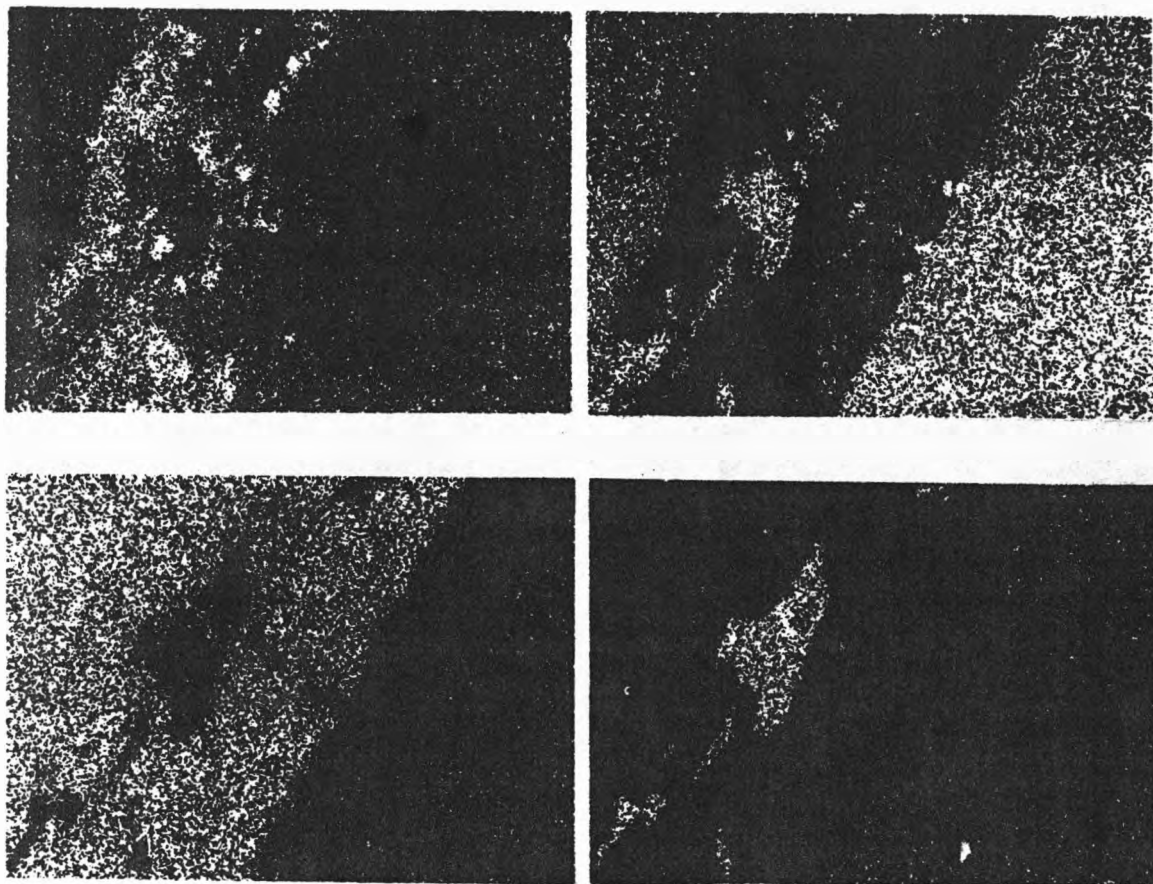
K	Ca
Al	Fe



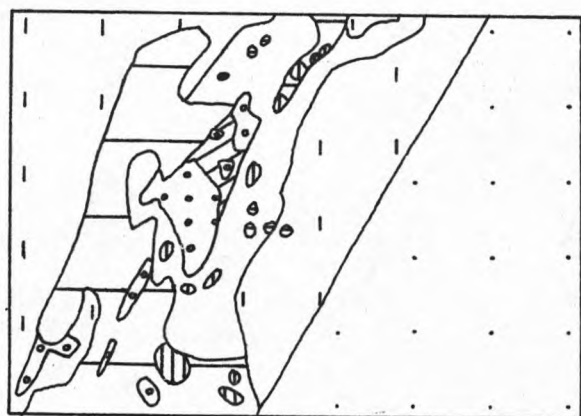
- Potassium feldspar
- High-potassium feldspar
- Low-potassium feldspar
- Biotite mica
- Pyroxene
- Iron oxide
- Apatite/Calcite

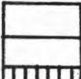

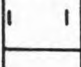

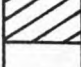
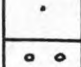
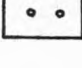
50 $\mu$

Fig. A6:10 Example X-ray maps for Killala Bay gabbro sample 124NA (1)



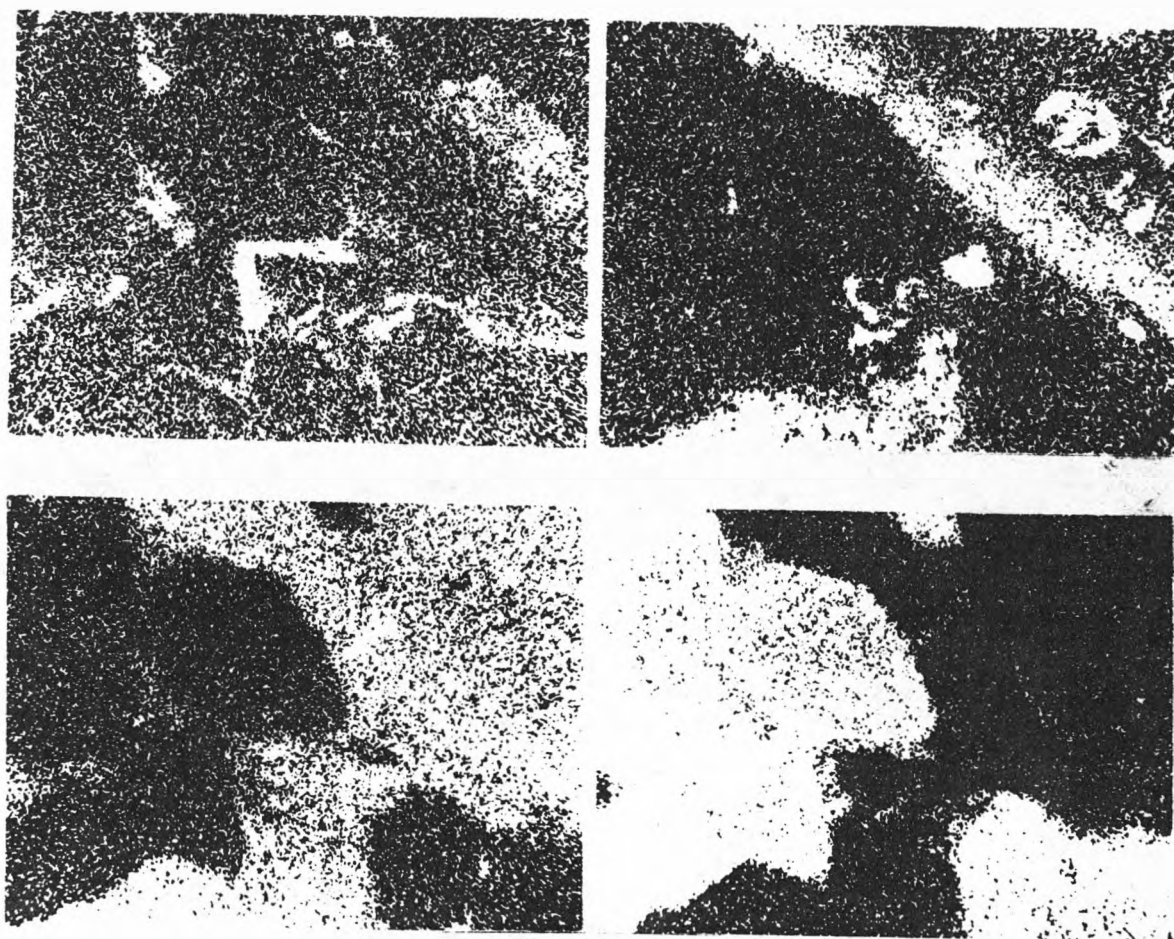
K	Ca
Al	Fe



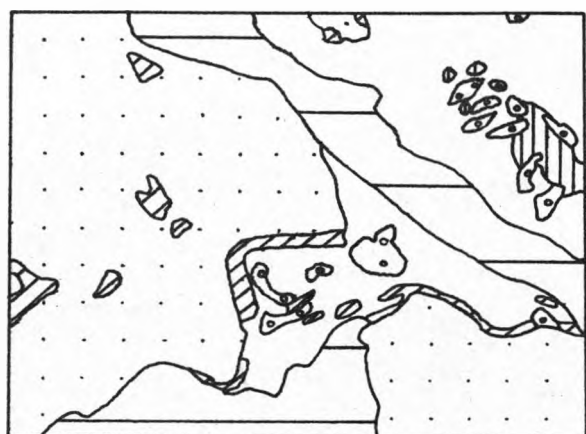
-  Potassium feldspar
-  High-potassium feldspar
-  Calcium feldspar
-  Sodium feldspar
-  Biotite
-  Titanaugite
-  Iron-rich pyroxene

50μ

Fig. A6:11 Example X-ray maps for Killala Bay gabbro sample 124NA (2)



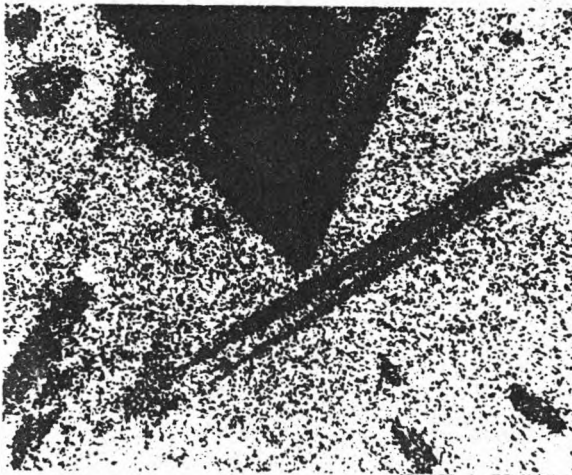
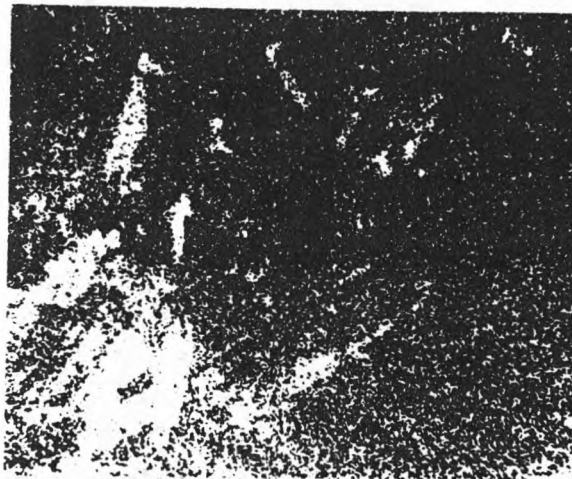
K	Ca
Al	Fe



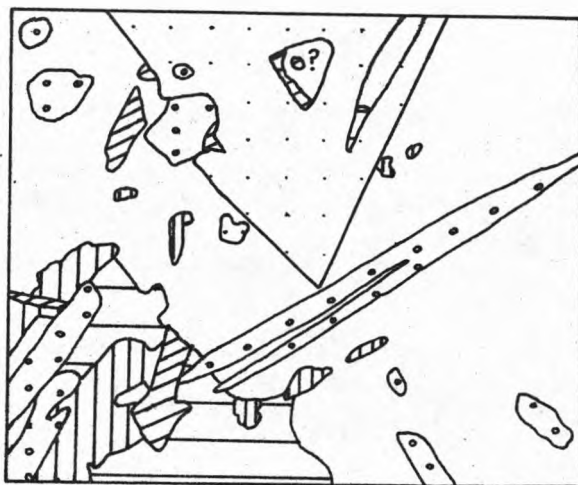
Potassium feldspar  
 Calcium feldspar  
 Sodium feldspar  
 Biotite mica  
 Olivine  
 Apatite

100 $\mu$

Fig. A6:12 Example X-ray maps for Killala Bay gabbro sample 128B (1)



K	Ca
Al	Fe



- Potassium feldspar
- High-potassium feldspar
- Plagioclase feldspar
- Biotite mica
- Iron oxide
- Apatite
- Unidentified mineral

100μ

Fig. A6:13 Example X-ray maps for Killala Bay gabbro sample 128B (2)



however, there are zones of a 10 - 50 $\mu$  dimension which contain extra-high potassium concentrations. It is thought that the dominant potassium-bearing phase would be the feldspar because it is found in much larger areas than the mafic potassium mineral.

Two further observations are worthy of note. Firstly, Fig. A6:12 clearly displays the zoned nature of the plagioclase feldspars in Killala Bay gabbro sample 128B. Lath cores are rich in calcium, with the rims being sodium rich (normal zoning). Secondly, it was only through the SEM work that apatite was identified in this sample. The phosphorous X-ray map (not shown), for the area analysis displayed in Fig. A6:13, is very similar to that for calcium. The only common mineral, which is both high in calcium and phosphorous, is apatite. The apatite crystals are between 10 - 50 $\mu$  across; however, the majority of the calcium in the sample is contained within very large plagioclase and pyroxene grains (100's  $\mu$  across).

Blind Rock dyke "normal dolerite" sample G049M

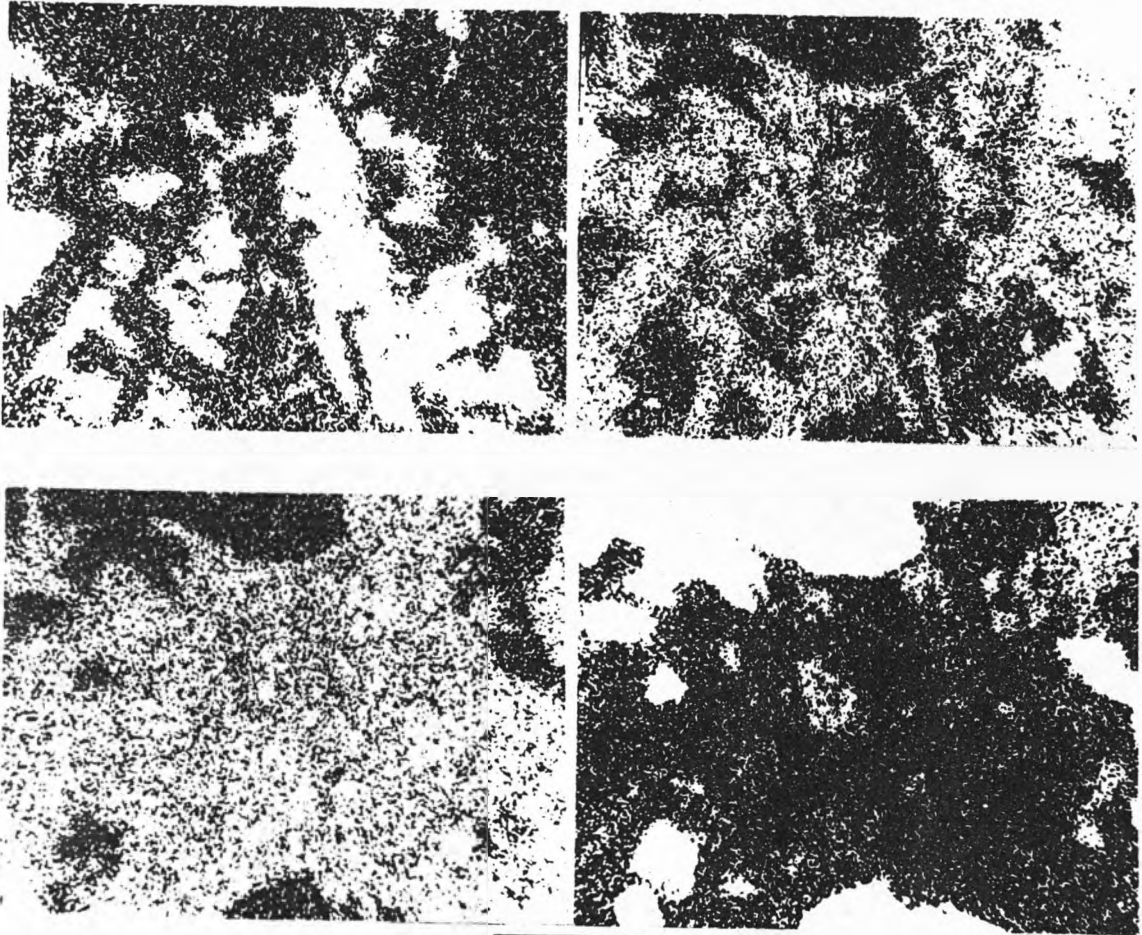
The potassium in this sample resides in feldspathic areas typically 50 $\mu$  wide (see Fig. A6:14).

Blind Rock dyke tholeiitic dolerite sample G049C

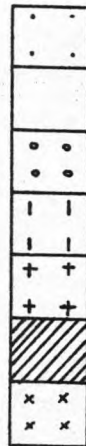
The potassium-bearing feldspathic zones in this, the more coarse-grained of the two Blind Rock dyke samples, are as large as 50 $\mu$ . However, a large proportion of the potassium appears to reside in smaller feldspathic areas less than 20 $\mu$  across (see Fig. A6:15).

Lower Basalt Formation olivine basalt sample I001

The potassium in this sample is concentrated in the zeolite amygdales. Fig. A6:16 clearly shows that the potassium concentration is higher in the zeolite than in the groundmass, and also that the zeolite rims possess an extra-high potassium content compared to the core. The zeolites themselves are typically > 0.5mm in diameter; however, the potassium-rich rims are only of the order of 50 $\mu$ .



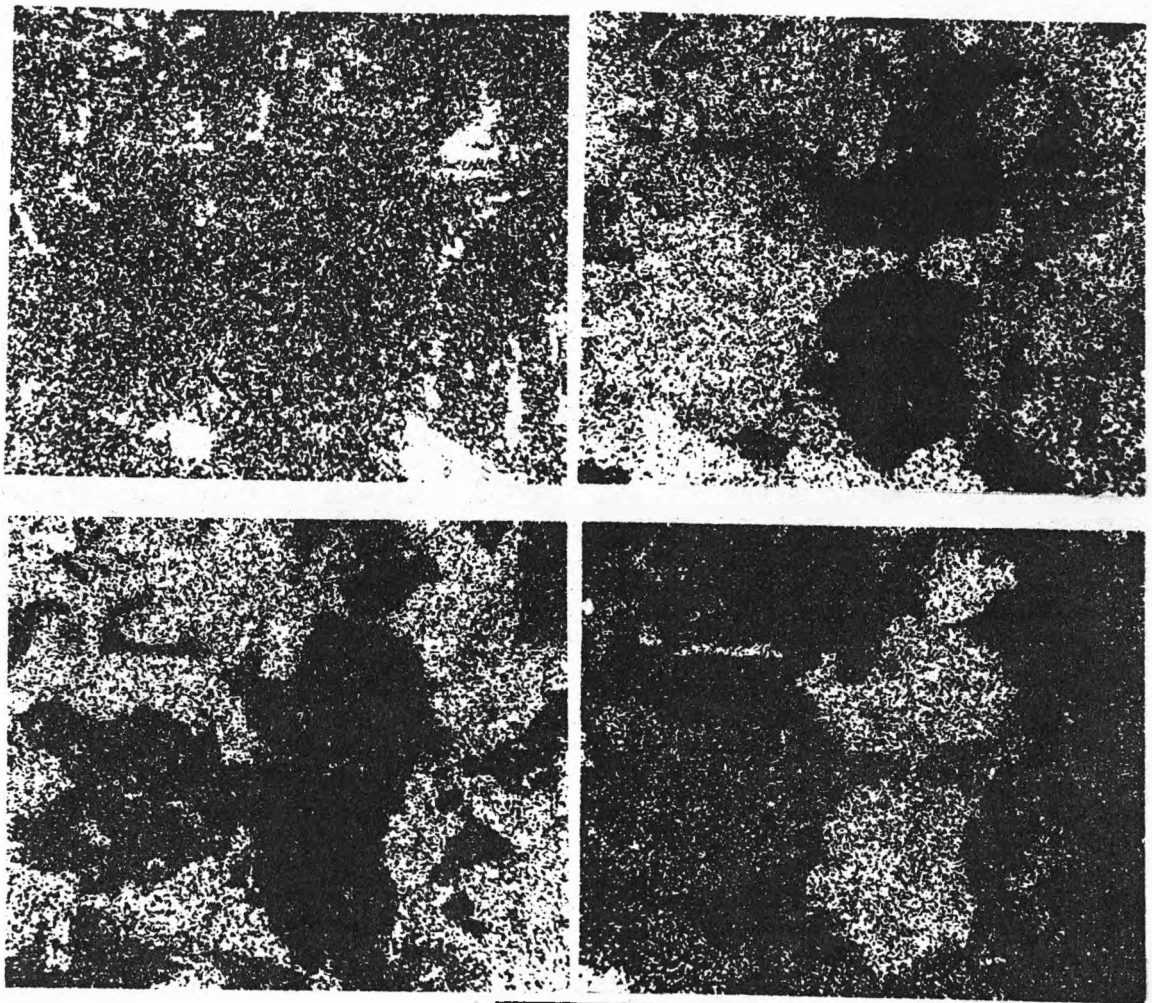
K	Ca
Al	Fe



- Potassium feldspar
- Calcium feldspar
- Pyroxene
- Olivine
- Iron oxide
- Calcite
- Unidentified mineral

50μ

Fig. A6:14 Example X-ray maps for Blind Rock dyke "normal dolerite" sample G049M



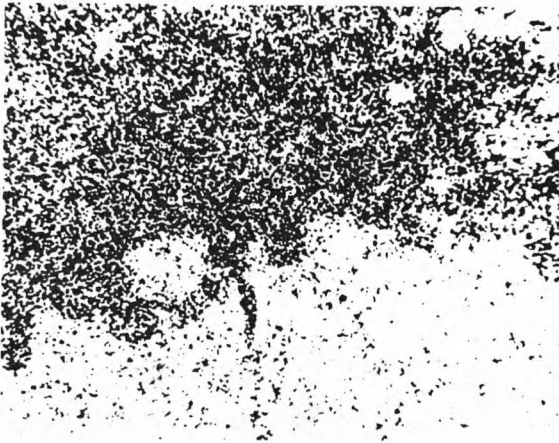
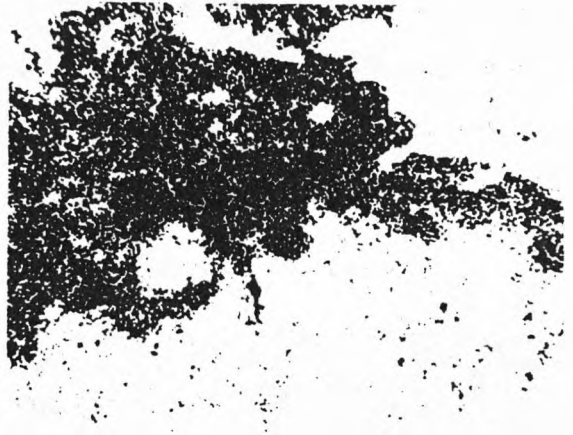
K	Ca
Al	Fe



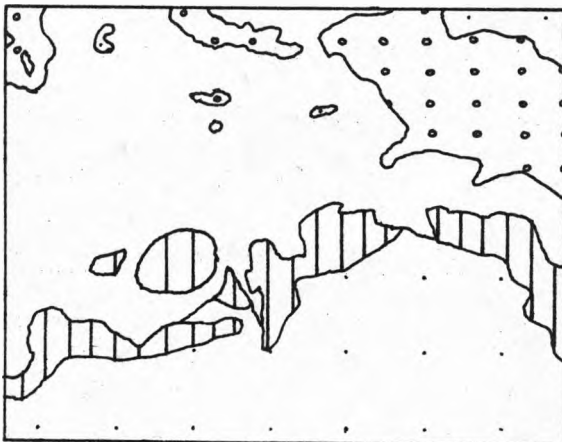
Potassium feldspar  
 Calcium feldspar  
 Pyroxene  
 Olivine  
 Iron oxide

200μ

Fig. A6:15 Example X-ray maps for Blind Rock dyke tholeiitic dolerite sample G049C



K	Ca
Al	Fe



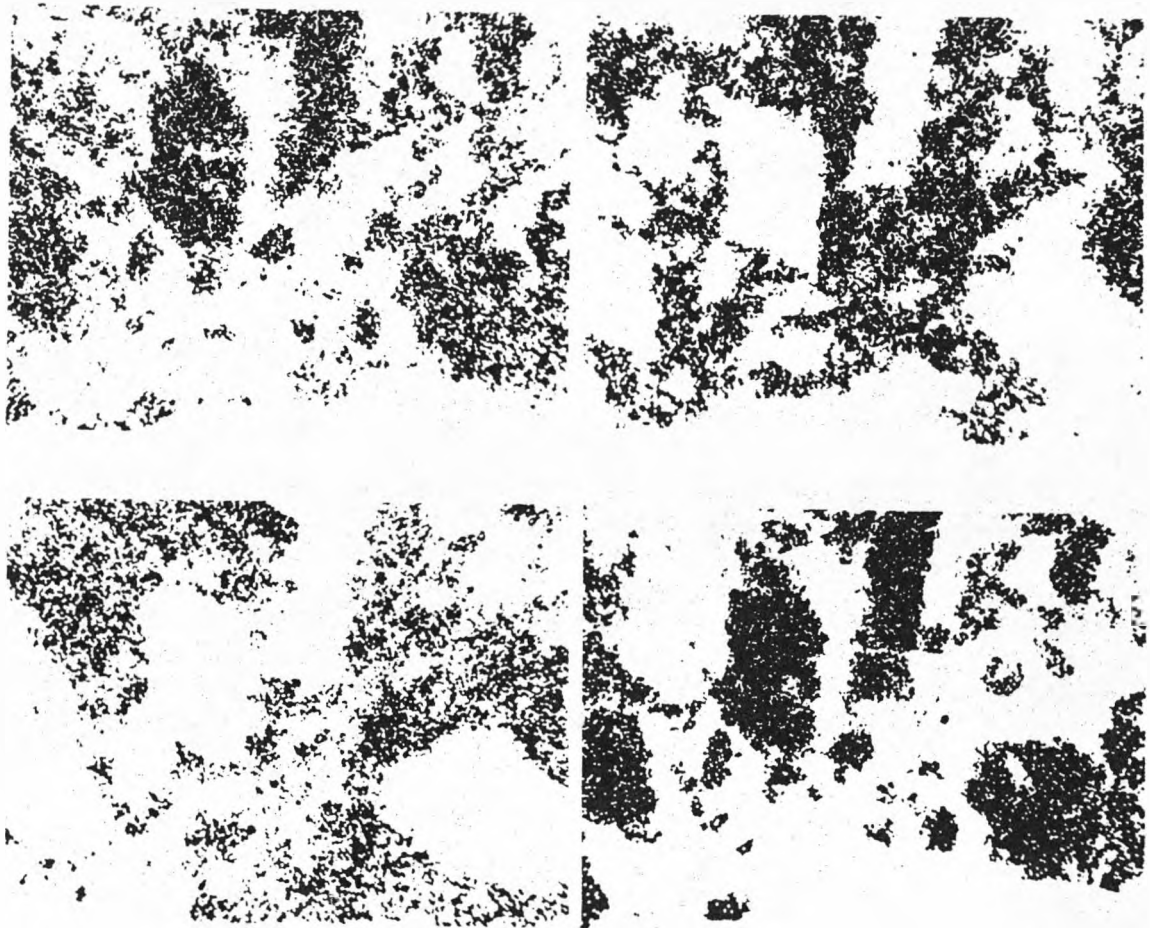
Zeolite  
 High-potassium zeolite  
 Pyroxene  
 Olivine/Iron oxide

100μ

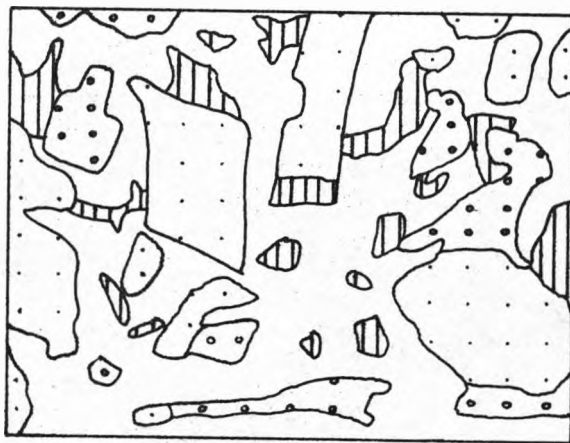
Fig. A6:16 Example X-ray maps for Lower Basalt Formation olivine basalt sample I001

Mourne dyke swarm feldspar porphyry sample N003A

The majority of the potassium in this sample lies in mafic grains which show reasonably high levels of aluminium (see Fig. A6:17). The mineral concerned is identified as hornblende - this choice is justified by the elemental composition, as deduced from the X-ray maps, and by reference to Tomkeieff & Marshall's (1935) petrographic description of samples from the same dyke. The hornblende, which is thought to represent the alteration product of augite (Tomkeieff & Marshall, 1935), is found as areas typically 25 $\mu$  across (see Fig. A6:17). Other minerals identified are augite, calcium feldspar and minor potassium feldspar. These constitute the areas between the hornblende grains and are often only 10 - 25 $\mu$  across, although much larger feldspar phenocrysts are also prominent (see Fig. A6:17).



K	Ca
Al	Fe



Hornblende

Augite

Enstatite and/or Serpentine

Calcium feldspar

50μ

Fig. A6:17 Example X-ray maps for Mourne dyke swarm feldspar porphyry sample N003A

APPENDIX 7

Petrographic Sample Descriptions

(i) Kerry Dyke System

R1470 (DDF) [Grid Ref. 0523 0427]

Consists of roughly 50% feldspar (mostly plagioclase), 25% olivine, 10% pyroxene, 5% opaque and 10% calcite/zeolite contained in spherical amygdales. All phases seem to be altered to some extent although many feldspar laths are quite fresh. The mafic minerals typically have a grain size less than 0.1mm, the feldspar is found in laths up to 0.5mm long, and the amygdales are commonly 0.5mm in diameter.

R1575 (DDC) [Grid Ref. 0523 0427]

Very similar to R1470 (DDF) except that mineral grain sizes are larger - mafics and feldspar laths typically 0.5mm and 2mm respectively.

R1579 (187) [Grid Ref. 0478 0610]

Consists of roughly 60% zoned plagioclase, 20% pyroxene, 20% olivine and less than 5% opaque. Feldspar is fairly fresh although there is evidence of alteration along cracks and in discrete blotches. The olivine shows only peripheral alteration and the pyroxene is fresh. Plagioclase laths are less than 1mm long, olivine and pyroxene grains are typically < 0.25mm and 0.5 - 1.0mm across respectively.

(ii) Intrusive Systems of West-Central Ireland

R1576 (DHP) [Grid Ref. 0590 2427]

50% plagioclase feldspar, 30% pyroxene, 10% olivine and 10% opaque approximately. 30% of the slide consists of fine-grained areas containing olivine, pyroxene, opaque and a black-grey grainy material. The latter consists of microscopic opaque grains and feldspathic material. All the olivine is heavily altered; however, both pyroxene and plagioclase feldspar are fresh. The plagioclase is found in laths up to 1mm long, pyroxene is sub-ophitic areas 1- 5mm across or discrete grains < 0.5mm across, olivine in grains < 0.5mm across, and opaque in laths and grains < 0.5mm and < 0.25mm across respectively.



R1384 (253), R1504 (253) [Grid Ref. 0603 2591]

Consists of roughly 40 - 50% plagioclase feldspar, 30% olivine, 20% pyroxene, 5% opaque, with perhaps some accessory biotite (as a secondary alteration). Olivine is heavily altered, pyroxene is fresh and plagioclase displays fine-grained alteration along cracks. Olivine and pyroxene grains are typically < 0.25mm and 0.5mm across respectively. Plagioclase laths reach 2mm in length, however, commonly they are 0.5 - 1mm long.

R1610 (211NWC) [Grid Ref. 0898 2686]

Consists of 70% feldspar (mainly plagioclase), 20% pyroxene and 10% olivine. All phases are fresh except that the olivine displays some alteration along internal cracks. Pyroxene and olivine grains are typically 0.5 - 2mm across. Feldspar is found in 0.5 - 1mm long laths or 1 - 2mm areas.

(iii) Droimchogaidh Sill

R1381 (238P), R1473 (238P) [Grid Ref. 1075 2702]

Consists of 85% untwinned zoned feldspar, 10% pyroxene and 5% opaque. Prominent within the feldspar are concentric square-zoned crystals. Mottled nature of the feldspar suggests a secondary alteration. Pyroxene shows slight alteration at rims. Square feldspars typically 1mm across and the more common laths are up to 4mm long. Both pyroxene and opaque grains are commonly 0.5 - 1mm, however, for the latter small grains 0.1mm across are also prominent.

R1612 (238P) [Grid Ref. 1075 2702]

Very similar to the first Droimchogaidh sill thin section.

R1530 (238) [Grid Ref. 1075 2702]

Consists of 50% feldspar (identified as labradorite), 25 - 30% ophitic pyroxene, 15 - 20% ophitic olivine and less than 5% opaque. All phases reasonably fresh except that olivine and pyroxene do show some

marginal alteration. Feldspar laths are up to 2mm long (typically < 1mm) and pyroxene/olivine ophitic areas are up to 5mm across. The opaque grains are typically  $\approx$  1mm across. There is evidence of xenocrystal material in the form of a 2mm area of feldspar surrounded by ophitic olivine masses.

R1583 (243) [Grid Ref. 1078 2708]

Very difficult to judge mineral proportions in this slide. Perhaps 40% of subhedral olivine grains displaying alteration in cracks and at margins. A 1- 2mm grain size for olivine is not untypical. The proportion of ophitic pyroxene areas (1 - 2mm) is estimated to be 20%. This mineral is fresh. Aside from the mafic minerals, there is also a high proportion of indistinguishable fine-grained ( $\ll$  0.1mm) material which constitutes the matrix. Much of this probably represents the altered remnants of minerals. The majority of the plagioclase feldspar is contained within the ophitic pyroxene as laths < 0.55mm long, however, there are occasional laths 1 - 2mm long independent of the pyroxene.

R1506 (234), R1581 (234) [Grid Ref. 1090 2728]

Consists of roughly 60% plagioclase feldspar, 30% pyroxene, 10% olivine and 5% opaque material. Both the feldspar and pyroxene are fresh, however, olivine is heavily altered and in some cases entirely pseudomorphed. Plagioclase laths are typically 1mm long and the sub-ophitic pyroxene is commonly found in patches 1 - 2mm across. Both the olivine and the opaque are found as smaller grains (0.5mm and 0.1mm are typical respective sizes).

(iv) Lough Key Dyke

R1611 (G048) [Grid Ref. 1820 3055]

A highly altered thin section with only the outlines of primary minerals visible. 70% consists of an indistinguishable dark brown material. Round grains, typically 0.1 - 0.2mm across and which probably represent

former olivine, form 25% of the slide. Rectangle/square shapes (5%) probably represent former plagioclase feldspar. These grains are typically of a 0.4 - 0.5mm dimension. Also observed in the thin section are small (0.1mm across) calcite veinlets.

(v) Killala Bay

R1383 (105A), R1503 (105A) [Grid Ref. 1221 3333]

This very fine-grained sample consists of 60 - 70% feldspar and 30 - 40% mafic minerals (5% opaque). Pyroxene probably represents the majority of the mafic material, although olivine is positively identified. All mineral phases appear to be fresh. Feldspar laths are typically 1 - 2mm long and mafic minerals are very much less than 1mm across.

R1526 (G013) [Grid Ref. 1221 3330]

Consists of roughly 50% altered mafic material and 50% feldspar which is in varying stages of alteration. Grain sizes are larger than above.

R1613 (G029) [Grid Ref. 1221 3333]

Consists of 85% large untwinned feldspar grains. Many of the rectangular feldspars show a distinct zoning with the rims displaying a markedly higher relief than the cores. The majority of the feldspars are fresh but there are occasional patches displaying a speckly birefringence. This probably represents a slight sericitisation. Some feldspar areas are as large as 1 - 3mm across but a more typical size is 0.5mm. 15% of the slide consists of altered mafic minerals (< 0.5mm across).

R1466 (106A) [Grid Ref. 1221 3333]

Consists of roughly 60% feldspar (mostly plagioclase), 30% olivine, 5% titanite and 1% opaque. Accessory biotite was also identified. The feldspar is for the most part fresh, as is the pyroxene, but the olivine commonly displays crack and grain margin alteration. A few

small regions of high alteration, with no discernable primary structures, are also seen in thin section. Twinned feldspar laths are typically 1- 3mm long, however, untwinned areas are often much smaller. The subhedral olivine grains are as large as 3 - 5mm and the pyroxene grains are from 1 - 5mm.

R1520 (RG) [Grid Ref. 1221 3333]

This thin section consists of over 30% altered olivine and pyroxene, however, the feldspar, which represents 60 - 70% is fresh. A few discrete fresh pyroxene grains and about 5% opaque materials are also observed. The areas of alteration are up to 1mm across and the feldspar laths/areas are typically 3 - 4/1- 2mm in dimension respectively.

R1571 (RG-pyroxene), R1621 (RG-plagioclase feldspar) [Grid Ref. 1221 3333]

Consists of 40 - 50% feldspar, 40 - 50% titanite and 10% biotite mica/opaque. The feldspar is largely fresh but there are some grains which display a development of analcite. Laths are up to 10mm long but more typically are only 5mm. The fresh, sometimes ophitic, titanite grains are often of the order of 5 - 10mm across.

R1382 (124NA), R1505 (124NA), R1577 (124NA) [Grid Ref. 1288 3317]

This very fresh thin section consists of 50 - 65% labradorite feldspar, 20 - 25% titanite, 10 - 15% olivine and 5 - 10% opaque. The only sign of alteration is found along the cracks and margins of olivine grains. The plagioclase, displaying distinct normal zoning, is found in laths typically 1.0 x 0.2mm, however, some as large as 5.0 x 1.5mm were also observed. The sub-ophitic and sometimes zoned pyroxene is found as areas 5 - 15mm across. Rounded olivine grains are typically 1mm across and the subhedral opaque areas, which are often found in association with the titanite, are typically 0.5mm across.

R1467 (128B) [Grid Ref. 1291 3322]

This thin section displays a more even grain size than that for

feeder dyke 124NA, with a typical dimension being 0.25 - 1mm.

128B displays an intergranular texture. The labradorite (35 - 45%), the olivine (30 - 40%) and pyroxene (15 - 20%) are all very fresh.

(vi) Blind Rock Dyke

R1524 (G049M) [Grid Ref. 1850 3744]

Consists of about 50% << 0.5mm long labradorite feldspar laths which in some cases appear to show signs of slight alteration. The remaining 50% consists of ophitic pyroxene (0.5 - 1.5mm), subhedral olivine (0.5 - 1.5mm), opaque and some minor zeolite.

R1521 (G049C) [Grid Ref. 1850 3744]

Very similar to R1524 (G049C), except that grain sizes are markedly larger - olivine and pyroxene areas typically 2mm across, and feldspar laths commonly 0.4 x 0.1mm. The olivine shows strong alteration along cracks and grain boundaries.

(vii) Antrim Lava Group

R1527 (I001) [Grid Ref. 3434 3981]

Olivine phenocrysts abundant in poikilitic ophitic matrix. Zeolite amygdales prominent. The olivine is strongly altered along cracks and margins. Groundmass also shows strong alteration. Olivine phenocrysts are typically 0.2 - 0.7mm across, ophitic pyroxene commonly found in areas of dimension 0.1mm, and the matrix plagioclase laths are up to 0.15mm long. The zeolite amygdales range in size from 0.6 - 1mm.

R1522 (K2A) [Grid ref. 2882 4389]

This very fine-grained (sizes generally << 0.1mm) tholeiitic basalt consists of about 30% plagioclase feldspar with the rest being made up by olivine, pyroxene and opaque. Because of the very fine grain size, it was difficult to assess the state of freshness of the constituent minerals; however, the larger feldspar laths were reasonably fresh.

R1532 (TPO) [Grid Ref. 3206 3957]

Consists of 70% homogeneous brown glass, displaying well-developed perlitic fractures, and 30% rounded phenocrysts of quartz, feldspar and mafic material. The glass is very fresh with no signs of devitrification. Feldspar is observed to display a speckly sericitisation and the mafic grains are also altered. Phenocrysts range in size from 0.5 - 4mm.

R1523 (G062) [Grid Ref. 3217 4192]

Consists of olivine and plagioclase phenocrysts set in a fine-grained matrix, plus vesicles infilled with zeolite. The rounded rims of the olivines are altered, but as a whole, this mineral is reasonably fresh. The plagioclase phenocrysts are also fairly fresh, but the matrix material appears to be quite heavily altered.

R1617 (L009) [Grid Ref. 3220 4057]

Consists of roughly 50% feldspar and 50% mafic (largely olivine and ophitic pyroxene). All phases are very fresh. The feldspar laths are up to 2mm in length (more typically 0.5mm); the olivine grains are up to 1mm across and the ophitic pyroxene plates are as large as 4mm.

(viii) Mourne Mountains

R1572 (G2M-biotite) [Grid Ref. 3366 3267]

Larger biotite plates are very fresh.

R1573 (G4-orthoclase feldspar) [Grid Ref. 3225 3188]

The orthoclase feldspar grains (up to 5mm across) are homogeneous and very fresh.

R1578 (N022) [Grid Ref. 3253 3213]

Phenocrysts of olivine and feldspar (up to about 1mm size) set in a very fine-grained matrix. All phases appear to be altered with olivine phenocrysts being pseudomorphed by green amphibole and the plagioclase

feldspar phenocrysts being speckled with sericite.

R1614 (N003A) [Grid Ref. 3387 3246]

Consists of very large, generally fresh, plagioclase feldspar phenocrysts set in a matrix showing strong alteration. The plagioclase phenocrysts are anything from 0.5 - 2.5mm long and the matrix plagioclase laths are typically 0.05mm in length. The hornblende, which is the product of mafic alteration, is found as grains 0.1mm across and less (see scanning electron microscope work in Appendix 6).

R1615 (N003B) [Grid Ref. 3387 3246]

60 - 70% feldspar (largely plagioclase) and 30% secondary hornblende and opaque. The larger feldspar laths (0.25mm) are reasonably fresh but the smaller ones (< 0.1mm) appear to be altered. The hornblende grains are typically < 0.25mm across and the opaque areas range from 0.25 - 1mm.

R1620 (N002) [Grid Ref. 3387 3246]

Very similar to R1615 (N003B), except there is only 50% feldspar.

R1616 (P001) [Grid Ref. 3529 3335]

Phenocrysts of olivine set in a fine-grained sub-ophitic pyroxene and plagioclase matrix. Calcite mineralisation is also prominent. Generally altered, however, the larger feldspar laths are quite fresh.

(ix) Carlingford Complex

R1574 (R028) [Grid Ref. 3130 3137]

Consists of 70% feldspar (with quartz intergrowths), 20 - 30% quartz grains and < 5% disseminated opaque and amphibole grains. The feldspar displays alteration in parts. The laths of feldspar are up to 1mm long, quartz grains are typically 0.1 - 0.25mm across and the mafic grains are all less than 0.1mm in size.

R1618 (R031) [Grid Ref. 3133 3137]

80% feldspar, 10% olivine, 5% pyroxene and 5% opaque. The feldspar areas (1 - 5mm) are often fresh in the interior, but altered at the

margins. The olivine (1- 2mm) is highly altered along cracks and margins; however, the pyroxene (1 - 2mm) appears to be fairly fresh. There are also very fine-grained (sizes of the order of 10's of  $\mu$ ) patches of alteration with no determinable primary form.

R1619 (R048) [Grid Ref. 3098 3102]

Consists of 80% pyroxene and 20% plagioclase feldspar (< 5% opaque). The pyroxene is very pitted and blotchy and the feldspar is also heavily altered. Typical grain sizes are 1 - 4mm and 1 - 2mm respectively.



APPENDIX 8

The  $^{40}\text{Ar}$ - $^{39}\text{Ar}$  Stepwise Degassing Data Tables for the Samples Analysed  
in this Study

The basic data tables (produced by the computer program "STEPAGE"  
- see Section 5:7 and Appendix 5) for all the samples analysed in  
this study are on the microfiche card contained in this pocket:



REFERENCES

- Albarede, F., Feraud, G., Kaneoka, I., Allegre, C.J. (1973).  
The polytectonic record in K-feldspars from the Eastern Pyrenees  
by the  $^{39}\text{Ar}$ - $^{40}\text{Ar}$  method (abstract). 3rd. Europ. Coll. Geochron.  
Oxford.
- Albarede, F., Feraud, G., Kaneoka, I., Allegre, C.J. (1978).  
 $^{40}\text{Ar}$  -  $^{39}\text{Ar}$  dating: The importance of K-feldspars on multi-mineral  
data of polyorogenic areas.  
J.Geol. 86: 581-598.
- Albarede, F. (1978). The recovery of spatial isotope distributions from  
stepwise degassing data. Earth Planet. Sci. Lett. 39:387-391.
- Alexander, E.C. Jr., Davis, P.K. (1974).  $^{40}\text{Ar}$ - $^{39}\text{Ar}$  ages and trace  
element contents of Apollo 14 breccias; an interlaboratory cross-  
calibration of Ar- Ar standards. Geochim. Cosmochim. Acta.  
38:911-928.
- Alexander, E.C. Jr., Davis, P.K., Reynolds, J.H., Srinivasan, B. (1973).  
Radiogenic xenon and argon in 14318 and implications (abstract).  
Lunar Science IV:30-32. Lunar Science Institute, Houston.
- Baksi, A.K. (1973). Quantitative unspiked argon runs in K-Ar dating.  
Can. J. Earth Sci. 10:1415-1419.
- Baksi, A.K. (1974). Isotopic fractionation of a loosely held atmospheric  
argon component in the Picture Gorge Basalts. Earth Planet. Sci.  
Lett. 21:431-438.
- Beckinsale, R.D., Thompson, R.N., Durham, J.J. (1974). Petrogenetic  
significance of initial  $^{87}\text{Sr}/^{86}\text{Sr}$  ratios in the North Atlantic  
Tertiary Igneous Province in the light of Rb-Sr, K-Ar and  $^{18}\text{O}$   
abundance studies in the Sarqâta qâqâ intrusive complex, Ubekendt,  
Ejland, West Greenland. J. Petrol. 15:525-538.
- Bennett, D.J. (1972). Elements of nuclear power. Longman.
- Berger, G.W. (1975).  $^{40}\text{Ar}/^{39}\text{Ar}$  step heating of thermally overprinted  
biotite, hornblende and potassium feldspar from Eldora, Colorado.  
Earth Planet. Sci. Lett. 26:387-408.
- Berger, G.W., York, D. (1979).  $^{40}\text{Ar}$ - $^{39}\text{Ar}$  dating of multicomponent  
magnetizations in the Archean Shelley Lake granite, northwestern  
Ontario. Can. J. Earth Sci. 16:1933-1941.
- Berger, G.W., York, D. (1981). Geothermometry from  $^{40}\text{Ar}/^{39}\text{Ar}$  dating  
experiments. Geochim. Cosmochim. Acta. 45:795-811.
- Berger, G.W., York, D., Dunlop, D.J. (1979). Calibration of Grenvillian  
paleopoles by  $^{40}\text{Ar}/^{39}\text{Ar}$  dating. Nature, 277:46-48.
- Bernatowicz, T.J., Hohenberg, C.M., Hudson, B., Kennedy, B.M., Podosek,  
F.A. (1978). Argon ages for lunar breccias 14064 and 15405. Proc.  
9th Lunar Planet. Sci. Conf. :905-919.

- Bogard, D.D., Husain, L., Wright, R.J. (1976).  $^{40}\text{Ar}$ - $^{39}\text{Ar}$  dating of collisional events in chondrite parent bodies. *J. Geophys. Res.* 81:5664-5678.
- Bottomley, R.J., York, D. (1976).  $^{40}\text{Ar}$ - $^{39}\text{Ar}$  age determinations on the Owyhee Basalt of the Columbia Plateau. *Earth Planet. Sci. Lett.* 31:75-84.
- Brandt, S.B., Voronovsky, S.N. (1967). Dehydration and diffusion of argon in micas. *Int. Geol. Rev.* 9:1504.
- Brereton, N.R. (1970). Corrections for interfering isotopes in the  $^{40}\text{Ar}/^{39}\text{Ar}$  dating method. *Earth Planet. Sci. Lett.* 8:427-433.
- Brereton, N.R., (1972). A reappraisal of the  $^{40}\text{Ar}/^{39}\text{Ar}$  stepwise degassing technique. *Geophys. J.R. astr. Soc.* 27:449-478.
- Briden, J.C., Henthorn, D.I., Rex, D.C. (1971). Palaeomagnetic and radiometric evidence for the age of the Freetown igneous complex, Sierra Leone. *Earth Planet. Sci. Lett.* 12:385-391.
- Brook, M. (1984). The age of the Corrachair Granite. In Harding, R.R., Merriman, R.J., Nancarrow, P.H.A. *St. Kilda: an illustrated account of the geology.* Rep. Br. Geol. Surv. 16(7).
- Brooks, C., Hart, S.R., Wendt, I. (1972). Realistic use of two-error regression treatments as applied to rubidium-strontium data. *Rev. Geophys. Space Phys.* 10:551-577
- Brooks, C.K. (1973). The Tertiary of Greenland: a volcanic record of continental break-up. In Pitcher, M.G., Ed. *Artic geology.* Mem. Am. Ass. Petrol. Geol. 19:150-160.
- Buchan, K.L., Berger, G.W., McWilliams, M.O., York D., Dunlop, D.J. (1977). Thermal overprinting of natural remanent magnetization and K/Ar ages in metamorphic rocks. *J. Geomagn. Geoelectr.* 29:401-410.
- Cadogan, P.H., Turner, G. (1976). The chronology of the Apollo 17 station 6 boulder. *Proc. 7th. Lunar Sci. Conf.* 2:2267-2285.
- Cameron, I.B., Sabine, P.A. (1969). The Tertiary welded-tuff vent agglomerate and associated rocks at Sandy Braes, Co. Antrim. *Inst. Geol. Sci. Rep.* 69/6
- Chandler, J.A. (1977). X-ray microanalysis in the electron microscope. In Glauert, A.M., Ed. *Practical methods in electron microscopy.* North-Holland.
- Clague, D.A., Dalrymple, G.B., Moberly, R. (1975). Petrography and K-Ar ages of dredged volcanic rocks from the western Hawaiian Ridge and the Southern Emperor Seamount Chain. *Bull. Geol. Soc. Am.* 86:991-998.
- Cliff, R.A. (1985). Isotopic dating in metamorphic belts. *J. geol. Soc. Lond.* 142:97-110.

- Crank, J. (1975). The mathematics of diffusion. 2nd. ed. O.U.P.
- Dagley, P., Mussett, A.E. (1985). Palaeomagnetism and radiometric dating of the British Tertiary Igneous Province: Muck and Eigg. In preparation.
- Dallmeyer, R.D. (1975).  $^{40}\text{Ar}/^{39}\text{Ar}$  ages of biotite and hornblende from a progressively remetamorphosed basement terrane: their bearing on interpretation of release spectra. *Geochim. Cosmochim. Acta.* 39: 1655-1669
- Dallmeyer, R.D. (1978).  $^{40}\text{Ar}/^{39}\text{Ar}$  incremental-release ages of hornblende and biotite across the Georgia Inner Piedmont: their bearing on Late Palaeozoic-Early Mesozoic tectono-thermal history. *Am. J. Sci.* 278:124-149.
- Dallmeyer, R.D. (1979).  $^{40}\text{Ar}/^{39}\text{Ar}$  dating: principles, techniques and applications in orogenic terrains. In Jäger, E. and Hunziker, J.C. *Lectures in isotope geology*: 77-104. Springer.
- Dallmeyer, R.D., Rivers, T. (1983). Recognition of extraneous argon components through incremental-release  $^{40}\text{Ar}/^{39}\text{Ar}$  analysis of biotite and hornblende across the Grenvillian metamorphic gradient in southeastern Labrador. *Geochim. Cosmochim. Acta.* 47:413-428.
- Dalrymple, G.B. (1969).  $^{40}\text{Ar}/^{36}\text{Ar}$  analysis of historic lava flows. *Earth Planet. Sci. Lett.* 6:47-55.
- Dalrymple, G.B., Clague, D.A. (1976). Age of the Hawaiian-Emperor bend. *Earth Planet. Sci. Lett.* 31:313-329
- Dalrymple, G.B., Clague, D.A., Lanphere, M.A. (1977). Revised age for Midway volcano, Hawaiian volcanic chain. *Earth Planet. Sci. Lett.* 37: 07-116.
- Dalrymple, G.B., Grommé, C.S., White, R.W. (1975). Potassium-argon age and paleomagnetism of diabase dikes in Liberia: initiation of central Atlantic rifting. *Bull. Geol. Soc. Am.* 86:399-411.
- Dalrymple, G.B., Lanphere, M.A. (1969). Potassium-argon dating: principles, techniques and applications to geochronology. Freeman.
- Dalrymple, G.B., Lanphere, M.A. (1971).  $^{40}\text{Ar}/^{39}\text{Ar}$  technique of K-Ar dating: a comparison with the conventional technique. *Earth Planet. Sci. Lett.* 12:300-308.
- Dalrymple, G.B., Lanphere, M.A. (1974).  $^{40}\text{Ar}/^{39}\text{Ar}$  age spectra of some undisturbed terrestrial samples. *Geochim. Cosmochim. Acta.* 38:713-738.
- Dalrymple, G.B., Moore, J.G. (1968). Argon-40 excess in submarine pillow basalts from Kilauea Volcano Hawaii. *Science.* 161:1132-1135.
- Damon, P.E., Laughlin, A.W., Percious, J.K. (1967). Problem of excess argon-40 in volcanic rocks. In *Radioactive dating and methods of low-level counting*: 468-481. Int. At. En. Agency, Vienna.

- Davis, P.K. (1977). Effects of shock pressure on  $^{40}\text{Ar}$ - $^{39}\text{Ar}$  radiometric age determinations. *Geochim. Cosmochim. Acta.* 41:195-205.
- Davis, P.K., Lewis, R.S., Reynolds, J.H. (1971). Stepwise heating analyses of rare gases from pile-irradiated rocks 10044 and 10057. *Proc. 2nd. Lunar Sci. Conf. Geochim. Cosmochim. Acta. Suppl.* 2:1693-1703.
- Del Moro, A., Puxeddu, M., Radicati di Brozolo, F., Villa, I.M. (1982). Rb-Sr and K-Ar ages on minerals at temperatures of 300°-400° from deep wells in the Larderello geothermal field (Italy). *Contrib. Mineral. Petrol.* 81:340-349.
- Dickin, A.P. (1981). Isotope geochemistry of Tertiary igneous rocks from the Isle of Skye, N.W. Scotland. *J. Petrol.* 22:155-189.
- Dickin, A.P., Jones, N.W. (1983). Isotopic evidence for the age and origin of pitchstones and felsites, Isle of Eigg, N.W. Scotland. *J. geol. Soc. Lond.* 140:691-700.
- Dodson, M.H. (1973). Closure temperature in cooling geochronological and petrological systems. *Contrib. Mineral. Petrol.* 40:259-274.
- Dodson, M.H., Long, L.E. (1962). Age of Lundy granite, Bristol Channel. *Nature.* 195:975-976.
- Dymond, J. Hogan, L. (1973). Noble gas abundance patterns in deep sea basalts - primordial gases from the mantle. *Earth Planet. Sci. Lett.* 20:131-139.
- Emeleus, C.H. (1955). The granites of the Western Mourne Mountains, County Down. *Sci. Proc. R. Dubl. Soc.* 27:35-50.
- Evans, A.L., Fitch, F.J., Miller J.A. (1973). Potassium-argon age determinations on some British Tertiary igneous rocks. *J. geol. Soc. Lond.* 129:419-443.
- Faller, A.M. (1975). Palaeomagnetism of the oldest Tertiary basalts in the Kangerdlugssuaq area of east Greenland. *Bull. Geol. Soc. Denmark.* 24:173-178.
- Feraud, G., Gastaud, J., Audenze, J-M, Olivet, J-L., Cornen, G. (1982).  $^{40}\text{Ar}/^{39}\text{Ar}$  ages for the alkaline volcanism and the basement of Gorrington Bank, North Atlantic Ocean. *Earth Planet. Sci. Lett.* 57:211-226.
- Fitch, F.J., Hooker, P.J., Miller, J.A., Brereton, N.R. (1978). Glauconite dating of Palaeocene-Eocene rocks from East Kent and the timescale of Palaeogene volcanism in the North Atlantic region. *Jl. geol. Soc. Lond.* 135:499-512.
- Fitch, F.J., Hurford, A.J. (1977). Fission track dating of the Tardree rhyolite, Co. Antrim. *Proc. Geol. Ass.* 88:267-274.
- Fitch, F.J., Miller, J.A., Hooker, P.H. (1976). Single rock K-Ar isochrons. *Geol. Mag.* 113:1-10.

- Fitch, F.J., Miller, J.A., Mitchell, J.G. (1969). A new approach to isotopic dating in orogenic belts. In Kent, P.E., et al., Eds. Time and place in orogeny: 157-196. Geol. Soc., London.
- Fleck, R.J., Sutter, J.F., Elliott, D.H. (1977). Interpretation of discordant  $^{40}\text{Ar}/^{39}\text{Ar}$  age-spectra of Mesozoic tholeiites from Antarctica. *Geochim. Cosmochim. Acta.* 41:15-32.
- Flisch, M (1982). Potassium-argon analysis. In Odin, G.S., Ed. Numerical dating and stratigraphy: 151-158. Wiley.
- Foland, K.A. (1974).  $\text{Ar}^{40}$  diffusion in homogeneous orthoclase and an interpretation of Ar diffusion in K-feldspars. *Geochim. Cosmochim. Acta.* 38:151-166.
- Foland, K.A. (1979). Limited mobility of argon in a metamorphic terrain. *Geochim. Cosmochim. Acta.* 43:793-801.
- Fowler, A. (1957). *Summ. Prog. geol. Surv. Lond.*, 1956: 48-49.
- French, A.P. (1968). *Special Relativity.* Nelson.
- Gale, N.H. (1982). The physical decay constants. In Odin, G.S., Ed. Numerical dating and stratigraphy. 107-138. Wiley.
- Giletti, B.J. (1974). Diffusion related to geochronology. In Hofmann, A.W. et al., Eds. *Geochemical transport and kinetics:* 61-76. Carnegie Inst. of Washington.
- Goldstein, J.I., Newbury, D.E., Echlin, P., Joy, D.C., Fiori, C., Lifshin, E. (1981). *Scanning electron microscopy and X-ray microanalysis: a text for biologists, materials scientists, and geologists.* Plenum.
- Hall, C.M., York, D. (1978). K-Ar and  $^{40}\text{Ar}/^{39}\text{Ar}$  age of the Laschamp geomagnetic polarity reversal. *Nature.* 274:462-464.
- Halsall, T.J. (1974). The minor intrusions and structure of the Carlingford complex, Eire. Ph.D thesis. Univ. Leicester.
- Hanes, J.A., York, D. (1979). A detailed  $^{40}\text{Ar}/^{39}\text{Ar}$  age study of an Abitibi dike from the Canadian Superior Province. *Can.J. Earth Sci.* 16:1060-1070.
- Hanson, G.N., Simmons, K.R., Bence, A.E. (1975).  $^{40}\text{Ar}/^{39}\text{Ar}$  spectrum ages for biotite hornblende and muscovite in a contact metamorphic zone. *Geochim. Cosmochim. Acta.* 39:1269-1278.
- Harland, W.B., Cox, A.V., Llewellyn, P.G., Pickton, C.A.G., Smith, A.G., Walters, S.R. (1982). *A geologic time scale.* C.U.P.
- Harrison, T.M. (1981). Diffusion of  $^{40}\text{Ar}$  in hornblende. *Contrib. Mineral. Petrol.* 78:324-331.
- Harrison, T.M., Armstrong, R.L., Naeser, C.W., Harakal, J.E. (1979). Geochronology and thermal history of the Coast Plutonic Complex, near Prince Rupert, British Columbia. *Can. J. Earth Sci.* 16:400-410.



- Harrison, T.M., McDougall, I. (1980a). Investigations of an intrusive contact, northwest Nelson, New Zealand(1). Thermal, Chronological and isotopic constraints. *Geochim. Cosmochim. Acta.* 44:1985-2003.
- Harrison, T.M., McDougall, I. (1980b). Investigations of an intrusive contact, northwest Nelson, New Zealand(2). Diffusion of radiogenic and excess Ar in hornblende revealed by  $^{40}\text{Ar}/^{39}\text{Ar}$  age spectrum analysis. *Geochim. Cosmochim. Acta.* 44:2005-2020.
- Harrison, T.M., McDougall I. (1981). Excess  $^{40}\text{Ar}$  in metamorphic rocks from Broken Hill, New South Wales: implications for  $^{40}\text{Ar}/^{39}\text{Ar}$  age spectra and the thermal history of the region. *Earth Planet. Sci. Lett.* 55:123-149.
- Harrison, T.M., McDougall, I. (1982). The thermal significance of potassium feldspar K-Ar ages inferred from  $^{40}\text{Ar}/^{39}\text{Ar}$  age spectrum results. *Geochim. Cosmochim. Acta.* 46:1811-1820.
- Hart, S.R. (1960). Extracts from the thesis investigations of S.R. Hart, Eighth Ann. Prog. Report. U.S. Atomic Energy Commission Contract, M.I.T., 87.
- Hart, S.R. (1964). The petrography and isotopic-mineral age relations of a contact zone in the Front Range, Colorado. *J. Geol.* 72:493-525.
- Hart, S.R. (1981). Diffusion compensation in natural silicates. *Geochim. Cosmochim. Acta.* 45:279-291.
- Hawkes, J.R., Merriman, R.J., Harding, R.R., Derbyshire, D.P.F. (1975). In Harrison, R.K., Ed. Expeditions to Rockall, 1971-2. Rep. Inst. geol. Sci. No. 75/1.
- Horn, P., Jessberger, E.K., Kirsten, T., Richter, H. (1975).  $^{39}\text{Ar}/^{40}\text{Ar}$  dating of lunar rocks: effects of grain size and neutron irradiation. Proc. 6th Lunar Sci. Conf. *Geochim. Cosmochim. Acta. Suppl.* 6:1563-1591.
- Horne, R.R., Macintyre, R.M. (1975). Apparent age and significance of Tertiary dykes in the Dingle Peninsula, S.W. Ireland. *Sci. Proc. R. Dubl. Soc.* 5:293-299.
- Huneke, J.C. (1976). Diffusion artefacts in dating by stepwise thermal release of rare gases. *Earth Planet. Sci. Lett.* 28:407-417.
- Huneke, J.C., Podosek, F.A., Turner, G., Wasserburg, G.J. (1972).  $^{40}\text{Ar}$ - $^{39}\text{Ar}$  systematics in lunar rocks and separated minerals of lunar rocks from Apollo 14 and 15 (abstract). In *Lunar Science III*:367-368. Lunar Science Institute, Houston.
- Huneke, J.C., Smith, S.P. (1976a).  $^{39}\text{Ar}$  recoil out of small grains and implications for  $^{40}\text{Ar}/^{39}\text{Ar}$  dating. *Lunar Science VII*:402-404. Lunar Science Institute, Houston.
- Huneke, J.C., Smith, S.P. (1976b). The realities of recoil:  $^{39}\text{Ar}$  recoil out of small grains and anomalous age patterns in  $^{39}\text{Ar}$ - $^{40}\text{Ar}$  dating. Proc. 7th Lunar Sci. Conf.:1987-2008

- Hunziker, J.C. (1979). Potassium argon dating. In Jäger, E. and Hunziker, J.C. Lectures in isotope geology:52-76. Springer.
- Jäger, E. (1973). Die Alpine Orogenese im Lichte der Radiometrischen Alterbestimmung. *Eclogae Geol. Helv.* 66,1:11-21.
- Jessberger, E.K. (1977). Comment on "Identification of excess  $^{40}\text{Ar}$  by the  $^{40}\text{Ar}/^{39}\text{Ar}$  age spectrum technique" by M.A. Lanphere and G.B. Dalrymple. *Earth Planet. Sci. Lett.* 37:167-168.
- Jessberger, E.K., Horn, P., Kirsten, T. (1975).  $^{39}\text{Ar}$ - $^{40}\text{Ar}$ -dating of lunar rocks: A methodical investigation of mare basalt 75075. Lunar Science VI. Part 1:441-443. Lunar Science Institute, Houston.
- Jessberger, E.K., Huneke, J.C., Podosek, F.A., Wasserburg, G.J. (1974). High resolution argon analysis of neutron-irradiated Apollo 16 rocks and separated minerals. *Proc. 5th Lunar. Sci. Conf. Geochim. Cosmochim. Acta. Suppl.* 5,2:1419-1449.
- Jones, E.J.W., Mitchell, J.G., Shido, F., Phillips, J.D. (1972). Igneous rocks dredged from the Rockall Plateau. *Nat. phys. Sci.* 237:118-120.
- Kaneoka, I. (1974). Investigation of excess argon in ultramafic rocks from the Kola Peninsula by the  $^{40}\text{Ar}/^{39}\text{Ar}$  method. *Earth Planet. Sci. Lett.* 22:145-156.
- Kaneoka, I. (1975). Non-radiogenic argon in terrestrial rocks. *Geochem. J.* 9:113-124.
- Kaneoka, I. (1980). Rare gas isotopes and mass fractionation: an indicator of gas transport into or from a magma. *Earth Planet. Sci. Lett.* 48:284-292.
- Kelly, W.R.E. (1973). Geochronological studies of the Tertiary igneous activity on the Isle of Skye, north-west Scotland. M. Sc. dissertation. Univ. Newcastle.
- Kirsten, T., Deubner, J., Horn, P., Kaneoka, I., Schaeffer, O.A. (1972). The rare gas record of Apollo 14 and 15 samples. *Proc. 3rd Lunar Sci. Conf. Geochim. Cosmochim. Acta. Suppl.* 3:1865-1891.
- Krummenacher, D. (1970). Isotopic composition of argon in modern surface volcanic rocks. *Earth Planet. Sci. Lett.* 8:109-117.
- Lanphere, M.A., Dalrymple, G.B. (1971). A test of the  $^{40}\text{Ar}/^{39}\text{Ar}$  age spectrum technique on some terrestrial materials. *Earth Planet. Sci. Lett.* 12:359-372.
- Lanphere, M.A., Dalrymple, G.B. (1976). Identification of excess  $^{40}\text{Ar}$  by the  $^{40}\text{Ar}/^{39}\text{Ar}$  age spectrum technique. *Earth Planet. Sci. Lett.* 32:141-148.
- Lanphere, M.A., Dalrymple, G.B. (1978). The use of  $^{40}\text{Ar}/^{39}\text{Ar}$  data in evaluation of disturbed K-Ar systems. USGS Open-file rep. 78-710 :241-243
- Lippolt, H.J. (1970). Argon-Isotopen-Anomalien in Gesteinen. Habilitationsschrift Universität Heidelberg.

- Long, L.E. (1964). Preliminary Rb-Sr investigation of Tertiary granite and granophyre from Skye. *Geochim. Cosmochim. Acta.* 28:1870-1873.
- Lopez-Martinez, M., York, D. (1983). Further thermochronometric unravelling of the age and palaeomagnetic record of the southwest Grenville Province. *Can. J. Earth Sci.* 20:953-960.
- McDougall, I. (1981).  $^{40}\text{Ar}/^{39}\text{Ar}$  age spectra for the KBS Tuff, Koobi Fora Formation. *Nature*, 294:120-124.
- McDougall, I., Polach, H.A., Stipp, J.J. (1969). Excess radiogenic argon in young subaerial basalts from the Auckland volcanic field, New Zealand. *Geochim. Cosmochim. Acta.* 33:1485-1520.
- McDougall, I., Roksandic, Z. (1974). Total fusion  $^{40}\text{Ar}/^{39}\text{Ar}$  ages using HIFAR reactor. *J. Geol. Soc. Aust.* 21:81-89.
- McIntyre, G.A., Brooks, S.C., Compston, W., Turek, A. (1966). The statistical assessment of Rb-Sr isochrons. *J. Geophys. Res.* 71:5459-5468.
- Macintyre, R.M. (1973). Lower Tertiary geochronology of the North Atlantic continental margins. In *Geochronology and isotope geology of Scotland, field guide, reference.* Pidgeon et al., K1-25, ECOG Oxford, Sept, 1973.
- Macintyre, R.M., McMenamin, T., Preston, J. (1975). K-Ar results from Western Ireland and their bearing on the timing and siting of Thulean magmatism. *Scott. J. Geol.* 2:227-249.
- Mankinen, E.A., Dalrymple, G.B. (1972). Electron microprobe evaluation of terrestrial basalts for whole-rock K-Ar dating. *Earth Planet. Sci. Lett.* 17:89-94.
- Meighan, I.G., Gamble, J.A. (1972). Tertiary acid magmatism in N.E. Ireland. *Nat. phys. Sci.* 240:183-184.
- Mellor, D.W., Mussett, A.E. (1975). Evidence for initial  $^{36}\text{Ar}$  in volcanic rocks, and some implications. *Earth Planet. Sci. Lett.* 26:312-318.
- Merrihue, C. (1965). Trace-element determinations and potassium-argon dating by mass spectroscopy of neutron-irradiated samples. *Eos.* 46:125.
- Merrihue, C., Turner, G., (1966). Potassium-argon dating by activation with fast neutrons. *J. Geophys. Res.* 71:2852-2857.
- Miller, E.L., Sutter, J.F. (1982). Structural geology and  $^{40}\text{Ar}-^{39}\text{Ar}$  geochronology of the Goldstone-Lane Mountain area, Mojave Desert, California. *Bull. Geol. Soc. Am.* 93:1191-1207.
- Miller, J.A. (1965). Geochronology and continental drift - the North Atlantic. *Phil. Trans. R. Soc.* A258:180-191.
- Miller, J.A., Brown, P.E. (1963). An absolute age determination in the Mourne Mountains granite. *Geol. Mag.* 100:93.

- Miller, J.A., Fitch, F.J. (1962). Age of the Lundy granites. *Nature*. 195:553-555.
- Miller, J.A., Mitchell, J.G., Evans, A.L1. (1970). The argon-40/argon-39 dating method applied to basic rocks. In Runcorn, S.K., Ed. *Palaeogeophysics:481-489*. Academic Press.
- Miller, J.A., Mohr, P.A. (1965). Potassium-argon age determinations on rocks from St. Kilda and Rockall. *Scott. J. Geol.* 1:93-99.
- Mitchell, G.F. (1980). The search for Tertiary Ireland. *J. Earth. Sci. R. Dub. Soc.* 3:13-33.
- Mitchell, J.G. (1968). Potassium-argon dating of neutron-irradiated minerals. Ph.D thesis. Univ. Cambridge.
- Mitchell, J.G., Mohr, P. (1985). K-Ar ages of Tertiary dolerites from west Connacht, Ireland, show regional gradients. In preparation.
- Mohr, P. (1982). Tertiary dolerite intrusions of west-central Ireland. *Proc. R. Ir. Acad.* 82b:53-82.
- Mohr, P., Mussett, A.E., Kennan, P.S. (1984). The Droimchogaidh sill, Connacht, Ireland. *Geol. J.* 19:1-21.
- Morris, P. (1974). A Tertiary dyke system in south-west Ireland. *Proc. R. Ir. Acad.* 74b:179-184.
- Mussett, A. E. (1969). Diffusion measurements and the potassium-argon method of dating. *Geophys. J. R. astr. Soc.* 18:257-303.
- Mussett, A.E. (1980). British Tertiary Igneous Province probably not associated with East Greenland lavas. *Nature*. 284:376-377.
- Mussett, A.E. (1982). Paleomagnetism and dating of the British Tertiary Igneous Province. *Open Earth*. 15:29-30.
- Mussett, A.E. (1984). Time and duration of Tertiary igneous activity of Rhum and adjacent areas. *Scott. J. Geol.* 20(3):273-279.
- Mussett, A.E. (1985).  $^{40}\text{Ar}$ - $^{39}\text{Ar}$  step-heating ages of the Tertiary igneous rocks of Mull, Scotland. Submitted to *J. geol. Soc. Lond.*
- Mussett, A.E., Brown, G.C., Eckford, M., Charlton, S.R. (1973). The British Tertiary Igneous Province: K-Ar ages of some dykes and lavas, from Mull, Scotland. *Geophys. J. R. astr. Soc.* 30:405-414.
- Mussett, A.E., Dalrymple, G.B. (1968). An investigation of the source of air Ar contamination in K-Ar dating. *Earth Planet, Sci. Lett.* 4:422-426.
- Mussett, A.E., McCormack, A.G. (1978). On the use of 3-dimensional plots in K-Ar dating. *Geochim. Cosmochim. Acta.* 42:1877-1883.
- Mussett, A.E., Ross, J.G., Gibson, I.L. (1980).  $^{40}\text{Ar}/^{39}\text{Ar}$  dates of eastern Iceland lavas. *Geophys. J. R. astr. Soc.* 60:37-52.
- Nier, A.O. (1950). A redetermination of the relative abundances of carbon, nitrogen, oxygen, argon and potassium. *Phys. Rev.* 77:789-793.

- Old, R.A. (1975). The age and field relationships of the Tardree Rhyolite Complex. Co. Antrim, Northern Ireland. Bull. geol. Surv. Gt. Br. 51:21-40.
- Ozima, M. (1973). Was the evolution of the atmosphere continuous or catastrophic? Nature. 246:41-42.
- Ozima, M. (1975). Ar isotopes and Earth-atmosphere evolution models. Geochim. Cosmochim. Acta. 39:1127-1134.
- Ozima, M., Honda, M., Saito, K. (1977).  $^{40}\text{Ar}$ - $^{39}\text{Ar}$  ages of guyots in the western Pacific and discussion of their evolution. Geophys. J. R. astr. Soc., 51:475-485.
- Ozima, M., Kaneoka, I., Yanagisawa, M. (1979). Temperature and pressure effects on  $^{40}\text{Ar}$ - $^{39}\text{Ar}$  systematics. Earth Planet. Sci. Lett. 42:463-472.
- Ozima, M., Takigami, Y. (1980). Activation energy for thermal release of Ar from some DSDP submarine rocks. Geochim. Cosmochim. Acta. 44:141-144.
- Pankhurst, R.J., Moorbath, S., Rex, D.C., Turner, G. (1973). Mineral age patterns in ca. 3700 my old rocks from West Greenland. Earth Planet. Sci. Lett. 20:157-170.
- Podosek, F.A., Huneke, J.C. (1973). Argon 40-Argon 39 chronology of four calcium-rich achondrites. Geochim. Cosmochim. Acta. 37:667-684.
- Preston, J. (1965). Tertiary feeder dykes in the west of Ireland. Proc. geol. Soc. Lond. 1626:149-150.
- Preston, J. (1967). The Blind Rock dyke, Co. Donegal. Ir. Nat. J. 15:286-293.
- Preston, J. (1981). Tertiary igneous activity. In Holland, C.H., Ed. A geology of Ireland:213-223. Scottish Academic Press.
- Purdy, J.W., Jäger, E. (1976). K-Ar ages on rock-forming minerals from the central Alps. Mem. 1st. Geol. Mineral. Univ. Padova. 30:3-31.
- Purdy, J.W., Mussett, A.E., Charlton, S.R., Eckford, M.J., English, N.H.N. (1972). The British Tertiary Igneous Province: Potassium-Argon ages of the Antrim basalts. Geophys. J. R. astr. Soc. 27:327-335.
- Radicati di Brozolo, F., Huneke, J.C., Papanastassiou, D.A., Wasserburg, J.G. (1981).  $^{40}\text{Ar}$ - $^{39}\text{Ar}$  and Rb-Sr age determinations on Quaternary volcanic rocks. Earth Planet. Sci. Lett. 53:445-456.
- Reffay, A., Ricq de Bonard, M., Tanpirard, J. (1974). Mise en point sur la datation des basaltes irlandais (1). Norois. 21:411-426.
- Reynolds, J.H., Turner, E. (1964). Rare gases in the chondrite Renasso. J. Geophys. Res. 69:3263-3281.

- Richey, J.E. (1928). The structural relations of the Mourne Granites, (Northern Ireland). *Quart. J. geol. Soc. Lond.* 83:653-688.
- Riddihough, R.P., Max, M.D. (1976). A geological framework for the continental margin to the west of Ireland. *Geol. J.* 11:109-120.
- Roddick, J.C. (1978). The application of isochron diagrams in  $^{40}\text{Ar}$ - $^{39}\text{Ar}$  dating: a discussion. *Earth Planet, Sci. Lett.* 41:233-244.
- Roddick, J.C. (1983). High precision intercalibration of  $^{40}\text{Ar}$ - $^{39}\text{Ar}$  standards. *Geochim. Cosmochim. Acta.* 47:887-898.
- Roddick, J.C., Cliff, R.A., Rex, D.C. (1980). The evolution of excess argon in Alpine biotites - A  $^{40}\text{Ar}$ - $^{39}\text{Ar}$  analysis. *Earth Planet. Sci. Lett.* 48:185-208.
- Ross, J.G. (1976). The validation and application of the  $^{40}\text{Ar}/^{39}\text{Ar}$  dating technique to eastern Iceland lavas and the geological and geophysical significance of the results. Ph.D thesis. Univ. Liverpool.
- Saito, K., Ozima, M. (1977).  $^{40}\text{Ar}$ - $^{39}\text{Ar}$  geochronological studies on submarine rocks from the western Pacific area. *Earth Planet. Sci. Lett.* 33:353-369
- Sarda, P., Staudacher, T., Allègre, C.J. (1985).  $^{40}\text{Ar}/^{36}\text{Ar}$  in MORB glasses: constraints on atmosphere and mantle evolution. *Earth Planet. Sci. Lett.* 72:357-375.
- Schilling, J.G., Noe-Nygaard, A. (1974). Faeroe-Iceland plume: rare-earth evidence. *Earth Planet. Sci Lett.* 24: 1-14.
- Scrutton, P.A. (1973). The age relationship of igneous activity and continental break up. *Geol. Mag.* 110:227-234.
- Seidemann, D. (1978).  $^{40}\text{Ar}/^{39}\text{Ar}$  studies of deep-sea rocks. *Geochim. Cosmochim. Acta.* 42:1721-1734.
- Soper, N.J., Higgins, A.C., Downie, C., Matthews, D.W., Brown, P.E. (1976). Late Cretaceous-early Tertiary stratigraphy of the Kangerdlugssuak area, east Greenland, and the age of the opening of the north-east Atlantic. *J. geol. Soc. Lond.* 132:85-104.
- Steiger, R.H., Jäger, E. (1977). Subcommittee on geochronology: convention on the use of decay constants in geo- and cosmo-chronology. *Earth Planet. Sci. Lett.* 36:359-362.
- Stettler, A., Bochsler, P. (1979). He, Ne and Ar composition in a neutron activated sea-floor basalt glass. *Geochim. Cosmochim. Acta.* 43:157-169.
- Stukas, V., Reynolds, P.H. (1974).  $^{40}\text{Ar}$ - $^{39}\text{Ar}$  dating of the Long Range dykes, Newfoundland. *Earth Planet, Sci. Lett.* 22:256-266.
- Tetley, N., McDougall, I. (1978). Anomalous  $^{40}\text{Ar}/^{39}\text{Ar}$  release spectra for biotites from the Berridale Batholith, New South Wales, Australia. USGS Open-file rep. 78-701:427-430.

- Tetley, N., McDougall, I., Heydegger, H.R. (1980). Thermal neutron interferences in the  $^{40}\text{Ar}/^{39}\text{Ar}$  dating technique. *J. Geophys. Res.* 85:7201-7205.
- Tomkeieff, S.I., Marshall, C.E. (1935). The Mourne dyke swarm. *Quart. J. geol. Soc.* 91:251-292.
- Tomkeieff, S.I., Marshall, C.E. (1940). The Killough-Ardglass dyke swarm. *Quart. J. geol. Soc.* 96:321-338.
- Topping, J. (1972). Errors of observation and their treatment. 4th. ed. Chapman and Hall.
- Turner, D.L., Forbes, R.B. (1976). K-Ar studies in deep basement drill holes: a new geological estimate of argon blocking in biotite (abstract). *Eos.* 57:353.
- Turner, G. (1968). The distribution of potassium and argon in chondrites. In Ahrens, L.H., Ed. *Origin and distribution of the elements:387-398*. Pergamon.
- Turner, G. (1969). Thermal history of meteorites. In Millman, Ed., *Meteorite research:407-417*. Reidel.
- Turner, G. (1970). Argon-40/argon-39 dating of lunar rock samples. *Geochim. Cosmochim. Acta. Suppl.* 2:1665
- Turner, G. (1971a). Argon 40- argon 39 dating: The optimization of irradiation parameters. *Earth Planet. Sci. Lett.* 10:227-234.
- Turner, G. (1971b).  $^{40}\text{Ar}/^{39}\text{Ar}$  ages from the lunar maria. *Earth Planet. Sci. Lett.* 11:169-191.
- Turner, G. (1979). A Monte Carlo fragmentation model for the production of meteorites: Implications for gas retention ages. *Proc. 10th. Lunar Sci. Conf.:*1917-1941.
- Turner, G., Cadogan, P.H. (1974). Possible effects of  $^{39}\text{Ar}$  recoil in  $^{40}\text{Ar}-^{39}\text{Ar}$  dating. *Proc. 5th. Lunar Sci. Conf. Geochim. Cosmochim. Act. Suppl.* 5,2:1601-1615.
- Turner, G., Cadogan, P.H., Yonge, C.J. (1973). Argon selenochronology. *Proc. 4th. Lunar Sci. Conf. Geochim. Cosmochim. Acta. Suppl.* 4,2:1889-1914.
- Turner, G., Cadogan, P.H., Yonge, C.J. (1974). The early chronology of the moon and meteorites (abstract). In *Lunar Science V:807-808*. Lunar Science Institute, Houston.
- Turner, G., Enright, M.C., Cadogan, P.H. (1978). The early history of chondrite parent bodies inferred from  $^{40}\text{Ar}-^{39}\text{Ar}$  ages. *Proc. 9th. Lunar Planet. Sci. Conf.:* 989-1025.
- Turner, G., Huneke, J.C., Podosek, F.A., Wasserburg, G.J. (1972).  $\text{Ar}^{40}-\text{Ar}^{39}$  systematics in rocks and separated minerals from Apollo 14. *Proc. 3rd. Lunar Sci. Conf. Geochim. Cosmochim. Acta Suppl.* 3,2:1589-1612.

- Turner, G., Jones, C.M., Butterfield, A.W. (1983). Ancient atmospheric argon in cherts. In Pepin, R.O., O'Connell, R. Eds. Conference on Planetary volatiles. LPI Tech. Rep. 83-01:188.
- Turner, G., Miller, J.A., Grasty, R.L. (1966). The thermal history of the Bruderheim meteorite. *Earth Planet. Sci. Lett.* 1:155-157.
- Vogt, P.R., Avery, O.E., (1974). Detailed magnetic surveys in the northeast Atlantic and Labrador Sea. *J. Geophys. Res.* 79:363-389.
- Wagner, G.A., Reimer, G.M., Jäger, E. (1977). Cooling ages derived by apatite fission track mica Rb-Sr and K-Ar dating: the uplift and cooling history of the central Alps. *Univ. Padua Mem.* 30:1-27.
- Walker, D.A., McDougall, I. (1982).  $^{40}\text{Ar}/^{39}\text{Ar}$  and K-Ar dating of altered glassy volcanic rocks: the Dabi Volcanics, P.N.G. *Geochim. Cosmochim. Acta.* 46:2181-2190.
- Walker, G.P.L. (1951). The amygdale-minerals in the Tertiary lavas of Ireland. 1. The distribution of chabazite habits and zeolites in the Garron Plateau area. *Mineral. Mag.* 29:773-791.
- Walker, G.P.L. (1959). Some observations on the Antrim basalts and associated dolerite intrusions. *Proc. Geol. Ass.* 70:179-205.
- Walker, G.P.L. (1960). The amygdale minerals in the Tertiary lavas of Ireland. 3: Regional distribution. *Mineral. Mag.* 32:503-527.
- Walsh, J.N., Beckinsale, R.D., Thorpe, R.S., Skelhorn, R.R. (1979). Geochemistry and petrogenesis of Tertiary granitic rocks from the Island of Mull, northwest Scotland. *Contrib. Mineral. Petrol.* 71:99-116.
- Wang, S., McDougall, I., Tetley, N., Harrison, T.M. (1980).  $^{40}\text{Ar}/^{39}\text{Ar}$  age and thermal history of the Kirin chondrite. *Earth Planet. Sci. Lett.* 49:117-131.
- Wapstra, A.H., Bos, K. (1976). 1975 mass-excess predictions. *Atomic Data and Nuclear Data Tables.* 17:474-475.
- Weast, R.C. (1983). Handbook of chemistry and physics. 64th. ed. CRC Press Inc.
- Wilson, R.L. (1970). Palaeomagnetic stratigraphy of Tertiary lavas from Northern Ireland. *Geophys. J. R. astr. Soc.* 20:1-9.
- Wolberg, J.R. (1967). Prediction analysis. Van Nostrand.
- York, D. (1969). Least squares fitting of a straight line with correlated errors. *Earth Planet. Sci. Lett.* 6:320-324.